## AD NUMBER

**AD867307**

## NEW LIMITATION CHANGE

TO

**Approved for public release, distribution unlimited**

FROM

**Distribution authorized to U.S. Gov't. agencies and their contractors; Administrative/Operational Use; Feb 1970. Other requests shall be referred to Air Force Materials Lab., Attn: MAMC, Wright-Patterson AFB, OH 45433.**

## AUTHORITY

**AFML ltr, 29 Mar 1972**

AFML-TR-69-84
PART III, VOLUME III



# STABILITY CHARACTERIZATION OF REFRACTORY MATERIALS UNDER HIGH VELOCITY ATMOSPHERIC FLIGHT CONDITIONS

## PART III, VOLUME III: EXPERMENTAL RESULTS OF HIGH VELOCITY HOT GAS/COLD WALL TESTS

*LARRY KAUFMAN*
*HARVEY NESOR*
*ManLabs, Inc.*

TECHNICAL REPORT AFML-TR-69-84, PART III, VOLUME III

FEBRUARY 1970



AIR FORCE MATERIALS LABORATORY
AIR FORCE SYSTEMS COMMAND
WRIGHT-PATTERSON AIR FORCE BASE, OHIO

NOTICE

When Government drawings, specifications, or other data are
or any purpose other than in connection with a definitely related
ument procurement operation, the United States Government
y incurs no responsibility nor any obligation whatsoever; and the
fact that the Government may have formulated, furnished, or in any way supplied the said drawings, specifications, or other data, is not to be regarded by implication or otherwise as in any manner licensing the holder or any other person or corporation, or conveying any rights or permission to manufacture, use, or sell any patented invention that may in any way be related thereto.

This document is subject to special export controls and each transmittal to foreign governments or foreign nationals may be made only with prior approval of the Air Force Materials Laboratory (MAMC), Wright-Patterson Air Force Base, Ohio 45433.

Distribution of this report is limited for the protection of technology related to critical materials restricted by the Export Control Act.

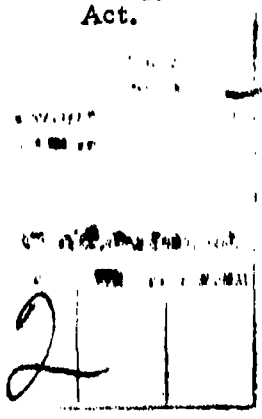

Copies of this report should not be returned unless return is required by security considerations, contractual obligations, or notice on a specific document.

700 - March 1970 - CO455 - 112-2464

# STABILITY CHARACTERIZATION OF REFRACTORY MATERIALS UNDER HIGH VELOCITY ATMOSPHERIC FLIGHT CONDITIONS

## PART III, VOLUME III: EXPERMENTAL RESULTS OF HIGH VELOCITY HOT GAS/COLD WALL TESTS

*LARRY KAUFMAN*

*HARVEY NESOR*

## FOREWORD

This report was prepared by ManLabs, Inc., Cambridge, Mass., with the assistance of Avco/SSD, Wilmington, Mass. (H. Hoercher, Project Director, supported by J. Recesso, R. Abate and R. Broughton) under Project 7312, "Metal Surface Deterioration and Protection," Task 731201, "Metal Surface Protection," and Project 7350, "Refractory Inorganic Nonmetallic Materials," Task Numbers 735001, "Refractory Inorganic Nonmetallic Materials: Nongraphitic," and 735002, "Refractory Inorganic Nonmetallic Materials: Graphitic," under AF33(615)-3859, and was administered by the Metals and Ceramics Division of the Air Force Materials Laboratory (MAMC), with J. D. Latva, J. Krochmal and N. M. Geyer acting as Project Engineers.

This report covers the period from April 1966 to July 1969.

ManLabs' personnel participating in this study included L. Kaufman, H. Nesor, H. Bernstein, J.R. Baron, G. Stepakoff, R. Hopper, R. Yeaton, S. Wallerstein, E. Sybicki, J. Davis, K. Meaney, K. Ross, J. Dudley, E. Offner, A. Macey, A. Silverman and A. Constantino.

The following reports will be issued under this contract.

| Part/Volume | |
|---|---|
| I-I | Summary of Results |
| II-I | Facilities and Techniques Employed for Characterization of Candidate Materials |
| II-II | Facilities and Techniques Employed for Cold Gas/Hot Wall Tests |
| II-III | Facilities and Techniques Employed for Hot Gas/Cold Wall Tests |
| III-I | Experimental Results of Low Velocity Cold Gas/Hot Wall Tests |
| III-II | Experimental Results of High Velocity Cold Gas/Hot Wall Tests |
| III-III | Experimental Results of High Velocity Hot Gas/Cold Wall Tests |
| IV-I | Theoretical Correlation of Material Performance with Stream Conditions |
| IV-II | Calculation of the General Surface Reaction Problem |

This report was released by the authors in December 1969.

This technical report has been reviewed and is approved.

W. G. RAMKE
Chief, Ceramics and Graphite Branch
Metals and Ceramics Divisions
Air Force Materials Laboratory

## ABSTRACT

The oxidation of refractory borides, graphites and JT composites, hypereutectic carbide-graphite composites, refractory metals, coated refractory metals, metal oxide composites, and iridium coated graphites in air over a wide range of conditions was investigated over the spectrum of conditions encountered during reentry or high velocity atmospheric flight, as well as those employed in conventional furnace tests. Elucidation of the relationship between hot gas/cold wall (HG/CW) and cold gas/hot wall (CG/HW) surface effects in terms of heat and mass transfer rates at high temperatures was a principal goal.

Arc plasma exposures have been performed at Mach Numbers between 0.1 and 3.2 stagnation pressures between 0.01 and 1.0 atm., stagnation enthalpies up to 16,000 BTU/lb, cold wall heat flux up to 1200 BTU/ft$^2$sec, exposure times up to 23,400 seconds and surface temperatures between 2100$^\circ$ and 6500$^\circ$F. Data include material recession, metallographic and X-ray analysis, radiated heat flux and normal total emittance. In addition, color motion picture coverage was provided. Materials forming solid oxides show lower recessions in the HG/CW tests at a stated surface temperature than in CG/HW tests. The reverse is true for ablating materials. Temperature gradients of 800$^\circ$ to 1500$^\circ$F through 30-50 mil oxides are observed. The practical implications of this finding are substantial (if the gradients exist under free flight conditions). Since the temperature level experienced by the substrate is substantially below that predicted, strength and load carrying capacity of the substrate would be much higher than for the case where gradients are ignored. Long-time cyclic exposures of diboride composites in the Model 500 and ROVERS facilities for trajectories typified by FDL-7MC provide a striking illustration of the reuse capability of boride composites for lifting reentry applications.

A $HfB_2$+SiC composite was exposed for thirteen cycles at 0.07 atm (1 psi) stagnation pressure, a stagnation enthalpy of 10,200 BTU/lb and a cold wall heat flux of 495 BTU/ft$^2$sec. Each cycle was about 1800 seconds long with a total exposure time of 22,500 seconds at a surface temperature near 5300$^\circ$R. Total material recession was 15 mils. A $ZrB_2$+SiC composite was exposed for four cycles at 1.0 atm (15 psi) stagnation pressure, a stagnation enthalpy of 5000 BTU/lb and a cold wall heat flux of 380 BTU/ft$^2$sec. Each cycle was 1800 seconds long, total exposure time was 7200 seconds. The surface temperatures were near 5000$^\circ$R. Total material recession was 26 mils. Under similar conditions graphite and tungsten would exhibit recessions of 7 to 14 inches.

These results illustrate the reuse capability of boride composites for lifting reentry application, since they exceed the range of conditions for FDL-7MC. This capability is unrivaled by any other materials system.

Surface temperatures calculated from stream conditions and radiation equilibrium agree with observed temperatures on melting. When solid coatings are present, surface temperatures are below computed values. Silicon carbide bearing materials achieve lower temperatures than predicted from stream conditions and exhibit superior behavior.

TABLE OF CONTENTS

## LIST OF ILLUSTRATIONS

## LIST OF TABLES

# I. INTRODUCTION AND SUMMARY

## A. Introduction

The response of refractory materials to high temperature oxidizing conditions imposed by furnace heating has been observed to differ markedly from the behavior in arc plasma "reentry simulators." The former evaluations are normally performed for long times at fixed temperatures and slow gas flows with well defined solid/gas-reactant/product chemistry. The latter on the other hand are usually carried out under high velocity gas-flow conditions in which the energy flux rather than the temperature is defined and significant shear forces can be encountered. Consequently, the differences in philosophy, observables and techniques used in the "material centered" regime and the "environment centered-reentry simulation" area differ so significantly as to render correlation of material responses at high and low speeds difficult if not impossible in many cases. Under these circumstances, expeditious utilization of the vast background of information available in either area for optimum matching of existing material systems with specific missions or prediction and synthesis of advanced material systems to meet requirements of projected missions is sharply curtailed.

In order to progress toward the elimination of this gap, an integrated study of the response of refractory materials to oxidation in air over a wide range of time, gas velocity, temperature and pressure has been designed and implemented. This interdisciplinary study spans the heat flux and boundary-layer-shear spectrum of conditions encountered during high velocity atmospheric flight as well as conditions normally employed in conventional materials centered investigations. In this context, significant efforts have been directed toward elucidating the relationship between hot gas/cold wall (HG/CW) and cold gas/hot wall (CG/HW) surface effects in terms of heat and mass transfer rates at high temperatures, so that full utilization of both types of experimental data can be made. The elucidation of mass transfer reactions has been studied in regimes where gaseous and solid oxide formation occurs.

The principal goal of this study is the coupling of the material-centered and environment-centered philosophies in order to gain a better insight into systems behavior under high-speed atmospheric flight conditions. This coupling function has been provided by an interdisciplinary panel composed of scientists representing the component philosophies. The coupling framework consists of an intimate mixture of theoretical and experimental studies specifically designed to overlap temperature/energy and pressure/velocity conditions. This overlap has provided a means for the evaluation of test techniques and the performance of specific materials systems under a wide range of flight conditions. In addition, it provides a base for developing an integrated theory of modus operandi capable of translating

reentry systems requirements such as velocity, altitude, configuration and life time into requisite materials properties as vaporization rates, oxidation kinetics, density, etc., over a wide range of conditions.

The correlation of heat flux, stagnation enthalpy, Mach No., stagnation pressure and specimen geometry with surface temperature through the utilization of thermodynamic, thermal and radiational properties of the material and environmental systems used in this study was of prime importance in defining the conditions for overlap between materials-centered and environment-centered tests.

Significant practical as well as fundamental progress along the above mentioned lines necessitated evaluation of refractory material systems which exhibit varying gradations of stability above 2700°F. Emphasis was placed on candidates for 3400° to 6000°F exploitation. Thus, borides, carbides, boride-graphite composites (JTA), JT composites, carbide-graphite composites, pyrolytic and bulk graphite, PT graphite, coated refractory metals/alloys, oxide-metal composites, oxidation resistant refractory metal alloys and iridium-coated graphites were considered (See Table 1). Similarly, a range of test facilities and techniques including oxygen pickup measurements, cold sample/hot gas and hot sample/cold gas devices at low velocities, as well as different arc plasma facilities capable of covering the 50-2500 BTU/ft$^2$sec flux range under conditions equivalent to speeds up to Mach 12 at altitudes up to 200,000 ft were employed. Stagnation pressures between 0.001 and 10 atmsopheres were covered. Splash and pipe tests were performed in order to evaluate the effects of aerodynamic shear. Based on the present results, this range of heat flux and stagnation enthalpy produced surface temperatures between 2000° and 6500°F.

## B. Summary

The present report is one of a series (1 - 6)* and describes the results of Hot Gas/Cold Wall exposures performed at Avco/SSD and at the Wave Superheater Arc Tunnel of Cornell Aeronautical Laboratory. The testing at Avco/SSD was performed under the direction of H. Hoercher. J. Recesso, R. Broughton and R. Abate were actively engaged in performing these tests. Exposures were carried out in the Model 500, ROVERS and Ten Megawatt Arc Facilities. The range of conditions employed in these tests covered stagnation pressures between 0.002 and 4.0 atm., stagnation enthalpy between 2000 and 16,000 BTU/lb, cold wall heat flux between 100 and 1500 BTU/ft$^2$sec and exposure times between 20 seconds and 23,000 seconds. A full spectrum of diagnostic measurements including surface temperature and radiated heat flux was continuously monitored during the exposures. Complete color film coverage were reported for selected models. A complete description of the techniques employed in these tests has been presented (3).

*Underscored numbers in parentheses indicate references given at the end of this report.

Testing in the Cornell Wave Superheater was performed under the direction of S. Tate, D. Colosimo and K. Graves. The Wave Superheater offers the possibility of exposing samples at very high velocity for short times. The heat flux levels can be varied by changing the position of the specimen relative to the nozzle. In this manner variable heat flux/temperature levels can be attained. Multiple-sample runs can be made using samples in the size range programmed. CAL furnished data on gas enthalpy, heat flux, surface temperature, stagnation pressure as well as colored motion pictures of the test samples. A complete description of testing methods has been presented (3). All test samples were returned to ManLabs for post-mortem metallography conducted under the direction of H. Nesor.

Current results for boride-base materials indicate substantially lower recession rates in the HG/CW arc plasma tests than in the CG/HW furnace tests. This difference is most striking for $HfB_{2.1}$ (A-2) and $ZrB_2$(A-3) where an order of magnitude difference is observed at surface temperatures of 4000°F. This difference is reduced by the addition of SiC to the boride. Thus, the HG/CW and CG/HW results for $HfB_2$ + SiC(A-4) and (A-7) agree more closely than do the corresponding data for the pure diborides. Results of "in-depth" temperature measurements during arc plasma tests indicate that these differences are principally due to temperature gradients through the oxide. Direct measurements indicate that temperature gradients of 1500°F can exist through a 100 mil wall thickness of boride plus oxide.

Gradients have also been observed for $HfB_{2.1}$(A-2) and $ZrB_2$(A-3) in the high velocity CG/HW tests (5). In these tests the temperature of the CG/HW interface is lower than that of the substrate. Moreover, the rate of oxidation observed in these high velocity CG/HW tests agreed with results of CG/HW furnace tests (in which virtually no gradients exist) run at temperatures corresponding to the surface temperatures observed in the high velocity CG/HW tests. In the HG/CW arc plasma tests, however, the temperature is highest at the HG/CW interface. The rate of oxidation observed in the arc plasma tests at a stated HG/CW surface temperature is much less than that observed in furnace tests at the same surface temperature. Moreover, the gradients appear to exist for long periods of time. These findings are in general agreement with the deductions based on post-mortem metallography and comparison of arc plasma and furnace oxidation tests. The figure shown below offers a schematic representation of the behavior of oxide forming refractory materials in the CG/HW and HG/CW tests.

The central figure represents the oxide and matrix of a solid oxide forming material (i.e., $HfB_{2.1}$(A-2), $ZrB_2$(A-3) or Hf-20Ta-2Mo(I-23) in a CG/HW furnace test at 3900°R. The temperature distribution across the oxide and matrix zones is assumed to be constant. In the figure at the right, which represents the temperature gradients through a high velocity CG/HW sample (inductively heated), the temperature is lowest at the CG/HW surface. Conversely, in the figure at the left representing a HG/CW arc plasma test sample, the temperature is highest at the HG/CW surface. These schematic figures suggest, that if the observed recession is limited by the minimum temperature in the oxide (where diffusion rates

of oxygen and components of the substrate would be slowest) the present HG/CW and high velocity CG/HW results could be brought into line with the CG/HW furnace results where temperature gradients are largely absent.

SCHEMATIC REPRESENTATION OF

MINIMUM OXIDE TEMPERATURE LIMIT CRITERION

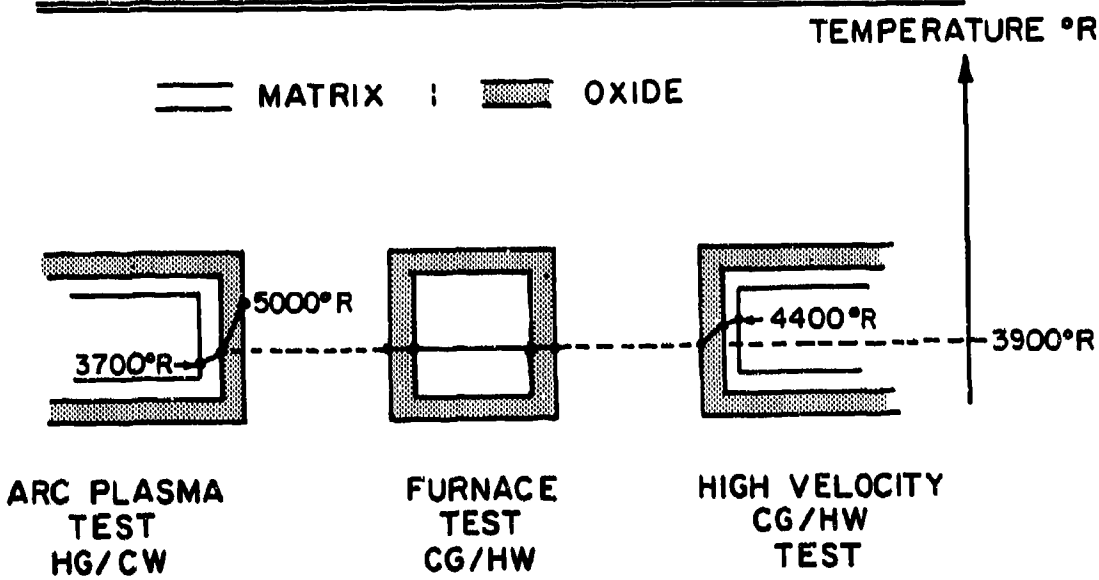


The practical implications of this finding are quite substantial since if thin layers of these solid oxides can result in such large gradients (and if the gradients exist under free flight conditions), the temperature level experienced by the substrate is substantially below the temperature at the HG/CW surface. Under such circumstances, the predicted strength and load carrying capacity of the substrate would be much higher than for the case where gradients are ignored.

As a direct illustration of the implications of these findings a number of long-time cyclic exposures of diboride composites have been performed in the Model 500 and ROVERS facilities to evaluate reuse capabilities for trajectories typified by FDL-7MC which is shown in the figure below. The results provide a striking illustration of the reuse capability of these materials for lifting reentry applications.

Sample $HfB_{2.1}$ + 20%SiC(A-7)-28R was exposed for thirteen cycles at 0.07 atm (1 psi) stagnation pressure, a stagnation enthalpy of 10,200 BTU/lb and a cold wall heat flux of 495 BTU/$ft^2$sec. Each cycle

# REUSE CAPABILITY OF BORIDE COMPOSITES DEVELOPED UNDER AIR FORCE MATERIALS LABORATORY PROGRAMS BY MANLABS INC.

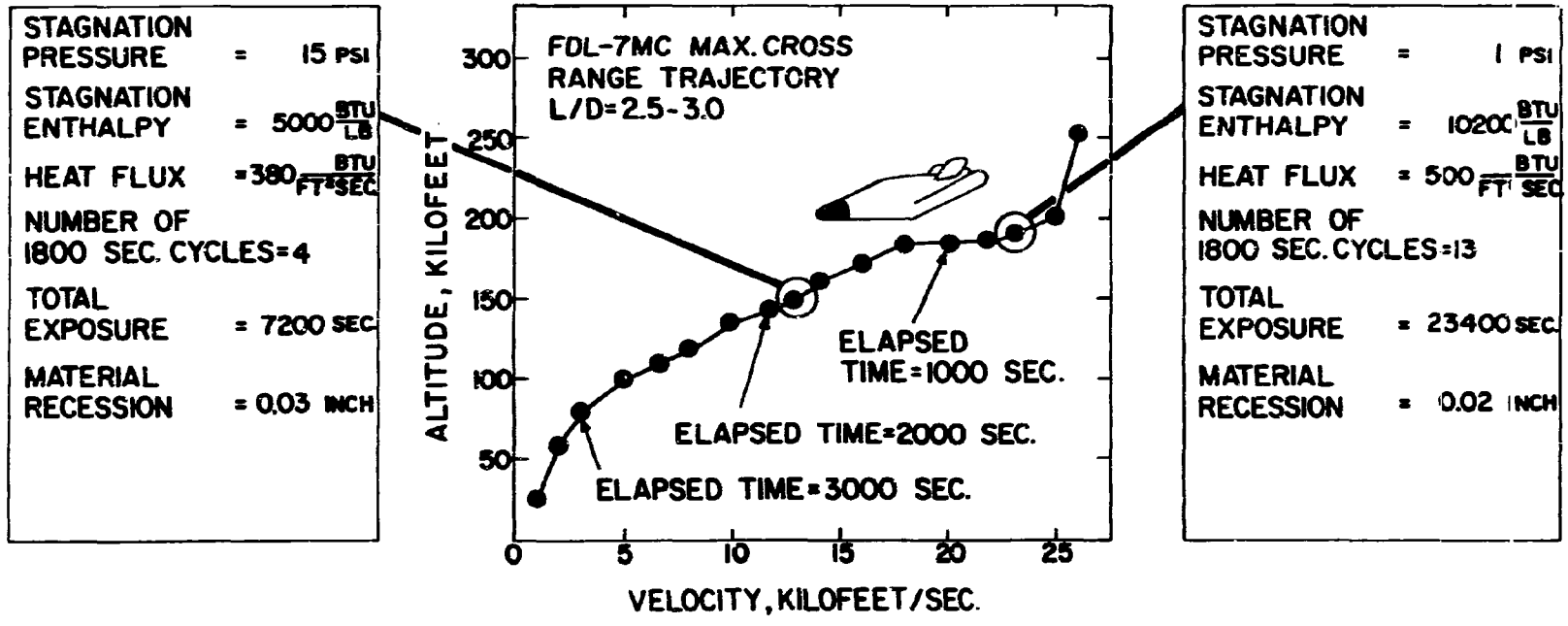


SCHEMATIC REPRESENTATION OF REUSE CAPABILITIES OF BORIDE COMPOSITES

was about 1800 seconds long with a total exposure time of 22,500 seconds. The surface temperature increased from one cycle to the next starting at 3500°R and holding near 5300°R for cycles 5 through 13. Total material recession was 15 mils after this extremely long exposure. Sample $ZrB_{2.1}$ + 20%SiC(A-8)-15M was exposed for four cycles at 1.0 atm (15 psi) stagnation pressure, a stagnation enthalpy of 5000 BTU/lb and a cold wall heat flux of 380 BTU/ft$^2$sec. Each cycle was 1800 seconds long, total exposure time was 7200 seconds. The surface temperatures were near 5000°R. Total material recession was 26 mils. Finally, sample $ZrB_2$+SiC+C (A-10)-26R (which is not illustrated on the accompanying figure) was exposed at 0.236 atmospheres (3 psi) stagnation pressure, a stagnation enthalpy of 7700 BTU/lb and a cold wall heat flux of 455 BTU/ft$^2$sec. This test covered eleven cycles of approximately 1800 seconds duration for a total exposure time of 18,900 seconds. Surface temperature held near 5100°R after the first cycle. Total material recession was 83 mils.

These results illustrate the reuse capability of boride composites for lifting reentry application, since their range of applicability exceeds the range of conditions and flight times of the FDL-7MC trajectory shown above. This capability is unrivaled by any other materials system.

The candidate $ZrB_2$(A-3) material did not exhibit any thermal stress failures at flux levels as high as 950 BTU/ft$^2$sec. However, Boride Z(A-5) exhibited thermal shock cracks after exposure at flux levels above 200-250 BTU/ft$^2$sec.

Boride composites $HfB_2$+20%SiC(A-4) and (A-7), and $ZrB_2$+ 20%SiC(A-8) were found to exhibit remarkable oxidation and thermal stress resistance in HG/CW arc plasma tests. Although these materials display temperature gradients in the oxides, the difference between the arc plasma and furnace oxidation depths are small. The adherent oxide which forms on these composites results in low recessions observed after exposures in the 3500°-4500°F temperature range. In addition, (A-4) exhibited no thermal shock failures at flux levels up to 1000 BTU/ft$^2$sec. Radiation equilibrium calculations performed for exposures of these materials showed that the ratio T(CALC)/T(OBS) for (A-2), (A-3) and (A-4) exceeds unity thus the observed temperature was 16% lower than expected for (A-2), 9% lower than expected for (A-3) and 22% lower than expected (based on radiation equilibrium) for (A-4). Similarly, the other boride composites containing SiC, i.e., $HfB_2$+20%SiC(A-7), $ZrB_2$+20%SiC(A-8) and $HfB_2$+ 35%SiC(A-9) yielded ratios of 1.25, 1.34 and 1.17. Moreover, exposure of hemispherical models exhibited lower surface temperatures than those observed for flat faced cylinders.

Examination of $HfB_2$+SiC(A-7) after 14,030 seconds exposure in eight-1800 second cycles at a stagnation pressure of 1.03 atmospheres a cold wall heat flux of 450 BTU/ft$^2$sec and an enthalpy level of 4180 BTU/lb, showed a total recession of 329 mils or about 0.32 inches. Under similar conditions graphite and tungsten would exhibit recessions of 14 to 28 inches. $ZrB_2$+20%SiC(A-8) displays all of the same features shown by $HfB_2$+SiC(A-7) although it is not as refractory as its hafnium base counterpart. However, the decrease in temperature resistance is compensated for by the reduced density and cost. Zirconium diboride is roughly one

half the density and one tenth the price of hafnium diboride. Measurements of the temperature gradients through oxide coatings formed on $ZrB_2$+SiC (A-8) yielded results which are smaller than exhibited by $ZrB_2$(A-3). This finding appears to be due to the higher thermal conductivity of the oxide formed on (A-8) (as compared with (A-3)). $ZrB_2$+SiC(A-8) exhibits the same tendency to develop low temperatures as (A-4) and (A-7). The behavior of $HfB_2$+35%SiC(A-9) was found to be similar to (A-4) and (A-7). The major difference is that (A-9) is less refractory than (A-4) and (A-7).

Recession rates observed for graphites in HG/CW arc plasma tests are substantially higher than thos observed in CG/HW furnace tests at 1-9 ft/sec in air flow rate. This indicates that the latter are supply limited. The results of high velocity CG/HW tests on graphite at air flow rates near 250 ft/sec approach the results obtained in the arc plasma exposures. Modest temperature gradients were measured through graphite samples during HG/CW tests. Limiting survival conditions for Si/RVC(B-8) determined under HG/CW conditions depart from the behavior in furnace tests and correspond to the failure characteristics observed for silicon carbide in HG/CW tests. In the arc plasma tests, Si/RVC(B-8) exhibits protective oxidation up to surface temperatures near 3800°F, some 700°F above the failure temperature in furnace tests. Graphite-type behavior occurs above this temperature. The recession rates of all of the graphites are inversely proportional to material density.

Hypereutectic carbides HfC+C(C-11) and ZrC+C(C-12) exhibited excellent oxidation resistance at surface temperatures below 5000°F and melted under very high temperature conditions in line with reported melting points. The present results are consistent with the eutectic temperatures but show little dependence on the melting point of the oxides. Current data indicate comparable oxidation rates in the CG/HW and HG/CW tests. No thermal shock failures were noted at flux levels up to 750 BTU/$ft^2$sec. In line with the oxidation behavior noted in furnace tests, the HG/CW arc plasma tests show a "puffy" oxide which forms at the lower temperatures investigated. This oxide has been noted in air oxidation tests performed in furnaces below 3400°F. Rapid oxidation occurs at the back of samples where the surface temperature is lower than at the front face. This is another characteristic of the HfC+C (C-11) oxidation which is in line with the furnace test results (4). The oxidation behavior of samples containing 13.6 w/o C does not appear to differ materially from samples fabricated from the billets which contain 14.0 to 15.6 w/o carbon. The behavior of ZrC+C(C-12) in the HG/CW arc plasma tests was found to be similar to that of HfC+C(C-11).

KT-SiC(E-14) exhibited rapid recession rates at surface temperatures above 3900°F. This is some 400°F above the limit observed in furnace tests and in line with the results obtained for Si/RVC(B-8).

Composites of borides, carbides and graphites including $ZrB_2$+SiC+C(A-10), JTA(C-$ZrB_2$-SiC)(D-13), JT0992(C-HfC-SiC)(F-15) and JT0981(C-ZrC-SiC)(F-16) exhibited HG/CW tests results which were comparable to their CG/HW behavior. At elevated temperatures, destruction of the protective oxide coatings leads to graphite-type recession behavior. $ZrB_2$+SiC+C(A-10) exhibits the best oxidation resistance in this group owing to the fact that is is a boride-base rather than a graphite base composite. It

also shows lower recession rates in the HG/CW tests than in the CG/HW tests as is the case for $ZrB_2$(A-3). Melting of $ZrB_2$+SiC+C(A-10) is encountered near 5000°F where substantial differences between low pressure and one atmosphere oxidation rates are observed. Thermal shock failures were not observed at flux levels up to 1010 BTU/ft$^2$sec. The low density (4.5 gms/cm$^3$), high strength, low modulus and good machinability exhibited by this composite, when coupled with its oxidation resistance up to 5000°F, offer an exceptional combination of properties.

In general, the behavior of the (A-10) composite is quite similar to that exhibited by (A-4), (A-7) and (A-8). Although (A-10) is not as refractory as (A-4) and (A-7) the lower density, cost, thermal stress resistance and machining characteristics of this composite provide compensating advantages for application in reusable lifting reentry spacecraft.

Extensive precautions were taken in order to insure that temperature measurements of the model surface are accurate. In general, the comparison of observed surface temperatures in HG/CW arc plasma tests with values calculated from stream conditions are in relatively good agreement. Moreover, a number of temperature measurements employing two color pyrometers yielded good results. Additional verification was obtained by measuring the melting points of tungsten and molybdenum in the arc facilities using pure nitrogen streams for comparison with accepted values. The relatively good agreement obtained in these tests should eliminate concern over the accuracy of surface temperature measurements due to interference of the arc with optical observations.

A substantial number of thermal shock failures of JTA(D-13) and JT0981(F-16) have been observed. For JTA(D-13), these failures occurred in random fashion at flux levels above 500 BTU/ft$^2$sec. The samples which failed by thermal shock were machined from 2-1/2" diameter x 2" long billets of JTA(D-13) in an orientation which corresponded to the hot pressing direction. Thus, the axis of the arc plasma test sample was parallel to that of the hot pressed cylinder. Under these conditions, residual strain present in the billets and in the samples could provide a source of the failures. However, a series of samples oriented with their axes perpendicular to the pressing direction showed no thermal shock failures at flux levels in excess of 500 BTU/ft$^2$sec. This finding has particular relevance to applications in which JTA(D-13) parts are exposed to severe environmental heat fluxes. JT0992(F-15) did not exhibit sensitivity to thermal shock.

The behavior of these composites is characterized by low recession rates at temperatures between 3000°F and 4000°F, best illustrated in $ZrB_2$+SiC+C(A-10) and JT0992(F-15) at temperatures up to 4500°F. Above 5000°F, the protection afforded by formation of $ZrO_2$ (or $HfO_2$) and $SiO_2$ is eliminated and oxidation rates which are characteristic of graphite are encountered.

Failure limits for the coated refractory metals $WSi_2$/W (G-18) and Sn-Al/Ta-10W(G-19) have been established in general agreement with furnace tests. Maximum survival conditions for $WSi_2$/W(G-18)

are 450 BTU/ft$^2$sec and 3100 BTU/lb at $P_e$ = 1 atm. At lower pressures, failure was observed at 458 BTU/ft$^2$sec and 11,420 BTU/lb. Coating failure conditions were established for Sn-Al/Ta-10W(G-19) at lower flux and enthalpy levels. Modest temperature gradients were measured through $WSi_2$/W(G-18) arc plasma test samples.

Current results for W+Zr+Cu(G-20) indicate relatively good resistance to oxidation at 10,000 BTU/lb and 500 BTU/ft$^2$sec at 0.100 atm. However, at 1 atmosphere stagnation pressure, very rapid degradation was observed at much lower flux and enthalpy levels. This behavior indicates that the mechanism of degradation is sensitive to pressure in the 0.1-1.0 atmosphere range. The precise nature of the degradation mechanism which is operative is not clear at present. The results obtained for W+Ag (G-21) in the Model 500 tests at stagnation pressures of one atmosphere were comparable to the results for (G-20).

The silica-tungsten composites $SiO_2$+68.5 w/o W(H-22) and $SiO_2$+60 w/o W(H-23) exhibited similar recession behavior in the one atmosphere HG/CW arc plasma tests as encountered in the CG/HW furnace tests. At low pressures, higher recession rates were observed due to instability of $SiO_2$ relative to SiO. At temperatures above 4000°F, extensive flow of this composite was observed, in agreement with the furnace test findings. Samples exposed at one atmosphere showed sting hole cracking.

Arc plasma exposures of Hf-20Ta-2Mo(I-23) exhibited lower oxidation rates than in the CG/HW tests at comparable surface temperatures. In addition, several samples with indicated surface temperatures in excess of the melting point of the alloy did not melt. Current results indicate that gradients of 1500°F can exist through 100 mils of alloy and oxide. This behavior is the basis for the surface temperature in the 4000°-5000°F range which were not accompanied by melting of the alloy.

Hf-Ta-Mo(I-23) was exposed to seven cyclic exposures at a stagnation pressure of 1.05 atmospheres, a stagnation enthalpy of 3300 BTU/lb and a cold wall heat flux of 410 BTU/ft$^2$sec. The observed surface temperature was 4230°F and a recession of 138 mils was observed after an exposure of 11,600 seconds in cycles of 1800 second duration. This behavior is not quite as good as that exhibited by $ZrB_2$+20%SiC(A-8) or $ZrB_2$+SiC+C(A-10) which were exposed under more severe conditions than (I-23)-27M and exhibited less recession. Nevertheless, Hf-20Ta-2Mo (I-23) is metallic and as such offers advantages as regards fabricability and resistance to thermal stress. On the other hand (A-8) and (A-10) possess higher strength and more temperature capability than (I-23). Hf-20Ta-2Mo(I-23) was also exposed to a 4 cycle exposure at a stagnation pressure of 0.132 atm, an enthalpy of 7600 BTU/lb and a cold wall heat flux of 398 BTU/ft$^2$sec. Total exposure time was 7220 seconds yielding a recession of 55 mils. As indicated above, boride composites exposed to more severe conditions in the ROVERS facility exhibited less recession. However, the behavior of Hf-Ta-Mo(I-23)-38R is outstanding for a metallic structure.

Present results for Ir/C(I-24) are in general agreement with the CG/HW tests, which showed that iridium exhibits very low oxidation rates up to its melting temperature at 4430°F. The temperature of the iridium-carbon eutectic is 4175°F. Samples exposed to higher conditions exhibited melting of the coating and ablation of the graphite. The major drawback of this coating system is the low emittance of the iridium ($\epsilon = 0.30$). However, addition of $HfO_2$ raised the emittance to values near 0.50 and extended the range of conditions under which the coating can be used. Thus, the pure coating is destroyed at flux levels in excess of 310 BTU/ft$^2$sec. At flux levels below 300 BTU/ft$^2$sec the coating is hardly affected; however, at higher levels, melting followed by rapid ablation occurs. In contrast, when $HfO_2$ is added to increase the emittance, failure does not occur until the flux level reaches 510 BTU/ft$^2$sec. Thus, although Ir/C(I-24) has excellent temperature capability to temperatures near 4200°F, it has very low resistance to stream conditions. In fact if heat flux/enthalpy characteristics are used as a yardstick, Ir/C(I-24) ranks below Si/RVC(B-8), even though the latter has a temperature limit near 3200°F.

Temperature gradients have been measured through 100 and 400 mil walls of $ZrB_2$(A-3), $HfB_2$+20%SiC(A-7), $ZrB_2$+20%SiC(A-8), $ZrB_2$+SiC+C(A-10), RVA(B-5), $WSi_2$/W(G-18) and Hf-20Ta-2Mo(I-23). Calculations of the temperature gradients through the test cylinders described have been presented. These calculations are based on side losses due to radiation and conduction down the length of the model but no heat loss via conduction. In general, relatively good agreement between observed and calculated temperature gradients has been obtained in view of the simple model employed.

Measurements of total normal emittance have been provided for all of the candidate materials based on radiated heat flux observations during HG/CW exposures. Averaged values obtained for solid oxides formed during exposure are higher than normal emittance values observed for melting surfaces. Comparison of calculated surface temperatures based on stream conditions with those observed yields relatively good results. However, systematic differences worthy of note have been observed. Calculated temperatures are quite close to those observed when melting occurs, but when solid coatings are present, actual temperatures are below values computed from stream conditions and the assumption of radiation equilibrium. Moreover, materials containing silicon carbide achieve lower surface temperatures during exposure than predicted on the basis of stream conditions. As a consequence, the overall behavior of these materials under HG/CW conditions appears to be better than under CG/HW furnace test conditions.

The present results illustrate the difference between solid oxide formers and graphites. The latter group exhibit increasing oxidation rates with increasing pressure while the former show little pressure effect. When the solid oxide formers are exposed to stream conditions at one atm, which result in surface temperatures below their

melting points, they exhibit recession rates 100 to 1000 times less than graphites do under comparable conditions. Coated metals and silicon carbide degrade at temperatures comparable to those observed in CG/HW furnace tests. These limits are due to melting or rapid vaporization. However, at a given surface temperature, the solid oxide formers exhibit much lower recession rates under HG/CW arc plasma test conditions than in a CG/HW air oxidation furnace test. This may be due to large temperature gradients across the oxide which occur in the HG/CW arc plasma tests than in the CG/HW furnace tests due to artificial oxygen supply limits imposed by the air flow limitations of the latter tests.

Ten Megawatt Arc exposures of 1/2" diameter and 7/8" diameter cylinders of diboride materials have been employed in splash tests to establish thermal shock thresholds at stagnation pressures of 4.3 atm under Mach 2 flow conditions. The best results were obtained with $HfB_2$+SiC(A-4) and (A-7), which survived fluxes at 950 BTU/$ft^2$sec and 790 BTU/$ft^2$sec at 1/2" and 7/8" diameters respectively. Failures were noted at 970 BTU/$ft^2$sec and 840 BTU/$ft^2$sec for the 1/2" and 7/8" diameter cylinders. A limited number of ten megawatt arc pipe tests were conducted in order to evaluate the combined effects of exposure to heat flux and high shear. Unfortunately one design aspect of the test generated a substantial thermal stress condition which caused this failure mode to dominate. Si/RVC(B-8) was found to be more thermal stress resistant than boride composites while $ZrB_2$+SiC+C(A-10) proved most thermal stress resistant of all of the boride composites exposed in the pipe tests.

Sixteen samples were exposed to Mach 6 tests in the Cornell Aeronautical Laboratory Wave Superheater Tunnel, including $HfB_{2.1}$, $ZrB_2$, $HfB_2$+SiC, RVA, PG, BPG, JTA, KT-SiC, JT0992, JT0981, W, Sn-Al/Ta-10W and Hf-20Ta-2Mo. Stagnation pressure and enthalpy levels of one atmosphere and 2200 BTU/lb at a cold wall heat flux level of 600 BTU/$ft^2$sec were applied to one half inch hemispherical cap specimens. Total exposure time was 15 seconds. Radiometer measurements of surface temperature indicated that the heat up time was much shorter than calculated, but surface temperature levels achieved compared reasonably with computed levels near 4000°F. In contrast, a one inch hemispherical cap Hf-20Ta-2Mo alloy showed evidence for melting (melting temperature, 3850°F) while a one half inch diameter cap of the same material showed no signs of melting and little oxidation.

## II. RESULTS OF HG/CW ARC PLASMA TESTING IN THE AVCO MODEL 500 AND ROVERS FACILITIES

### A. Introduction

More than 700 arc plasma exposures (HG/CW) have been performed in the Avco-SSD Model 500 and ROVERS (Radiation Orbital Vehicle Re-entry Simulator) in air between Mach 0.1 and 3.2. Almost all of the candidate materials listed in Table 1 were tested. Detailed descriptions of the testing facilities and techniques employed are given in Part II-Volume III of this series ( 3 ). Stagnation pressures and enthalpies ranged between 0.01 and 1 atmosphere and 1,000 to 16,000 BTU/lb, respectively. Cold wall heat fluxes between 35 and 1200 BTU/ft$^2$sec were employed for times up to 1800 seconds per test with aggregate times of up to 23,400 seconds per sample for those undergoing multiple exposure tests. Surface temperatures ranging between 1700$^o$ and 7000$^o$F were generated and radiated heat flux measurements were performed in order to obtain estimates of normal total emittance for the candidate materials. Post-mortem metallographic and x-ray studies have been employed to characterize material behavior. The HG/CW arc plasma exposures are compared with CG/HW air oxidation test results reported in Part III-Volume I of this series ( 4 ). The results of temperature gradient measurements through oxide films formed during exposure are presented for flat-faced, hemispherical tipped and shrouded samples of several of the candidate materials. These results are compared with theoretical calculations based on stream conditions and material properties. A theoretical correlation of material performance with stream conditions is presented in Part IV-Volume I of this series ( 7 ).

### B. Presentation of Arc Plasma Test Conditions and Results

The test conditions and results are presented in Tables 2-39. A description of the facilities and techniques for performing measurements of stream conditions and sample temperatures is presented elsewhere ( 3 ). The tabulated information presented for each exposure includes the Mach number, stagnation pressure, $P_e$, stagnation enthalpy, $i_e$, initial diameter of the samples, cold wall heat flux, $q_{cw}$, and the observed surface temperature. The latter values were obtained by employing the emittance values for $\lambda = 0.65\mu$ which are contained in Tables 2-39 for each material. It should be noted that employing a constant value of emittance at $\lambda = 0.65\mu$ for the wide range of temperatures and pressures encountered in the present tests represents an over-simplification. However, the current values are employed as a first approximation to the problem at hand.

In addition to the foregoing, Tables 2-39 contain measurements of the surface radiation, $q_r$, and the total normal emittance, $\epsilon_N$, computed on the basis of Eq. (1):

$$\epsilon_N = q_r(\text{BTU/ft}^2\text{sec})\,(0.47)^{-1}\,(T^oR/1000)^{-4} \qquad (1)$$

Measurements of surface radiation emitted from samples having 1/2 inch diameter faces requires special alignment of the optical system. Initial measurements in the ROVERS facility were performed with an optical system which was designed for measuring surface radiation from 3/4 inch diameter models. These measurements are expected to be lower than values obtained with an optical system specifically designed to measure radiation from 1/2 inch diameter samples. This system was employed for all measurements. In addition, comparison of test data obtained with 1/2 inch and 3/4 inch diameter samples has been performed and will be discussed below.

It should be pointed out that measurement of the surface brightness temperature carried out in the ROVERS facility is converted to true temperature by employing the emittance at 0.65μ and a transmissivity factor to correct for the window material. The correction factor is the product of the surface emittance and the transmissivity factor of the window. A transmissivity factor of 0.86 was used for the sapphire windows employed.

In addition to the foregoing set of "stream conditions" and surface radiation and temperature data, Tables 2-39 contain data on initial and final lengths, exposure time and recession rates for each sample. Also included are ratios of the calculated surface temperature, $T_{CALC}$ and the observed surface temperature, $T_{OBS}$, which are based on radiation equilibrium as indicated by Eq. (2):

$$0.47\epsilon \, (T_{CALC}{}^{\circ}R/1000)^4 = h_e \, (i_e - i_w \, [T_{CALC}, P_e]) \qquad (2)$$

where $h_e$ is the heat transfer coefficient, $\epsilon$ is the total normal emittance, and $i_w[T_{CALC}, P_e]$ (BTU/lb) is the enthalpy of air at $T_{CALC}$ and $P_e$ ( 6 ). In the first order calculations presented in Tables 2-39, the normal total emittance, $\epsilon_N$, is assumed to be equal to the emittance at $\lambda = 0.65\mu$. Thus, these calculations ignore the measured $q_r$ and normal emittance values. Part IV-Volume I of the present series ( 6 ) repeats the calculation including the measured emittance. The first order calculations are presented for comparison with results obtained earlier. Finally, the heat transfer coefficient, $h_e$, in Eq. (2) is calculated in two ways. The cold wall heat transfer coefficient is defined by Eq. (3) as:

$$h_e = q_{cw}/i_e \qquad (3)$$

while the Fay-Riddell heat transfer coefficient is given by Eq. (4) ( 6 ), as:

$$h_e = 0.0386 \, (1 + 0.17M^{-1})^{-1} \, (24 \, P_e/D)^{1/2} \text{ lbs/ft}^2\text{sec} \qquad (4)$$

where M is the Mach No., and D is the diameter of a hemispherical tipped cylinder in inches. For flat faced samples an effective diameter was used, where (6)

$$D_{eff} = 2.5 D_{cylinder} \quad (5)$$

Evaluation of the sample recession was performed by measuring the overall length of the test cylinders as well as the depth of the sting hole drilled in the back. The difference is the thickness. Measurement of the thickness after exposure is carried out by sectioning the sample and metallographic analysis. This procedure is preferable to measurements of the overall length before and after test. The latter are also made and are presented in Tables 2-39 for reference. Initially, measurements of the sting hole depth were not performed and final dimensions were obtained by sectioning the exposed cylinders and comparing the overall length of the sectioned sample with the initial length. As a consequence, some of the materials contained in Tables 2-39 show identical values of initial length and thickness*.

Figures 1-8 show the results graphically as compared with the behavior in furnace tests, while Figures 9-301 show post exposure photographs of the samples tested as well as typical photomicrographs.

1. $HfB_{2.1}$(A-2)

The results obtained for $HfB_{2.1}$(A-2) are contained in Table 2 and compared in Figure 1 with the results of CG/HW furnace tests in air at a flow rate of 1 ft/sec (4). The melting point of this material shown in Figure 1 is based on the work of E. Rudy (7). Figures 9-11 show post exposure macrographs of all of the samples after test. As indicated above, all of the samples were sectioned after exposure and examined metallographically. Typical sections are shown in Figures 12-23 illustrating the most severe test where minimal recession occurred (Figures 12-15) and the least severe test where rapid recession occurred (Figures 16-19) in the Model 500. Similarly Figures 20-23 show maximum "survival" and minimum "failure" conditions in the ROVERS arc. Figures 16, 17, 22 and 23 (when compared with the microstructural features of virgin material (1)) show that rapid recession coincides with melting of the boride. This conclusion is reinforced by Figure 1 where the measured recession results at high temperatures are compared with the published melting point (7).

*Tests where changes occurred due to arc or sample conditions are denoted by A and B. Thus, in Table 2, $HfB_{2.1}$(A-2)-18MA refers to melting at the beginning of the exposure, while (A-2)-18MB refers to the behavior after melting ceased. Multiple exposures such as $HfB_{2.1}$+20 v/o SiC(A-7)-23M in Table 6 are denoted by roman numerals I, II, etc. Finally, hemispherical capped cylinders and shrouded samples are denoted by MH and MS as shown in Table 6 for tests $HfB_{2.1}$ + 20 v/o SiC(A-7)-36MH and 44MS.

Figures 24-27 illustrate the excellent oxidation resistance of $HfB_{2.1}$(A-2) at temperatures in the 4500°F range. Although the mechanical integrity of the (A-2) samples was poor (see Section IV.C and Table 16 of Reference (1) for details) no thermal stress failures were noted below a heat flux of 770 BTU/ft$^2$sec. In particular dye penetrant tests of sample (A-2)-8R exhibited a band of high porosity near the center while sample (A-2)-9R was sound. At a heat flux of 772 BTU/ft$^2$sec, the former exhibited thermal shock failure while the latter did not. As indicated in Section II.B-4, 6 and 7, addition of silicon carbide materially improved the mechanical integrity and increased the resistance to thermal stress failures. This finding has been extensively documented in a companion study of fabrication characteristics and mechanical, thermal and physical properties (8, 14). The most striking feature of the present result for $HfB_{2.1}$(A-2) in the HG/CW tests is the difference between the recession rates encountered at a given surface temperature in these exposures and those observed at the same surface temperature in furnace tests (4). This difference is shown in Figure 1 which indicates that an oxidation depth of 20 mils in 30 minutes is obtained in an arc plasma test at 5000°F while the same oxidation depth can be produced at 3500°F in a furnace test. Alternatively a 100 mil oxidation depth is observed in a furnace test at 4000°F after 30 minutes while comparable oxidation depths are not obtained in arc plasma tests below 5500°F. The source of this difference is the temperature gradient through the oxide as indicated in Section I.B. Reference to Figure 1 also indicates no significant effect of oxygen pressure on the oxidation rate of this material in the pressure range between 0.002 and 1.0 atmospheres (air). This finding is in keeping with previous results (15, 16).

Table 2 shows the results of several test samples (A-2)-16M, 17M and 18M which were preoxidized at 1930°C (3500°F) for ten minutes to form a 10 mil oxide (4) and subsequently exposed under marginal survival conditions. These tests were performed to ascertain whether a high normal emittance coating (oxide = 0.50, bare boride = 0.40) could extend the operating range. Comparison of (A-2)-16M with (A-2)-1M and (A-2)-4M indicates little or no improvement. In addition, cyclic exposure of (A-2)-13M, 14M and 15M to three cycles which were each of 600 second duration (interrupted by cooling to room temperature) produced no accelerated oxidation over uninterrupted 1800 second tests (i.e., see (A-2)-1M)).

2. $ZrB_2$(A-3)

Table 3 summarizes the results obtained for $ZrB_2$(A-3). As before, Figures 28 and 29 show post exposure photographs of all samples, while Figures 30-39 illustrate "maximum severity survivals" and "minimum failures" in the Model 500 and ROVERS. The melting point (7) shown in Figure 1 as well as Figures 32, 33, 37 and 38 indicate that melting of the boride is the cause of rapid recession. The excellent long time oxidation resistance of this material at 4000°F is illustrated in Figures 40 and 41. Graphical comparison of CG/HW furnace test data (4) with the current results in Figure 1 shows evidence for temperature gradients and the

"minimimum oxide temperature limit criterion" discussed in Section I.B. Tests (A-3)-1MC, 2MC, 3MC and 4MC were designed to measure the temperature gradients through 100 mil wall thicknesses of oxide and boride. Thus, reference to Table 3 shows that nose thicknesses of 104, 101, 102 and 104 mils were machined in samples (A-3)-1MC, 2MC, 3MC and 4MC. In-depth temperature measurements were performed at these stations along the lines previously indicated (3). Figure 42 shows post exposure photographs of all these "in-depth temperature" tests, while Figure 43 shows a section through (A-3)-2MC which exhibited a 1500°F temperature gradient. Reference to Table 3 and Figure 43 shows that the final boride thickness was 87 mils. The time-temperature history at the "in-depth" station is documented in Table 40. This illustrates the long time stability of this effect which will be discussed in further detail in Section II.C. Figure 43 also shows the tungsten sting in place. Close examination illustrates the small contact area between sting and sample designed to minimize heat transfer by conduction. In view of the 9:1 length/diameter ratio of the "sighting hole" the "blackbody" assumption of Table 40 is justified. Additional experimental justification is presented in Section II.C. Comparison of the observed temperature gradients with calculations based on a simple one dimensional model which allows for side losses due to radiation (6) yields good agreement with observations. For the case of (A-3)-2MC shown in Figure 43 the computed surface and internal temperatures were 4170°F (4470°F observed) and 2910°F (2930°F observed), respectively.

Cyclic exposures of $ZrB_2$(A-3)-52M, 53M and 54M were performed along the lines previously indicated for $HfB_{2.1}$(A-2) to assess the effects of heating and cooling in three-600 second cycles. The results showed that at the lowest level $ZrB_2$(A-3) exhibited a recession equivalent to that observed in an 1800 second test. At higher levels $ZrB_2$(A-3) exhibited larger recessions for cyclic exposures than in the case of uninterrupted 1800 second tests. By contrast, the cyclic tests performed on $HfB_2$ did not result in larger recessions than the uninterrupted tests. The motion picture coverage indicated that the oxide formed on $HfB_{2.1}$(A-2) exhibited greater tenacity under these conditions than did the oxide formed on $ZrB_2$(A-3). The latter flaked off between cycles. As indicated in Section II.B.1, preoxidation of $HfB_2$(A-2) to form a 10 mil coating did not result in noticeable changes in behavior.

Reference to Table 3 shows that the $ZrB_2$(A-3) material employed in these tests did not exhibit any thermal stress failures at flux levels as high at 950 BTU/ft$^2$sec. In contrast to the $HfB_{2.1}$(A-2) material discussed in Section II.B.1, the (A-3) material was mechanically sound and did not exhibit the flaws shown by the (A-2) in the nondestructive tests prior to exposure (see Sections IV.B,C and Tables 15, 16 of Reference 1).

3. $HfB_2$ + SiC(A-4)

Table 4 contains the results obtained for $HfB_2$+SiC(A-4) which has the same composition as $HfB_2$+SiC(A-7) (1) but was prepared by

an alternate supplier (Table 1). Post exposure photographs of all test samples are shown in Figures 44 and 45. Figure 2 compares the furnace tests results (4) with the current HG/CW arc plasma data. Metallographic sections of "maximum severity survivals" and "minimum failure" tests in the Model 500 and ROVERS are shown in Figures 46-53. Figures 47, 52 and 53 show the "silicon carbide depletion zone" which is observed (4) when this composite is exposed to oxidizing environments at high temperature. The depletion depths for various exposures of (A-4) are shown in Table 15 and displayed in Figure 1. Thus, a ten mil depletion depth was observed in $HfB_2$+SiC(A-4)-2M (Figure 47) after 30 minutes in an arc plasma test where the surface temperature was 5020°F. By contrast Figure 1 of Reference (4) shows that a ten mil depletion depth is attained in 30 minutes near 3500°F in a CG/HW furnace test. Although these observations suggest the existence of temperature gradients in the boride-silicon carbide composites, the difference between the arc plasma and furnace oxidation depths are small (Figure 2). This finding is in contrast to the results obtained for $HfB_{2.1}$(A-2) and $ZrB_2$(A-3) shown in Figure 1. This subject will be discussed in greater detail in Sections II.B-5, II.B-7 and II.C. The adherent oxide which forms on this composite is shown clearly in Figures 47 and 53. Figures 54-57 show the low recessions observed after exposures in the 3500°-4500°F temperature range. Reference to Table 4 shows that no thermal shock failures were noted at the highest flux levels employed in these tests (1000 BTU/ft$^2$sec).

As indicated above (Section II.B) radiation equilibrium calculations were performed for each exposure to compare observed and computed temperatures as a general check on the internal consistency of the data. An extensive comparison of the data collected in the present study with the results obtained in other investigations is presented in Reference (6). Although the significance of these comparisons in terms of the ratio T(CALC)/T(OBS) will be discussed in some detail below (Section II.D) it is worth noting at this point that the average values of this ratio (for cases where melting does not occur) for (A-2), (A-3) and (A-4) are 1.16, 1.09 and 1.22, respectively. The significance of this result will become evident if one considers that on the average, the observed temperature was 16% lower than expected for (A-2), 9% lower than expected for (A-3) and 22% lower than expected (based on radiation equilibrium) for (A-4).

4. Boride Z (A-5)

Table 5 and Figures 1 and 58 show the results obtained for Boride Z(A-5). Samples Boride Z(A-5)-2M, 5M, 6M, 7R, 8R and 12R all showed thermal shock behavior. All of the remaining samples except 9R were observed to contain large cracks after sectioning. Samples Boride Z(A-5)-7R and 8R cracked after the exposures were completed. Consequently, the current results indicate that Boride Z(A-5) is very susceptible to thermal shock failure. Figures 59a and 59b show Boride Z(A-5)-4M and 8R which

exhibit thermal shock cracks after exposure at 348 BTU/ft$^2$sec and 3215 BTU/lb and 262 BTU/ft$^2$sec and 9200 BTU/lb, respectively. Thus, flux levels above 200-250 BTU/ft$^2$sec appear to result in thermal shock failures of Boride Z. By contrast $ZrB_2$(A-3) discussed in Section II.B.2 and $ZrB_2$+SiC(A-8) to be discussed in Section II.B.6 did not exhibit thermal shock failures at these levels.

5. $HfB_2$ + 20%SiC(A-7)

Tables 6, 7, 8 and 15 summarize the results observed for $HfB_2$+20%SiC(A-7). As indicated earlier, this material has the same composition as (A-4). This composite was exposed to extensive evaluation since it exhibited the most outstanding high temperature-long time oxidation resistance. Exposure (A-7)-28R details the 23,400 second exposure noted in Section 1B. As indicated earlier, multiple exposures are denoted by roman numerals, i.e., (A-7)-24MI, 24MII, 24MIII, 24MIV. Hemispherical capped samples and shrouded samples are designated by the suffix H and S respectively as can be seen by comparing the tables with Figures 60-62. The latter illustrate all of the samples after exposure. Thus, (A-7)-45MS is shown in Figure 60 (sample 45M) to consist of the (A-7) cylinder with a 437 mil diameter in a 875 mil shroud. The shroud material was $ZrB_2$+SiC+C(A-10). This material was employed because it is machinable and quite oxidation resistant. Reference to Figure 60 shows qualitatively that (A-7) is more resistant to oxidation than (A-10). Figure 61 shows the hemispherical samples (A-7)-36MH, 37MH, 38RH, 39RH, 48RH and 50RH. Finally a few of the hemispherical samples were shrouded in order to evaluate the effect of such shrouds on internal temperature distributions. Samples 49RHS and 51RHS shown in Figure 61 are examples of this configuration. Little effect was noted due to shrouding of hemispherical models. However, hemispherical models and shrouded flat faced models resulted in lower temperature levels. This aspect of the testing program will be discussed later.

Finally samples (A-7)-38RH and (A-7)-46RS were run twice. The second exposures are denoted as (A-7)-38RR and (A-7)-46RR. Sample (A-7)-39RH was run three times with the second and third exposures designated as (A-7)-39RRI and (A-7)-39RRII.

Figures 63-70 show the "maximum severity survival" and "minimum failure" conditions in the Model 500 and ROVERS facility. As in the case of $HfB_{2.1}$(A-2) and $ZrB_2$(A-3), rapid recession appears to result from melting. However, since the composite does not melt as sharply as the pure diboride, the transition in Figure 2 is not very sharp. The temperature limit appears to be 5000°F. Figures 71 and 72 show metallographic sections of (A-7)-28R exposed for thirteen cycles (each of 1800 second duration) at a stagnation pressure of 0.07 atm, an average heat flux of 495 BTU/ft$^2$sec and an enthalpy near 10,300 BTU/lb. Reference to Table 7 shows that the temperature increased progressively during

the first four cycles even though the stream conditions were constant. Cycle number five exhibited a large temperature increase which was maintained through the remaining eight exposures. This behavior is characteristic of all of the multicycle exposures of boride composite samples. The difference in temperature between cycles (A-7)-28RIII and (A-7)-28RV is real since it is reflected in the measured value of radiated flux as well as in the surface temperature. Physically, the increase in temperature appears to be connected with the presence of an oxide over the entire surface of the sample. Thus, in cycles (A-7)-28RI through (A-7)-28RIII little or no oxide is visible (see Film Description) and the observed surface temperature and radiated flux is low. Similarly, in cycle X the oxide has fallen off exposing the bare composite. Here again the surface temperature and radiation are low. Apparently then, the oxide sustains a large temperature gradient over a very small thickness (1500°F over 5-10 mils in the present case). Reference to Figure 72 indicates minimal depletion of SiC. The depletion depth was of the order of 1-2 mils.

Another interesting feature is the ratio T(CALC)/T(OBS) and its variation from one cycle to the next. This ratio is near 1.18 when the oxide is present. However, when the bare boride composite is exposed, the ratio is near 1.70. Thus, the boride composite exhibits surface temperatures which are much lower than expected on the basis of radiation equilibrium. When the oxide is present, calculated temperatures are closer to (but still 15% below) the observed values. Although the cause of this behavior is not known at present (6) part of the difference is undoubtedly due to conduction losses and side radiation (6). Thus, if the conduction between the oxide and the boride is very low the radiation equilibrium calculation applies well to the oxide layer. However, when the bare boride composite surface is exposed conduction losses coupled with side radiation (6) and other factors lead to much lower surface temperatures than expected.

Apart from these fine points, the gross behavior of $HfB_2$+20%SiC(A-7)-28R is quite remarkable. Table 7 and Figure 71 show that the total recession after the thirteen cycle exposure was 15 mils. This behavior is unrivaled by any other known material system.

Figures 73 and 74 show post exposure sections through (A-7)-52M after 14,030 seconds exposure in eight-1800 second cycles at a stagnation pressure of 1.03 atmospheres. The average cold wall heat flux was 450 BTU/ft$^2$sec at an enthalpy level of 4180 BTU/lb. Total recession was 329 mils or about 0.33 inches. Under similar conditions graphite and tungsten would exhibit recessions of 14 to 28 inches.

Figures 75-78 show post exposure metallographic sections through samples (A-7)-37MH and (A-7)-39RH which were employed for in-depth temperature measurements. Table 41 shows the

time temperature histories of the internal temperature measurements which will be discussed in Section II. C. However, several points are worth noting currently. First, the temperature gradients observed for (A-7) are not as large as those observed for (A-2). Part of the reason for this behavior is believed to be due to the fact that the oxide which forms on (A-7) is much more adherent than that which forms on (A-2). Consequently, this oxide has a higher thermal conductivity which reduces the temperature gradient (6). As a consequence, the difference between the recession rates observed in HG/CW arc plasma tests and CG/HW furnace tests is smaller for (A-7) than for (A-2). This can be observed by comparing Figures 1 and 2.

As indicated above, (A-4) and (A-7) exhibit lower temperatures than anticipated from radiation equilibrium considerations (i.e., T(CALC)/T(OBS) is much larger than unity). This conclusion was derived by considering flat faced cylinders in the earlier discussion. Consideration of the hemispherical capped specimen tests indicates an additional lowering of the surface temperature. Thus, the T(CALC)/T (OBS) ratios for tests (A-7)-38RH, 39RH, 48RH, 49RHS, 50RH and 51RHS are near 2.0. A graphical illustration of this phenomena is afforded by tests (A-7)-39RRI and 39RRII shown at the end of Table 8. As indicated above, these tests were re-runs of sample (A-7)-39RH. The sample is shown sectioned after exposure in Figures 77 and 78. Here, exposure at 965 BTU/ft$^2$sec and 7290 BTU/lb resulted in a surface temperature of 4285$^\circ$F for the hemispherical model. By contrast, exposure of a flat faced sample (A-7)-34R to milder conditions (720 BTU/ft$^2$sec, 8040 BTU/lb) resulted in a surface temperature of 5005$^\circ$F. Moreover, at 791 BTU/ft$^2$sec and 9030 BTU/lb, flat faced sample (A-7)-35R reached 5350$^\circ$F and receded 315 mils in 90 seconds.

### 6. $ZrB_2$ + 20%SiC(A-8)

Tables 9, 10, 15 and 42 and Figures 1, 2 and 79-92 detail all of the results obtained for $ZrB_2$+20%SiC(A-8). This composite exhibits all of the same features shown by $HfB_2$+SiC(A-7) although it is not as refractory as its hafnium base counterpart. However, the decrease in temperature resistance is compensated for by the reduced density and cost. Zirconium diboride is roughly one half the density and one tenth the price of hafnium diboride. Reference to Tables 9 and 10 and the post exposure photographs shown in Figures 79 and 80 indicates that most of the tests were conducted with flat faced cylinders. A few tests were shrouded with $ZrB_2$+14%SiC+30%C(A-10). As in the case of (A-7), the $ZrB_2$+20%SiC (A-8) material is more oxidation resistant than (A-10) as indicated by samples 30M and 32R in Figure 80. In addition, it is interesting to note the results of (A-8)-29M in which a graphite shroud was employed (Tables 9 and 42). Although the boride exhibited minimal recession (8 mils in 1800 seconds) the graphite shroud which was one inch long ablated completely in 500 seconds.

Table 15 and Figure 1 show the depletion depths for $ZrB_2$+ SiC(A-8) as a function of temperature. This material exhibited the lowest

depletion rate of all the boride composites as shown in Figure 1. In addition, the depletion rate in the current HG/CW tests was much less than the corresponding rates ( for a given surface temperature) in CG/HW furnace tests (4). Metallographic sections were prepared for all of the exposures. Figures 83-88 show the "maximum severity survivals" and "minimum exposure failures" in the Model 500 and ROVERS tests.

Figures 89-92 illustrate the results of long exposure cyclic tests in the Model 500 and ROVERS. Test (A-8)-15M shown in Figures 89 and 90 was discussed previously in Section I.B. The sting section of (A-8)-16R shown in Figure 91 was cracked on removal from the sting. Both tests show excellent long time oxidation resistance. Reference to Table 42 shows that temperature gradients through one hundred and four hundred mil walls exist in these materials which are comparable to those observed in (A-7). However, the gradients appear to be smaller than exhibited by $ZrB_2$(A-3). This finding apparently results from the higher thermal conductivity of the oxide formed on (A-8) (as compared with (A-3))(6). Consideration of Tables 9 and 10 shows that $ZrB_2$+SiC(A-8) exhibits the same tendency to develop low temperatures as (A-4) and (A-7). Thus, tests in the ROVERS facility at flux levels below 500 BTU/ft$^2$sec and in the Model 500 facility at flux levels below 350 BTU/ft$^2$sec develop ratios of T(CALC)/T(OBS) which are of the order of 1.5. This feature of the boride composites which contain SiC permits a wider range of applicability than materials which exhibit (T(CALC)/T(OBS)) near unity.

7. $HfB_{2.1}$+35v/oSiC(A-9)

A limited set of exposures of $HfB_{2.1}$+35v/oSiC(A-9) was conducted in the Model 500 facility. The results are summarized in Tables 11 and 15 and in Figures 1 and 2. Figure 93 shows post exposure photographsof all the test samples while Figures 94-97 show "maximum severity survival" and "minimum failure" conditions in the Model 500. The nonuniform recession exhibited by (A-9)-5M is due to misalignment of the sample in the arc. These results show that the features of (A-9) are similar to (A-4) and (A-7)(i.e., T(CALC)/T(OBS) comparison, recession rate vs. temperature for HG/CW arc plasma tests and furnace exposures, depletion depth vs. temperature in HG/CW tests as a function of temperature, etc.). The major difference is that (A-9) is less refractory than (A-4) and (A-7). Thus, (A-9) exhibits melting in Model 500 exposures when the flux level exceeds 500 BTU/ft$^2$sec at enthalpy levels near 4000 BTU/lb. By contrast, (A-7)-23M receded 193 mils after 7200 seconds at flux levels near 600 BTU/ft$^2$sec and 4500 BTU/lb. Similar thermal stability is evidenced by (A-4)-2M and (A-4-2)-3M. A method for comparing the recession rate as a function of flux and enthalpy, rather than exclusively in terms of surface temperature as in Figures 1 and 2, is described in Reference (6).

8. $ZrB_2$+14%SiC+30%C(A-10)

This composite has been developed (8-14) in order to improve the thermal stress resistance of boride composites (by lowering

of the elastic modulus) without sacrificing oxidation resistance. Moreover, (A-10) is machinable with carbide tools while (A-8) is not. Tables 12-15 and 43 summarize the results of an extensive series of tests conducted on $ZrB_2$+SiC+C(A-10). Figures 1 and 6 display the results in graphical form. Reference to Figure 6 shows that at surface temperatures between 3000°and 5000°F. (A-10) exhibits a much slower rate of oxidation in HG/CW arc plasma tests than in CG/HW furnace tests. This result is undoubtedly a manifestation of the MOTEL criterion presented in Section I.B.

Figures 98-100 are post exposure photographs of all of the samples after testing. Shrouded samples shown in Figure 99 consisted of the test model jacketed in a cylinder of (A-10) with a 3/16 inch wall thickness. Utilization of the shrouds did not have a substantial effect on model behavior or temperature (6).

In general, the behavior of this composite is quite similar to that exhibited by (A-4), (A-7) and (A-8) discussed earlier in Sections II.B-3, 5 and 6. However, (A-10) is not as refractory as (A-4) and (A-7). Nevertheless, the lower density, cost, thermal stress resistance and machining characteristics of this composite provide compensating advantages.

The series of photographs of tests (A-10)-30R, 31R, 32R and 33R shown in Figure 100 are extremely revealing when examined along with the data shown in Table 14. Test (A-10)-30R exhibits the connection between oxide coating and surface temperature described in Section II.B.4 for (A-7). During the first 428 seconds of this long test (1669 seconds total) the oxide slowly covered the face and the observed surface temperature of 3650°R was 75% lower than expected from radiation equilibrium. The radiated flux was 33 BTU/ft$^2$sec. However, once the thin oxide coating covered the surface, the temperature increased to 5455°R and the radiated flux level jumped to 196 BTU/ft$^2$sec. Under these circumstances the observed surface temperature was only 17% lower than expected on the basis of Eqs. 2 and 3. The total conversion of boride to oxide during the 1669 second exposure was 26 mils. However, reference to Table 14 shows that the total length of the sample actually increased by 10 mils. Thus, the oxide thickness was probably of the order of 36 mils. Figure 100 shows the oxide cover which separated from the sample on cooling. This cover was 35 mils thick. Test (A-10)-31R exposed at identical conditions as (A-10)-30R except that the flux was 596 BTU/ft$^2$sec instead of 551 BTU/ft$^2$sec, melted.

Figures 101-108 show the "maximum severity survival" and "minimum failure" tests in the Model 500 and ROVERS facilities. Figures 109-112 show sections through (A-10)-24M and (A-10)-26R which were exposed for times up to 21,600 seconds near 4500°F with total recession of the order of 100 mils. This behavior, which was discussed in Section I.B, shows striking evidence for the applicability of these composites in reusable lifting reentry spacecraft. The sting leg portion of sample (A-10)-26R was cracked on removal after completion of the test.

Table 43 details the results of in-depth temperature measurements. These tests will be discussed later in Section II. C. Comparison of the results with calculations based on side losses due to radiation is presented in a companion report in this series (6). Relatively good agreement between observed and calculated gradients has been obtained (6).

Reference to Table 14 shows that (A-10)-36RH and (A-10)-37RH (hemispherical capped models with in-depth temperature holes) were exposed at flux levels near 500 BTU/ft$^2$sec. Table 43 details the time-temperature history for these exposures. Reference to Table 14 indicates that the observed temperature for these exposures was 60% lower than calculated on the basis of Eqs. 2 and 3. This behavior (noted earlier with (A-7) and (A-8) in Sections II. B. 4 and II. B. 6), characterized by lower temperatures achieved with hemispherical models than with flat faced models is not understood at present. Nevertheless, the practical implications of this finding are substantial. For example, (A-10)-25R, 26R, 40R and 41R (which were flat faced models) exposed at conditions similar to (A-10)-37R and 38R (i. e., 500 BTU/ft$^2$sec, 7700 BTU/lb, 0.15 atm.) exhibited temperatures near 5000°R in contrast to (A-10)-37R and 38R which exhibited temperatures near 3700°R. Naturally the hemispherical models exhibited lower recession rates. Sample (A-10)-37RH is shown after sectioning in Figures 113 and 114.

Similarly, sample (A-10)-48RH was exposed to four exposures at ascending flux levels until evidence of melting was noted. Melting of this hemispherical capped model was not observed to occur until fluxes near 850 BTU/ft$^2$sec were attained. Flat faced models melted near 650 BTU/ft$^2$sec.

### 9. Pure Graphite Materials -RVA(B-5), PG(B-6) and BPG (B-7)

Figures 3, 4 and 115-137 compare the results of (HG/CW) Arc Plasma Tests with the results of (CG/HW) Air Oxidation Furnace Tests (4). Figures 3 and 4 also contain a number of results reported by Kendall et al. (17) and by Tanzilli (18) for comparison. The results of these studies are in general agreement with present findings. The general behavior indicated by Figures 3 and 4 is that the supply limited (oxidation rates observed to increase as air flow rate increases) oxidation rates observed in the furnace tests are much lower than observed in the one atmosphere (HG/CW) Arc Plasma Tests. Recession rates in the latter exposures are dependent on pressure and weakly temperature dependent. In general, the results are in keeping with the theoretical description (6). Thus, it appears that the oxidation of graphite observed in the arc plasma exposures is limited by diffusion of oxygen and oxidation products in the boundary layer. This is certainly the case at lower pressures. Reference to Figures 3 and 4 shows that little if any temperature dependence of the

recession rate is noted in the Mach 3.2 exposures at 0.01 to 0.03 atmospheres. However, at higher pressures the temperature dependence becomes more pronounced. The one atmosphere subsonic exposures exhibit a definite temperature dependence of the recession rate particularly in the temperature range between 2500°F and 3500°F. This result is in keeping with the observations derived from high velocity CG/HW tests (5) and theoretical studies (6). The pressure dependence of the recession rate appears to agree with the $P_e^{1/2}$ relation predicted by theory (6). The present results shown in Figures 3 and 4 (Tables 16-18) indicate that PG (B-6) and BPG(B-7) are comparable in oxidation resistance to RVA(B-5) in the (HW/CG) Arc Plasma Tests and the the "C" plane recedes more slowly than the "A" plane of PG(B-6) and BPG(B-7). This is readily evident in Figure 4 for the Mach 0.30-0.50 exposures at one atmosphere.

It should be noted that the observation of enhanced "A" plane recession indicates that while gaseous boundary layer diffusion exercises dominant control, surface reactions do exert some influence on the overall rate.

Reference to Tables 17 and 18 indicates that thermal shock delaminations were noted along the "C" plane for samples of PG (B-6) and BPG(B-7) exposed normal to the "C" axis. Thermal shock failures were not noted for RVA or PG(B-6) and BPG(B-7) when samples of the latter were exposed perpendicular to their "C" axes. This was evidently due to nonuniform heating of samples so exposed due to enhanced conductivity parallel to "C" planes. Motion picture footage clearly illustrated this behavior in which central bands of material which were parallel to the "C" plane and parallel to the cylinder axis heated up before the cylinder surface heated. Figures 123, 126, 131, 134 and 135 illustrate the thermal shock failures of (B-6) and (B-7). Photographs of (B-5), (B-6) and (B-7) samples exposed in the Model 500 illustrate "necking" of the test samples due to oxidation on the sides. This behavior is seen in Figures 115, 118, 122-126, 130 and 132-134.

Comparison of the T(CALC)/T(OBS) ratios obtained for (B-5), (B-6) and (B-7) with those noted for other materials will be performed in Section II. D. For the present however, reference to Tables 16-18 shows that this ratio is approximately 1.18 for these materials. Thus, observed temperatures are about 18% less than expected based on radiation equilibrium. In addition, the ratios are nearer unity for (B-6) and (B-7) when the "C" axis is parallel to the arc (i.e., when the basal planes of graphite are exposed). Table 44 details the results of two exposures of RVA(B-5) in which internal temperatures were recorded. Comparison of the results with calculated values yield relatively good results (6). Temperature gradients are modest due to the bare surface and high thermal conductivity of graphite. Section II. C will provide an additional discussion of these findings.

In comparing the behavior of the foregoing boride materials to the pure graphites RVA(B-5), PG(B-6) and BPG(B-7), it is

evident that the former group (i.e., the borides) exhibit substantially lower recession rates than the graphites at temperatures below the melting temperatures of the borides. This is the case at atmospheric pressures. Thus, at 5000°F and 1 atmosphere, graphite recessions of the order of 3000-6000 mils in 30 minutes are observed as compared to boride recessions in the 30-60 mils in 30 minute range. Even at 0.01 atmosphere stagnation pressures, graphites recede at rates of 1000 mils in 30 minutes. However, once the melting temperature of the borides is exceeded, their advantage is lost.

### 10. Siliconized RVC Graphite, Si/RVC(B-8)

Table 19 documents the results of the HG/CW arc plasma tests performed on Si/RVC(B-8). Figure 5 compares the results of these tests with CG/HW furnace tests, while post exposure photographs and "maximum severity survivals" are illustrated in Figures 138-142. The present results demonstrate that Si/RVC(B-8) exhibits protective oxidation for short periods of time up to surface temperatures near 3800°F. This is some 700°F above the coating failure temperature observed in the CG/HW furnace tests (4). Above this temperature coating-breakdown occurs and samples exhibit typical graphite behavior. As noted previously, graphite oxidation rates in the arc plasma tests are 20 times larger than the rates observed in the furnace indicating that the latter are supply limited. In particular, exposure Si/RVC(B-8)-5M (Table 19) shows coating burn-off after 735 seconds at 470 BTU/ft$^2$sec and 3720 BTU/lb corresponding to a surface temperature of 3790°F. At low pressure, Si/RVC(B-8)-7R showed protective behavior at 210 BTU/ft$^2$sec and 8850 BTU/lb corresponding to a surface temperature of 2740°F.

Exposures (B-8)-4M and (B-8)-5M discussed above represent short time survival conditions. Survival for 30 minutes was exhibited at slightly lower levels by (B-8)-18M at 362 BTU/ft$^2$sec. A surface temperature of 3110°F was observed in this test in accordance with the CG/HW furnace results (4). Reference to Table 19 indicates that T(CALC)/T(OBS) ratios for this material are high (approximately equal to 1.36) when the coating is intact. This result is in keeping with the behavior noted for other SiC bearing materials ((A-4), (A-7), (A-8), (A-9) and (A-10)) discussed above. Thus (6), Si/RVC(B-8) exhibits enhanced temperature resistance.

### 11. Special Graphites PT0178(B-9), POCO(B-10) and Glassy Carbon (B-11)

Tables 20 and 21 as well as Figures 3, and 143-155 display the results obtained for the fibrous graphite composite PT0178(B-9), fine grained graphite, Poco (B-10) and glassy carbon (B-11). As in the case of RVA(B-5), PG(B-6) and PG(B-7), the oxidation rates observed in the furnace tests are 20 times smaller than those observed in the arc plasma tests, indicating that the former are supply limited. In line with the high velocity CG/HW test results (5) and the theoretical findings (6), the recession rates of the graphites are inversely proportional to density ($\Gamma$). The motion picture coverage of test (B-11)-1M shown in Table 21 indicates melting during

the exposure. No post exposure examination could be made since the sample ablated completely. Since glassy carbon is not reported to melt at one atmosphere, the only possible explanation that can be advanced at present for this observation is based on surface contamination of the sample by tungsten from the arc or sting (Reference 5, pages 28 and 29).

Figures 143-146 indicate the extensive "necking" of PT0178(B-9) in the Model 500 tests which resulted from side wall oxidation. Although Poco Graphite (B-9) showed similar characteristics (see Figure 148) the necking was less pronounced.

Section II. D will present a complete discussion of the emittance and T(CALC)/T(OBS) ratios for these materials. For the present, it is sufficient to note that the T(CALC)/T(OBS) ratios for PT0178(B-9) and Glassy Carbon (B-11) are near unity while the average ratio for Poco Graphite (B-10) is near 1.15.

12. Arc Cast Hypereutectic Carbides HfC+C(C-11) and ZrC+C(C-12)

Tables 22 and 23 along with Figures 5 and 156-179 detail the results obtained for the arc cast hypereutectic carbides HfC+C(C-11) and ZrC+C(C-12). The melting points shown in Figure 5 are taken from the work of Rudy (7). Reference to Figure 5 indicates that the present results on melting of (C-11) and (C-12) are in keeping with Rudy's results. In addition, the values of T(CALC)/T(OBS) for (C-11) and (C-12) are found to lie near 1.0. Although the temperature range of the present HC/CW arc plasma tests were not overlapped with CC/HW furnace tests, Figure 5 indicates the two sets of results are comparable. This is due in part to the unusual oxidation characteristics of (C-11) and (C-12) (4). These materials do not form protective oxides below 3300°F. At lower temperatures they form porous flakey oxides which do not suppress the oxidation rate. Thus, arc plasma samples which are hotter at the front than at the back are expected to exhibit variable oxidation characteristics. This behavior is shown clearly in the post exposure photographs which constitute Figures 156, 157, 168 and 169. Thus, the post exposure pictures of (C-11)-17M and (C-12)-15M are quite reminiscent of the structures shown on page 64 of Reference (4). Figures 158, 170 and 178 illustrate the rapid oxidation of the sting leg region where a thick nonprotective oxide forms. Figures 171 and 179 show preferential oxidation along the graphite flakes in the hypereutectic structure. As indicated in Figure 5, HfC+C(C-11) is more refractory than ZrC+C(C-12) and is thus capable of withstanding higher flux and enthalpy levels before melting (6). Figures 158-178 illustrate the "maximum severity survival" and "minimum failure" condition in the Model 500 and ROVERS facilities. The latter are associated with melting of the carbide. This conclusion is based on the large number of survivals (recession rates of 100 mils or less in

30 minutes) observed for (C-11) above the melting point of $HfO_2$ near 5100°F, and the clear difference in resistance to stream conditions evidenced by (C-11) and (C-12) despite the fact that the melting points of $HfO_2$ and $ZrO_2$ are nearly equal.

The samples employed in tests HfC+C(C-11)-10R and 12R (Figures 160-163) were fabricated from billet 1422A (Table 8 of Reference 1) which is lowest in carbon. Consequently, these samples do not exhibit large graphite flakes. Nonetheless, the oxidation behavior of samples from Billet 1422A does not appear to differ materially from samples fabricated from the billets which are higher in carbon. Figure 163 shows the microstructure which is characteristic of billet 1422A.

Figures 170-175 show post exposure photomicrographs of ZrC+C(C-12)-15M, 10R and 7R. A recession of 64 mils was observed for (C-12)-15M after 1800 seconds at 3900°F. Figure 170 shows the "puffy" attack of the hypereutectic carbides. Figure 172 displays the structure of (C-12)-10R after 1800 seconds at 5030°F. A recession of 32 mils was observed subsequent to this exposure. At 4955°F (C-12)-7R exhibited a total recession of 209 mils in 1800 seconds at 5030°F. The apparent reversal in behavior of (C-12)-10R and (C-12)-7R indicates that these conditions are borderline relative to melting of $ZrO_2$ as shown in Figure 5. Both HfC+C(C-11) and ZrC+C(C-12) are resistant to thermal shock over the range of conditions employed.

Cyclic exposures of (C-11) and (C-12) were not carried out due to the problems associated with the poor low temperature oxidation behavior. Under these conditions it is expected that excessive side oxidation at cooler locations on the sample would lead to rapid oxidation.

### 13. JTA(C+$ZrB_2$+SiC) (D-13)

The results of the present arc plasma testing programs for JTA(D-13) (which is predominantly a graphite in contrast to (A-10) which is mostly boride) is shown in Tables 24 and 25. Figure 6 compares the HG/CW results with furnace test data, while Figures 180-197 show post exposure photographs and metallographic sections of selected test samples. Experimental results obtained in HG/CW tests by Kendal et al. (17), Criscione et al. (19) and by Buckley and Stein (20) are included for comparison in Figure 6.

The ratio of T(CALC)/T(OBS) for most exposures of this material was near 1.10. Comparison of the temperature calculations and emittance values for this material will be compared with the results obtained for other candidate materials in Section II.D.

A substantial number of thermal shock failures were observed in these tests. These failures, noted in Table 24, occurred in random fashion at flux levels above 500 BTU/ft$^2$sec. The samples which failed by thermal shock were machined from 2-1/2" diameter x 2" long billets of JTA(D-13) in an orientation which corresponds to the hot pressing direction. Thus, the axis of the arc plasma test sample was parallel to that of the hot pressed cylinder. Under these conditions, residual strains present in the billets and in the samples could provide a source for the failures. In order to investigate this possibility a second series of samples were machined from additional billets. These sample cylinders were oriented with their axes perpendicular to the pressing direction. Nondestructive testing of these cylinders showed no nonuniformities or imperfections (see Page 19 of Reference 1). The above mentioned samples are designated as (D-13)-31MX through (D-13)-41MX in Table 24. Significantly, no thermal shock failures were noted for these samples even at flux levels in excess of 500 BTU/ft$^2$sec. This finding has particular relevance to applications in which JTA(D-13) parts are exposed to severe environmental heat fluxes. A preoxidized coating on (D-13)-43M, 44M and 45M had no noticeable effect.

Reference to Figure 6 shows that the results obtained for JTA(D-13) in HG/CW arc plasma tests and CG/HW furnace tests "dove tail." By contrast the HG/CW results for (A-10) lie below the CG/HW rates at temperatures up to 5000°F as shown in Figure 6. At 4500°F and one atmosphere stagnation pressure, JTA(D-13) behaves like a graphite exhibiting recession of 2-4 inches in thirty minutes, while (A-10) behaves like a boride and exhibits recessions of 10-20 mils in thirty minutes.

A post exposure metallographic section of JTA(D-13)-22M is shown in Figures 185 and 186 to illustrate a "maximum severity survival" in the Model 500. Rapid recession is illustrated by Figures 188 and 189 for JTA(D-13)-4M after rapid oxidation at 660 BTU/ft$^2$sec and 4320 BTU/lb (surface temperature equals 4560°F). ROVERS exposures at low pressure lead to protective oxidation at a surface temperature of 4665°F (500 BTU/ft$^2$sec and 9520 BTU/lb) as shown in JTA(D-13)-7R illustrated by Figures 190 and 191. At higher levels (770 BTU/ft$^2$sec, 7310 BTU/lb and surface temperature equal to 5305°F) rapid oxidation rates are observed as shown in Figures 192 and 193 for JTA(D-13)-8R.

Figures 194 and 195 show sample (D-13)-48MX after 4 cyclic exposures at a stagnation enthalpy of 4350 BTU/lb, stagnation pressure of 1.01 atm and a cold wall heat flux of 380 BTU/ft$^2$sec. Each exposure was 1800 seconds long making the total exposure time 7200 seconds. The average recession was 118 mils. This test can be compared with (A-10)-24 shown in Figure 109 which exhibited a recession of 104 mils after 12 cycles (1800 seconds each) totalling 21,600 seconds under comparable conditions.

Figures 196 and 197 show sample (D-13)-49RX after 4 cyclic exposures at a stagnation pressure of 0.057 atmospheres at a stagnation enthalpy of 9600 BTU/lb and a cold wall heat flux of 440 BTU/ft$^2$sec. Each exposure was 1800 seconds long making the total exposure time 7200 seconds. Total recession for this test was 45 mils. By comparison, (A-10)-26R exposed for 18,951 seconds at comparable heat flux and enthalpy and a higher pressure (0.238 atm) exhibited a recession of 83 mils as shown in Figure 111.

14. KT-SiC(E-14)

The behavior of KT-SiC in (HG/CW) exposures is compared with the (CG/HW) tests in Figure 5. Detailed results are contained in Table 26. Rapid oxidation rates are observed at temperatures above 4000°F, or 500°F higher than observed in (CG/HW) tests (4). Although a complete discussion of the emittance and calculated temperatures for this material will be postponed to Section II. D, it should be noted that the computed ratios $T_{CALC}/T_{OBS}$ exceed unity with typical values near 1.5. This indicates that the observed surface temperature is substantially less than anticipated on the basis of radiation equilibrium. Thus, heat absorbtion due to vaporization or degradation of the heat transfer coefficient due to injection or blocking is operative. At 4500°F, significant vaporization of KT-SiC leads to rapid rates of recession.

Figure 5 shows a slightly higher failure temperature for KT-SiC(E-14) in the HG/CW Arc Plasma Tests at one atmosphere than in the CG/HW furnace tests. At lower pressures, higher oxidation rates are observed as expected. This is due to the instability of $SiO_2$ (relative to SiO) at low pressure (4).

Post exposure photographs of all samples are shown in Figures 198 and 199. Figures 200 and 201 show metallographic sections through sample (E-14)-4M after survival at 3670°F for 1835 seconds. At higher levels rapid ablation is illustrated. Figures 202 and 203 show KT-SiC(E-14)-5M after exposure for 165 seconds at 4440°F. A total recession of 425 mils was observed. Under these conditions recession occurs by ablation and vaporization.

Samples KT-SiC(E-14)-3R, 5R and 7R exhibited low oxidation rates but showed internal cracks on sectioning as indicated in Figure 204.

15. JT-0992(C-HfC-SiC)(F-15) and JT-0981(C-ZrC-SiC)(F-16)

The results obtained for the graphite composites JT-0992(C-HfC-SiC)(F-15) and JT-0981(C-ZrC-SiC)(F-16) are summarized

in Tables 27 and 28. These composites, like JTA(C-$ZrB_2$-SiC)(D-13), are mainly graphite (1). Unlike the former, however, they do not contain boron and are therefore susceptible to rapid oxidation at temperatures below 2800°F. This fact is illustrated in Figure 6 which compares the current results of HC/CW arc plasma tests with furnace tests conducted under CG/HW conditions. Reference to Tables 27 and 28 shows that the ratio T(CALC)/T(OBS) is near 1.05 for (F-15) and 1.10 for (F-16). These findings and the results of the emittance measurements presented in Tables 27 and 28 will be discussed in Section II. D. Post exposure photographs and metallographic sections are shown in Figures 206-229. Photographs of all the exposures of (F-15) shown in Figures 206-208 and (F-16) shown in Figures 218-220 illustrate a large number of thermal shock failures particularly in the case of JT0981(F-16). As indicated earlier in Section II. B-13 (Table 24), JTA(D-13) also exhibited thermal shock failures when exposed to heat flux levels above 600 BTU/$ft^2$sec. This failure mode was eliminated (for JTA) by orienting the pressing axis of the billets perpendicular to the arc (Section II. B-13). All of the samples of (F-15) and (F-16) discussed in Tables 27 and 28 were oriented so that the pressing axis was parallel to the arc since testing was completed before the effect of orientation was established for JTA(D-13).

After initial observation of thermal shock failures in exposures JTA(D-13)-23M and 24M (Table 24) and JT0981(F-16)-21M, 22M, 23M and 24M, a second set of samples was prepared and submitted for nondestructive testing as noted on p. 19 of Reference 1. The NDT results indicated that JTA(D-13)-1, 6 and 9 and JT0981(F-16)-1, 4, 9 and 11 gave extreme values in the ultrasonic velocity and eddy current measurements. No nonuniformities or surface cracks were disclosed by radiographic or dye penetrant methods. Reference to Tables 24 and 28 show that none of these extreme samples exhibited thermal shock failures.

If the results are taken at face value, it appears that JT0981 exhibits a high thermal shock failure rate at flux levels in excess of 400 BTU/$ft^2$sec. The failure level for JTA appears to be in the vicinity of 600 BTU/$ft^2$sec, while JT0992 exhibited only two random failures when exposed at flux levels up to 1145 BTU/$ft^2$sec. Examination of the microstructures of the test cylinders with Mr. S.E. Slosarik, Applications Manager of the Aerospace and Nuclear Products Division of Union Carbide Corp., showed some preliminary evidence for carbon and carbide grain size differences between test cylinders which seemed to correlate with the occurrence of thermal shock failures. However, subsequent extensive metallographic investigation of this factor did not verify the hypothesis that fine grained structures exhibit a higher flux tolerance than coarse grain structures. Since all of the 1/2 inch diameter x 1 inch long cylinders were cut from one 2 inch diameter x 2-1/2 inch billet which

in turn were cut from 7 inch diameter x 7 inch pressings, grain size variations between test cylinders were not ancitipated. The axes of the test cylinders, billets and pressings were identical and thermal shock failures were found to occur by delaminations along planes perpendicular to the cylinder axis.

Reference to Figure 6 shows that the 30 minute oxidation depths exhibited by JT0992(F-15) and JT0981(F-16) in the (HW/CG) Arc Plasma Tests at Mach 0.3-0.5 and one atmosphere agree with the (CG/HW) Air Oxidation Furnace Tests (4). These rates are 30 times less than those encountered for RVA(B-5) Graphite at temperatures below 4000°F indicating some beneficial effect of the solid oxide formers contained in the composites. A substantial lowering of the 30 minute conversion depth was observed at stagnation pressures in the 0.01-0.03 atmosphere range at temperatures below 5500°F. Melting was observed at this temperature.

Figures 209-217 illustrate "maximum severity survivals" and "minimum failures" for JT0992(F-15). Figure 211 in this group illustrates the low temperature susceptibility to rapid oxidation of JT0992 (C-HfC-SiC)(F-15) which was noted earlier for HfC+C(C-11) and ZrC+C (C-12) in Section II.B-12. This low temperature attack (which is eliminated when boron is present) is clearly seen in Figure 211. Here,test (F-15)-2M exhibited a 34 mil recession on the hot face at a surface temperature of 3470°F after an 1173 second exposure at one atmosphere stagnation pressure. However, the oxidation depth increases along the sides of the model as the distance from the hot face increases (due to the fact that the temperature decreases) in accordance with Figure 6. Thus, oxidation depths of 100 mils are seen at a distance of 750 mils from the front face where the temperature level dropped below 2800°F.

Post exposure metallographic sections for JT0981(F-16) shown in Figures 221 and 222 present additional graphic evidence of the rapid low temperature oxidation. This behavior is absent at low pressure (0.075 atm) as shown in Figure 226. Figures 224 and 228 illustrate rapid recession at temperatures near 5000°F due to melting.

### 16. Molybdenum and Tungsten Melting Tests and Exposures of $WSi_2$/W(G-18) and Sn-Al/Ta-10W(G-19)

As indicated in Reference (3) extensive precautions have been taken in order to insure that temperature measurements of the model surface are accurate. In general, the comparison of observed surface temperatures in HG/CW arc plasma tests with values calculated from stream conditions are in relatively good agreement. Moreover, a number of temperature measurements employing two color pyrometers yielded good results (page 8 of Reference (3)). In order to obtain additional verification of the surface temperature measurements, the melting points of tungsten and molybdenum were measured in the arc facilities using pure nitrogen streams

for comparison with accepted values. The results of these tests are shown in Table 29 and in Figure 230. The relatively good agreement obtained in these tests should eliminate concern over the accuracy of surface temperature measurements due to interference of the arc with optical observations.

The results of arc plasma testing of the coated refractory metals $WSi_2/W$(G-18) and Sn-Al/Ta-10W(G-19) is shown in Tables 30-32 and 45. Both of these materials exhibit high ratios of T(CALC)/T(OBS) when the coating is intact. Thus, ratios near 1.55 are typical for (G-18) and 1.40 for (G-19). As indicated earlier, ratios which are larger than 1.0 indicate enhanced temperature resistance. This behavior will be discussed in Section IID. Modest temperature gradients observed for (G-18) are shown in Table 45. The results will be discussed in Section IIC. These data agree with computed results (6). Figure 6 compares the results for (G-18) and (G-19) obtained in the current HG/CW arc plasma tests with those obtained in CG/HW furnace tests. Post exposure photographs and metallographic sections of "maximum severity survivals" and "minimum failures" are shown in Figures 231-246.

It should be noted that (G-18)-19M and (G-18)-20M which were shrouded in cylinders of $ZrB_2$+SiC+C(A-10) as indicated in Table 30 and Figure 233 showed no sign of reaction with the shroud. This indicates compatability between the coated tungsten and boride composite under these conditions.

Figures 234 and 235 show post exposure metallographic sections through sample $WSi_2/W$(G-18)-4M which represent a "maximum severity survival" condition in the Model 500 at one atmosphere stagnation pressure. This test conducted at a flux level of 460 BTU/ft$^2$sec and 2785 BTU/lb survived the full 1800 second exposure as did tests (G-18)-21M and 22M at slightly lower flux levels and slightly higher enthalpies. In all three cases, the observed surface temperatures were below 3450$^\circ$F which corresponds to the survival limit noted in the furnace tests (4). In addition, in each case the calculated temperature based on Eqs. 2 and 3 was 40% to 60% higher than observed. This finding is in keeping with the behavior noted for SiC, SiC coated graphite and SiC bearing composites discussed earlier.

Raising the conditions slightly as in (G-18)-14M at 440 BTU/ft$^2$sec and 3485 BTU/lb results in coating burn-off and tungsten ablation. This test resulted in complete ablation of the sample in 1032 seconds. The initial length of 452 mils leads to a rate of about 0.44 mils/sec under these conditions or a 30 minute recession depth of 790 mils. These rates are in good agreement with calculated recession rates for tungsten ablation (6). It should be noted that once the $WSi_2$ coating is burned off (as in (G-18)-14M) the ratio T(CALC)/T(OBS) drops to unity. This finding offers strong support for the calculation and the conclusion that silicious materials act to lower the surface temperature. It also mitigates against errors due to conduction losses. Figure 235 shows the $W_5Si_3$ zone formed during Test (G-18)-4M. The width of this zone is seen to be 0.55 mils. Table 31 summarizes the $W_5Si_3$ zone widths measured after exposure of all the $WSi_2/W$(G-18) samples. The results are plotted in Figure 237 for comparison with

published values (21, 22) and complementary values obtained during CC/HW tests of this material (4, 5). Figure 236b shows a similar measurement of $W_5Si_3$ zone width for exposure (G-18)-6R in the Rovers arc.

Reference to Figure 237 shows that the zone width data obtained in arc plasma tests under HC/CW conditions at temperatures above 3050°F are in good agreement with the observations obtained using other exposure techniques; however, at lower temperatures, substantial discrepancies exist as shown in Figure 237. These differences cannot be attributed to errors in zone width measurement or temperature measurement. At present the source of these differences is unknown.

The data presented in Table 30 show that Mach 3.2 exposures at $P_e$ = 0.082, $i_e$ = 8310 BTU/lb and $q_{cw}$ = 554 (Sample No. 6RB, Table 30) did not lead to failure. However, exposures 7RA-7RB and 8RA-8RB described in Table 30 clearly describe failure conditions. In the former case, the five mil coating of $WSi_2$ burned off after 300 seconds at a surface temperature of 3610°F generated by $P_e$ = 0.158 atm, $i_e$ = 8020 BTU/lb and $q_{cw}$ = 781 BTU/ft$^2$sec. Subsequently, the surface temperature rose to 5420°F as the tungsten began to burn and 40 mils of tungsten were lost during the 50 second exposure of the bare tungsten. Exposures 8RA and 8RB repeat the 7RA-7RB conditions and extend the exposure time for oxidation of the bare tungsten surface. These exposures (7RB-8RB) indicate a recession rate of 0.80-0.95 mils/sec. The computed rate (6) is 0.35 mils/sec under these conditions. The comparsion of tungsten recession rates observed in this study with those reported in the literature (17) shown in Figure 7 is quite reasonable. These failure conditions are in agreement with the air oxidation, oxygen pickup and high velocity (CG/HW) tests which indicated failure of the $WSi_2$/W coating system at 3450°F to 3680°F. Table 30 illustrates the effects of the $WSi_2$ coating on the surface temperature. For these cases (in contrast to the aforementioned behavior of the boride, graphite and graphite composite materials) the T(CALC)/T(OBS) ratios are much larger than unity. Exposures 7RA-7RB and 8RA-8RB are particularly illuminating in this regard in that 7RB and 8RB, corresponding to the bare tungsten surface after $WSi_2$ burn-off, yield ratios much more typical of the borides and graphites. As indicated earlier, SiC(E-14), Table 26, exhibited high values of T(CALC)/T(OBS).

Exposures (G-18)-23R and (G-18)-24R bracket failure conditions at a stagnation pressure near 0.25 atm. In this case, (G-18)-24R survived a full 30 minute time period characteristic of a hot gas/cold wall exposure at a heat flux of 653 BTU/ft$^2$sec and an enthalpy of 7460 BTU/lb. Raising the stream conditions slightly to 699 BTU/ft$^2$sec and 8180 BTU/lb results in coating failure.

The behavior of Sn-Al/Ta-10W(G-19) shown in Table 32 and Figures 7 and 238-246 compares HG/CW arc plasma test results with furnace data obtained under CG/HW conditions. In addition, post exposure photographs of all samples are presented along with "maximum severity survival" and "minimum failure conditions".

The behavior of Sn-Al/Ta-10W(G-19) indicates failure at temperatures above 3000°F in agreement with the results of CG/HW tests (4, 5). Examination of Table 32 shows that the subsonic exposures (G-19)-2M, 3M and 4M resulted in protection at surface temperatures up to 3000°F. In the last case illustrated in Figures 239 and 240, flux-enthalpy conditions at 350 BTU/ft$^2$sec and 2980 BTU/lb were not sufficient to degrade the coating in 1830 seconds. These conditions lead to a computed temperature, $T_{CALC}$ = 4590°F, on the basis of Eqs 23-25. However, at slightly higher conditions of 390 BTU/ft$^2$sec and 2880 BTU/lb (exposure (G-19)-1M) shown in Figures 241 and 242 which correspond to $T_{CALC}$ = 4640°F, complete degradation of the coating occurs. As in the case of $WSi_2$/W(G-18) and KT-SiC(E-14) the ratios of T(CALC)/T(OBS) are much larger than unity when the coating is retained. When the coating is eliminated (i.e., (G-18)-1M, 5M and 6R), the T(CALC)/T(OBS) ratios are closer to unity. Table 32 contains the values of total normal emittance for Sn-Al-Mo coated Ta-10W as determined from measurements of surface radiation as $\epsilon_N$ = 0.59. Values of $\epsilon_N$ = 0.44 and $\epsilon_N$ = 0.17 were measured for $Ta_2O_5$ and liquid tantalum. These values will be discussed in Section II. D.

The results contained in Table 32 lead to the following characterization of survival and failure conditions for Sn-Al/Ta-10W (G-19):

PASS

| No. | $P_e$ (atm) | Mach No. | $q_{cw}$ (BTU/ft$^2$sec) | $i_e$ (BTU/lb) |
|---|---|---|---|---|
| 9R | 0.010 | 3.2 | 158 | 10,520 |
| 7R | 0.050 | 3.2 | 355 | 7,100 |
| 4M | 1.0 | 0.29 | 350 | 2,980 |

FAIL

| No. | $P_e$ (atm) | Mach No. | $q_{cw}$ (BTU/ft$^2$sec) | $i_e$ (BTU/lb) |
|---|---|---|---|---|
| 8R | 0.011 | 3.2 | 200 | 11,440 |
| 6R | 0.063 | 3.2 | 504 | 8,740 |
| 1M | 1.0 | 0.32 | 390 | 2,880 |

These results show the expected decrease in coating stability with decreasing pressure. Rovers exposures Sn-Al/Ta-10W(G-19)-9R and 8R shown in Figures 243-246 illustrate survival and failure under low pressure conditions.

17. W+Zr+Cu(G-20) and W+Ag(G-21)

Table 33 summarizes the tests conducted on the tungsten composites W+Zr+Cu(G-20) obtained from Rocketdyne (23) and W+Ag(G-21) obtained from Wah Chang. The latter material was only exposed at one atmosphere stagnation pressure. CG/HW tests were not performed for these materials. Reference to Table 33 shows that values of T(CALC)/T(OBS) near 1.3 were obtained for these materials. This result is not surprising in view of the fact that the heat resisting mechanism involves vaporization of Cu or Ag. This behavior will be discussed further in Section II. D. Figures 7 and 247-260 show the recession in thirty minutes as a function of temperature for the current set of tests as well as post exposure photographs of all exposures and examples of "maximum severity survivals" and "minimum failure conditions".

Arc plasma tests have been reported for W+Zr+Cu (G-20) by Schwarzkopf (23) who observed a gross recession of 91 mils after a 720 second exposure at a stagnation pressure of 0.121 atmospheres, a stagnation enthalpy of 10,520 BTU/lb and a cold wall heat flux of 535 BTU/ft$^2$sec at Mach 3.2. One half inch diameter flat faced samples were employed in these tests (Reference 23, pages 62-63). Reference to Table 33 and Figure 252 show the results of a comparable exposure, W+Zr+Cu (G-20)-9R, run at a stagnation pressure of 0.1 atm, a stagnation enthalpy of 10,680 BTU/lb, and cold wall heat flux of 585 BTU/ft$^2$sec at Mach 3.2. A gross recession of 17 mils was observed after 775 seconds. Total recession of 22 mils was observed. Exposure (G-20)-7R was performed at 0.075 atm, 9,280 BTU/lb and 489 BTU/ft$^2$sec resulted in a gross recession of 28 mils and a total recession of 43 mils after 1800 seconds. However, when the conditions were increased to 0.135 atm, 11,980 BTU/lb and 662 BTU/ft$^2$sec melting was observed initially followed by oxidation. The gross recession was 253 mils and the total recession was 257 mils after an exposure time of 500 seconds as shown in Figure 254. In the Model 500 tests at one atmosphere stagnation pressure extremely rapid degradation was observed at much lower flux and enthalpy levels. Thus, W+Zr+Cu(G-20)-1M exhibited a recession of 147 mils after 157 seconds at 1.03 atm, 2970 BTU/lb and 315 BTU/ft$^2$sec. This behavior indicates that the mechanism of degradation is sensitive to pressure in the 0.1-1.0 atmosphere range. The precise nature of the degradation mechanism which is operative is not clear at present. Figures 247-251 illustrate the behavior at one atmosphere stagnation pressure.

The results obtained for W+AG(G-21) in the Model 500 tests at stagnation pressures of one atmosphere were comparable to the results for (G-20). Figures 256-260 illustrate the high rate of oxidation at one atmosphere.

18. Silica-Tungsten Composites $SiO_2$+68.5 w/o W(H-22) and $SiO_2$+60 w/o W(H-23)

The current results for $SiO_2$+68.5 w/o W(H-22) and $SiO_2$+60 w/o W(H-23) are shown in Tables 34 and 35 and in Figure 8.

Post exposure macrographs as well as "maximum severity survivals" and "minimum failure exposures" are shown in Figures 261-272. The behavior of these materials is quite similar. Figure 8 shows good correspondence between the CG/HW furnace tests and the HG/CW arc plasma tests. In particular, exposures at one atmosphere which achieved surface temperatures in excess of 4000°F all exhibit viscous flow. Higher oxidation rates are observed at lower pressure due to instability of $SiO_2$ relative to SiO (Section VI of Reference 4). All samples exposed in the Model 500 showed sting hole cracking. In addition, all samples which flowed and mushroomed during exposure increased in front face diameter and were exposed to lower effective flux levels. Microstructural features shown in Figure 270 illustrate depletion of tungsten particles from the surface of the one atmosphere tests. The low pressure exposures showed no tungsten depletion, sting hole cracking or viscous flow. Test $SiO_2$ + 68.5 w/o W(H-22)-4M in Figure 262 shows rapid recession at a surface temperature of 5205°F and one atmosphere. At a lower temperature (Test (H-22)-2M, Figure 263) the recession rate is much lower but sting leg oxidation is observed due to the lack of $SiO_2$ viscosity (see Section III. K of (5)). Figures 264 and 265 show tests (H-22)-10R and (H-22)-7R which illustrate the zones depleted of tungsten particles. The latter figure shows the $SiO_2$ zone (depleted of tungsten) actually separated and "peeled back" from the sample.

Reference to Table 35 shows that tests $SiO_2$+60 w/oW (H-23)-6M, 7M, 15M, 16M, 17M, 18M, 19M and 20 M which achieved surface temperatures in excess of 4000°F all exhibit viscous flow. Higher oxidation rates are observed at lower pressure due to instability of $SiO_2$ relative to SiO (Section VI of Reference 3). All samples exposed in the Model 500 showed sting hole cracking. In addition, all samples which flowed and mushroomed during exposure increased in front face diameter and were exposed to lower effective flux levels. Figures 267-270 show exposures $SiO_2$+60 w/oW (H-23)-2M and 15M. Figure 270 shows the zone depleted of tungsten particles. Figures 271 and 272 show Rovers exposures $SiO_2$+60 w/o W(H-23)-8R. The low pressure exposures showed no tungsten depletion, sting hole cracking or viscous flow.

The T(CALC)/T(OBS) ratios shown in Tables 34 and 35 indicate values of 1.10 for $SiO_2$+68.5 w/o W(H-22) and 1.25 for $SiO_2$ + 60 w/o W(H-23). These values will be discussed further in Section II. D. However, the former appears low, while the latter seems consistent with values obtained for other silicon bearing materials. It appears difficult to blame the small difference in tungsten content between (H-22) and (H-23) for the disparity in T(CALC)/T(OBS) ratios.

### 19. Hf-20Ta-2Mo(I-23)

The results obtained for Hf-20Ta-2Mo(I-23) are summarized in Tables 36, 37, 38, 46 and 47. Figure 8 compares the HG/CW test data with results obtained in CG/HW furnace tests. Photographs of all test samples after exposure and metallographic sections of selected samples are displayed in Figures 273-293. Reference to Tables 36-38 indicates that the ratio T(CALC)/T(OBS) for this refractory metal alloy is near 1.20 when

melting does not occur. This characteristic will be discussed in Section II. D. As shown in Tables 46 and 47, temperature gradients of 1500°R or more exist through 100 and 400 mil wall thicknesses of this material during oxidation. Measurement of these gradients has been discussed in Section II. B. 4 of Reference 3. Large gradients have also been observed in high velocity CG/HW tests (5).

Reference to Figure 8 shows that Hf-20Ta-2Mo(I-23) exhibits the same characteristics shown by the diborides $HfB_{2.1}$(A-2) and $ZrB_2$(A-3) where the rate of recession in the CG/HW furnace test exceeds that in the HG/CW arc plasma test at a given surface temperature. As indicated above, the source of this behavior are the temperature gradients and operation of the MOTEL criterion discussed in Section I. B. Indeed, the gradients are so severe that surface temperatures up to 5000°F are observed over long periods of time even though the alloy melts at 3860°F (Reference 2, page 5) in furnace tests. This behavior is indicated in 24M, 44R and 1MC shown in Tables 36 and 37. Reference to Figure 8 does not indicate any effect of stagnation pressure on oxidation rate in the 0.01-1.0 atmosphere range covered by these tests. This result is in keeping with earlier observations (24). Figures 274 and 275 show post exposure photographs of (I-23)-45M, 46M, 47R and 48R which were shrouded in $ZrB_2$+ SiC+C(A-10) cylinders. Post exposure examination showed no interaction indicating compatibility between (I-23) and (A-10).

Figures 276 and 277 show the low recession observed for test (I-23)-1M at an observed temperature of 4030°F on the front face of the sample at the air/oxide interface. This temperature is 170°F above the melting point of 3860°F observed for samples of this alloy. This result is due to the occurrence of temperature gradients in the HG/CW tests. Exposure Hf-20Ta-2Mo(I-23)-14M at 605 BTU/ft$^2$sec and 3965 BTU/lb corresponding to a surface temperature of 4620°F melted in 30 seconds. By contrast, (I-23)-15M (shown in Figures 278 and 279) at 515 BTU/ft$^2$sec and 3735 BTU/lb exhibited a surface temperature of 4645°F and did not melt. Nonetheless, (I-23)-15M showed melting of the oxide but not of the metal. This would imply a temperature gradient of more than 700°F through the oxide. In contrast to (I-23)-15M, exposure (I-23)-1M at 530 BTU/ft$^2$sec and 3295 BTU/lb exhibited a surface temperature of 4030°F. ROVERS exposures Hf-20Ta-2Mo(I-23)-12R and 9R are shown in Figures 280-283. The former shows protective oxidation at 378 BTU/ft$^2$sec and 12,710 BTU/lb (surface temperature equals 3755°F). Surprisingly, (I-23)-9R at 337 BTU/ft$^2$sec and 11,250 BTU/lb (surface temperature equals 4220°F) showed signs of melting. This could be due to the formation of a very thin oxide at low pressure which was not an effective insulator.

Figures 284 and 285 show post exposure photographs of several (I-23) samples which were employed for measurements of internal temperature. Sample (I-23)-3MC shows the results of a burn-through after 1455 seconds. The time-temperature history of this exposure which is documented in Table 46 shows that the internal temperature reached 3800°F

(melting point equals 3860°F) at this point. Sample (I-23)-1MC is shown after sectioning in Figure 285. The tungsten sting is in place in this figure to illustrate the small contact area for conduction losses.

Figures 286-293 illustrate samples exposed to multiple cycles and in the hemispherical configuration after sectioning.

Test (I-23)-27M was exposed to seven cyclic exposures at a stagnation pressure of 1.05 atmospheres, a stagnation enthalpy of 3300 BTU/lb and a cold wall heat flux of 410 BTU/ft$^2$sec. The observed surface temperature was 4230°F and a recession of 138 mils was observed after an exposure of 11,600 seconds in cycles of 1800 second duration. This behavior is not quite as good as that exhibited by $ZrB_2$+20%SiC(A-8)-17M shown in Figure 83 or $ZrB_2$+SiC+C(A-10)-24M shown in Figure 109. These samples ran for longer times under more severe conditions than did (I-23)-27M and exhibited less recession. Nevertheless, Hf-20Ta-2Mo(I-23) is metallic and as such offers advantages as regards fabricability and resistance to thermal stress. On the other hand (A-8) and (A-10) possess higher strength and more temperature capability (6) than (I-23).

Figure 288 illustrates the results obtained with Hf-Ta-Mo (I-23)-28R after a 4 cycle exposure at a stagnation pressure of 0.132 atm., an enthalpy of 7600 BTU/lb and a cold wall heat flux of 398 BTU/ft$^2$sec. Total exposure time was 7220 seconds yielding a recession of 55 mils. As indicated above, boride composites shown in Figures 71, 91 and 111 exposed to more severe conditions in the ROVERS facility exhibited less recession. However, the behavior of Hf-Ta-Mo(I-23)-28R is outstanding for a metallic structure.

The earlier discussions of cyclic boride exposures presented in Sections II.B.5, 6 and 8 made note of the fact that the temperature increased from one cycle to the next. Reference to Tables 37 and 38 indicates that although tests (I-23)-27M exhibited an increase in surface temperature during the first two cycles, the temperature was relatively stable from cycle III to cycle VII with T(CALC)/T(OBS) ratios near 1.08. Surface temperature held steady during cyclic exposure of (I-23)-28R with T(CALC)/T(OBS) ratios near 1.27.

Figures 290-293 show the results obtained with hemispherical capped samples of (I-23)-38MH and 39RH. Reference to Tables 37 and 38 show that T(CALC)/T(OBS) for these tests were 1.12 and 1.44, respectively. Although the latter value is higher than the typical ratios observed for this material (1.20) the former value is lower. In any case, the magnitude of temperature reduction observed with hemispherical caps is smaller than observed for (A-8), (A-8) and (A-10) (c.f., (A-7)-36MH, Table 6; (A-7)-48RH, Table 8; (A-10)-35MH, Table 13; and (A-10)-46RH, Table 14).

### 20. Iridium Coated Poco Graphite Ir/C (I-24)

Iridium coated Poco graphite samples furnished by Battelle Memorial Institute (25) were tested in the Model 500 and Rovers facilities. In view of the high cost of these samples an attempt was made to use them for several runs and to avoid sectioning(thus destroying the sample) where possible. Accordingly, techniques were employed for nondestructively measuring coating thickness (Reference(1), pages 7, 8, 24 and 25). Most of the coatings were of the order of 20 mils thick based on the NDT results and the observations made on sectioned samples. The sample numbers supplied by Battelle were retained in order to permit cross referencing with the fabrication report (25). In addition to the samples of Ir/C(I-24) listed in Reference (1), Battelle supplied two cylinders of iridium coated graphite in which an Iridium-50 v/o $HfO_2$ coating was applied to improve the oxidation resistance. Photographs of these samples are shown on page 101 of Reference (25). Fabrication is discussed on page 89 of Reference (25). In accordance with the Battelle designation, these samples are numbered Ir/C(I-24)-36 and 37.

The results obtained in arc plasma testing of Ir/C(I-24) are summarized in Table 39. Figure 8 shows the temperature dependence of the oxidation behavior, while Figures 294-301 display post exposure photographs of all test samples and sections through a failure and a survival. In line with the CG/HW tests reported earlier (4), iridium exhibits very low oxidation rates up to its melting temperature at 4430°F. The temperature of the iridium-carbon eutectic (4) is 4175°F. Reference to Figure 8 shows that samples exposed to higher conditions exhibited melting of the coating and ablation of the graphite. The major drawback of this coating system is the low emittance of the iridium ($\epsilon \approx 0.30$). However, addition of $HfO_2$ raised the emittance to values near 0.50 and extended the range of conditions under which the coating can be used. Thus, examination of Table 39 shows that the pure coating is destroyed at flux levels in excess of 310 BTU/ft$^2$sec. At flux levels below 300 BTU/ft$^2$sec the coating is hardly affected; however at higher levels, melting followed by rapid ablation occurs.

However, when $HfO_2$ is added to increase the emittance, failure does not occur until the flux level reaches 510 BTU/ft$^2$sec (i.e., see tests 36MRA and 36MRB).

In summary, although Ir/C(I-24) has excellent temperature capability to temperatures near 4200°F, it has very low resistance to stream conditions. In fact (6), if heat flux/enthalpy characteristics are used as a yardstick, Ir/C(I-24) ranks below Si/RVC(B-8), described in Table 19, even though the latter has a temperature limit near 3200°F. The difference is caused by the fact that (B-8) has a higher emittance than (I-24), 0.69 vs. 0.36, and a higher T(CALC)/T(OBS) ratio, 1.36 vs. 1.21. These factors will be discussed in further detail in Section II. D.

C. Results of Temperature Gradient Measurements

As indicated above, temperature gradients have been measured through 100 and 400 mil walls of $ZrB_2$(A-3), $HfB_{2.1}$+20%SiC(A-7), $ZrB_2$+20%SiC(A-8), $ZrB_2$+SiC+C(A-10), RVA(B-5), $WSi_2$/W(G-18) and Hf-20Ta-2Mo(I-23). Tables 40-47 detail the time-temperature histories obtained in these tests. Figures 302-312 show the time-temperature data graphically. Calculations of the temperature gradients through the test cylinders described by Figures 302-312 are presented in Section VII of Reference (6). These calculations are based on side losses due to radiation and conduction down the length of the model but no heat loss via conduction. Thus, the model employed implies a modification of Eqs. (2) and (3) to reflect side losses.

The materials chosen for examination actually cover a wide range of characteristics. Thus RVA(B-5) represents an ablator with no coating. On the other hand $WSi_2$/W(G-18) provides an alternative situation where the bulk thermal conductivity is nearly three times that of RVA(B-5) at the temperature of interest. However, $WSi_2$/W(G-18) has a 5 mil $WSi_2$ coating which has a thermal conductivity approximately one third that of RVA(B-5). The remaining materials, (A-3), (A-7), (A-8), (A-10) and (I-23) have bulk thermal conductivities ranging between 0.5 to 0.8 that of tungsten. However, they all form oxide coatings which have very low thermal conductivities. Thus, the coating which forms on $ZrB_2$ (A-3), which is quite flakey, is estimated to have a thermal conductivity of $10^{-4}$ BTU/ft sec$^{o}$R or 65 times less than RVA(B-5).

The thermal conductivity of the oxides formed on (A-7), (A-8), (A-10) and (I-23), which are more adherent, was estimated to be five times larger than the oxide formed on (A-3).

Examination of Figures 302-312 shows that with few exceptions, the internal temperatures remain fairly constant over long periods of time. The exceptions are cases in which fairly rapid degradation is occurring. Thus, the principal exception is test (I-23)-3MC discussed earlier in Section II.B.18 where the melting point was achieved at 1455 seconds. As a consequence, comparison of the computed values, which are based on a steady state condition, with the observed temperatures appears justified. This description is contained in Tables 23-28 of Reference (6) which compare the observed internal temperatures with calculated values for $ZrB_2$+SiC(A-8), $ZrB_2$(A-3), $HfB_2$+SiC(A-7), RVA(B-5), $ZrB_2$+SiC+C(A-10), $WSi_2$/W(G-18) and Hf-Ta-Mo(I-23). Data include measured front face and internal temperatures, $T_f$ and $T_d$, the cold wall heat flux, $q$, the stagnation enthalpy, $i_e$, and the stagnation pressure, $P_e$. In addition, these tables show the radius, R, length, L, and oxide coating thickness, I. The latter was equated to the conversion depth for the oxide formers. For $WSi_2$/W, I was equated to the $WSi_2$ coating thickness and I=0 for RVA(B-5) graphite which ablates without coating formation. Values of the emittance, $\epsilon_S$ (see Section II.D) as well as suitable values of the thermal conductivities characteristic of each material for the coating $k_F$ and the substrate $k_S$ are also shown in Tables 23-28 of Reference (6).

The computed results are displayed in terms of the ratio of calculated front face temperature to observed front face temperature $T_f(CALC)/T_f(OBS)$ and the ratio of computed in-depth temperature $T_d(CALC)$ to computed front face temperature $T_f(CALC)$. If the agreement is exact (e.g., Hf-Ta-Mo(I-23)-43R in Figure 311), the ratio of $T_f(CALC)/T_f(OBS)$ would be 1.00. In the example, $T_f(CALC)$ is 4440°R vs. 4530°R = $T_f(OBS)$. Similarly the measured temperature at 109 mils is 3560°R vs. $T_d(CALC)$ = 3380°R. In this case, the observed gradient is 960°R while the calculated gradient is 1060°R in 109 mils.

All of the runs shown in Tables 41-47 were performed on flat faced cylinders except those designated by a suffix H (hemisphere) or S (cylindrical shroud with a 200 mil wall). Photographs of these models have been presented. The shrouds and hemispherical caps did not alter the gradients observed for flat faced cylinders. Thus, all of the calculations were based on flat faced cylinders ignoring the hemispherical caps and the shrouds. Reference to Tables 23-28 of Reference (6) indicates relatively good agreement between calculation and observation, in view of the simple model employed and the complexities of the experiments.

The largest deviations occur at low surface temperatures (i.e., $T_f$ < 3300°R) for the materials which form $SiO_2$ as an oxidation product. Thus, in cases where samples of $HfB_2$+SiC(A-7), $ZrB_2$+SiC(A-8), $ZrB_2$+SiC+C(A-10) or $WSi_2$/W(G-18) were exposed with shrouds or as large diameter hemispheres $T_f$ (CALC) is considerably larger than $T_f$(OBS). However, this difference is smaller than obtained when $T_f$ is computed on the basis of radiation equilibrium. The cause of this behavior is presently unknown (6). Reference to Tables 23-28 of Reference (6) shows that the calculated and observed ratios of $T_d/T_f$ are in general agreement.

### D. Average Values of Normal Total Emittance and T(CALC)/T(OBS) Ratios for the Candidate Materials

Tables 2-39 contain values of the radiated heat flux, $q_r$, observed during the arc plasma exposures. These values are employed to compute total normal emittance on the basis of Eq. 1. The resultant values are contained in Tables 2-39 along side each exposure. As noted earlier (3), the surface temperature which appears in Tables 2-39 and in Eq. 1 is measured optically (at $\lambda$ = 0.65μ) and converted to a true temperature by employing specific values of the normal spectral emittance at $\lambda$ = 0.65μ (5).

In addition to the measurements presented in Tables 2-39, two-color pyrometer measurements were performed during the course of exposures $HfB_2$+SiC(A-4)-2M, PG(B-6)-9M, BPG(B-7)-6M, JTA(D-13)-2M, $HfB_2$+35%SiC(A-9)-6M and Si RVC(B-8)-13M. The results were combined with the brightness temperatures in order to obtain spectral emittance values at $\lambda$ = 0.65μ. The results were found to agree reasonably with the current values assumed for $\epsilon_N$ at $\lambda$ = 0.65, (3, 5).

Table 48 summarizes the average of all the $\epsilon_N$ results for each material. Tests conducted on flat faced cylinders without shrouds were employed exclusively in taking the averages. Separate averaged $\epsilon_N$ values are presented for conditions where melting was observed and conditions whwere a coated surface was removed. Most of the results for the solid oxidized surfaces are between 0.6 + 0.2. Lower values are obtained for those cases where melting occurs (i.e., $\epsilon_N$ = 0.32 for tungsten ($WSi_2$/W)(G-18)).

In view of the relatively low values of $\epsilon_N$ observed for 0.500 inch diameter graphite samples, a series of exposures were performed employing samples which were 0.740 inch in diameter. In the latter case, the image fills a larger fraction of the Eppley thermopile viewing area (3). As shown in Table 16, larger values of $\epsilon_N$ were observed with the larger diameter samples. Similar experiments performed with $ZrB_2$ (A-3) and Hf-20Ta-2Mo(I-23) where solid oxides form (Tables 3 and 36) did not show this behavior. For such cases, difference in $\epsilon_N$ are not anticipated since changes in diameter are not encountered during exposure.

Table 48 summarizes averaged ratios of T(CALC)/T(OBS) derived on the basis of Eqs. 2 and 3 and the stream conditions and surface temperatures contained in Tables 2-39. Ideally, if radiation equilibria were the dominant factor and all measurements were accurate, these ratios should be unity. Although there are departures, it is satisfying to note that the differences are small compared to those obtained by considering the results of other studies (i.e., Figures 16-21 of Reference (6)). Reference to Table 48 shows that ratios of T(CALC)/T(OBS) are lower for cases where melting is observed than for cases where a solid oxide (or coating) is present. Moreover, Table 48 shows that large values of T(CALC)/T(OBS) are characteristic for some of the materials. The occurrence of ratios which are larger than unity implies resistance to energy absorption by the material. Thus, exposure of $HfB_2$+SiC(A-4) and HfC+C(C-11) to identical stream conditions (i.e., stagnation pressure, enthalpy and cold wall heat flux) would result in an observed surface temperature for the former which is 1.10/1.22 = 0.90, or 11% lower than the surface temperature reached by HfC+C(C-11). This conclusion would apply if stream conditions were not sufficient to produce melting of $HfB_2$ + SiC(A-4). At lower levels, KT-SiC(E-14), $WSi_2$/W(G-18) and Sn-Al/Ta-10W(G-19), which exhibit T(CALC)/T(OBS) ratios of 1.43, 1.54 and 1.41, respectively, demonstrate similar resistance to energy transfer. Although the origin of this resistance is not clear at present, it is probably due to blocking effects caused by evolution of gaseous oxides. These observations suggest a method of ranking the behavior of the refractory materials which differs from the present recession vs. temperature curves (Figures 1-8). In Reference (6), an alternative method of presentation which compares recession rate as a function of heat flux and enthalpy for the candidate materials is considered. This method does not require a knowledge of the spectral or the normal emittance and integrates the blocking effects characteristic of each material.

E. Summary

Present results for $HfB_{2.1}$(A-2) and $ZrB_2$(A-3) in the HG/CW arc plasma tests show a marked difference between the recession rates at a given surface temperature and those observed at the same surface temperature in furnace tests (4). As shown in Figure 1, an oxidation depth of 20 mils in 30 minutes is obtained in an arc plasma test at 5000°F while the same oxidation depth can be produced at 3500°F in a furnace test. Alternatively a 100 mil oxidation depth is observed in a furnace test at 4000°F after 30 minutes while comparable oxidation depths are not obtained in arc plasma tests below 5500°F. The source of this difference is the temperature gradient through the oxide as indicated in Section I.B. Thus, oxidation occurs slowly until temperatures are high enough to cause melting of the boride. The excellent long-time oxidation resistance of this material at 4000°F is illustrated in Figures 40 and 41.

Cyclic exposures of $ZrB_2$(A-3) and $HfB_{2.1}$(A-2) were performed to assess the effects of heating and cooling in three 600-second cycles. At the lowest level $ZrB_2$(A-3) exhibited a recession equivalent to that observed in an 1800 second test. At higher levels $ZrB_2$(A-3) exhibited larger recessions for cyclic exposures than in the case of uninterrupted 1800 second tests. By contrast, the cyclic tests performed on $HfB_2$ did not result in larger recessions than the uninterrupted tests. Motion picture coverage indicated that the oxide formed on $HfB_{2.1}$(A-2) exhibited greater tenacity under these conditions than did the oxide formed on $ZrB_2$(A-3). The latter flaked off between cycles. As indicated in Section II.B.1, preoxidation of $HfB_2$(A-2) to form a 10 mil coating did not result in noticeable changes in behavior.

Reference to Table 3 shows that the $ZrB_2$(A-3) material employed in these tests did not exhibit any thermal stress failures at flux levels as high at 950 BTU/ft$^2$sec. In contrast to the $HfB_{2.1}$(A-2) material discussed in Section II.B.1, the (A-3) material was mechanically sound and did not exhibit the flaws shown by the (A-2) in the nondestructive tests prior to exposure (see Sections IV.B,C and Tables 15, 16 of Reference 1). However, Boride Z(A-5) was found to be very susceptible to thermal shock failure. Figures 59a and 59b show Boride Z(A-5)-4M and 8R which exhibit thermal shock cracks after exposure at 348 BTU/ft$^2$sec and 3215 BTU/lb and 262 BTU/ft$^2$sec and 9200 BTU/lb, respectively. Thus, flux levels above 200-250 BTU/ft$^2$sec appear to result in thermal shock failures of Boride Z.

Boride composites $HfB_2$+20%SiC(A-4) and (A-7), $ZrB_2$+20% SiC(A-8) and $HfB_2$+35%SiC(A-9) were found to exhibit remarkable oxidation and thermal stress resistance in HG/CW arc plasma tests. Although these materials display temperature gradients in the oxides, the difference between the arc plasma and furnace oxidation depths are small (Figure 2). This finding is in contrast to the results obtained for $HfB_{2.1}$(A-2) and $ZrB_2$(A-3) shown in Figure 1. The adherent oxide which forms on these composites results in low recessions observed after

exposures in the 3500°-4500°F temperature range. In addition, (A-4) exhibited no thermal shock failures at flux levels up to 1000 BTU/ft$^2$sec. Radiation equilibrium calculations performed for exposures of these materials showed that the ratio T(CALC)/T(OBS) for (A-2), (A-3) and (A-4) exceed unity. Thus, the observed temperature was 16% lower than expected for (A-2), 9% lower than expected for (A-3) and 22% lower than expected (based on radiation equilibrium) for (A-4). Similarly, the other boride composites containing SiC, i.e., $HfB_2$+20%SiC(A-7), $ZrB_2$+20%SiC(A-8) and $HfB_2$+35%SiC(A-9) yielded ratios of 1.25, 1.34 and 1.17. Moreover, exposure of hemispherical models exhibited lower surface temperatures than those observed for flat faced cylinders.

Figures 71 and 72 show metallographic sections of (A-7)-28R exposed for thirteen cycles (each of 1800 second duration) at a stagnation pressure of 0.07 atm, an average heat flux of 495 BTU/ft$^2$sec and an enthalpy near 10,300 BTU/lb. Reference to Table 7 and Figure 71 show that the total recession after the thirteen cycle exposure was 15 mils. This behavior is unrivaled by any other known material system.

Figures 73 and 74 show post exposure sections through (A-7)-52M after 14,030 seconds exposure in eight 1800-second cycles at a stagnation pressure of 1.03 atmospheres. The average cold wall heat flux was 450 BTU/ft$^2$sec at an enthalpy level of 4180 BTU/lb. Total recession was 329 mils or about 0.33 inches. Under similar conditions graphite and tungsten would exhibit recessions of 14 to 28 inches. $ZrB_2$+20%SiC(A-8) displays all of the same features shown by $HfB_2$+SiC(A-7) although it is not as refractory as its hafnium base counterpart. However, the decrease in temperature resistance is compensated for by the reduced density and cost. Zirconium diboride is roughly one half the density and one tenth the price of hafnium diboride. A few tests of (A-8) were shrouded and it is interesting to note the results of (A-8)-29M in which a graphite shroud was employed (Tables 9 and 42). Although the boride exhibited minimal recession (8 mils in 1800 seconds) the graphite shroud which was one inch long ablated completely in 500 seconds.

Table 15 and Figure 1 show the depletion depths for $ZrB_2$+SiC(A-8) as a function of temperature. This material exhibited the lowest SiC depletion rate of all the boride composites. In addition, the depletion rate in the current HG/CW arc plasma tests were observed to be less than depletion rates in CG/HW furnace tests at comparable surface temperatures.

Measurements of the temperature gradients through oxide coatings formed on $ZrB_2$+SiC(A-8) yielded results which are smaller than exhibited by $ZrB_2$(A-3). This finding appears to be due to the higher thermal conductivity of the oxide formed on (A-8) (as compared with (A-3)) (6). Consideration of Tables 9 and 10 shows that $ZrB_2$+SiC (A-8) exhibits the same tendency to develop low temperatures as (A-4) and (A-7). Thus, tests in the ROVERS facility at flux levels below 500 BTU/ft$^2$sec and in the Model 500 facility at flux levels below

350 BTU/ft$^2$sec develop ratios of T(CALC)/T(OBS) which are of the order of 1.50. This feature of the boride composites which contain SiC permits a wider range of applicability than materials which exhibit (T(CALC)/T(OBS)) near unity.

The behavior of $HfB_2$+35%SiC(A-9) was found to be similar to (A-4) and (A-7) as regards the T(CALC)/T(OBS) comparison, recession rate vs. temperature for HG/CW arc plasma tests and furnace exposures, depletion depth vs. temperature in HG/CW tests as a function of temperature, etc. The major difference is that (A-9) is less refractory than (A-4) and (A-7).

Recession rates observed for graphites in HG/CW arc plasma tests are substantially higher than those observed in CG/HW furnace tests at 1-9 ft/sec air flow rate (4). This indicates that the latter are supply limited. As indicated earlier (5), the results of high velocity CG/HW tests on graphite at air flow rates near 250 ft/sec approach the results obtained in the arc plasma exposures. Modest temperature gradients were measured through graphite samples during HG/CW tests. Limiting survival conditions for Si/RVC(B-8) determined under HG/CW conditions depart from the behavior in furnace tests and correspond to the failure characteristics observed for silicon carbide in HG/CW tests. In the arc plasma tests, Si/RVC (B-8) exhibits protective oxidation up to surface temperatures near 3800°F, some 700°F above the failure temperature in furnace tests. Graphite-type behavior occurs above this temperature. At one atmosphere stagnation pressure, coating burn-off occurs after 735 seconds at 470 BTU/ft$^2$sec and 3720 BTU/lb. At a stagnation pressure of 0.01 atmospheres protective behavior was observed in a 30 minute exposure at 210 BTU/ft$^2$sec and 8850 BTU/lb.

The recession rates of all of the graphites are inversely proportional to material density. Glassy Carbon (B-11) appeared to melt during exposure. No post exposure examination could be made since the sample was completely destroyed. Since glassy carbon is not reported to melt at one atmosphere, the only explanation of such an observation must be made on the basis of surface contamination of the sample by tungsten or copper (from the arc electrodes) and melting of the alloy. This conclusion is based on the findings at Lockheed (5).

Hypereutectic carbides HfC+C(C-11) and ZrC+C(C-12) exhibited excellent oxidation resistance at surface temperatures below 5000°F and melted under very high temperature conditions in line with reported melting points. The present results are consistent with the eutectic temperatures but show little dependence on the melting point of the oxides. Current data indicate comparable oxidation rates in the CG/HW and HG/CW tests. No thermal shock failures were noted at flux levels up to 750 BTU/ft$^2$sec. In line with the oxidation behavior noted in furnace tests, the HG/CW arc plasma tests show a "puffy" oxide which forms at the lower temperatures investigated. This oxide has been noted in air oxidation tests

performed in furnaces below 3400°F (4). Rapid oxidation occurs at the back of samples where the surface temperature is lower than at the front face. This is another characteristic of the HfC+C(C-11) oxidation which is in line with the furnace test results (4). The oxidation behavior of samples containing 13.6 w/oC does not appear to differ materially from samples fabricated from the billets which contain 14.0 to 15.6 w/o carbon. The behavior of ZrC+C(C-12) in the HG/CW arc plasma tests was found to be similar to that of HfC+C(C-11).

KT-SiC(E-14) exhibited rapid recession rates at surface temperatures above 3900°F. This is some 400°F above the limit observed in furnace tests and in line with the results obtained for Si/RVC (B-8).

Composites of borides, carbides and graphites including $ZrB_2$+SiC+C(A-10), JTA(C-$ZrB_2$-SiC)(D-13), JT0992(C-HfC-SiC)(F-15) and JT0981(C-ZrC-SiC)(F-16) exhibited HG/CW test results which were comparable to their CG/HW behavior. At elevated temperatures, destruction of the protective oxide coating leads to graphite-type recession behavior. $ZrB_2$+SiC+C(A-10) exhibits the best oxidation resistance in this group owing the fact that it contains the largest percentage of boride. In addition, it exhibits lower recession rates in the HG/CW tests than in the CG/HW tests as is the case for $ZrB_2$(A-3). Melting of $ZrB_2$+SiC+C(A-10) is encountered near 5000°F where substantial differences between low pressure and one atmosphere oxidation rates are observed. Thermal shock failures were not observed at flux levels up to 1010 BTU/ft$^2$sec. The low density (4.5 gms/cm$^3$), high strength, low modulus and good machinability exhibited by this composite, when coupled with its oxidation resistance up to 5000°F, offer an exceptional combination of properties.

In general, the behavior of the (A-10) composite is quite similar to that exhibited by (A-4), (A-7) and (A-8) discussed earlier in Sections II.B-3, 5 and 6. However, (A-10) is not as refractory as (A-4) and (A-7). However, the lower density and cost as well as the thermal stress resistance and machining characteristics of this composite provide compensating advantages. Figures 109-112 show sections through (A-10)-24M and (A-10)-26R after exposure for times up to 21,600 seconds near 4500°F with total recessions of the order of 100 mils. This behavior, which was discussed in Section I.B shows striking evidence for the applicability of this material in reusable lifting reentry spacecraft.

Exposures of hemispherical models of (A-10) indicate that the observed temperature was 60% lower than expected. This behavior (noted earlier with (A-7) and (A-8) in Sections II.B.4 and II.B.6), characterized by lower temperatures achieved with hemispherical models than with flat faced models is not understood at present. Nevertheless, the practical implications of this finding are substantial. For example, (A-10)-25R, 26R, 40R and 41R (which were flat faced models) exposed at conditions similar to (A-10)-37R and 38R (i.e., 500 BTU/ft$^2$sec, 7700 BTU/lb, 0.15 atm) exhibited temperatures near 5000°R in contrast to (A-10)-37R and 38R which exhibited temperatures near 3700°R. Naturally the hemispherical models exhibited lower recession rates. Sample (A-10)-37RH is shown after sectioning in Figures 113 and 114.

Similarly, sample (A-10)-48RH was exposed to four exposures at ascending flux levels until evidence of melting was noted. Melting of this hemispherical capped model was not observed to occur until fluxes near 850 BTU/ft$^2$sec were attained. Flat faced models melted near 650 BTU/ft$^2$sec.

Figures 194 and 195 show sample (D-13)-48MX after 4 cyclic exposures at a stagnation enthalpy of 4350 BTU/lb, stagnation pressure of 1.01 atm and a cold wall heat flux of 380 BTU/ft$^2$sec. Each exposure was 1800 seconds long making the total exposure time 7200 seconds. The average recession was 118 mils. This test can be compared with (A-10)-24 shown in Figure 109 which exhibited a recession of 104 mils after 12 cycles (1800 seconds each) totalling 21,600 seconds under comparable conditions.

Figures 196 and 197 show sample (D-13)-49RX after 4 cyclic exposures at a stagnation pressure of 0.57 atmospheres at a stagnation enthalpy of 9600 BTU/lb and a cold wall heat flux of 440 BTU/ft$^2$sec. Each exposure was 1800 seconds long making the total exposure time 7200 seconds. Total recession for this test was 45 mils. By comparison, (A-10)-26R exposed for 18,951 seconds at comparable heat flux and enthalpy and a higher pressure (0.238 atm) exhibited a recession of 83 mils as shown in Figure 111.

As indicated in Reference (3) extensive precautions have been taken in order to insure that temperature measurements of the model surface are accurate. In general, the comparison of observed surface temperatures in HG/CW arc plasma tests with values calculated from stream conditions are in relatively good agreement. Moreover, a number of temperature measurements employing two color pyrometers yielded good results (page 8 of Reference (3)). In order to obtain additional verification of the surface temperature measurements, the melting points of tungsten and molybdenum were measured in the arc facilities using pure nitrogen streams for comparison with accepted values. The results of these tests are shown in Table 29 and in Figure 230. The relative good agreement obtained in these tests should eliminate concern over the accuracy of surface temperature measurements due to interference of the arc with optical observations.

A substantial number of thermal shock failures of JTA(D-13) and JT0981(F-16) have been observed. For JTA(D-13), these failures occurred in random fashion at flux levels above 500 BTU/ft$^2$sec. The samples which failed by thermal shock were machined from 2-1/2" diameter x 2" long billets of JTA(D-13) in an orientation which corresponded to the hot pressing direction. Thus, the axis of the arc plasma test sample was parallel to that of the hot pressed cylinder. Under these conditions, residual strain present in the billets and in the samples could provide a source of the failures. However, a series of samples oriented with their axes prependicular to the pressing

direction showed no thermal shock failures at flux levels in excess of 500 BTU/ft$^2$sec. This finding has particular relevance to applications in which JTA(D-13) parts are exposed to severe environmental heat fluxes. JT0992(F-15) did not exhibit sensitivity to thermal shock.

The behavior of these composites is characterized by low recession rates at temperatures between 3000°F and 4500°F, best illuatrated in $ZrB_2$+SiC+C(A-10) and JT0992(F-15) at temperatures up to 4500°F. Above 5000°F, the protection afforded by formation of $ZrO_2$ (or $HfO_2$) and $SiO_2$ is eliminated and oxidation rates which are characteristic of graphite are encountered.

Failure limits for the coated refractory metals $WSi_2$/W (G-18) and Sn-Al/Ta-10W(G-19) have been established in general agreement with furnace tests. Maximum survival conditions for $WSi_2$/W (G-18) are 450 BTU/ft$^2$sec and 3100 BTU/lb at $P_e$ = 1 atm. At lower pressures, failure was observed at 458 BTU/ft$^2$sec and 11,420 BTU/lb. Coating failure conditions were established for Sn-Al/Ta-10W(G-19) at lower flux and enthalpy levels. Modest temperature gradients were measured through $WSi_2$/W(G-18) arc plasma test samples.

Current results for W+Zr+Cu(G-20) indicate relatively good resistance to oxidation at 10,000 BTU/lb and 500 BTU/ft$^2$sec at 0.100 atm in agreement with the findings of Schwarzkopf (5). However, in the Model 500 tests at 1 atmosphere stagnation pressure, very rapid degradation was observed at much lower flux and enthalpy levels. Thus W + Zr+Cu(G-20)-1M exhibited a recession of 147 mils after 157 seconds at 1.03 atm, 2970 BTU/lb and 315 BTU/ft$^2$sec. This behavior indicates that the mechanism of degradation is sensitive to pressure in the 0.1-1.0 atmosphere range. The precise nature of the degradation mechanism which is operative is not clear at present. The results obtained for W+Ag(G-21) in the Model 500 tests at stagnation pressures of one atmosphere were comparable to the results for (G-20).

The silica-tungsten composites $SiO_2$+68.5 w/o W(H-22) and $SiO_2$+60 w/oW (H-23) exhibited similar recession behavior in the one atmosphere HG/CW arc plasma tests as encountered in the CG/HW furnace tests. At low pressures, higher recession rates were observed due to instability of $SiO_2$ relative to SiO. At temperatures above 4000°F, extensive flow of this composite was observed, in agreement with the furnace test findings. Samples exposed at one atmosphere showed sting hole cracking.

Arc plasma exposures of Hf-20Ta-2Mo(I-23) exhibited lower oxidation rates than in the CG/HW tests at comparable surface temperatures. In addition, several samples with indicated surface temperatures in excess of the melting point of the alloy did not melt. Current results indicate that gradients of 1500°F can exist through 100 mils of alloy and

oxide. This behavior is the basis for the surface temperature in the 4000°-5000°F range which were not accompanied by melting of the alloy.

Test (I-23)-27M was exposed to seven cyclic exposures at a stagnation pressure of 1.05 atmospheres, a stagnation enthalpy of 3300 BTU/lb and a cold wall heat flux of 410 BTU/ft$^2$sec. The observed surface temperature was 4230°F and a recession of 138 mils was observed after an exposure of 11,600 seconds in cycles of 1800 second duration. This behavior is not quite as good as that exhibited by $ZrB_2$+20%SiC (A-8)-17M shown in Figure 83 or $ZrB_2$+SiC+C(A-10)-24M shown in Figure 109. These samples ran for longer times under more severe conditions than did (I-23)-27M and exhibited less recession. Nevertheless, Hf-20Ta-2Mo(I-23) is metallic and as such offers advantages as regards fabricability and resistance to thermal stress. On the other hand (A-8) and (A-10) possess higher strength and more temperature capability (6) than (I-23).

Figure 288 illustrates the results obtained with Hf-Ta-Mo (I-23)-28R after a 4 cycle exposure at a stagnation pressure of 0.132 atm, an enthalpy of 7600 BTU/lb and a cold wall heat flux of 398 BTU/ft$^2$sec. Total exposure time was 7220 seconds yielding a recession of 55 mils. As indicated above, boride composites shown in Figures 71, 91 and 111 exposed to more severe conditions in the ROVERS facility exhibited less recession. However, the behavior of Hf-Ta-Mo(I-23)-38R is outstanding for a metallic structure.

Present results for Ir/C(I-24) are in general agreement with the CG/HW tests (4), which showed that iridium exhibits very low oxidation rates up to its melting temperature at 4430°F. The temperature of the iridium-carbon eutectic is 4175°F. Reference to Figure 8 shows that samples exposed to higher conditions exhibited melting of the coating and ablation of the graphite. The major drawback of this coating system is the low emittance of the iridium ($\epsilon$ = 0.30). However, addition of $HfO_2$ raised the emittance to values near 0.50 and extended the range of conditions under which the coating can be used. Thus, examination of Table 39 shows that the pure coating is destroyed at flux levels in excess of 310 BTU/ft$^2$sec. At flux levels below 300 BTU/ft$^2$sec the coating is hardly affected. However, at higher levels melting followed by rapid ablation occurs.

In contrast, when $HfO_2$ is added to increase the emittance, failure does not occur until the flux level reaches 510 BTU/ft$^2$sec (i.e., Table 39 - 36MRA and 36MRB). Thus, although Ir/C(I-24) has excellent temperature capability to temperatures near 4200°F, it has very low resistance to stream conditions. In fact (6), if heat flux/enthalpy characteristics are used as a yardstick, Ir/C(I-24) ranks below Si/RVC (B-8), described in Table 19, even though the latter has a temperature limit near 3200°F. The difference is caused by the fact that (B-8) has a higher emittance than (I-24), 0.69 vs. 0.36, and a higher T(CALC)/T(OBS) ratio, 1.36 vs. 1.21.

Temperature gradients have been measured through 100 and 400 mil walls of $ZrB_2$(A 3), $HfB_{2.1}$+20%SiC(A-7), $ZrB_2$+20% SiC(A-8), $ZrB_2$+SiC+C(A-10), RVA(B-5), $WSi_2$/W(G-18) and Hf-20Ta-2Mo(I-23). Tables 40-47 detail the time-temperature histories obtained in these tests. Figures 302-312 show the time-temperature data graphically. Calculations of the temperature gradients through the test cylinders described by Figures 302-312 are presented in Section VII of Reference (6). These calculations are based on side losses due to radiation and conduction down the length of the model but no heat loss via conduction. In general, relatively good agreement between observed and calculated temperature gradients has been obtained in view of the simple model employed.

Measurements of total normal emittance have been provided for all of the candidate materials based on radiated heat flux observations during HG/CW exposures. Averaged values obtained for solid oxides formed during exposure are higher than normal emittance values observed for melting surfaces. Comparison of calculated surface temperatures based on stream conditions with those observed yields relatively good results. However, systematic differences worthy of note have been observed. Calculated temperatures are quite close to those observed when melting occurs, but when solid coatings are pres... actual temperatures are below values computed from stream cond... as and the assumption of radiation equilibrium. Moreover, materials containing silicon carbide achieve lower surface temperatures during exposure than predicted on the basis of stream conditions. As a consequence, the overall behavior of these materials under HG/CW conditions appears to be better than under CG/HW furnace test conditions.

The present results illustrate the difference between solid oxide formers and graphites. The latter group exhibit increasing oxidation rates with increasing pressure while the former show little pressure effect. When the solid oxide formers are exposed to stream conditions at one atm, which result in surface temperatures below their melting points, they exhibit recession rates 100 to 1000 times less than graphites do under comparable conditions. Coated metals and silicon carbide degrade at temperatures comparable to those observed in CG/HW furnace tests. These limits are due to melting or rapid vaporization. However, at a given surface temperature, the solid oxide formers exhibit much lower recession rates under HG/CW arc plasma test conditions than in a CG/HW air oxidation furnace test. This may be due to large temperature gradients across the oxide which occur in the HG/CW tests. Conversely, graphites exhibit higher recession rates in the HG/CW arc plasma tests than in the CG/HW furnace tests due to artificial oxygen supply limits imposed by the air flow limitations of the latter tests.

## III. RESULTS OF HC/CW ARC PLASMA SPLASH TESTS IN THE AVCO TEN MEGAWATT FACILITY

A limited number of tests were conducted early in the program to establish thermal stress failure thresholds at low enthalpy levels. Although this phenomena is quite complex, the tests were conducted in order to determine flux thresholds for shock failure for cylinders of borides and boride composites with different diameters. Subsequent results obtained for hemispherical caps (vs. flat faced cylinders) which are reported in Section IIB indicate that these thresholds will depend upon sample shape as well as sample diameter. Descriptions of the facilities, techniques and samples employed in these tests have been presented in Sections IID-1 and IID-2 of reference (3) and Section VIE of reference (1).

### A. Results of Ten Megawatt Arc Exposures

#### 1. Calculation of Transient Thermal Gradients in Boride Cylinders

Since the present series of exposures were of relatively short duration (maximum of twenty seconds) a series of one dimensional heat transfer calculations were performed for hafnium diboride and zirconium diboride in order to compute the transient thermal gradients through the cylinders. The values of density, $\rho$, specific heat, $c_p$, and thermal conductivity, k, employed in these calculations are shown in Figure 313, while the results are shown in Figures 314a and 314b and in Table 49. The calculations were performed for one inch thick samples employing the properties of diboride compounds (12). Figure 314 and Table 49 indicate that temperature gradients of 2100°F in 250 mils can exist at a flux level of 1000 BTU/ft$^2$sec and an enthalpy of 2000 BTU/lb at two seconds. These gradients are most severe near the front (hot face) of the cylinder. After twenty seconds, the thermal gradients are reduced to 800°F in 250 mils. Reference to Table 50 indicates that the ratio of the computed temperature for radiation equilibrium (Eqs. 2, 3) divided by the observed surface temperature is approximately 1.3.

#### 2. Test Results

Table 50 summarizes the results of the present tests. Headings include stream conditions, sample diameter, cold wall heat flux, maximum observed surface temperature and computed surface temperatures based on radiation equilibrium (Eqs. 2 and 3). In addition, exposure time, recession depth, degradation mode and metallographic features are summarized. The result of pre- and post-exposure nondestructive test data are given in reference (1). Cases where samples are numbered A and B (i.e., $HfB_{2.1}$ + 20%SiC(A-4)(HF-25A and 25B)) indicate situations where a sample was run consecutively under two different conditions. Samples $ZrB_2$ (HF-17) and $HfB_{2.1}$(A-6)(HF-20) were the only models exhibiting cracks prior to testing. Neither sample failed because of these flaws. Figures 315-317 show post exposure photographs of the 10MW samples. Reference to Figure 315 shows obvious thermal shock failure of $HfB_{2.1}$(A-2)(HF-1), $HfB_{2.1}$(A-6)(HF-20),

$HfB_{2.1}$ + 20%SiC(A-4)(HF-25,26,36 and 38). Similarly, Figure 316 shows that $HfB_{2.1}$ + 20%SiC(A-7)(HF-19B and 33) and $ZrB_2$(A-3)(HF-5,6 and 7B) failed by thermal shock. Finally, Figure 317 shows thermal shock failures for $ZrB_2$(A-3)(HF-13,14 and 15), $ZrB_2$(ManLabs-Avco)(HF-22), Boride Z(A-5)(HF-11 and 12) and $ZrB_2$ + 20%SiC(A-8)(HF-23B). The occurrence of clear thermal shock failures appears to depend on material and sample diameter. Table 51 summarizes the results and states tentative fracture thresholds for the boride samples tested. For example, $HfB_2$ + SiC(A-7) survived a flux of 948 BTU/$ft^2$sec in the one half inch diameter size but fractured at 840 BTU/$ft^2$sec in the 7/8 inch diameter size. Boride Z(A-5) did not survive the lowest fluxes employed. This is in line with the results of Model 500 and ROVERS exposures discussed in Section IIB-4. In line with the above mentioned effect of sample size, specimens of $ZrB_2$ + SiC(A-8) have been tested under AF33(615)3671 at flux levels of 2200-2400 BTU/$ft^2$sec, stagnation pressures of 17-18 atm and enthalpies near 1450 BTU/lb. Surface temperatures between 3700°F and 4000°F were noted for symmetrical wedge models of a sharp leading edge. The models were two inches long, one half inch wide and one quarter inch thick. Thirty and forty-five degree wedge angles were employed with a 30 mil radius of curvature. Three samples of $ZrB_2$ + SiC (A-8) were exposed for 15 seconds and survived with little erosion and no thermal shock failures (8).

Subsequent to exposure, samples were examined nondestructively by dye penetrant techniques and then sectioned for metallographic investigation. This procedure showed the presence of fine cracks which were not evident after exposure. The observations made after sectioning confirmed the NDT results shown in reference (1) and Table 50. Figures 318-323 show post exposure sections of $HfB_{2.1}$ (A-2)(HF-2), $HfB_{2.1}$(A-6)(HF-21), $HfB_2$ + 20%SiC(A-4)(HF-37), $HfB_2$ + 20%SiC(A-7)(HF-32 and 18) and $ZrB_2$(ManLabs-Avco)(HF-17) which did not thermal shock. As indicated in Table 50, all of the 7/8 inch diameter samples contain cracks. As indicated in Table 50 and in Figures 318-323, most of these cracks are between 100 and 400 mils from the front face of the samples. Reference to Figure 314 and Table 49 indicates thermal gradients of 1400°F in 500 mils in the vicinity of the fracture point.

## IV. HOT GAS/COLD WALL ARC PLASMA PIPE TESTS IN THE AVCO TEN MEGAWATT FACILITY

### A. Introduction

The purpose of this phase of the program was to examine experimentally the performance of selected candidate materials in high shear, turbulent flow steady-state heating environments. In particular, these tests attempted to simulate conditions at points beyond the sonic point where turbulent boundary layer flow prevails over the major heating period. A description of the experimental and calibration techniques employed is given elsewhere (see pp. 21-24 of Reference 3).

Pipes of selected materials which were 1-1/4" long with a 75 mil wall were exposed.* The candidate materials tested were $HfB_{2.1}$+20%SiC(A-7), $ZrB_{2.1}$+20%SiC(A-8), $ZrB_2$+SiC+C(A-10), Si/RVC(B-8)*, KT-SiC(E-14) and Hf-20Ta-2Mo(I-23). One pair of pipe samples of each material was tested at the initial test conditions of 3960 BTU/lb, $q_{cw}$ = 480 BTU/ft$^2$sec, $\gamma$ = 26.8 lbs/ft$^2$. Based on visual inspection of the results, conditions for the second pair of pipe samples were either increased to 6000 BTU/lb, 590 BTU/ft$^2$sec and 26.4 lbs/ft$^2$ or decreased to 3520 BTU/lb, 410 BTU/ft$^2$sec and 24.4 lbs/ft$^2$.

### B. Results of Pipe Tests

Table 52 and Figures 324-326 summarize the results of these exposures. The material designation, sample number, position in the stream, heat flux, enthalpy and shear stress are given in Table 52. As indicated earlier (3), two pipes were run simultaneously. In each case the pipe closest to the exit plane of the arc is designated as occupying the UP position. The pipe farthest from the exit plane is designated as occupying the DOWN position. The down section is regarded as the test section. The purpose of the upstream section is to allow damping of flow irregularities and weak shock waves arising from the supersonic expansion processes in the pipe (3).

Table 52 also contains information covering pre and post exposure weight and dimensions for each sample. Visual observations and description of motion picture film coverage are also summarized. Reference to Table 52 and Figures 324-326 indicate that Si/RVC(B-8) was the only candidate material to survive the starting and "high" test condition. Post exposure examination indicated that the coating was burned off but that the pipes remained intact.

All other candidate materials completely failed the starting condition except for $ZrB_2$+SiC+C(A-10). The upstream pipe survived as

*The wall thickness of the Si/RVC(B-8) pipes were 140 mils. The pipe lengths were 1.5 inches.

shown in Figure 325. Thus, $ZrB_2$+SiC+C(A-10) was also exposed to the "high" condition at 590 BTU/ft$^2$sec, 6000 BTU/lb and 26.4 lbs/ft$^2$ shear stress. Under these conditions the downstream sample survived while the upstream sample thermal shocked.

The Hf-Ta-Mo(I-23) pipes exposed to the starting conditions of 480 BTU/ft$^2$sec, 3960 BTU/lb and 26.4 lbs/ft$^2$ shear stress melted badly as indicated in Figure 326. However, the Hf-Ta-Mo(I-23) pipe which occupied the upstream position in the "low test condition" did not fail.

Post test examination of the pipes reinforced the observations made during the exposures which indicated that heat conduction at the "O" ring resulted in severe temperature gradients (see Figure 64 of Reference (3)). As a result of this feature of the tests, it is difficult to make any firm quantitative conclusions about the results.

Qualitatively, the results indicate the fact that the thermal stress resistance of graphite exceeds that of the boride composites, and that $ZrB_2$+SiC+C(A-10) is more resistant to thermal stress failure than $HfB_2$+SiC(A-7) and $ZrB_2$+SiC(A-8) which do not contain graphite and have higher moduli of elasticity than (A-10) (11).

## V. RESULTS OF TESTS CONDUCTED IN THE CORNELL AERONAUTICAL LABORATORY WAVE SUPERHEATER

A limited number of samples were exposed in the CAL Wave Superheater. A description of the nondestructive tests performed on the models employed is contained in Section IV. D of Reference (1). Section IV. D of Reference (3) describes the facilities and techniques employed in performing the exposures.

Analysis of the result obtained from models exposed in the Mach 6 Wave Superheater Hypersonic Tunnel are consistent with the behavior of these materials in the HG/CW tests in the Model 500 and ROVERS facilities. Limited recession was observed due to the short exposure time (15 seconds) and moderate temperatures (4000°F) encountered in these tests. Analytical and experimental studies of the relative importance of conduction losses for hemispherical shells have been performed in order to determine the origin of the unexpected behavior of 1/2" and 1" hemispherical cap models of Hf-20Ta-2Mo(I-23) and KT-SiC(E-14) in these tests. Surprisingly, it was noted that the 1" diameter caps attained a higher temperature level than the 1/2" diameter caps. Although the origin of this result is not definitely established, experimental simulation of these tests produced a similar result in torch tests on steel samples, and analysis has defined appropriate shell thickness/shell diameter ratios required to avoid such effects.

### A. Description of Tests

Sixteen refractory material models were exposed (HG/CW) to the high velocity flow of air in the Mach 6 Wave Superheater Hypersonic Tunnel. Data were taken in two 15 second tests of eight models, each at a velocity of $10^4$ft/sec, a stagnation pressure (at the model nose) of one atmosphere, and a tunnel flow rate of 2.5 lb/sec. The models were designed to permit their surface temperature to approach the radiation/aerodynamic heating equilibrium value during each exposure to the test stream at $q(R)^{1/2} = 90$ BTU/ft$^{3/2}$ sec. As indicated earlier (3), the models were expected to reach temperatures in excess of 4000°R.

All sixteen models tested were hollow hemispherical cylinders. The "elox" process was used to bore from the aft end to provide a uniform material thickness which was nominally 1/8 inch. The diameter of the bore was a nominal 1/4 inch for the thirteen 1/4 inch nose radius models and 3/4 inch for the three 1/2 inch nose radius models. The purpose of the shell or "thimble" design was to promote faster wall temperature response so as to approach the radiation equilibrium wall temperature as rapidly as possible. A sketch showing the typical model features and the typical attachment to their stings is presented in Figure 327. Eight models and a single 1/4 inch nose radius steady-heating copper calorimeter were mounted in the tunnel by a multiple sting arrangement as shown in Figure 328. Tables 53 and 54 list the initial dimensions and sting positions occupied by each model.

Motion picture coverage of the tests was provided as indicated earlier (3). Table 55 lists the camera settings employed for the motion picture coverage. The methods employed for establishing heat flux, enthalpy and stagnation pressure were described in Section III of Reference (3). Tables 56 and 57 summarize the results.

As indicated above, model surface temperatures in excess of 4000°R were anticipated. Calculations based on a transient heat flux calculation were presented in Section III.C of Reference (3). The results of these calculations are reproduced in Tables 58 and 59 and are shown graphically in Figures 329 and 330.

The models were not, in themselves, instrumented. The calorimeter had one chromel/alumel thermocouple welded to the back face of the thermal element. The models were observed individually by miniature radiometers. In addition to individual model radiometers, one ManLabs Milletron two-color pyrometer and one microphotographic camera (Photosonics #4) were arranged to observe the stagnation point of the model on sting number one. Two Photosonics cameras (#2 and #3) were arranged to observe all models from the right (pilot's view) during both runs. To obtain test conditions, the normal complex of Wave Superheater cycle instrumentation data were recorded as well as the tunnel throat and nozzle exit static pressure, and the test section cabin pressures. All data were recorded on EFB or ERB 16 mm film and a CEC optical galvonometer paper recorder.

Eight hemisphere-cylinder models and one calorimeter, as listed in Tables 53 and 54 were exposed in each (CAL 67-473 and 67-747) test. Tabulated camera settings are presented in Table 55. The facility functioned normally in both tests. However, the model instrumentation suffered some difficulties. In particular, the two-color Milletron gave no deflection, the microphotographic film was blank, and the test section windows became cloudy during the first test. The JT0992(F-15), KT-SiC(E-14) (one inch diameter) and Hf-20Ta-2Mo(I-23) models were lost during the first test, but the latter two were recovered from the floor of the test cabin, and some (but not all) measurements were made on these (see Tables 53 and 54).

The nozzle, sting assembly and windows were removed and the models replaced in preparation for the second test. The Milletron two color pyrometer was switched to a lower scale to improve its sensitivity. The second set of models, the nozzle and the cleaned test section windows were installed. The facility functioned normally for the second test. Again, however, there were difficulties in obtaining model data. The windows clouded early and a heavy dust deposit was found throughout the test cabin, which has never before been observed. This dust appeared to be asbestos. The recorded data show no deflection on any of the nine radiometers. The dust was also deposited on the lenses of the miniature radiometers. The microphotographic film was blank for the second tests, also.

The miniature radiometer data are presented in Figure 331. Model pre and post-test measurements are included for convenience in the model identification and location data of Tables 53 and 54. No data were obtained from the Milletron two-color pyrometer or the microphotography in either test. No data were obtained from the miniature radiometer during the second test.

The one inch diameter Hf-20Ta-2Mo(I-23) model which was exposed in the first run (473) has a melting temperature of 3860°F. The post-test examination of this model revealed evidence of the melt having formed during the test. Since it is evident that the model I-23-4 surface temperature was at least 3860°F during the test, a comparison of this result with that of Figure 331 ($T_W$ MAX = 2750°F) produces the conclusion that the radiometer data are in error. This is indeed unfortunate because it invalidates the only temperature data obtained. The failure of this data can be attributed most probably to the dust in the test cabin. X-ray analysis of the dust indicated that it was asbestos. By contrast, the one half inch diameter Hf-20Ta-2Mo(I-23) model exposed in the second rung (474) showed no signs of melting.

Because of the relatively small heat absorption capacity of the models, at the rate of heating produced by the stream, the surface temperature should have approached the equilibrium value for the heat balance between aerodynamic heating and radiation dissipation (see Tables 58 and 59). For a one inch diameter model at an emittance of 0.55, equilibrium temperature is 4700°R. For a 1/2 inch diameter model it is 5000°R (Figure 330). Figures 332 and 333 compare the calculated time-temperature histories with the values contained in Figure 331. The latter have been "corrected" to true temperature by employing the values of normal total emittance measured in the Avco Arc Plasma Tests (i.e., Table 48). In comparing the observed and computed time/temperature histories, it should be noted that coating of the radiometers by asbestos dust as the exposure proceeded undoubtedly reduced the radiation received. Thus, the one inch diameter hemispherical cap sample Hf-20Ta-2Mo(I-23)-4-19 must have reached 4310°R during the exposure even though the maximum radiometer temperature was 3650°R. Secondly, the computations were performed for $ZrB_2$ which has different thermophysical and radiative properties than the samples shown in Figures 332 and 333. However, the product of $\rho C_p K$ (density x specific heat x thermal conductivity) for these materials is quite similar so that substitution of the specific values in each case would not alter the results. However, the value of normal emittance employed would have an important bearing. Thus, tungsten and RVA graphite having values of $\epsilon_N$ = 0.32 and 0.52 differ most from the $\epsilon_N$ = 0.55 employed in the calculations. Reference to Figures 332 and 333 indicates that the models were heated more rapidly than anticipated but did not reach the anticipated radiation equilibrium temperature levels. Although the later discrepancy may be due to coating of the radiometers, the observation that ($T_{CALC}/T_{OBS}$) is more than unity is in line with the results of the Avco

exposures where ($T_{CALC}/T_{OBS}$) is approximately 1.17 for RVA, 1.43 for KT-SiC, 1.04 for JT0992 at one atmosphere stagnation pressures. Bare tungsten yields ($T_{CALC}/T_{OBS}$) at 1.15 at $P_e$ = 0.16 atm (see Table 30).

B. Metallographic Examination of the Test Models after Exposure

Figures 334 and 335 show post exposure photographs of all the models. In addition, Tables 53 and 54 summarize the dimensional changes which were very minor due to the short exposure time. The zirconium diboride (A-3)-1-2 model in the sting 1 position showed no recession and little change in structure. This finding is in general agreement with the results obtained at Mach 0.3 and $P_e$ = 1 atm presented earlier for 1800 second exposures (Figure 1). Unfortunately no radiometer measurements were obtained for this model but it is doubtful that the surface temperature exceeded 4000°F. The KT-SiC models which were positioned at the sting 2 and sting 3 positions in run 67-473 exhibited recessions of 18 mils and 2 mils during the fifteen second exposures. In this case, the smaller model (488 mil diameter) reached a lower surface temperature than the larger model (944 mil diameter) as indicated in Figures 331-333. The cap of the larger model fractured on cooling (Figure 334). The observed recession rates of 0.1-1 mils per second or 180-1800 mils in 30 minutes are higher than indicated in Figure 5 for KT-SiC exposed at $P_e$ = 1 atm at Mach 0.3. The RVA(B-5), PG(B-6) and BPG(B-7) samples which were exposed at the sting 6 position in Run 67-473 and sting 4 and 5 positions in Run 67-474 exhibited recessions of 30, 8 and 32 mils in the present runs which is comparable to the results shown in Figures 3 and 4; however, the tungsten model, Run 67-473 sting 5 showed virtually no recession. Recession rates near 1 mil/sec were anticipated on the basis of results at $P_e$ = 1 atm and a Mach Number of 0.9 and the present results for bare tungsten shown in Figure 7. The Sn-Al/Ta-10W coated model, sting 8 Run 67-474, exhibited melting of the Sn outer layer but no degradation of the inner layer. However, this model probably attained a much lower surface temperature than the other models due to high values of ($T_{CALC}/T_{OBS}$).

The models which formed solid oxides on exposure (i.e., Hf-20Ta-2Mo(I-23) sting 1 Run 67-474 and sting 4 Run 67-474, $ZrB_2$(A-3) sting 1 Run 67-473, $HfB_{2.1}$(A-3) sting 2 Run 674, $HfB_2$+SiC(A-4) sting 3 Run 67-474) showed little recession in line with the temperature and time of exposure. Similar behavior was noted for JTA(D-13) sting 7 Run 67-473; JT0981(F-16) sting 6 Run 67-474 exhibited a recession comparable to the pure graphites.

The thermal shock failures noted for JT0992(F-16) sting 8, Run 67-473 and $ZrB_2$(A-3)-24-3 sting 7 Run 67-474 are surprising since these materials have survived flux levels in excess of the current values without failing. However, they were not tested as hollow shells. It is possible that the defects present in the later model (1) may have contributed to failure. Although $HfB_2$(A-2) samples have exhibited thermal shock failures at levels above 770 BTU/ft$^2$sec, no failures were observed below this level in the Avco tests (Table 2) nor were any obvious defects noted for this sample as a result of nondestructive tests (1).

Figures 334 and 335 shows post exposure photographs of these models. Post exposure longitudinal sections are shown in Figures 336-347. Figure 336 shows Model $ZrB_2$(A-3)-1-2 which experienced a negligible recession during exposure and no change in surface structure was observed. Figures 337 and 338 illustrate KT-SiC(E-14)-1-8 and 3-18. Both models exhibit melting of the silicon binder and depletion through the nose section. Figure 339 shows Hf-20Ta-2Mo(I-23)-4-19 which melted during exposure. Model W (uncoated) (G-18)-X-11 presented in Figure 340 showed no change in structure as did RVA(B-5)-X-5 and JTA(D-13)-X-7 which are illustrated in Figure 341. This set of figures covers all of the models in Run No. 1. JT0992(F-15)-X-9 which occupied Sting 8 in Run No. 1 thermal shocked.

Figure 342 displays Model Hf-20Ta-2Mo(I-23)-I-12 and shows no melting (in contrast to the one inch model exposed in Run No. 1 shown in Figure 339). The one half inch diameter Hf-20Ta-2Mo(I-23) model is coated with suboxide containing tantalum stringers throughout. Figures 343-346 show models, $HfB_{2.1}$(A-2)-X-1, $HfB_2$+SiC(A-4)-X-4, PG(B-6)-X-6, BPG(B-7)-X-16 and JT0981(F-16)-X-10 which exhibited very minor changes during exposure. Model $HfB_{2.1}$(A-2)-X-1 (Figure 343) exhibited a thermal shock failure at the end of Run No. 2 when the cap broke off. Model $HfB_2$+SiC(A-4)-X-4 (Figure 344) shows no SiC depletion at the surface. Models PG(B-6)-X-6 and BPG(B-7)-X-16 experienced recessions of 8 and 32 mils respectively, (Figure 345). Model JT0981(F-16)-X-10 shown in Figure 346 exhibited a conversion depth of 19 mils and a very light oxide. Sting position 7 of Run No. 2 was occupied by $ZrB_2$(A-3)-23-3 which thermal shocked during exposure. The last position (Sting 8) in Run No. 2 was filled by Model Sn-Al/Ta-10W(G-19)-3-22 shown in Figure 347a. Melting and removal of the Sn cover of the duplex coating (page 55, Reference 1) is shown in Figure 347b.

## C. Analysis of the Relative Conduction Losses for Spherical Shells

In the discussion of the Wave Superheater exposures presented above, the observation that the one inch diameter models Hf-20Ta-2Mo(I-23)-4-19 (Sting 4 Run 1) and KT-SiC(E-14)-3-18 (Sting 3 Run 1) achieved higher temperatures than one half inch diameter models of the same material (Hf-20Ta-2Mo(I-23)-1-12 (Sting 1 Run 2) and KT-SiC(E-14)-1-8) Sting 2 Run 1) was noted. This was deemed to be unusual since the heat flux to the larger model is 70% of that experienced by the smaller model. One possible source of this difference was considered to be the losses due to conduction through the models. In particular, the models are hollow shells. Consequently to consider the relative conduction losses it is necessary to introduce the ratio of shell thickness to model diameter as an additional factor.

A suitable analysis of the problem has been performed (3) based on the relative importance of conduction and aerodynamic heating for a model represented by the sketch shown in Figure 348, where the aerodynamic heating is given as a function of $\theta$ by $q[\theta] = q_s \cos\theta$. In

order to obtain experimental data on the relative conduction losses for spherical shells, one inch and one half inch diameter models having a wall thickness of 1/8" were fabricated from SAE1020 steel. This material was employed since its thermal conductivity is approximately one third that of KT-SiC(E-14) at temperatures between 500° and 2000°R. As a consequence, the heat flux level for this experiment was maintained at 1/3 the level of the Wave Superheater exposures described in Section V.B.

Accordingly, models were exposed in an oxyacetylene torch situated in the Wave Superheater Hypersonic Tunnel for convenience in utilizing the required test equipment. Separate copper calorimeters were employed to determine cold wall heat flux. Heat fluxes of 150 BTU/ft$^2$sec and 220 BTU/ft$^2$sec were applied to the one inch and one-half inch diameter models, respectively. Thermocouples which were spring mounted in contact with the inner wall directly behaind the stagnation point were employed to measure the thermal response of the models. The results are shown in Figure 349. These data indicate that the larger model reached 1900°F in 11.4 seconds; the smaller models reached 1900°F in 13.8 + 1.0 seconds. At shorter times, the rise rate for the smaller models is greater than for the larger models as expected. At longer times, the larger model does heat up more rapidly than the smaller model does. However, it is surprising that the crossover occurs at low temperatures near 600°F where the magnitudes of dT/d0 are smaller than the values assumed in the foregoing calculation. Finally, it should be noted that the k/q matching is partially satisfied for KT-SiC but not satisfactory for Hf-20Ta-2Mo.

## REFERENCES


1. Kaufman, L. and Nesor, H., "Stability Characterization of Refractory Materials under High Velocity Atmospheric Flight Conditions," AFML-TR-69-84, Part II Volume I: Facilities and Techniques Employed for Characterization of Candidate Materials, ManLabs, Inc., Cambridge, Mass. (September 1969).

2. Kaufman, L. and Nesor, H., "Stability Characterization of Refractory Materials under High Velocity Atmospheric Flight Conditions," AFML-TR-69-84, Part II Volume II: Facilities and Techniques Employed for Cold Gas/Hot Wall Tests, ManLabs, Inc., Cambridge, Mass. (September 1969).

3. Kaufman, L. and Nesor, H., "Stability Characterization of Refractory Materials under High Velocity Atmospheric Flight Conditions," AFML-TR-69-84, Part II Volume III: Facilities and Techniques Employed for Hot Gas/Cold Wall Tests, ManLabs, Inc., Cambridge, Mass. (September 1969).

4. Kaufman, L. and Nesor, H., "Stability Characterization of Refractory Materials under High Velocity Atmospheric Flight Conditions," AFML-TR-69-84, Part III Volume I: Experimental Results of Low Velocity Cold Gas/Hot Wall Tests, ManLabs, Inc., Cambridge, Mass. (September 1969).

5. Perkins, R., Kaufman, L. and Nesor, H., "Stability Characterization of Refractory Materials under High Velocity Atmospheric Flight Conditions," AFML-TR-69-84, Part III, Volume II: Experimental Results of High Velocity Cold Gas/Hot Wall Tests, ManLabs, Inc., Cambridge, Mass. (September 1969).

6. Kaufman, L. Nesor, H., Bernstein, H. and Baron, J.R., "Stability Characterization of Refractory Materials under High Velocity Atmospheric Flight Conditions," AFML-TR-69-84, Part IV Volume I: Theoretical Correlation of Material Performance with Stream Conditions, ManLabs, Inc., Cambridge, Mass. (September 1969).

7. Rudy, E., "Ternary Phase Equilibria in Transition Metal-Boron-Carbon-Silicon Systems: Part V, Compendium of Phase Diagram Data," AFML-TR-65-2, Part V, June 1969.

8. Clougherty, E. V., "Research and Development of Refractory Oxidation-Resistant Diborides, Part II Volume I: Summary," AFML-TR-68-190 Part II Volume I, December 1969.

9. Clougherty E.V., Hill, R.H., Rhodes, W.R., and Peters, E.T., "Research and Development of Refractory Oxidation-Resistant Diborides, Part II Volume II: Processing and Characterization," AFML-TR-68-190 Part II Volume II, November 1969.

10. Clougherty, E.V. and Peters, E.T., "Research and Development of Refractory Oxidation-Resistant Diborides, Part II Volume III: Thermochemical Stability Characteristics," AFML-TR-68-190, Part II Volume II, November 1969.

11. Rhodes, W.H., Clougherty, E.V., and Kalish, D., "Research and Development of Refractory Oxidation-Resistant Diborides, Part II Volume IV; Mechanical Properties," AFML-TR-68-190 Part II Volume IV, November 1969.

12. Clougherty, E.V., Wilkes, K.E., and Tye, R.P., "Research and Development of Refractory Oxidation-Resistant Diborides, Part II Volume V: Physical, Thermal, Electrical and Optical Properties," AFML-TR-68-190, Part II Volume V, November 1969.

13. Clougherty, E.V., Niesz, D.E., Mistretta, A.L., "Research and Development of Refractory Oxidation-Resistant Diborides, Part II Volume VI: Thermal Stress Resistance," AFML-TR-68-190, Part II Volume VI, November 1969.

14. Clougherty, E.V., "Research and Development of Refractory Oxidation-Resistant Diborides, Part II Volume VIII: Application Evaluations and Design Considerations," AFML-TR-68-190, Part II Volume VII, November 1969.

15. Kaufman, L., Clougherty, E.V. and Berkowitz-Mattuck, J.B., Trans. Met. AIME (1967) 239, 458.

16. Kaufman, L. and Clougherty, E.V., "Investigation of Boride Compounds for Very High Temperature Applications," RTD-TDR-63-4096, Part III, March 1966.

17. Kendall, E.G., Slaughter, J.I. and Riley, W.C., "A New Class of Hypereutectic Carbide Composites," Aerospace Corp., June 1965, TDR-469 (52500-10)-11 (SSD-TR-65-78).

18. Tanzilli, R.A., "Evaluating of Graphite Composites in Reentry Environments," AFML-TR-65-328, October 1965.

19. Criscione, J.M., et al., "High Temperature Protective Coatings for Graphite," ML-TDR-64-173, Part II, October 1964.

20. Buckley, J.D. and Stein, B.A., "Preliminary Investigation of the Dynamic Oxidation of JT Graphite Composites at Surface Temperatures between 4000°F and 5000°F," Summary of the Eleventh Refractory Composites Working Group Meeting, AFML-TR-66-179, July 1966.

21. Bartlett, R.W. and Gage, P/R., "Investigation of Mechanisms for Oxidation Protection and Failure of Intermetallic Coatings for Refractory Metals", ASD-TDR-63-753 Part II, July 1964.

22. Perkins, R. and Packer, C.M., "Coatings for Refractory Metals in Aerospace Environments", AFML-TR-65-351, September 1965.

23. Schwartzkopf, P., "Evaluation of Tungsten Composites for Hypersonic Vehicles", AFML-TR-67-272, Rocketdyne Division of North American Aviation, Inc., Canoga Park, California, June 1967.

24. Berkowitz-Mattuck, J.B., Kaufman, L., Clougherty, E.V. and Hopper, R., Trans. Met. Soc. AIME (1967) 239, 750.

25. Wright, T.R., Braeckel, T.R., Kizer, D.E., et al., "The Fabrication of Iridium and Iridium-Alloy Coatings on Graphite by Plasma-Arc Deposition and Gas-Pressure Bonding", AFML-TR-68-6, Battelle Memorial Institute, Columbus, Ohio, February 1968.

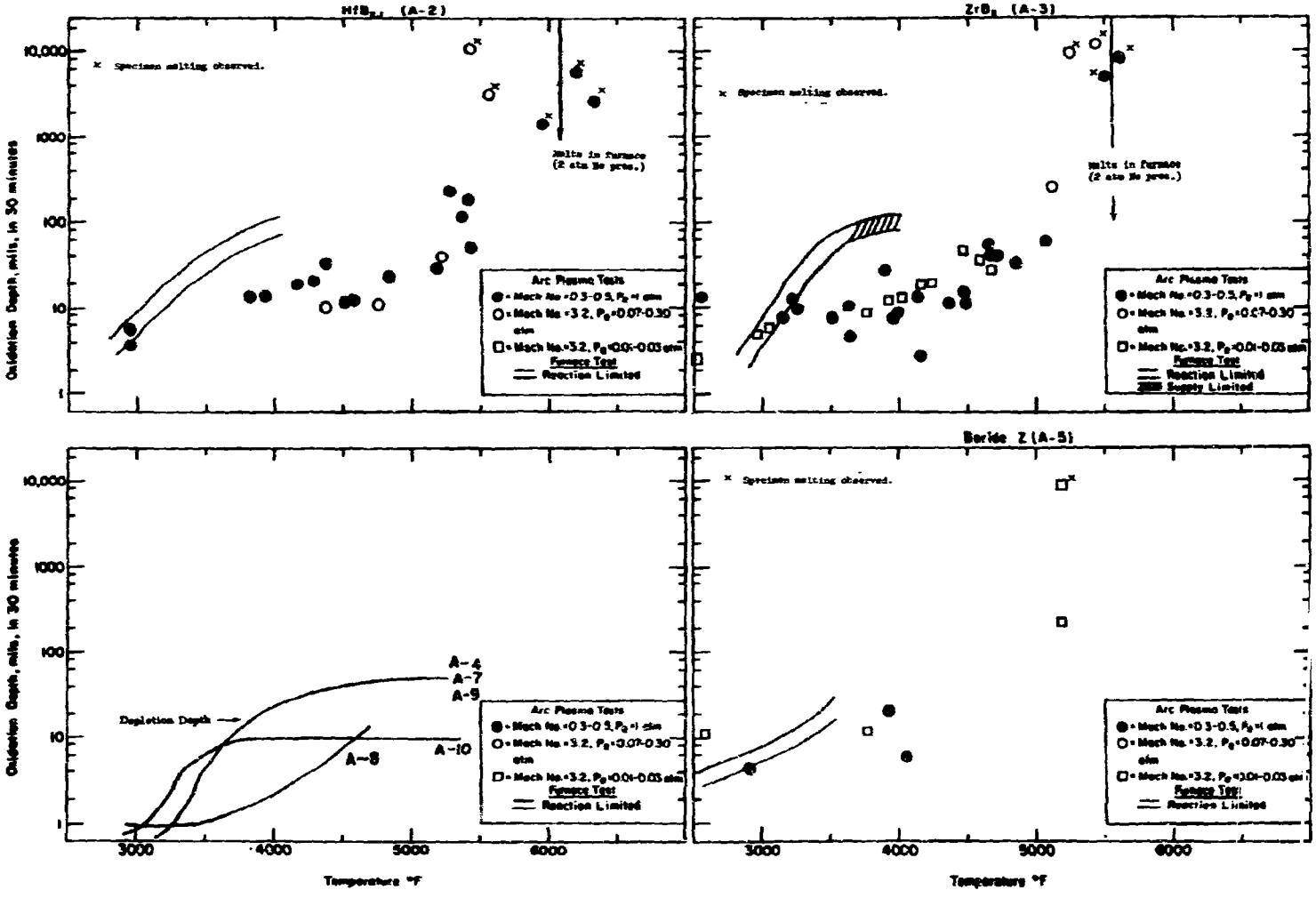


Figure 1. Comparison of Arc Plasma (HG/CW) Tests with Furnace Oxidation (CG/HW) Tests at 1.8 ft/sec for $HfB_{2.1}$(A-2), $ZrB_2$(A-3) and Boride Z(A-5) Plus Typical SiC Depletion Depths for Diboride-Silicon Carbide Composites.

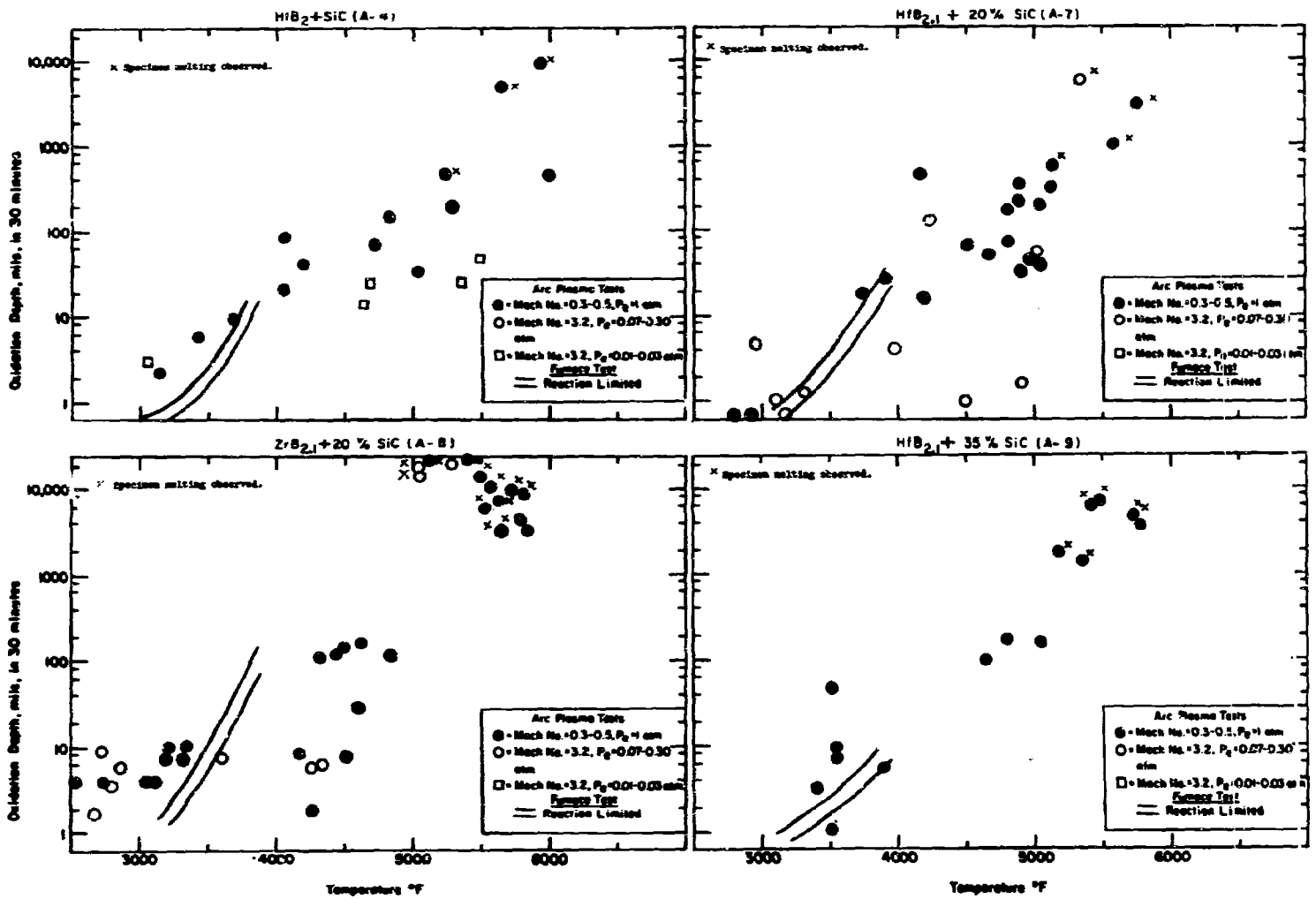


Figure 2. Comparison of Arc Plasma (HG/CW) Tests with Furnace Oxidation (CG/HW) Tests at 1.8 ft/sec for $HfB_2$+SiC(A-4), $HfB_{2.1}$+20v/oSiC(A-7), $ZrB_{2.1}$+20v/oSiC(A-8), and $HfB_{2.1}$+35v/oSiC(A-9).

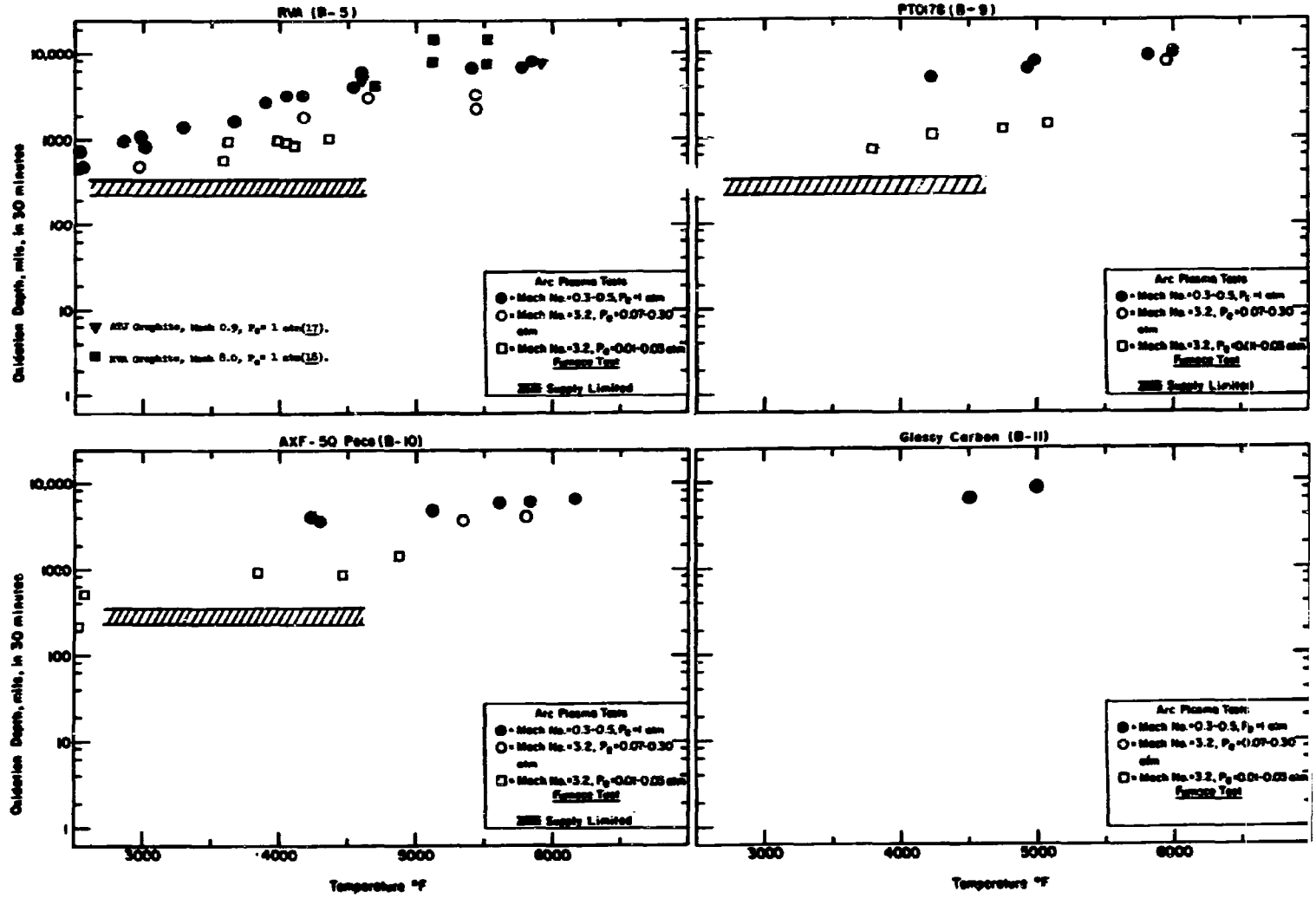


Figure 3. Comparison of Arc Plasma (HG/CW) Tests with Furnace Oxidation (CG/HW) Tests at 1.8 ft/sec for RVA(B-5), PTO178(B-9), AXF-5Q Poco(B-10) and Glassy Carbon (B-11).

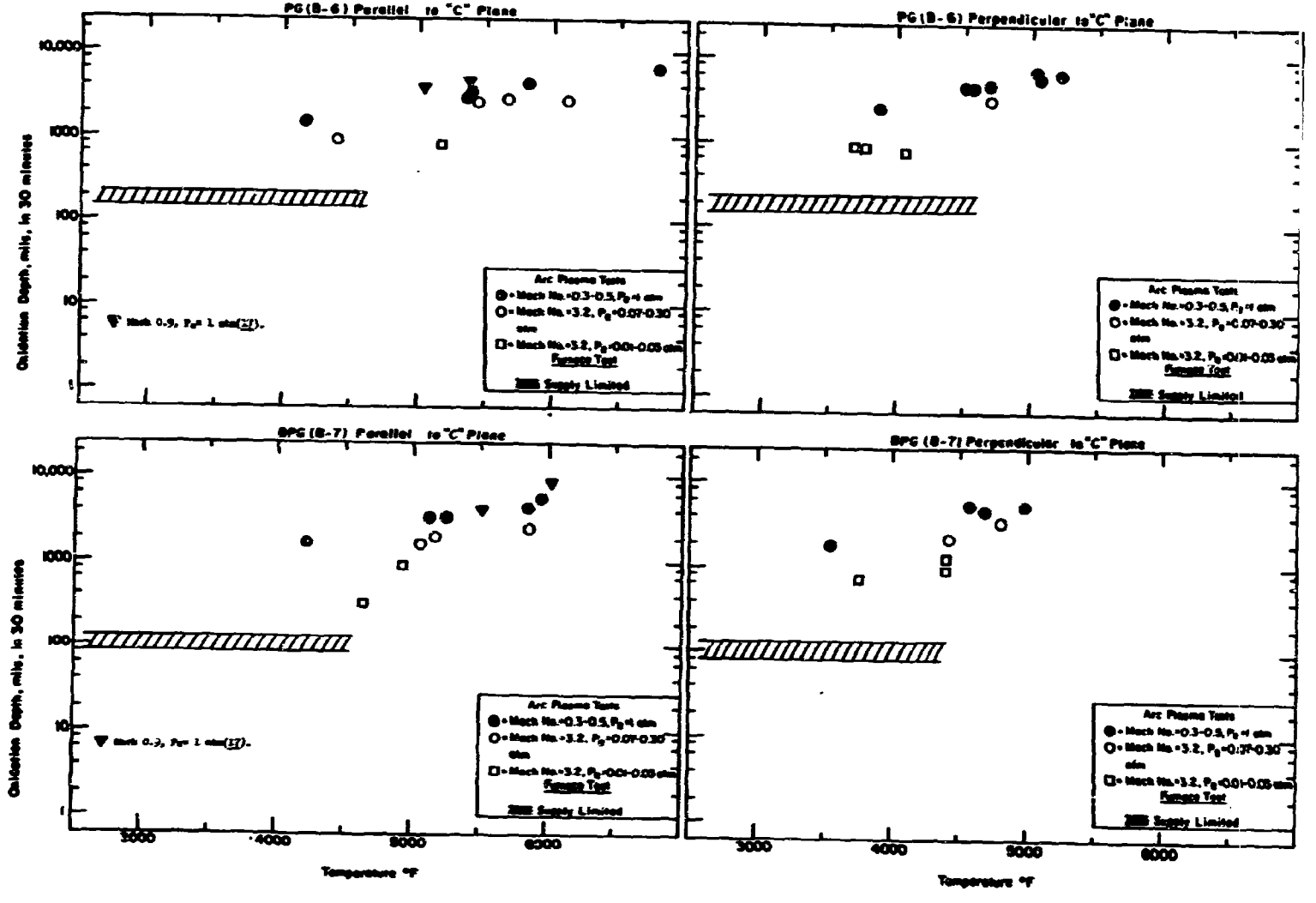


Figure 4. Comparison of Arc Plasma (HG/CW) Tests with Furnace Oxidation (CG/HW) Tests at 1.8 ft/sec for PG(B-6) and BPG(B-7).

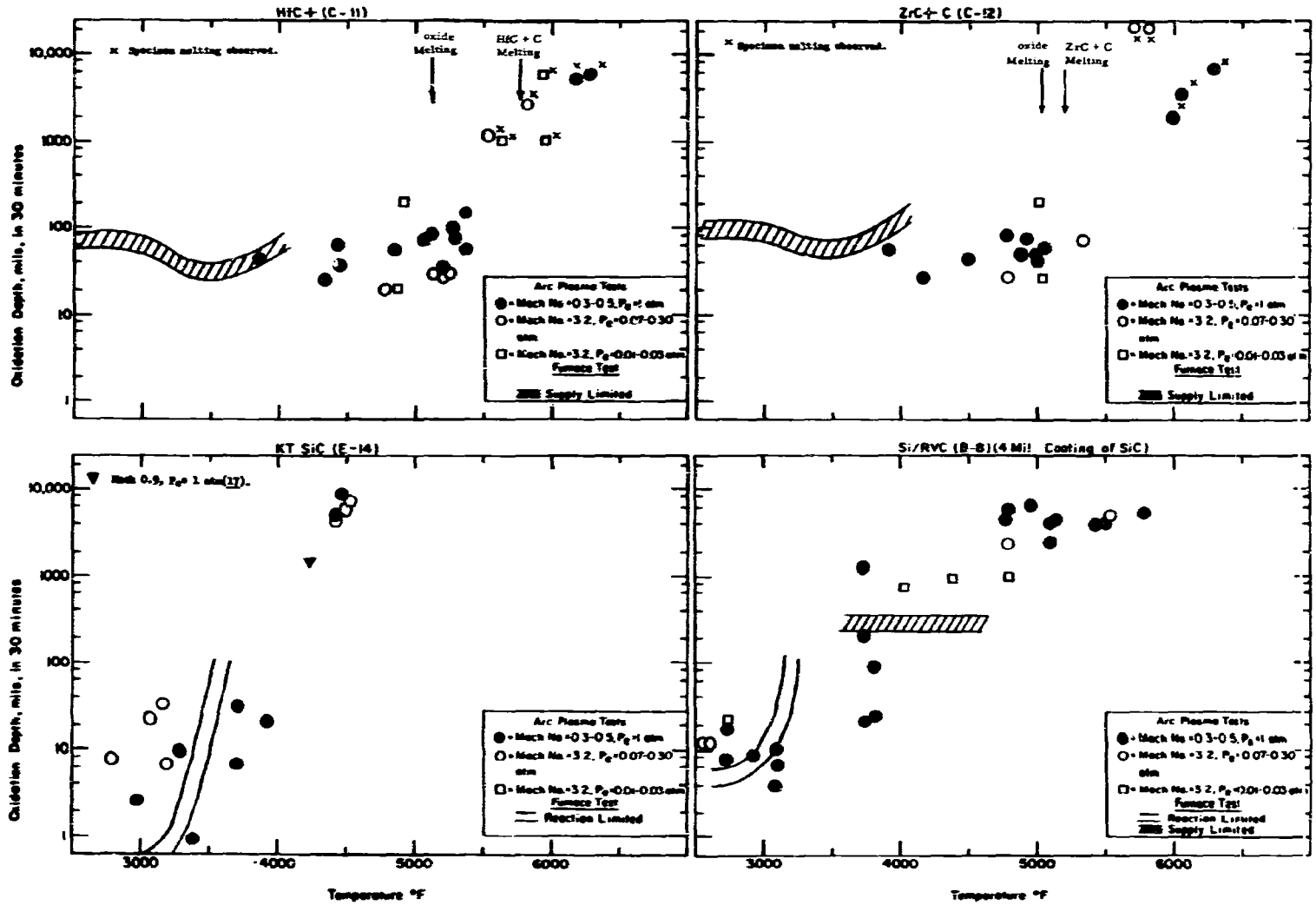


Figure 5. Comparison of Arc Plasma (HG/CW) Tests with Furnace Oxidation (CG/HW) Tests at 1.8 ft/sec for HfC+C(C-11), ZrC+C(C-12), KT-SiC(E-14), and Si/RVC(B-8).

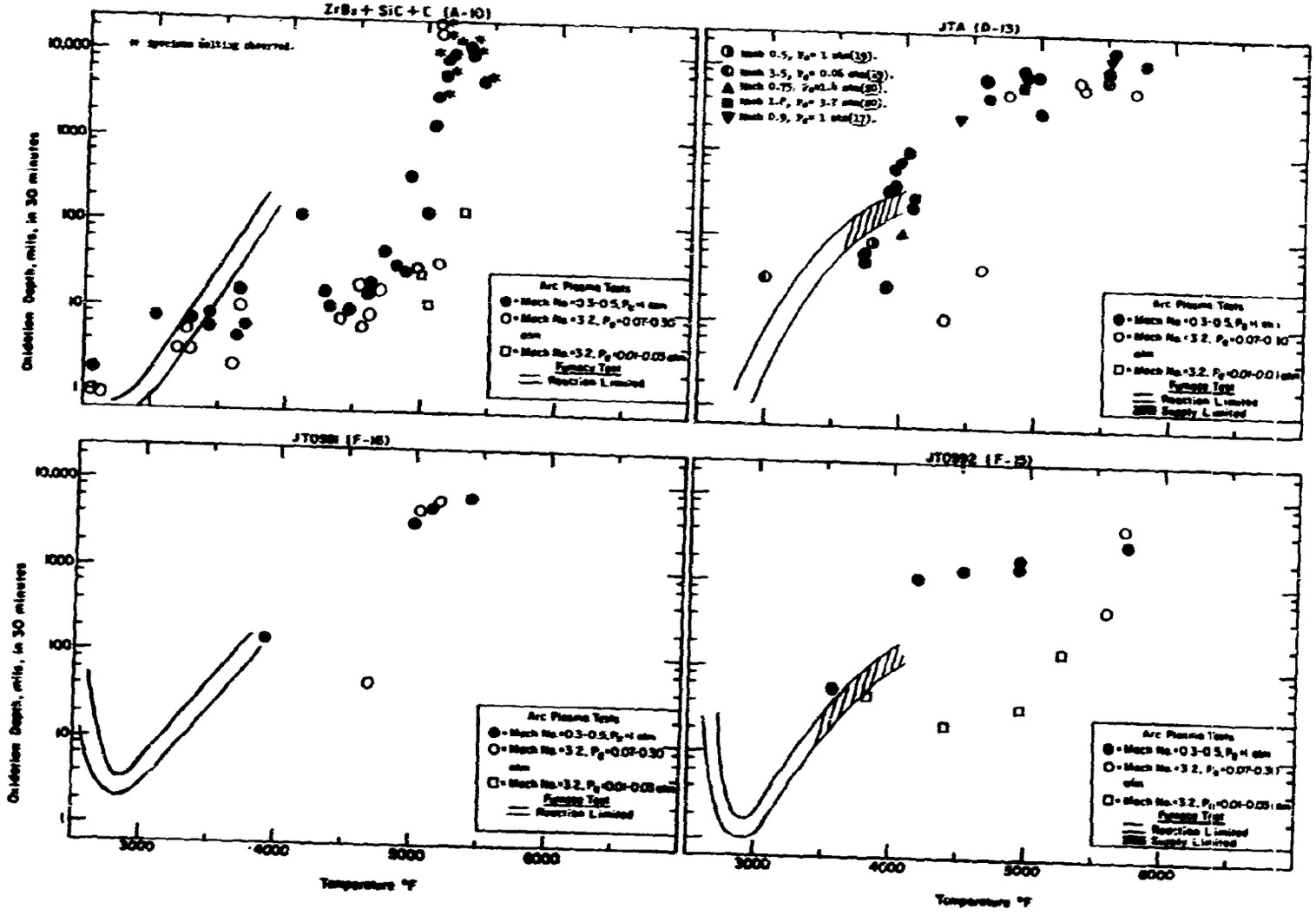


Figure 6. Comparison of Arc Plasma (HG/CW) Tests with Furnace Oxidation (CG/HW) Tests at 1.8 ft/sec for $ZrB_2$+SiC+C(A-10), JTA(D-13), JT 0981(F-16), and JT 0992(F-15).

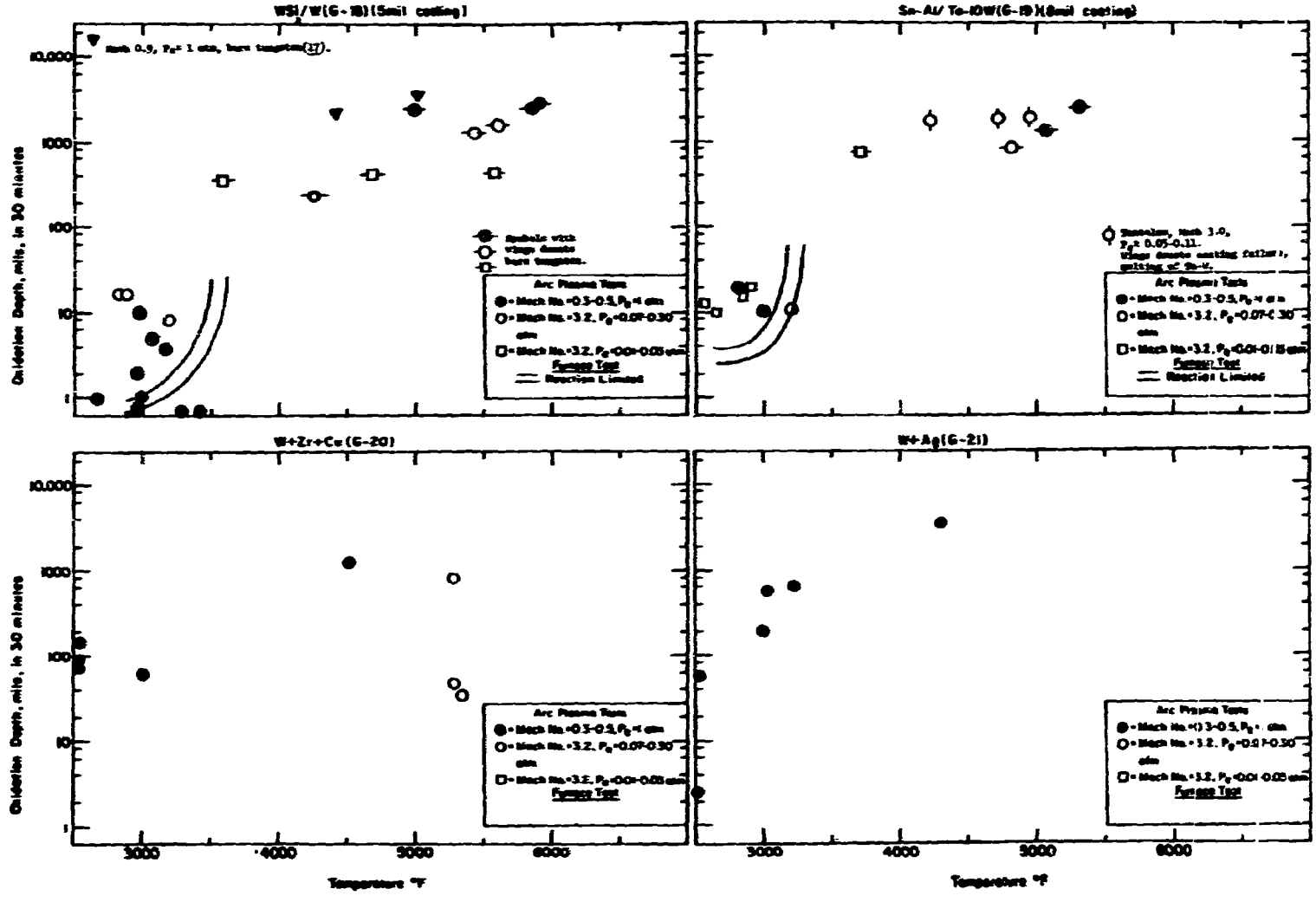


Figure 7. Comparison of Arc Plasma (HG/CW) Tests with Furnace Oxidation (CG/HW) Tests at 1.8 ft/sec for $WSi_2$/W(G-18), Sn-Al/Ta-10W(G-19), W+Zr+Cu(G-20), and W+Ag(G-21).

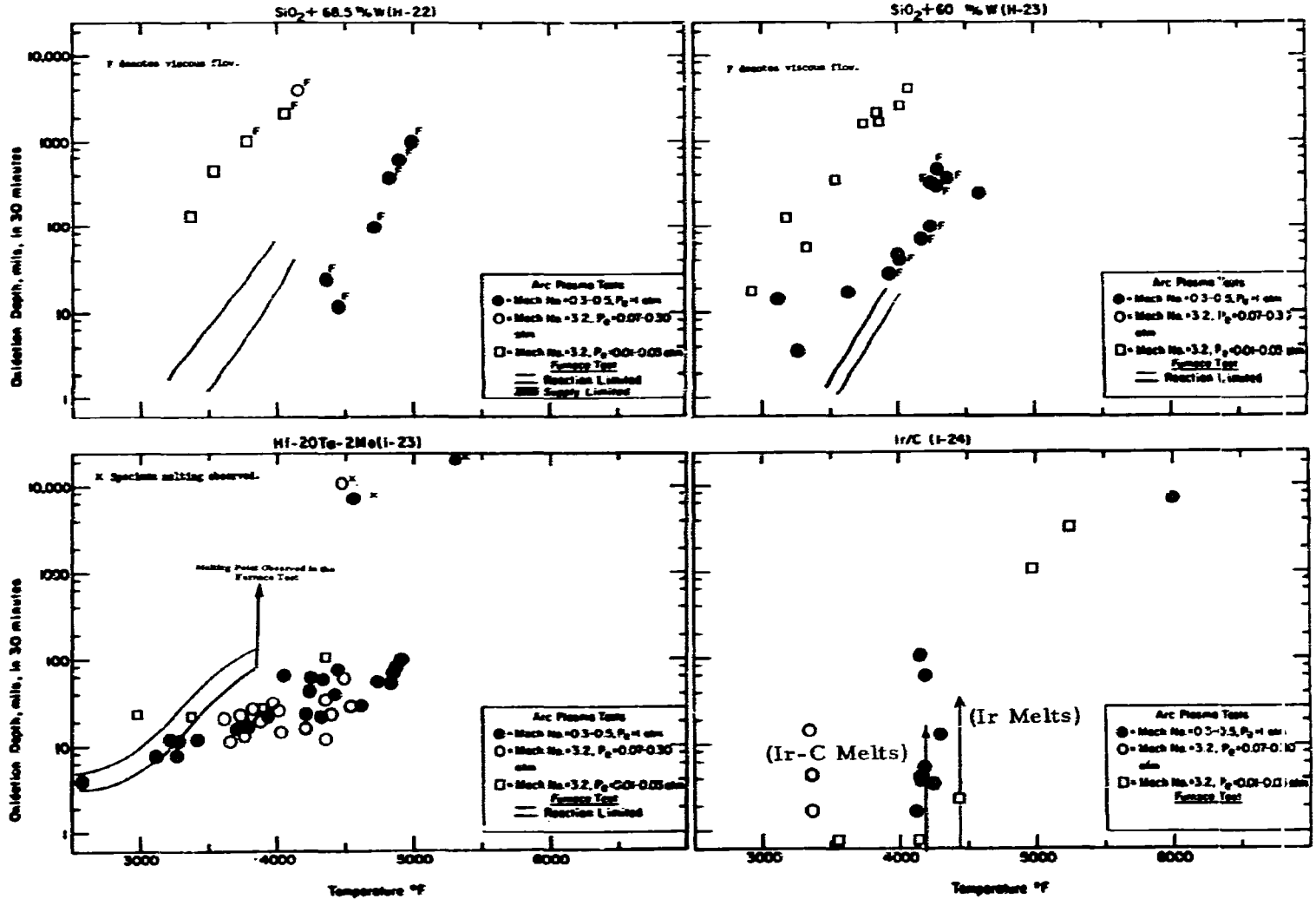


Figure 8. Comparison of Arc Plasma (HG/CW) Tests with Furnace Oxidation (CG/HW) Tests at 1.8 ft/sec for $SiO_2$+68.5w/oW(H-22), $SiO_2$+60w/oW(H-23), Hf-20Ta-2MO(I-23), and Ir/C(I-24).

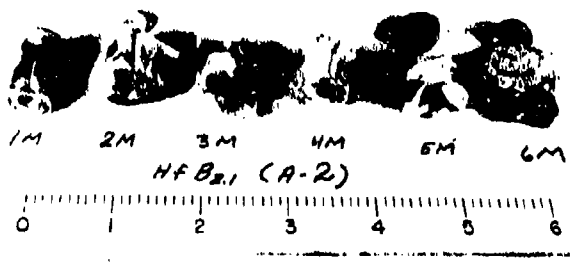


Plate 1-4225

Figure 9. Post Exposure Photographs of Arc Plasma Tests $HfB_{2.1}$(A-2)-1M, 2M, 3M, 4M, 5M and 6M. Samples 1M, 2M, 3M and 4M were Cracked During Removal of Tungsten Sting. Samples 5M and 6M Showed Initial Thermal Shock Delaminations and Were Cracked After Sting Removal. Samples 3M and 5M Melted. Scale is One Inch. Hot Face is Pointing Up.

Plate 1-4250

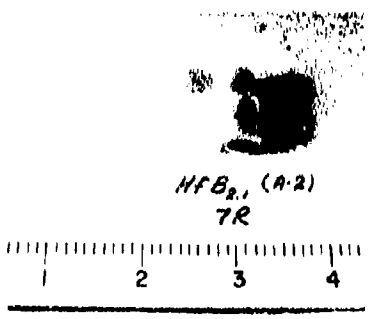


Plate 1-4254

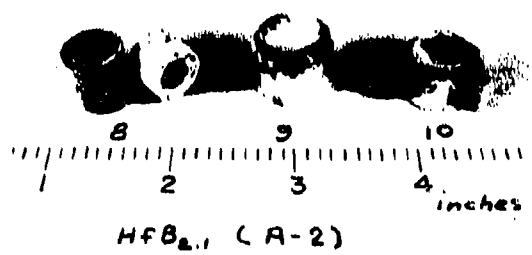


Figure 10. Post Exposure Photographs of Arc Plasma Tests $HfB_{2.1}$(A-2)-7R, 8R, 9R and 10R. Sample 8R showed an Initial Thermal Shock Failure While Samples 9R and 10R exhibited Melting. Scale is One Inch. Hot Face is Pointing Up.

*Distance between numbered divisions is equal to one inch.

Plate No. 1-8750

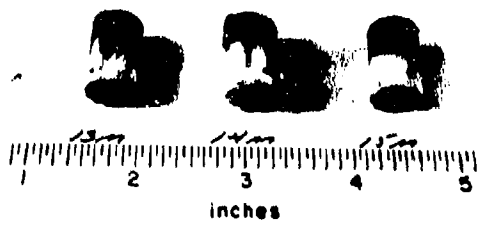


Plate No. 1-9521

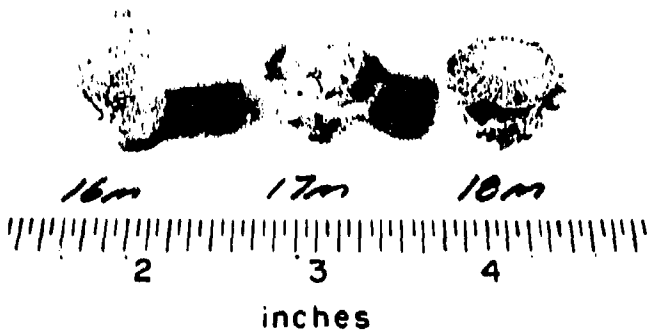


Plate No. 1-4992

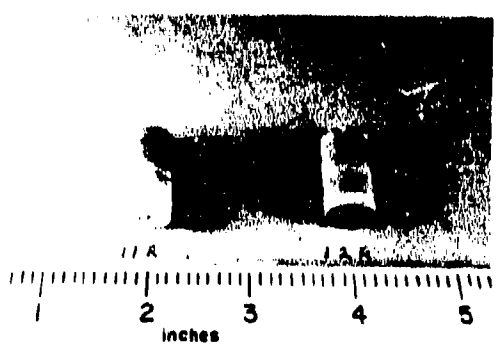


Figure 11. Post Exposure Photographs of Arc Plasma Tests $HfB_{2.1}$(A-2)-13M, 14M, 15M, 16M, 17M and 18M, 11R and 12R.

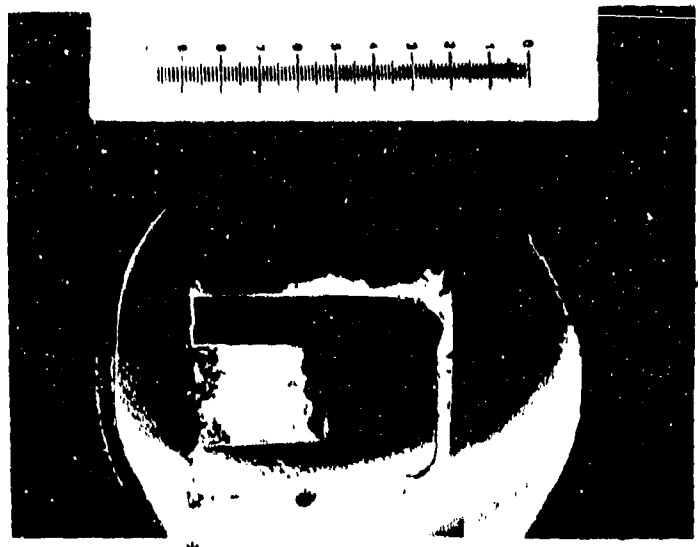

Plate 1-4238

Oxide Coating

One Inch Scale* X 2.5

Figure 12. Arc Plasma Test $HfB_2$ 1 (A-2)-4M, Surface Temperature 5270°F, Stagnation Enthalpy 5570 BTU/lb, Stagnation Pressure 1 atm, Cold Wall Heat Flux 760 BTU/$ft^2$, Exposure Time 1830 Seconds, Initial Thickness 557 Mils, Final Thickness 286 Mils. Hot Face at Right.

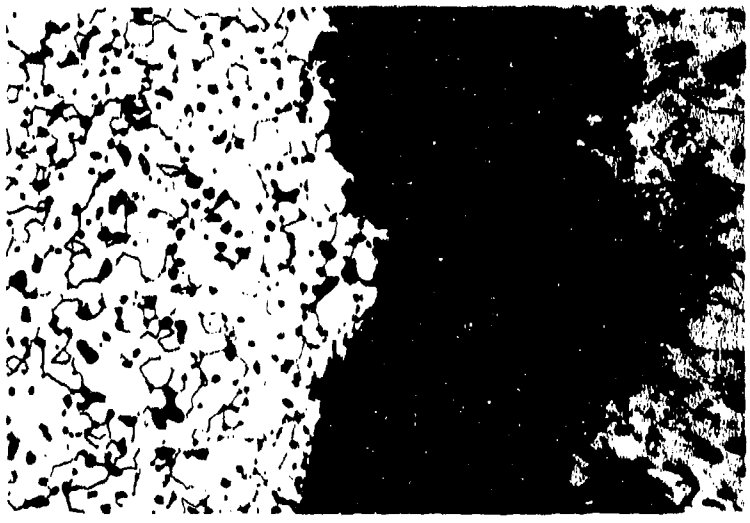

Plate 1-4239

Etched with 10 Glycerine 5 $HNO_3$ 3HF X160

Figure 13. Arc Plasma Test $HfB_2$ 1 (A-2)-4M, Hot Face, Showing Boride at Left, Oxide at Right with 10 Mil Separation.

*Distance between numbered divisions is equal to one hundred mils.

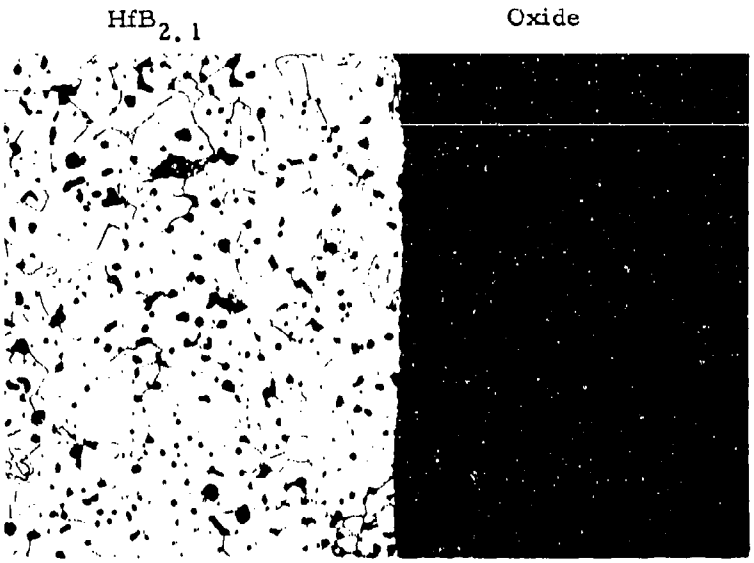


Plate 1-4240

Etched with 10 Glycerine $5HNO_3$ 3HF X250

Figure 14. Arc Plasma Test $HfB_{2.1}$ (A-2)-4M, Side Face of Test Sample Showing Adherent Oxide.

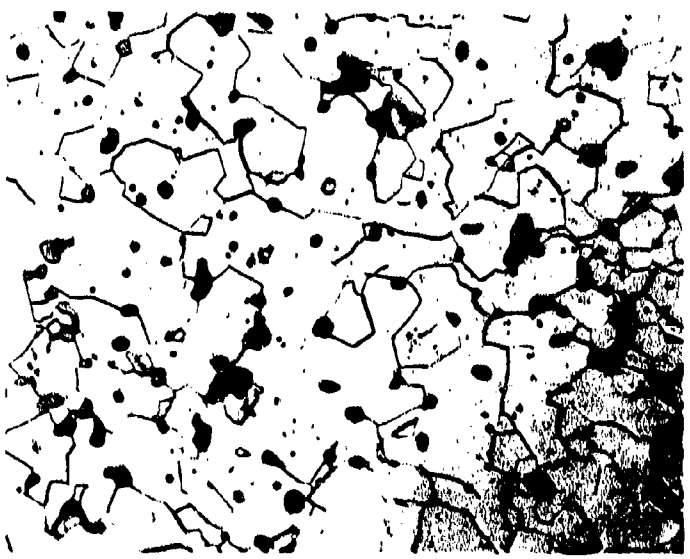

Plate 1-4241

Etched with 10 Glycerine $5HNO_3$ 3HF X500

Figure 15. Arc Plasma Test $HfB_{2.1}$ (A-2)-4M, Matrix Sting Leg Showing Matrix Grain Size.

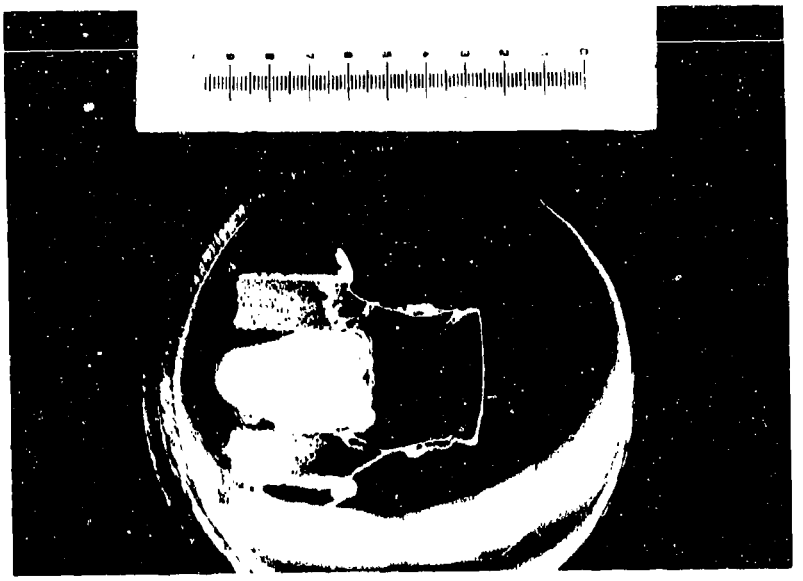

Plate 1-4233

One Inch Scale X2.5

Figure 16. Arc Plasma Test $HfB_{2.1}$(A-2)-3M, Surface Temperature 6010°F, Stagnation Enthalpy 6585 BTU/lb, Stagnation Pressure 1 atm, Cold Wall Heat Flux 1060 BTU/$ft^2$sec, Exposure Time 82 Seconds, Initial Thickness 542 Mils, Final Thickness 281 Mils. Melting Observed. Hot Face on Right.

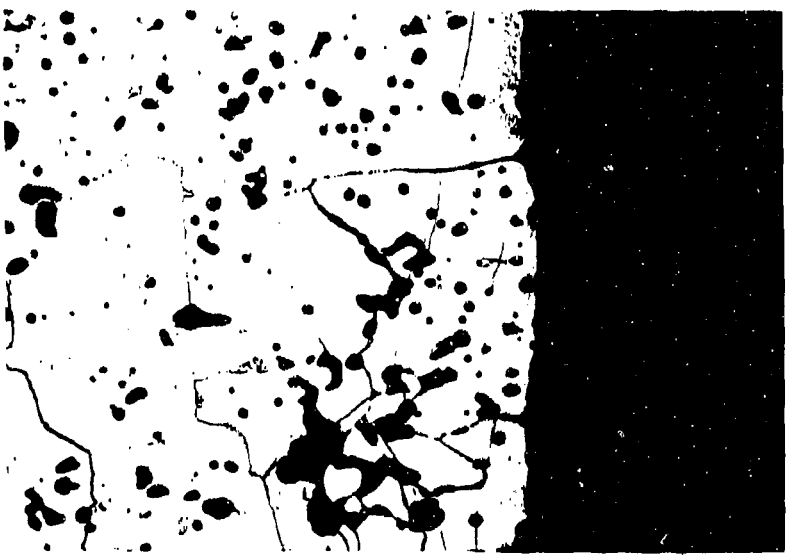

Plate 1-4234

Etched with 10 Glycerine $5HNO_3$ 3HF X250

Figure 17. Arc Plasma Test $HfB_{2.1}$(A-2)-3M, Hot Face, Showing Boride with Extremely Large Grain Size at Left.

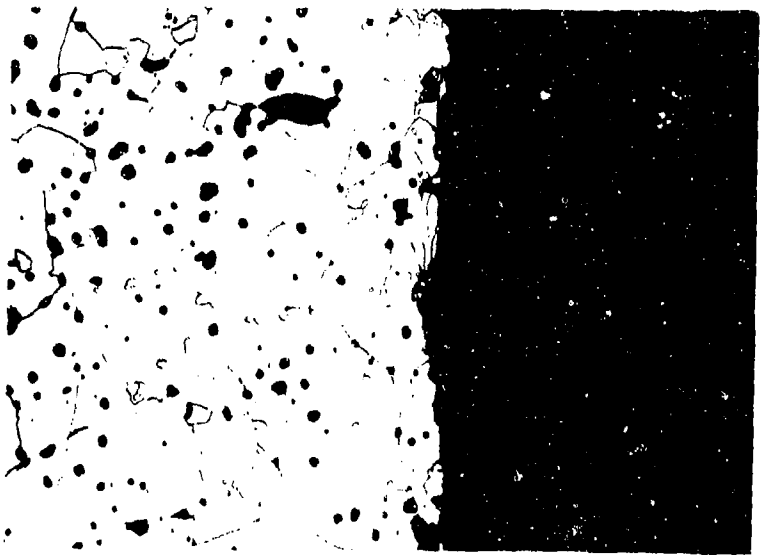

Plate 1-4236

Etched with 10 Glycerine 5$HNO_3$ 3HF X250

Figure 18. Arc Plasma Test $HfB_{2.1}$(A-2)-3M, Side Face Showing Adherent Oxide and Boride at Left.

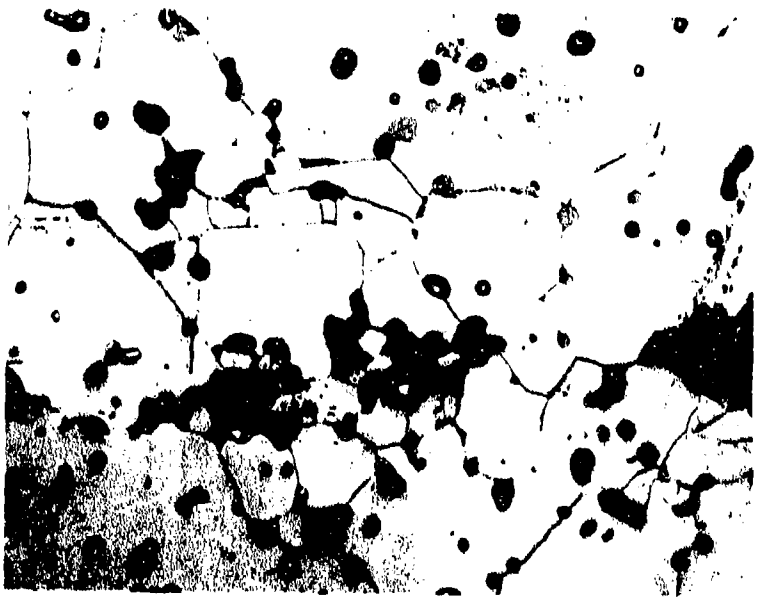

Plate 1-4237

Etched with 10 Glycerine 5$HNO_3$ 3HF X500

Figure 19. Arc Plasma Test $HfB_{2.1}$(A-2)-3M, Matrix Sting Leg.

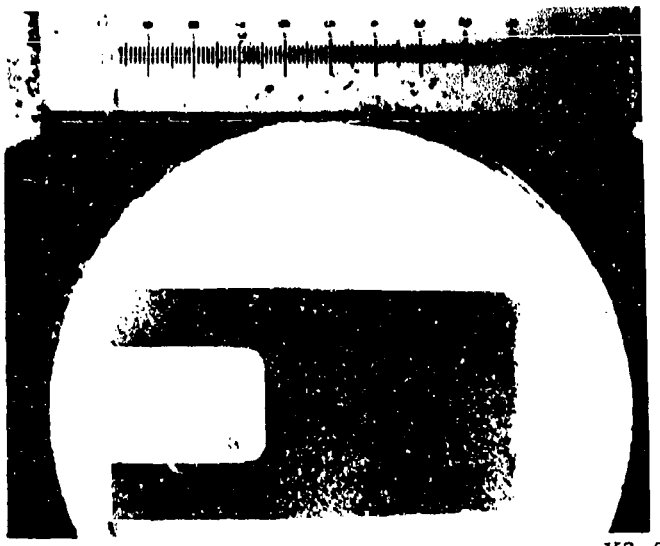

Plate No. 1-4993

X2.81

Figure 20. Arc Plasma Test $HfB_{2.1}$(A-2)-11R, Surface Temperature 5040°F, Exposure Time 1800 Seconds, Stagnation Pressure 0.097 atm, Stagnation Enthalpy 10730 BTU/lb, Cold Wall Heat Flux 651 BTU/ft$^2$sec., Initial Length 605 Mils, Final Length 566 Mils. Hot Face at Right. One Inch Scale.

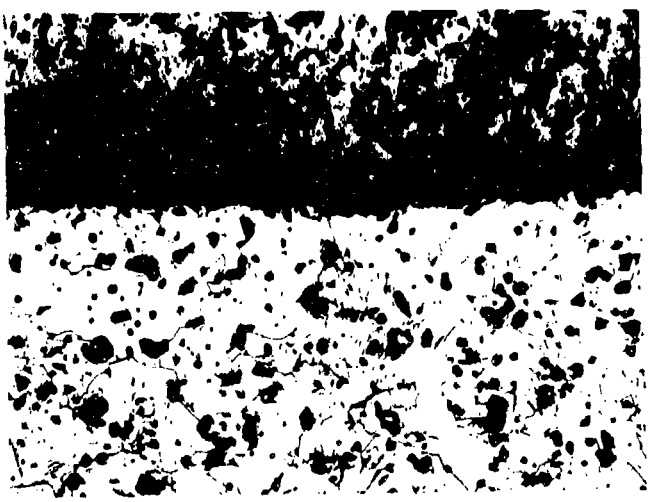

Plate No. 1-4994

Etched with 10 Glycerine 5$HNO_3$ 3HF X250

Figure 21. Arc Plasma Test $HfB_{2.1}$(A-2)-11R. Interface of Oxide (Top) and Matrix.

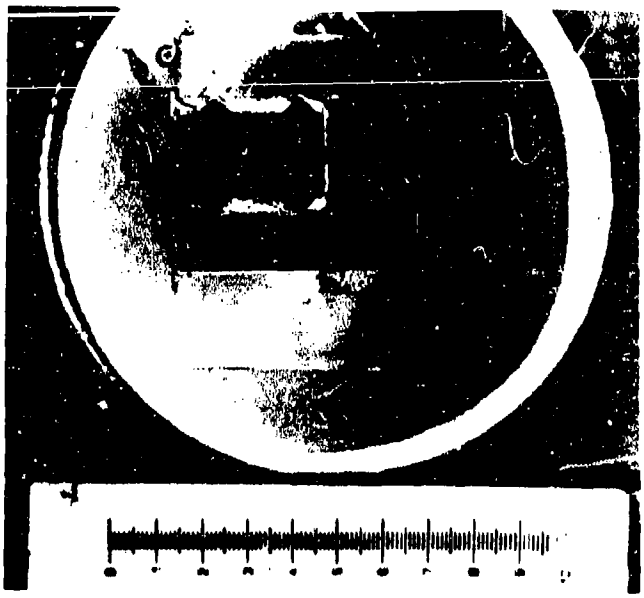

Plate No. 1-4264

X2.81

Figure 22. Arc Plasma Test $HfB_{2.1}$(A-2)-10R, Surface Temperature 5290°F, Exposure Time 60 Seconds, Stagnation Pressure 0.158 atm, Stagnation Enthalpy 7260 BTU/lb, Cold Wall Heat Flux 781 BTU/ft$^2$sec, Initial Length 558 Mils, Final Length 174 Mils. Hot Face at Right. One Inch Scale.

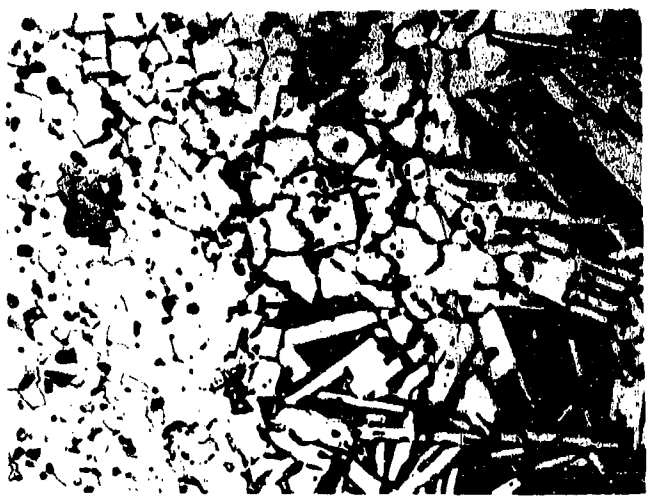

Plate No. 1-4265

Etched with 10 Glycerine $5HNO_3$ 3HF X250

Figure 23. Arc Plasma Test $HfB_{2.1}$(A-2)-10R. Rapid Melting was Observed. Interface of Melted Region (Right) and Matrix.

X2.44

Plate No. 1-4226

Figure 24. Arc Plasma Test $HfB_{2.1}$ (A-2)-1M, Surface Temperature 4060°F, Exposure Time 1800 Seconds, Stagnation Pressure 1.06 Atm., Stagnation Enthalpy 3270 BTU/lb, Cold Wall Heat Flux 520 $BTU/ft^2$ sec, 21 Mils Recession. Hot Face at Right. One Inch Scale.

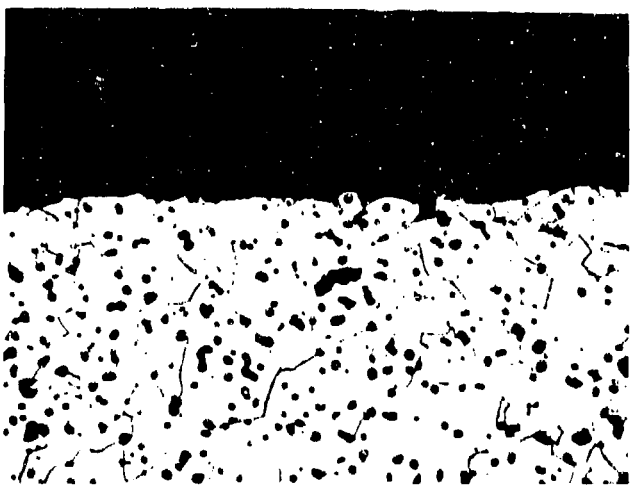

Etched with 10 Glycerine $5HNO_2$ 3H F X250

Plate No. 1-4227

Figure 25. Arc Plasma Test $HfB_{2.1}$ (A-2)-1M, Hot Surface.

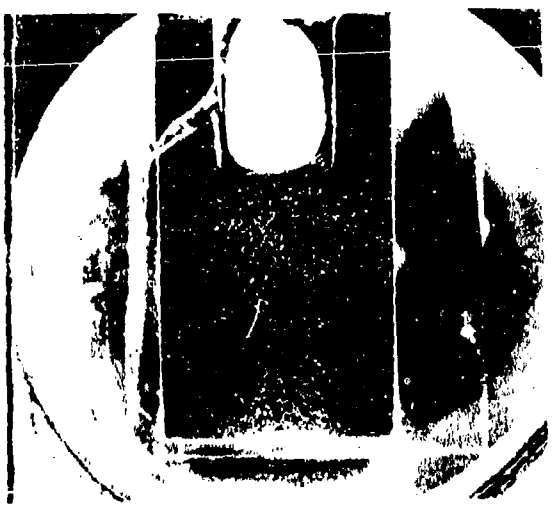

Plate No. 1-4996

X2.82

Figure 26. Arc Plasma Test $HfB_{2.1}$ (A-2) - 12R, Surface Temperature 4640°F, Exposure Time 1800 Seconds, Stagnation Pressure 0.095 Atm., Stagnation Enthalpy 9830 BTU/lb, Cold Wall Heat Flux 573 BTU/ft$^2$ sec, 11 Mils Recession, Hot Face Down. One Inch Scale.

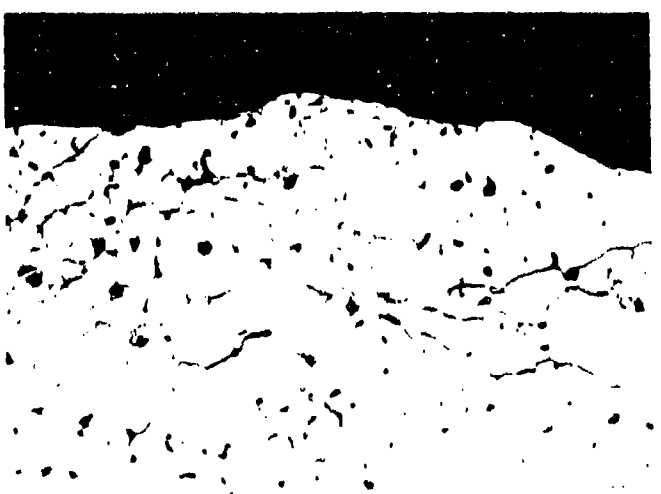

Plate No. 1-4997

Etched with 10 Glycerine $5HNO_3$ 3HF

Figure 27. Arc Plasma Test $HfB_{2.1}$ (A-2) -12R, Hot Surface.

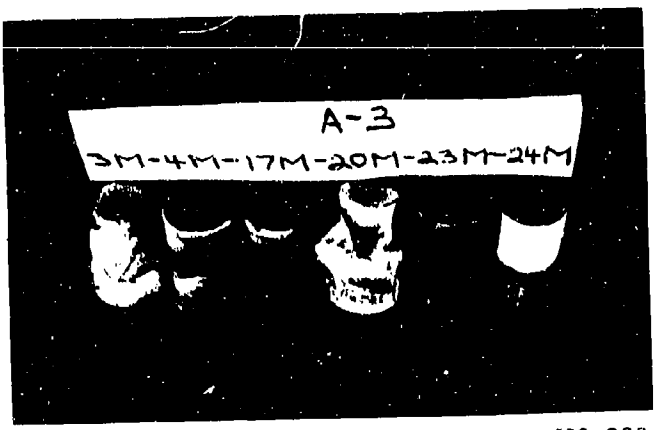


Plate No.
1-2803

X0.938

Figure 28. Post Exposure Photographs of Arc Plasma Tests $ZrB_2$ (A-3)-3M, 4M, 17M, 20M, 23M and 24M. Samples 3M and 20M Exhibited Melting. Sting End of 8M was Cracked During Removal from Sting. Hot Face is Pointing Up.

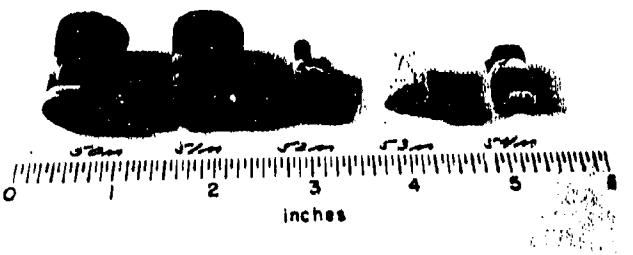


Plate No.
1-8734

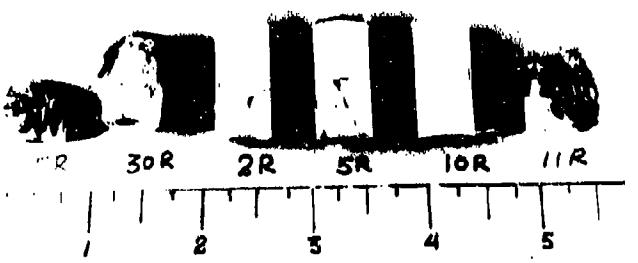


Plate No.
1-3595-A

Figure 29. Post Exposure Photographs of Arc Plasma Tests $ZrB_2$ (A-3)-50M, 51M, 52M, 53M, 54M, 15R, 30R, 2R, 5R, 10R and 11R. Samples 15R, 30R and 11R Exhibited Melting. Sting Ends of 30R, 2R and 5R were Cracked During Removal from Sting. Scale is One Inch. Hot Face is Pointing Up.

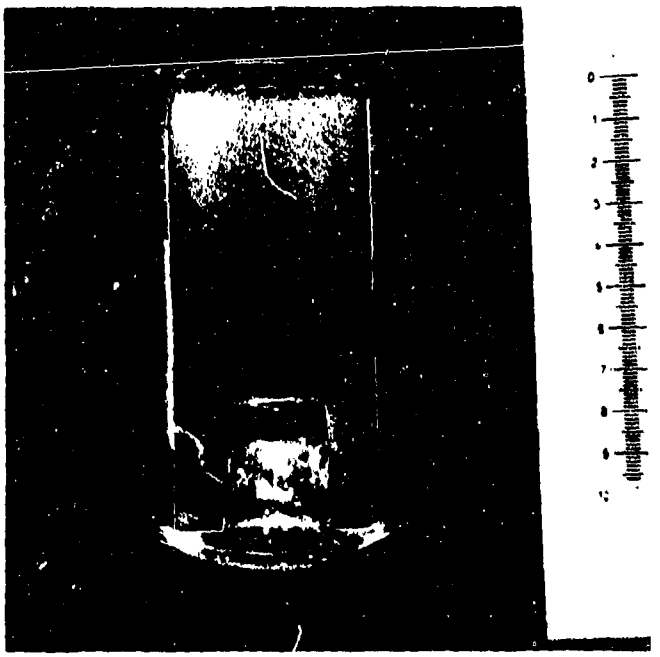

Plate No.
1-2810

X2.60

Figure 30. Arc Plasma Test $ZrB_2$(A-3)-4M, Surface Temperature 4505°F, Stagnation Enthalpy 3990 BTU/lb, Stagnation Pressure 1.07 Atm., Cold Wall Heat Flux 560 BTU/ft$^2$ sec, Exposure Time 1860 Seconds, Initial Length 1062 Mils, Final Length 1048 Mils. Hot Face Up. One Inch Scale

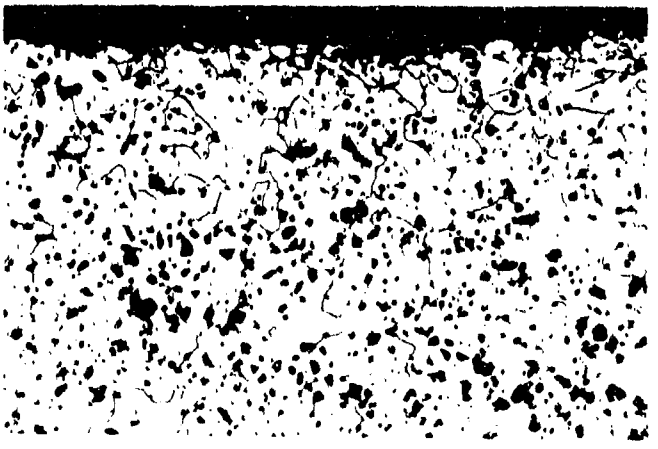

Plate No.
1-2811

Etched with 10 Glycerine
5$HNO_3$3HF

X250

Figure 31. Arc Plasma Test $ZrB_2$(A-3)-4M, Hot Face at Top.

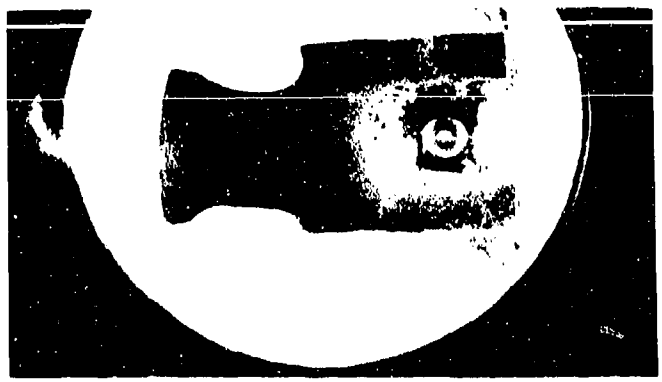

Plate No. 1-2814

X2.50

Figure 32 Arc Plasma Test $ZrB_2$(A-3)-20M, Surface Temperature 5530°F Exposure Time 90 Seconds, Stagnation Pressure 1.11 Atm. Stagnation Enthalpy 4665 BTU/lb, Cold Wall Heat Flux 840 BTU/$ft^2$ sec, 204 Mils Recession, Hot Face at Left. One Inch Scale.

Plate No. 1-2816

Etched with 10 Glycerine $5HNO_3$ 3HF X250

Figure 33. Arc Plasma Test $ZrB_2$ (A-3)-20M, Hot Surface.

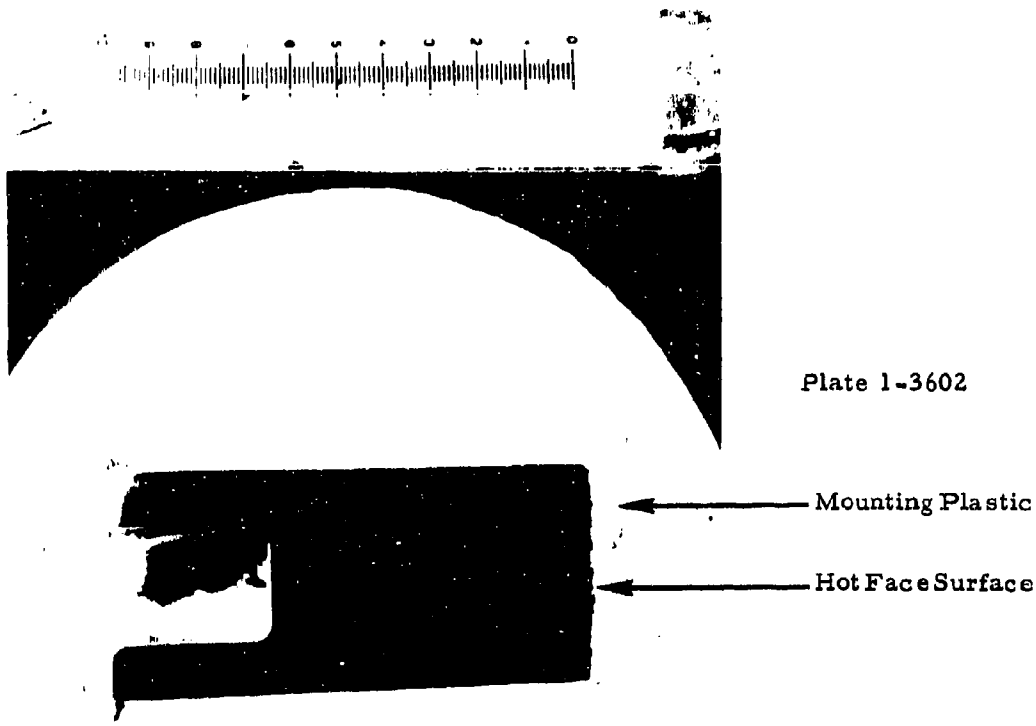


Figure 34. Arc Plasma Test $ZrB_2$(A-3)-10R, Surface Temperature 4345°F, Stagnation Enthalpy 9530 BTU/lb, Stagnation Pressure 0.021 atm., Cold Wall Heat Flux 520 BTU/$ft^2$ sec, Exposure Time 1802 Seconds, Initial Length 1045 Mils, Final Length 1027 Mils. Hot Face at Right.

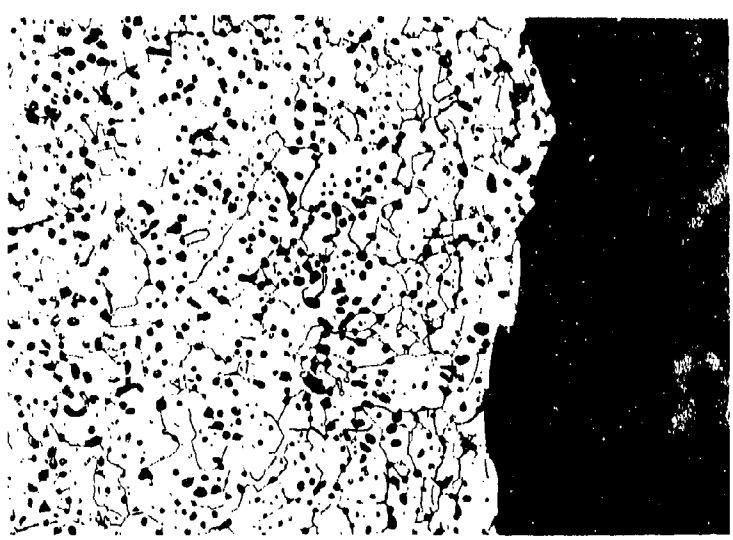


Figure 35. Arc Plasma Test $ZrB_2$(A-3)-10R, Hot Face, Showing Boride at Left.

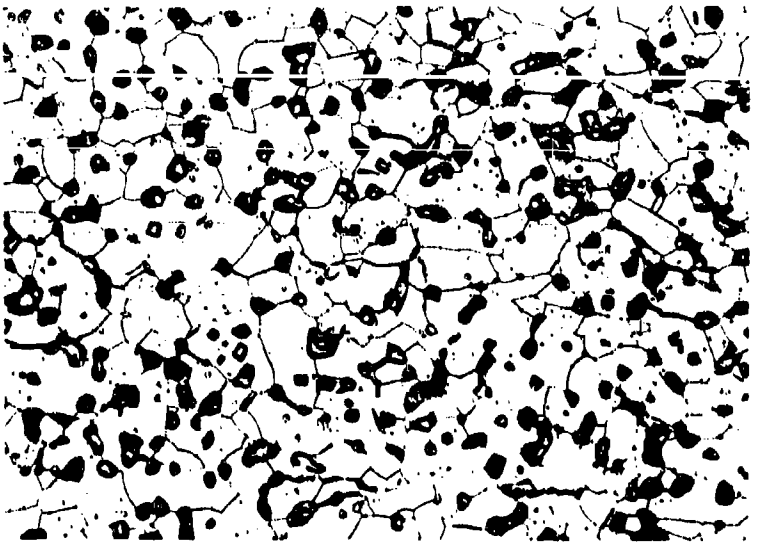

Plate 1-3604

Etched with 10 Glycerine 5$HNO_3$ 3HF X500

Figure 36. Arc Plasma Test $ZrB_2$(A-3)-10R, Matrix Sting Leg, Showing Matrix Grain Size.

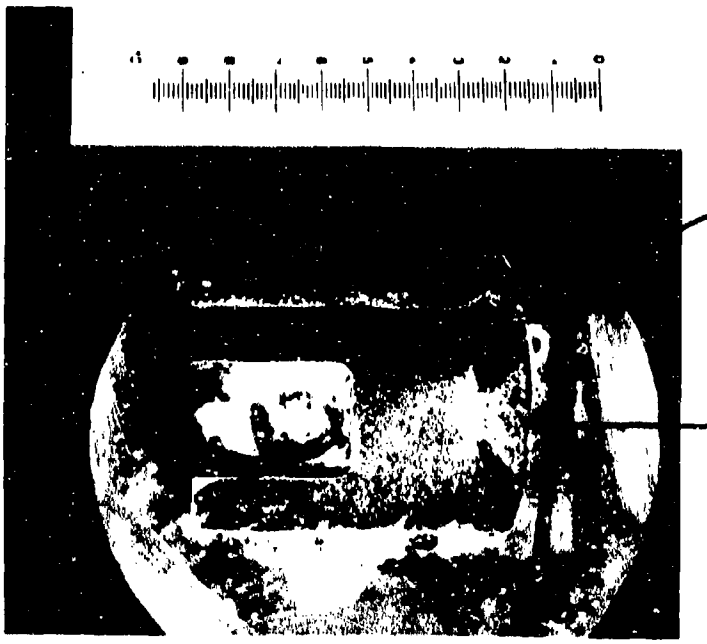


X3

Figure 37. Arc Plasma Test $ZrB_2$(A-3)-11R, Surface Temperature 5435°F, Stagnation Enthalpy 9270 BTU/lb, Stagnation Pressure 0.187 atm, Cold Wall Heat Flux 950 BTU/$ft^2$ sec, Exposure Time 51 Seconds, Initial Length 1063 Mils, Final Length 728 Mils. Hot Face at Right Illustrates Melting. One Inch Scale.

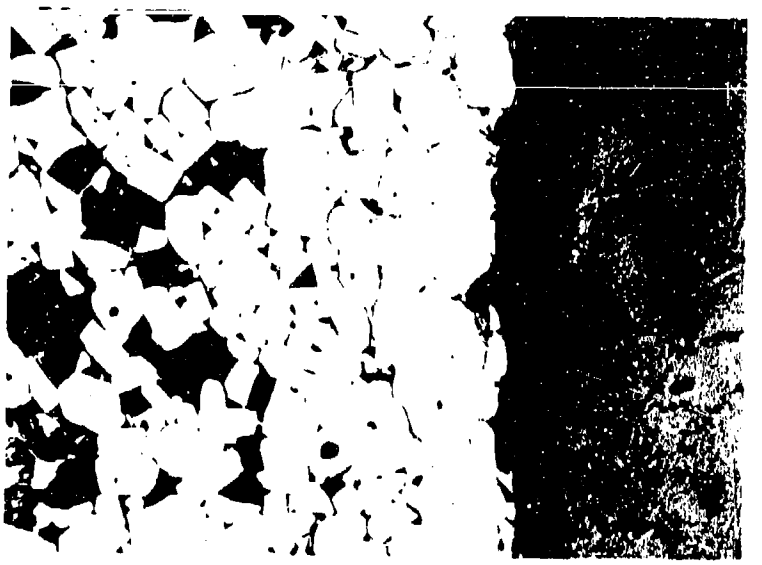

Plate 1-3606

Etched with 10 Glycerine $5HNO_3$ 3HF X250

Figure 38. Arc Plasma Test $ZrB_2$ (A-3)-11R, Hot Face, Showing Solidified Grain Structure in Core Region of Hot Face (See Figures 141 and 143).

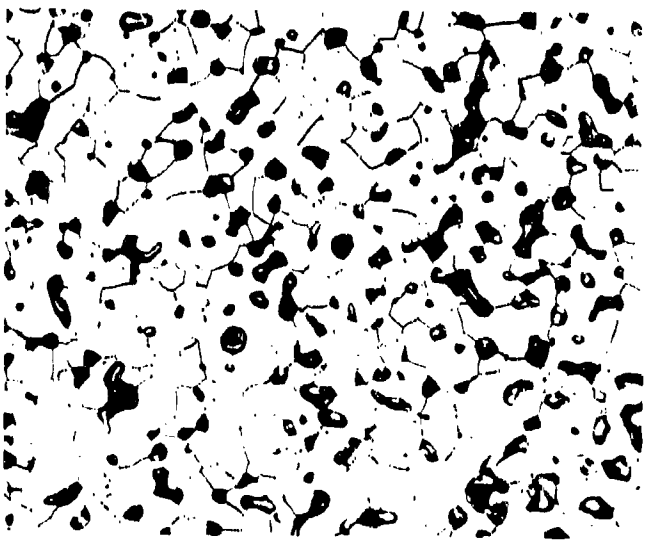

Plate 1-3595

Etched with 10 Glycering $5HNO_3$ 3HF X500

Figure 39. Arc Plasma Test $ZrB_2$(A-3)-11R, Matrix Sting Leg, Showing Matrix Grain Size.

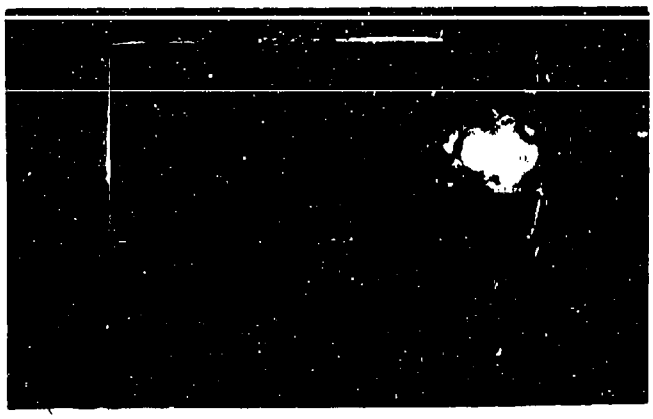

Plate No. 1-2821

X2.55

Figure 40. Arc Plasma Test $ZrB_2$(A-3)-23M, Surface Temperature 3990°F, Exposure Time 1860 Seconds, Stagnation Pressure 1.06 Atm., Stagnation Enthalpy 3345 BTU/lb, Cold Wall Heat Flux 460 BTU/ft$^2$sec, 8 Mils Recession. Hot Face at Left. One Inch Scale.

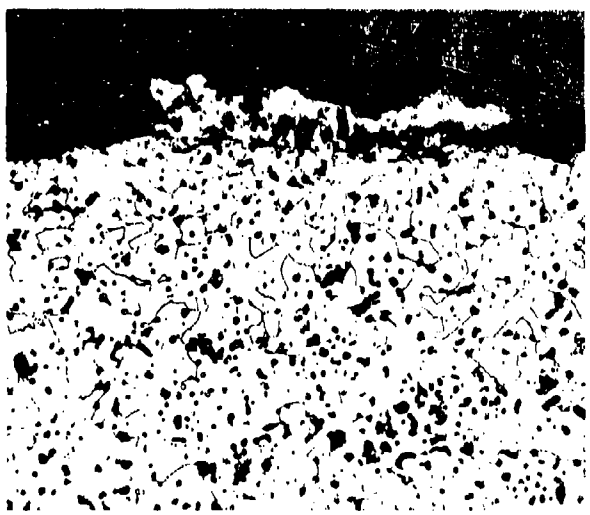

Plate No. 1-2822

X250

Etched with 10 Glycerine 5$HNO_3$ 3HF

Figure 41. Arc Plasma Test $ZrB_2$(A-3)-23M, Hot Surface.

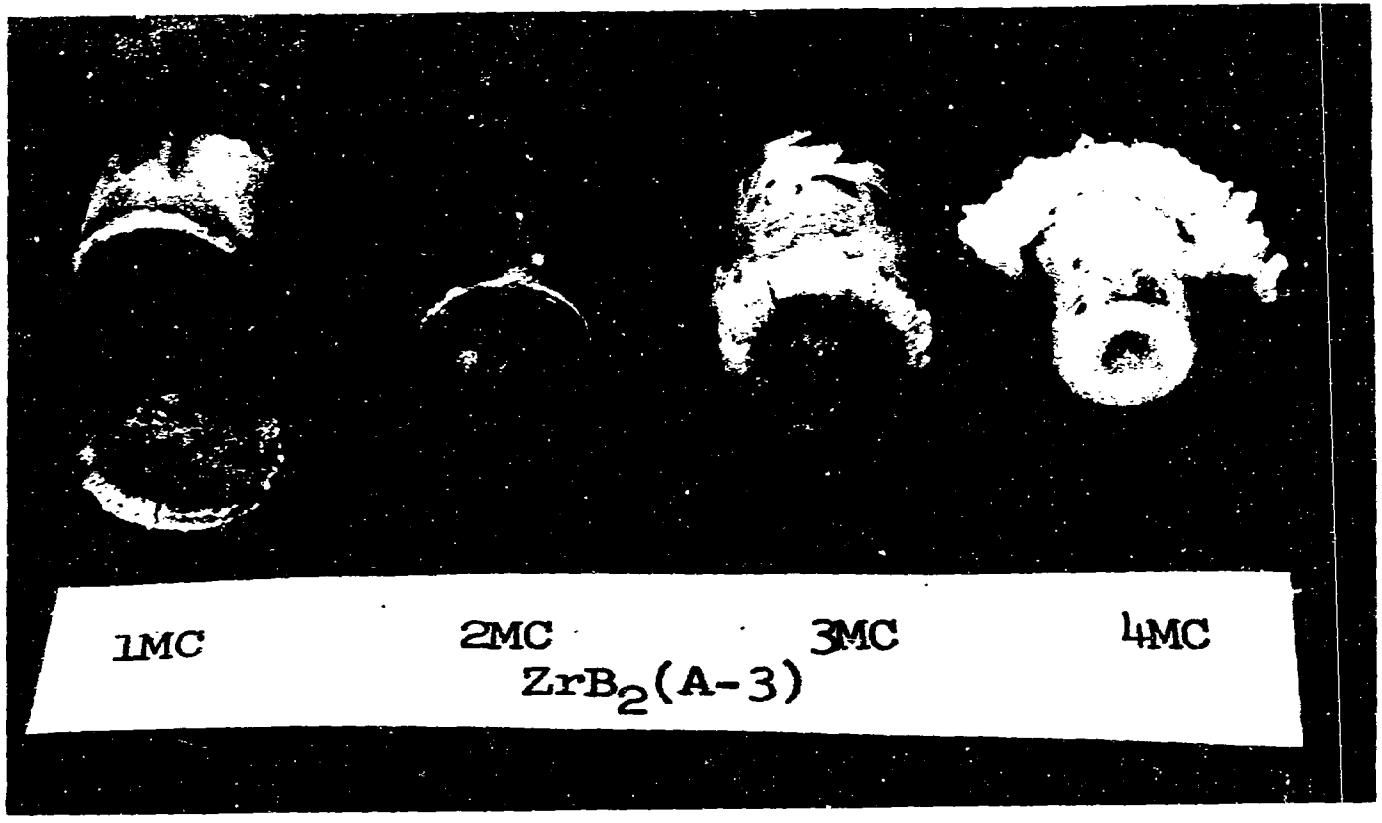


Figure 42. Post Exposure Photographs of Samples $ZrB_2$(A-3)-1MC, 2MC, 3MC and 4MC.

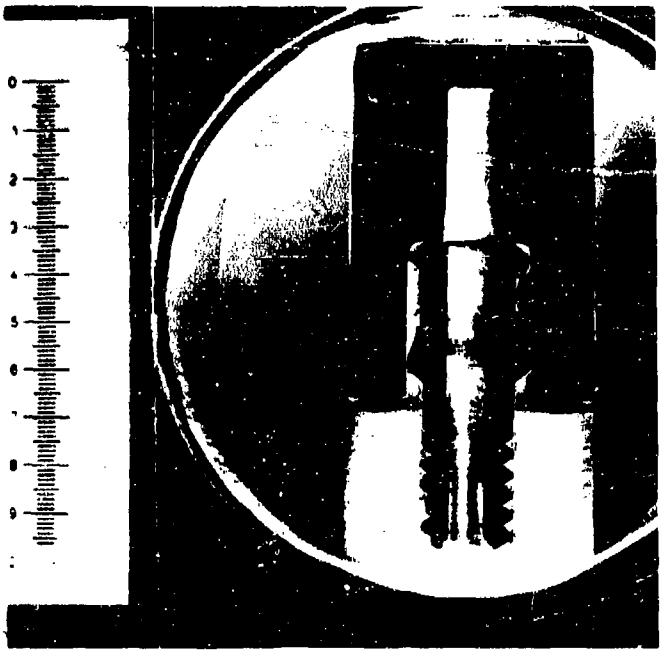

Plate No.
1-9213

X3.00

Figure 43. Arc Plasma Test $ZrB_2$(A-3)-2MC, Surface Temperature 4470°F, Internal Temperature 2940°F, Exposure Time 1800 Seconds, Stagnation Pressure 1.05 Atm., Stagnation Enthalpy 3230 BTU/lb, Cold Wall Heat Flux 365 $BTU/ft^2sec$, 14 Mil Recession. Hot Face Up. One Inch Scale.

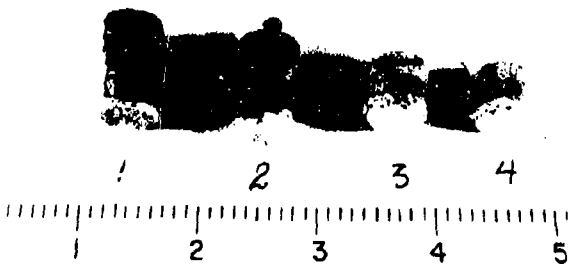


Figure 44. Post Exposure Photographs of Arc Plasma Tests $HfB_2$+ SiC(A-4)-1M, 2M, 3M and 4M. Samples 3M and 4M Exhibited Melting. Hot Face is Pointing Down. Tungsten Sting was not Removed from Sample 2M and is Protruding from Sting Hole

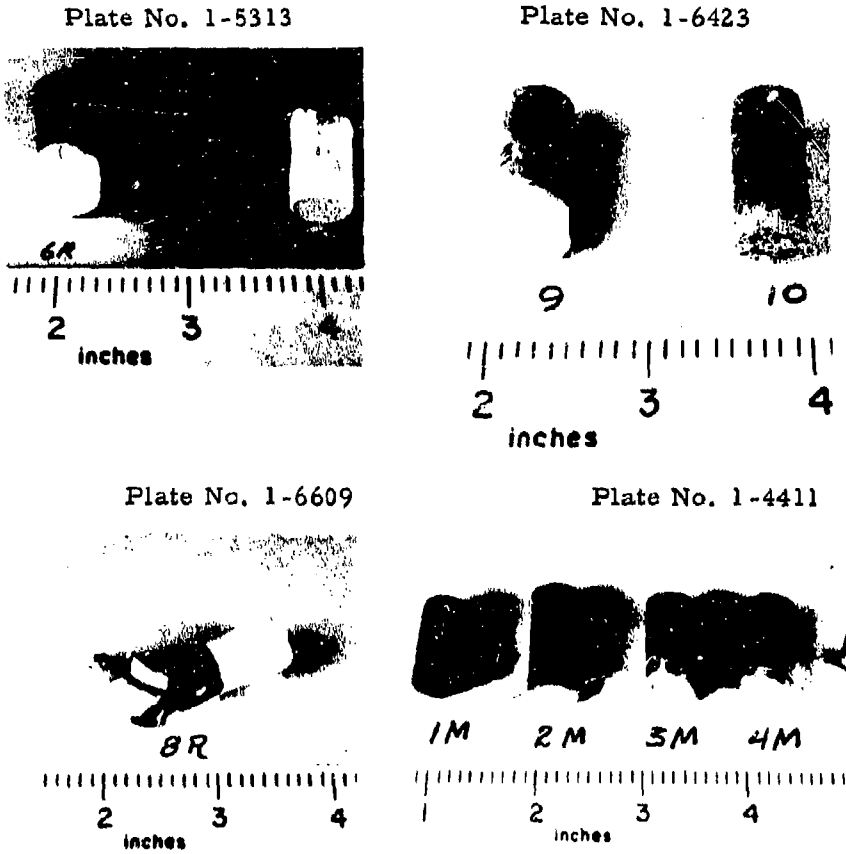


Figure 45. Post Exposure Photographs of Arc Plasma Tests $HfB_2$+ SiC(A-4)-2-6R, 7R, 9R, 10R, 8R, 1M, 2M, 3M, 4M and 5M.

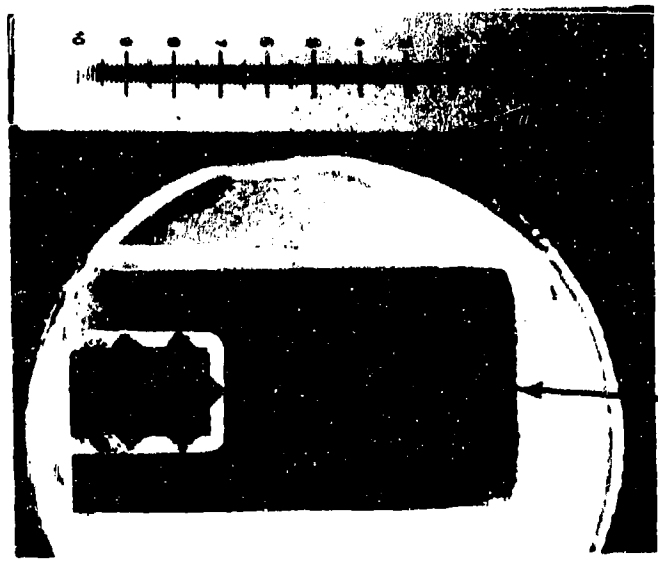


Figure 46. Arc Plasma Test $HfB_2$+SiC(A-4)-2M, Surface Temperature 5020°F, Exposure Time 1830 Seconds, Stagnation Pressure One Atm., Stagnation Enthalpy 5105 BTU/lb, Cold Wall Heat Flux 670 BTU/$ft^2$sec, Initial Thickness 675 Mils, Final Thickness 643 Mils. Hot Face at Right, One Inch Scale. Tungsten Sting is Seen in the Sting Hole.

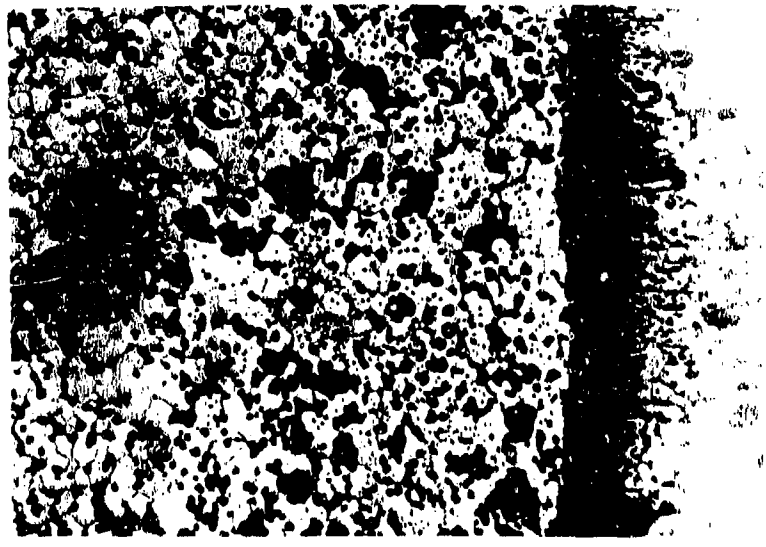


Figure 47. Arc Plasma Test $HfB_2$+SiC(A-4)-2M, Hot Face, Showing Boride at Left, Oxide at Right and Ten Mil Boride Zone Depleted of Silicon Carbide in Center. Note Adherence of Oxide.

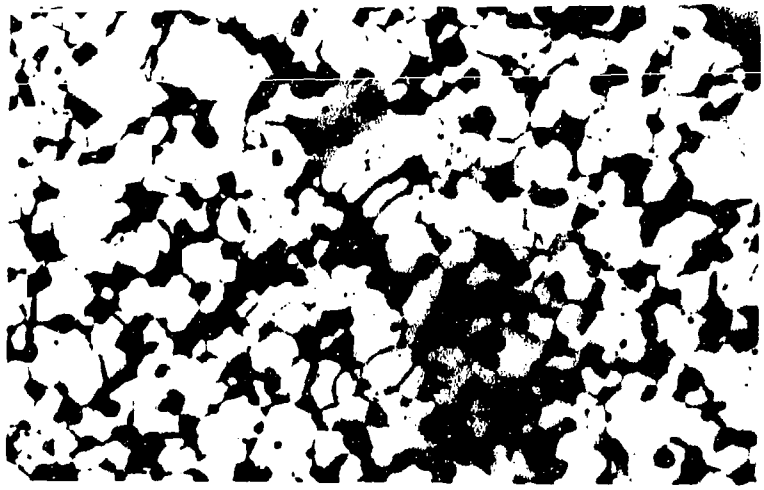

Plate 1-4441

Etched with 10 Glycerine 5$HNO_3$ 3HF X500

Figure 48. Arc Plasma Test $HfB_2$+SiC(A-4)-2M, Matrix Sting Leg, Showing $HfB_2$ and SiC Grain Structure.

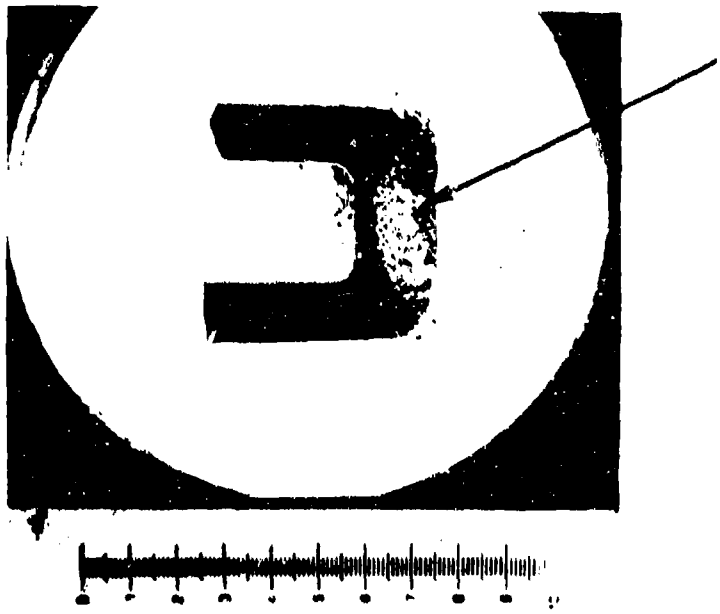


Plate 1-4446

X3

Figure 49. Arc Plasma Test $HfB_2$+SiC(A-4)-4M, Surface Temperature 5160°F, Exposure Time 1608 Seconds, Stagnation Pressure One Atm., Stagnation Enthalpy 5410 BTU/lb, Cold Wall Heat Flux 900 BTU/$ft^2$ sec, Initial Thickness 644 Mils, Final Thickness 175 Mils. Hot Face on Right Illustrates Melting. One Inch Scale.

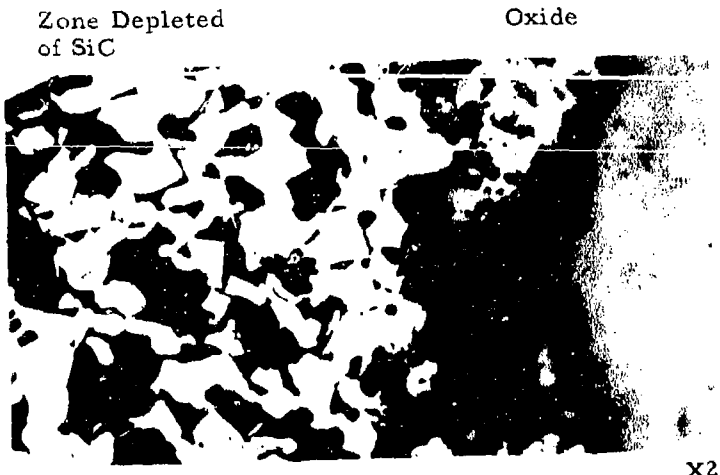


Plate 1-4447

X250

Figure 50. Arc Plasma Test $HfB_2$+SiC(A-4) Showing Hot Face.

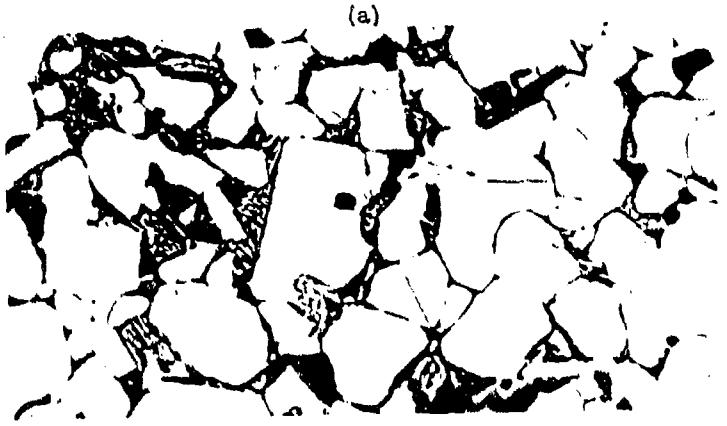


Plate 1-4449

Etched with 10 Glycerine 5$HNO_3$ 3HF X500

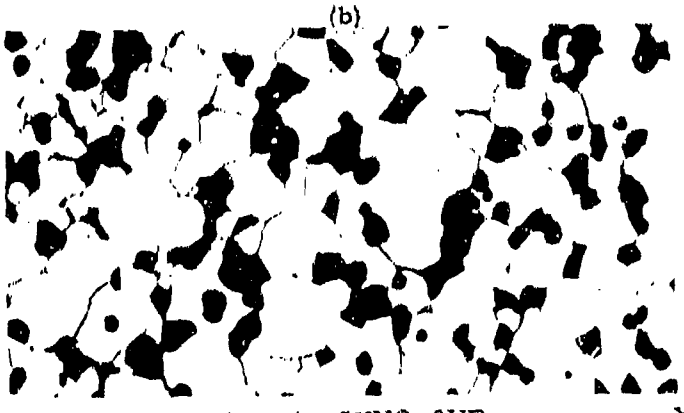


Plate 1-4448

Etched with 10 Glycerine 5$HNO_3$ 3HF X500

Figure 51. Arc Plasma Test $HfB_2$ + SiC (A-4)-4M, (a) Matrix Near Top of Sting Hole, (b) Matrix at Sting Leg Showing Diboride Plus Silicon Carbide.

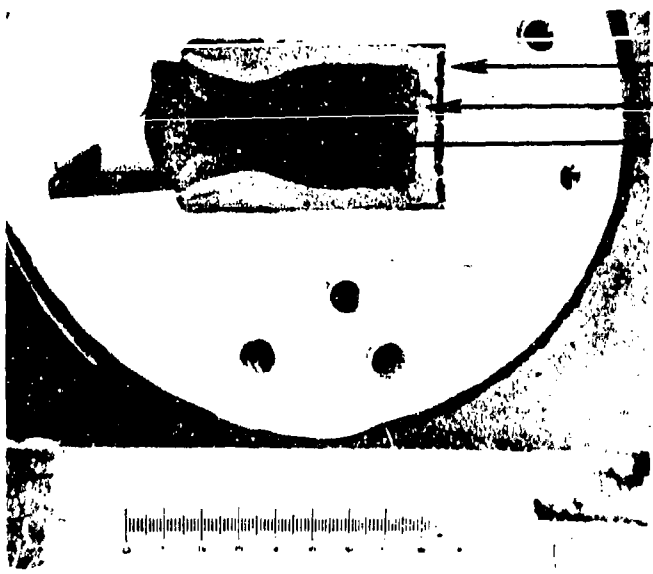


Plate No. 1-6610

X2.3

Figure 52. Arc Plasma Test $HfB_2$+20%SiC(A-4)-2-8R, Surface Temperature 5480°F, Exposure Time 1800 Seconds, Stagnation Pressure 0.027 Atm, Stagnation Enthalpy 13540 BTU/lb, Cold Wall Heat Flux 700 BTU/$ft^2$sec. Initial Length 781 Mils, Final Length 738 Mils. Hot Face at Right. One Inch Scale. Rear Broke on Removal After Test.

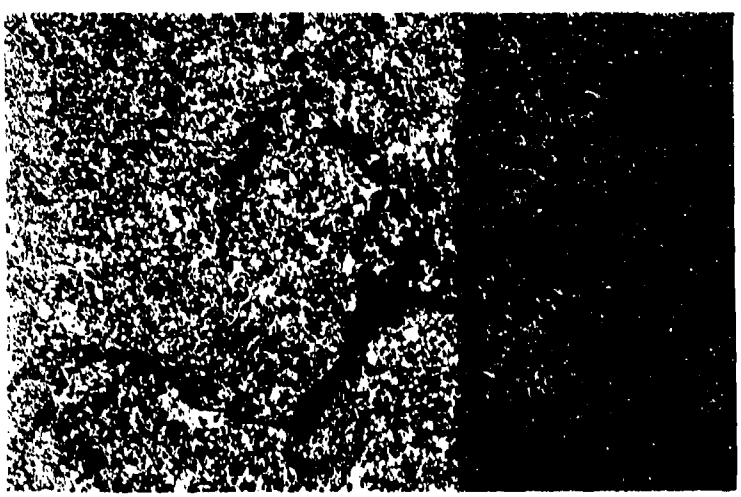

Plate No. 1-6611A

Etched with 10 Glycerine 5$HNO_3$ 3HF X50

Figure 53. Arc Plasma Test $HfB_2$+20%SiC(A-4)-2-8R. Oxide at Right, Depletion Zone Center. Matrix at Left.

Plate No. 1-4435

X2.9

Figure 54. Arc Plasma Test $HfB_2$ + SiC(A-4)-1M, Surface Temperature 3450°F, Exposure Time 1830 Seconds, Stagnation Pressure 1.08 Atm., Stagnation Enthalpy 3915 BTU/lb, Cold Wall Heat Flux 570 BTU/$ft^2$sec, 6 Mil Recession. Hot Face Down. One Inch Scale.

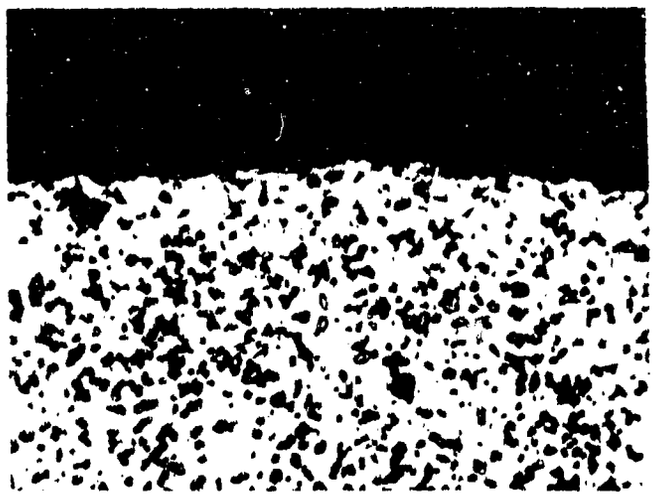

Plate No. 1-4436

Etched with 10 Glycerine 5$HNO_3$ 3HF X250

Figure 55. Arc Plasma Test $HfB_2$ + SiC(A-4)-1M, Hot Surface Showing Oxide (Top) and Depletion Zone (Center).

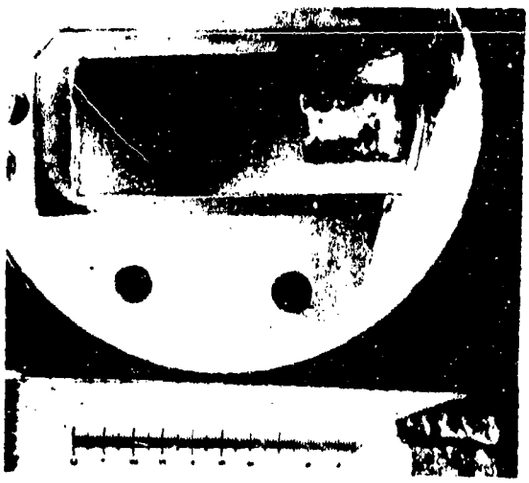

Plate No. 1-6424

X1.88

Figure 56. Arc Plasma Test $HfB_2$ + SiC (A-4)-2-9R, Surface Temperature 4680°F, Exposure Time 1800 Seconds, Stagnation Pressure 0.023 Atm., Stagnation Enthalpy 8920 BTU/lb, Cold Wall Heat Flux 402 BTU/ft$^2$ sec, 23 Mils Recession. Hot Face at Left. One Inch Scale.

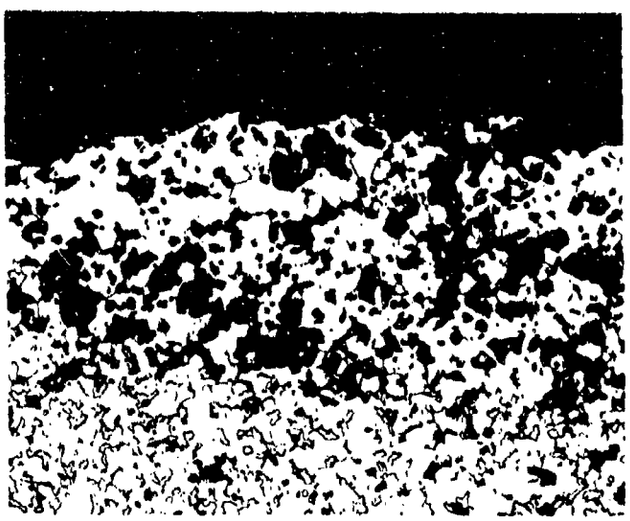

Plate No. 1-6425

Etched with 10 Glycerine $5HNO_3$ 3HF X250

Figure 57. Arc Plasma Test $HfB_2$ + SiC(A-4)-2-9R, Hot Surface Showing Depletion Zone at Top.

Plate No. 1-4971

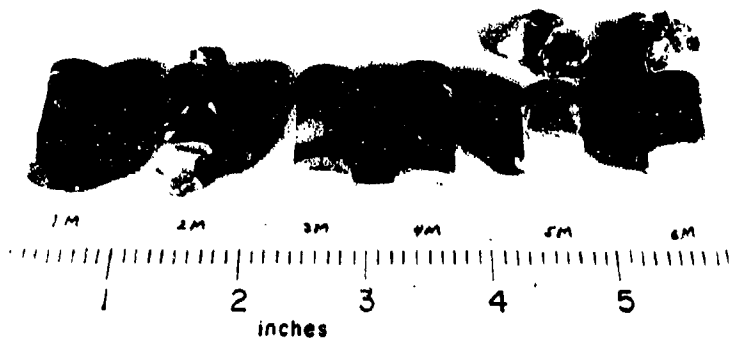


Plate No. 1-6614


Plate No. 1-6441

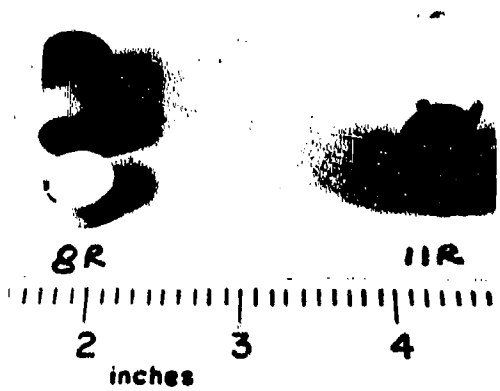


Plate No. 1-7622

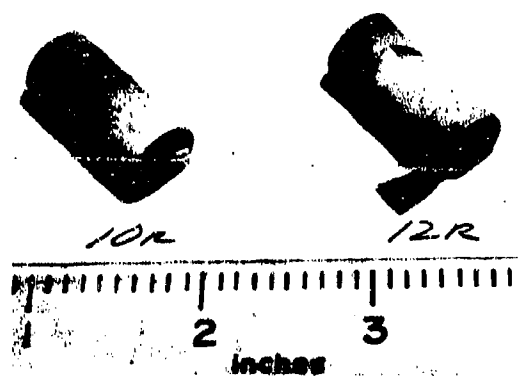


Figure 58. Post Exposure Photographs of Arc Plasma Tests Boride Z(A-5)-1M, 2M, 3M, 4M, 5M, 6M, 7R, 9R, 8R, 11R, 10R and 12R.

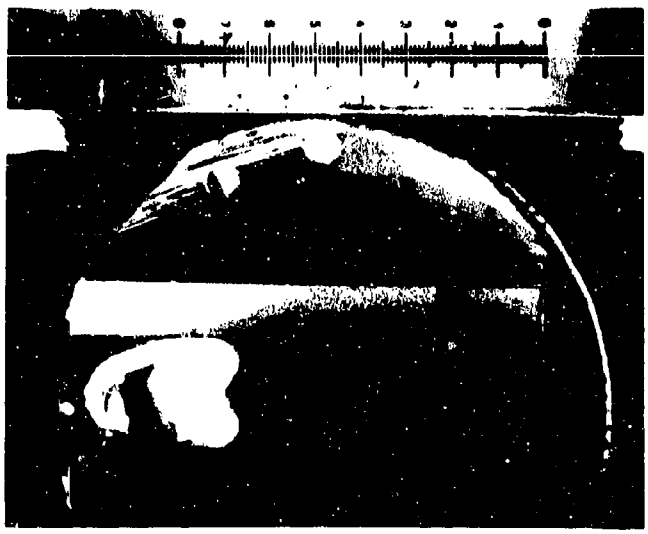

Plate No. 1-4981

X2.81

Figure 59a. Arc Plasma Test Boride Z(A-5)-4M, Surface Temperature 2920°F, Exposure Time 1830 Seconds, Stagnation Pressure 1.05 Atm, Stagnation Enthalpy 2500 BTU/lb, Cold Wall Heat Flux 350 BTU/ft$^2$sec, Initial Length 663 Mils, Final Length 659 Mils. Hot Face at Right. Specimen Thermal Shocked. One Inch Scale

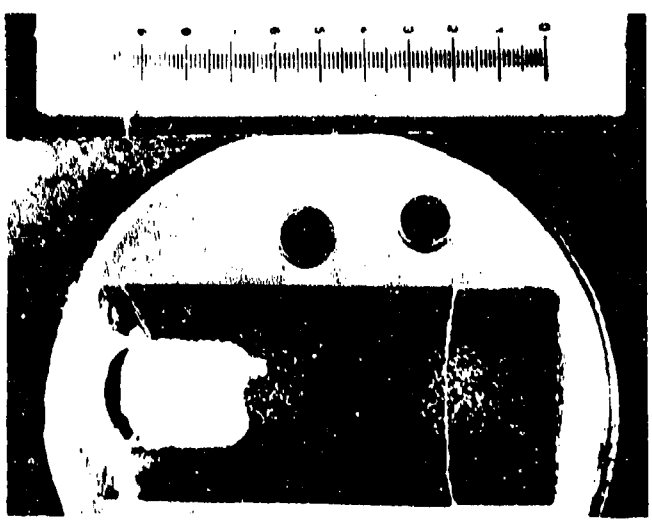

Plate No. 1-6442

X2.75

Figure 59b. Arc Plasma Test Boride Z(A-5)-8R, Surface Temperature 3790°F, Exposure Time 1800 Seconds, Stagnation Pressure 0.018 Atm, Stagnation Enthalpy 9200 BTU/lb, Cold Wall Heat Flux 262 BTU/ft$^2$sec, Inital Length 690 Mils, Final Length 680 Mils. Hot Face at Right. Specimen Thermal Shocked. One Inch Scale.

Plate No. 1-6574

Plate No. 1-7396

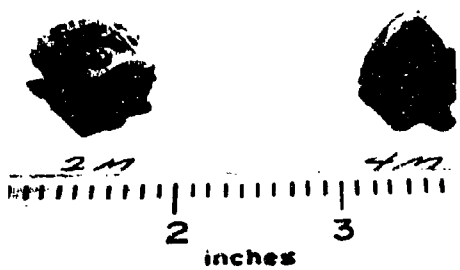


Plate No. 1-9526

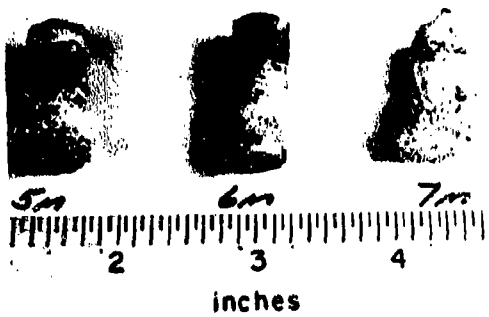


Plate No. 1-9586

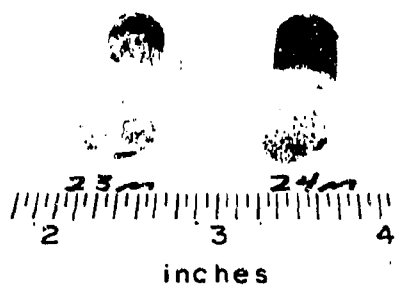


Plate No. 2-0190

Plate No. 2-0666

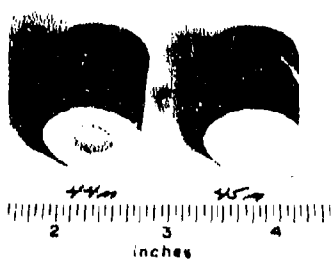


Figure 60. Post Exposure Photographs of Arc Plasma Tests $HfB_{2.1}$ + 20%SiC(A-7)-1M, 3M, 2M, 5M, 6M, 7M, 23M, 24M, 25M, 30M, 31M, 32M, 44M and 45M.

Plate No. 2-0583

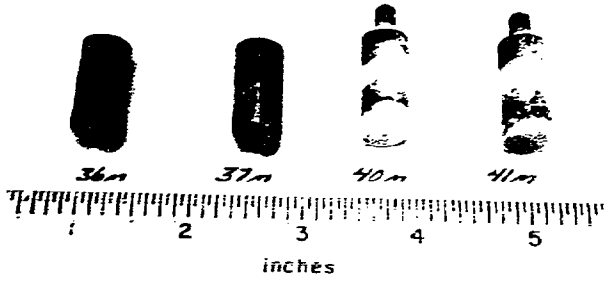


Plate No. 2-0581

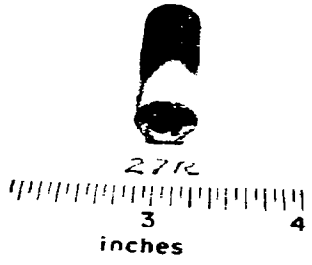


Plate No. 2-0191

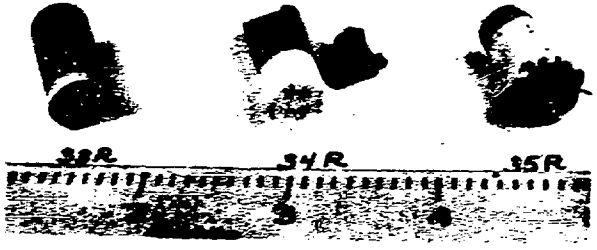


Plate No. 2-0667


Plate No. 2-0703

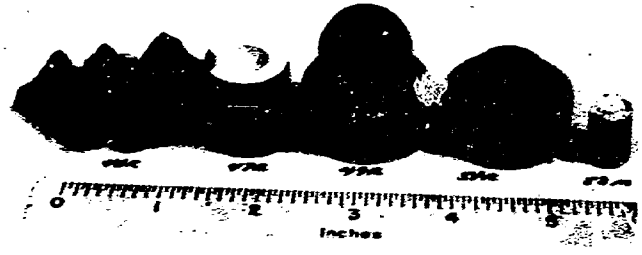


Figure 61. Post Exposure Photographs of Arc Plasma Tests $HfB_2$+20%SiC(A-7)-36M, 37M, 40M, 41M 27R, 33R, 34R, 5R, 29R, 38R, 39R, 42R, 43R, 48R, 50R, 46R, 47R, 49R, 51R and 52M.

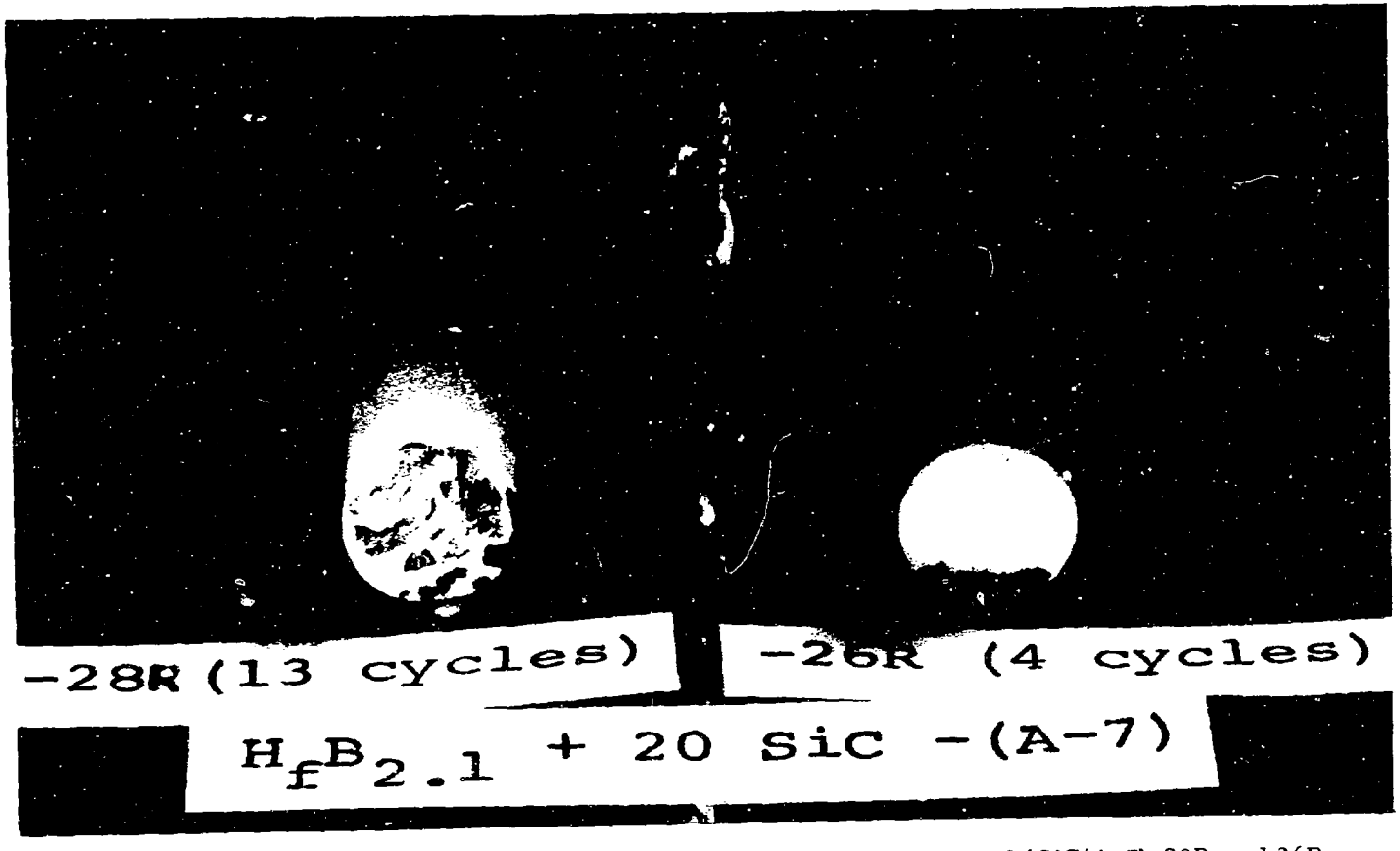


Figure 62. Post Exposure Photographs of Arc Plasma Tests $HfB_{2.1}$ + 20%SiC(A-7)-28R and 26R.

Plate No. 1-7397

X2.75

Figure 63. Arc Plasma Test $HfB_{2.1}$ + 20 v/o SiC(A-7)-2M, Surface Temperature 4800°F, Exposure Time 1745 Seconds, Stagnation Pressure 1.08 Atm. Stagnation Enthalpy 5055 BTU/lb, Cold Wall Heat Flux 715 BTU/$ft^2$ sec, 157 Mils Recession, Hot Face at Left. One Inch Scale.

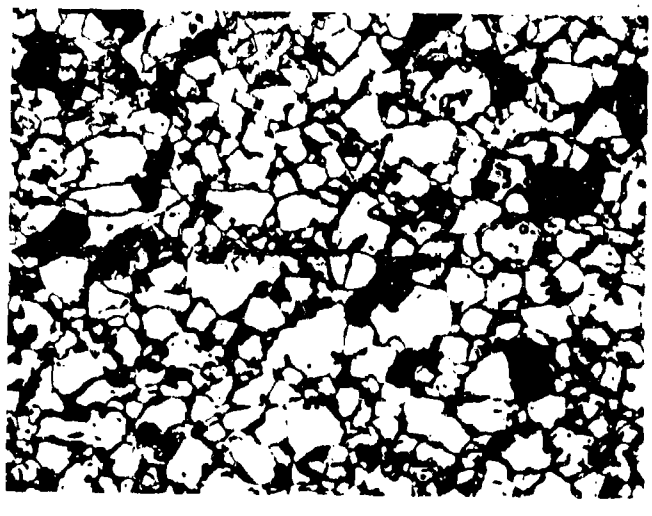

Plate No. 1-7398

Etched with 10 Glycerine $5HNO_3$ 3HF X250

Figure 64. Arc Plasma Test $HfB_{2.1}$ + 20 v/o SiC(A-7)-2M, Interface Between Depleted Zone and Matrix.

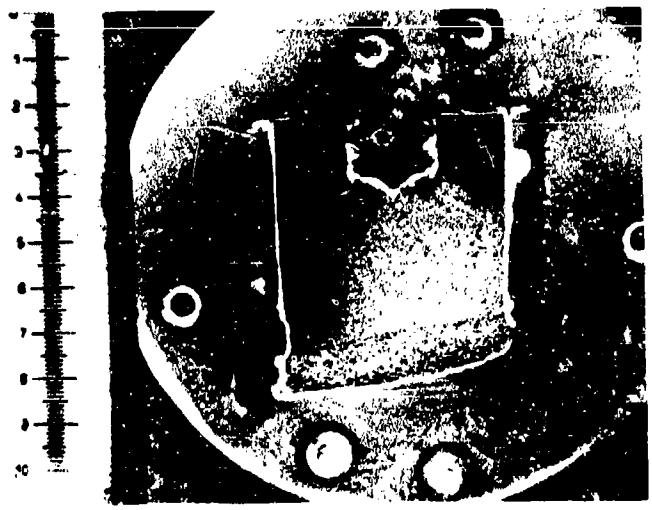

X2.75

Plate No. 1-6575

Figure 65. Arc Plasma Test $HfB_{2.1}$ + 20 v/o SiC(A-7)-1M Surface Temperature 5760°F, Exposure Time 56 Seconds, Stagnation Pressure 1.11 Atm. Stagnation Enthalpy 3915 BTU/lb, Cold Wall Heat Flux 810 BTU/$ft^2$ sec, 110 Mils Recession, Hot Face Down. One Inch Scale.

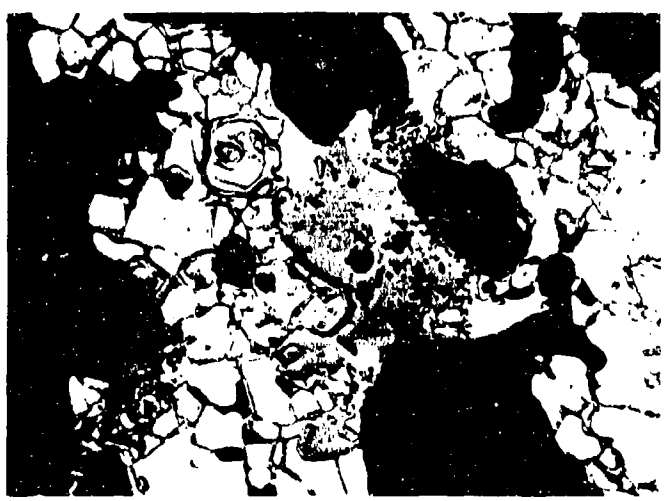

Etched with 10 Glycerine 5$HNO_3$ 3HF X 250

Plate No. 1-6576

Figure 66. Arc Plasma Test $HfB_{2.1}$ + 20 v/o SiC(A-7)-1M, Hot Surface.

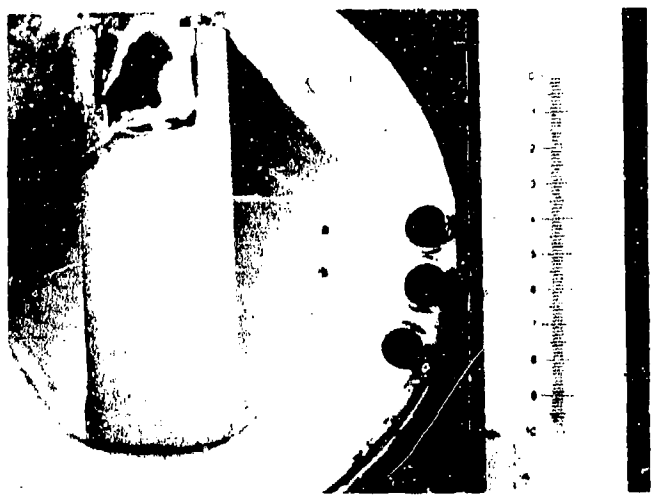

Plate No.
2-0211

X2.25

Figure 67. Arc Plasma Test $HfB_{2.1}$+20%SiC(A-7)-34R, Surface Temperature 5005°F, Exposure Time 1200 Seconds, Stagnation Pressure 0.160 Atm., Stagnation Enthalpy 8040 BTU/lb, Cold Wall Heat Flux 720 BTU/$ft^2$sec., Initial Length 920 Mils, Final Length 889 Mils, Hot Face Down. One Inch Scale. Oxide Broke Off on Handling.

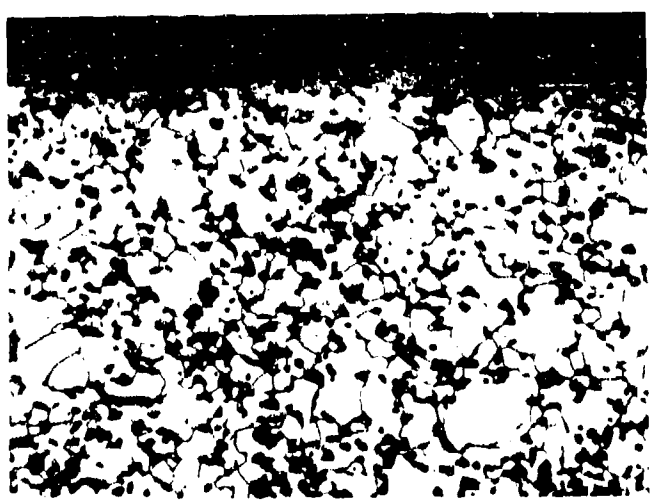

Plate No.
2-0212

Etched with 10 Glycerine
$5HNO_3 3HF$

X250

Figure 68. Arc Plasma Test $HfB_{2.1}$+20%SiC(A-7)-34R. Hot Interface Up.

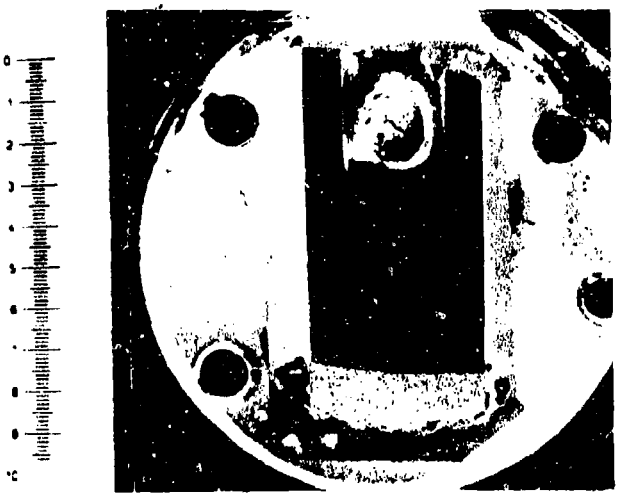

Plate No.
2-0214

X2.60

Figure 69. Arc Plasma Test $HfB_{2.1}$+20%SiC(A-7)-35R, Surface Temperature 5350°F, Exposure Time 90 Seconds, Stagnation Pressure 0.180 Atm., Stagnation Enthalpy 9030 BTU/lb, Cold Wall Heat Flux 791 BTU/ft$^2$sec, Initial Length 921 Mils, Final Length 606 Mils, Depletion Depth 130 Mils. Hot Face Down. One Inch Scale.

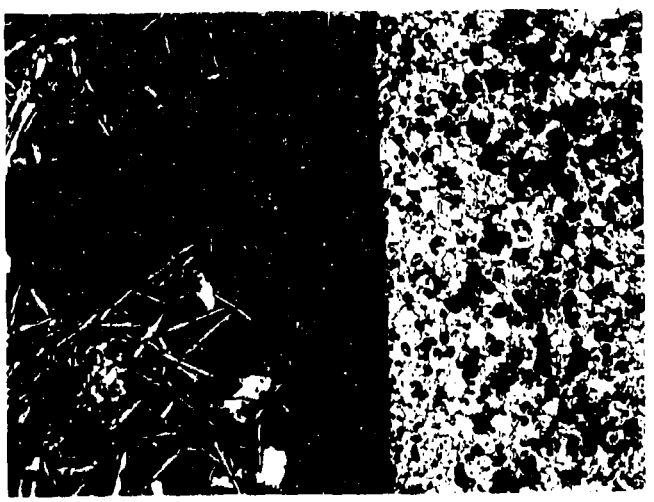

Plate No.
2-0215

Etched with 10 Glycerine
5$HNO_3$3HF

X250

Figure 70. Arc Plasma Test $HfB_{2.1}$+20%SiC(A-7)-35R. Side Interface, Depleted Matrix at Right, Melted Material at Left. Hot Face Up.

X 2.35

Plate No. 2-0675

Figure 71. Arc Plasma Test $HfB_{2.1}$ + 20 v/o SiC(A-7)-28R Average Surface Temperature 4650°F, Exposure Time 22, 400 Seconds (13 cyclic exposures each of approximately 1800 seconds), Stagnation Pressure 0.07 Atm. Stagnation Enthalpy 10300 BTU/lb, Cold Wall Heat Flux 495 BTU/$ft^2$sec, 15 Mils Recession, Hot Face Up. One Inch Scale.

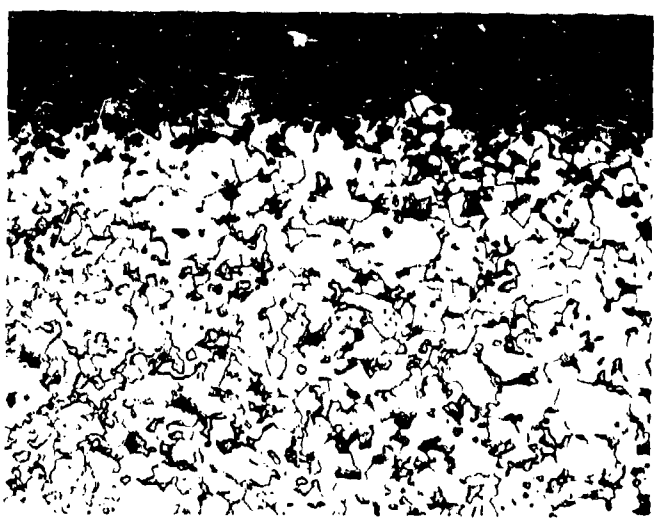

Plate No. 2-0676

Etched with 10 Glycerine 5$HNO_3$ 3HF X250

Figure 72. Arc Plasma Test $HfB_{2.1}$ + 20 v/o SiC(A-7)-28R, Hot Surface.

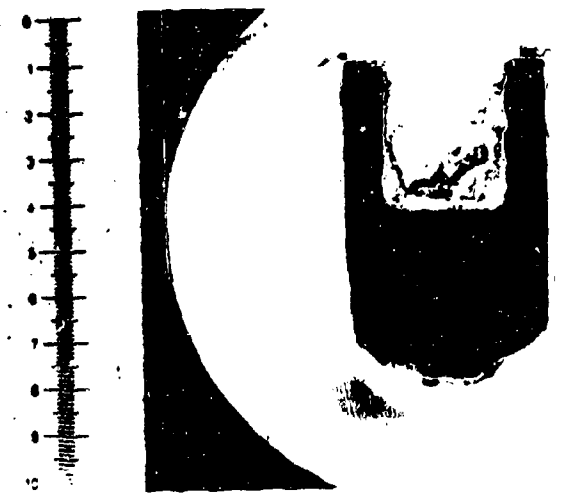

Plate No.
2-0681

Figure 73. Arc Plasma Test $HfB_{2.1}$+20 v/o SiC(A-7)-52M. Surface Temperature 4600°F, Exposure Time 14,030 Seconds (8 Cyclic Exposures Each of Approximately 1800 Seconds), Stagnation Pressure 1.03 Atm., Stagnation Enthalpy 4180 BTU/lb, Cold Wall Heat Flux 450 BTU/$ft^2$ sec, 329 Mils Recession, Hot Face Down, One Inch Scale.

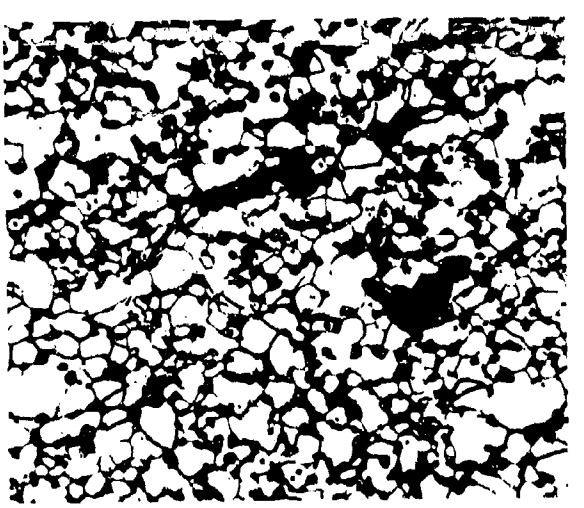

Plate No.
2-0682

Etched with 10 Glycerine
$5HNO_3 3HF$

X250

Figure 74. Arc Plasma Test $HfB_{2.1}$+20 v/o SiC(A-7)-52M Hot Surface.

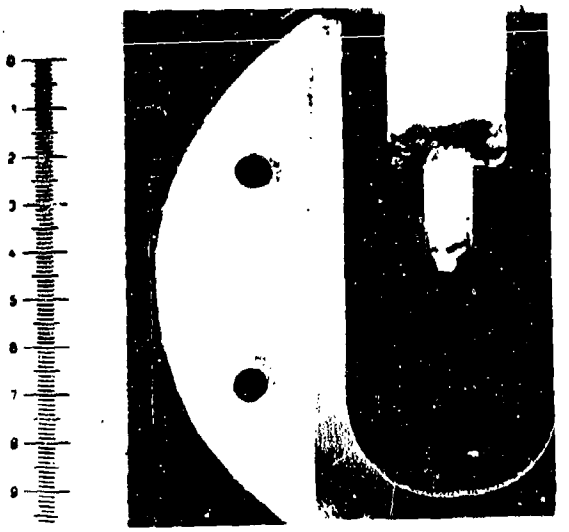

Plate No. 2-0677

X 2.95

Figure 75. Arc Plasma Test $HfB_{2.1}$ + 20 v/o SiC(A-7)-37MH Surface Temperature 3765°F, Exposure Time 1080 Seconds, Stagnation Pressure 1.02 Atm. Stagnation Enthalpy 3640 BTU/lb, Cold Wall Heat Flux 495 BTU/$ft^2$sec, 10 Mils Recession, Hot Face Down. One Inch Scale.

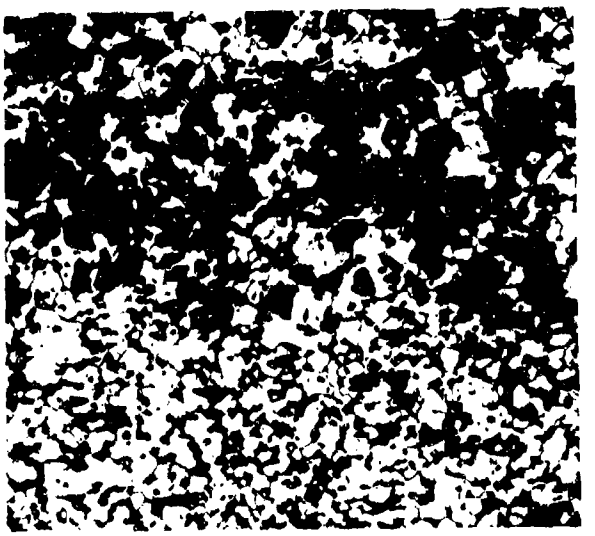

Plate No. 2-0678

Etched with 10 Glycerine $5HNO_3$ 3HF X 250

Figure 76. Arc Plasma Test $HfB_{2.1}$ + 20 v/o SiC(A-7)-37MH, Hot Surface.

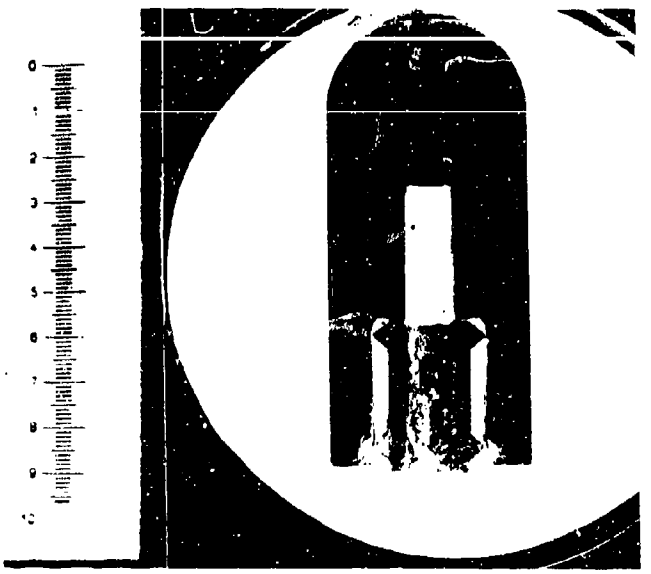

Plate No.
2-0679

X2.78

Figure 77. Arc Plasma Test $HfB_{2.1}$+20 v/o SiC(A-7)-39RH Surface Temperature 2710°F, Exposure Time 1812 Seconds, Stagnation Pressure 0.162 Atm., Stagnation Enthalpy 6540 BTU/lb, Cold Wall Heat Flux 487 BTU/$ft^2$sec, Second Exposure: Surface Temperature 2955°F, Exposure Time 1800 Seconds, Stagnation Pressure 0.053 Atm., Stagnation Enthalpy 8810 BTU/lb, Cold Wall Heat Flux 885 BTU/$ft^2$sec. Third Exposure: Surface Temperature 4285°F, Exposure Time 375 Seconds, Stagnation Pressure 0.105 Atm., Stagnation Enthalpy 7290 BTU/lb, Cold Wall Heat Flux 965 BTU/$ft^2$sec, 24 Mils Recession, Hot Face Up, One Inch Scale.

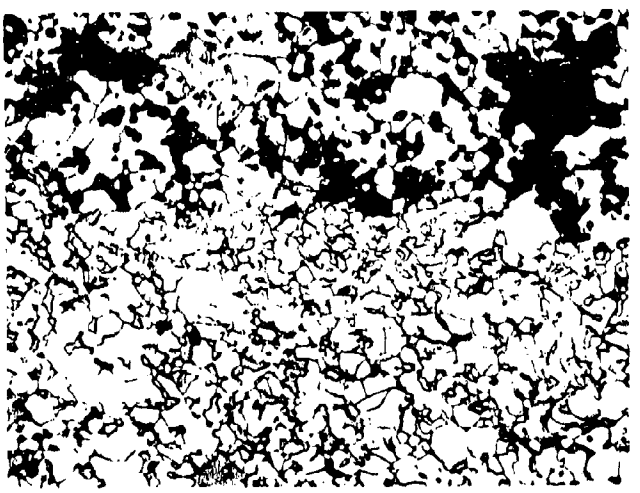

Plate No.
2-0680

Etched with 10 Glycerine
5$HNO_3$3HF

X250

Figure 78. Arc Plasma Test $HfB_{2.1}$+20 v/o SiC(A-7)-39RH, Hot Surface.

Plate No. 1-6563

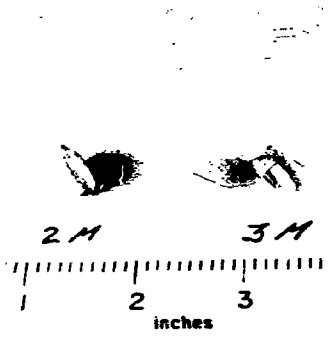


Plate No. 1-7387


Plate No. 1-9527

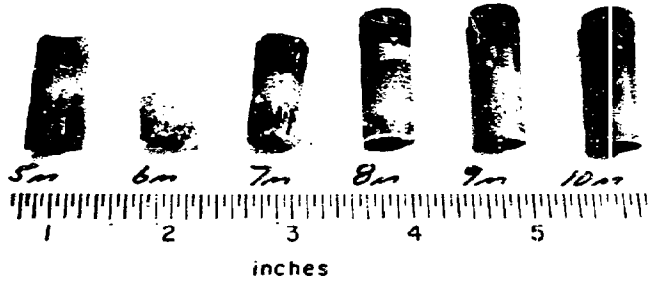


Plate No. 1-6582


Plate No. 1-7411

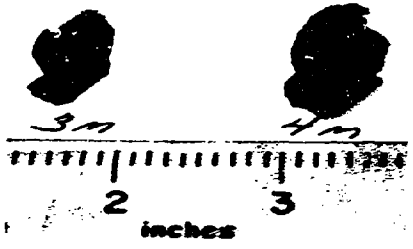


Plate No. 1-9522

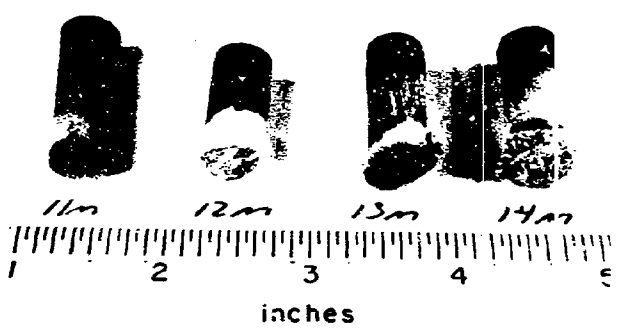


Figure 79. Post Exposure Photographs of Arc Plasma Tests $ZrB_2$+20%SiC(A-8)-1M, 2M, 3M, 4M, 5M, 6M, 7M, 8M, 9M, 10M, 11M, 12M, 13M, 14M, 40M, 41M, 42M and 43M.

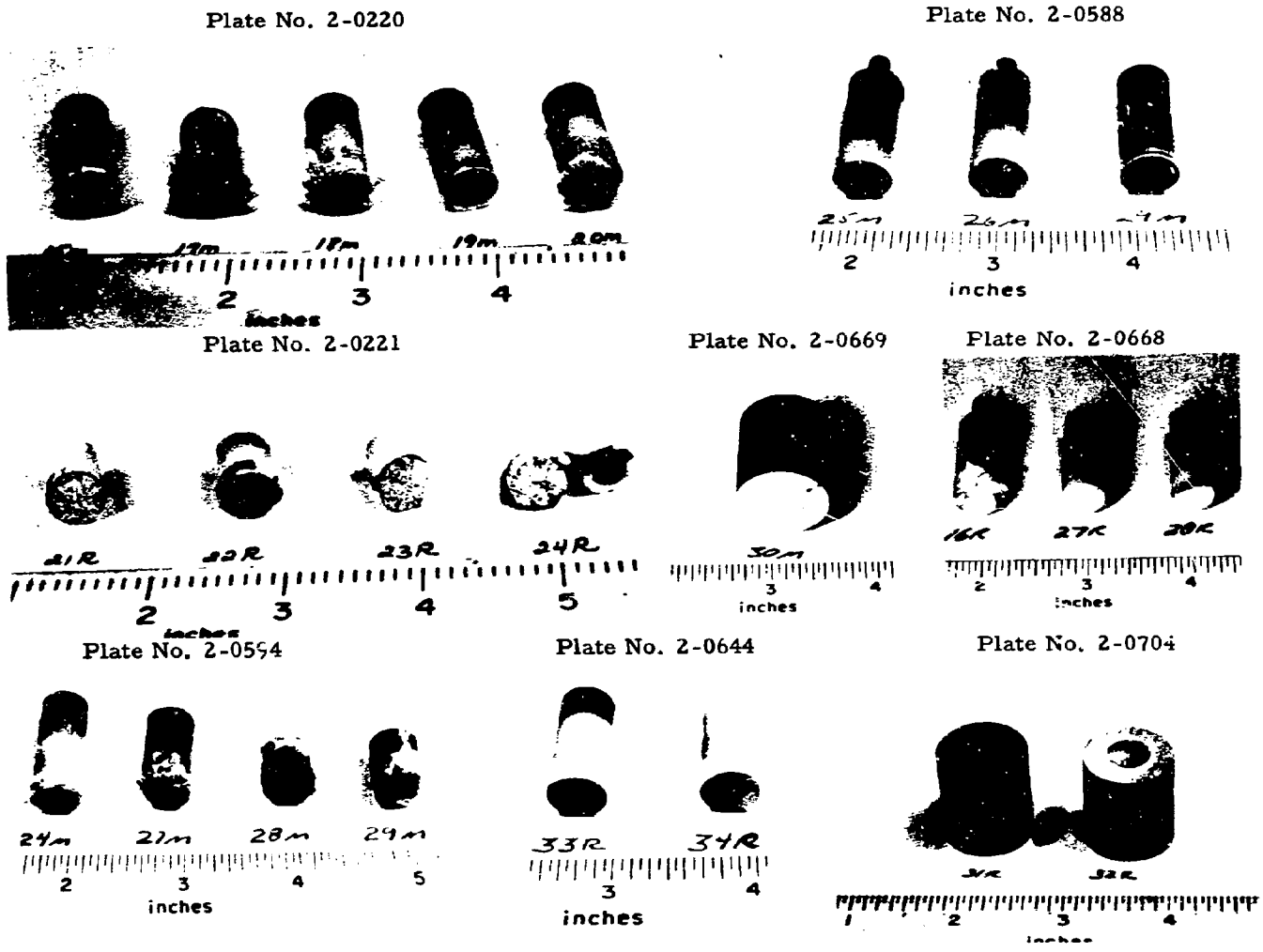


Figure 80. Post Exposure Photographs of Arc Plasma Tests $ZrB_2$+20%SiC(A-8)-15M, 17M, 18M, 19M, 20M, 25M, 26M, 29M, 30M, 21R, 22R, 23R, 24R, 16R, 27R, 28R, 24M, 27M, 28M, 29M, 33R, 34R, 31R, 32R.

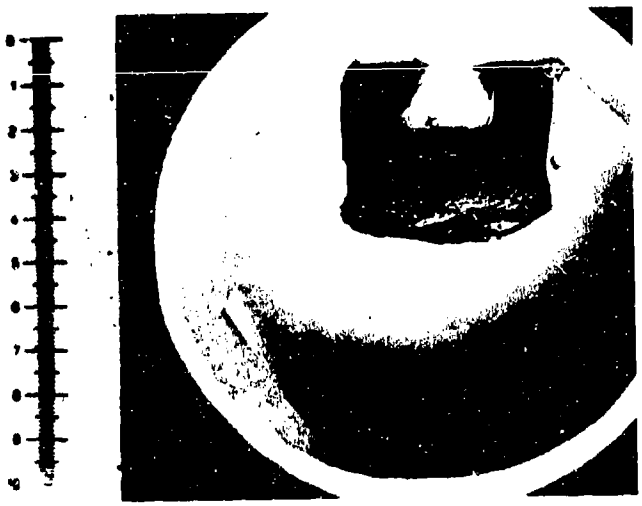

Plate No. 1-7415

X2.75

Figure 81. Arc Plasma Test $ZrB_2$ + 20 v/o SiC(A-8)-4M, Surface Temperature 5445°F, Exposure Time 327 Seconds, Stagnation Pressure 1.06 Atm. Stagnation Enthalpy 3915 BTU/lb, Cold Wall Heat Flux 515 BTU/$ft^2$ sec, 142 Mils Recession. Hot Face Down. One Inch Scale.

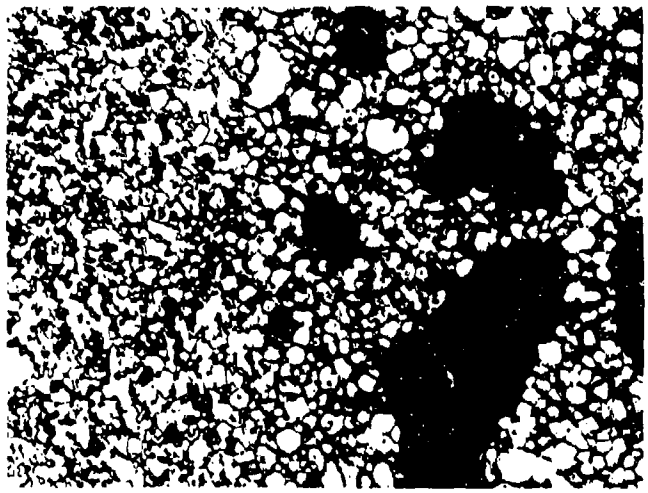

Plate No. 1-7416

Etched with 10 Glycerine 5$HNO_3$ 3HF X250

Figure 82. Arc Plasma Test $ZrB_2$ + 20 v/o SiC(A-8)-4M, Hot Surface.

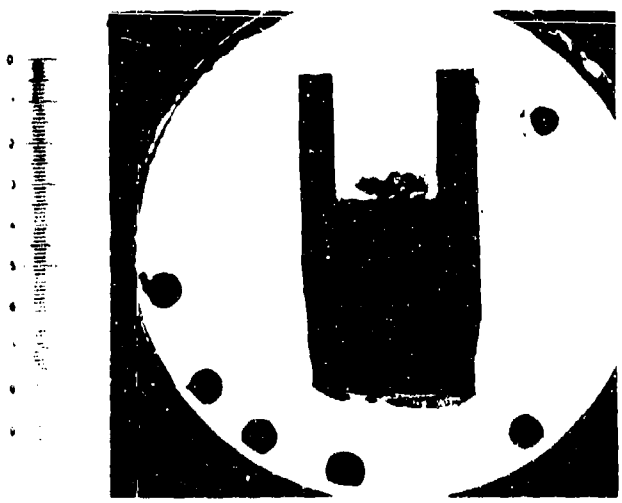

Plate No.
2-0225

X2.55

Figure 83. Arc Plasma Test $ZrB_{2.1}$+20%SiC(A-8)-17M, Surface Temperature 4880°F, Exposure Time 1800 Seconds, Stagnation Pressure 1.01 Atm., Stagnation Enthalpy 5700 BTU/lb, Cold Wall Heat Flux 503 BTU/ft$^2$sec, Initial Length 604 Mils, Final Length 494 Mils, Recession Depth 110 Mils. Hot Face Down. One Inch Scale.

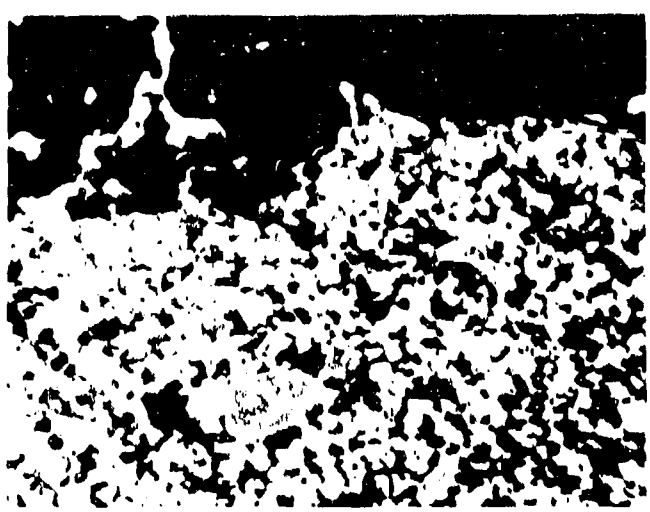

Plate No.
2-0686

Etched with 10 Glycerine
5HNO$_3$3HF

X250

Figure 84. Arc Plasma Test $ZrB_{2.1}$+20%SiC(A-8)-17M, Hot Interface at Top.

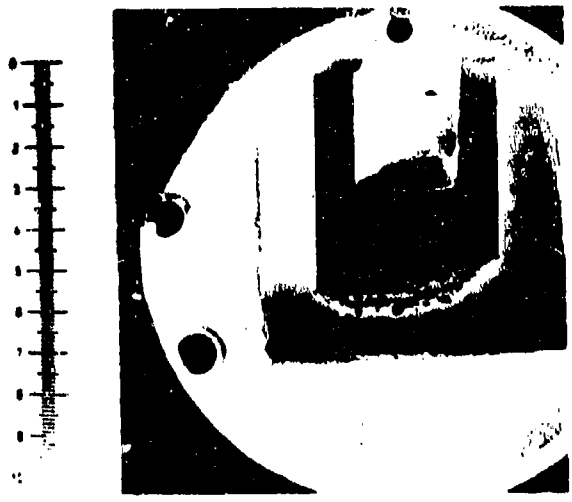

Plate No.
2-0237

X2.55

Figure 85. Arc Plasma Test $ZrB_{2.1}$+20%SiC(A-8)-21R, Surface Temperature 5280°F, Exposure Time 433 Seconds, Stagnation Pressure 0.095 Atm., Stagnation Enthalpy 10300 BTU/lb., Cold Wall Heat Flux 575 BTU/$ft^2$sec., Initial Length 838 Mils, Final Length 271 Mils. Hot Face Down. One Inch Scale.

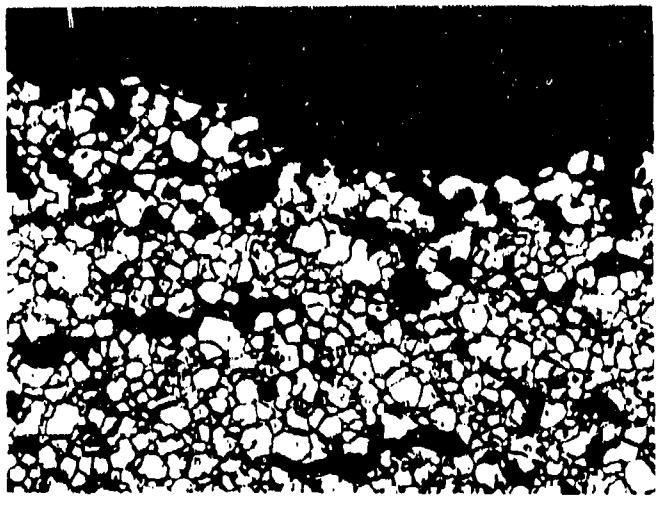

Plate No.
2-0238

Etched with 10 Glycerine
$5HNO_3 3HF$ X250

Figure 86. Arc Plasma Test $ZrB_{2.1}$+20%SiC(A-8)-21R, Hot Interface at Top.

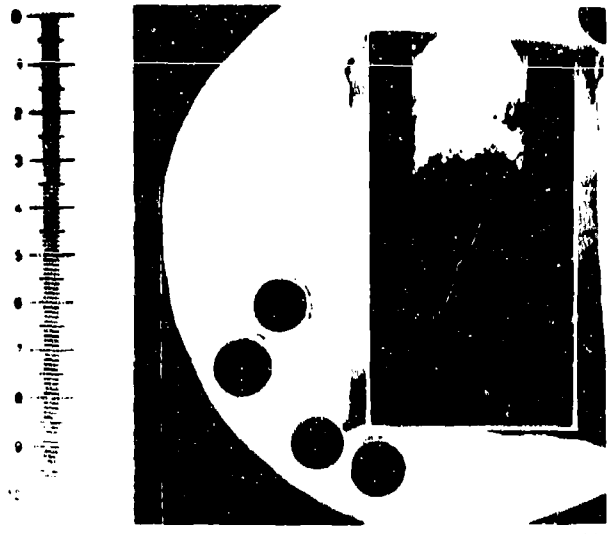

Plate No.
2-0648

X 2.95

Figure 87. Arc Plasma Test $ZrB_{2.1}$+20%SiC(A-8)-34R, Surface Temperature 4265°F, Exposure Time 1800 Seconds, Stagnation Pressure 0.063 Atm., Stagnation Enthalpy 10160 BTU/lb, Cold Wall Heat Flux 480 BTU/$ft^2$sec, Initial Length 503 Mils, Final Length 496 Mils, Total Recession 7 Mils. Hot Face Down. One Inch Scale.

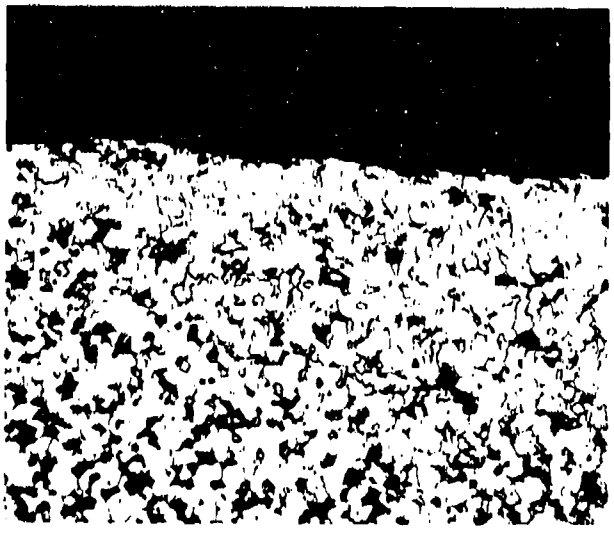

Plate No.
2-0687

Etched with 10 Glycerine
$5HNO_3$3HF

X250

Figure 88. Arc Plasma Test $ZrB_{2.1}$+20%SiC(A-8)-34R. Hot Interface at Top.

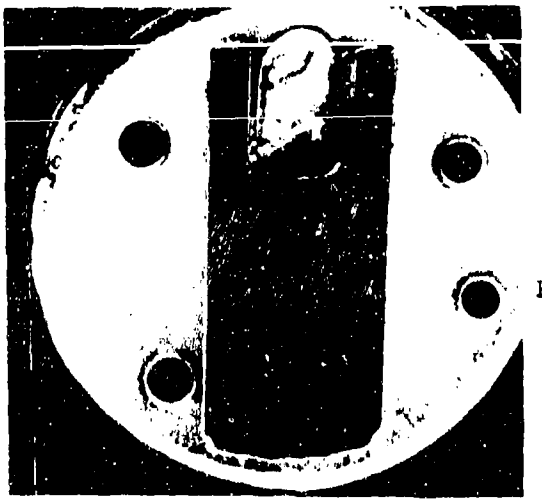

Plate No. 2-0222

X2.50

Figure 89. Arc Plasma Test $ZrB_{2.1}$ +20v/o SiC(A-8)-15M Average Surface Temperature 4350°F, Exposure Time 7200 Seconds, (4 cyclic exposure each of 1800 seconds) Stagnation Pressure 1.00 Atm. Stagnation Enthalpy 5000 BTU/lb, Cold Wall Heat Flux 385 BTU/$ft^2$sec, 26 Mils Recession, Hot Face Down. One Inch Scale.

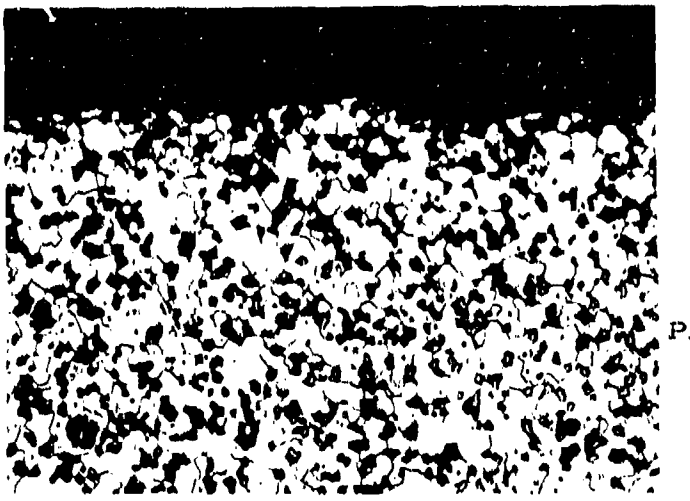

Plate No. 2-0223

Etched with 10 Glycerine 5$HNO_3$ 3HF X 250

Figure 90. Arc Plasma Test $ZrB_{2.1}$ +20v/o SiC(A-8)-15M, Hot Surface.

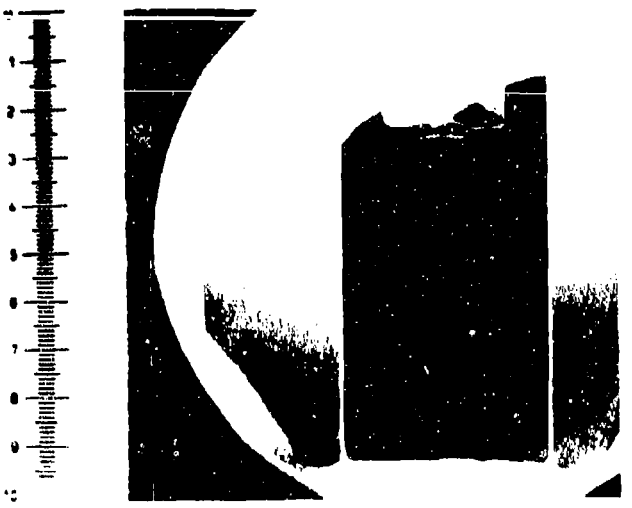

Plate No. 2-0683

X2.95

Figure 91. Arc Plasma Test $ZrB_{2.1}$+20v/o SiC(A-8)-16R Average Surface Temperature 4270°F, Exposure Time 7200 Seconds, (4 cyclic exposures, each of 1800 seconds) Stagnation Pressure 0.159 Atm. Stagnation Enthalpy 7000 BTU/lb, Cold Wall Heat Flux 450 BTU/$ft^2$sec, 27 Mils Recession, Hot Face Down. One Inch Scale.

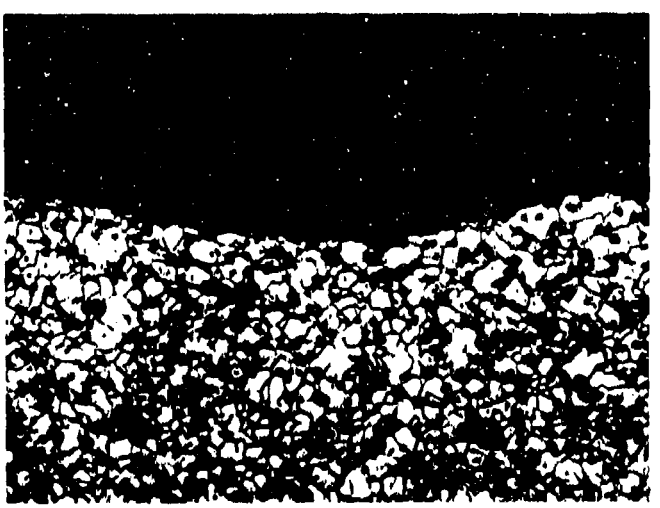

Plate No. 2-0684

Etched with 10 Glycerine 5$HNO_3$ 3HF X250

Figure 92. Arc Plasma Test $ZrB_{2.1}$+20v/o SiC(A-8)-16R, Hot Surface.

Plate No. 1-6592

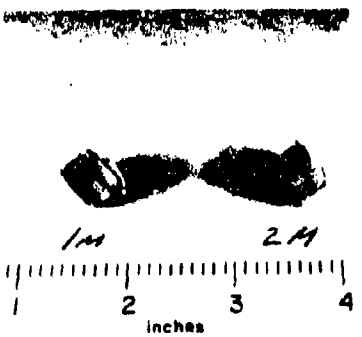


Plate No. 1-9528

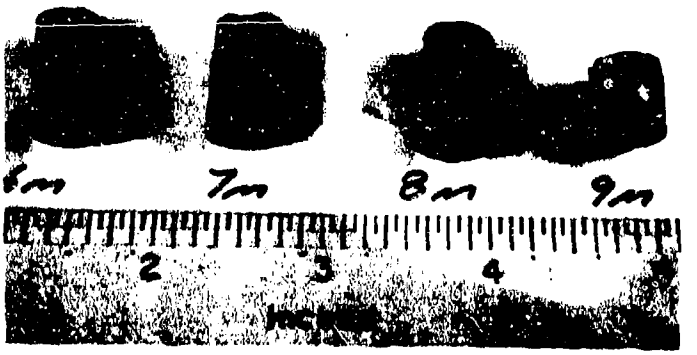


Plate No. 1-9529

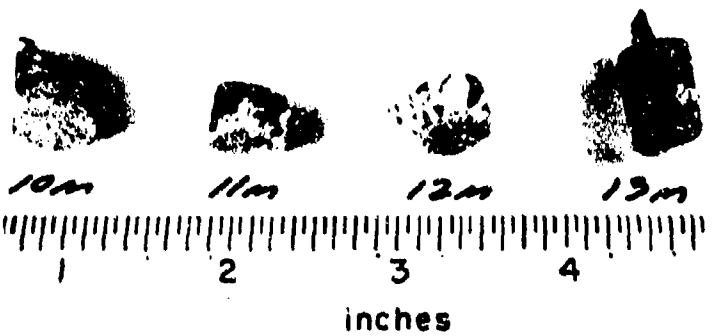


Plate No. 1-7404

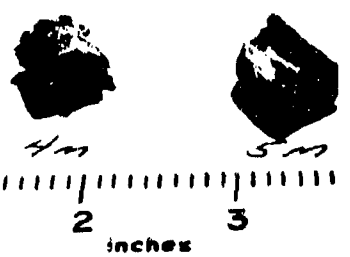


Plate No. 1-9523

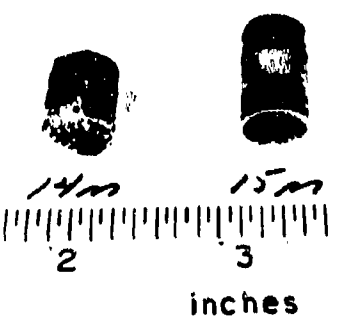


Figure 93. Post Exposure Photographs of Arc Plasma Tests $HfB_2$+ 35%SiC(A-9)-1M, 2M, 4M, 5M, 6M, 7M, 8M, 9M, 10M, 11M, 12M, 13M, 14M and 15M.

X2.75

Plate No. 1-7408

Figure 94. Arc Plasma Test $HfB_{2.1}$ + 35 v/o SiC(A-9)-5M, Surface Temperature 3540°F, Exposure Time 1800 Seconds, Stagnation Pressure 1.07 Atm, Stagnation Enthalpy 3665 BTU/lb, Cold Wall Heat Flux 530 BTU/ft$^2$ sec, 50 Mils Recession, Hot Face Down. One Inch Scale.

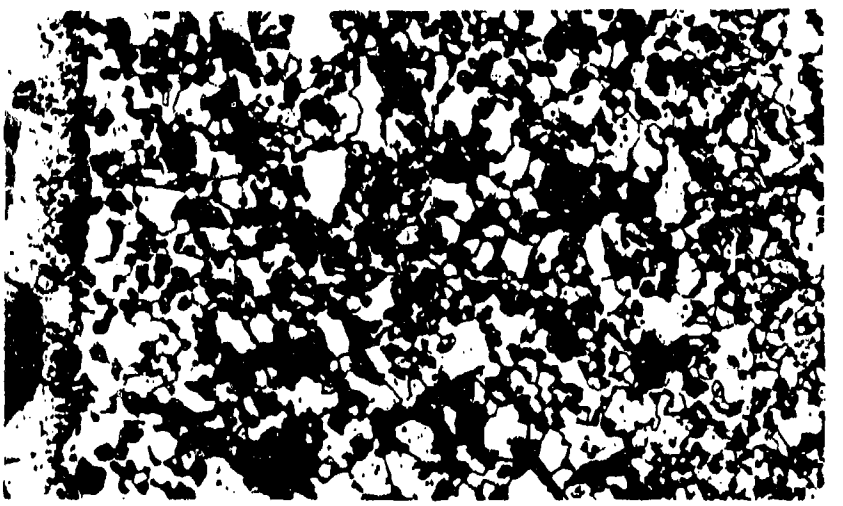

Etched with 10 Glycerine $5HNO_3$ 3HF X250

Plate No. 1-7409

Figure 95. Arc Plasma Test $HfB_{2.1}$ + 35 v/o SiC(A-9)-5M, Hot Surface at Left, Depletion Zone in Center, Matrix at Right.

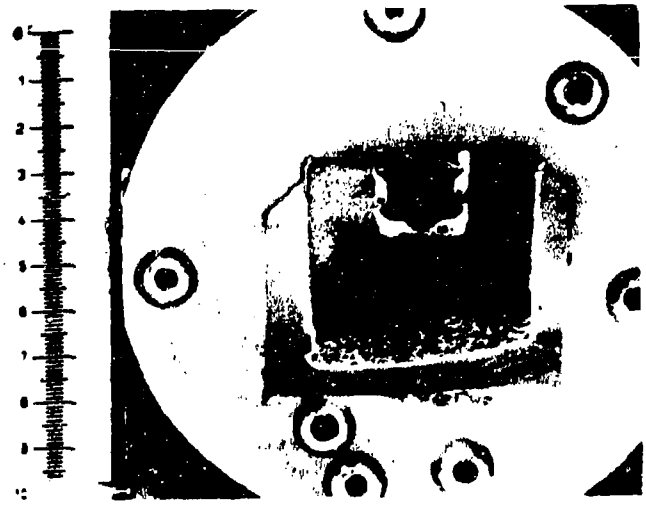

Plate No. 1-6598

X2.75

Figure 96. Arc Plasma Test $HfB_{2.1}$ + 35 v/o SiC(A-9)-2M, Surface Temperature 5840°F, Exposure Time 133 Seconds, Stagnation Pressure 1.12 Atm. Stagnation Enthalpy 4700 BTU/lb, Cold Wall Heat Flux 730 BTU/$ft^2$ sec, 231 Mils Recession. Hot Face Down. One Inch Scale.

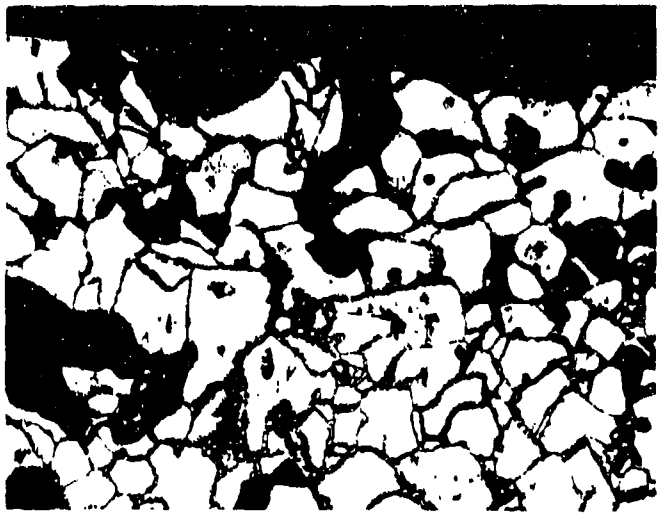

Plate No. 1-6599

Etched with 10 Glycerine 5$HNO_3$ 3HF X250

Figure 97. Arc Plasma Test $HfB_{2.1}$ + 35 v/o SiC(A-9)-2M, Hot Surface.

Plate No. 1-7418

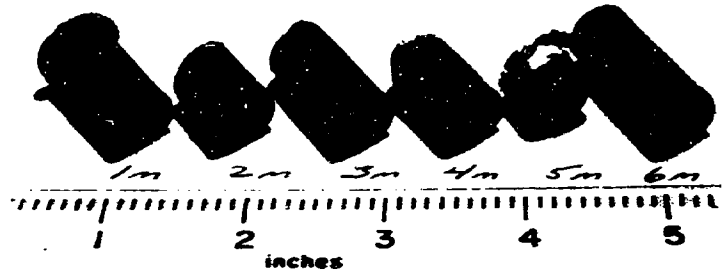


Plate No. 1-9516

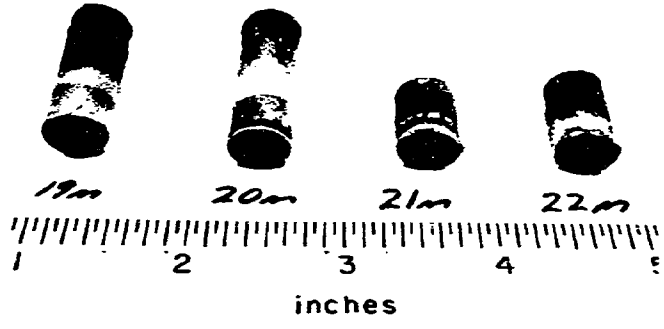


Plate No. 1-7640

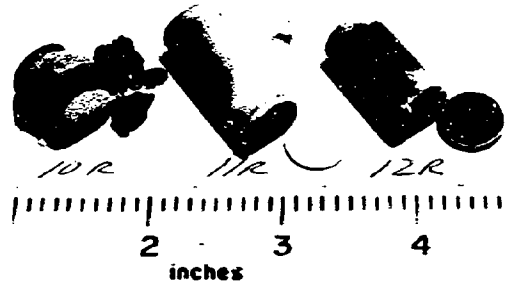


Plate No. 1-7629

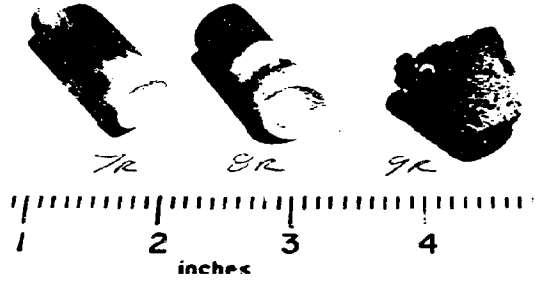


Plate No. 1-8770

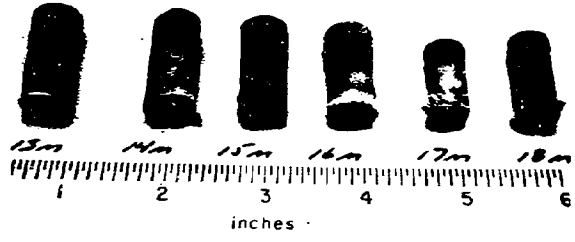


Figure 98. Post Exposure Photographs of Arc Plasma Tests $ZrB_2$+SiC+C(A-10)-10R, 11R, 12R, 7R, 8R, 9R, 1M, 2M, 3M, 4M, 5M, 6M, 13M, 14M, 15M, 16M, 17M, 18M, 19M, 20M, 21M and 22M.

Plate No. 2-0670

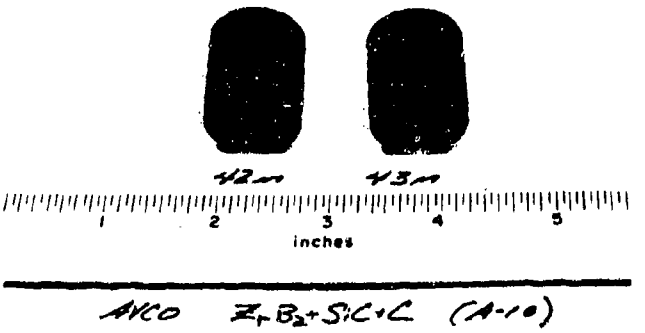


Plate No. 2-0705

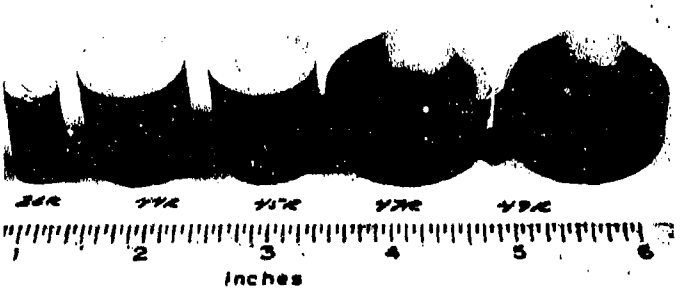


Figure 99. Post Exposure Photographs of Arc Plasma Tests $ZrB_2$+SiC+C(A-10)-42M, 43M, 26R, 44R, 45R, 47R and 49R.

Plate No. 2-0594

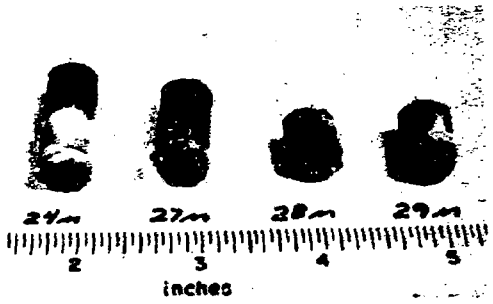


Plate No. 2-0255


Plate No. 2-0607

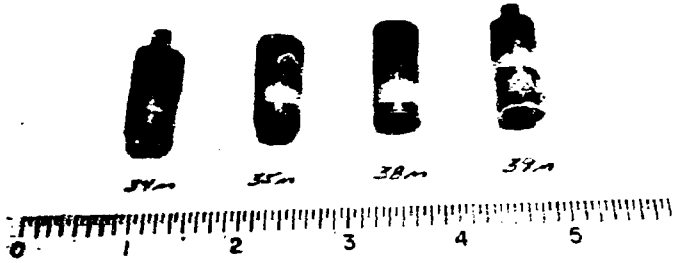


Plate No. 2-0671

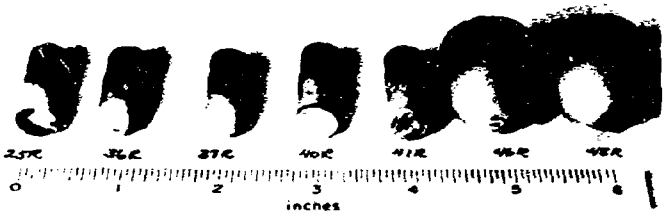


Figure 100. Post Exposure Photographs of Arc Plasma Tests $ZrB_2$+SiC+C(A-10)-24M, 27M, 28M, 29M, 30R, 31R, 32R, 33R, 34M, 35M, 38M, 39M, 23M, 25R, 36R. 37R, 40R, 41R, 46R and 48R.

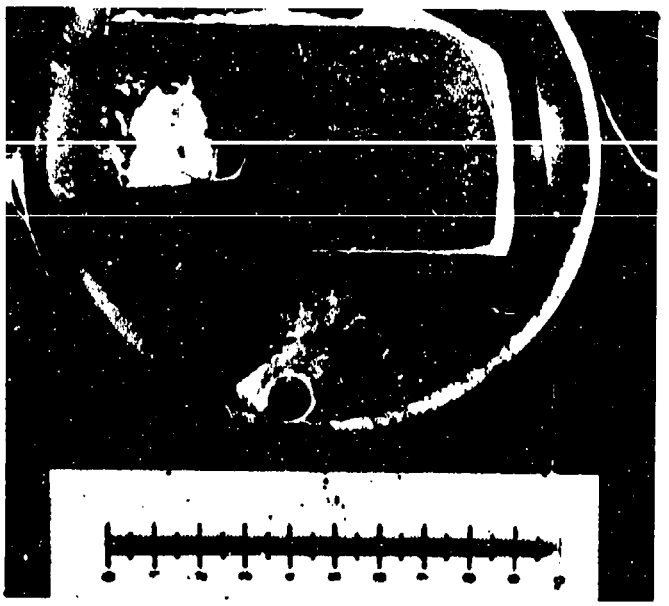

Plate No. 1-7428

X2.75

Figure 101. Arc Plasma Test $ZrB_2$+SiC+C(A-10)-4M, Surface Temperature 4870°F, Exposure Time 1800 Seconds, Stagnation Pressure 1.06 Atm, Stagnation Enthalpy 4075 BTU/lb, Cold Wall Heat Flux 620 BTU/$ft^2$sec, Initial Length 850 Mil, Final Length 504 Mil. Hot Face at Right. One Inch Scale.

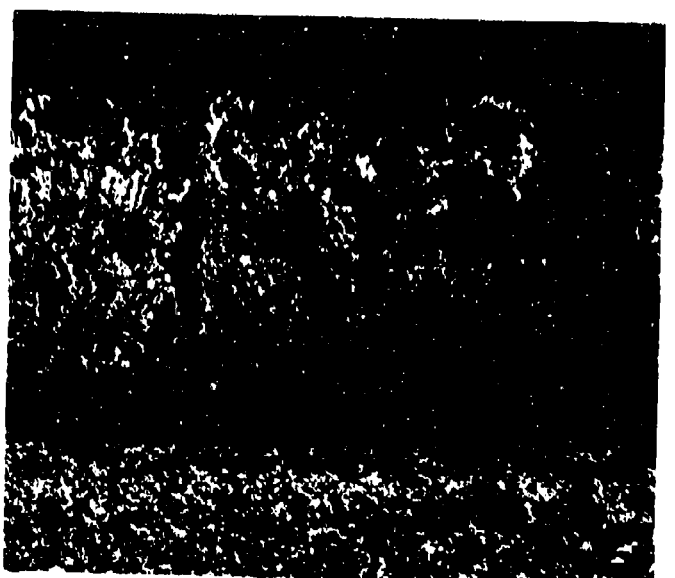

Plate No. 1-7429A

Unetched

X75

Figure 102. $ZrB_2$+SiC+C(A-10)-4M. Interface of Oxide (Top) and Matrix.

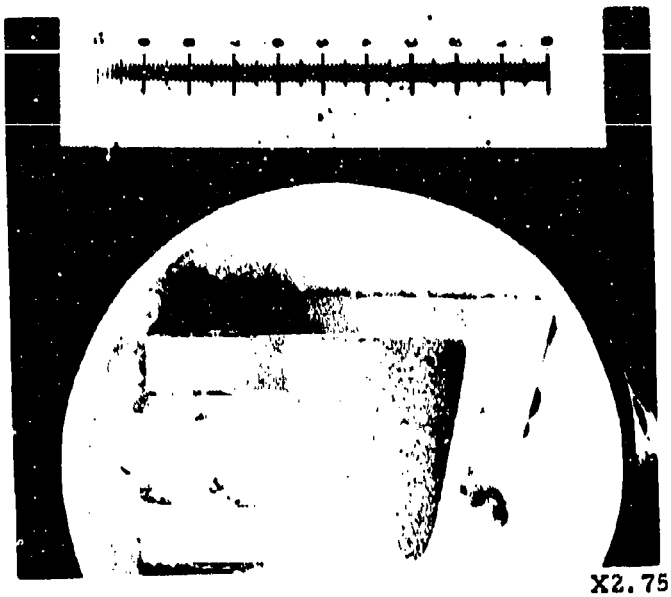

Plate No. 1-7422

X2.75

Figure 103. Arc Plasma Test $ZrB_2$+SiC+C(A-10)-2M, Surface Temperature 5110°F, Exposure Time 182 Seconds, Stagnation Pressure 1.07 Atm, Stagnation Enthalpy 4755 BTU/lb, Cold Wall Heat Flux 665 BTU/ft$^2$sec, Initial Length 848 Mil, Final Length 346 Mil, Hot Face at Right, One Inch Scale.

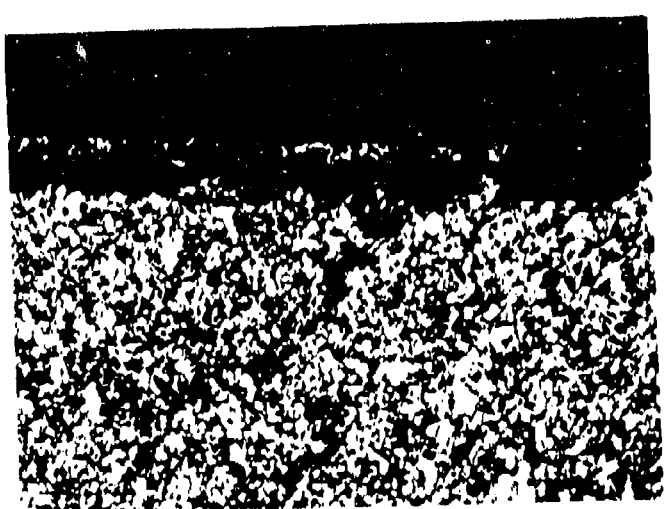

Plate No. 1-7423

Unetched

X250

Figure 104. $ZrB_2$+SiC+C(A-10)-2M. Melted Interface.

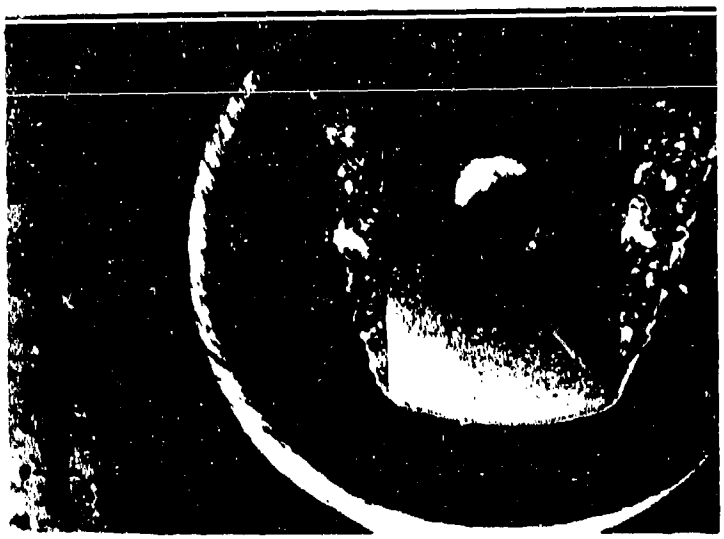

Plate No. 1-7637

X3

Figure 105. Arc Plasma Test $ZrB_2$+SiC+C(A-10)-9R, Surface Temperature 5065°F, Exposure Time 32 Seconds, Stagnation Pressure 0.222 Atm, Stagnation Enthalpy 10260 BTU/lb, Cold Wall Heat Flux 1010 BTU/ft$^2$sec, Initial Length 852 Mil, Final Length 277 Mil. Hot Face at Bottom, One Inch Scale. Melted Material on Sides.

Plate No. 1-7638

Unetched X250

Figure 106. $ZrB_2$ + SiC+C(A-10)-9R. Melted Interface.

Plate No. 1-7644

X3

Figure 107. Arc Plasma Test $ZrB_2$+SiC+C(A-10)-11R, Surface Temperature 5075°F, Exposure Time 1800 Seconds, Stagnation Pressure 0.084 Atm, Stagnation Enthalpy 10540 BTU/lb, Cold Wall Heat Flux 696 BTU/ft$^2$ sec, Initial Length 852 Mil, Final Length 816 Mils. Hot Face at Right. One Inch Scale. Rear Broke on Removal after Test.

Plate No. 1-7645

Unetched X250

Figure 108. Arc Plasma Test $ZrB_2$ + SiC+C(A-10)-11R. Hot Interface.

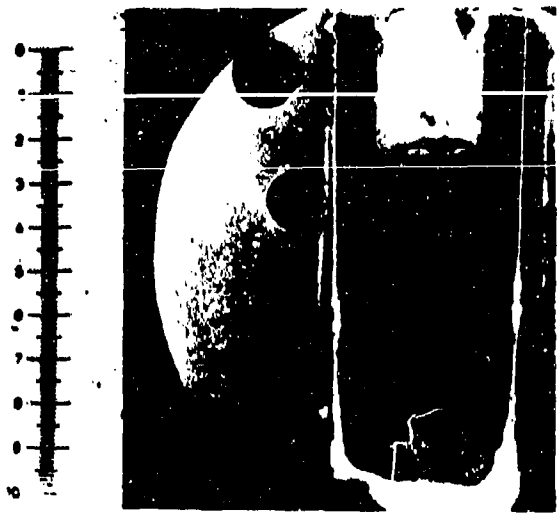

Plate No. 2-0595

X2.70

Figure 109. Arc Plasma Test $ZrB_2$+SiC+C(A-10)-24M Average Surface Temperature 4415°F, Exposure Time 21,600 Seconds (12 cyclic exposures each of 1800 seconds), Stagnation Pressure 1.02 Atm. Stagnation Enthalpy 4250 BTU/lb, Cold Wall Heat Flux 400 BTU/$ft^2$sec, 104 Mils Recession, Hot Face Down . One Inch Scale.

Plate No. 2-0596

Unetched X 250

Figure 110. Arc Plasma Test $ZrB_2$+SiC+C(A-10)-24M,Hot Surface.

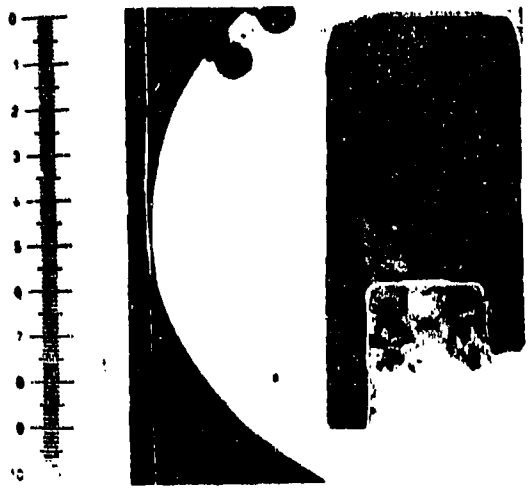

Plate No.
2-0688

Figure 111. Arc Plasma Test $ZrB_2$+SiC+C(A-10)-26R. Average Surface Temperature 4650°F, Exposure Time 18951 Seconds (11 Cyclic Exposures Each of Approximately 1800 Seconds), Stagnation Pressure 0.238 Atm., Stagnation Enthalpy 7750 BTU/lb, Cold Wall Heat Flux 460 BTU/ft$^2$sec, 83 Mils Recession, Hot Face Up. One Inch Scale.

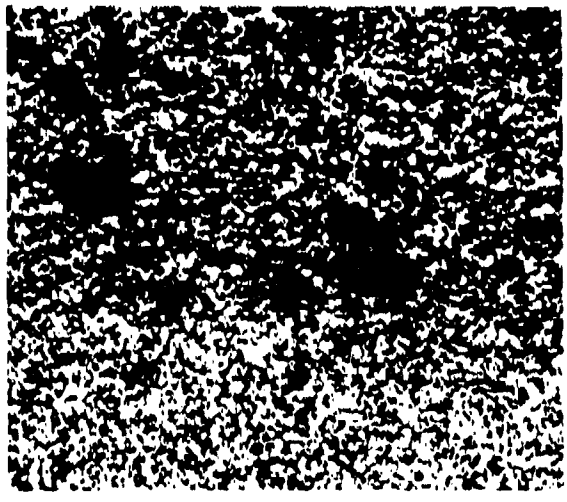

Plate No.
2-0689

Unetched X250

Figure 112. Arc Plasma Test $ZrB_2$+SiC+C(A-10)-26R, Hot Surface.

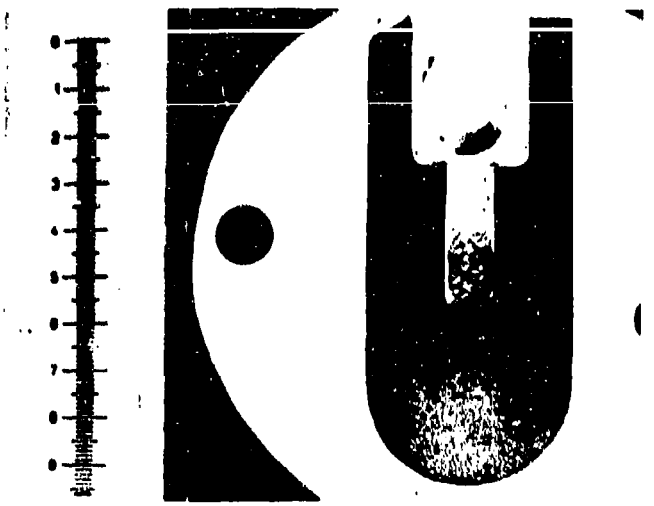

Plate No. 2-0690

X2.88

Figure 113. Arc Plasma Test $ZrB_2$+SiC+C(A-10)-37RH Surface Temperature 3235°F, Exposure Time 1800 Seconds, Stagnation Pressure 0.144 Atm. Stagnation Enthalpy 7710 BTU/lb, Cold Wall Heat Flux 482 BTU/$ft^2$sec, 3 Mils Recession, Hot Face Down. One Inch Scale.

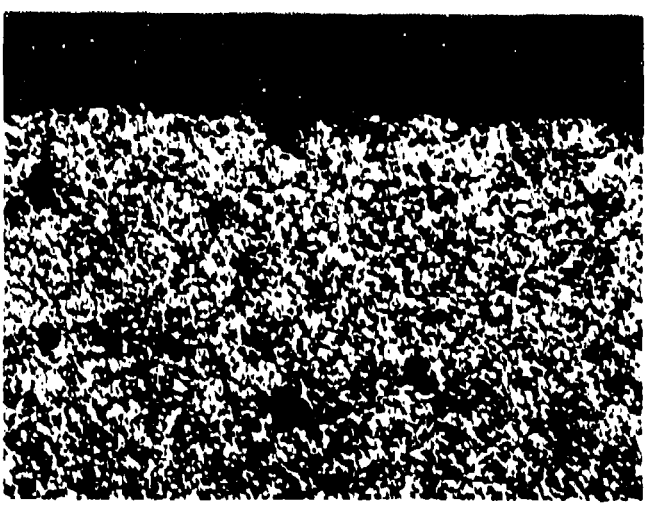

Plate No. 2-0691

Unetched X 250

Figure 114. Arc Plasma Test $ZrB_2$+SiC+C(A-10)-37RH, Hot Surface.

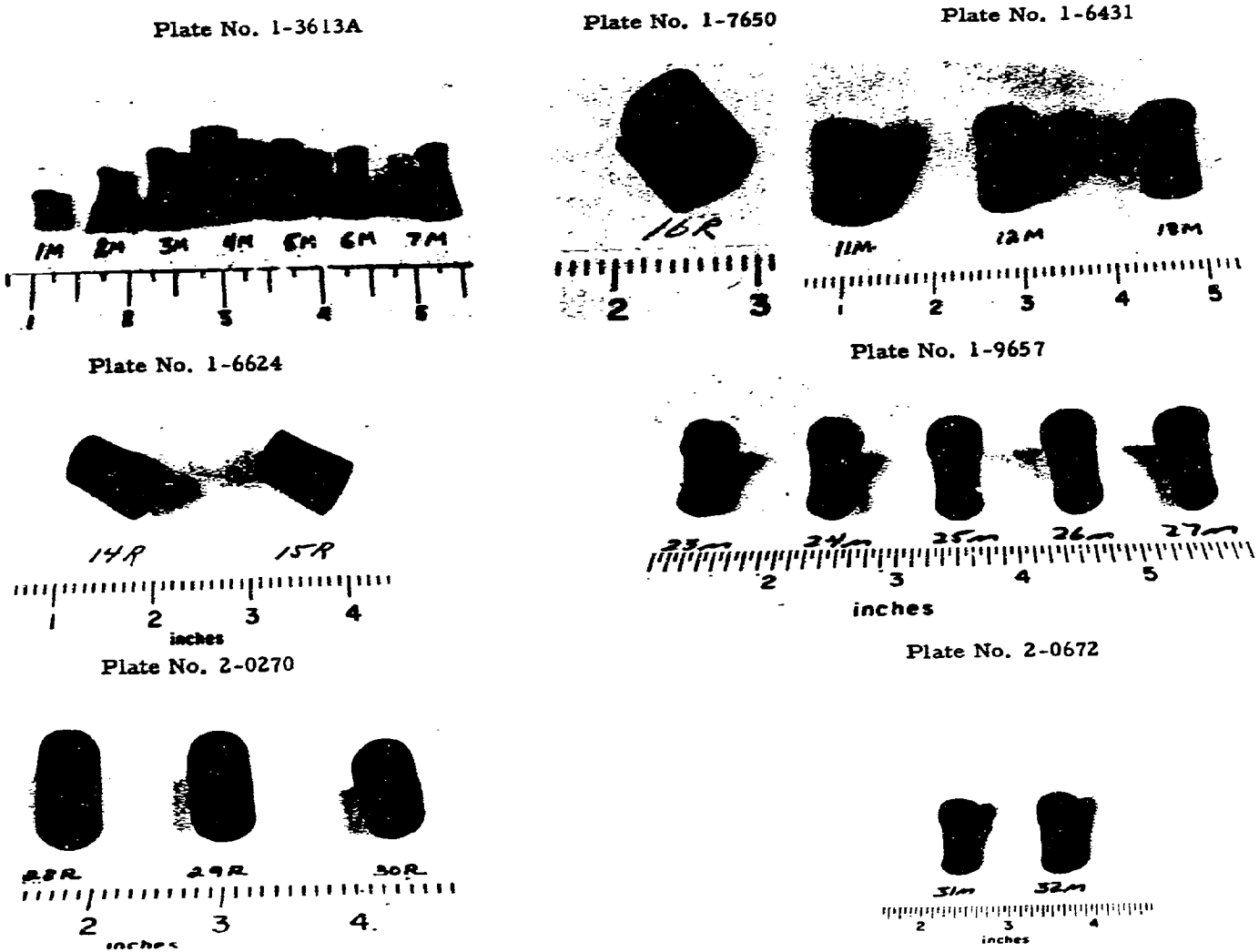


Figure 115. Post Exposure Photographs of Arc Plasma Tests RVA(B-5)-1M, 2M, 3M, 4M, 5M, 6M, 7M, 16R, 11M, 12M, 13M, 14R, 15R, 23M, 24M, 25M, 26M, 27M, 28R, 29R, 30R, 31M, 32M.

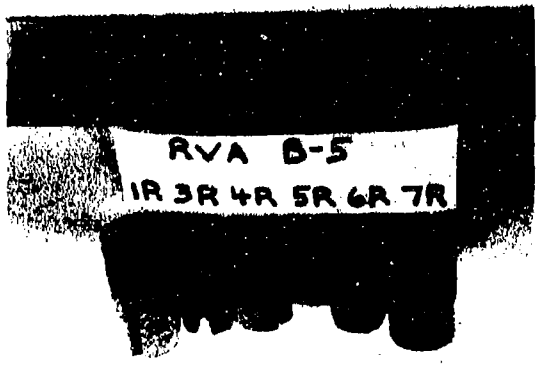


Plate 1-3429

Figure 116. Post Exposure Photographs of Arc Plasma Tests RVA (B-5)-1R, 3R, 4R, 5R and 7R. Hot Face is Pointing Up. Samples 1R and 3R Show Exposed Thermocouple Holes While 5R Shows Sting Hole Exposed Due to Side Ablation.

Plate 1-3432

X3.1

Figure 117. Post Exposure Photograph of Arc Plasma Test RVA (B-5)-2R Hot Face is Pointing Up.

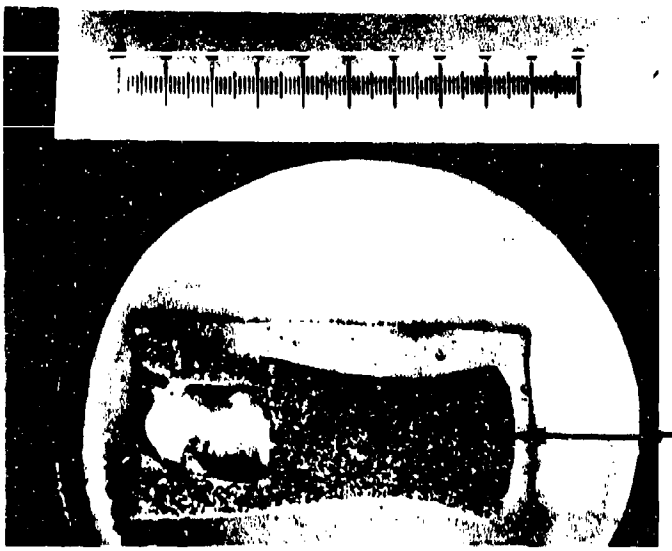


Plate 1-3697

X3

Figure 118. Arc Plasma Test RVA(B-5)-5M, Surface Temperature 5720°F. Exposure Time 58 Seconds, Stagnation Pressure 1 Atm, Stagnation Enthalpy 6455 BTU/lb, Cold Wall Heat Flux 1030 BTU/ft$^2$sec, Initial Length 1028 Mils, Final Length 830 Mils, Hot Face at Right. One Inch Scale. Side Ablation is Illustrated.

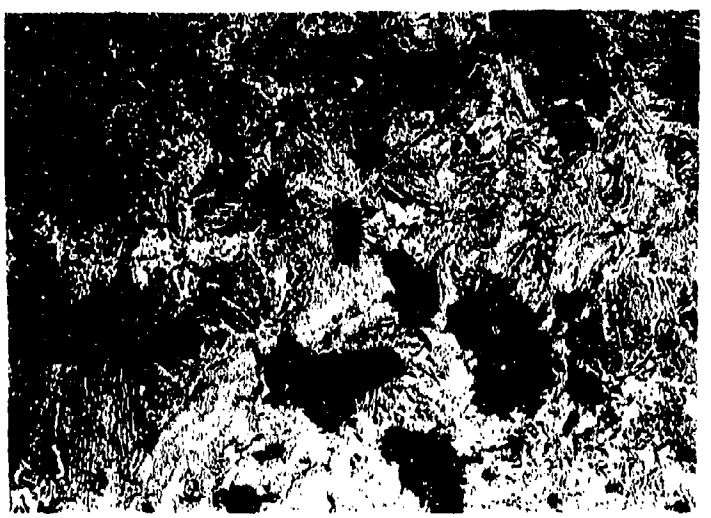

Plate 1-3619

X150

Figure 119. Arc Plasma Test RVA(B-5)-5M, Matrix Area. Little Difference Noted between Interface and Matrix.

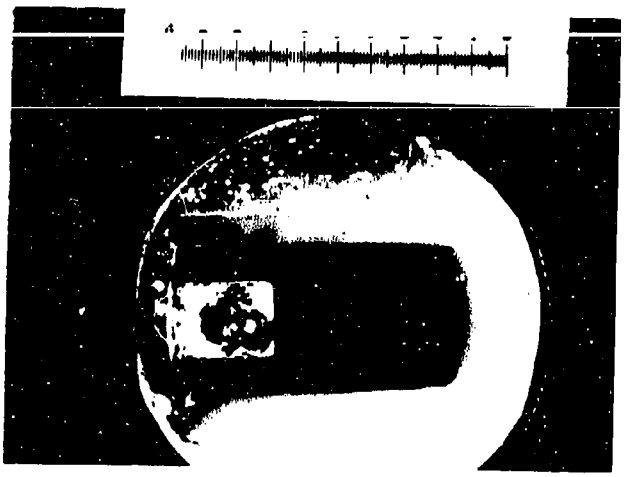

Plate 1

X2.1

Figure 120. Arc Plasma Test RVA(B-5)-7R, Surface Temperature 5430°F, Exposure Time 108 Seconds, Stagnation Pressure 0.299 Atm, Stagnation Enthalpy 10950 BTU/lb, Cold Wall Heat Flux 979 BTU/ft$^2$sec. Initial Length 1044 Mils, Final Length 839 Mils. Hot Face at Right. One Inch Scale.

Plate 1

X150

Figure 121. Arc Plasma Test RVA(B-5)-7R, Matrix Area. Little Difference Noted between Interface and Matrix.


Plate 1-3630-A

Figure 122. Post Exposure Photographs of Arc Plasma Tests PG(B-6)-1M, 2M, 3M,4M, 5M, 6M, 7M, "C" Axis Perpendicular to Arc. Hot Face Pointing Up. One Inch Scale. Samples 3M and 7M Show "C" Plane Delaminations.

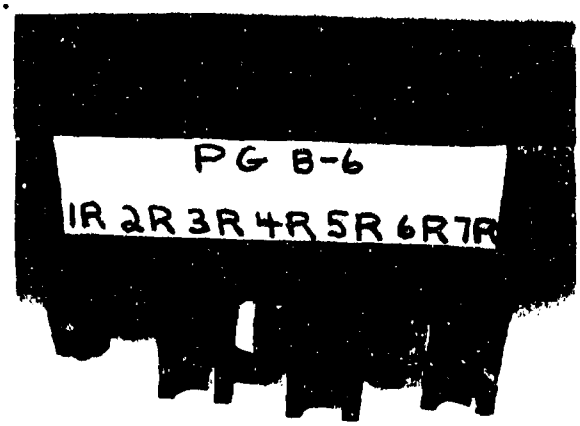


Plate 1-3446

Figure 123. Post Exposure Photographs of Arc Plasma Tests PG (B-6)-1R, 2R, 3R, 4R, 5R, 6R and 7R, "C" Axis Perpendicular to Arc. Hot Face Pointing Up. One Inch Scale. Samples 3R, 5R and 7R Show "C" Plane Delaminations. Sample PG(B-6)-5R Delaminated on "C" Plane During Installation Due to Interference Between Stinghole and Sting.

Plate No. 1-4270

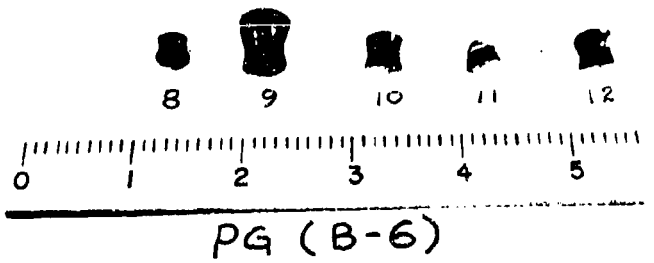


Figure 124. Post Exposure Photographs of Arc Plasma Tests PG (B-6)-8M, 9M, 10M, 11M and 12M, "C" Axis Parallel to Arc. Hot Face Pointing Down. One Inch Scale.

Plate No. 1-4271

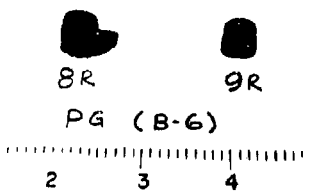


Plate No. 1-4932

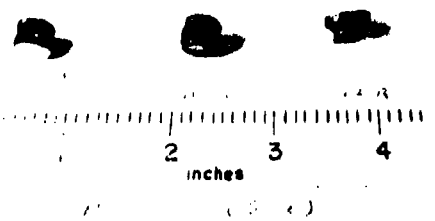


Figure 125. Post Exposure Photographs of Arc Plasma Tests PG (B-6)-8R, 9R, 10R, 11R and 12R, "C" Axis Parallel to Arc. Hot Face Pointing Down in All Cases. One Inch Scale.

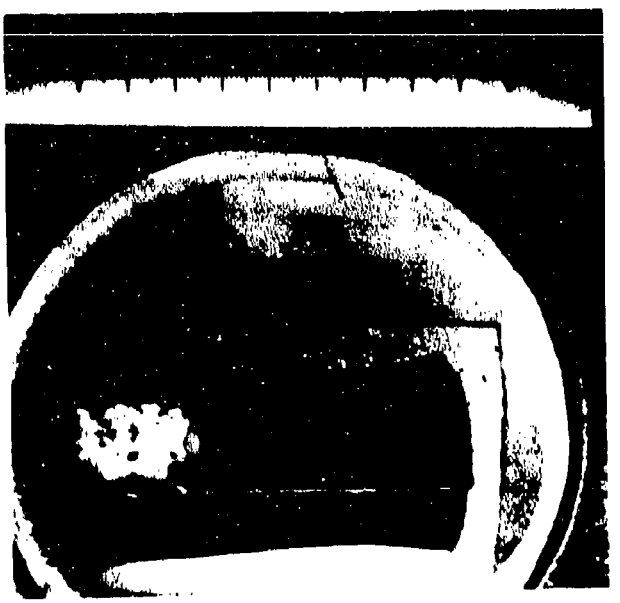

Plate 1-3634

X3

Figure 126. Arc Plasma Test PC(B-6)-3M, "C" Axis Perpendicular to Arc. Sample Delaminated on "C" Plane after Exposure. Surface Temperature 4530°F, Exposure Time 61 Seconds, Stagnation Pressure 1 Atm, Stagnation Enthalpy 4580 BTU/lb, Cold Wall Heat Flux 670 BTU/ft$^2$sec, Initial Length 999 Mils, Final Length 856 Mils. Hot Face at Right. One Inch Scale.

Plate 1-3635

X50

Figure 127. Arc Plasma Test PC(B-6)-3M, Matrix Area. Little Difference Noted between Matrix and Interface Areas.

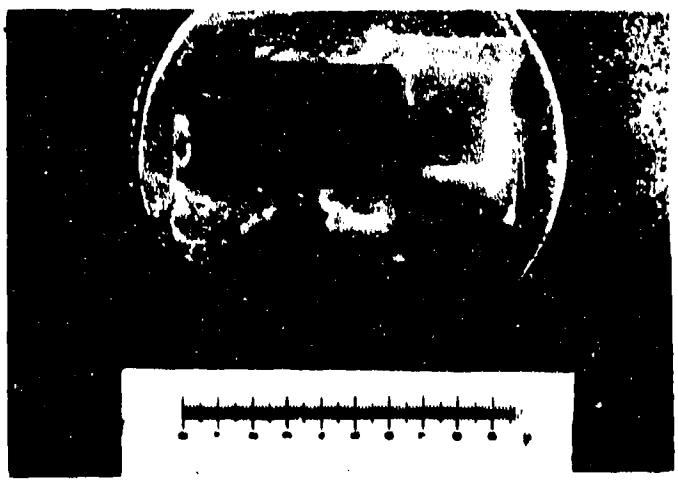

Plate 1-3453

Figure 128. Arc Plasma Test PG(B-6)-4R, "C" Axis Perpendicular to Arc. Surface Temperature 4650°F, Exposure Time 300 Seconds, Stagnation Pressure 0.187 atm, Stagnation Enthalpy 3440 BTU/lb, Cold Wall Heat Flux 852 BTU/ft$^2$, Initial Length 1084 Mils, Final Length 628 Mils. Hot Face at Right. One Inch Scale.

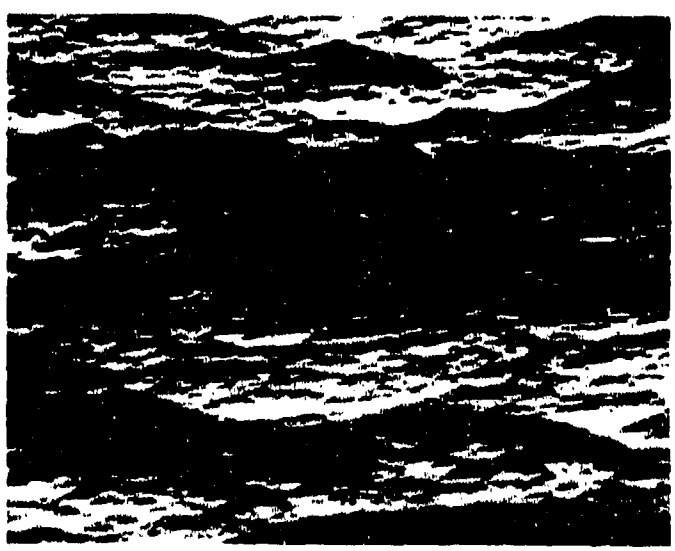

Plate 1-3454

Figure 129. Arc Plasma Test PG (B-6)-4R, Matrix Area. Little Difference Noted between Interface and Matrix Areas.

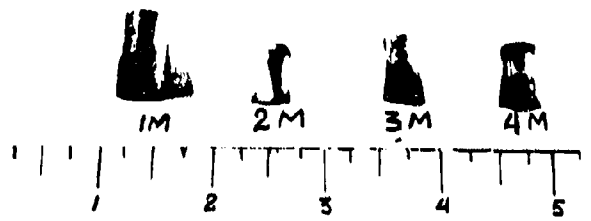


Plate 1-3622

Figure 130. Post Exposure Photographs of Arc Plasma Tests BPG (B-7)-1M, 2M, 3M and 4M, "C" Axis Perpendicular to Arc. Hot Face Pointing Up. One Inch Scale. Sample 3M Delaminated on "C" Plane, While Samples 1M and 3M show Incipient Delaminations.

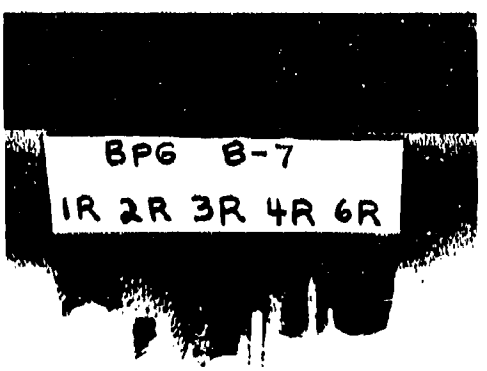


Plate 1-3416

Figure 131. Post Exposure Photographs of Arc Plasma Tests BPG (B-7)-1R, 2R, 3R, 4R and 6R, "C" Axis Perpendicular to Arc. Hot Face Pointing Up. One Inch Scale. Samples 1R and 2R Delaminated on "C" Plane During Test. Sample 3R, Showing Thermocouple Hole Delaminated on "C" Plane When Installed Due to Interference Fit of Sting and Tungsten Holder. Sample BPG (B-7)-5R Ablated Completely.

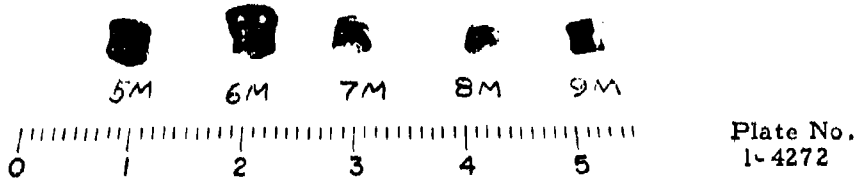


Figure 132. Post Exposure Photographs of Arc Plasma Tests BPG(B-7)-5M, 6M, 7M, 8M and 9M, "C" Axis Parallel to Arc. Hot Face Pointing Down. One Inch Scale.

Plate No. 1-4273 Plate No. 1-4274 Plate No. 1-4939

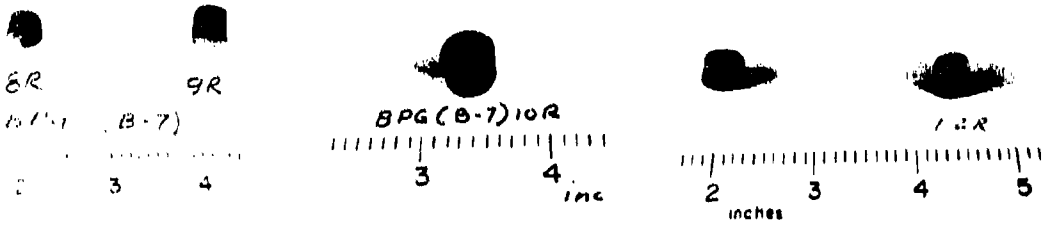


Figure 133. Post Exposure Photographs of Arc Plasma Tests BPG(B-7)-8R, 9R, 10R, 11R and 12R, "C" Axis Parallel to Arc. Hot Face Pointing Down except BPG(B-7)-10R, 11R and 12R Where It is Pointing Up. One Inch Scale.

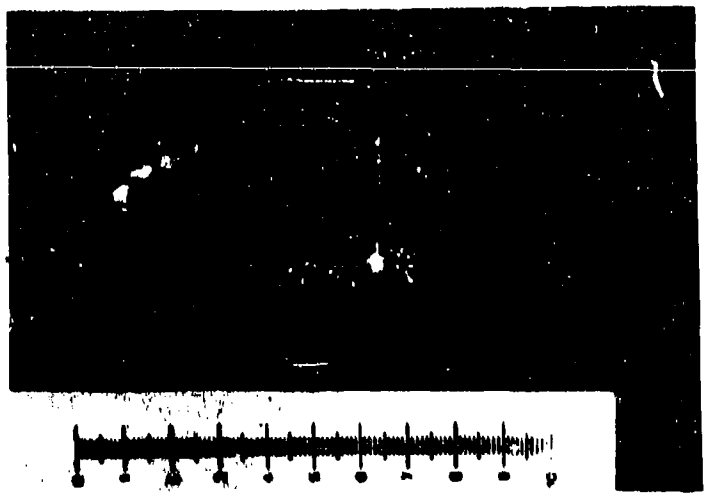

Plate 1-3701

X3

Figure 134. Arc Plasma Test BPG(B-7)-4M, "C" Axis Perpendicular to Arc. Incipient Delamination on "C" Plane. Side Ablation Present. Surface Temperature 4940°F, Exposure Time 75 Seconds, Stagnation Pressure 1 Atm, Stagnation Enthalpy 6500 BTU/lb, Cold Wall Heat Flux 760 BTU/ft$^2$sec. Initial Length 799 Mils, Final Length 575 Mils. Hot Face at Right. One Inch Scale.

Plate 1-3628

Figure 135. Arc Plasma Test BPG(B-7)-4M, Interface Area Showing Cracks Extending along "C" Plane.

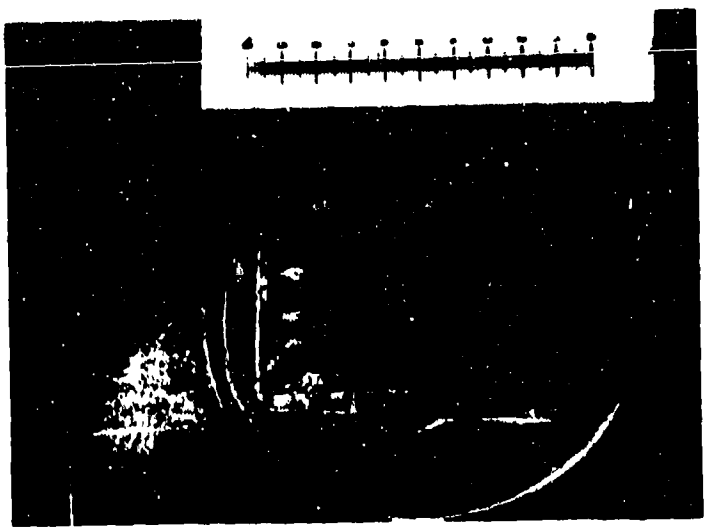

Plate 1-3427

Surface of
Hot Face

X2.1

Figure 136. Arc Plasma Test BPG(B-7)-6R, "C" Axis Perpendicular to Arc, Surface Temperature 3810°F, Exposure Time 600 Seconds, Stagnation Pressure 0.017 Atm, Stagnation Enthalpy 13890 BTU/lb, Cold Wall Heat Flux 321 BTU/ft²sec. Initial Length 785 Mils. Final Length 547 Mils. Hot Face at Right. One Inch Scale.

Plate 1-3428

X50

Figure 137. Arc Plasma Test BPG(B-7)-6R, Matrix Area. Little Difference between Interface and Matrix Areas.

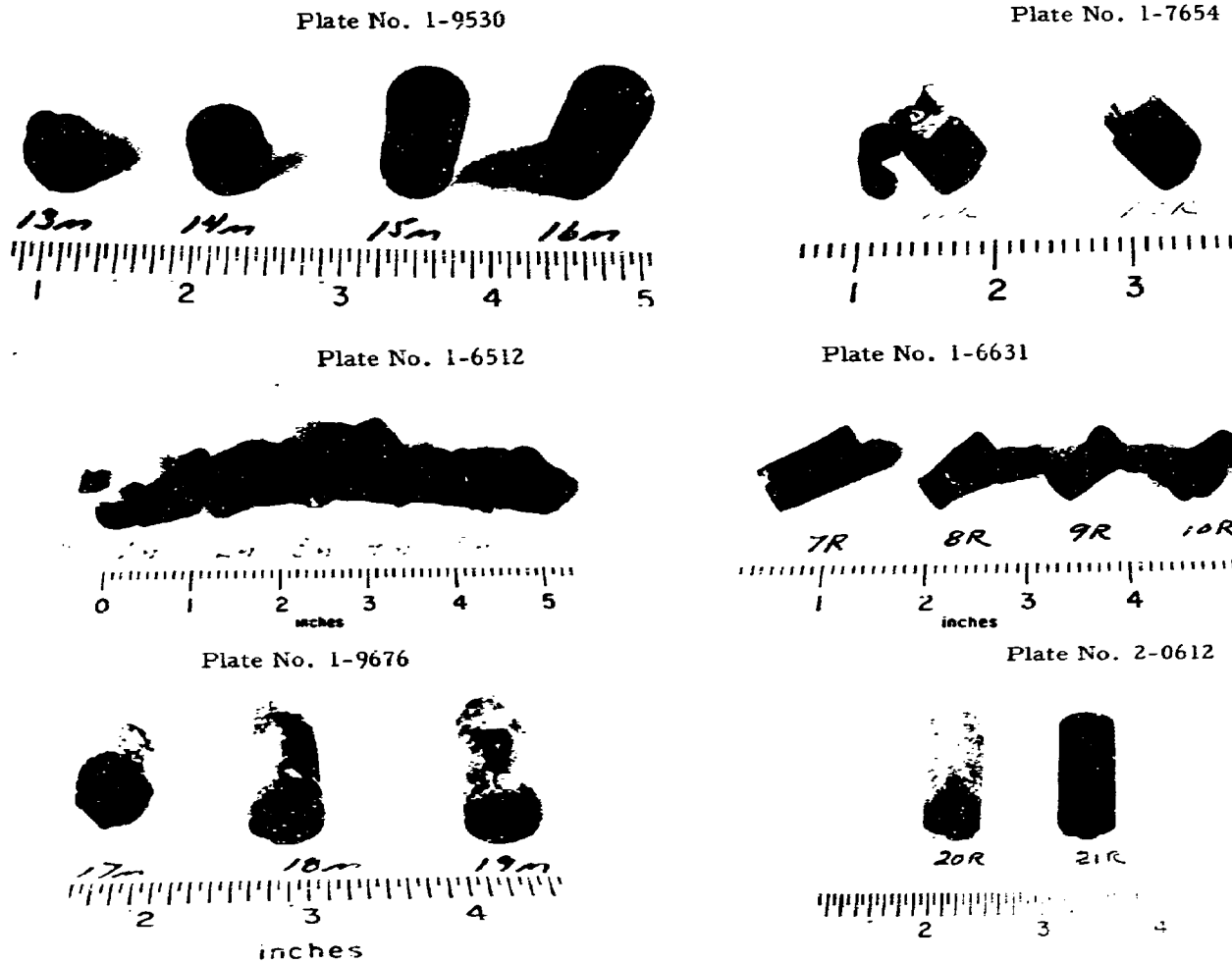


Figure 138. Post Exposure Photographs of Arc Plasma Tests Si/RVC(B-8)-1M, 2M, 3M, 4M, 5M, 6M, 7R 8R, 9R, 10R, 11R, 12R, 13M, 14M, 15M, 16M, 17M, 18M, 19M, 20R and 21R.

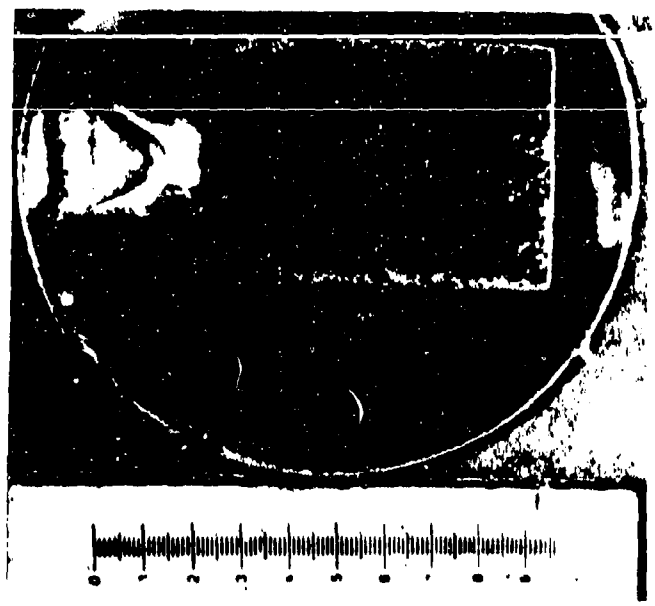

Plate No. 1-6632

X2.94

Figure 139. Arc Plasma Test Si/RVC(B-8)-7R, Surface Temperature 2740°F, Exposure Time 1800 Seconds, Stagnation Pressure 0.013 Atm, Stagnation Enthalpy 8850 BTU/lb, Cold Wall Heat Flux 210 BTU/ft$^2$sec, Initial Length 735 Mils, Final Length 714 Mils. Hot Face at Right. One Inch Scale.

Plate No. 1-6633

Unetched

X250

Figure 140. Arc Plasma Test Si/RVC(B-8)-7R, SiC Coating (Top) Did Not Fail.

Plate No. 1-6522

X2.69

Figure 141. Arc Plasma Test Si/RVC(B-8)-4M, Surface Temperature 3770°F, Exposure Time 240 Seconds, Stagnation Pressure 1.06 Atm, Stagnation Enthalpy 3270 BTU/lb, Cold Wall Heat Flux 475 BTU/ft$^2$sec, Intial Length 739 Mils, Final Length 727 Mils. Hot Face at Right. One Inch Scale.

Plate No. 1-6523

Unetched X250

Figure 142. Arc Plasma Test Si/RVC(B-8)-4M. SiC Coating (Top). Did Not Fail.

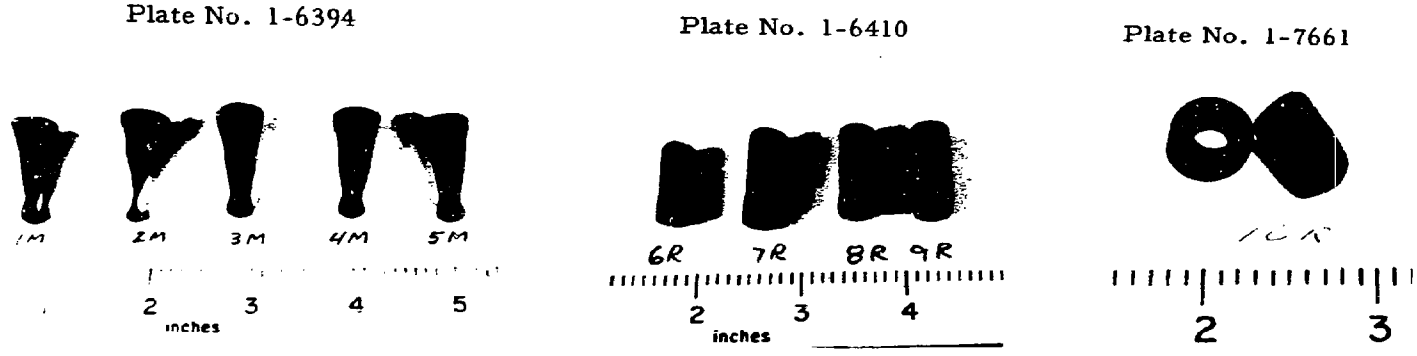




Figure 143. Post Exposure Photographs of Arc Plasma Tests PT0178(B-9)-1M, 2M, 3M, 4M, 5M, 6R, 7R, 8R, 9R and 10R.

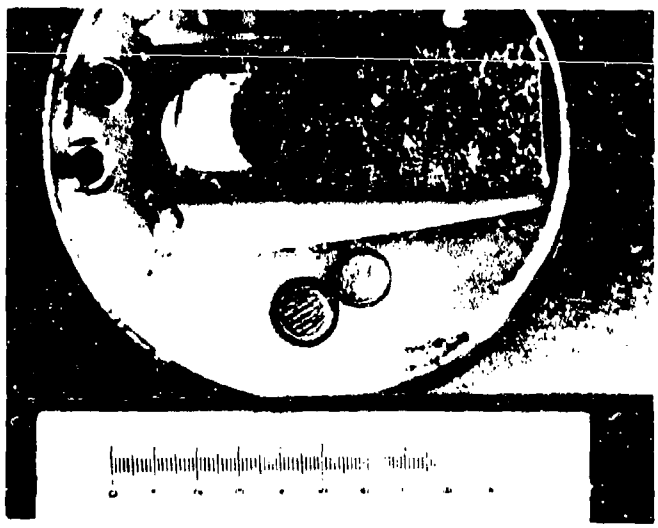

Plate No. 1-6420

X2.56

Figure 144. Arc Plasma Test PT0178(B-9)-9R, Surface Temperature 5040°F, Exposure Time 400 Seconds, Stagnation Pressure 0.030 Atm, Stagnation Enthalpy 16050 BTU/lb, Cold Wall Heat Flux 763 BTU/ft$^2$sec, Initial Length 1091 Mils, Final Length 675 Mils, Hot Face at Right. One Inch Scale.

Plate No. 1-6421

Unetched X250

Figure 145. Arc Plasma Test PT0178(B-9)-9R. Interface Showing Random Orientation of Fibers.

Plate No. 1-6407

X2.87

Figure 146. Arc Plasma Test PT0178(B-9)-5M, Surface Temperature 5985°F, Exposure Time 54 Seconds, Stagnation Pressure 1.07 Atm, Stagnation Enthalpy 5590 BTU/lb, Cold Wall Heat Flux 940 BTU/ft$^2$sec, Initial Length 1080 Mils, Final Length 801 Mils. Hot Face at Right. One Inch Scale.

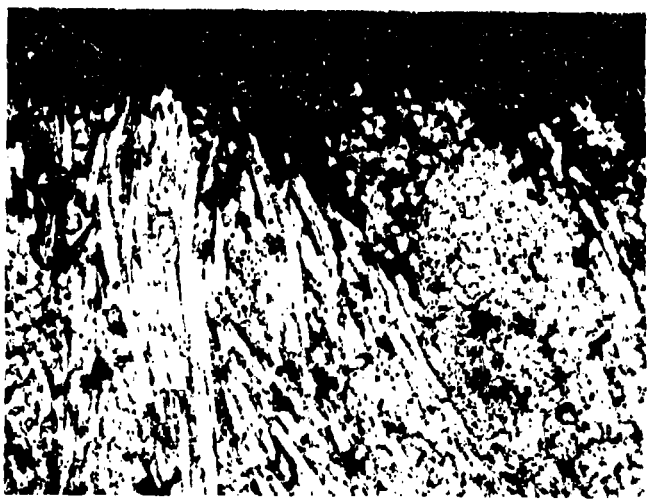

Plate No. 1-6408

Unetched X250

Figure 147. Arc Plasma Test PT0178(B-9)-5M. Interface Showing Random Orientation of Fibers.

Plate No. 1-4488

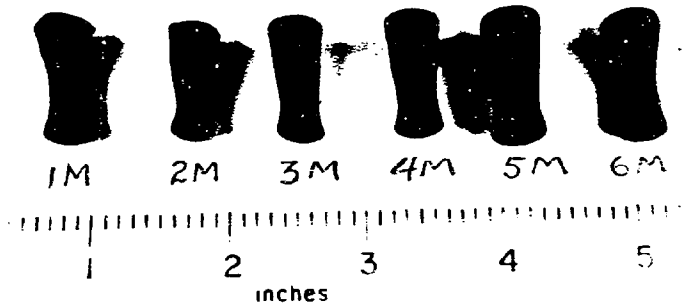


Plate No. 1-5106

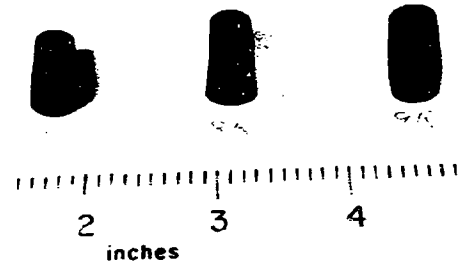


Plate No. 1-7665




Plate No. 1-9517

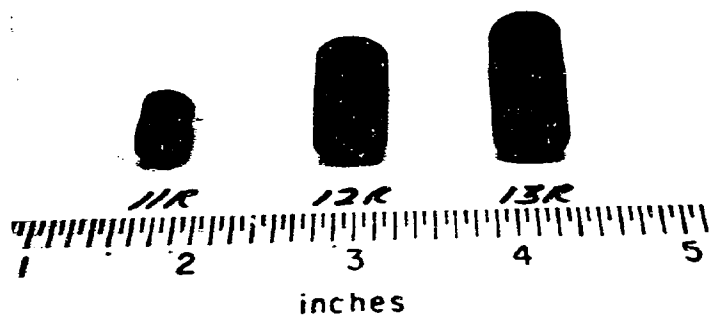


Figure 148. Post Exposure Photographs of Arc Plasma Tests Poco Graphite(B-10)-1M, 2M, 3M, 4M, 5M, 6M, 7R, 8R, 9R, 10R, 11R, 12R and 13R.

Plate No. 1-7666

X2.94

Figure 149. Arc Plasma Test POCO(B-10)-10R, Surface Temperature 5350°F, Exposure Time 250 Seconds, Stagnation Pressure 0.218 Atm, Stagnation Enthalpy 10890 BTU/lb, Cold Wall Heat Flux 1102 BTU/ft$^2$sec, Initial Length 836 Mils, Final Length 308 Mils. Hot Face at Right. One Inch Scale.

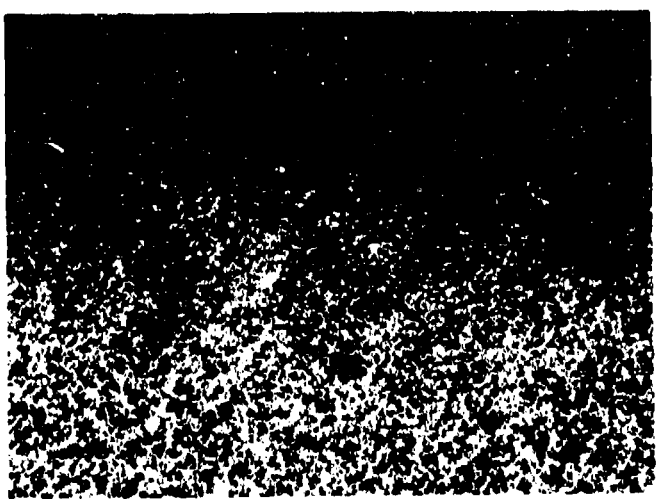

Plate No. 1-7667

Unetched X250

Figure 150. POCO(B-10)-10R. Hot Interface.

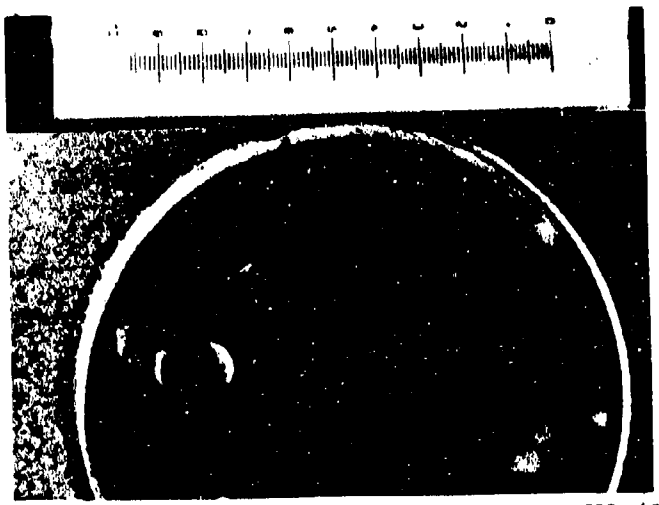

Plate No. 1-4497

X2.69

Figure 151. Arc Plasma Test POCO(B-10)-5M, Surface Temperature 6120°F, Exposure Time 44 Seconds, Stagnation Pressure 1.11 Atm, Stagnation Enthalpy 9195 BTU/lb, Cold Wall Heat Flux 1060 BTU/ft$^2$sec, Initial Length 841 Mils, Final Length 679 Mils. Hot Face at Right. One Inch Scale.

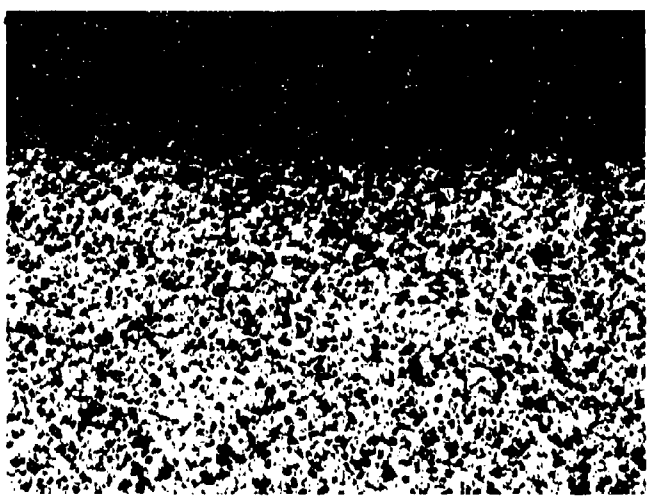

Plate No. 1-7762

Unetched X250

Figure 152. Arc Plasma Test POCO (B-10)-5M. Hot Interface.

Plate No. 1-8061

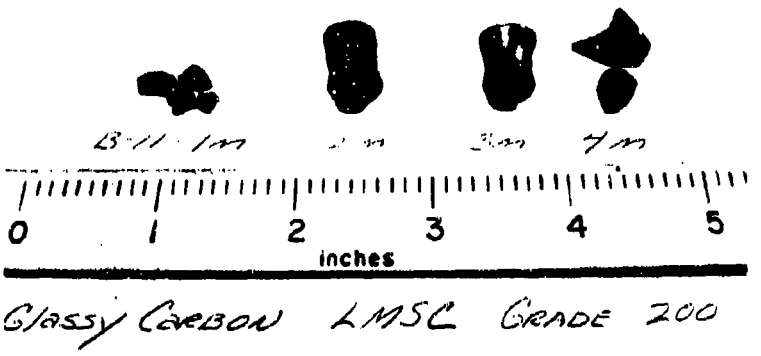


Figure 153. Post Exposure Photographs of Arc Plasma Tests Glassy Carbon(B-11)-1M, 2M, 3M and 4M.

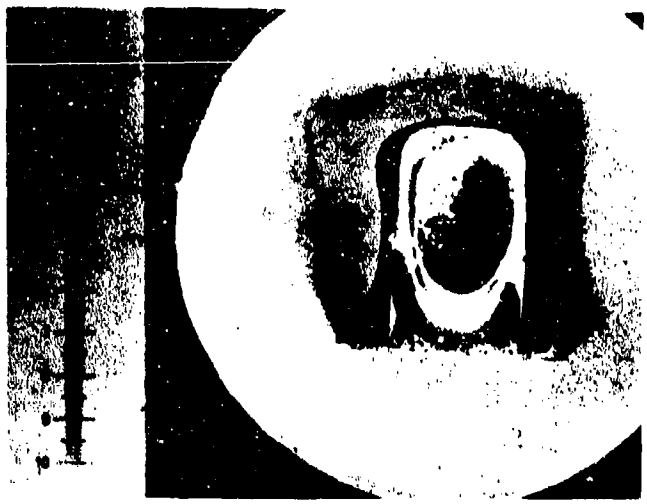

Plate No. 1-8065

X2.62

Figure 154. Arc Plasma Test Glassy Carbon (B-11)-3M, Surface Temperature 4540°F, Exposure Time 54 Seconds, Stagnation Pressure 1.03 Atm, Stagnation Enthalpy 3785 BTU/lb, Cold Wall Heat Flux 360 BTU/ft$^2$ sec, 125 Mils Recession, Hot Face Up. One inch Scale.

Plate No. 1-8063

Unetched X160

Figure 155. Arc Plasma Test Glassy Carbon (B-11)-3M, Hot Surface Down.

Plate No. 1-7438


Plate No. 2-0615


Plate No. 2-0625

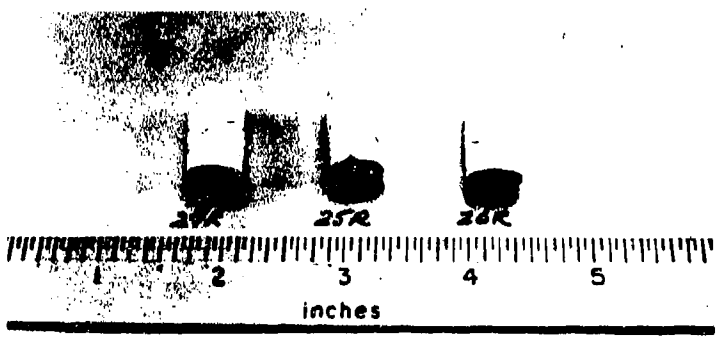


Figure 156. Post Exposure Photographs of Arc Plasma Tests HfC+C(C-11)-1M, 2M, 3M, 4M, 5M, 21M, 22M, 23M, 24R, 25R and 26R.

Plate No. 1-7669

Plate No. 1-8056

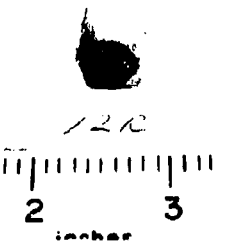


Plate No. 1-8760

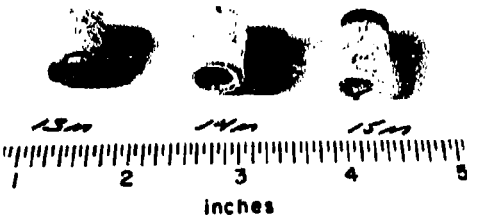


Plate No. 1-9493

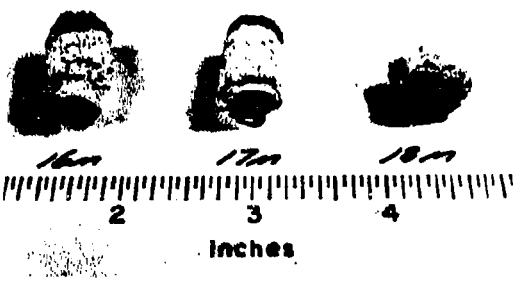


Plate No. 1-9520

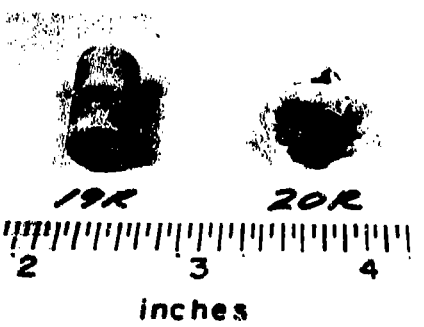


Figure 157. Post Exposure Photographs of Arc Plasma Tests HfC+C(C-11)-7R, 8R, 9R, 10R, 11R, 12R, 13M, 14M, 15M, 16M, 17M, 18M, 19R and 20R

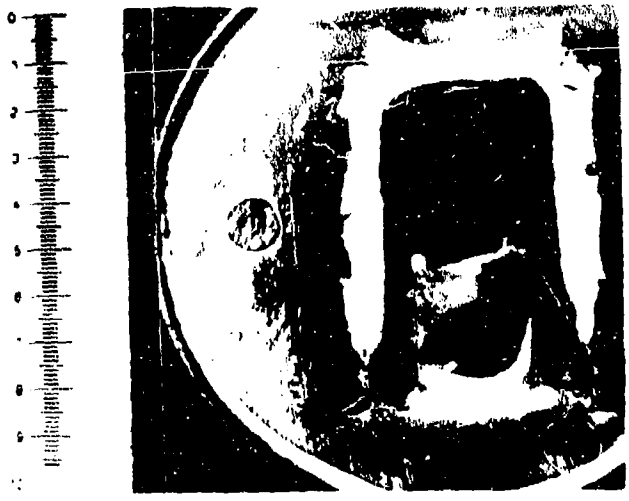

Plate No. 1-8767

X2.80

Figure 158. Arc Plasma Test HfC + C(C-11)-15M, Surface Temperature 3865°F, Exposure Time 1800 Seconds, Stagnation Pressure 1.01 Atm. Stagnation Enthalpy 2830 BTU/lb, Cold Wall Heat Flux 235 BTU/ft$^2$ sec, 47 mils Recession, Hot Face Up. One Inch Scale.

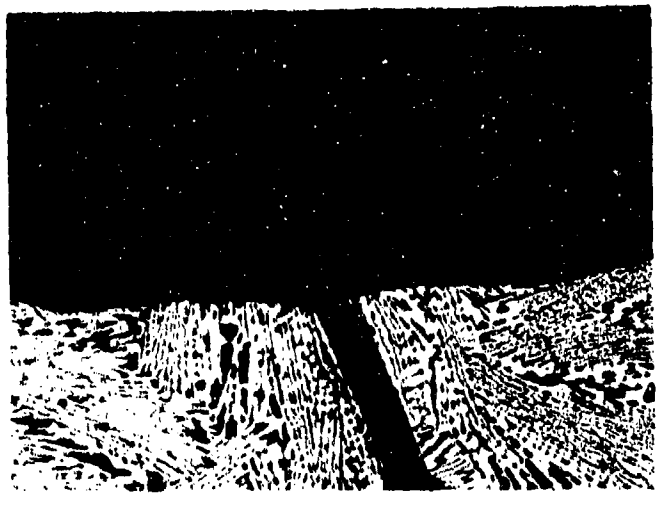

Plate No. 1-8768

Unetched

X250

Figure 159. Arc Plasma Test HfC + C (C-11)-15M, Hot Surface Oxide at Top.

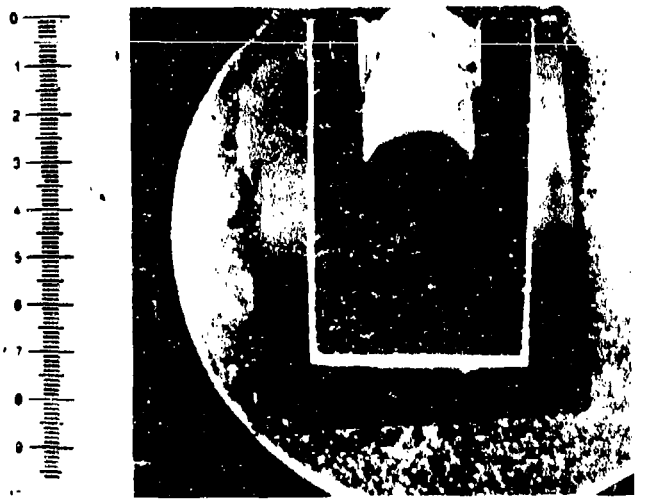

Plate No. 1-7676

X2.90

Figure 160. Arc Plasma Test HfC + C(C-11)-10R, Surface Temperature 4875°F Exposure Time 1800 Seconds, Stagnation Pressure 0.066 Atm. Stagnation Enthalpy 11,850 BTU/lb, Cold Wall Heat Flux 614 BTU/ft$^2$ sec, 20 Mil Recession, Hot Face Down, One Inch Scale.

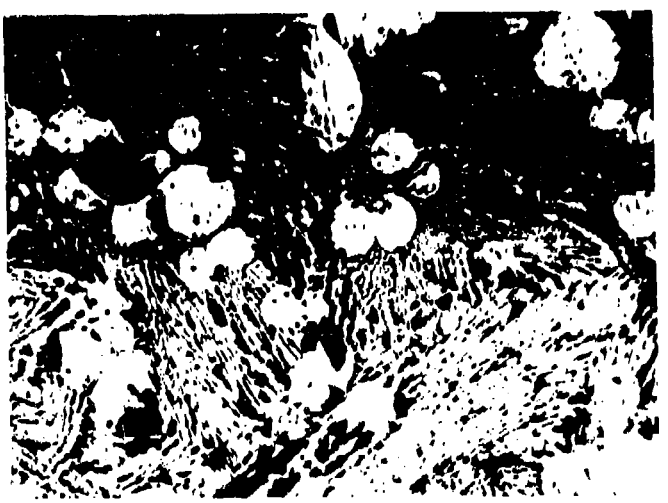

Plate No. 1-7677

Unetched X250

Figure 161. Arc Plasma Test HfC + C(C-11)-10R, Hot Surface, Oxide on Top.

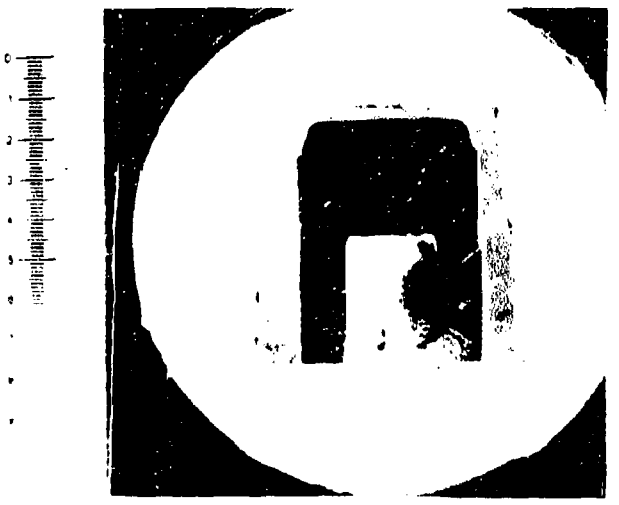

Plate No. 1-8057

X2.5

Figure 162. Arc Plasma Test HfC + C (C-11)-12R, Surface Temperature 5545°F, Exposure Time 180 Seconds, Stagnation Pressure 0.017 Atm. Stagnation Enthalpy 15,420 BTU/ft$^2$ sec, Cold Wall Heat Flux 756 BTU/ft$^2$ sec. 110 Mils Recession, Hot Face Up. One Inch Scale.

Plate No. 1-8059

Unetched X50

Figure 163. Arc Plasma Test HfC + C (C-11)-12R, Hot Surface.

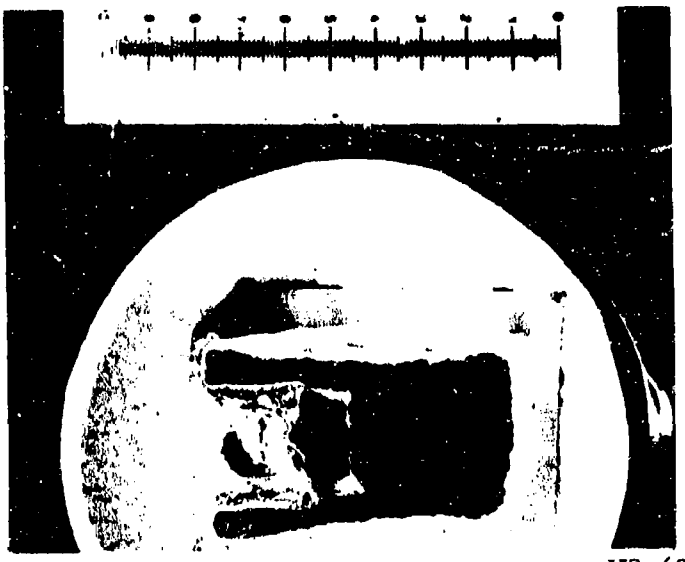

Plate No. 1-7439

X2.69

Figure 164. Arc Plasma Test HfC+C(C-11)-1M, Surface Temperature 5250°F, Exposure Time 1185 Seconds, Stagnation Pressure 1.07 Atm, Stagnation Enthalpy 4670 BTU/lb, Cold Wall Heat Flux 635 BTU/ft$^2$sec, Initial Length 407 Mils, Final Length 348 Mils. Hot Face at Right. One Inch Scale. White Oxide Clearly Visible.

Plate No. 1-7440

Unetched X250

Figure 165. HfC+C(C-11)-1M. Interface of Oxide (Top) and Carbide Matrix.

Plate No. 1-7448

X2.65

Figure 166. Arc Plasma Test HfC+C(C-11)-4M, Surface Temperature 6250°F, Exposure Time 45 Seconds, Stagnation Pressure 1.08 Atm, Stagnation Enthalpy 5200 BTU/lb, Cold Wall Heat Flux 755 BTU/ft$^2$sec, Initial Length 404 Mils, Final Length 256 Mils. Hot Face at Right. One Inch Scale.

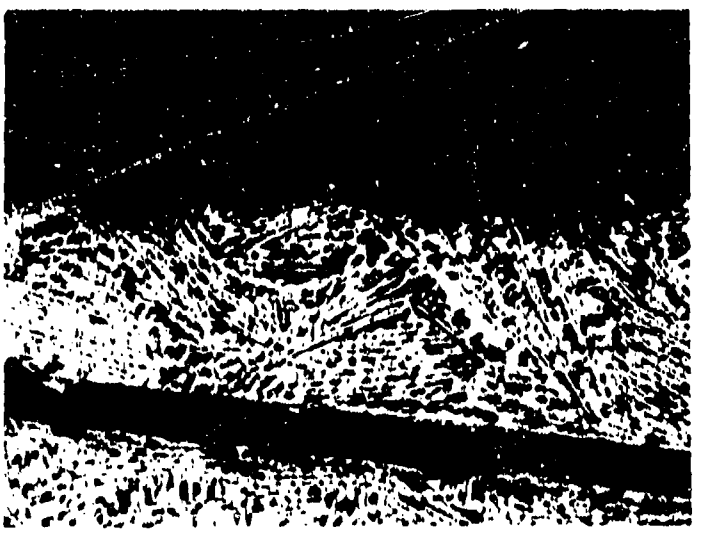

Plate No. 1-7449

Unetched X250

Figure 167. HfC+C(C-11)-4M. Interface of Oxide (Top) and Carbide Matrix.

Plate No. 1-7454

Plate No. 1-7467


Figure 168. Post Exposure Photographs of Arc Plasma Tests ZrC+C(C-12)-1M, 2M, 3M, 4M, 5M, 6M and 7M.

Plate No. 1-7683

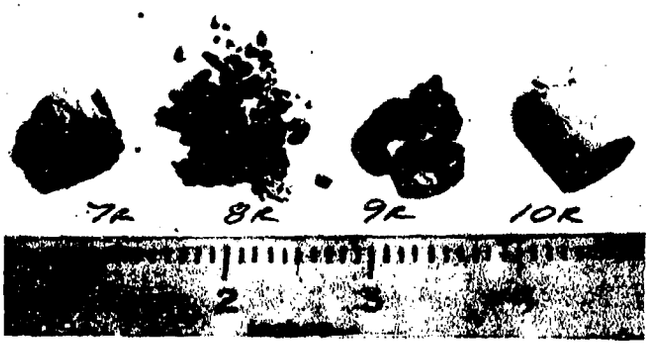


Plate No. 1-7822

Plate No. 1-8789

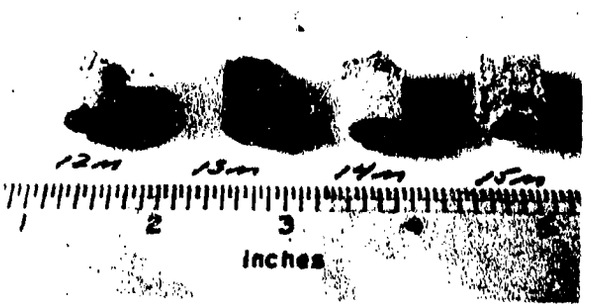


Plate No. 1-9489


Plate No. 1-9519

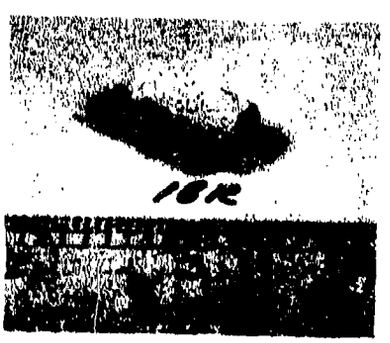


Figure 169. Post Exposure Photographs of Arc Plasma Tests ZrC+C(C-12)-7R, 8R, 9R, 10R, 11R, 12M, 13M, 14M, 15M, 16M, 17M and 18R

Plate No. 1-8796

X2.90

Figure 170. Arc Plasma Test ZrC + C(C-12)-15M, Surface Temperature 3900°F, Exposure Time 1800 Seconds, Stagnation Pressure 1.01 Atm. Stagnation Enthalpy 2750 BTU/lb, Cold Wall Heat Flux 235 BTU/ft$^2$ sec. 64 Mils Recession, Hot Face Up. One Inch Scale.

Plate No. 1-8797

Unetched X250

Figure 171. Arc Plasma Test ZrC + C(C-12)-15M, Hot Surface Oxide on Top.

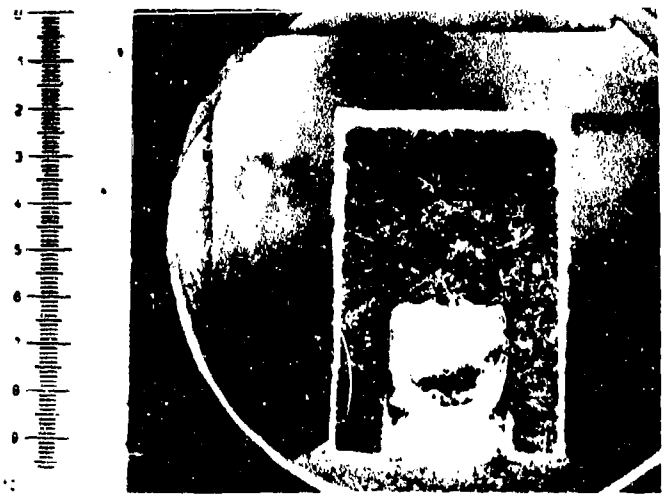

Plate No. 1-7688

X2.90

Figure 172. Arc Plasma Test ZrC + C(C-12)-10R, Surface Temperature 5030°F, Exposure Time 1800 Seconds, Stagnation Pressure 0.093 Atm. Stagnation Enthalpy 11,030 BTU/lb, Cold Wall Heat Flux 548 BTU/ft$^2$ sec, 32 Mils Recession, Hot Face Up. One Inch Scale.

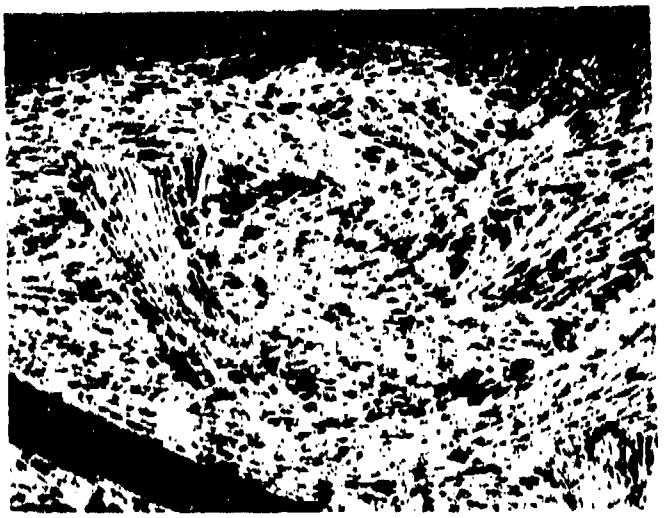

Plate No. 1-7689

Unetched X250

Figure 173. Arc Plasma Test ZrC+C(C-12)-10R, Hot Surface Oxide at Top.

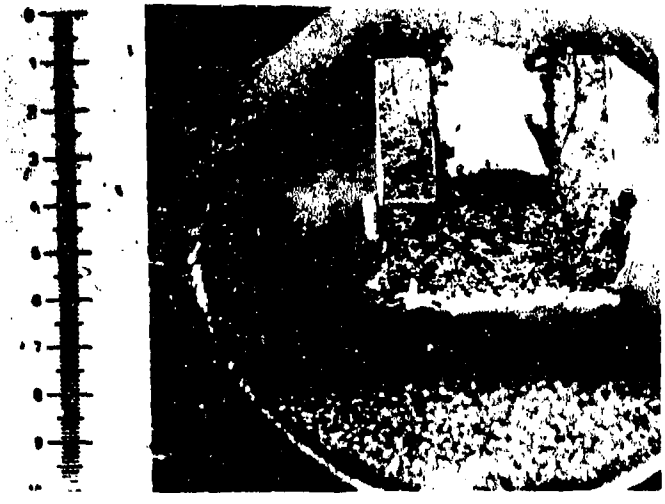

Plate No. 1-7684

X2.90

Figure 174. Arc Plasma Test ZrC+C(C-12)-7R, Surface Temperature 4955° F, Exposure Time 1800 Seconds, Stagnation Pressure 0.084 Atm. Stagnation Enthalpy 11,100 BTU/lb, Cold Wall Heat Flux 775 BTU/ft$^2$ sec, 209 Mils Recession, Hot Face Down. One Inch Scale.

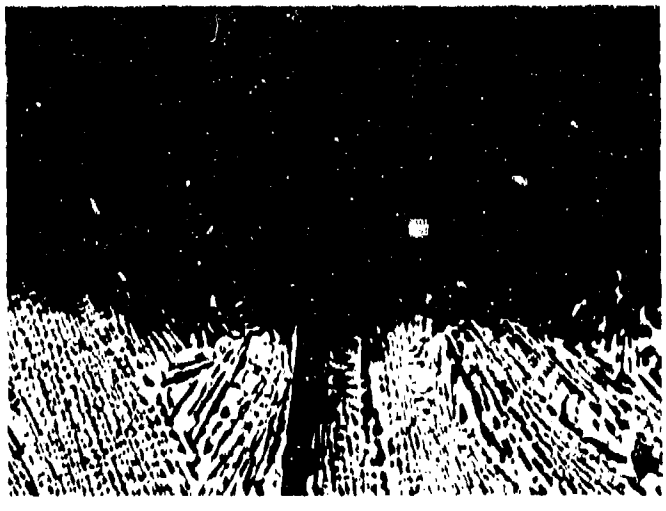

Plate No. 1-7685

Unetched X250

Figure 175. Arc Plasma Test ZrC+C(C-12)-7R, Hot Surface Oxide at Top.

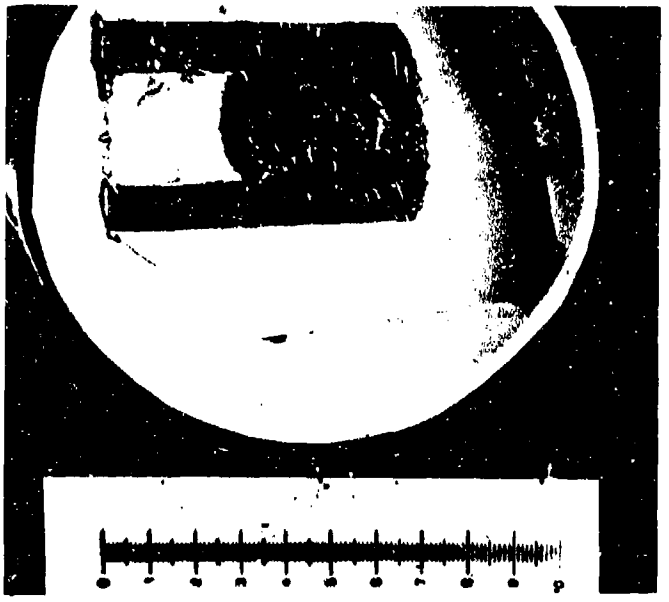

Plate No. 1-7461

X2.75

Figure 176. Arc Plasma Test ZrC+C(C-12)-3M, Surface Temperature 5970°F, Exposure Time 23 Seconds, Stagnation Pressure 1.08 Atm, Stagnation Enthalpy 4580 BTU/lb, Cold Wall Heat Flux 660 BTU/ft$^2$sec, Initial Length 404 Mils, Final Length 379 Mils. Hot Face at Right. One Inch Scale.

Plate No. 1-7462

Unetched X250

Figure 177. Arc Plasma Test ZrC+C(C-12)-3M. Interface of Melted Oxide (Top) and Carbide Matrix.

Plate No. 1-7468

X2.69

Figure 178. Arc Plasma Test ZrC+C(C-12)-5M, Surface Temperature 4860°F, Exposure Time 1800 Seconds, Stagnation Pressure 1.07 Atm, Stagnation Enthalpy 4460 BTU/lb, Cold Wall Heat Flux 620 BTU/ft$^2$sec, Initial Length 407 Mil, Final Length 341 Mils. Hot Face at Right. One Inch Scale. White Oxide Clearly Visible. Rear Broke on Removal after Test.

Plate No. 1-7469

Unetched X250

Figure 179. ZrC+C(C-12)-5M. Interface of Oxide (Top) and Carbide Matrix.

Plate 1-2782

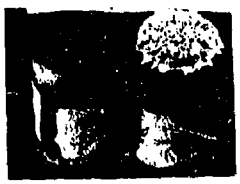

X0.88
(D-13)-21M and 22M
Hot Face Pointing Up

Plate 1-3510

(D-13)-23M X0.88

Hot Face On Right

Plate 1-3511

(D-13)-24M X0.88

Hot Face On Right

Figure 180. Post Exposure Photographs of Arc Plasma Tests JTA(C-$ZrB_2$-SiC) (D-13)-21M, 22M, 23M and 24M, Showing Thermal Shock Delaminations of JTA(D-13)-23M and 24M.

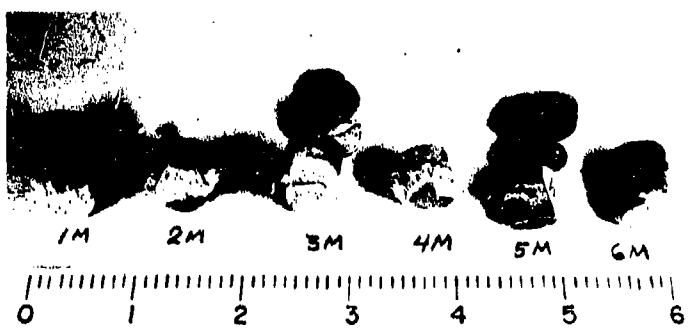


Plate 1-4275

Figure 181. Post Exposure Photographsof Arc Plasma Tests JTA(C-$ZrB_2$-SiC) (D-13)-1M, 2M, 3M, 4M, 5M and 6M. Hot Face Pointing Down. Samples 3M and 5M Show Thermal Shock Failures. Sample 2M is Propped on Support. One Inch Scale.

Plate 1-4277

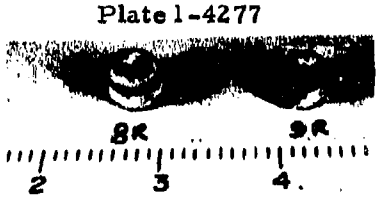


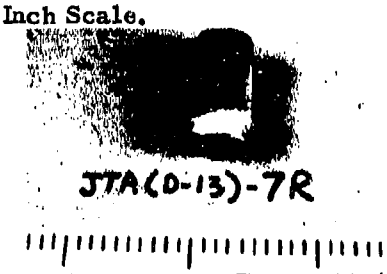


Plate -14276

Figure 182. Post Exposure Photographs of Arc Plasma Tests JTA(D-13)-8R and 9R (Hot Face Up) and 7R (Hot Face Down). One Inch Scale.

Plate No. 1-8068

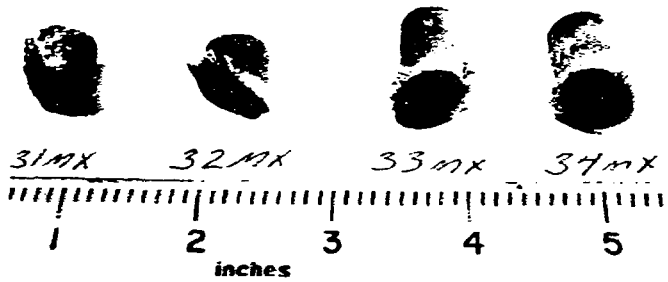


Plate No. 1-8082

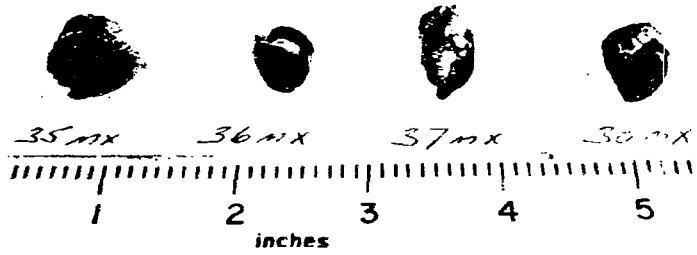


Plate No. 1-8101


Plate No. 1-9525

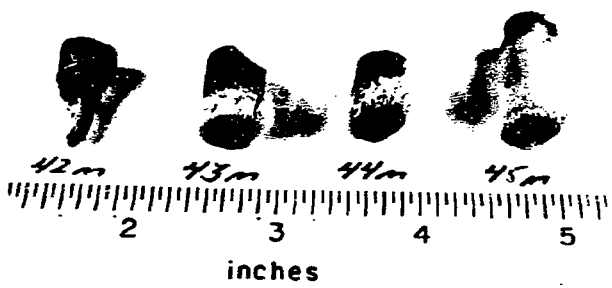


Figure 183. Post Exposure Photographs of Arc Plasma Tests JTA(D-13)-31MX, 32MX, 33MX, 34MX, 35MX, 36MX, 37MX, 38MX, 39MX, 40MX, 41MX, 42M, 43M, 44M and 45M

Plate No. 1-4944

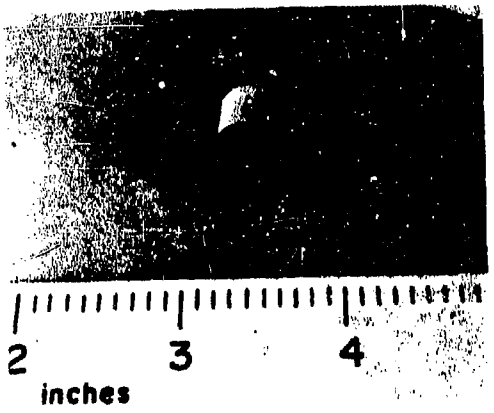


Plate No. 2-0418

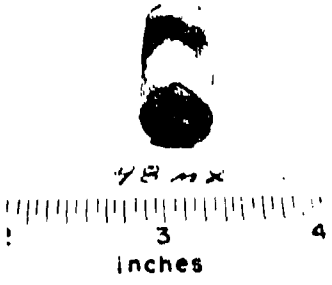


Plate No. 2-0277

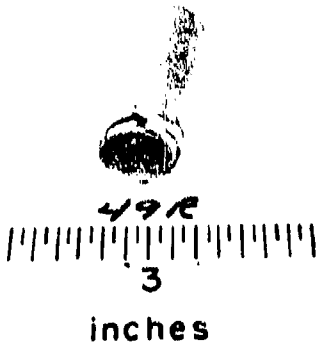


Figure 184. Post Exposure Photographs of Arc Plasma Tests JTA(D-13)-10R, 48MX and 49RX.

Plate 1-2786

X2.5

Figure 185. Arc Plasma Test JTA(C-$ZrB_2$-SiC)(D-13)-22M, Surface Temperature 3750°F, Exposure Time 1830 Seconds, Stagnation Pressure 1 Atm, Stagnation Enthalpy 3075 BTU/lb, Cold Wall Heat Flux 460 BTU/$ft^2$sec. Initial Length 1050 Mils, Final Length 977 Mils. Hot Face at Right, One Inch Scale.

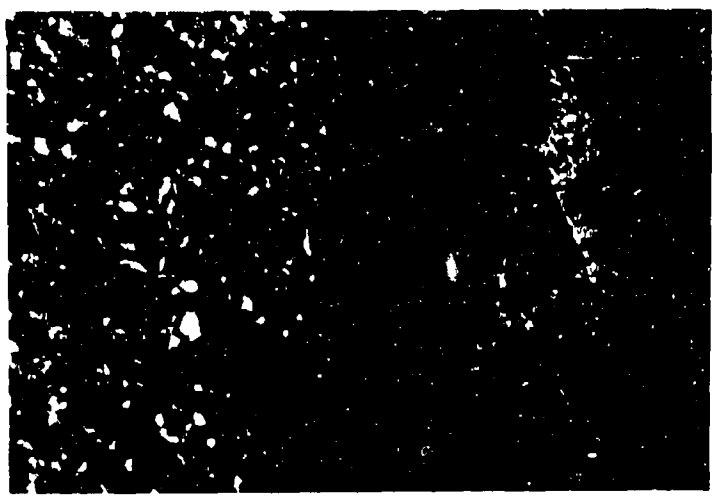

Plate 1-4466

X50

Figure 186. Arc Plasma Test JTA(C-$ZrB_2$-SiC)(D-13)-22M, Interface of Hot Face Showing Matrix on Left and Oxide on Right with Gap in Center.

Plate No.
1-2789

500X

Figure 187. Arc Plasma Test JTA(C-$ZrB_2$-SiC)(D-1?)-22M, Matrix Sting Leg Showing White $ZrB_2$ Grains and Light Grey SiC Grains in Dark Grey Graphite Matrix.

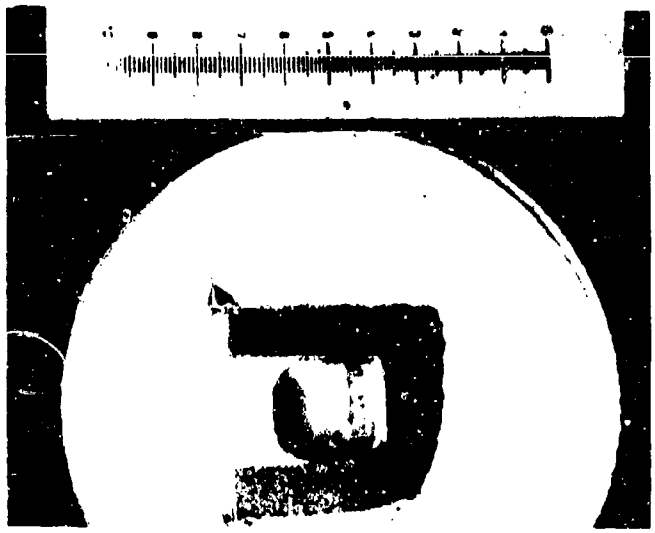

Plate No. 1-4511

X2.75

Figure 188. Arc Plasma Test JTA(D-13)-4M, Surface Temperature 4560°F, Exposure Time 214 Seconds, Stagnation Pressure 1.08 Atm, Stagnation Enthalpy 4320 BTU/lb, Cold Wall Heat Flux 660 BTU/ft$^2$sec, Initial Length 645 Mil, Final Length 125 Mil. Hot Face at Right. One Inch Scale.

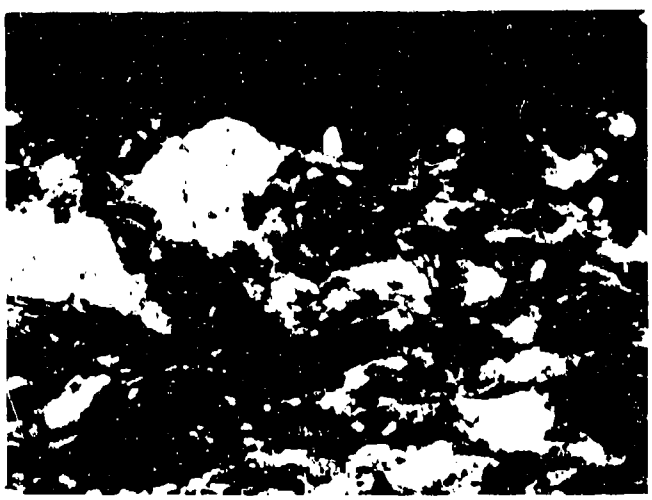

Plate No. 1-4512

Graphite

Boride

Unetched X250

Figure 189. Arc Plasma Tests JTA(D-13)-4M. Melted Interface.

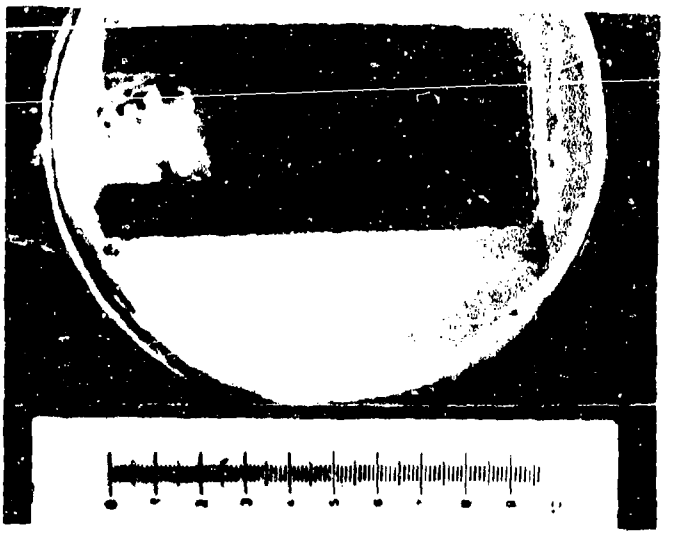

Plate No. 1-4520

X2.69

Figure 190. Arc Plasma Test JTA(D-13)-7R, Surface Temperature 4665°F, Exposure Time 1800 Seconds, Stagnation Pressure 0.074 Atm, Stagnation Enthalpy 9520 BTU/lb, Cold Wall Heat Flux 500 BTU/ft$^2$sec, Initial Length 681 Mil, Final Length 637 Mil, Hot Face At Right. One Inch Scale. White Oxide Clearly Visible.

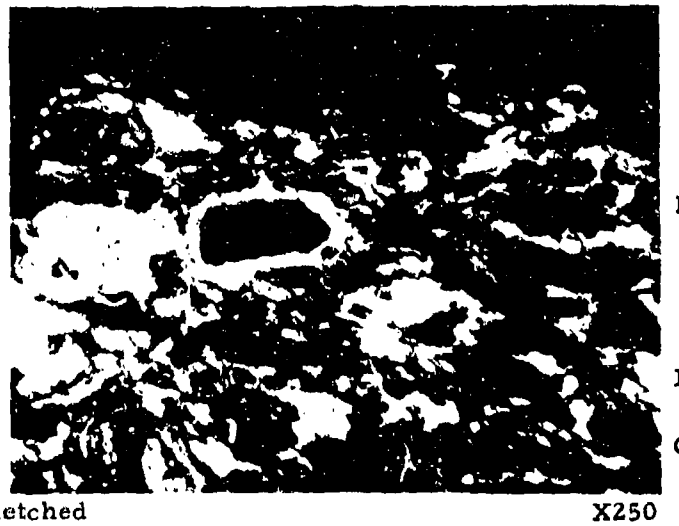

Plate No. 1-4521

Boride

Graphite

Unetched X250

Figure 191. Arc Plasma Test JTA(D-13)-7R. Oxide Detached at Top Interface.

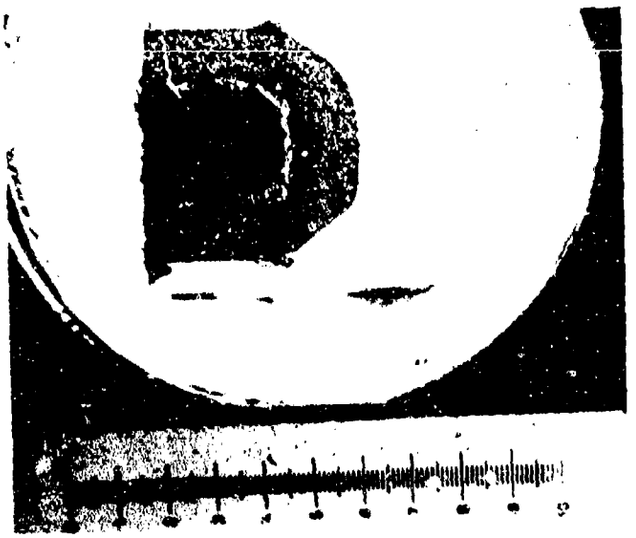

Plate No. 1-4523

X3.13

Figure 192. Arc Plasma Test JTA(D-13)-8R, Surface Temperature 5305°F, Exposure Time 180 Seconds, Stagnation Pressure 0.164 Atm, Stagnation Enthalpy 7310 BTU/lb, Cold Wall Heat Flux 770 BTU/ft$^2$sec, Initial Length 713 Mil, Final Length 132 Mil. Hot Face at Right. One Inch Scale.

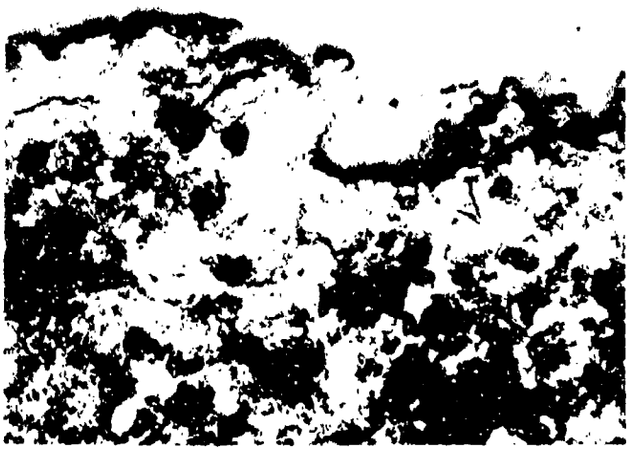

Plate No. 1-4525

Unetched X250

Figure 193. Arc Plasma Test JTA(D-13)-8R. Melted Interface.

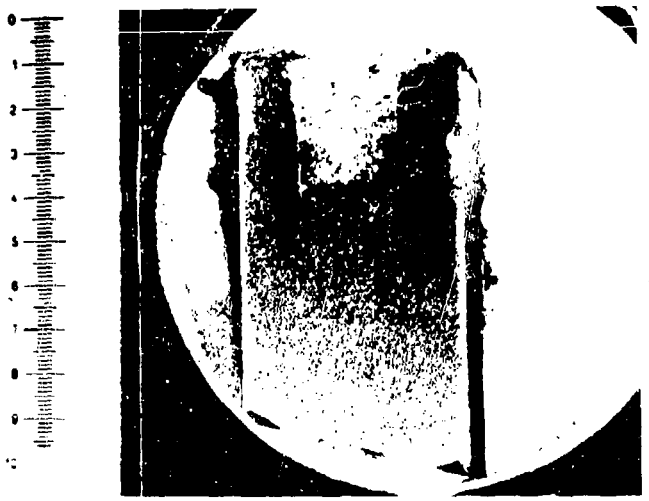

Plate No. 2-0419

X2.70

Figure 194. Arc Plasma Test JTA(D-13)-48MX Surface Temperature 4050°F, Exposure Time 7200 Seconds (4 cyclic exposures each of 1800 seconds), Stagnation Pressure 1.01 Atm. Stagnation Enthalpy 4350 BTU/lb, Cold Wall Heat Flux 380 BTU/ft$^2$sec, 118 Mils Recession, Hot Face Down, One Inch Scale.

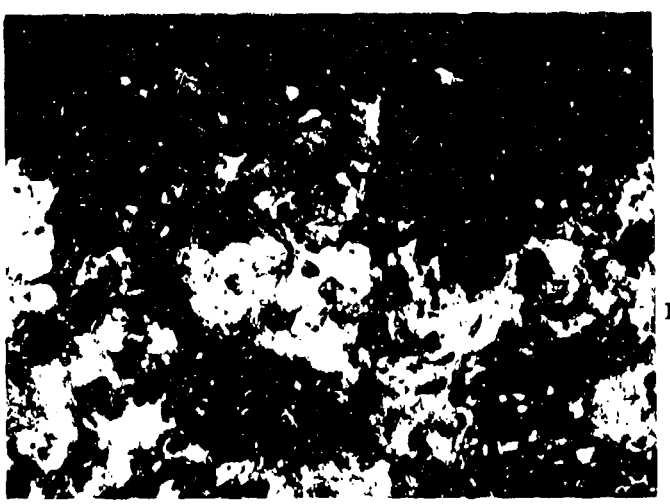

Plate No. 2-0420

Unetched X 250

Figure 195. Arc Plasma Test JTA(D-13)-48MX, Hot Surface.

Plate No. 2-0278

X2.60

Figure 196. Arc Plasma Test JTA(D-13)-49RX Surface Temperature 4425° F, Exposure Time 7200 Seconds (4 cyclic exposures each of 1800 seconds), Stagnation Pressure 0.057 Atm. Stagnation Enthalpy 9600 BTU/lb, Cold Wall Heat Flux 440 BTU/ft$^2$ sec, 45 Mils Recession, Hot Face Down, One Inch Scale.

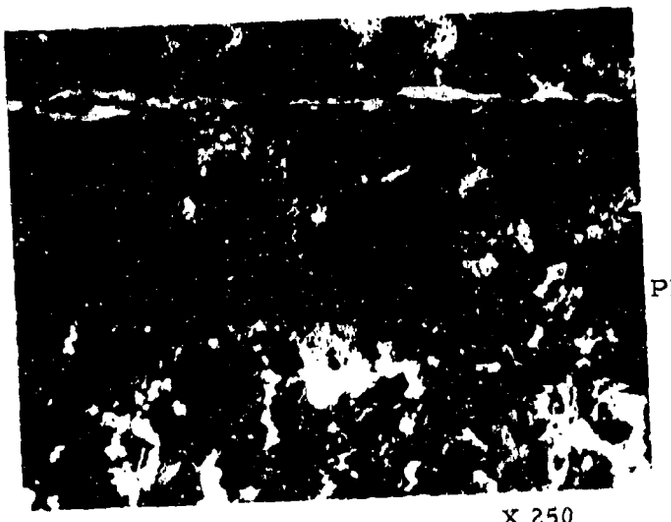

Plate No. 2-0279

Unetched

X 250

Figure 197. Arc Plasma Test JTA(D-13)-49RX, Hot Surface.


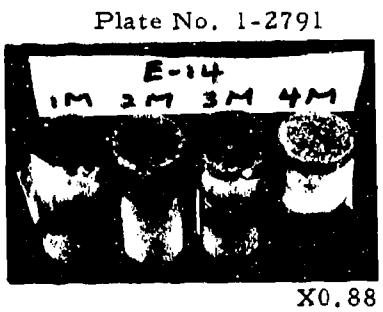


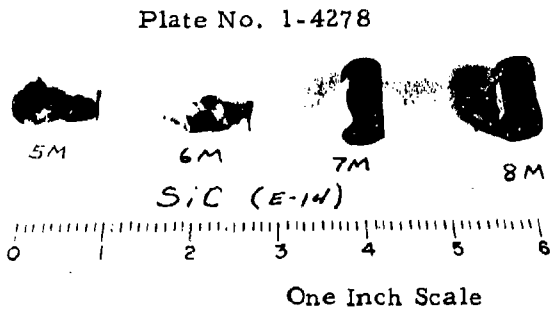


Figure 198. Post Exposure Photographs of Arc Plasma Tests KT-SiC(E-14)-3R, 4R, 5R, 6R, 7R, 1M, 2M, 3M, 4M, 5M, 6M, 7M and 8M. Hot Face Pointing Up. Sample 6M Ablated Completely While 7M and 8M showed Longitudinal Cracks.

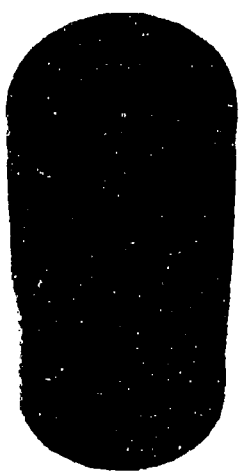

KT-SiC(E-14)-1R X3

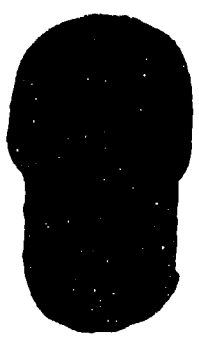

KT-SiC(E-14)-2R X2.5

Figure 199. Post Exposure Photographs of Arc Plasma Tests KT-SiC (E-14)-1R and 2R. Hot Face Pointed Up. Sample KT-SiC (E-14)-2R Ablated Completely and is Shown Mounted on Tungsten Sting.

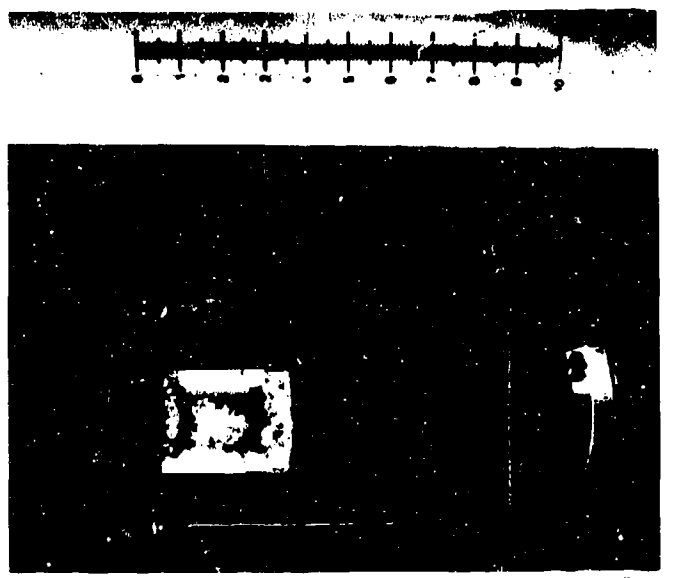

Plate No.
1-2801

X2.55

Figure 200. Arc Plasma Test KT-SiC(E-14)-4M, Surface Temperature 3670°F, Exposure Time 1835 Seconds, Stagnation Enthalpy 4155 BTU/lb, Stagnation Pressure 1 Atm, Cold Wall Heat Flux 600 BTU/ft$^2$sec, Initial Length 841 Mils, Final Length 834 Mils. Hot Face at Right. One Inch Scale.

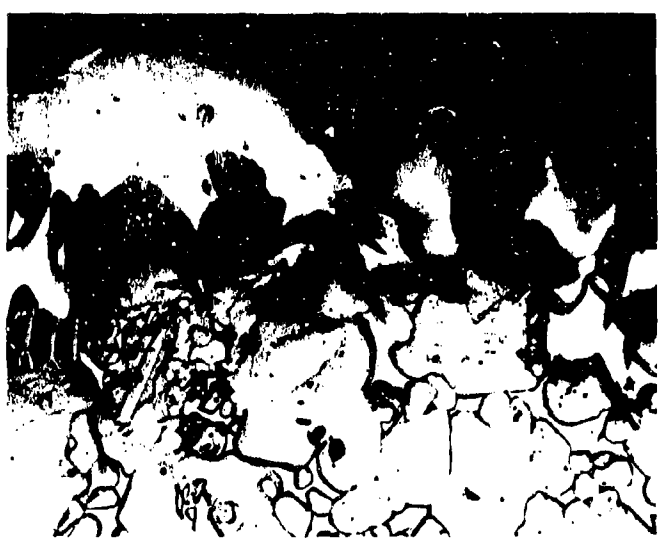

Plate No.
1-2802

X250

Figure 201. Arc Plasma Test KT-SiC(E-14)-4M, Hot Face Showing Light Grey, SiC Grains and White Silicon Binder Phase.

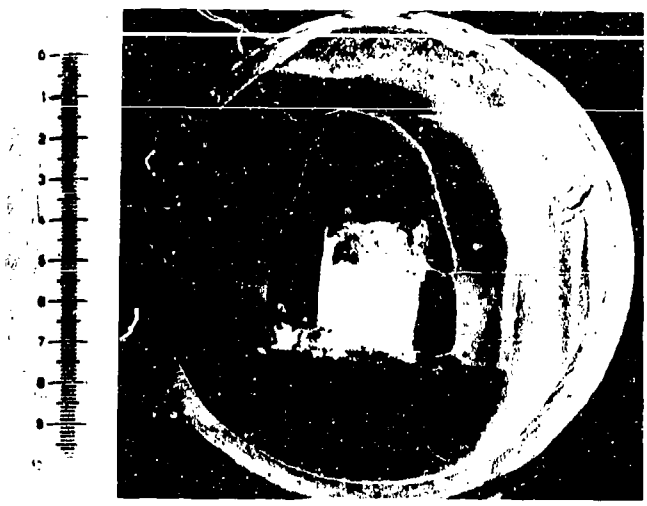

Plate No. 1-4738

X2.50

Figure 202. Arc Plasma Test KT-SiC(E-14)-5M, Surface Temperature 4440°F, Exposure Time 165 Seconds, Stagnation Pressure 1.08 Atm. Stagnation Enthalpy 4910 BTU/lb, Cold Wall Heat Flux 810 BTU/ft$^2$ sec, 425 Mil Recession, Hot Face Up. One Inch Scale.

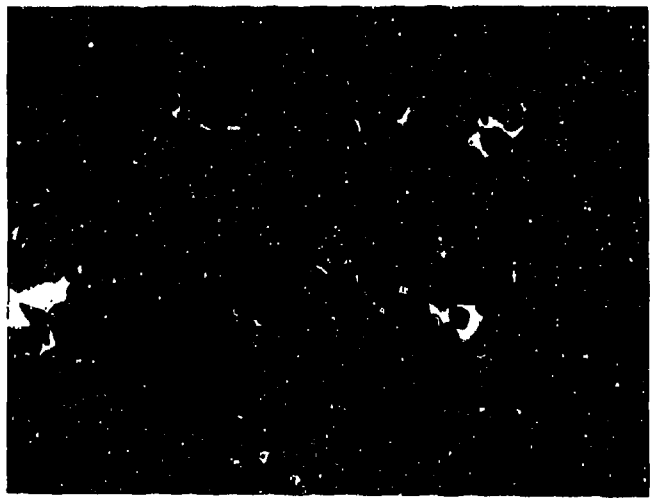

Plate No. 1-4739

Etched Electrolytically with 5% KOH Solution X 250

Figure 203. Arc Plasma Test KT-SiC(E-14)-5M, Hot Surface.

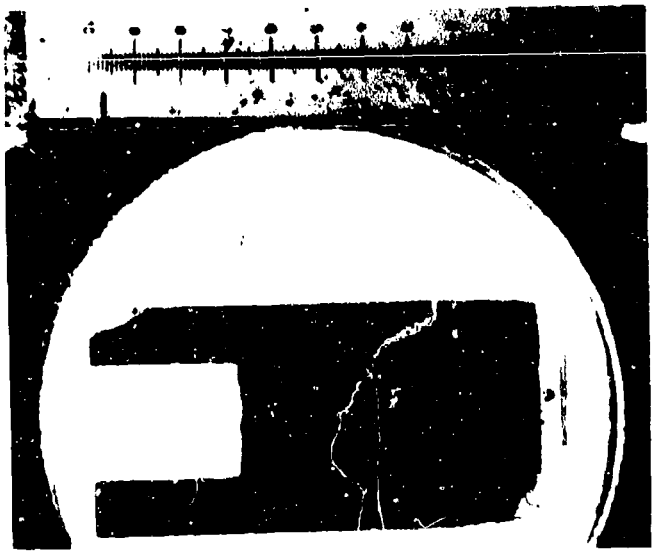

Plate No. 1-4957

X2.81

Figure 204. Arc Plasma Test KT-SiC(E-14)-7R, Surface Temperature 3060°F, Exposure Time 1800 Seconds, Stagnation Pressure 0.097 Atm, Stagnation Enthalpy 10880 BTU/lb, Cold Wall Heat Flux 652 BTU/ft$^2$sec, Initial Length 679 Mils, Final Length 655 Mils. Hot Face at Right. One Inch Scale. Specimen Cracked by Thermal Shock.

Plate No. 1-4958

Electrolytic Etch 5%KOH X250

Figure 205. Arc Plasma Test KT-SiC(E-14)-7R. Hot Interface.

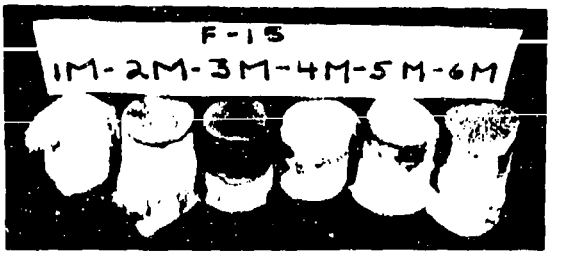


Plate 1-2762

X0.88

Figure 206. Post Exposure Photographs of Arc Plasma Tests JT0992 (C-HfC-SiC) (F-15)-1M, 2M, 3M, 4M, 5M and 6M. Hot Face Pointed Up.

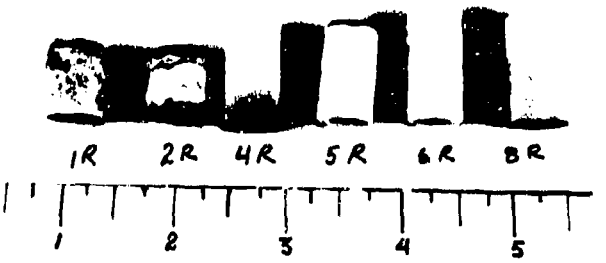


Plate 1-3642

Figure 207. Post Exposure Photographs of Arc Plasma Tests JT0992 (C-HfC-SiC) (F-15) (Billet 2/G/6)-1R, 2R, 4R, 5R, 6R and 8R. One Inch Scale. Hot Face Pointed Up.

Plate 1-3504

(F-15)-3R X0.88

Plate 1-3505

(F-15)-7R X0.88

Figure 208. Post Exposure Photographs of Arc Plasma Tests JT0992 (C-HfC-SiC) (F-15) (Billet 2/G/6)-3R and 7R. Hot Face at Right Pointed toward Left in 3R and Hot Face at Right in 7R Illustrating Thermal Shock Failures.

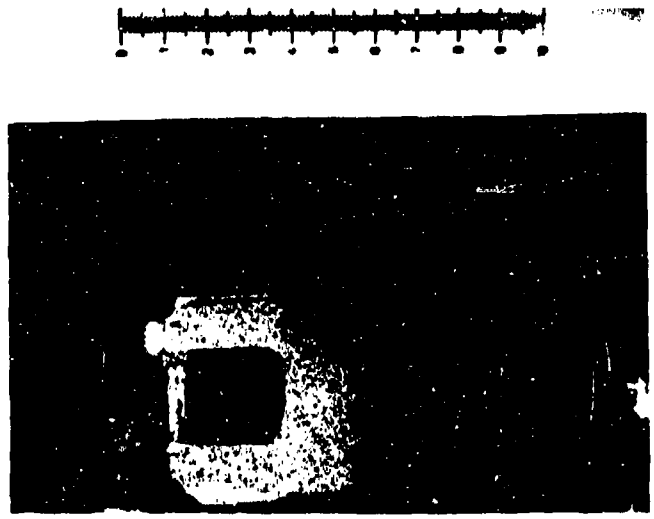

Plate No. 1-2769

X2.6

Figure 209. Arc Plasma Test JT0992(F-15)-3M, Surface Temperature 4930°F, Exposure Time 300 Seconds, Stagnation Pressure 1.10 Atm, Stagnation Enthalpy 4285 BTU/lb, Cold Wall Heat Flux 770 BTU/ft$^2$sec, Initial Length 1054 Mil, Final Length 692 Mil. Hot Face at Right. One Inch Scale. Some Side Recession.

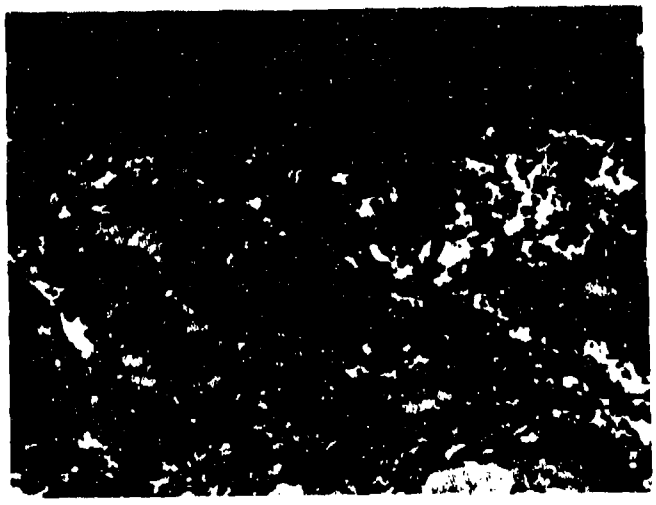

Plate No. 1-2770

Unetched X250

Figure 210. Arc Plasma Test JT0992(F-15)-3M. Melted Interface.

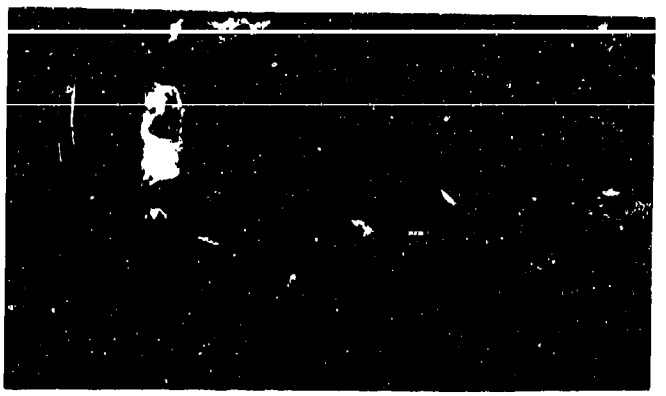

Plate No. 1-2766

X2.5

Figure 211. Arc Plasma Test JT0992(F-15)-2M, Surface Temperature 3470°F, Exposure Time 1173 Seconds, Stagnation Pressure 1.07 Atm, Stagnation Enthalpy 2105 BTU/lb, Cold Wall Heat Flux 430 BTU/ft$^2$sec, Initial Length 1033 Mil, Final Length 999 Mil. Hot Face at Right. One Inch Scale. Severe Recession at Sides and Rear.

Plate No. 1-2767

Unetched X250

Figure 212. Arc Plasma Test JT0992(F-15)-2M. Oxide (Top). Detached from Matrix at Hot Interface.

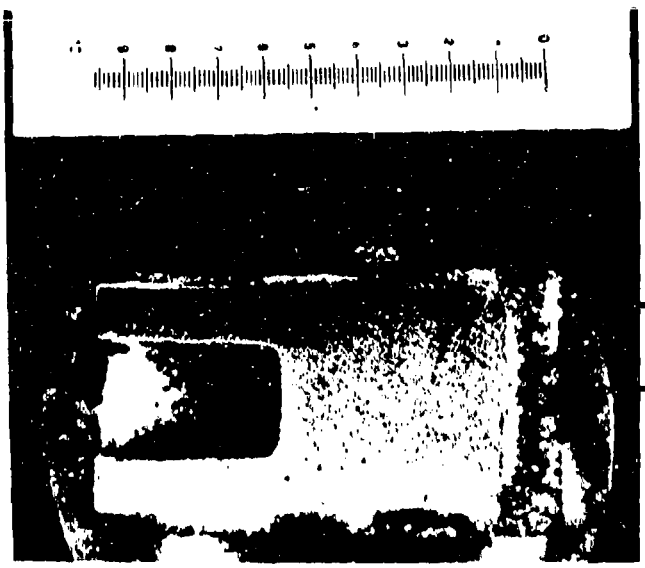


Figure 213. Arc Plasma Test JT0992(C-HfC-SiC)(F-15)-5R, Surface Temperature 5225°F, Exposure Time 1200 Seconds, Stagnation Pressure 0.027 atm, Stagnation Enthalpy 14550 BTU/lb, Cold Wall Heat Flux 500 BTU/ft$^2$sec, Initial Length 988 Mils, Final Length 865 Mils. Hot Face at Right. One Inch Scale.

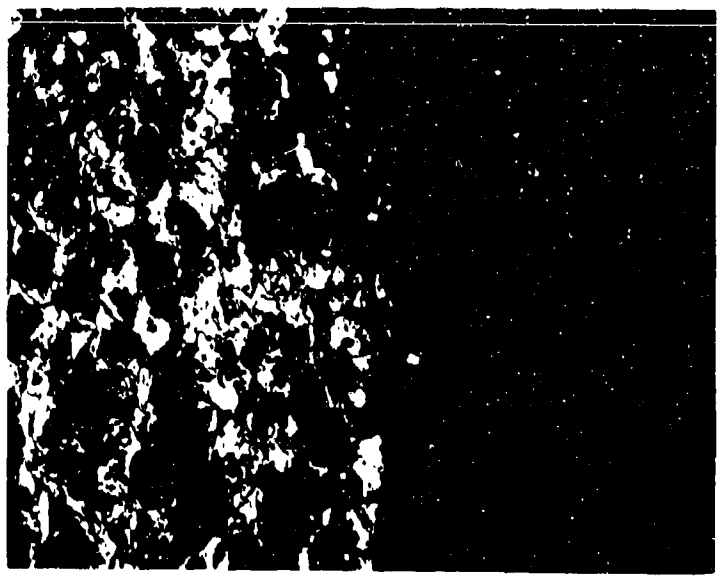

Plate 1-3653

X250

Figure 214. Arc Plasma Test JT0992(C-HfC-SiC)(F-15)-5R, Hot Face Interface. Matrix at Left Containing White HfC Grains and Light Grey SiC Grains in a Dark Grey Graphite Matrix. Oxide Skin is Out of Focus.

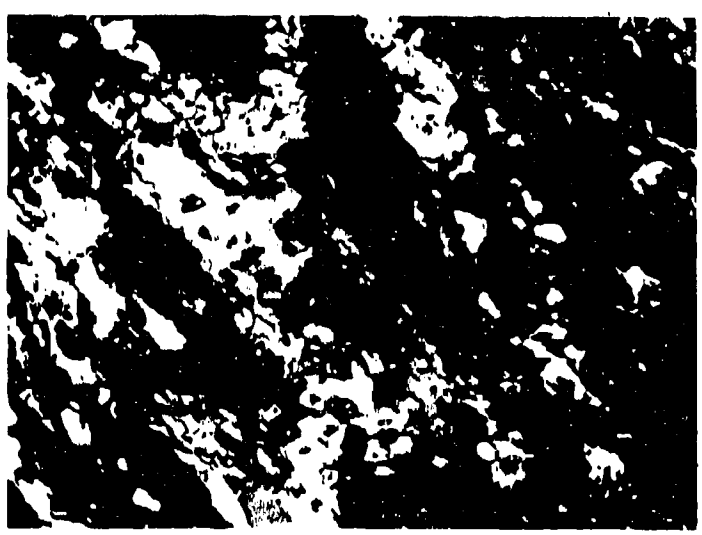

Plate 1-3655

X500

Figure 215. Arc Plasma Test JT0992 (C-HfC-SiC)(F-15)-5R, Sting Leg Matrix Showing White HfC Grains and Light Grey SiC Grains in a Dark Grey Graphite Matrix.

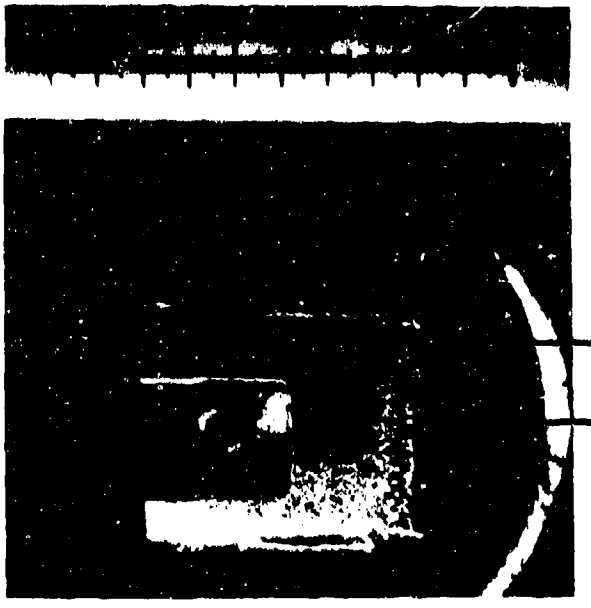


Figure 216. Arc Plasma Test JT0992(C-HfC-SiC)(F-15)-2R, Surface Temperature 5630°F, Exposure Time 110 Seconds, Stagnation Pressure 0.287 Atm, Stagnation Enthalpy 9390 BTU/lb, Cold Wall Heat Flux 1145 BTU/ft$^2$sec. Initial Length 994 Mils, Final Length 594 Mils. Hot Face at Right. One Inch Scale.

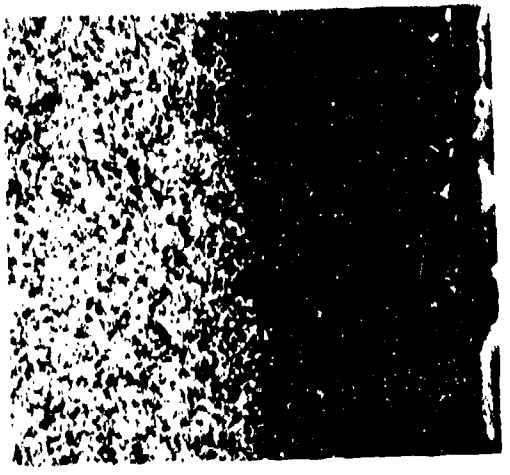


Figure 217. Arc Plasma Test JT0992 (C-HfC-SiC) (F-15)-2R, Hot Face Interface Zone, Matrix on Left, Zone Depleted of Carbides on Right.

Plate 1-3506

(F-16)-21M X0.88

Hot Face at Center Facing Right

Plate 1-3507

(F-16)-22M X0.88

Hot Face to Left

Plate 1-3508

(F-16)-23M X0.88

Hot Face to Right

Plate 1-3509

(F-16)-24M X0.88

Hot Face to Right

Figure 218. Post Exposure Photographs of JT0981 (C-ZrC-SiC) (F-16)-21M, 22M, 23M and 24M Showing Thermal Shock Failures. (F-16)-22M Experienced Low Temperature (3870°F) Oxidation for 1830 Seconds Prior to Failure.

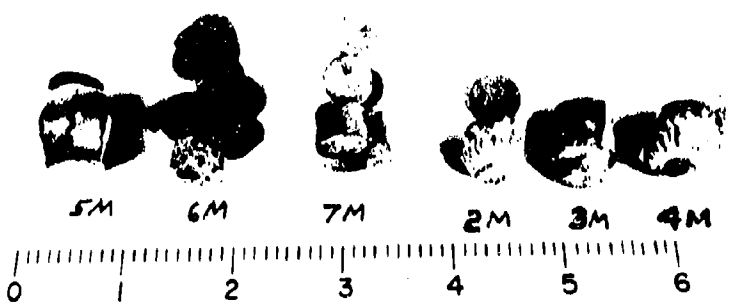


Plate 1-4280

Figure 219. Post Exposure Photographs of JT0981 (C-ZrC-SiC) (F-16)-2M, 3M, 4M, 5M, 6M and 7M. Samples 2M, 6M and 7M Exhibited Thermal Shock Failures While 5M Experienced Low Temperature (3910°F) Oxidation. One Inch Scale.

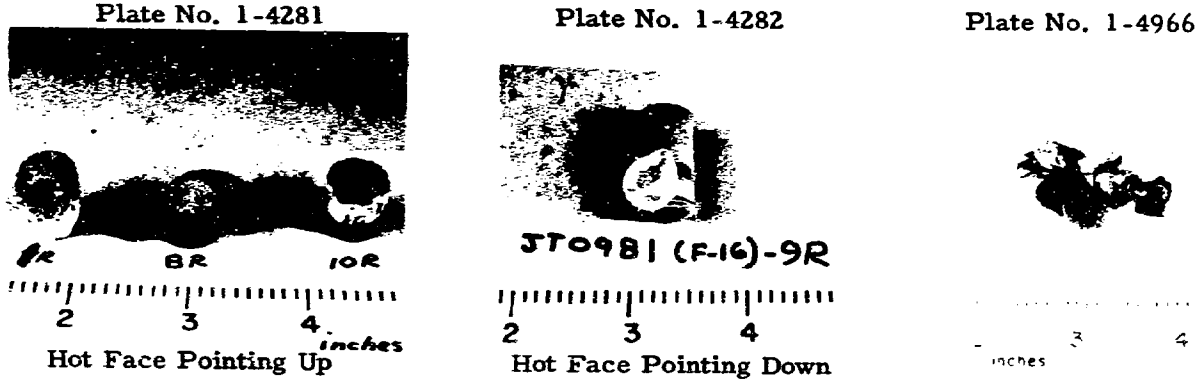




Figure 220. Post Exposure Photographs of JT0981(C-ZrC-SiC)(F-16)-1R, 8R, 10R, 9R and 11R. Samples 8R and 11R Exhibited Thermal Shock Failures. One Inch Scale.

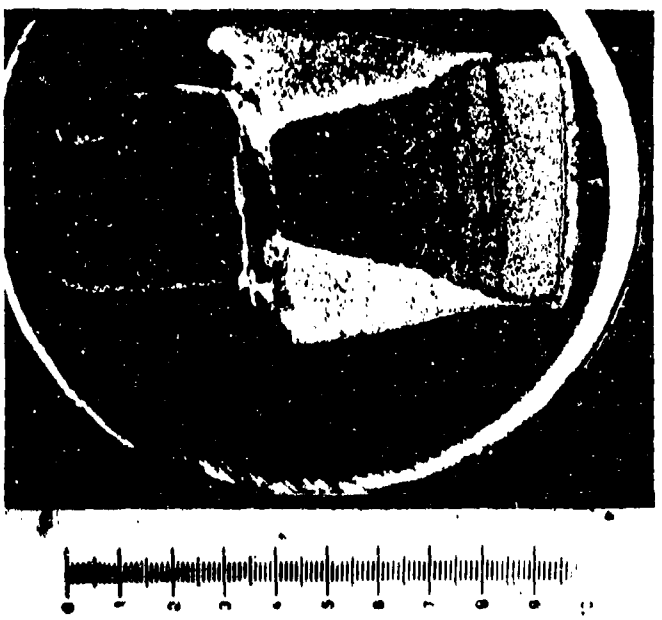

Plate No.
1-4183

X3

Figure 221. Arc Plasma Test JT0981(C-ZrC-SiC)(F-16)-22M, Surface Temperature 3870°F, Exposure Time 1830 Seconds, Stagnation Pressure 1 Atm., Stagnation Enthalpy 3230 BTU/lb, Cold Wall Heat Flux 460 BTU/ft²sec, Initial Length 1055 Mils. Hot Face at Right. One Inch Scale. Exposure Illustrates Extensive Side Face Oxidation Occurring at Low Temperature where Protective Oxide Formation does not Occur.

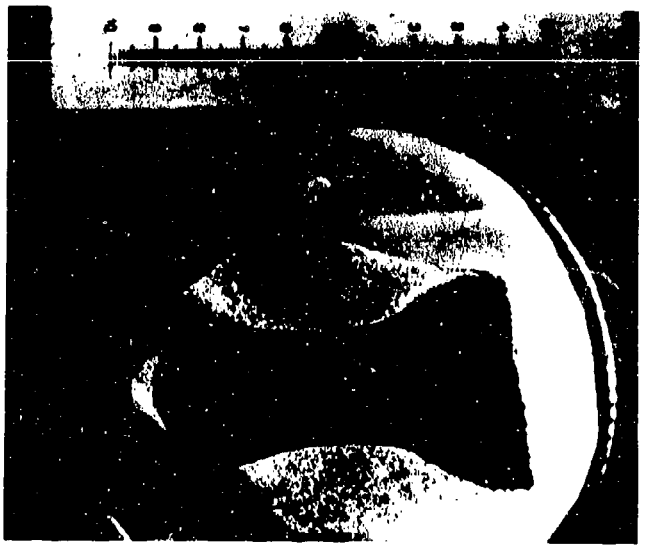

Plate No. 1-4614

X2.69

Figure 222. Arc Plasma Test JT0981(F-16)-5M, Surface Temperature 3910°F, Exposure Time 1830 Seconds, Stagnation Pressure 1.06 Atm, Stagnation Enthalpy 2485 BTU/lb, Cold Wall Heat Flux 390 BTU/ft$^2$sec, Initial Length 692 Mil, Final Length 586 Mil. Hot Face at Right. One Inch Scale. Severe Side Recession.


Plate No. 1-4616

Unetched X250

Figure 223. Arc Plasma Test JT0981(F-16)-5M. Interface of Oxide and Matrix.

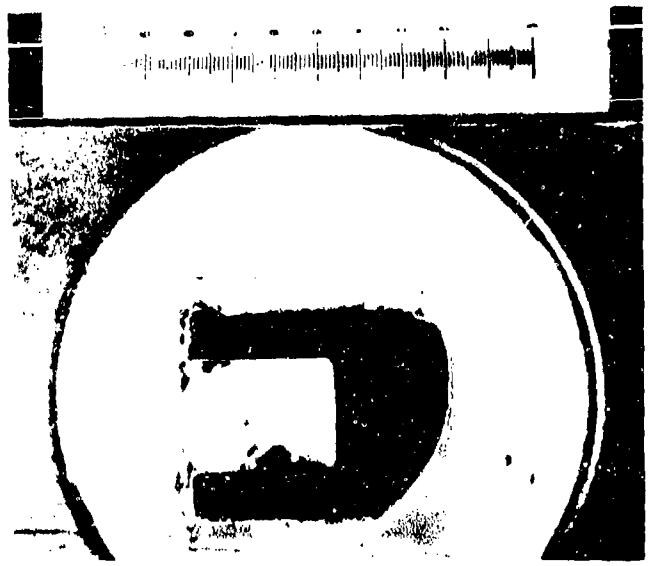

Plate No. 1-4610

X2.69

Figure 224. Arc Plasma Test JT0981(F-16)-4M, Surface Temperature 4990°F, Exposure Time 148 Seconds, Stagnation Pressure 1.08 Atm, Stagnation Enthalpy 3475 BTU/lb, Cold Wall Heat Flux 640 BTU/ft$^2$sec, Initial Length 565 Mil, Final Length 266 Mil. Hot Face at Right. One Inch Scale. Some Side Recession.

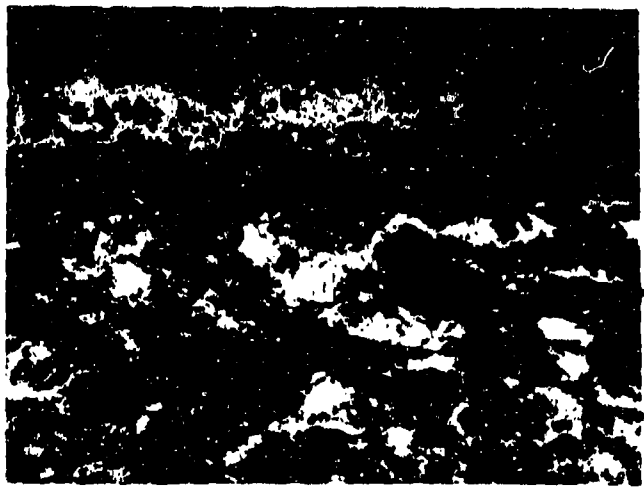


Plate No. 1-4612

Unetched X250

Figure 225. Arc Plasma Test JT0981(F-16)-4M. Interface of Oxide and Matrix.

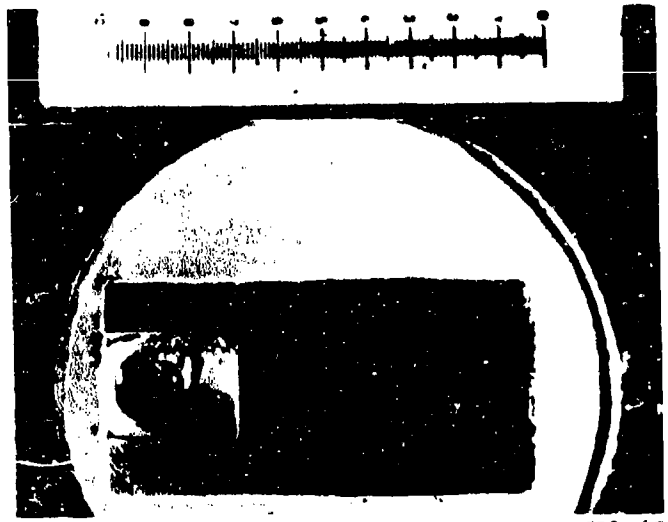

Plate No. 1-4636

X2.69

Figure 226. Arc Plasma Test JT0981(F-16)-9R, Surface Temperature 4695°F, Exposure Time 1800 Seconds, Stagnation Pressure 0.075 Atm, Stagnation Enthalpy 9120 BTU/lb, Cold Wall Heat Flux 523 BTU/ft$^2$sec, Initial Length 696 Mil, Final Length 655 Mil. Hot Face at Right. One Inch Scale.

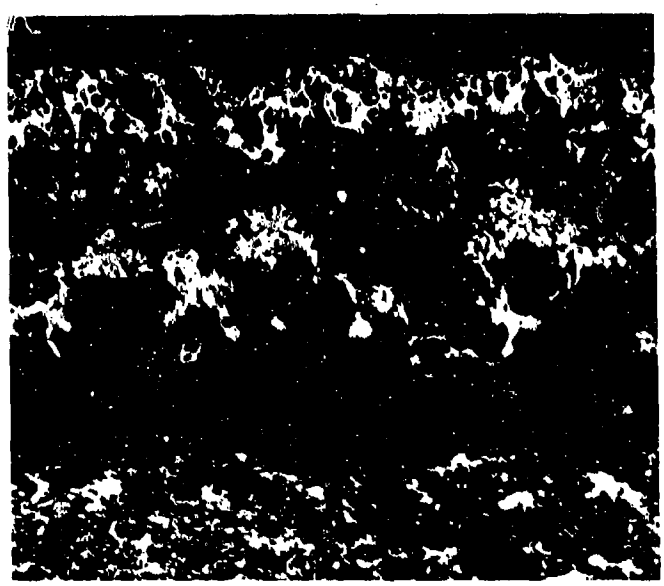

Plate No. 1-4637A

Unetched X75

Figure 227. JT0981(F-16)-9R. Oxide (Top). Detached from Matrix.

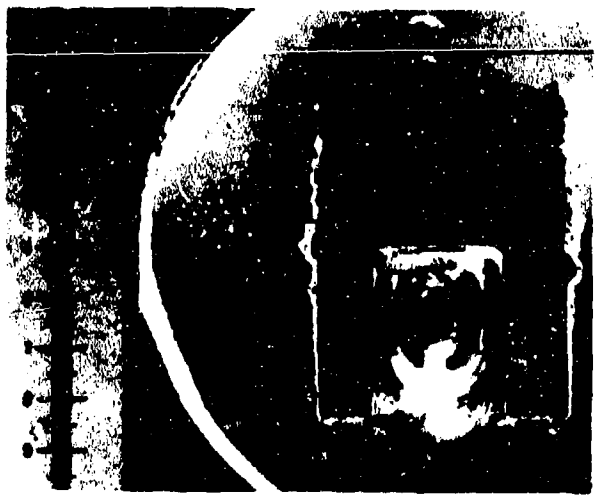

Plate No. 1-4624

X3.06

Figure 228. Arc Plasma Test JT0981(F-16)-1R, Surface Temperature 5065°F, Exposure Time 150 Seconds, Stagnation Pressure 0.179 Atm, Stagnation Enthalpy 7430 BTU/lb, Cold Wall Heat Flux 747 BTU/ft$^2$sec, Initial Length 694 Mil, Final Length 338 Mil. Hot Face at Top. One Inch Scale.

Plate No. 1-4626

Unetched X250

Figure 229. Arc Plasma Test JT0981(F-16)-1R, Melted Interface at Top.


Figure 230. Post Exposure Photographs of Tungsten and Molybdenum Samples Employed in Temperature Calibration Tests in the Model 500 (M) and ROVERS (R) Facilities.

Plate No. 1-6453

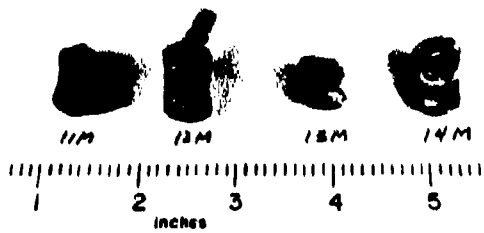


Plate No. 1-5417

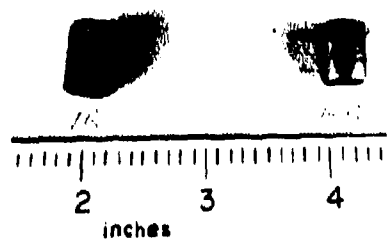


Plate No. 1-4283


Figure 231. Post Exposure Photographs of 5 Mil $WSi_2$ Coated W; $WSi_2$/W(G-18)-1M, 2M, 3M, 4M, 5M, 11M, 12M, 13M, 14M, 9R and 10R. Hot Face Pointed Down. One Inch Scale.

Plate No. 1-4284

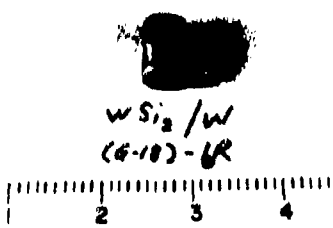


Plate No. 1-4285

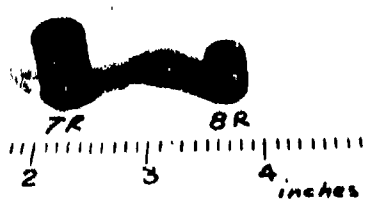


Figure 232. Post Exposure Photographs of 5 Mil $WSi_2$ Coated W; $WSi_2$/W(G-18)-6R, 7R and 8R. Hot Face Pointed Up. One Inch Scale.

Plate No. 2-0629

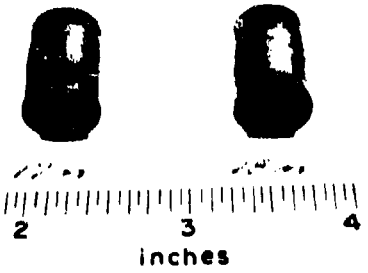


Plate No. 2-0713


Plate No. 2-0634

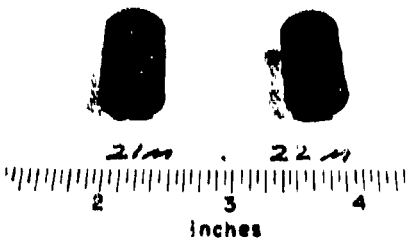


Plate No. 2-0639

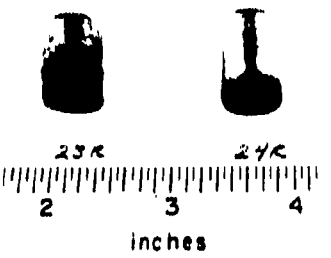


Figure 233. Post Exposure Photographs of 5 Mil $WSi_2$ Coated W $WSi_2$/W(G-18)-17M, 18M, 19M, 20M, 21M, 22M, 23R and 24R.

Plate No. 1-5363

X2.81

Figure 234. Arc Plasma Test $WSi_2$/W(G-18)-4M, Surface Temperature 3210°F, Exposure Time 1830 Seconds, Stagnation Pressure 1.05 Atm, Stagnation Enthalpy 2785 BTU/lb, Cold Wall Heat Flux 460 BTU/$ft^2$sec, Initial Length 449 Mil, Final Length 442 Mil. Hot Face at Right. One Inch Scale. No Coating Failure.


Plate No. 1-5364

Etched with Murakami's Reagent 0.394 Mils per Small Division (X200)

Figure 235. Arc Plasma Test $WSi_2$/W(G-18)-4M. Interface Showing $W_5Si_3$ Zone.

Plate No. 1-5411

X2.81

Figure 236a. Arc Plasma Test $WSi_2$/W(G-18)-6R, Surface Temperature 2830°F, Exposure Time 1800 Seconds, Stagnation Pressure 0.082 Atm, Stagnation Enthalpy 8310 BTU/lb, Cold Wall Heat Flux 554 BTU/$ft^2$sec, Initial Length 455 Mils, Final Length 434 Mils. Hot Face at Right. One Inch Scale Arc Conditions are for Most of Test (See Table 39). Coating Intact.

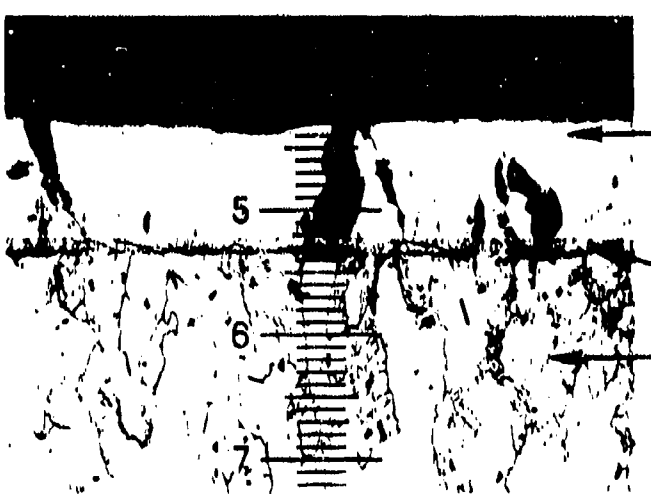


Etched with Murakami's Reagent, 0.394 Mils per Small Division (X200)

Figure 236b. Arc Plasma Test $WSi_2$/W(G-18)-6R. Interface Showing $W_5Si_3$ Zone.

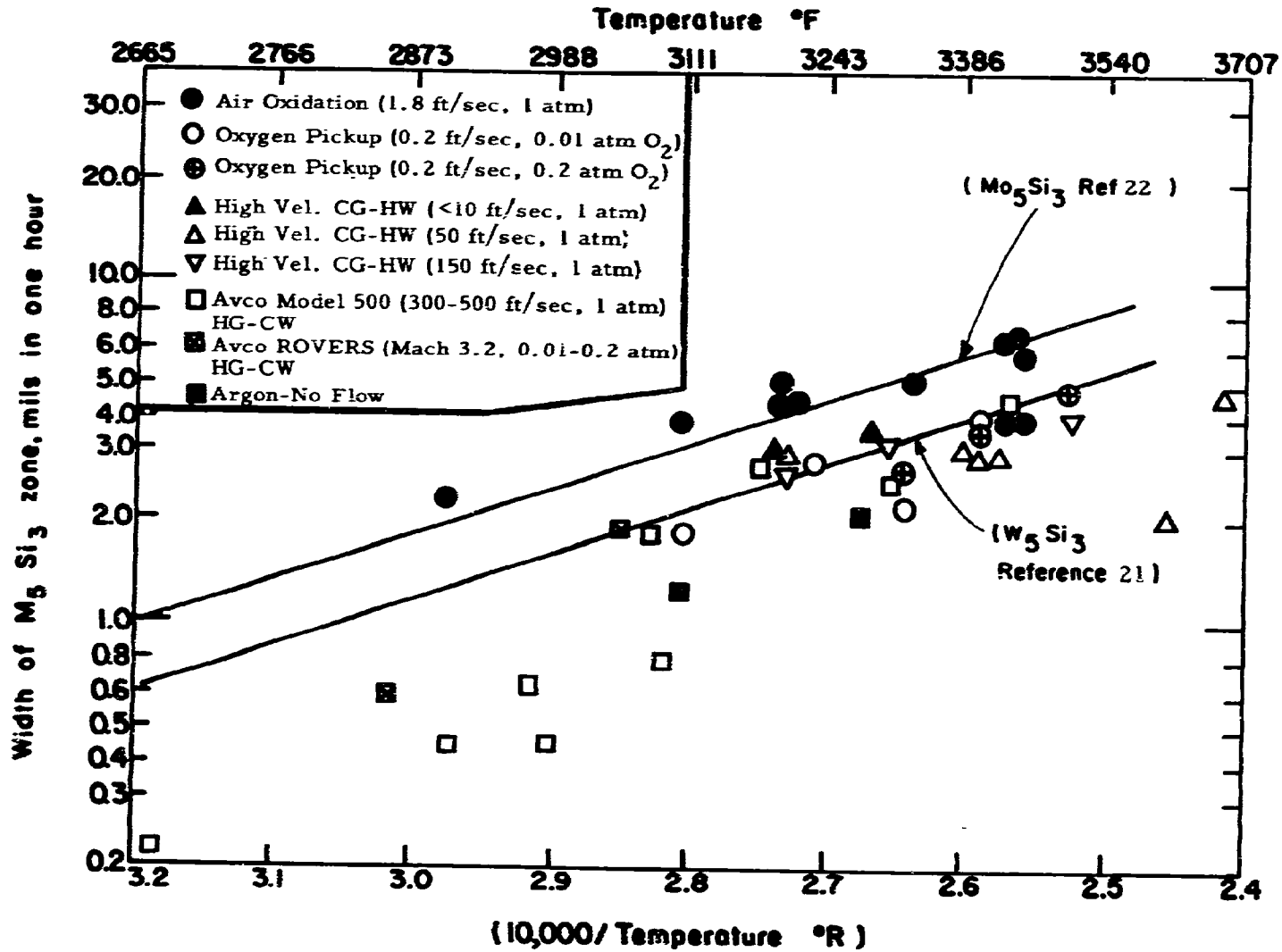


Figure 237. Growth of $W_5Si_3$ Zone on $WSi_2$/W(G-18) as a function of Flow Rate and Pressure Compared with the results of Bartlett and Gage (21) for $W_5Si_3$ and Perkins and Packer for $Mo_5Si_3$ (22).

Plate No. 1-5105

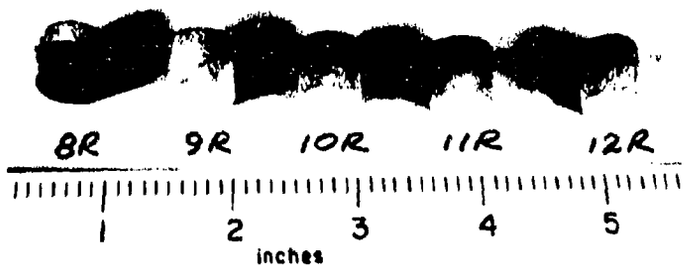


Plate No. 1-4286

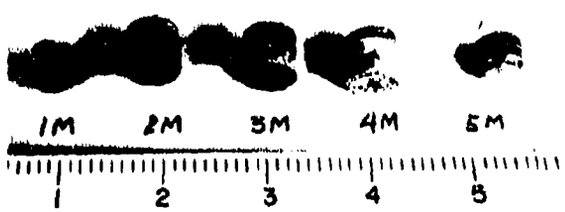


Plate No. 1-4287

Plate No. 1-4288

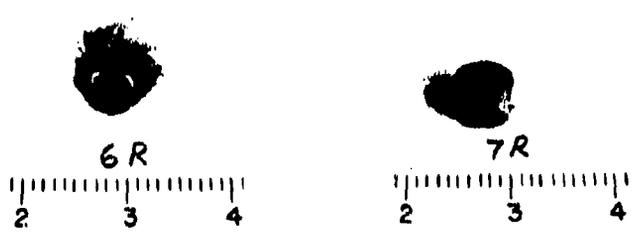


Figure 238. Post Exposure Photographs of 8 Mil Sn-Al-Mo Coated Ta-10W; Sn-Al/Ta-10W(G-19)-1M, 2M, 3M, 4M, 5M, 6R, 7R, 8R, 9R, 10R, 11R and 12R Arc Plasma Test Samples. Hot Face Pointing Down. Samples 1M and 5M Illustrate Coating Failure and Melting of $Ta_2O_5$. Samples 6R and 8R Illustrate Coating Failures and Melting of Tantalum. One Inch Scale.

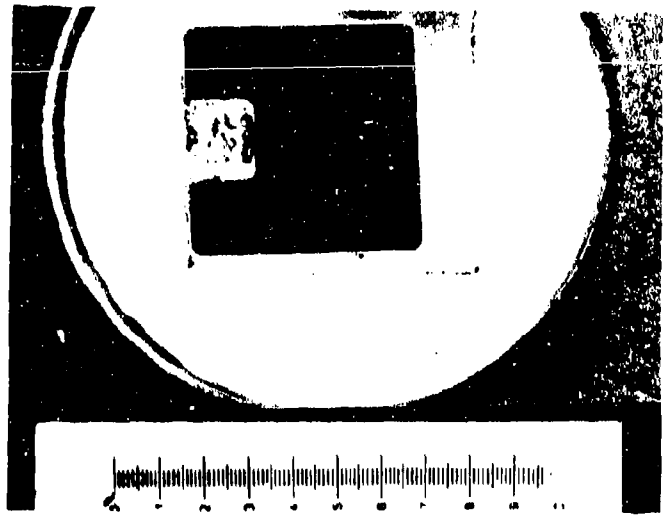

Plate No. 1-5040

X2.69

Figure 239. Arc Plasma Test Sn-Al/Ta-W(G-19)-4M, Surface Temperature 3000°F, Exposure Time 1830 Seconds, Stagnation Pressure 1.05 Atm, Stagnation Enthalpy 2980 BTU/lb, Cold Wall Heat Flux 350 BTU/ft$^2$sec, Initial Length 378 Mil, Final Length 367 Mil. Hot Face at Right. One Inch Scale. Coating Did not Fail.

Plate No. 1-5041

Unetched X250

Figure 240. Sn-Al/Ta-W(G-19)-4M. Interface of Sn-Al Coating (Top) and Ta-W Matrix.

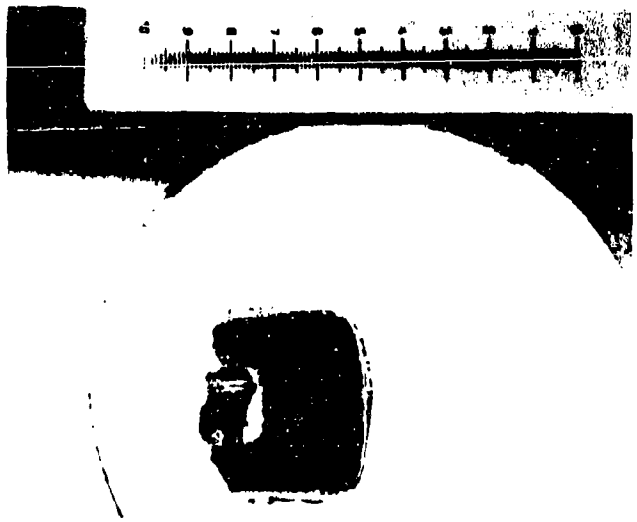

Plate No. 1-5031

X2.75

Figure 241. Arc Plasma Test Sn-Al/Ta-W(G-19)-1M, Surface Temperature 5090°F, Exposure Time 140 Seconds, Stagnation Pressure 1.06 Atm, Stagnation Enthalpy 2880 BTU/lb, Cold Wall Heat Flux 390 BTU/ft$^2$sec, Initial Length 368 Mil, Final Length 244 Mil. Hot Face at Right. One Inch Scale. Coating Failed.


Plate No. 1-5032

Unetched X250

Figure 242. Arc Plasma Test Sn-Al/Ta-W(G-19)-1M. Interface of Melted Region and Matrix.

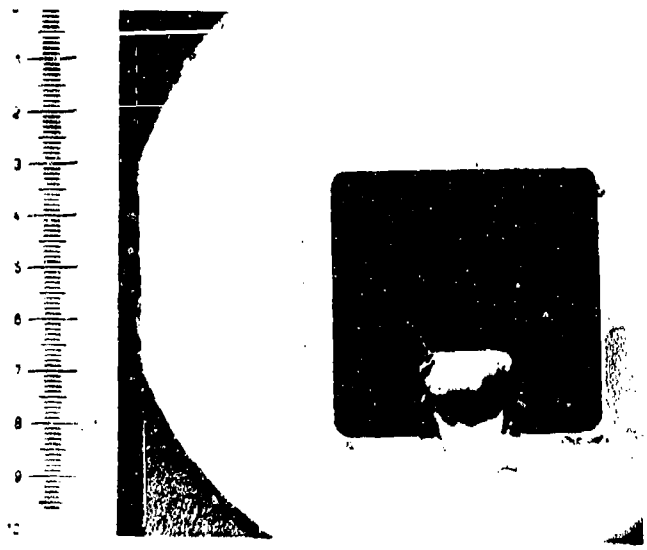

Plate No. 1-5019

X3.18

Figure 243. Arc Plasma Test Sn-Al/Ta-W(G-19)-9R, Surface Temperature 2950°F, Exposure Time 1800 Seconds, Stagnation Pressure 0.010 Atm, Stagnation Enthalpy 10520 BTU/lb, Cold Wall Heat Flux 158 BTU/ft$^2$sec, Initial Length 362 Mil, Final Length 342 Mil. Hot Face at Top. One Inch Scale. Coating Did Not Fail.

Plate No. 1-5020

Unetched X250

Figure 244. Arc Plasma Test Sn-Al/Ta-W(G-19)-9R. Interface of Coating (Right) and Matrix.

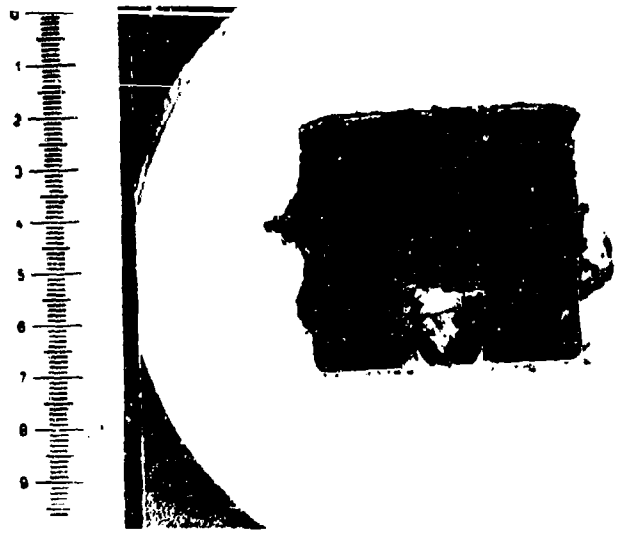

Plate No. 1-5016

X3.18

Figure 245. Sn-Al/Ta-W(G-19)-8R, Surface Temperature 3670°F, Exposure Time 400 Seconds, Stagnation Pressure 0.011 Atm, Stagnation Enthalpy 11440 BTU/lb, Cold Wall Heat Flux 200 BTU/ft$^2$sec, Initial Length 361 Mil, Final Length 322 Mil. Hot Face at Top. One Inch Scale. Coating Failed.

Plate No. 1-5018

Unetched X250

Figure 246. Arc Plasma Test Sn-Al/Ta-W(G-19)-8R. Interface of Melted Ta-W (Right) and Matrix.


W+Zr+Cu (G-20)



Figure 247. Post Exposure Photographs of Arc Plasma Tests W+Zr+Cu(G-20)-1M, 2M, 3M, 4M, 5M, 6M, 7R, 8R and 9R.

Plate No.
1-9729

X2.87

Figure 248. Arc Plasma Test W+Zr+Cu(G-20)-6M, Surface Temperature 2420°F, Exposure Time 1800 Seconds, Stagnation Pressure 1.01 Atm., Stagnation Enthalpy 1830 BTU/lb, Cold Wall Heat Flux 155 BTU/ft$^2$sec, Initial Length 427 Mils, Final Length 262 Mils. Hot Face Up. One Inch Scale.

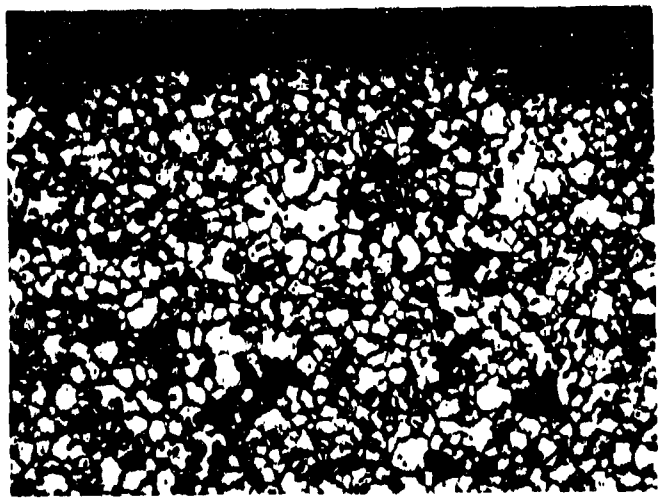

Plate No.
1-9731

Etched with Murikami's Reagent X250

Figure 249. Arc Plasma Test W+Zr+Cu(G-20)-6M, Hot Interface at Top.

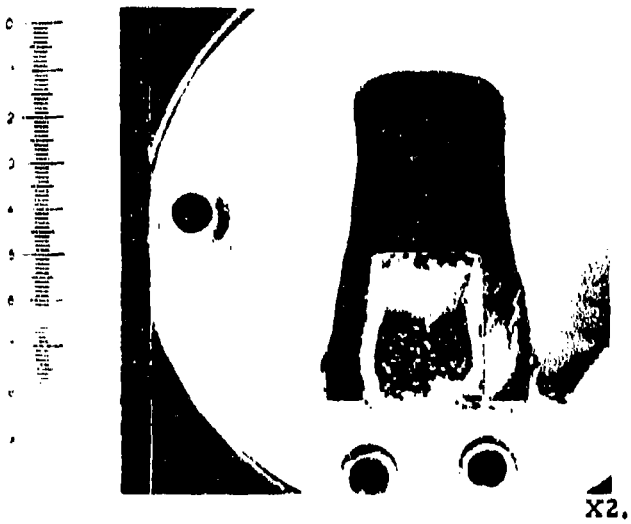

Plate No.
1-9712

X2.87

Figure 250. Arc Plasma Test W+Zr+Cu(G-20)-2M, Surface Temperature 3345°F, Exposure Time 324 Seconds, Stagnation Pressure 1.01 Atm., Stagnation Enthalpy 3030 BTU/lb, Cold Wall Heat Flux 170 BTU/ft$^2$sec, Initial Length 500 Mils, Final Length 388 Mils. Hot Face Up. One Inch Scale.

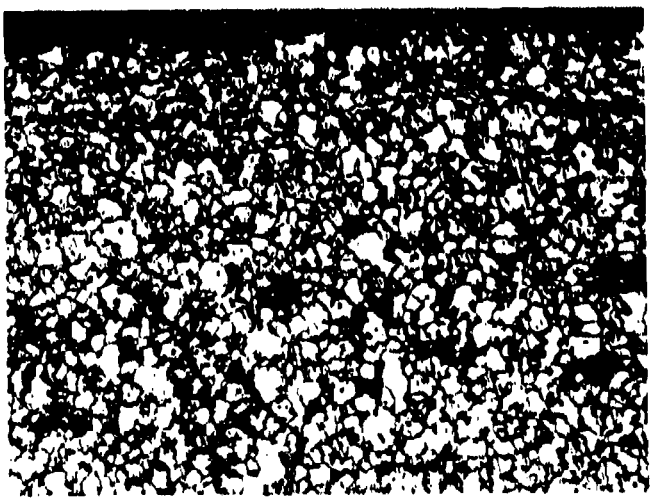

Plate No.
1-9713

Etched with Murikami's Reagent X250

Figure 251. Arc Plasma Test W+Zr+Cu(G-20)-2M, Hot Interface at Top.

Plate No.
1-9748

X2.80

Figure 252. Arc Plasma Test W+Zr+Cu(G-20)-9R, Surface Temperature 5300°F, Exposure Time 775 Seconds, Stagnation Pressure 0.100 Atm., Stagnation Enthalpy 10680 BTU/lb, Cold Wall Heat Flux 584 BTU/ft$^2$sec, Initial Length 433 Mils, Final Length 411 Mils. Hot Face Up. One Inch Scale.

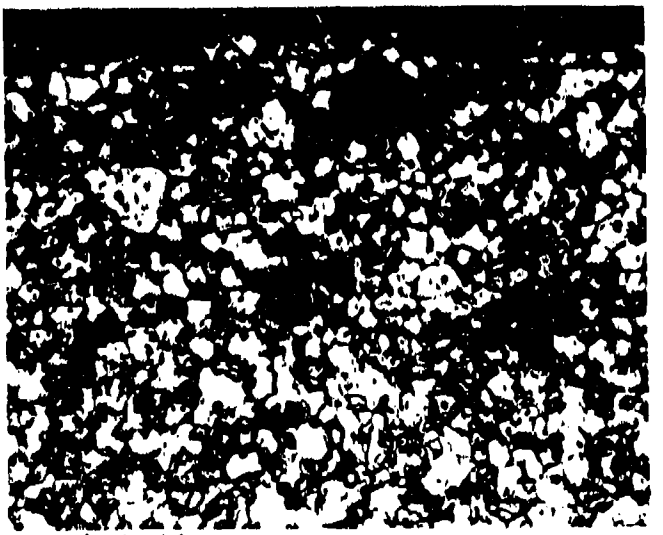

Plate No.
1-9749

Etched with Murikami's Reagent X250

Figure 253. Arc Plasma Test W+Zr+Cu(G-20)-9R. Hot Interface at Top.

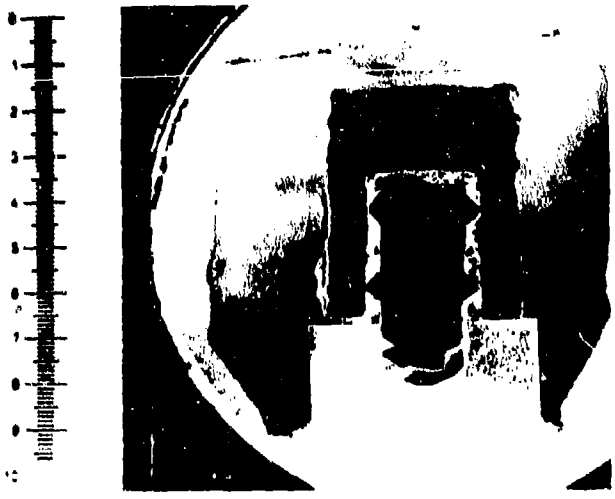

Plate No.
1-9742

X2.80

Figure 254. Arc Plasma Test W+Zr+Cu(G-20)-8R, Surface Temperature 5205°F, Exposure Time 500 Seconds, Stagnation Pressure 0.135 Atm., Stagnation Enthalpy 11980 BTU/lb, ColdWall Heat Flux 662 BTU/ft$^2$sec. Initial Length 438 Mils, Final Length 181 Mils. Hot Face Up. One Inch Scale. Sting Shown in Place.

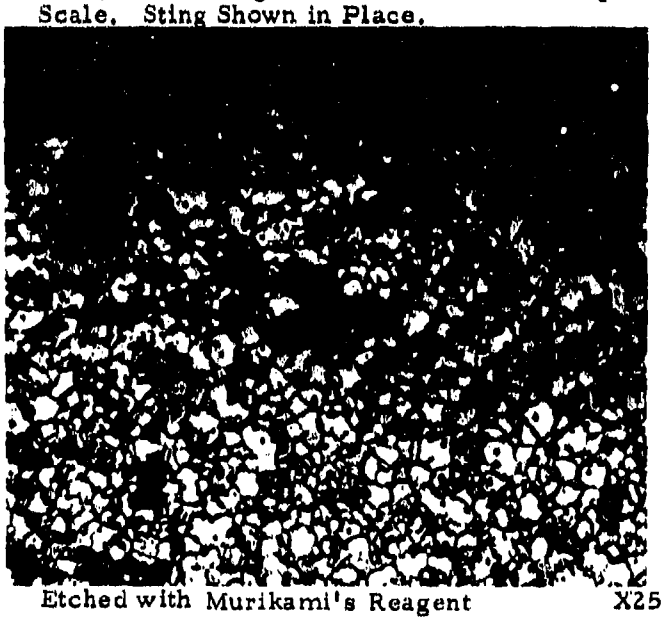

Plate No.
1-9743

Etched with Murikami's Reagent X250

Figure 255. Arc Plasma Test W+Zr+Cu(G-20)-8R Hot Interface at Top.

Plate No. 1-9532

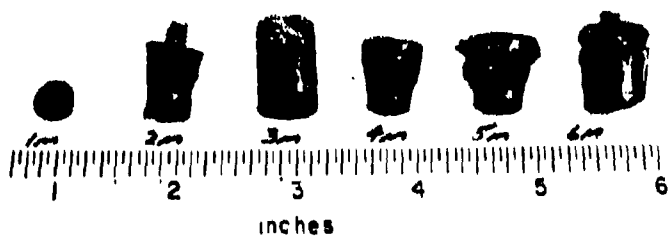


Figure 256. Post Exposure Photographs of Arc Plasma Tests W + Ag(G-21)-1M, 2M, 3M, 4M, 5M and 6M.

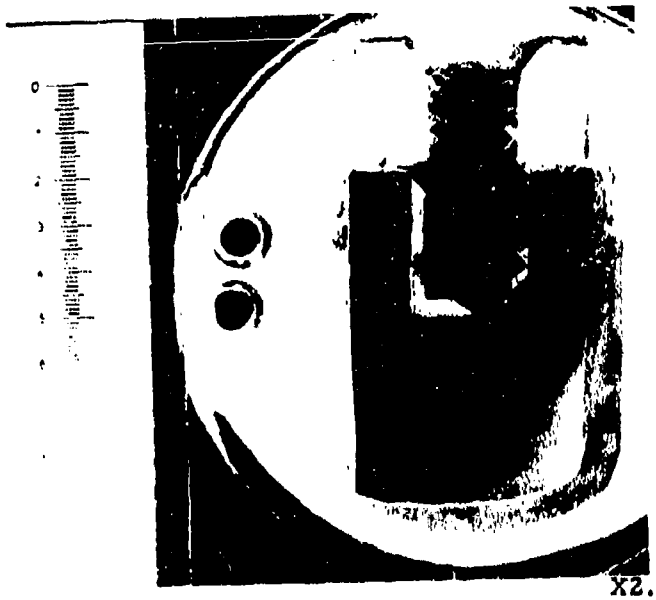

Plate No.
1-9773

X2.80

Figure 257. Arc Plasma Test W+Ag(G-21)-6M, Surface Temperature 2545°F, Exposure Time 1800 Seconds, Stagnation Pressure 1.01 Atm., Stagnation Enthalpy 2000 BTU/lb, Cold Wall Heat Flux 160 BTU/ft$^2$sec, Initial Length 445 Mils, Final Length 387 Mils. Hot Face Down. One Inch Scale

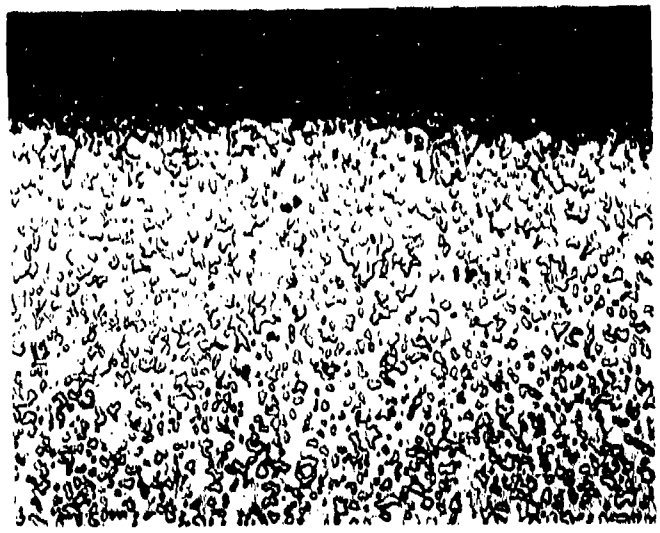

Plate No.
2-0693

Etched with Murikami's Reagent X250

Figure 258. Arc Plasma Test W+Ag(G-21)-6M. Hot Interface at Top.

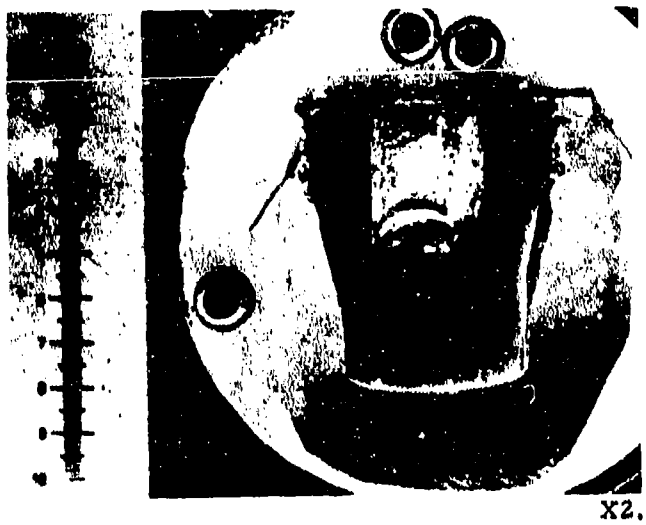

Plate No.
1-9768

X2.80

Figure 259. Arc Plasma Test W+Ag(G-21)-5M, Surface Temperature 3050°F, Exposure Time 460 Seconds, Stagnation Pressure 1.01, Stagnation Enthalpy 2760 BTU/lb, Cold Wall Heat Flux 210 BTU/ft$^2$sec, Initial Length 439 Mils, Final Length 301 Mils. Hot Face Down. One Inch Scale.

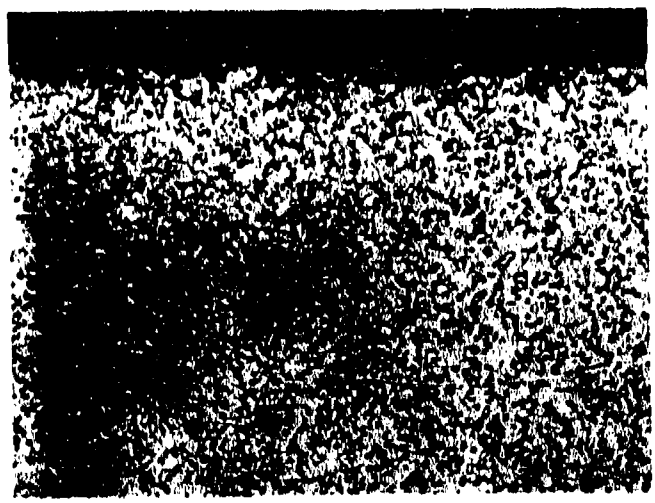

Plate No.
1-9769

Etched with Murikami's Reagent X250

Figure 260. Arc Plasma Test W+Ag(G-21)-5M. Hot Interface at Top.

Plate No. 1-7743


Plate No. 1-7691

Plate No. 1-7827


Figure 261. Post Exposure Photographs of Arc Plasma Tests $SiO_2$+ 68.5w/o(H-22)-1M, 2M, 3M, 4M, 5M, 6M, 7R, 8R, 9R, 10R and 11R.

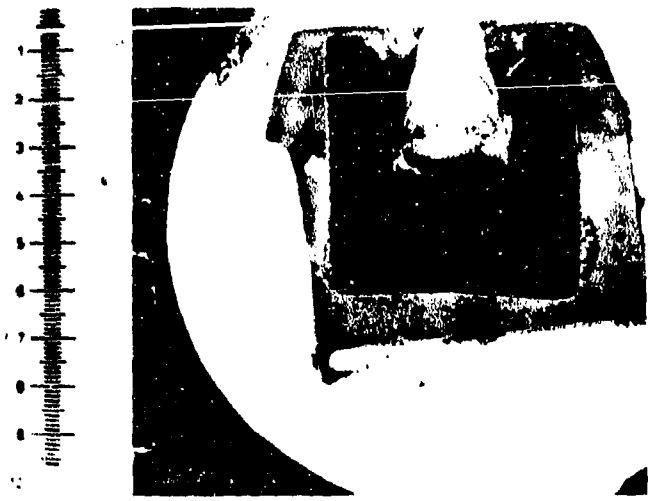

Plate No. 1-7753

X3.00

Figure 262. Arc Plasma Test $SiO_2$ + 68.5 w/o W(H-22)-4M, Surface Temperature 5205°F, Exposure Time 1800 Seconds, Stagnation Pressure 1.08 Atm. Stagnation Enthalpy 5500 BTU/lb Cold Wall Heat Flux 780 BTU/$ft^2$ sec, 428 Mil Recession, Hot Face Down. One Inch Scale.

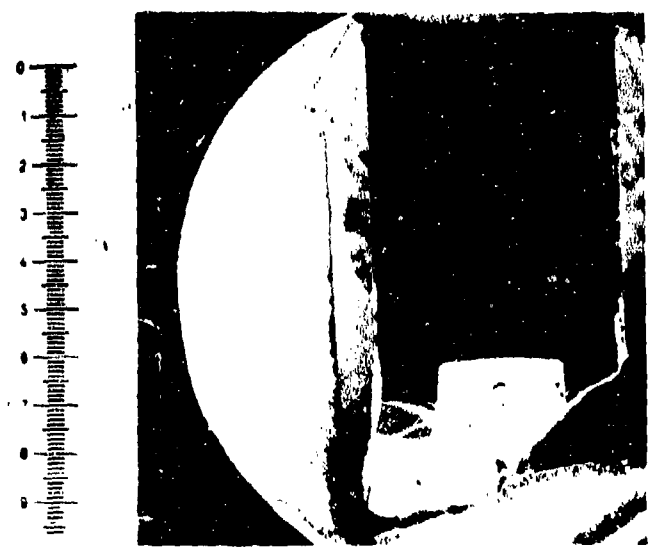

Plate No. 1-7747

X3.00

Figure 263. Arc Plasma Test $SiO_2$ + 68.5 w/o W(H-22)-2M, Surface Temperature 4505°F, Exposure Time 1557 Seconds, Stagnation Pressure 1.07 Atm, Stagnation Enthalpy 4110 BTU/lb, Cold Wall Heat Flux 580 BTU/$ft^2$ sec, 19 Mil Recession, Hot Face Up, One Inch Scale.

Plate No. 1-7701

X3.00

Figure 264. Arc Plasma Test $SiO_2$ + 68.5 w/o W(H-22)-10R, Surface Temperature 3750°F, Exposure Time 600 Seconds, Stagnation Pressure 0.009 Atm. Stagnation Enthalpy 13,100 BTU/lb, Cold Wall Heat Flux 230 BTU/$ft^2$ sec, 331 Mils Recession, Hot Face Up. One Inch Scale.

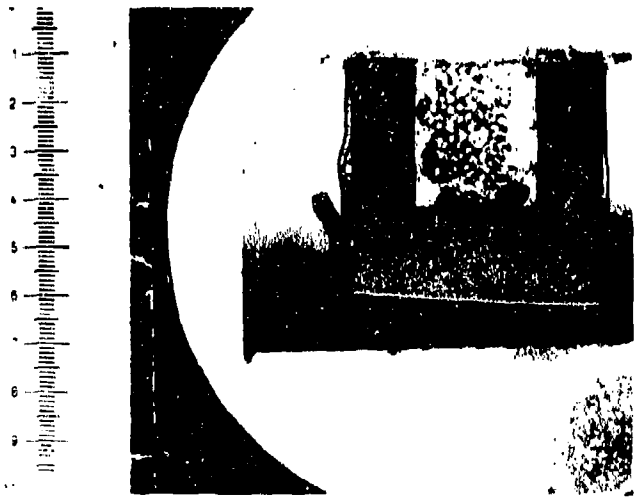

Plate No. 1-7692

X3.00

Figure 265. Arc Plasma Test $SiO_2$ + 68.5 w/o W(H-22)-7R, Surface Temperature 4175°F, Exposure Time 230 Seconds, Stagnation Enthalpy 10,580 BTU/lb, Cold Wall Heat Flux 526 BTU/$ft^2$ sec, 507 Mil Recession, Hot Face Down, One Inch Scale.

Plate No. 1-6602

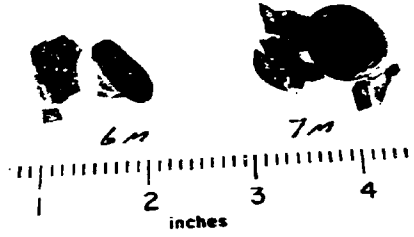


Plate No. 1-4756

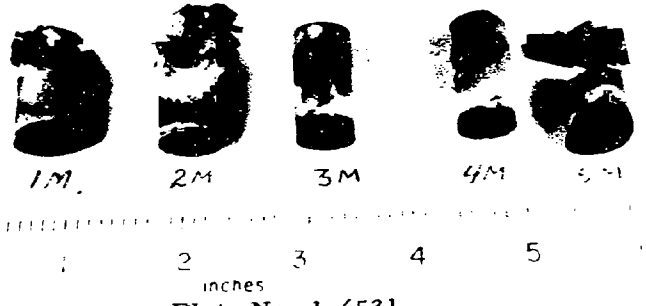


Plate No. 1-5317

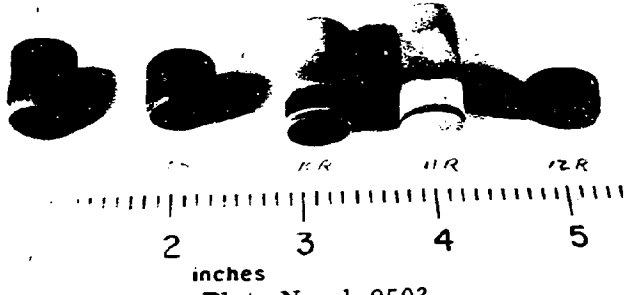


Plate No. 1-6531

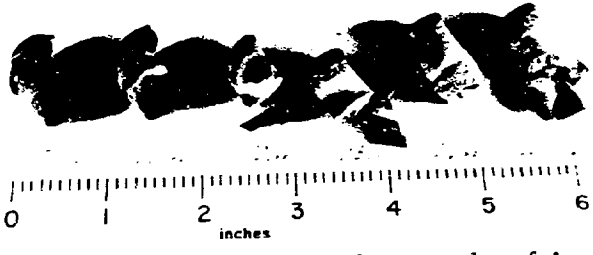


Plate No. 1-9503

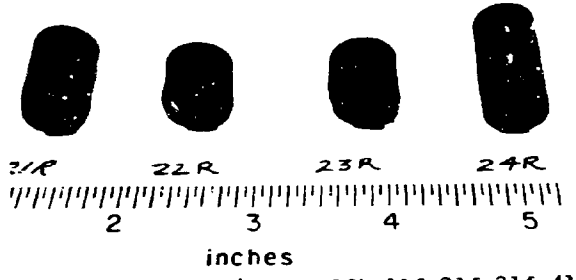


Figure 266. Post Exposure Photographs of Arc Plasma Tests $SiO_2$+60w/oW(H-23)-1M, 2M, 3M, 4M, 5M, 6M, 7M, 8R, 9R, 10R, 11R, 12R, 15M, 16M, 17M, 18M, 19M, 20M, 21R, 22R, 23R and 24R.

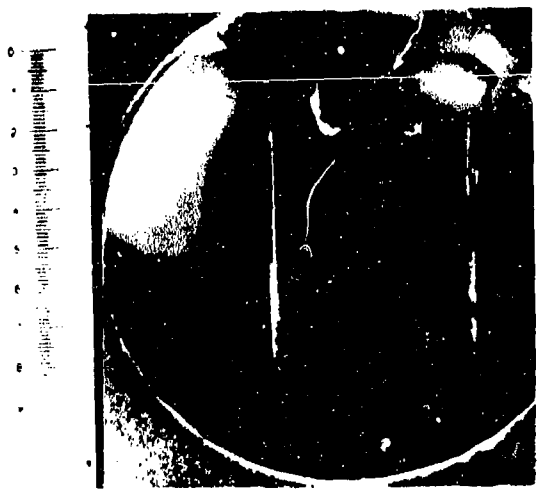

Plate No. 1-4760

X2.5

Figure 267. Arc Plasma Test $SiO_2$ + 60w/oW(H-23)-2M, Surface Temperature 3675°F, Exposure Time 1830 Seconds, Stagnation Pressure 1.06 Atm, Stagnation Enthalpy 3380 BTU/lb, Cold Wall Heat Flux 405 BTU/$ft^2$sec, Initial Length 700 Mil, Final Length 683 Mil. Hot Face at Bottom. One Inch Scale. Rear Broke on Removal after Test.


Plate No. 1-4762

Unetched X125

Figure 268. Arc Plasma Test $SiO_2$+60w/oW(H-23)-2M. Hot Interface.

Plate No. 1-6532

X2.69

Figure 269. Arc Plasma Test $SiO_2$+60w/oW(H-23)-15M, Surface Temperature 4210°F, Exposure Time 1286 Seconds, Stagnation Pressure 1.08 Atm, Stagnation Enthalpy 5440 BTU/lb. Cold Wall Heat Flux 855 BTU/$ft^2$sec, Initial Length 686 Mil, Final Length 318 Mils. Hot Face at Right. One Inch Scale. Specimen Broke on Removal after Test. Viscous Flow Observed.

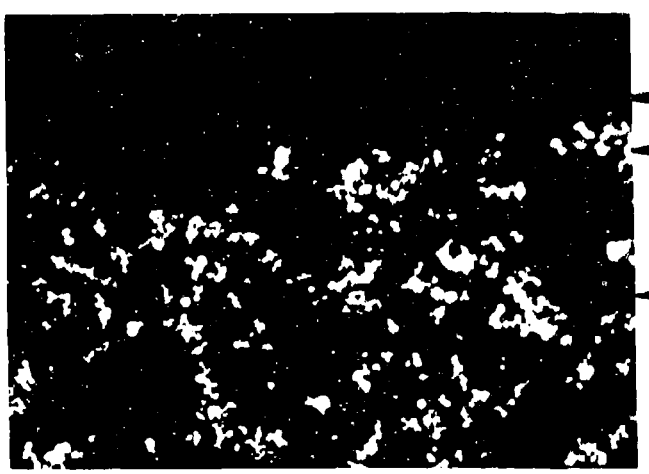


Plate No. 1-6533

Unetched X250

Figure 270. Arc Plasma Test $SiO_2$ + 60w/oW(H-23)-15M. Top Surface After Viscous Flow.

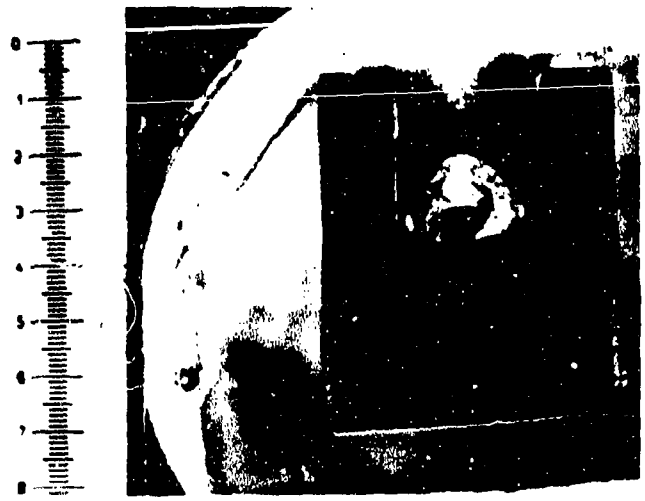

Plate No. 1-5318

X3.38

Figure 271. Arc Plasma Test $SiO_2$+60w/oW(H-23)-8R, Surface Temperature 3870°F, Exposure Time 325 Seconds, Stagnation Pressure 0.023 Atm, Stagnation Enthalpy 10860 BTU/lb, Cold Wall Heat Flux 475 BTU/$ft^2$sec, Initial Length 699 Mil, Final Length 320 Mil. Hot Face at Bottom. One Inch Scale.

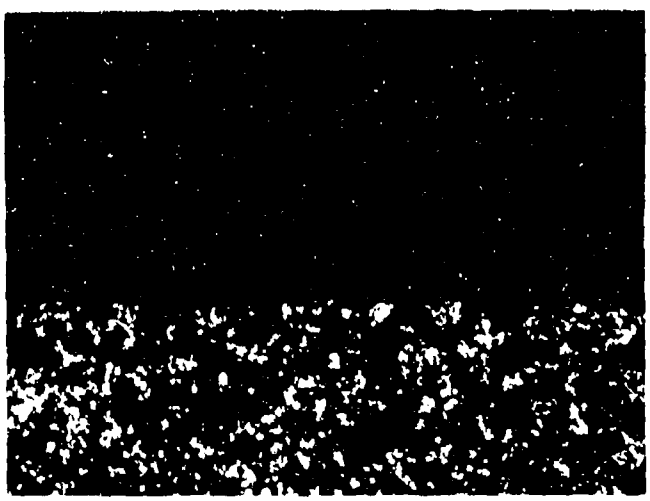

Plate No. 1-5319

Unetched X125

Figure 272. Arc Plasma Test $SiO_2$ + 60w/oW(H-23)-8R. Hot Interface Showing Some $SiO_2$ Reaction.

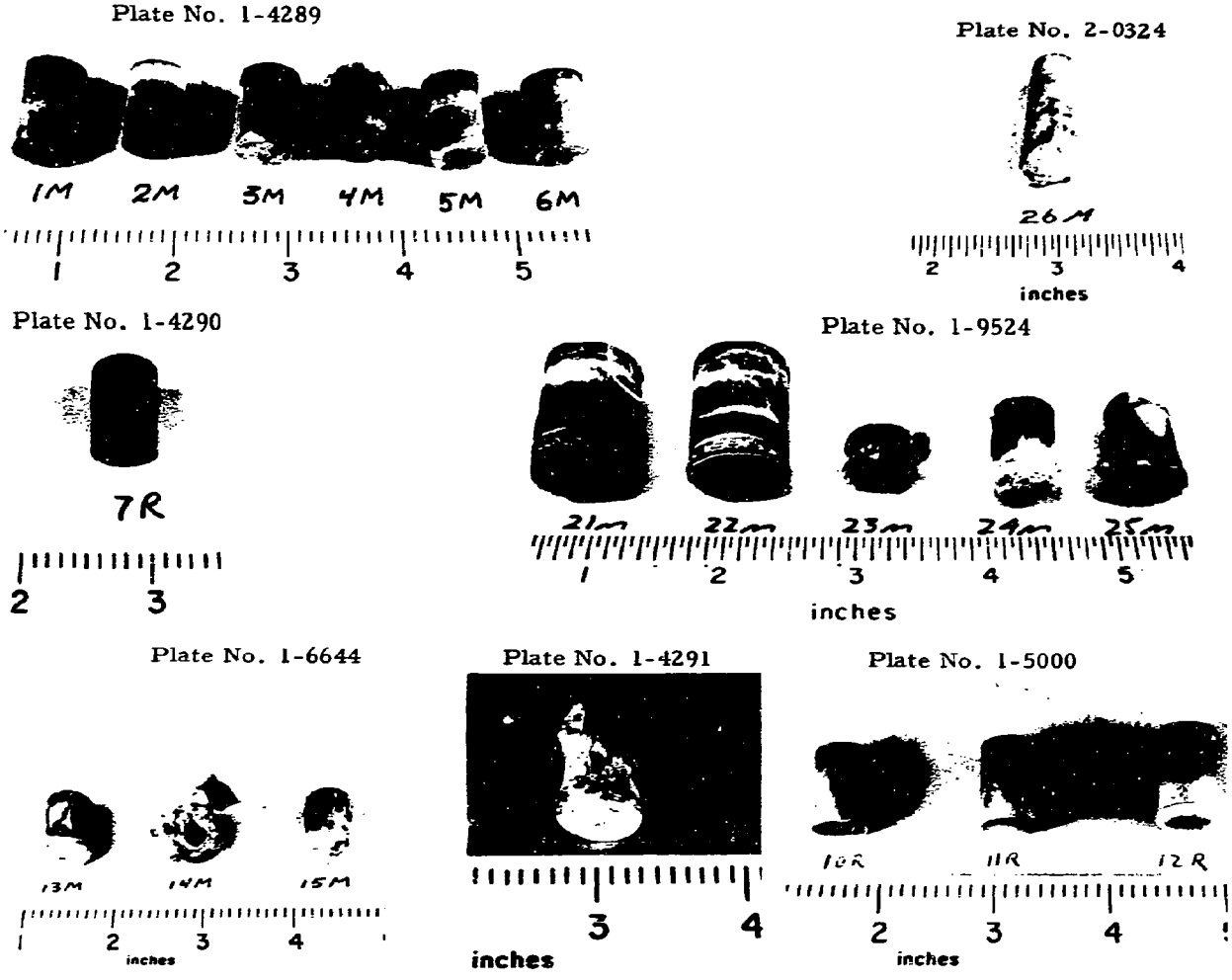


Figure 273. Post Exposure Photographs of Arc Plasma Tests Hf-Ta-Mo(I-23)-1M, 2M, 3M, 4M, 5M, 6M, 26M, 7R, 21M, 22M, 23M, 24M, 25M, 13M, 14M, 15M, 9R, 10R, 11R, 12R (8R Melted completely).

Plate No. 2-0706

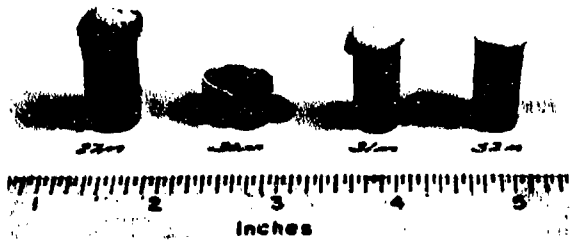


Plate No. 2-0674


Plate No. 2-0707

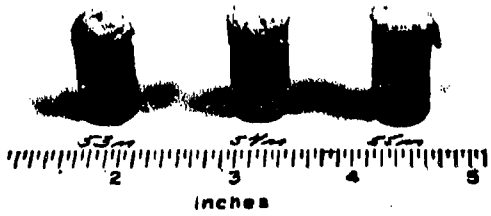


Plate No. 2-0708

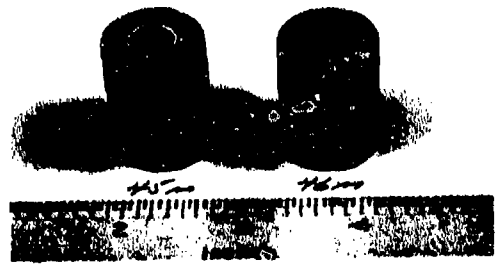

Figure 274. Post Exposure Photographs of Arc Plasma Tests Hf-Ta-Mo (1-23)-27M, 30M, 31M, 32M, 37M, 38M, 41M, 42M, 53M, 54M, 55M, 45M, 46M.

Plate No. 2-0649

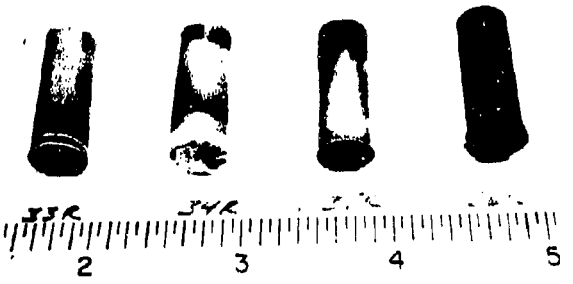


Plate No. 2-0673


Plate No. 2-0709

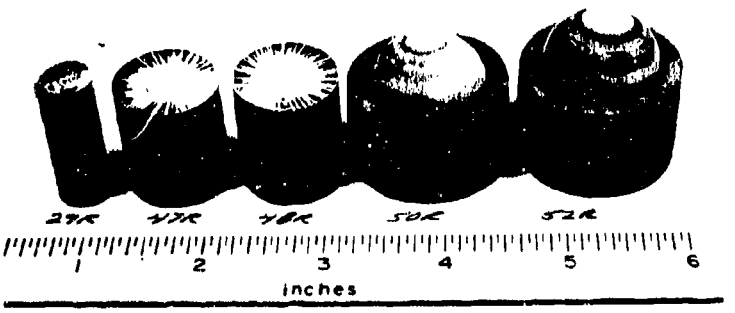


Figure 275. Post Exposure Photographs of Arc Plasma Tests Hf-Ta-Mo(I-23)-33R, 34R, 35R, 36R, 28R, 39R, 40R, 43R, 44R, 49R, 51R, 29R, 47R, 48R, 50R and 52R.

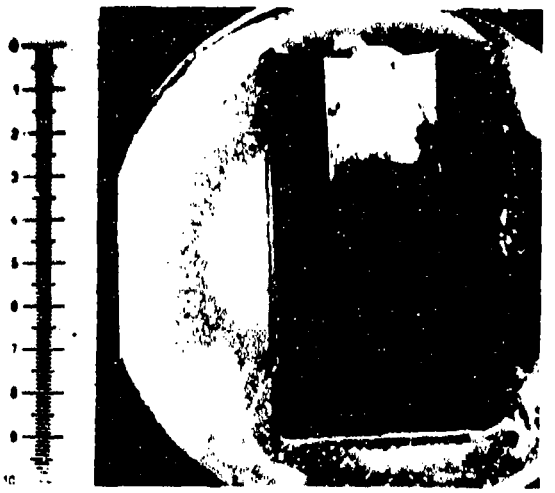

Plate No. 1-4785

X2.7

Figure 276. Arc Plasma Test Hf-Ta-Mo(I-23)-1M, Surface Temperature 4030°F, Exposure Time 1830 Seconds, Stagnation Pressure 1.08 Atm, Stagnation Enthalpy 3295 BTU/lb, Cold Wall Heat Flux 530 BTU/ft$^2$sec, Initial Length 578 Mil, Final Length 553 Mil. Hot Face at Bottom. One Inch Scale.

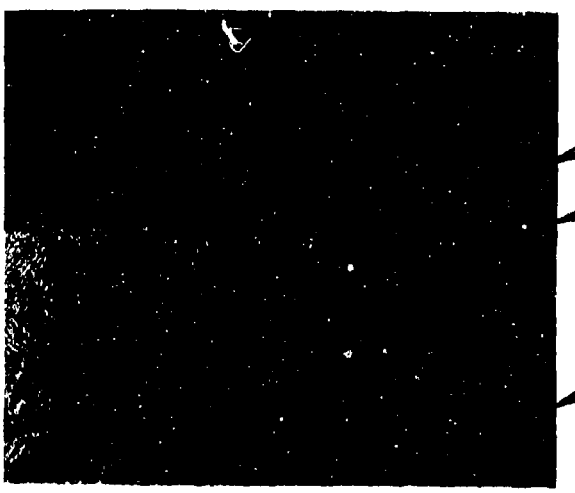


Plate No. 1-4786A

Etched with 15 Glycerine 5 $HNO_3$5HCl 3HF X75

Figure 277. Arc Plasma Test Hf-Ta-Mo(I-23)-1M. Interface Showing Oxide, Subscale and Matrix.

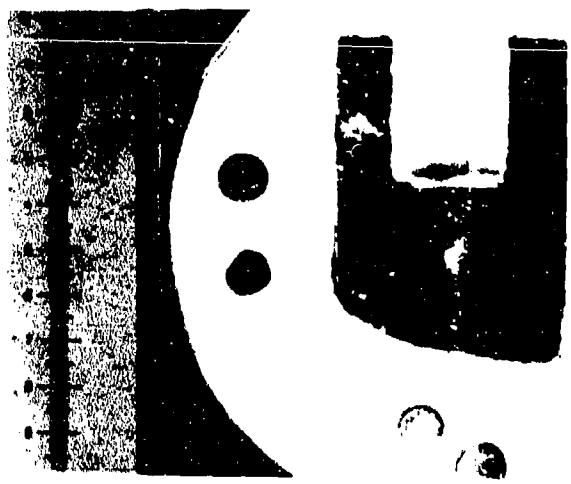

Plate No. 1-6652

X2.87

Figure 278. Arc Plasma Test Hf-Ta-Mo(I-23)-15M, Surface Temperature 4645°F, Exposure Time 1830 Seconds, Stagnation Pressure 1.06 Atm, Stagnation Enthalpy 3735 BTU/lb, Cold Wall Heat Flux 515 BTU/ft$^2$sec, Initial Length 421 Mil, Final Length 353 Mil. Hot Face at Bottom. One Inch Scale.


Plate No. 1-6653A

Etched with 15 Glycerine 5$HNO_3$5HCl 3HF X75

Figure 279. Arc Plasma Test Hf-Ta-Mo(I-23)-15M, Interface Showing Oxide, Subscale, Matrix, Some Melting of Oxide Has Occurred.

Plate No. 1-5007

X2.81

Figure 280. Arc Plasma Test Hf-Ta-Mo(I-23)-12R, Surface Temperature 3755°F, Exposure Time 1800 Seconds, Stagnation Pressure 0.018 Atm, Stagnation Enthalpy 12710 BTU/lb, Cold Wall Heat Flux 378 BTU/ft$^2$sec, Initial Length 560 Mil, Final Length 534 Mil. Hot Face at Bottom. One Inch Scale. Oxide and Subscale Clearly Visible at Hot Face.

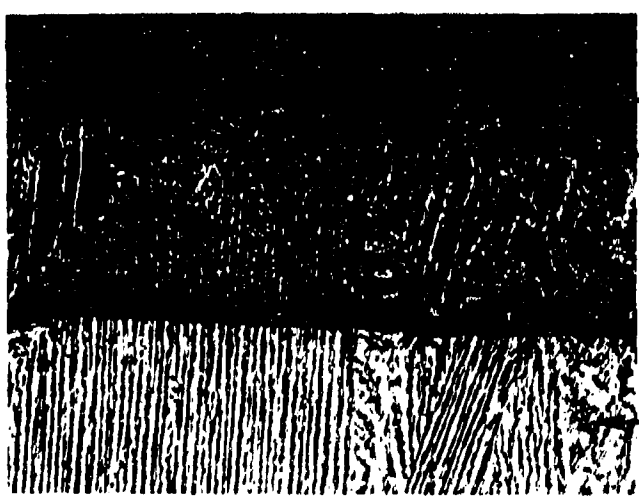


Plate No. 1-5008A

Etched with 15 Glycerine 5$HNO_3$HCl 3HF X75

Figure 281. Arc Plasma Test Hf-Ta-Mo(I-23)-12R, Interface Showing Oxide, Subscale and Matrix.

Plate No. 1-4807

X3.18

Figure 282. Arc Plasma Test Hf-Ta-Mo(I-23)-9R, Surface Temperature 4220°F, Exposure Time 1800 Seconds, Stagnation Pressure 0.022 Atm, Stagnation Enthalpy 11250 BTU/lb, Cold Wall Heat Flux 337 BTU/ft2sec, Initial Length 432 Mil, Final Length 326 Mil, Hot Face at Top, One Inch Scale. Oxide and Subscale Clearly Visible at Hot Face. Some Melting has Occurred.

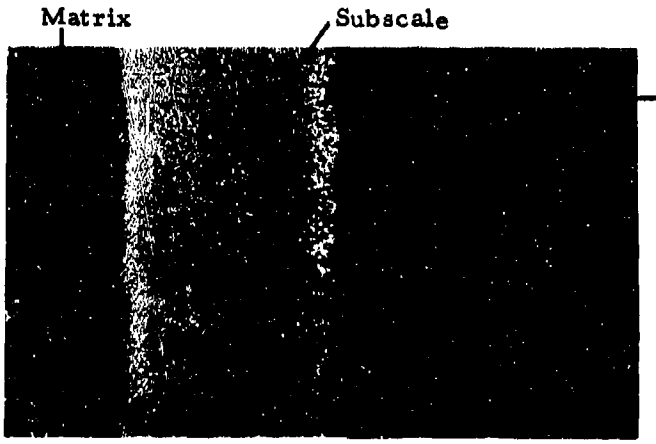


Plate No. 1-4808

Eteched with 15 Glycerine 5$HNO_3$ 5HCl 3HF X50

Figure 283. Arc Plasma Test Hf-Ta-Mo(I-23)-9R, Interface Showing Oxide, Subscale and Matrix, Some Melting of Oxide has Occurred.

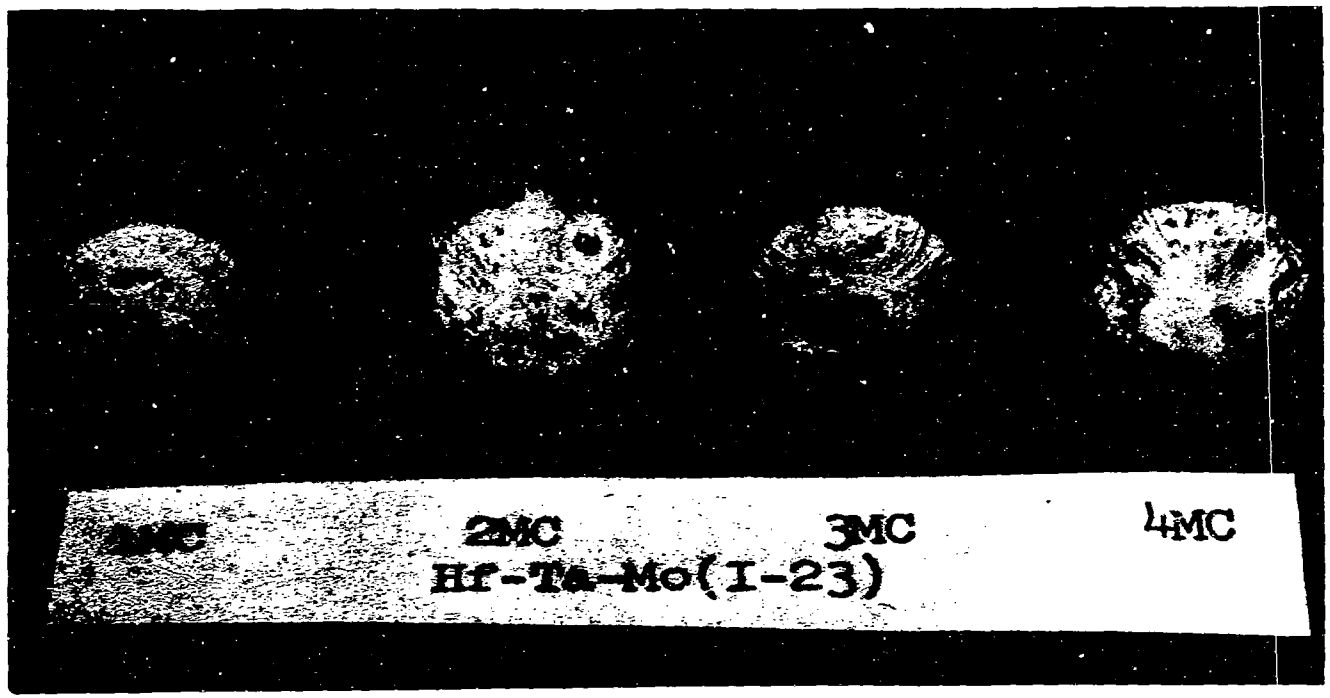


Figure 284. Post Exposure Photographs of Samples Hf-Ta-Mo(I-23) - 1MC, 2MC, 3MC and 4MC

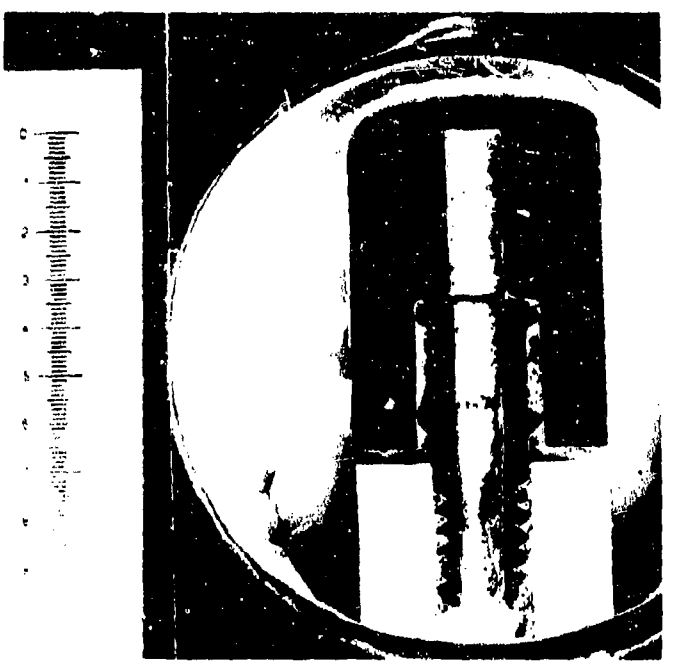

Plate No. 1-9224

X3.00

Figure 285. Arc Plasma Test Hf-20Ta-2Mo(I-23)-1MC, Surface Temperature 4760°F, Internal Temperature 3530°F, Exposure Time 1800 Seconds, Stagnation Pressure 1.05 Atm, Stagnation Enthalpy 3220 BTU/lb, Cold Wall Heat Flux 425 BTU/ft$^2$ sec, 46 Mil Recession, Hot Face Up. One Inch Scale.

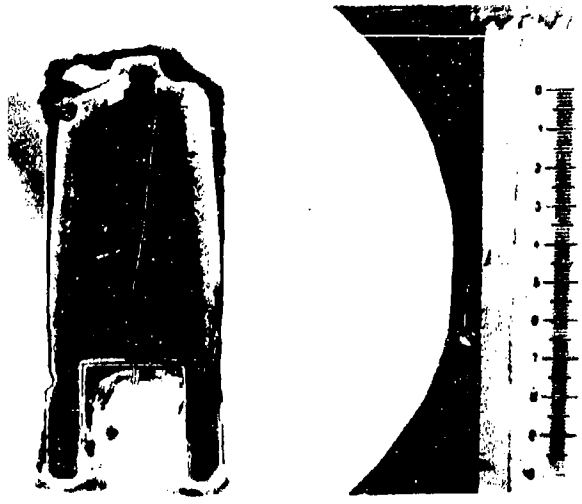

Plate No.
2-0694

X2.35

Figure 286. Arc Plasma Test Hf-Ta-Mo(I-23)-27M. Average Surface Temperature 4230°F, Exposure Time 11,600 Seconds (7 cyclic exposures each of approximately 1800 seconds), Stagnation Pressure 1.05 atm., Stagnation Enthalpy 3300 BTU/lb, Cold Wall Heat Flux 410 BTU/ft$^2$sec, 138 Mils Recession, Hot Face Up. One Inch Scale.

Plate No.
2-0695

Etched with 15 Glycerine
5$HNO_3$5HCl

X250

Figure 287. Arc Plasma Test Hf-Ta-Mo(I-23)-27M, Hot Surface.

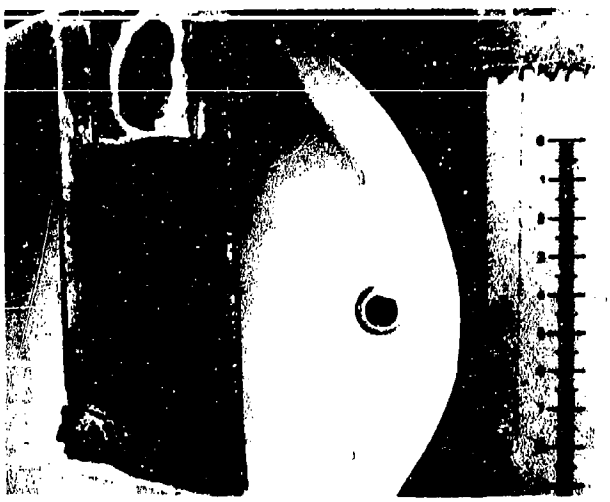

Plate No.
2-0696

X2.35

Figure 288. Arc Plasma Test Hf-Ta-Mo(I-23)-28R. Average Surface Temperature 4200°F, Exposure Time 7220 Seconds (4 cyclic exposures each of approximately 1800 seconds), Stagnation Pressure 0.132 Atm., Stagnation Enthalpy 7600 BTU/lb, Cold Wall Heat Flux 398 BTU/ft$^2$sec, 55 Mils Recession, Hot Face Down, One Inch Scale.

Plate No.
2-0697

Etched with 15 Glycerine
5HNO$_3$5HCl3HF

X250

Figure 289. Arc Plasma Test Hf-Ta-Mo(I-23)-28R, Hot Surface.

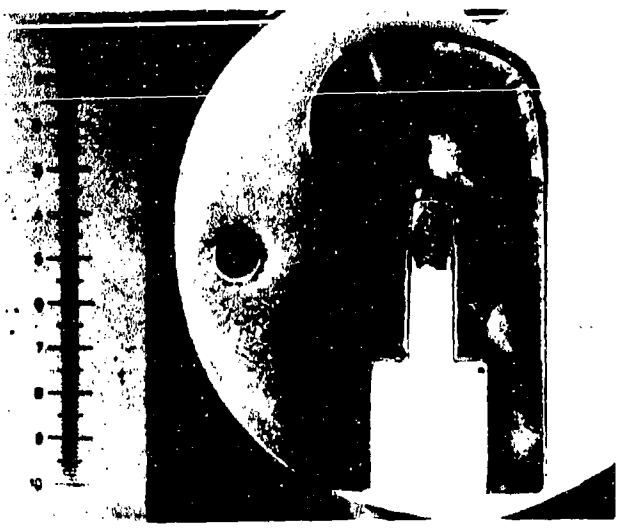

Plate No. 2-0699

X2.75

Figure 290. Arc Plasma Test Hf-Ta-Mo(I-23)-38MH Surface Temperature 4230°F, Exposure Time 1800 Seconds, Stagnation Pressure 1.02 Atm., Stagnation Enthalpy 3220 BTU/lb, Cold Wall Heat Flux 435 BTU/ft$^2$ sec, 48 Mils Recession, Hot Face Up. One Inch Scale

Plate No. 2-0700

Etched with 10 Glycerine
5$HNO_3$5HCl3HF

X250

Figure 291. Arc Plasma Test Hf-Ta-Mo(I-23)-38MH, Hot Surface.

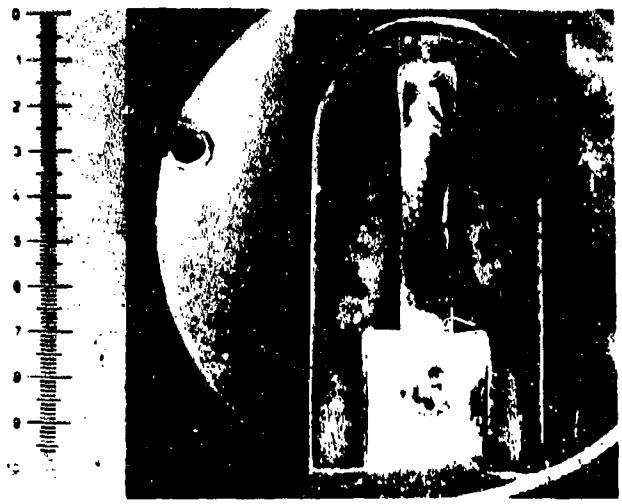

Plate No.
2-0701

X2.80

Figure 292. Arc Plasma Test Hf-Ta-Mo(I-23)-39RH. Surface Temperature 3620°F, Exposure Time 1800 Seconds, Stagnation Pressure 0.137 atm., Stagnation Enthalpy 6740 BTU/lb, Cold Wall Heat Flux 412 BTU/ft$^2$sec, 22 Mils Recession, Hot Face Up. One Inch Scale.

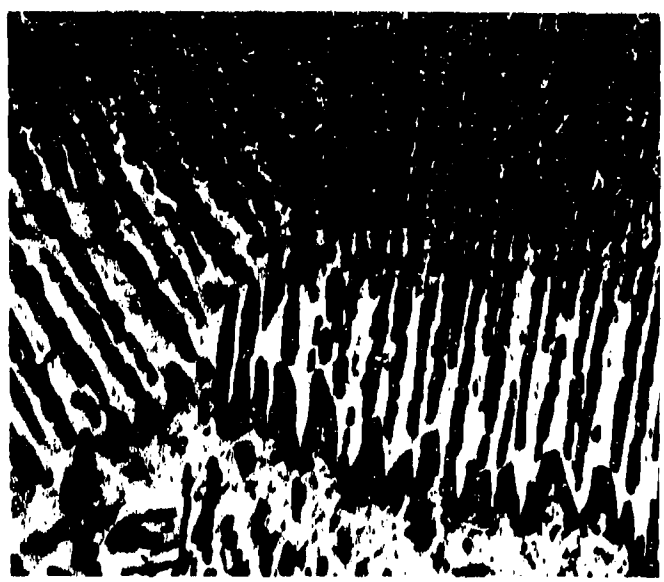

Plate No.
2-0702

Etched with 10 Glycerine
5$HNO_3$5HCl3HF

X250

Figure 293. Arc Plasma Test Hf-Ta-Mo(I-23)-39RH, Hot Surface.

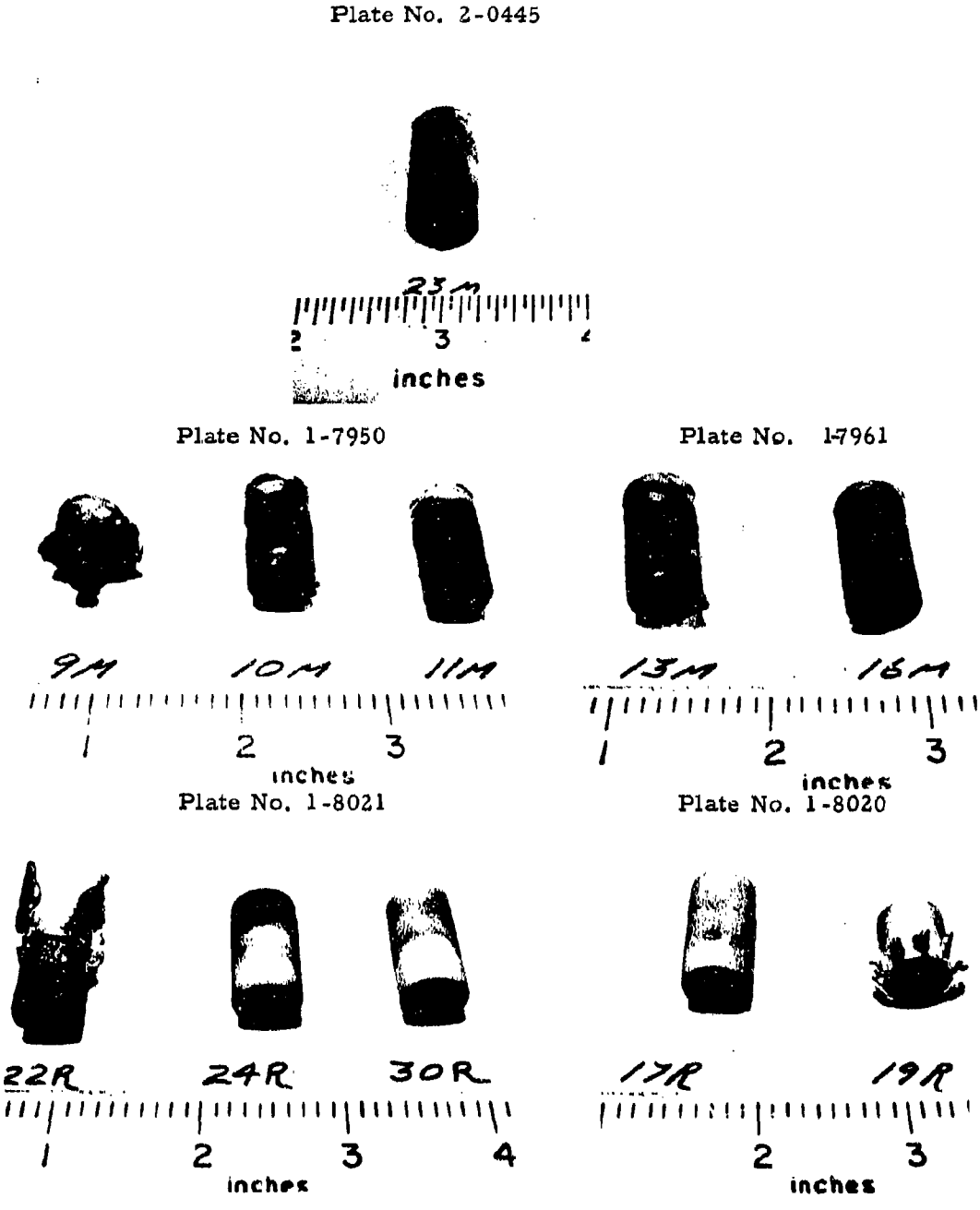


Figure 294. Post Exposure Photographs of Arc Plasma Tests IrC/C (I-24)-23M, 9M, 10M, 11M, 13M, 16M, 17R, 19R, 22R, 24R and 30R.

Plate No. 2-0710

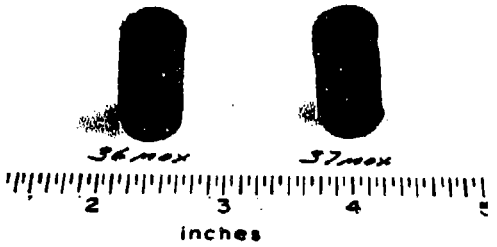


Plate No. 2-0711

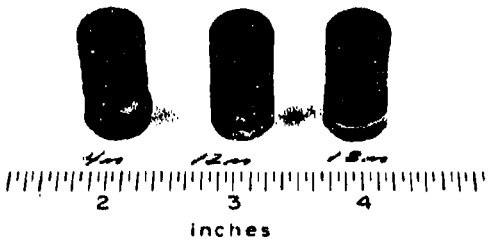


Plate No. 2-0712

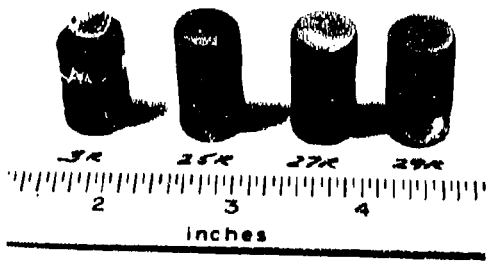


Figure 295. Post Exposure Photographs of Arc Plasma Tests Ir/C (I-24)-36MOX, 37MOX, 4M, 12M, 18M, 3R, 25R, 27R and 29R.

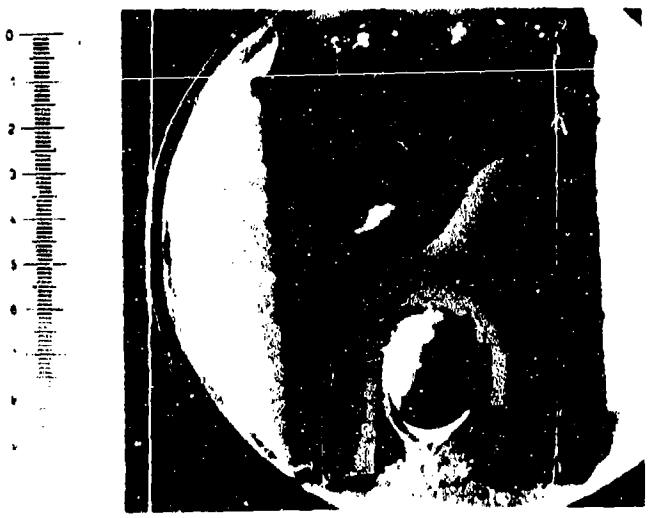

Plate No. 1-7962

X2.80

Figure 296. Arc Plasma Test Ir/C(I-24)-13M, Surface Temperature 4535°F, Exposure Time 1800 Seconds, Stagnation Pressure 1.02 Atm. Stagnation Enthalpy 3140 BTU/lb, Cold Wall Heat Flux 310 BTU/ft$^2$ sec, 16 Mil coating melted off. Hot Face Up. One inch Scale.

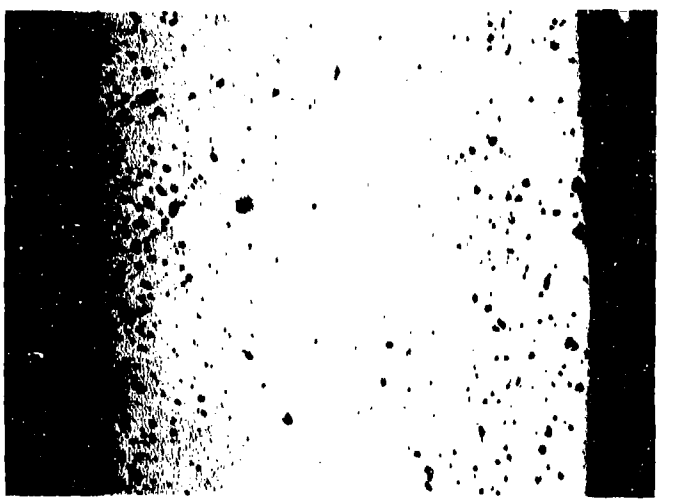

Plate No. 1-7966

Unetched X 200

Figure 297. Arc Plasma Test Ir/C(I-24)-13M, Location in Iridium Coating at Center of Side Wall.

Plate No. 1-7971

Etched Electrolytically in 20% HCl in Saturated Aqueous Solution of NaCl X500

Figure 298. Arc Plasma Test Ir/C(I-24)-13M, Location in Iridium Coating at Back of Sting Leg.

Plate No. 1-7970

Etched Electrolytically in 20% HCl in Saturated Aqueous Solution of NaCl. X500

Figure 299. Arc Plasma Test Ir/C (I-24)-13M, Location in Iridium Coating at Back Quarter of Side Wall.

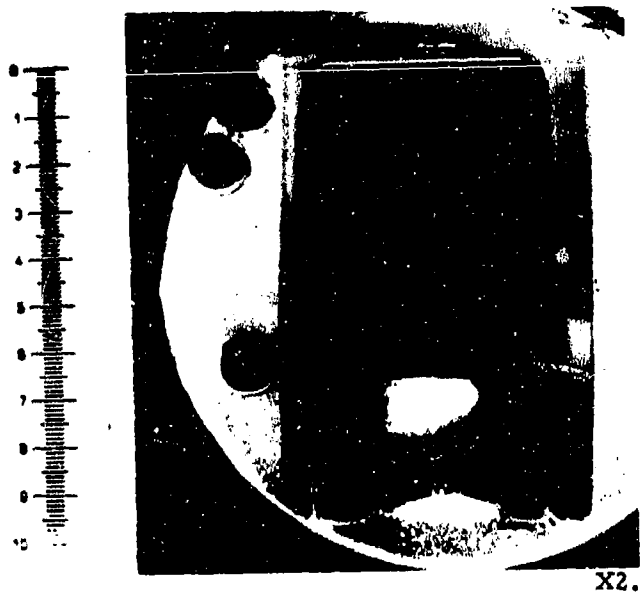

Plate No.
2-0446

X2.87

Figure 300. Arc Plasma Test Ir/C(I-24)-23M. Surface Temperature 4155°F, Exposure Time 1800 Seconds, Stagnation Pressure 1.01 Atm., Stagnation Enthalpy 2750 BTU/lb, Cold Wall Heat Flux 288 BTU/ft$^2$sec. Coating Survived Hot Face Up. One Inch Scale.

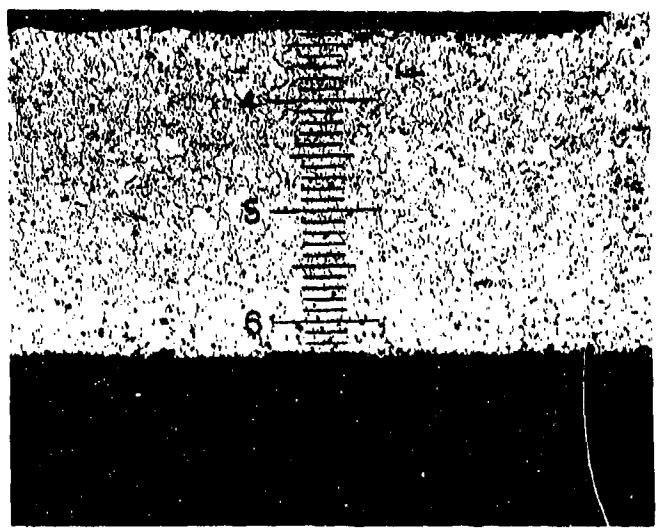

Plate No.
2-0447

Etched Electrolytically in 20% HCl in a Saturated Solution of NaCl in Water

X89

Figure 301. Arc Plasma Test Ir/C(I-24)-23M. Hot Interface at Top. One Division Equals 0.788 Mils. Coating Thickness Equals 23.6 Mils.

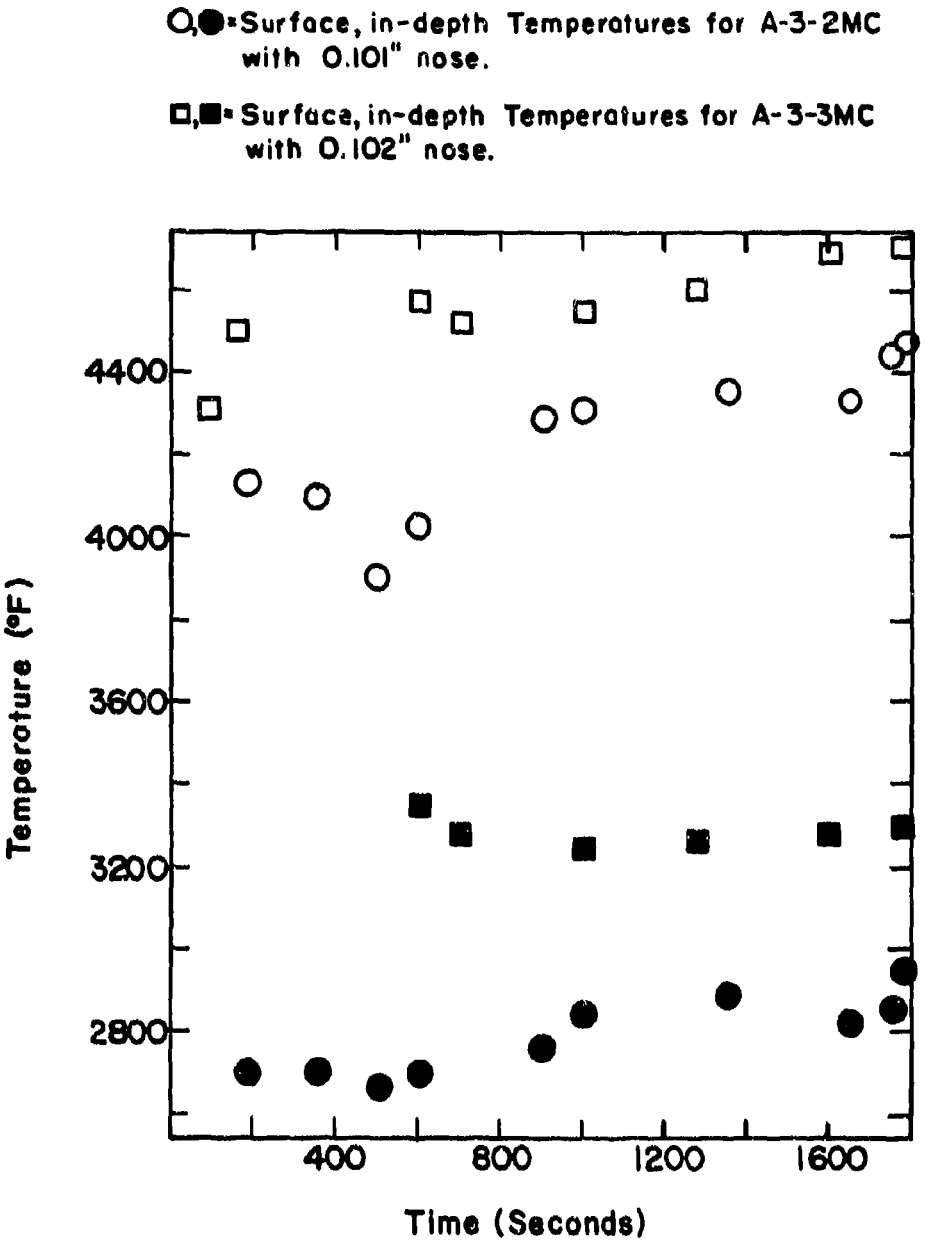


Figure 302. Time-Temperature Histories of Surface and In-Depth Temperatures for $ZrB_2$(A-3).

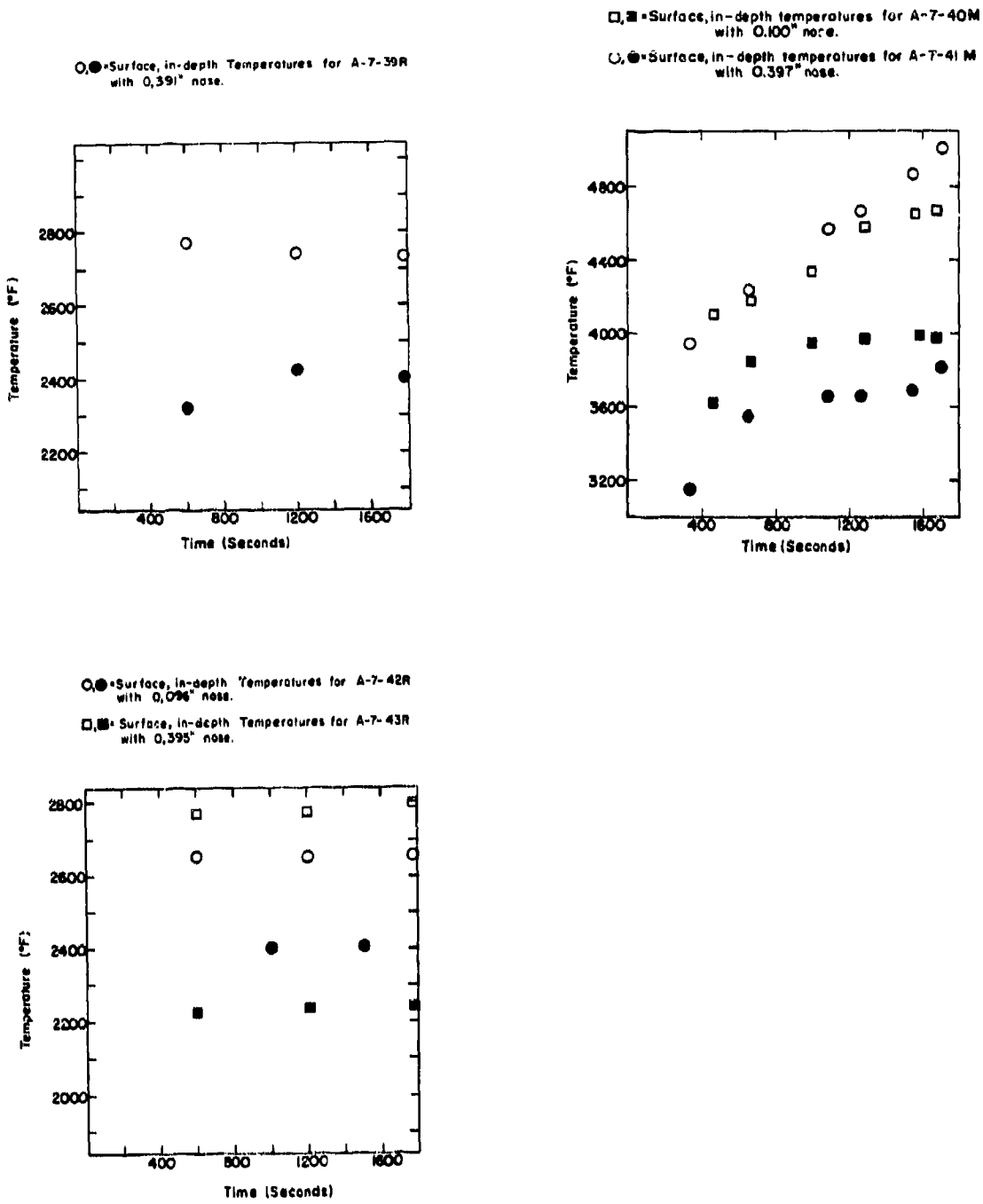


Figure 303. Time-Temperature Histories of Surface and In-Depth Temperatures for $HfB_2$+SiC(A-7).

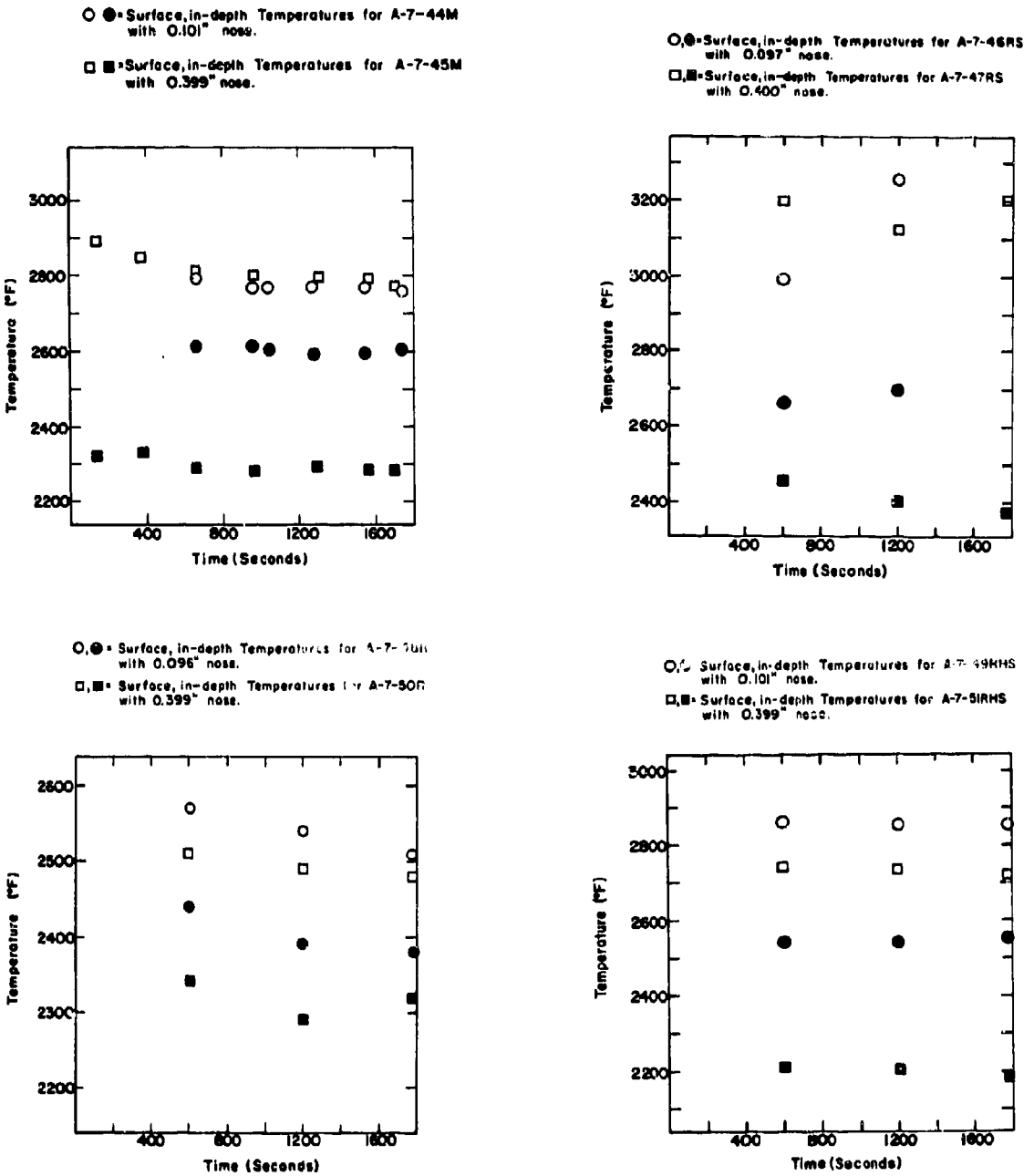


Figure 304. Time-Temperature Histories of Surface and In-Depth Temperatures for $HfB_2$+SiC(A-7).

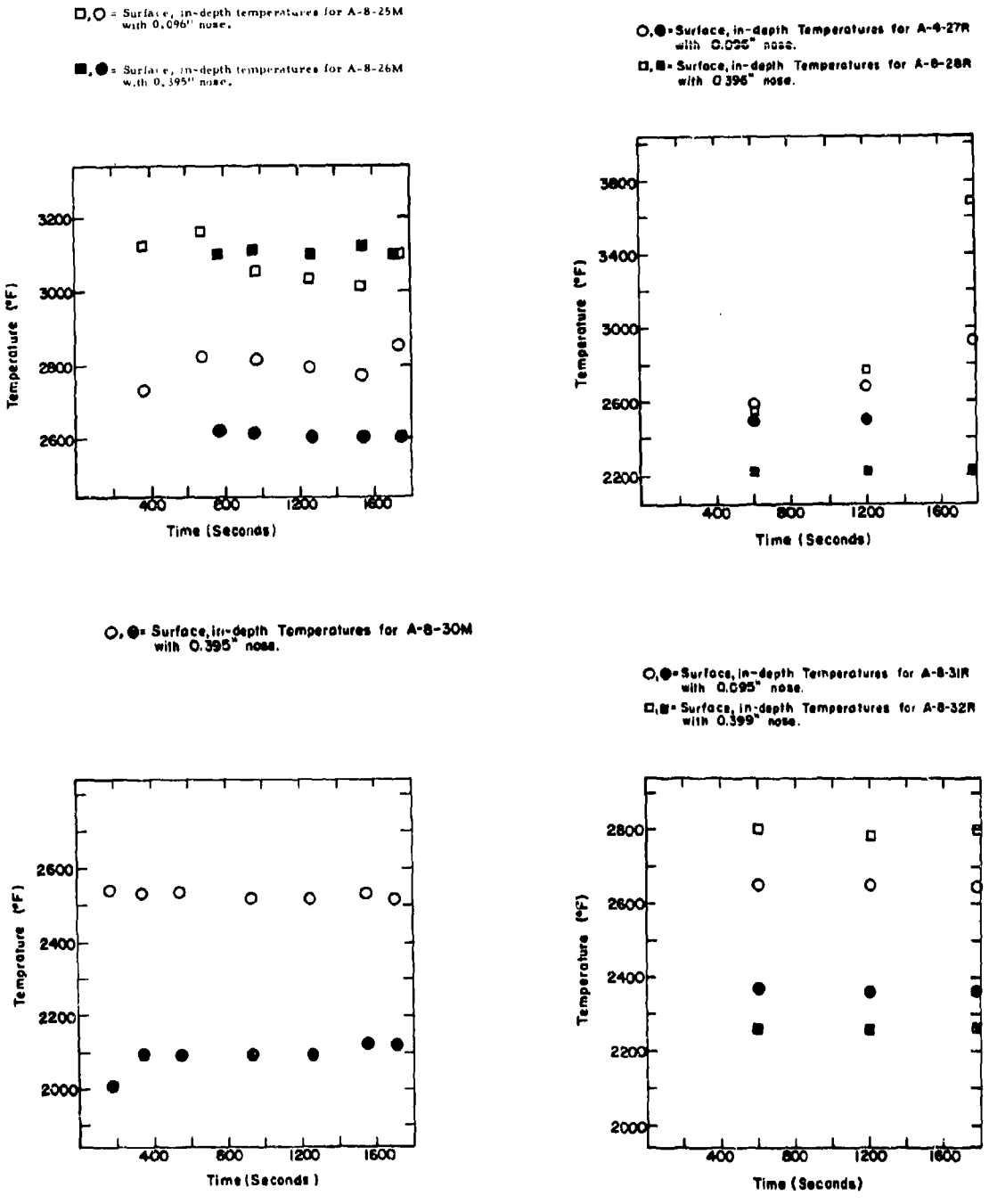


Figure 305. Time-Temperature Histories of Surface and In-Depth Temperatures for $ZrB_2$+SiC(A-8).

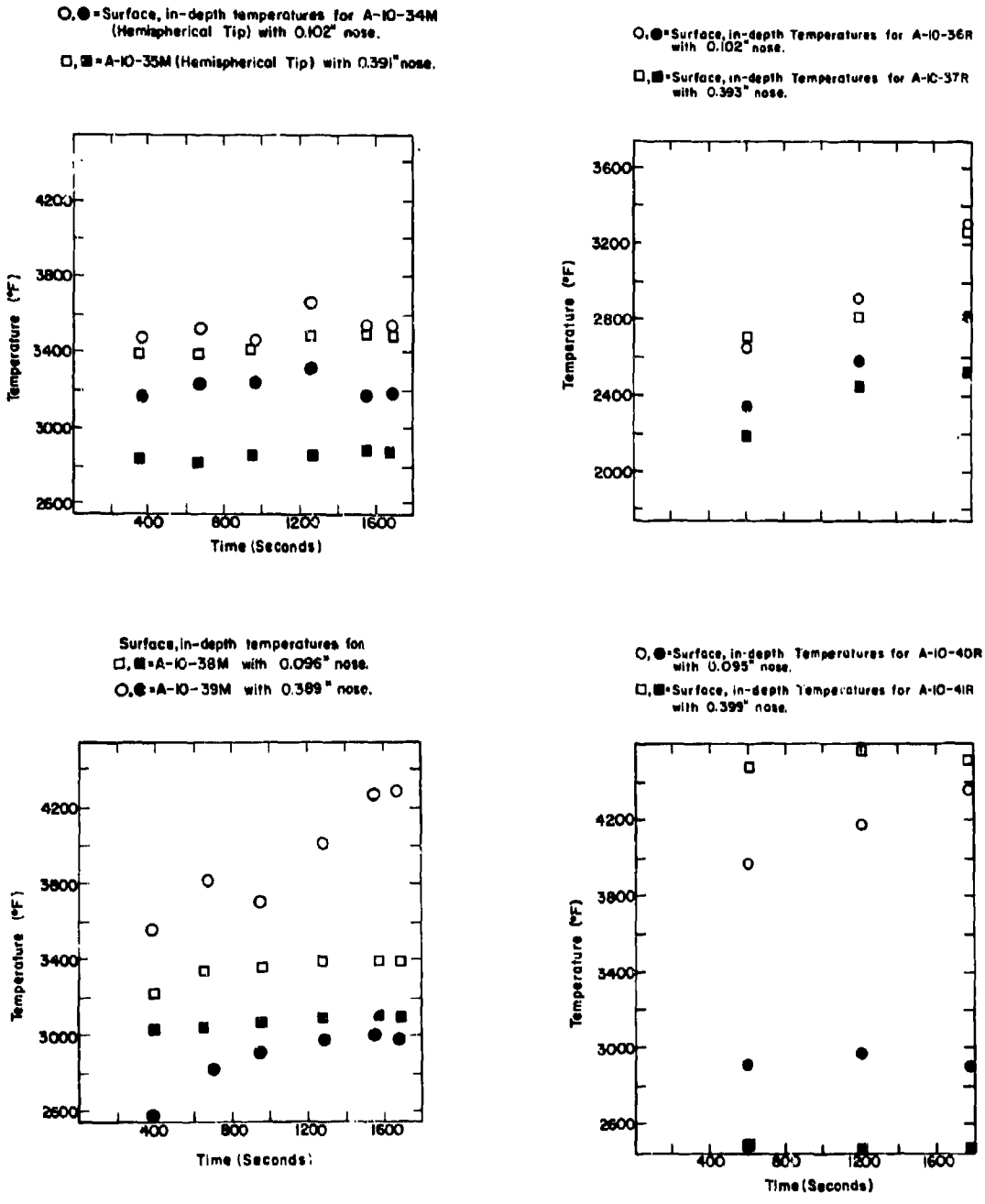


Figure 306. Time-Temperature Histories of Surface and In-Depth Temperatures for $ZrB_2$+SiC+C(A-10).

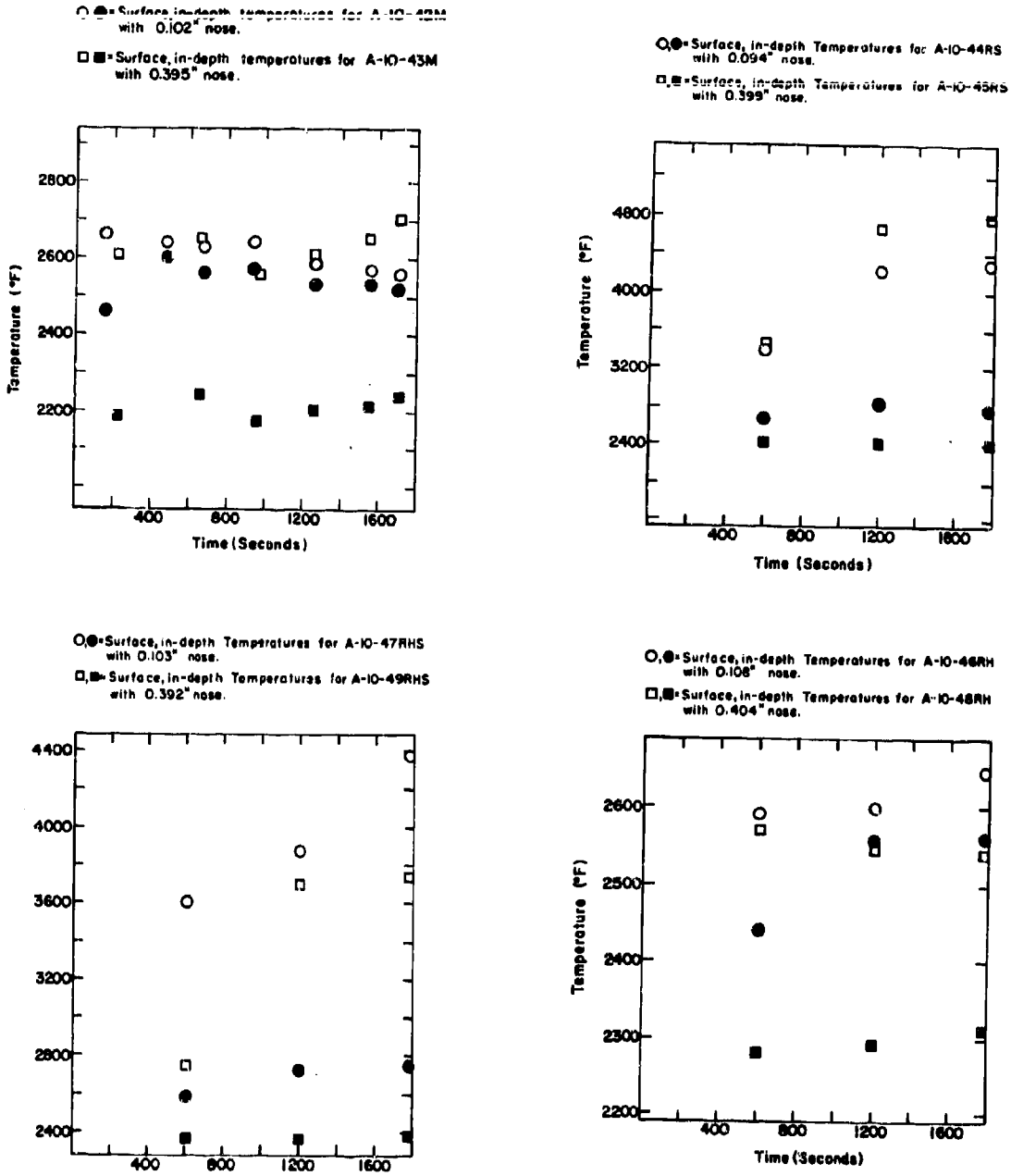


Figure 307. Time-Temperature Histories of Surface and In-Depth Temperatures for $ZrB_2$+SiC+C(A-10).

□, ○ = Surface, in-depth temperatures for B-5-31 M with 0.202" nose.

■, ● = Surface, in-depth temperatures for B-5-32 M with 0.463" nose.

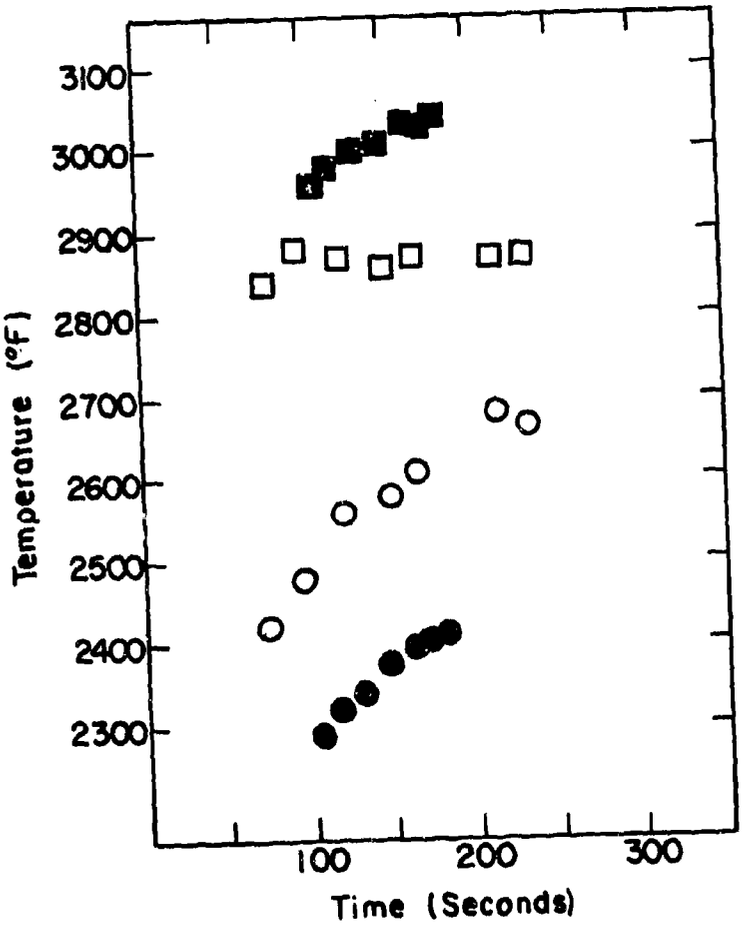


Figure 308. Time-Temperature Histories of Surface and In-Depth Temperatures for RVA(B-5).

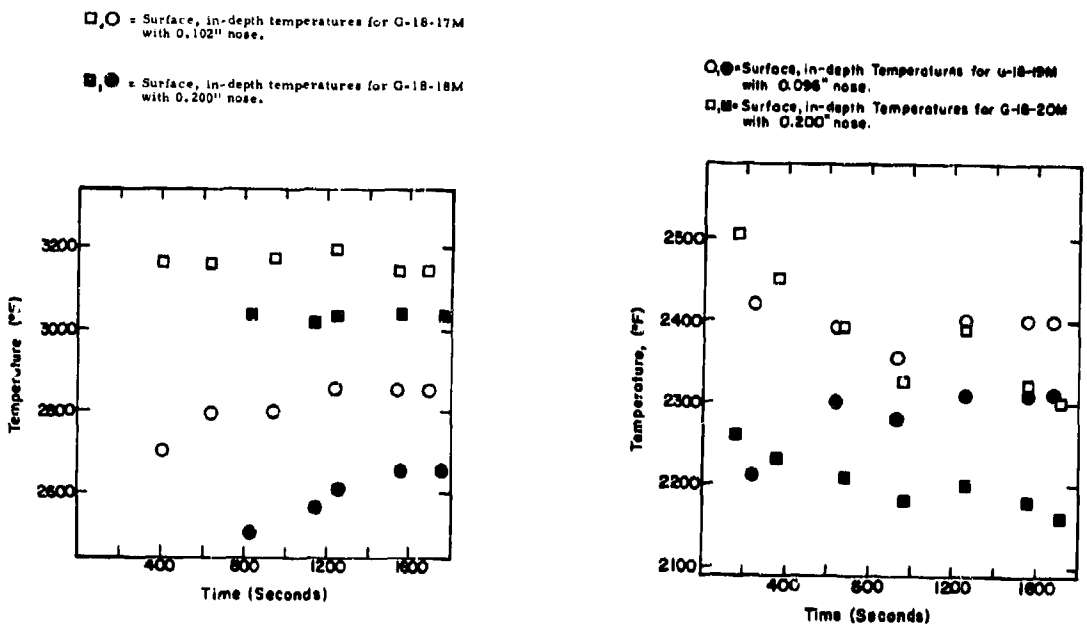


Figure 309. Time-Temperature Histories of Surface and In-Depth Temperatures for $WSi_2/W$(G-18).

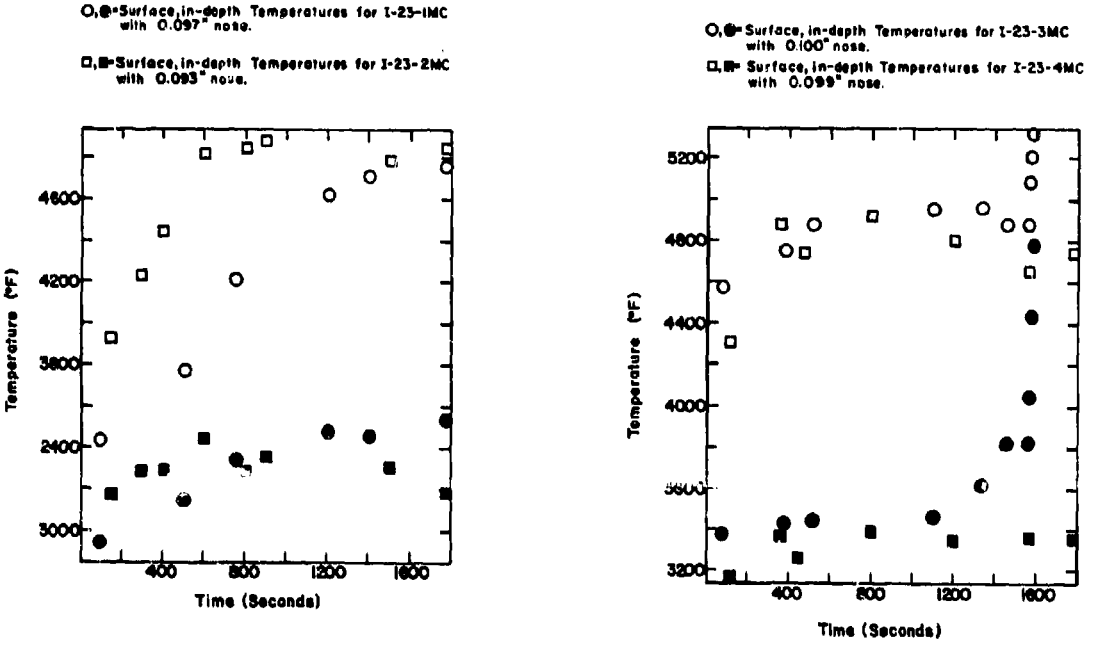


Figure 310. Time-Temperature Histories of Surface and In-Depth Temperatures for Hf-Ta-Mo(I-23).

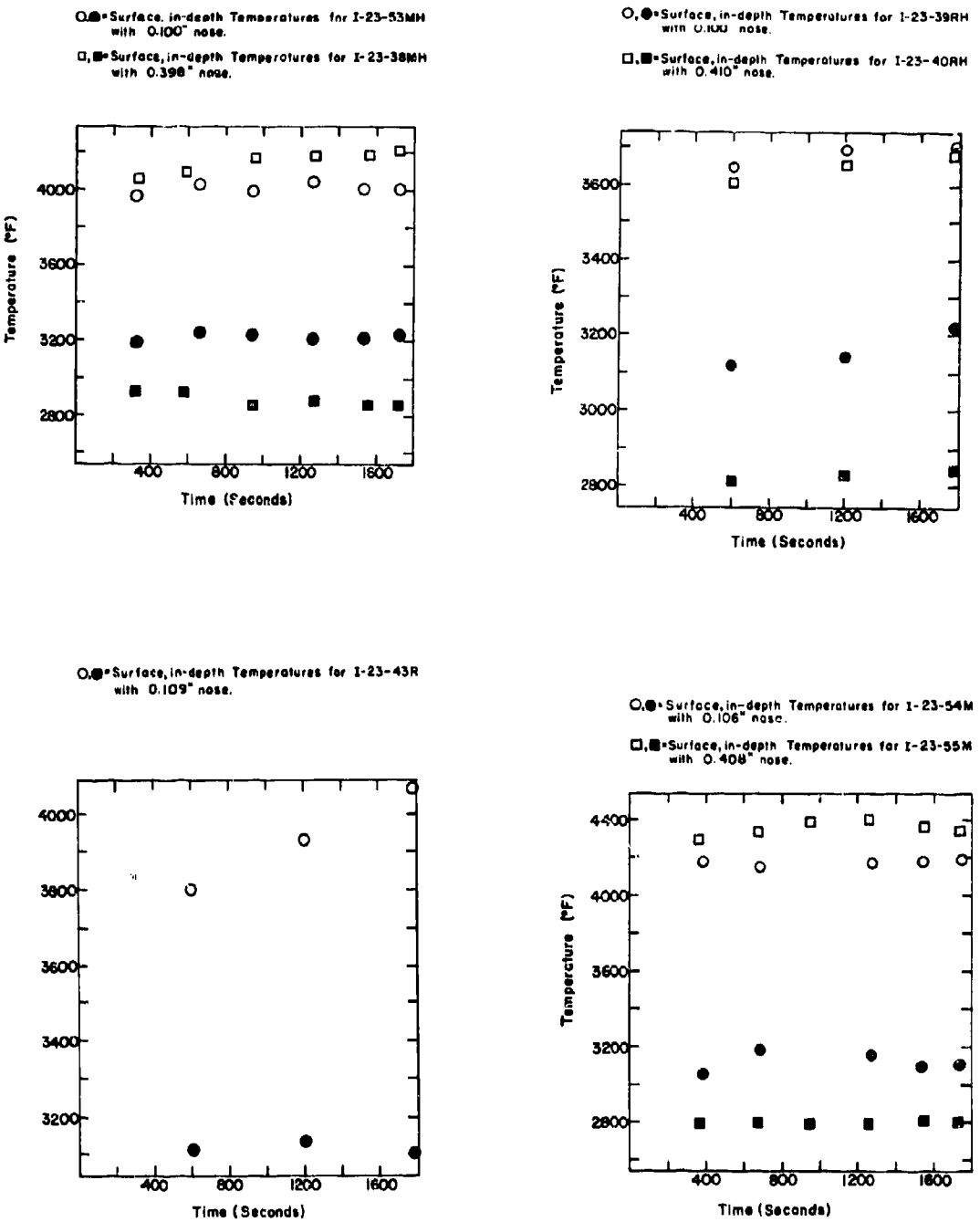


Figure 311. Time-Temperature Histories of Surface and In-Depth Temperatures for Hf-Ta-Mo(I-23).

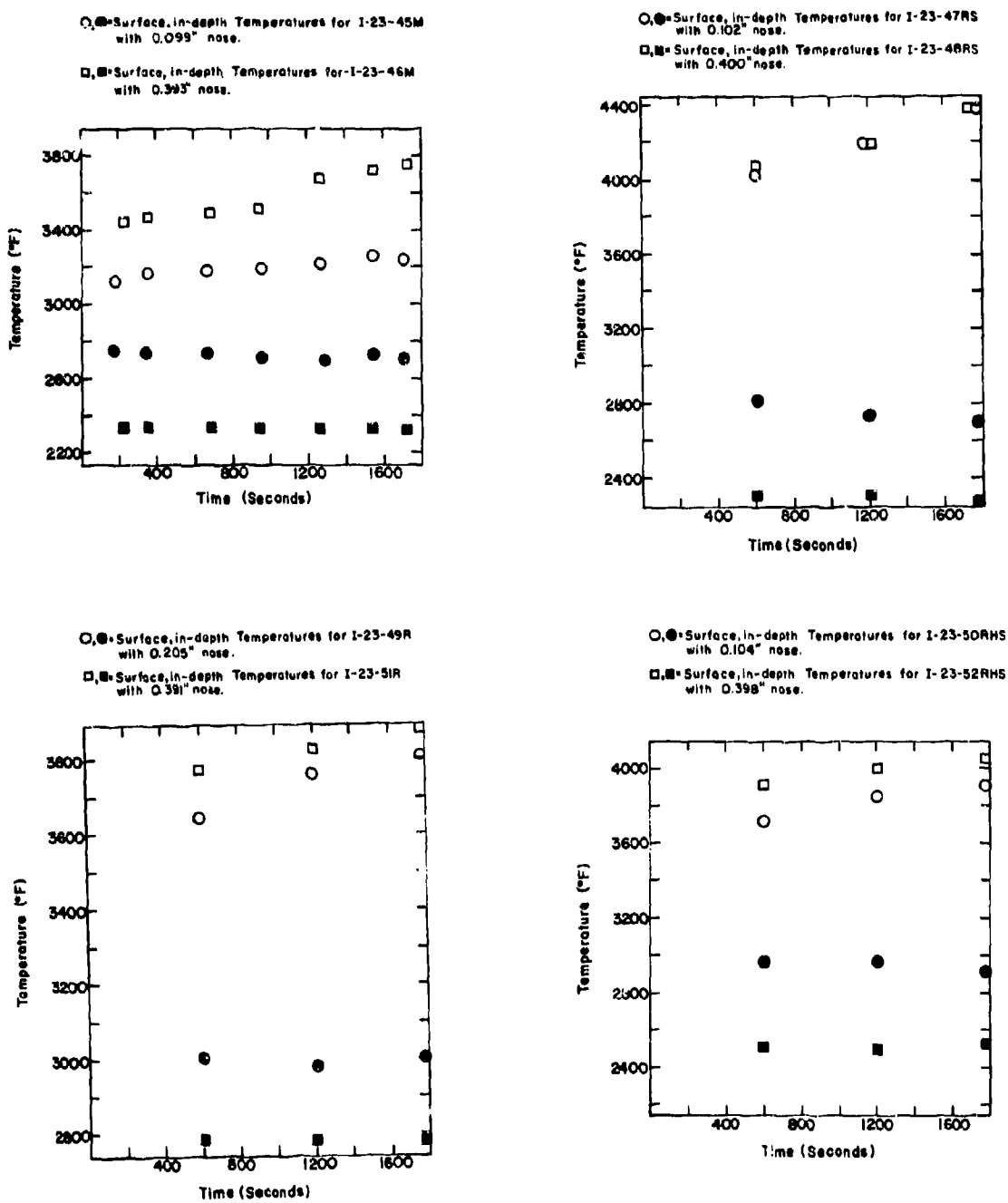


Figure 312. Time-Temperature Histories of Surface and In-Depth Temperatures for Hf-Ta-Mo(I-23).

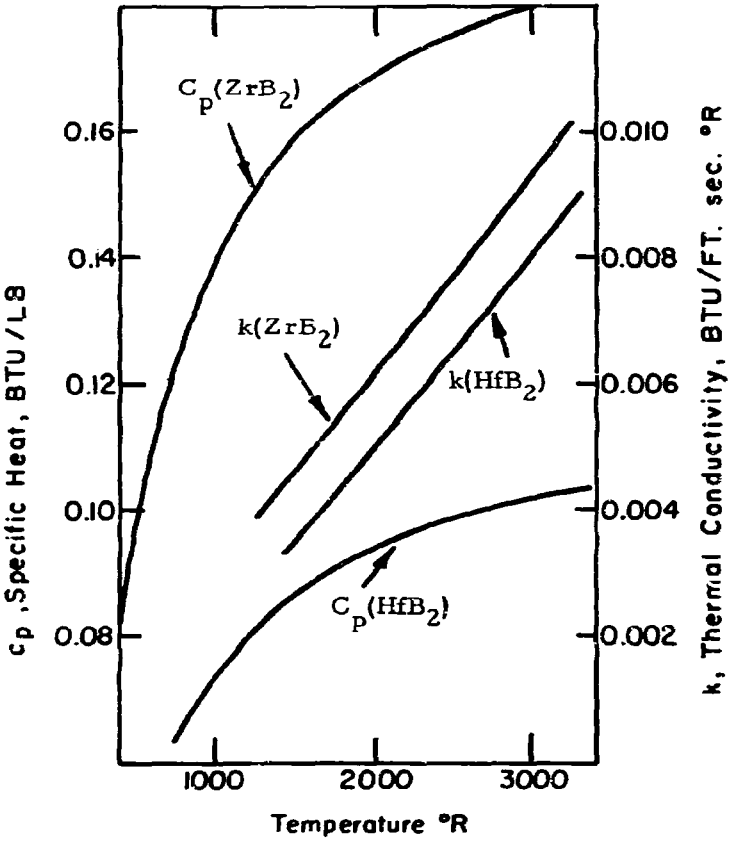


Figure 313. Thermal Properties of $ZrB_2$ (Density = 375 lbs/ft$^3$) and $HfB_2$ (Density = 625 lbs/ft$^3$) as a Function of Temperature.

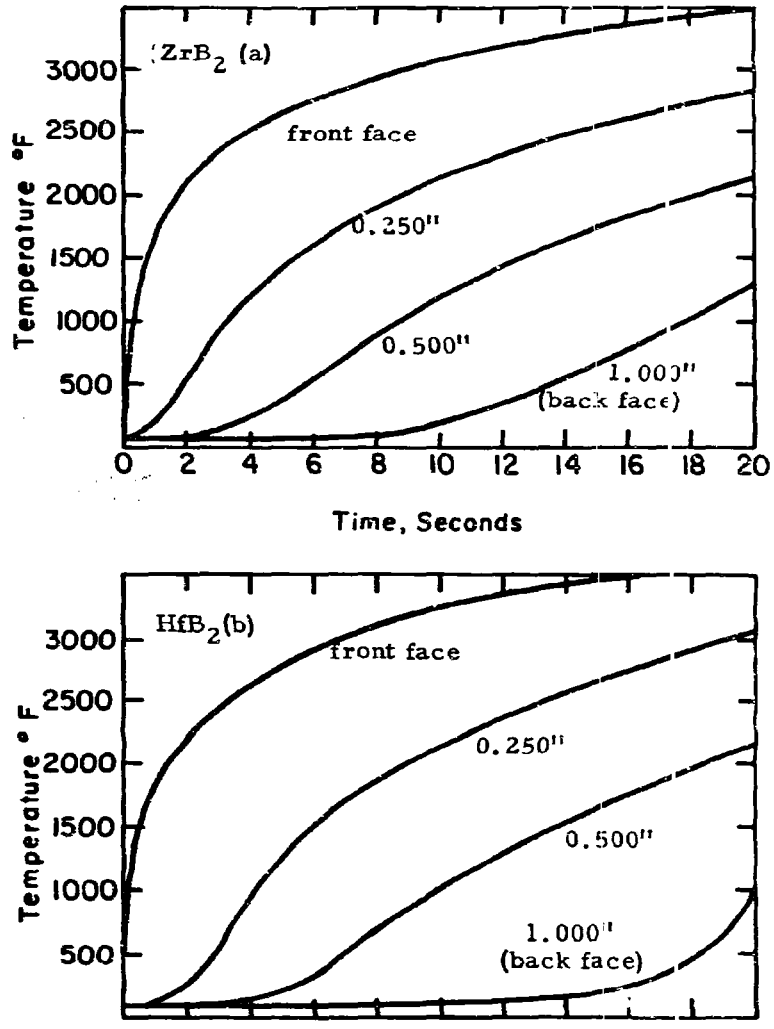


Figure 314 (a)(b). Calculated Thermal Gradients for $ZrB_2$ and $HfB_2$, q = 1000 BTU/ft$^2$sec, $i_e$ = 2000 BTU/lb.


Figure 315. Post Exposure Photographs of 10 MW Arc Exposures $HfB_{2.1}$ (A-2) and (A-6), and $HfB_2$ + 20% SiC (A-4).

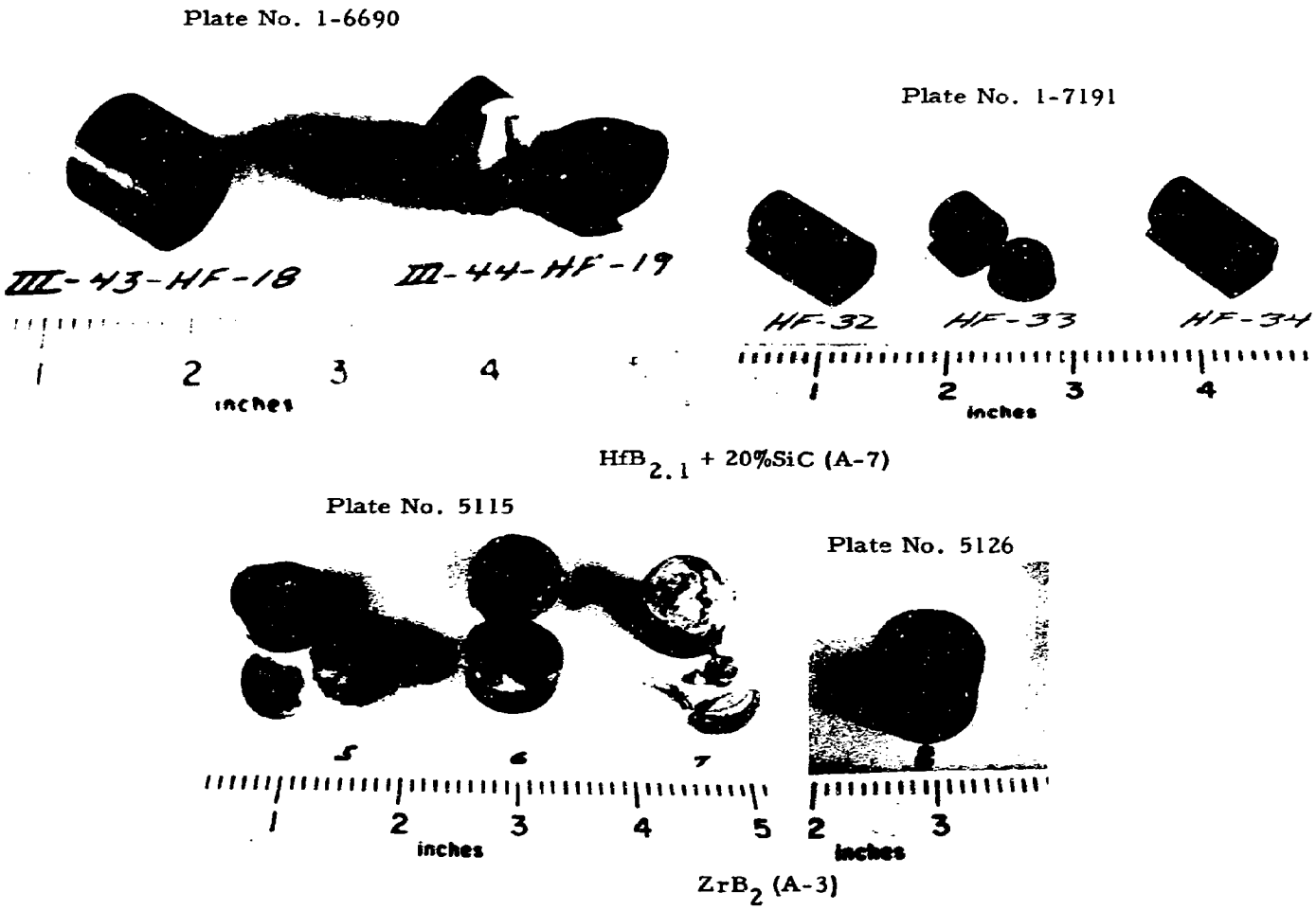


Figure 316. Post Exposure Photographs of 10 MW Arc Exposures $HfB_{2.1}$ + 20%SiC(A-7) and $ZrB_2$(A-3).

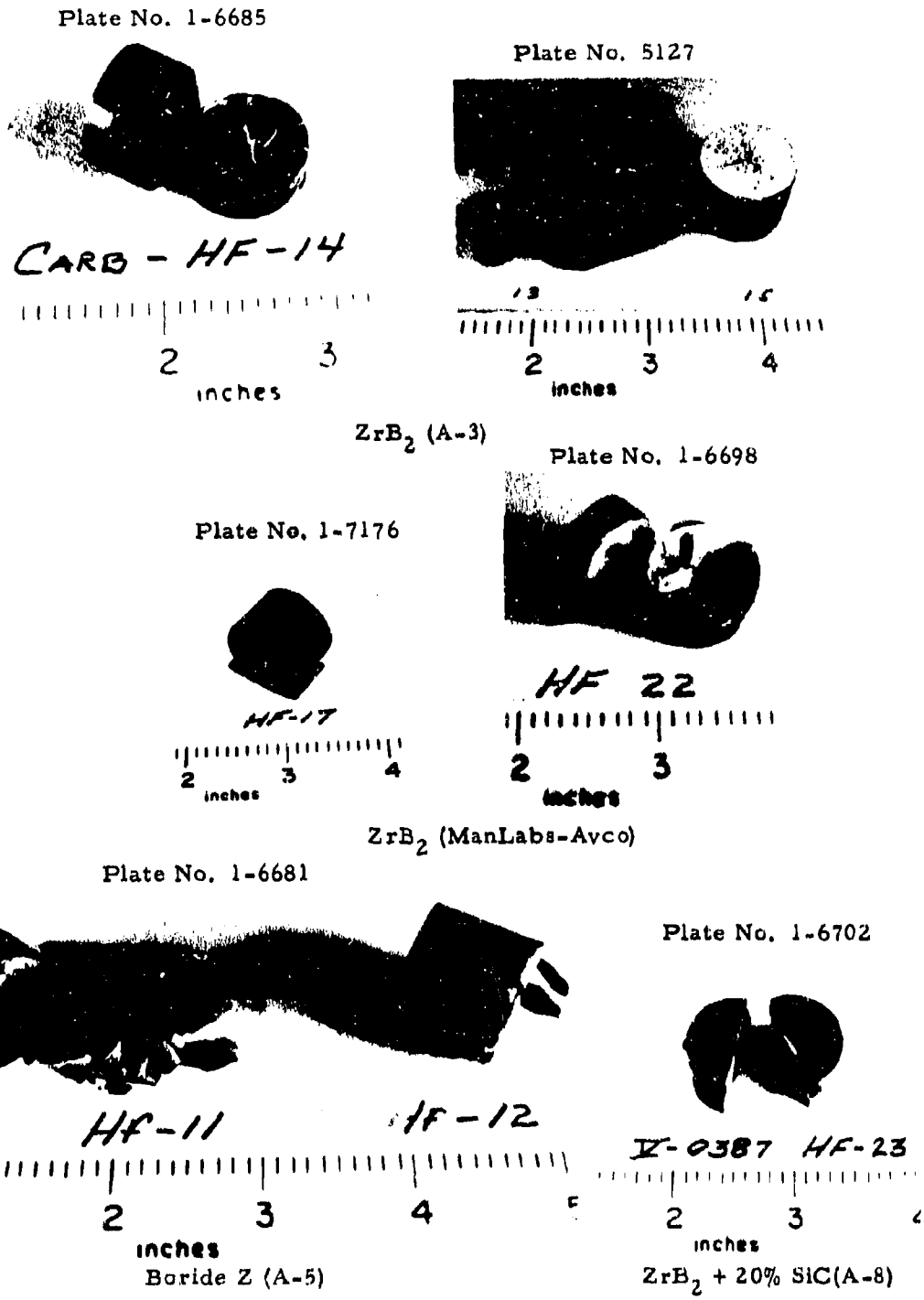


Figure 317. Post Exposure Photographs of 10MW Arc Exposures $ZrB_2$(A-3) and (ManLabs-Avco), Boride Z(A-5) and $ZrB_2$ + 20%SiC(A-8).

Plate No. 1-7173

X3.4

Figure 318. 10 MW Arc Test $HfB_{2.1}$ (A-2)-HF-2, Surface Temperature 3305°F, Exposure Time 20.1 Seconds, Stagnation Pressure 4.3 Atm, Stagnation Enthalpy 1930 BTU/lb, Cold Wall Heat Flux 695 BTU/ft$^2$sec. Hot Face at Top. One Inch Scale. Fine Cracks Observed.

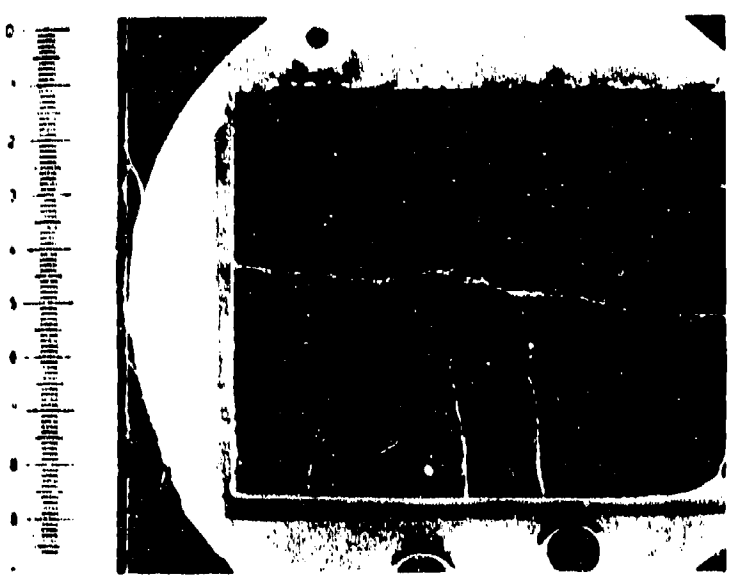

Plate No. 1-7188

X3.3

Figure 319. 10 MW Arc Test $HfB_{2.1}$ (A-6)-HF-21, Surface Temperature 3470°F, Exposure Time 20.1 Seconds, Stagnation Pressure 4.3 Atm, Stagnation Enthalpy 2030 BTU/lb, Cold Wall Heat Flux 733 BTU/ft$^2$sec. Hot Face at Bottom. One Inch Scale. Large Cracks Observed.

Plate No. 1-7212

X2.87

Figure 320. 10MW Arc Test $HfB_2$ +20%SiC(A-4)-HF-37, Surface Temperature 4790°F, Exposure Time 20.2 Seconds, Stagnation Pressure 4.3 Atm, Stagnation Enthalpy 2540 BTU/lb, Cold Wall Heat Flux 940 BTU/ft$^2$ sec. Hot Face at Top. One Inch Scale.

Plate No. 1-7192

X3.4

Figure 321. 10MW Arc Test $HfB_2$ +20%SiC(A-7)-HF-32, Surface Temperature 4610°F, Exposure Time 20.1 Seconds, Stagnation Pressure 4.3 Atm, Stagnation Enthalpy 2710 BTU/lb, Cold Wall Heat Flux 948 BTU/ft$^2$ sec. Hot Face at Right. One Inch Scale.

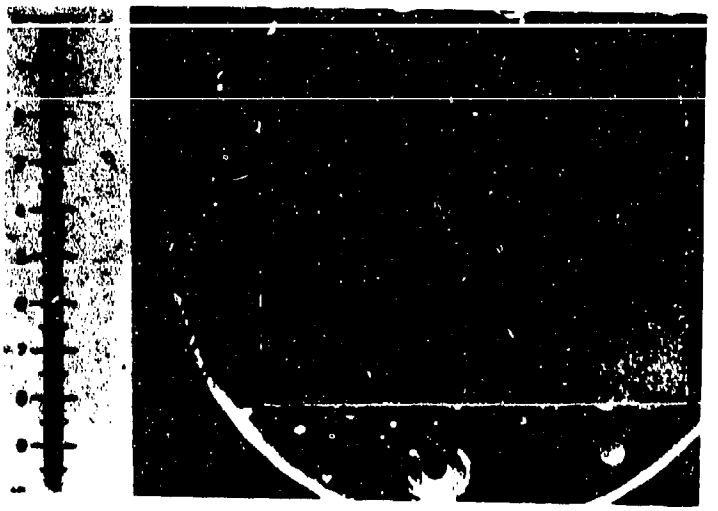

Plate No. 1-7202

X2.87

Figure 322. 10 MW Arc Test $HfB_{2.1}$+20%SiC(A-7)-HF-18, Surface Temperature 3500°F, Exposure Time 20.1 Seconds, Stagnation Pressure 4.3 Atm, Stagnation Enthalpy 2200 BTU/lb, Cold Wall Heat Flux 787 BTU/$ft^2$sec. Hot Face at Top. One Inch Scale. Fine Cracks Observed.

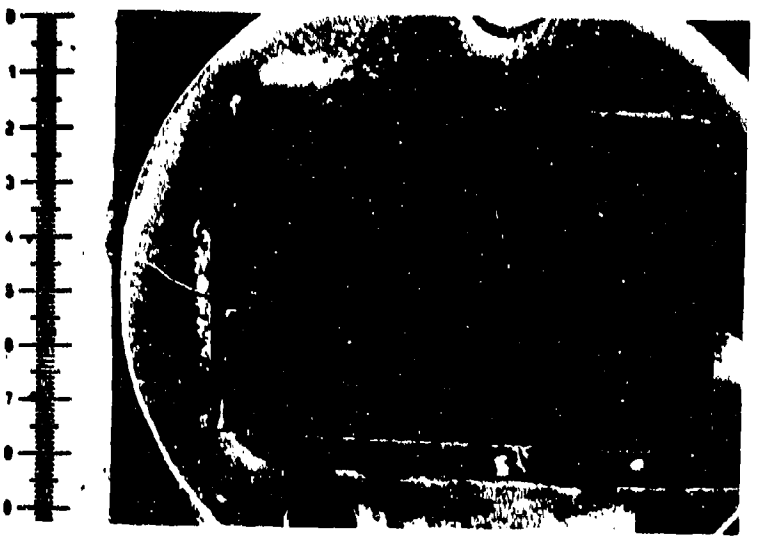

Plate No. 1-7177

X3.4

Figure 323. 10MW Arc Test $ZrB_2$ (ManLabs-Avco)-HF-17, Surface Temperature 3425°F, Exposure Time 20.1 Seconds, Stagnation Pressure 4.3 Atm, Stagnation Enthalpy 1964 BTU/lb, Cold Wall Heat Flux 714 BTU/$ft^2$sec. Hot Face at Bottom. One Inch Scale. Fine Cracks Observed.

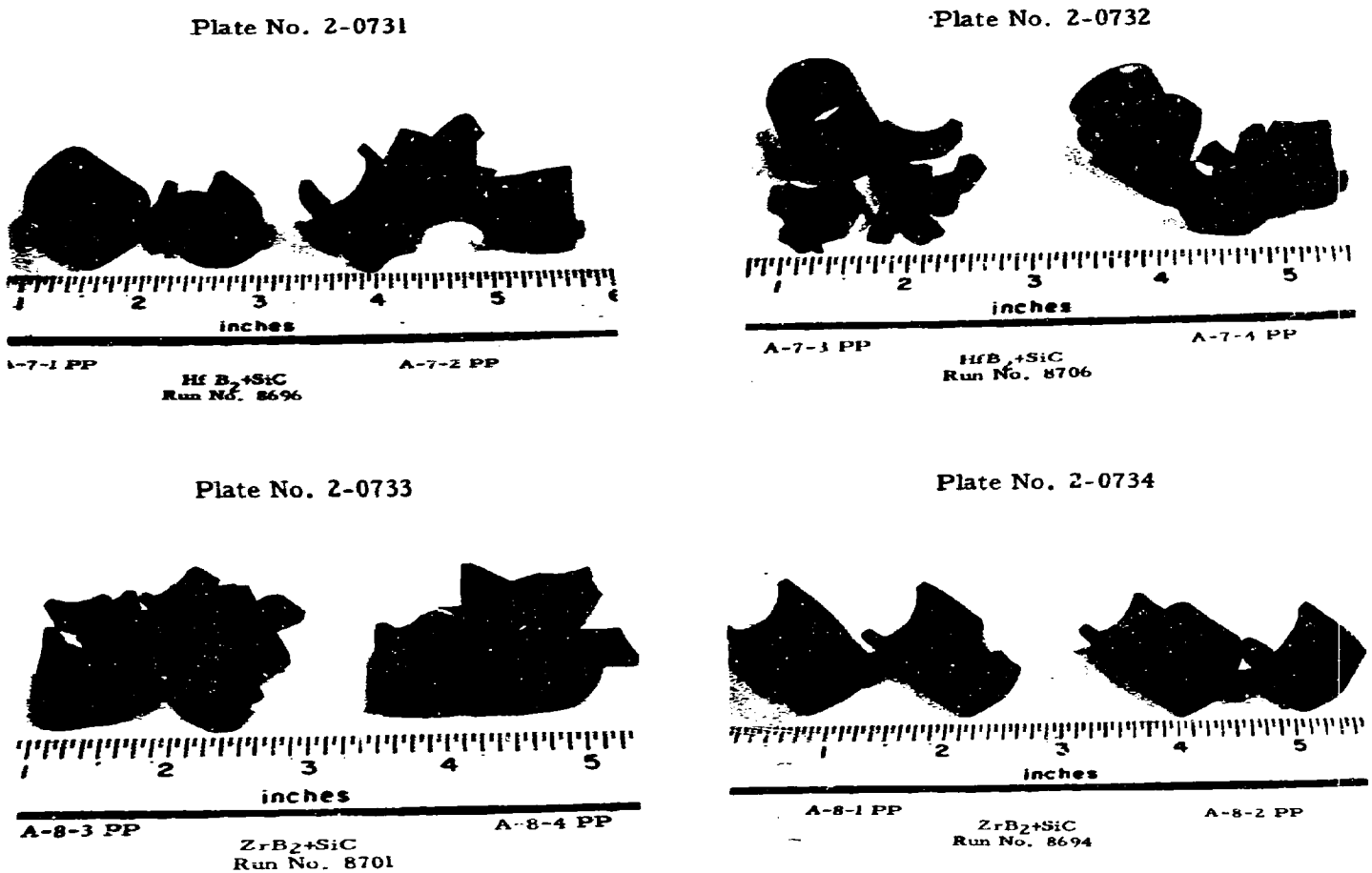


Figure 324. Post-exposure Photographs of $HfB_{2.1}$+20%SiC(A-7) and $ZrB_{2.1}$+20%SiC(A-8) Supersonic Pipe Test Samples Run in Avco 10-Megawatt Arc Facility.

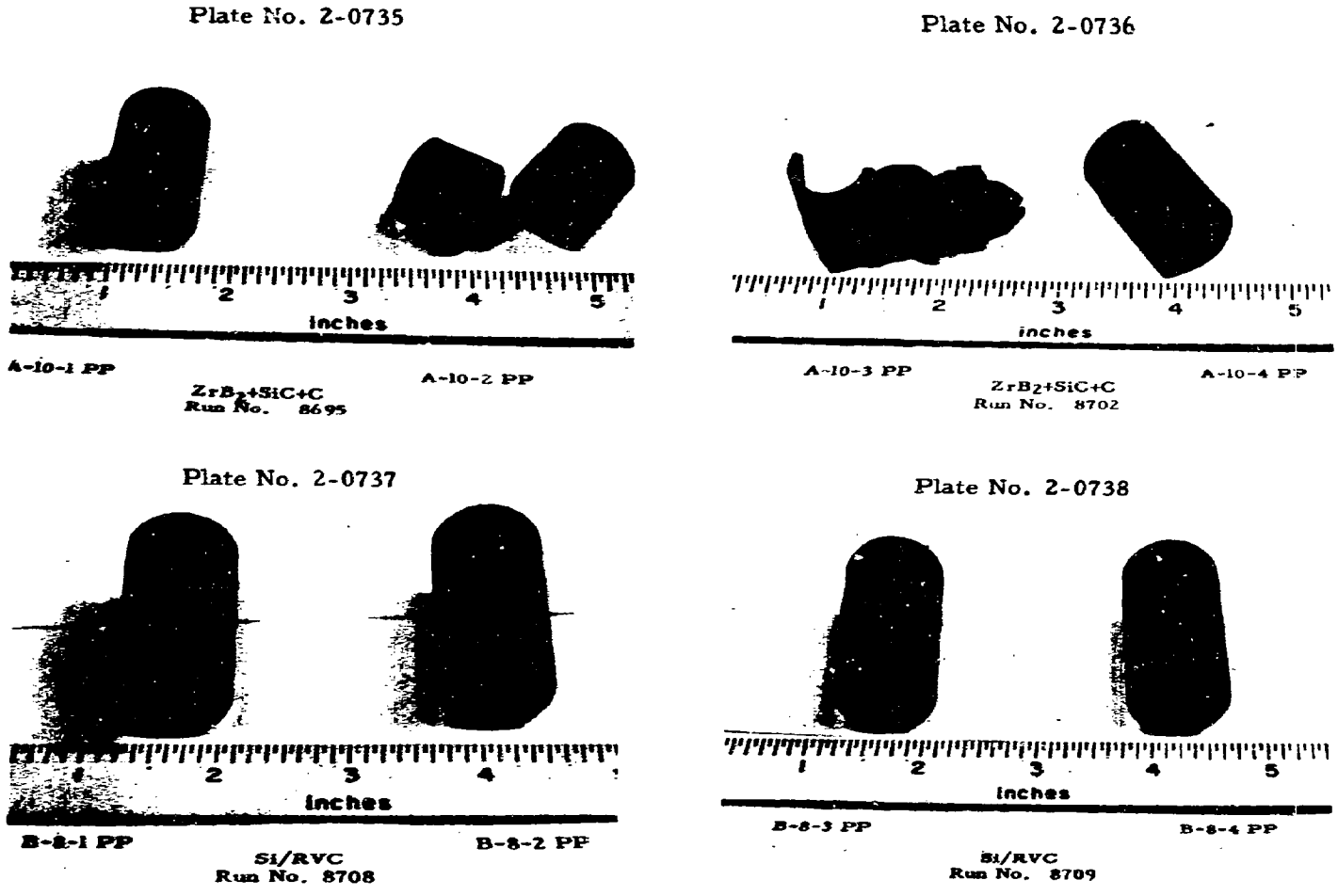


Figure 325. Post-exposure Photographs of $ZrB_2$+SiC+C(A-10) and Si/RVC(B-8) Supersonic Pipe Test Samples Run in Avco 10-Megawatt Arc Facility.

Plate No. 2-0739

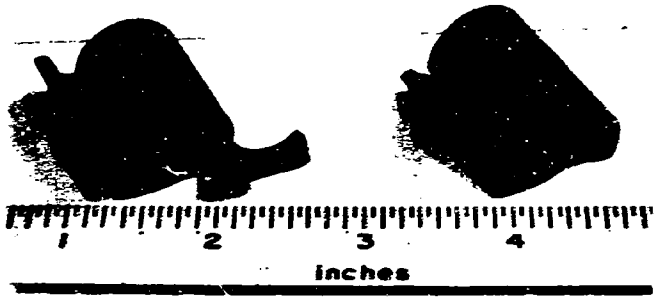


Plate No. 2-0740

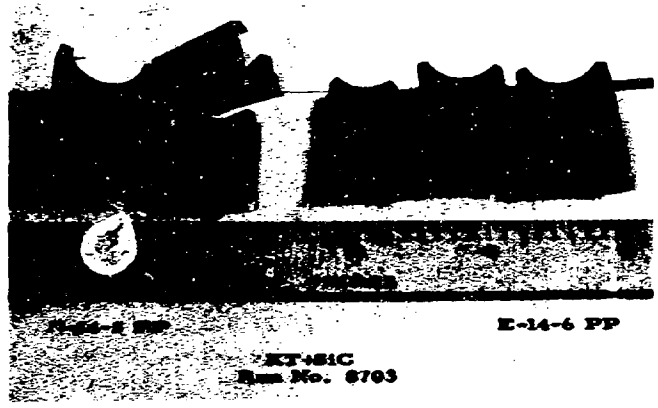


Plate No. 2-0741

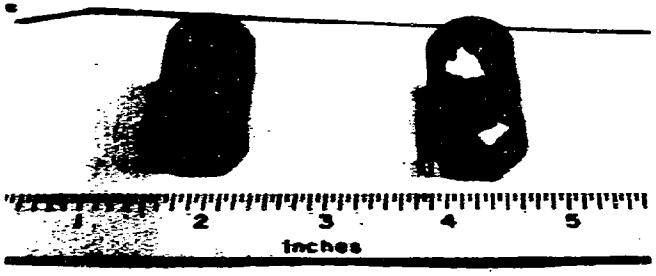


Plate No. 2-0742

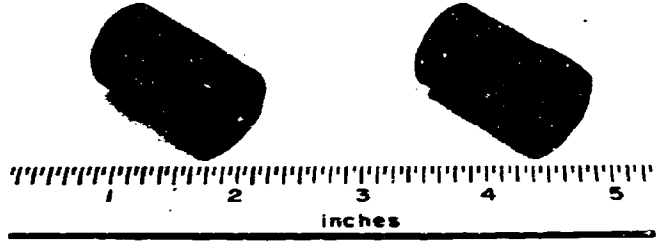


Figure 326. Post-exposure Photographs of KT-SiC(E-14) and Hf-Ta-Mo(I-23) Supersonic Pipe Test Samples Run in Avco 10-Megawatt Arc Facility.

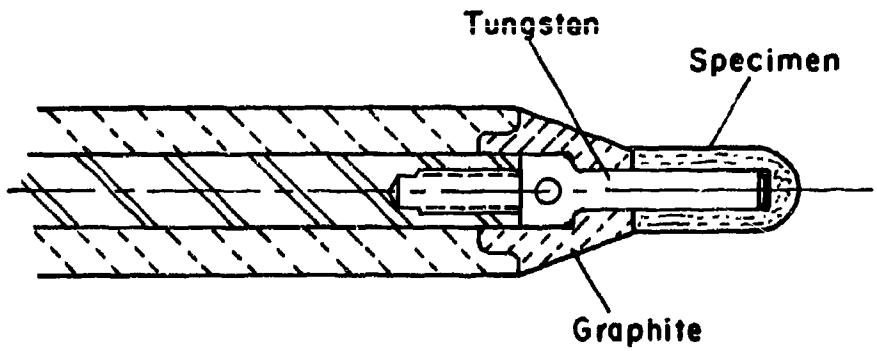


One Half Inch Diameter Specimens

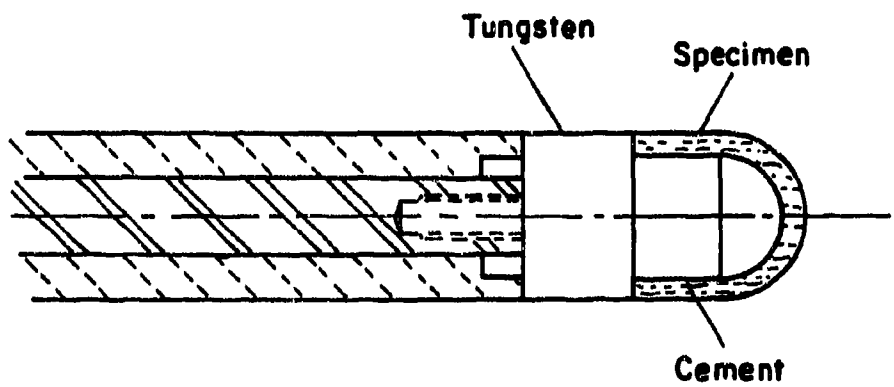


One Inch Diameter Specimens

Figure 327. Details of Specimen Holders Employed in Wave Superheater Tests.

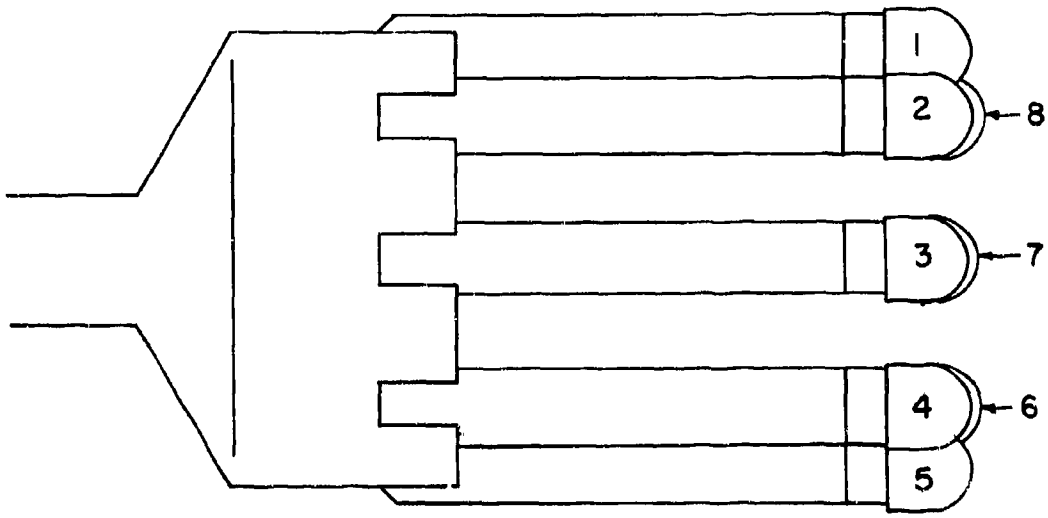


(a) View From Right Side
(Camera View)

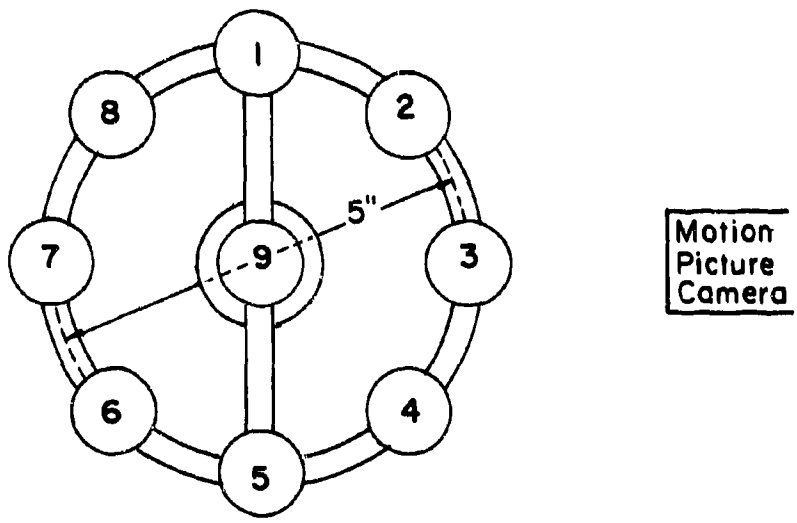


(b) Pilot's View (Looking Upstream)

Figure 328. Orientation of Calorimeter and Models in Wave Superheater Exposures.

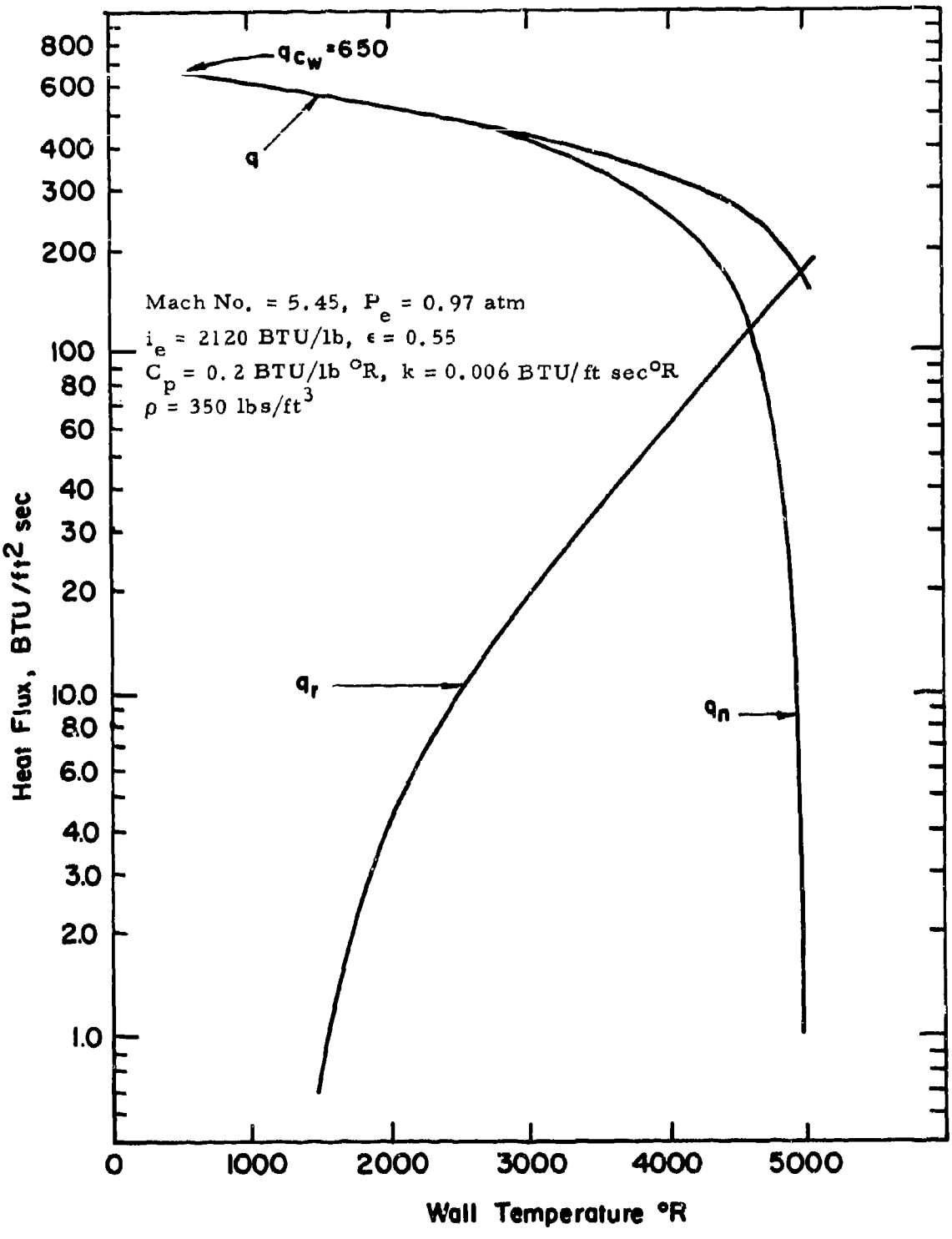


Figure 329. Calculated Heat Flux As A Function of Wall Temperature for A One-Half Inch Diameter Hemispherical Cap Shell of Zirconium Diboride One-Eighth Inch Thick in the Mach 6 Test Section of the Cornell Wave Superheater.

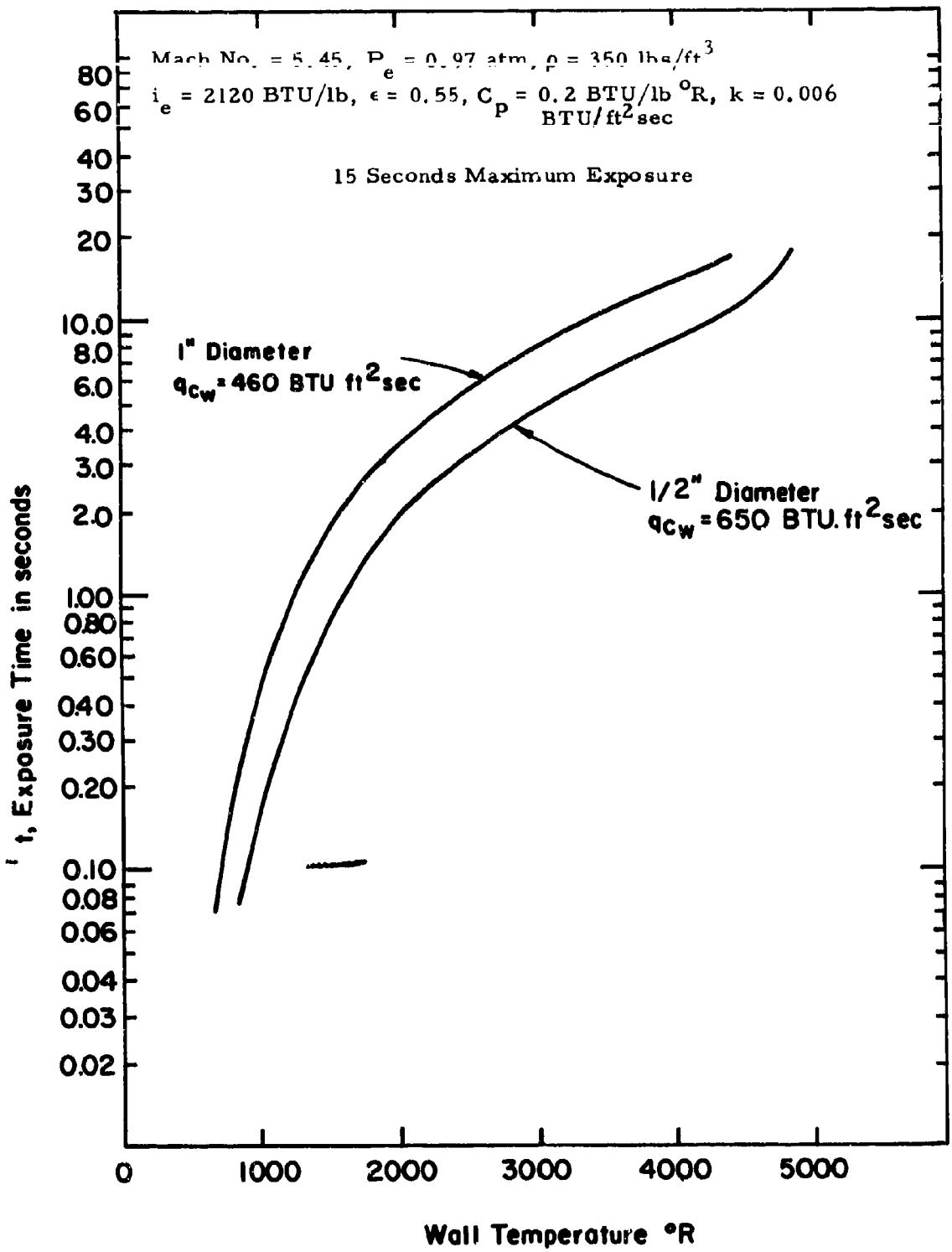


Figure 330. Calculated Wall Temperature As A Function of Time for A One Inch and a One-Half Inch Diameter Hemispherical Cap Shell of Zirconium Diboride One-Eighth Inch Thick in the Mach 6 Test Section of the Cornell Wave Superheater.

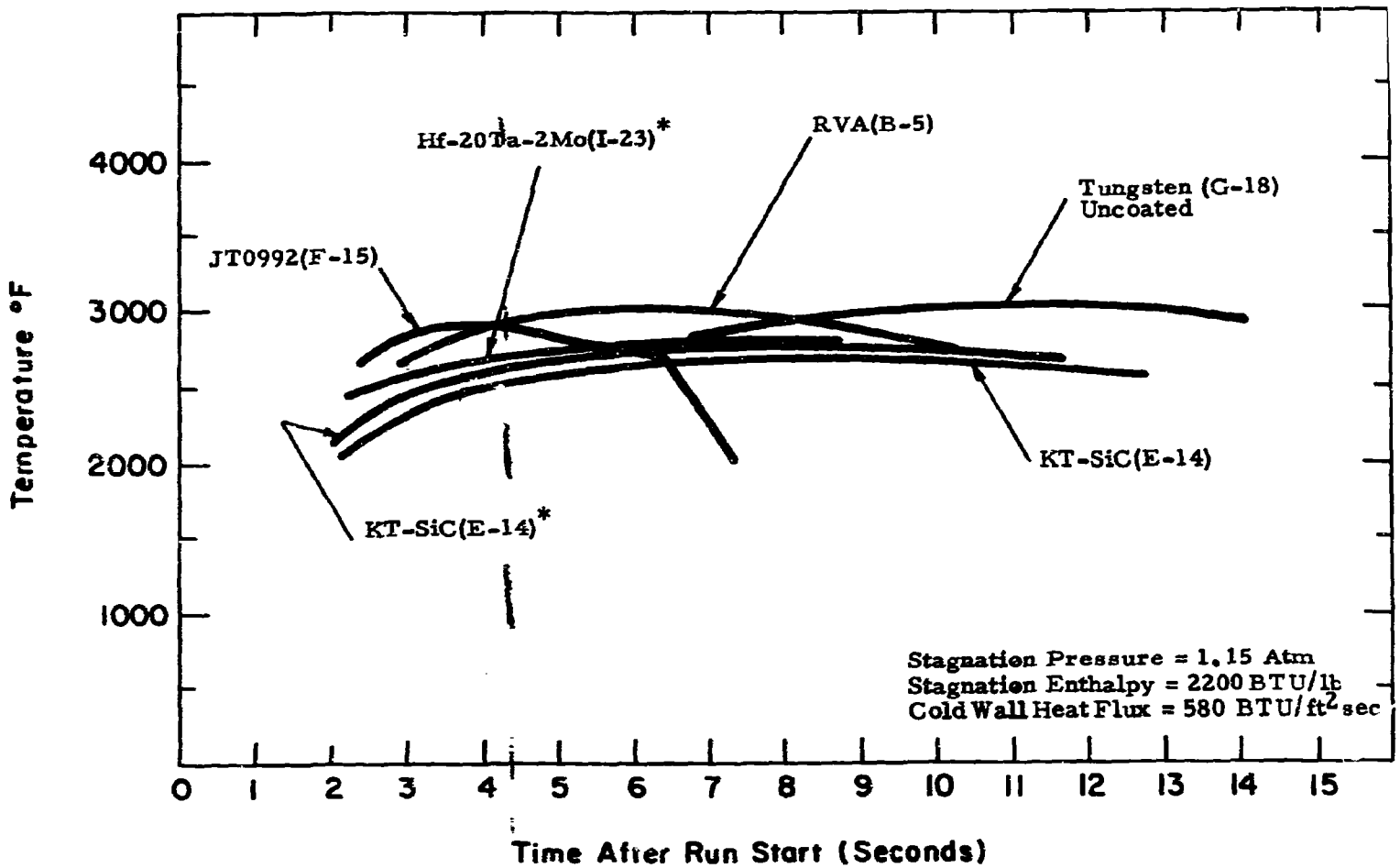


Figure 331. Brightness Temperature of Models as a Function of Time in the Wave Superheater at Mach 5.5 (Run 473). All Samples Were 1/2 Inch Diameter Hemispherical Caps except These Noted by an Asterisk Which Were One Inch Diameter Caps.

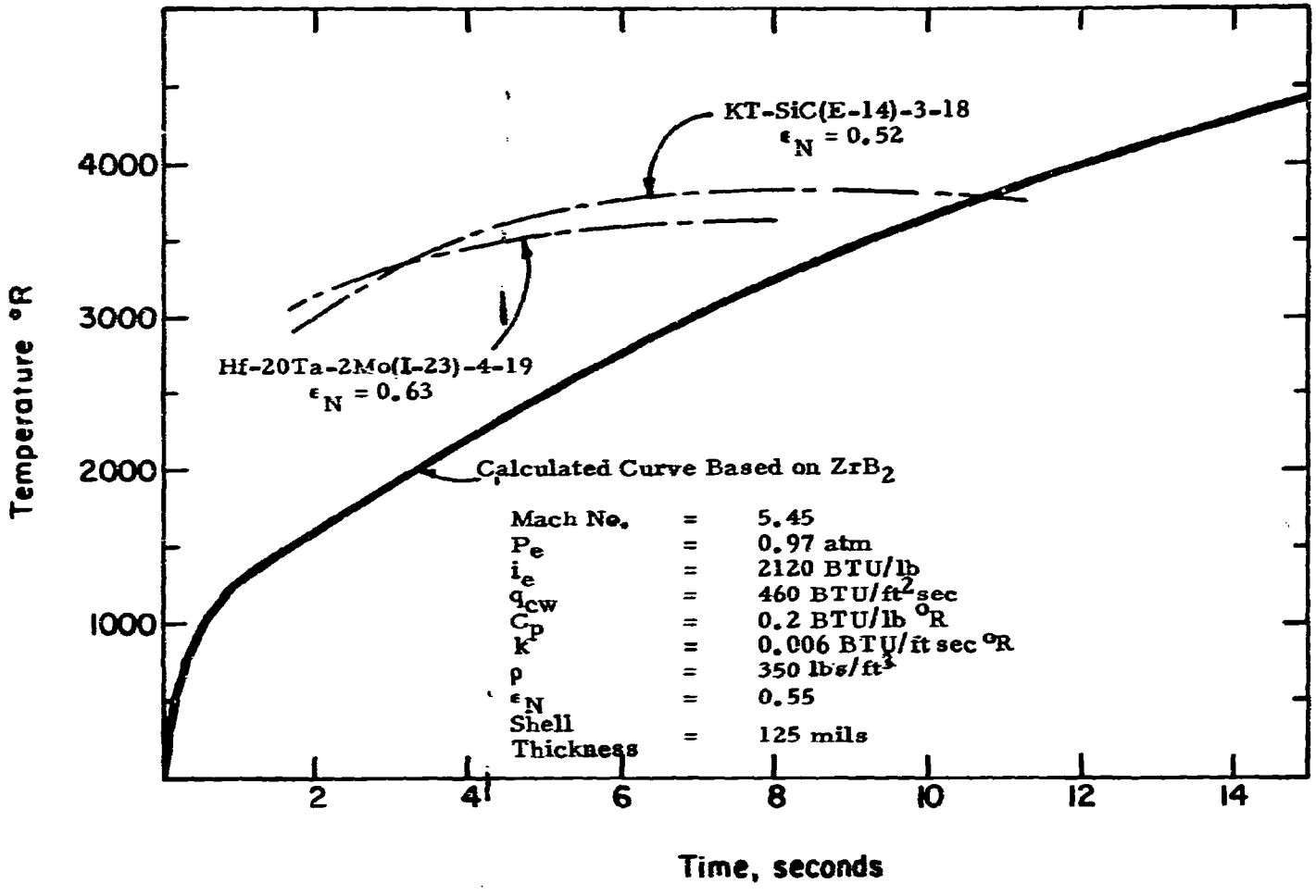


Figure 332. Comparison of Observed Time-Temperature Histories with Computed Values for One Inch Diameter Hemispherical Cap Models.

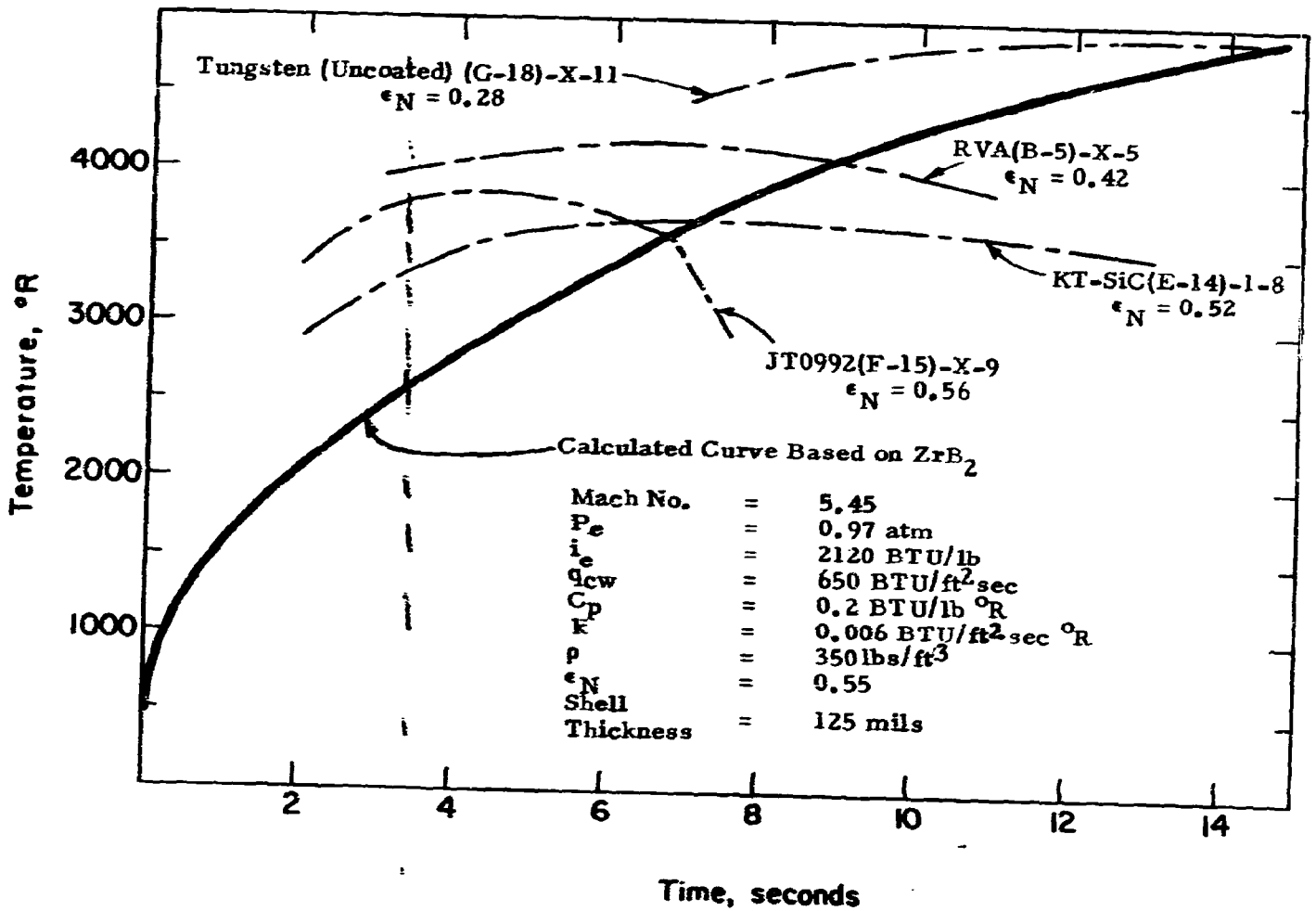


Figure 333. Comparison of Observed Time-Temperature Histories with Computed Values for One Half Inch Diameter Hemispherical Cap Models.

Plate 1-4483

| Sting Number | Material |
|---|---|
| 1 | $ZrB_2$(A-3)-1-2 |
| 2 | KT-SiC(E-14)-1-8 |
| 3 | KT-SiC(E-14)-3-18* |
| 4 | Hf-20Ta-2Mo(I-23)-4-19* |
| 5 | W(Uncoated)(G-18)-X-11 |
| 6 | RVA(B-5)-X-5 |
| 7 | JTA(D-13)-X-7 |
| 8 | JT0992(F-15)-X-9 |

*Denotes one inch diameter cap. All other models are one half inch diameter.

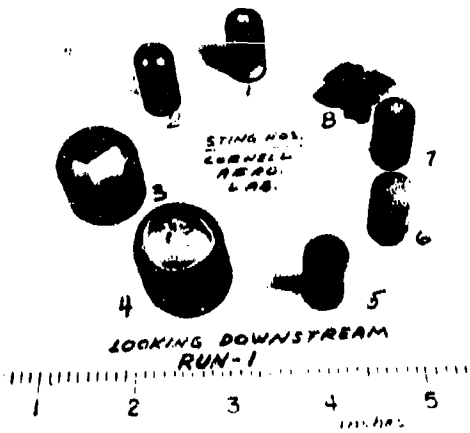


Figure 334. CAL Run 67-473, Mach Number 5.45, Stagnation Pressure 1.15 atm, Stagnation Enthalpy 2200 BTU/lb, Cold Wall Heat Flux 580 BTU/ft$^2$sec, Exposure Time 15 Seconds.

Plate 1-4884

| Sting Number | Material |
|---|---|
| 1 | Hf-20Ta-2Mo(I-23)-1-12 |
| 2 | $HfB_2$(A-2)-X-1 |
| 3 | $HfB_2$+SiC(A-4)-X-4 |
| 4 | PG(B-6)-X-6 |
| 5 | BPG(B-7)-X-16 |
| 6 | JT0981(F-16)-X-10 |
| 7 | $ZrB_2$(A-3)-24-3 |
| 8 | Sn-Al/Ta-10W(G-19)-3-22* |

*Denotes one inch diameter cap. All other models are one half inch diameter.

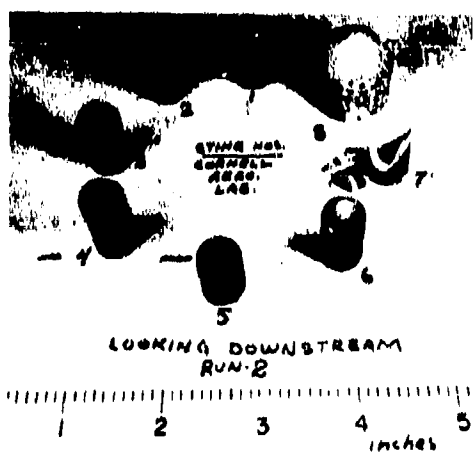


Figure 335. CAL Run 67-474, Mach Number 5.45, Stagnation Pressure 1.15 atm, Stagnation Enthalpy 2180 BTU/lb, Cold Wall Heat Flux 635 BTU/ft$^2$sec, Exposure Time 15 Seconds.

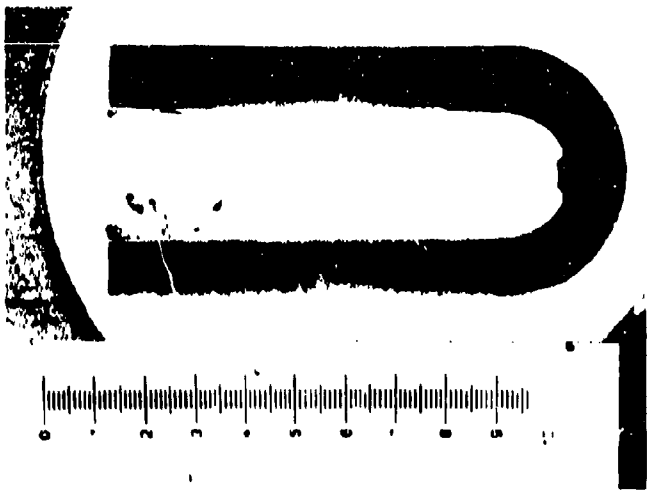

Plate No. 1-4691
a) One Inch Scale

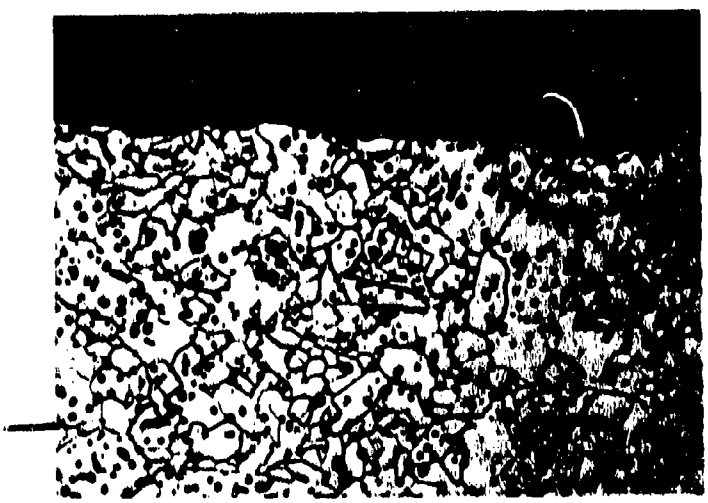

Plate No. 1-4692
b) X250, Etched with 10 Glycerine $5HNO_3$ 3HF. Hot Interface at Top.

Figure 336. Model $ZrB_2$(A-3)-1-2, Run #1, Sting #1.

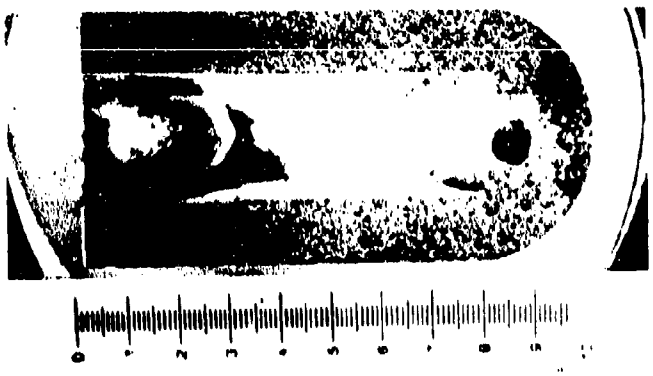

Plate No. 1-4708

a) One Inch Scale

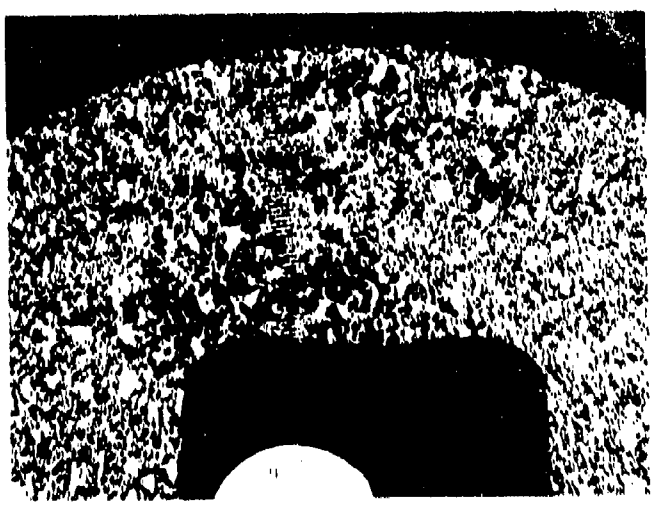

Plate No. 1-7767

b) 1.97 Mils per Small Division, Etched Electrolytically in 5% KOH, Hot Face at Top

Plate No. 1-5334

c) X250, Etched. Hot Interface at Top

Figure 337. Model KT-SiC(E-14)-1-8, Run #1, Sting #2.

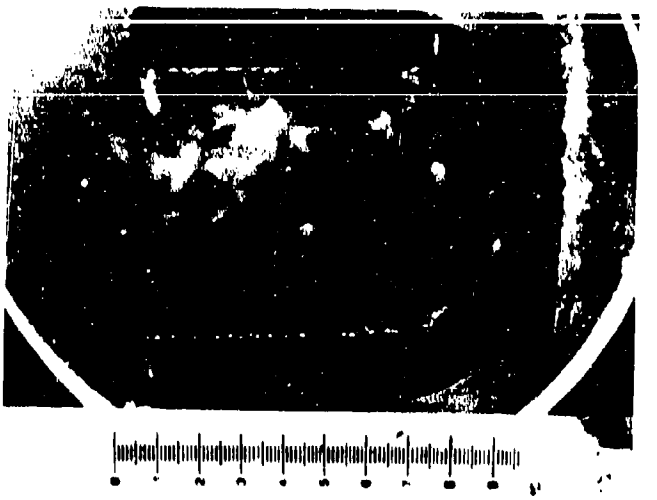

Plate No. 1-4709

a) One Inch Scale

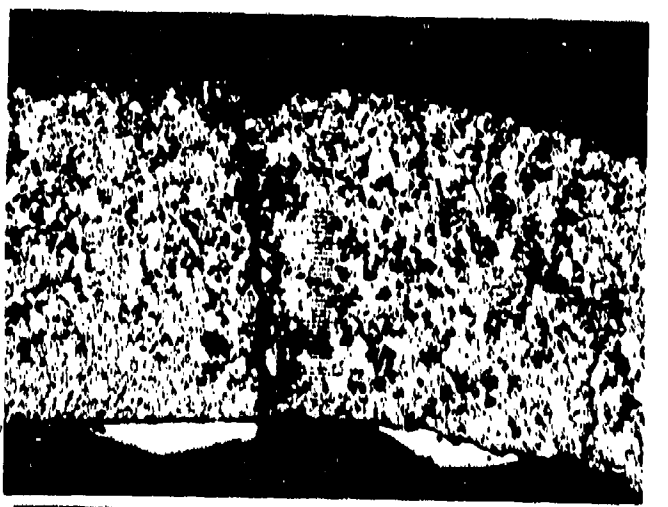

Plate No. 1-7768

b) 1.97 Mils per Small Division, Etched Electrolytically in 5% KOH. Hot Face at Top

Plate No. 1-4710

c) X250, Etched, Hot Interface at Top.

Figure 338. Model KT-SiC(E-14)-3-18, Run #1, Sting #3.

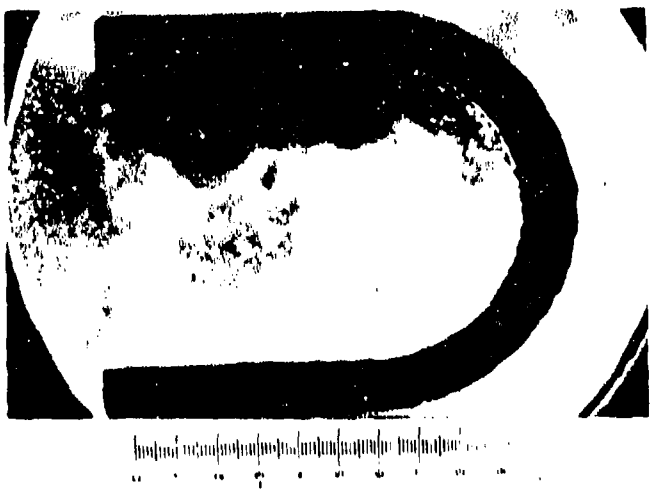

Plate No. 1-4719

a) One Inch Scale

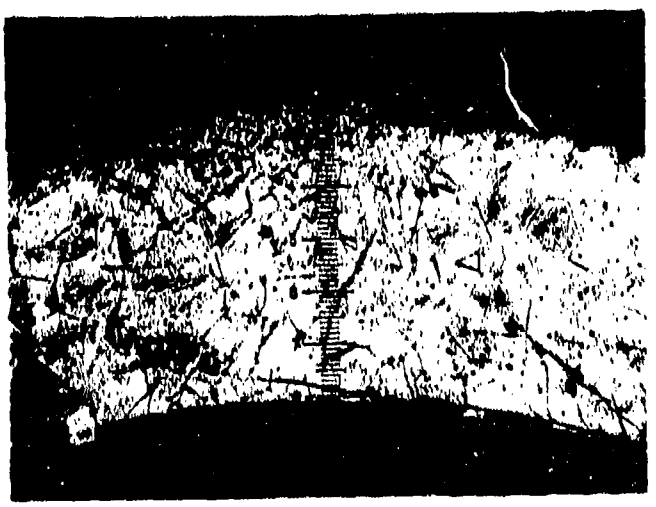

Plate No. 1-7766

b) 1.97 Mils per Small Division, Etched with 15 Glycerine $5HNO_3$ 5HCl 3HF, Hot Face at Top

Figure 339. Model Hf-20Ta-2Mo(I-23)-4-19, Run#1, Sting #4.

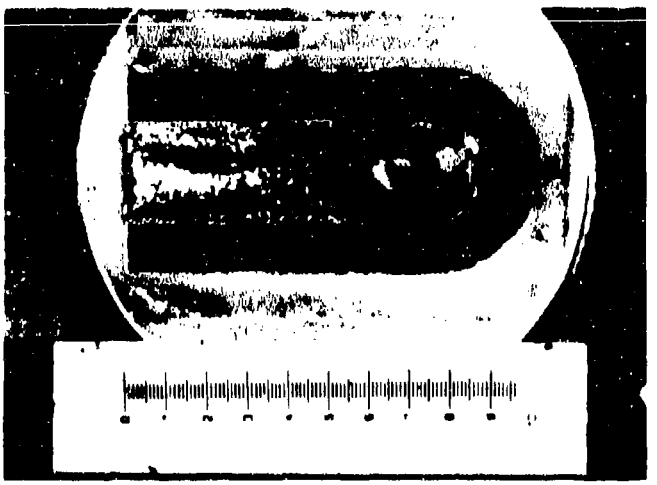

Plate No. 1-4716
a) One Inch Scale

Plate No. 1-5335
b) X200, Etched with
Murakami's Reagent
Hot Interface at Top

Figure 340. Model W(Uncoated) (G-18)-X-11, Run #1, Sting #5.

Plate No. 1-4698
a) One Inch Scale

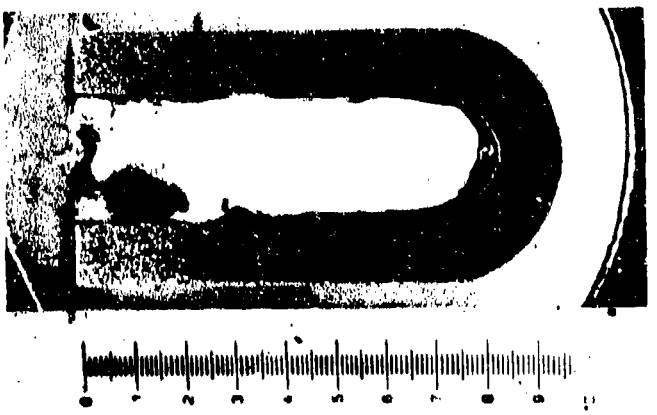

Plate No. 1-4705
b) One Inch Scale

Plate No. 1-4706
c) X250, Unetched.
Hot Interface at Top

Figure 341. a) Model RVA(B-5)-X-5, Run #1, Sting #6.
b & c) Model JTA(D-13)-X-7, Run #1, Sting #7.

Plate No. 1-4718

a) One Inch Scale

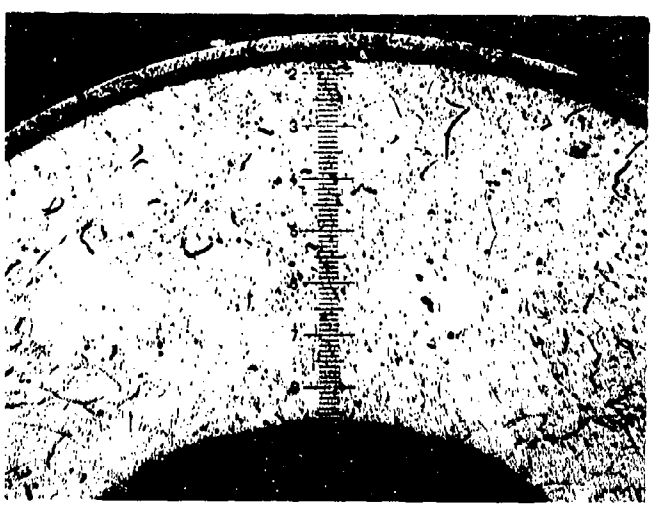

Plate No. 1-7765

b) 1.97 Mils per Small Division, Etched with 15 Glycerine 5$HNO_3$ 5HCl 3HF. Hot Face at top.

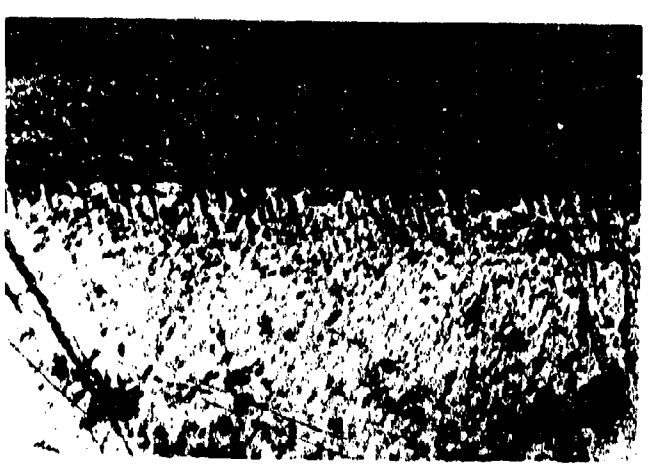

Plate No. 1-7763

c) X500, Etched, Interface of Suboxide (Top) and Matrix.

Figure 342. Model Hf-20Ta-2Mo(I-23)-1-12, Run #2, Sting #1.

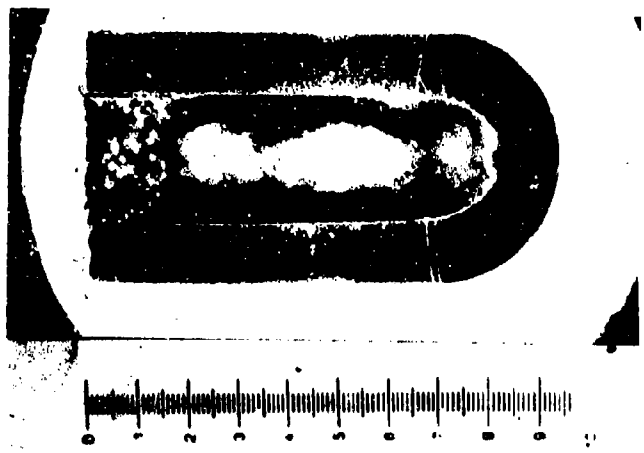

Plate No. 1-4688
a) One Inch Scale

Plate No. 1-4689
b) X250, Etched with
10 Glycerine $5HNO_3$
3HF. Hot Interface
at Top

Figure 343. Model $HfB_{2.1}$(A-2)-X-1, Run #2, Sting #2.

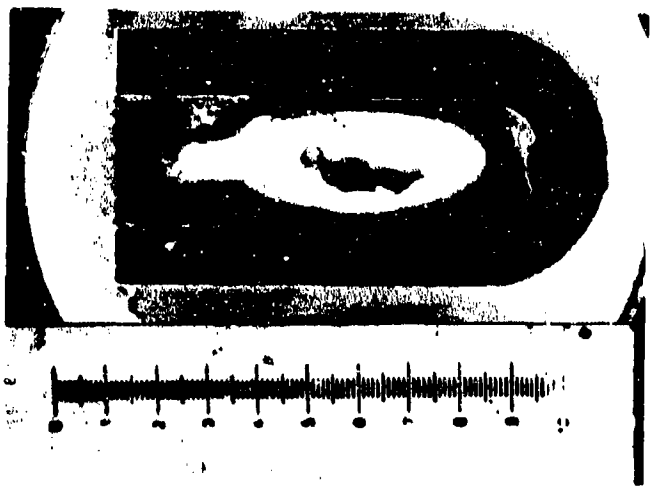

Plate No. 1-4694
a) One Inch Scale

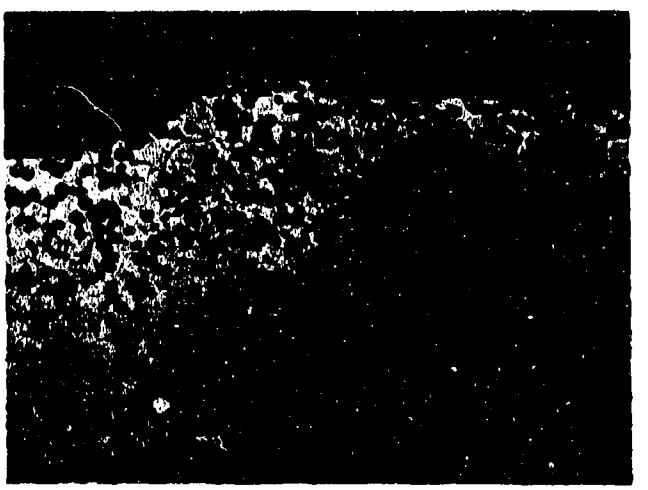

Plate NO. 1-4695
b) X250, Etched with
10 Glycerine 5$HNO_3$
3HF. Hot Interface
at Top

Figure 344. Model $HfB_2$ + SiC(A-4)-X-4, Run #2, Sting #3.

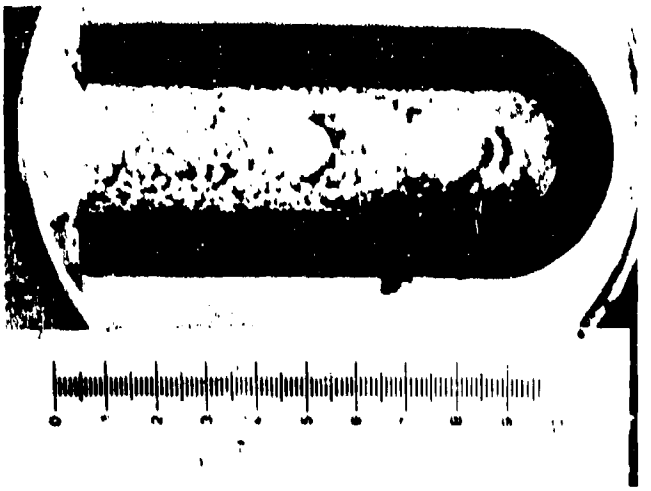

Plate No. 1-4701
a) One Inch Scale

Plate No. 1-4703
b) One Inch Scale

Figure 345. a) Model PG(B-6)-X-6, Run #2, Sting #4.
b) Model BPG(B-7)-X-16, Run #2, Sting #5.

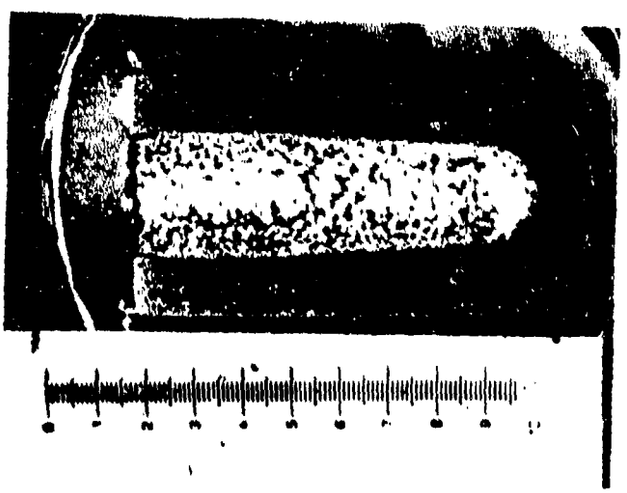

Plate No. 1-4713
a) One Inch Scale

Plate No. 1-4714
b) X250, Unetched.
Hot Interface at Top.

Figure 346. Model JT0981(F-16)-X-10, Run #2, Sting #6.

Plate No. 1-4717
a) One Inch Scale

Plate No. 1-5341
b) X250, Unetched.
Hot Interface at Top.

Figure 347. Model Sn-Al/Ta-W(G-19)-3-22, Run #2, Sting #8.

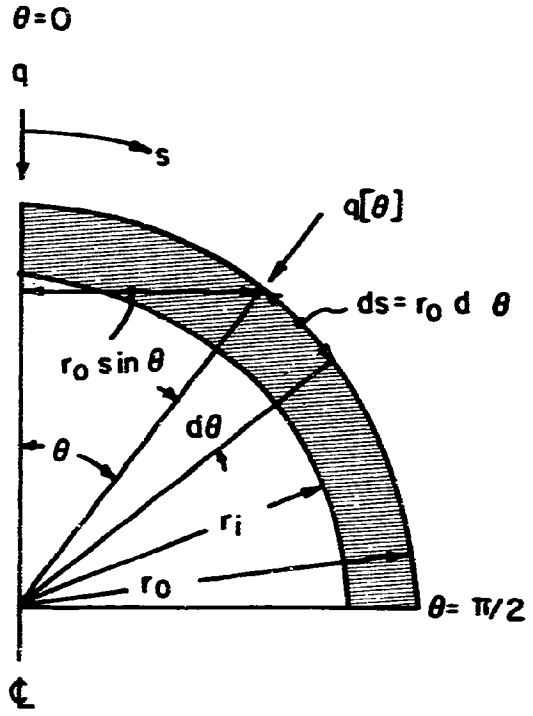


Figure 348. Geometrical Definitions for Analysis of Conduction Losses Through a Hemispherical Shell.

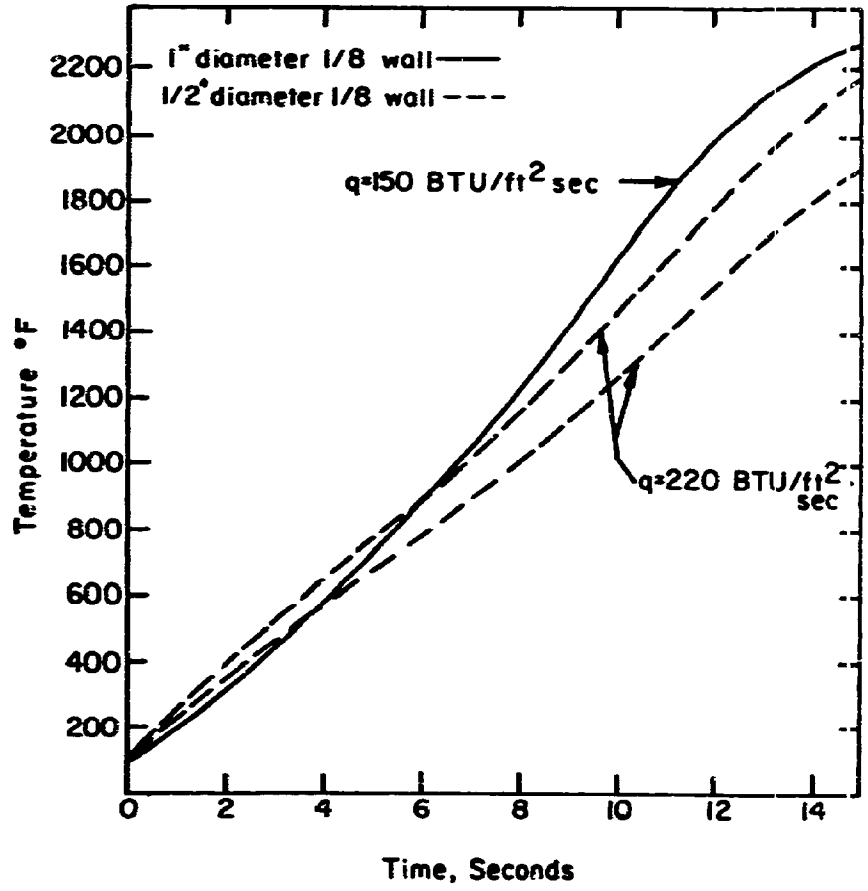


Figure 349. Temperature Response for Hemispherical Shells of 1020 Steel Exposed under Flux-Conductivity Conditions to Simulated Wave Superheater Tests.

## TABLE 1

## LIST OF CANDIDATE MATERIALS

| Material | Code | Supplier |
|---|---|---|
| $HfB_{2.1}$ | A-2 | Carborundum Co., Niagara Falls, New York |
| $ZrB_2$ | A-3 | Carborundum Co., Niagara Falls, New York |
| $HfB_2$ + 20v/o SiC | A-4 | Carborundum Co., Niagara Falls, New York |
| Boride Z | A-5 | Carborundum Co., Niagara Falls, New York |
| $HfB_{2.1}$ | A-6 | ManLabs-Avco AF33(615)-3671 |
| $HfB_{2.1}$ + 20v/o SiC | A-7 | ManLabs-Avco AF33(615)-3671 |
| $ZrB_{2.1}$ + 20 v/o SiC | A-8 | ManLabs-Avco AF33(615)-3671 |
| $HfB_{2.1}$ + 35 v/o SiC | A-9 | ManLabs-Avco AF33(615)-3671 |
| $ZrB_2$ + 14v/o SiC + 30 v/o C | A-10 | ManLabs-Avco AF33(615)-3671 |
| RVA | B-5 | Union Carbide Corp., New York, New York |
| PG | B-6 | General Electric Co., Detroit, Michigan |
| BPG | B-7 | High Temperature Materials, Lowell, Mass. |
| Si/RVC | B-8 | Union Carbide Corp., New York, New York |
| PT0178 | B-9 | Union Carbide Corp., New York, New York |
| Poco Graphite (AXF-5Q) | B-10 | Poco Graphite Inc., Garland, Texas |
| Glassy Carbon | B-11 | Lockheed M&SC, Palo Alto, California |
| HfC + C | C-11 | Battelle Memorial Institute, Columbus, Ohio |
| ZrC + C | C-12 | Battelle Memorial Institute, Columbus, Ohio |
| JTA (C-$ZrB_2$-SiC) | D-13 | Union Carbide Corp., New York, New York |
| KT-SiC | E-14 | Carborundum Co., Niagara Falls, New York |
| JT0992 (C-HfC-SiC) | F-15 | Union Carbide Corp., New York, New York |
| JT0981 (C-ZrC-SiC) | F-16 | Union Carbide Corp. New York, New York |
| $WSi_2$/W | G-18 | General Electric Co., Cleveland, Ohio (Type MK-W) |
| Sn-Al/Ta-W | G-19 | TRW, Cleveland, Ohio ($WSi_2$ coating) |
| W-Zr-Cu | G-20 | National Research Corp., Newton, Mass. (Ta-10W) |
| W-Ag | G-21 | GT&E, Hicksville, New York (Sn-Al coating) |
| $SiO_2$ + 68.5 w/o W | H-22 | Rocketdyne, Canoga Park, California |
| $SiO_2$ + 60 w/o W | H-23 | Wah Chang Corp., Albany, Oregon |
| $SiO_2$ + 35 w/o W | H-24 | Bjorksten Research Labs, Madison, Wisconsin |
| Hf-20Ta-2Mo | I-23 | General Electric Co., Willoughby, Ohio |
| Ir/Graphite | I-24 | General Electric Co., Willoughby, Ohio |
| | | Wah Chang Corp., Albany, Oregon |
| | | Battelle Memorial Institute, Columbus, Ohio |
| | | General Technologies Corp., Reston, Virginia |

# TABLE 2

## SUMMARY OF ARC PLASMA EXPOSURES OF $HfB_{2.1}$ (A-2)

| Material: Sample No. Assumed Emittance at $\lambda = 0.65\mu$ | Mesh No. | $P_u$ atm | $I_o$ BTU/lb | D (in) | $q_w$ BTU/ft²sec | $T_R$ abs | $q_r$ Surface Radiation BTU/ft²sec | $\epsilon_N$ Computed Normal Emittance |
|---|---|---|---|---|---|---|---|---|
| $HfB_{2.1}$ (A-2) $\epsilon = 0.80$ | | | | | | | | |
| -1M | 0.32 | 1.06 | 3270 | 0.500 | 820 | 4610 | 73 | 0.34 |
| -2M | 0.36 | 1.08 | 5020 | 0.500 | 730 | 5440 | 208 | 0.44 |
| -3M | 0.36 | 1.09 | 4885 | 0.500 | 1060 | 6640 | 343 | 0.37 |
| -4M | 0.36 | 1.09 | 4570 | 0.500 | 760 | 5888 | 129 | 0.23 |
| -5M | 0.37 | 1.09 | 4735 | 0.500 | 900 | 6400 | 94 | 0.18 |
| | 220 mil disk thermal checked off initially | | | | | | | |
| -6M | 0.39 | 1.10 | 5635 | 0.500 | 910 | 5840 | 169 | 0.31 |
| | 160 mil disk thermal checked off initially | | | | | | | |
| -7R[b] | 3.2 | 0.074 | 9470 | 0.500 | 492 | 5000 | 111 | 0.38 |
| -8R[b] | 3.2 | 0.168 | 7260 | 0.500 | 772 | ---- | --- | |
| | thermal shock failure | | | | | | | |
| -9R[b] | 3.2 | 0.168 | 7030 | 0.496 | 772 | 5995 | 299 | 0.49 |
| -10R[b] | 3.2 | 0.168 | 7260 | 0.500 | 781 | 5870 | 263 | 0.47 |
| -11R[b] | 3.2 | 0.097 | 10730 | 0.500 | 651 | 5440 | 329 | 0.69 |
| -12R[b] | 3.2 | 0.098 | 9830 | 0.500 | 573 | 5245 | 197 | 0.55 |
| -13M-1 | 0.30 | 1.05 | 2765 | 0.500 | 465 | 4660 | 74 | 0.33 |
| -13M-2 | 0.30 | 1.05 | 2765 | 0.500 | 465 | 4670 | 87 | 0.39 |
| -13M-3 | 0.30 | 1.05 | 2765 | 0.500 | 465 | 4975 | 124 | 0.45 |
| -14M-1 | 0.30 | 1.05 | 3870 | 0.500 | 510 | 5120 | 105 | 0.33 |
| -14M-2 | 0.30 | 1.05 | 3870 | 0.500 | 510 | 5380 | 130 | 0.35 |
| -14M-3 | 0.30 | 1.05 | 3870 | 0.500 | 510 | 5500 | 195 | 0.45 |
| -15M-1 | 0.21 | 1.03 | 2035 | 0.500 | 365 | 3390 | 41 | 0.66 |
| -15M-2 | 0.21 | 1.03 | 2035 | 0.500 | 365 | 3585 | 37 | 0.49 |
| -15M-3[b] | 0.21 | 1.03 | 2035 | 0.500 | 365 | 3625 | 51 | 0.62 |
| -16M[c] | 0.21 | 1.03 | 4930 | 0.507 | 588 | 5865 | 291 | 0.52 |
| -17M[c] | 0.30 | 1.05 | 4520 | 0.507 | 725 | 6700 | 431 | 0.66 |
| -18MA[c] | 0.33 | 1.07 | 4690 | 0.504 | 665 | 6665 | 423 | 0.65 |
| -18MB[c] | 0.33 | 1.07 | 4690 | 0.504 | 665 | 5695 | 287 | 0.58 |

[a] Preoxidized 10 minutes at 1930°C.

[b] Transmissivity factor equals 0.86 for sapphire window.

| Material Sample No. | Initial Length/Thickness (mils) | Final Length[c]/Thickness (mils) | Exposure Time (seconds) | Calculated Temperature Ratio T(CALC)/T(OBS) Cold Wall Heat Transfer Coefficient | Fay and Riddell Heat Transfer Coefficient |
|---|---|---|---|---|---|
| $HfB_{2.1}$ (A-2) | | | | | |
| -1M | 959/629 | 962/608 | 1800 | 1.13 | 1.19 |
| -2M | 930/585 | 973/556 | 1830 | 1.08 | 1.12 |
| -3M | 860/542 | ---/281 | 82 | 1.00 | 1.06 |
| -4M | 890/557 | 667/286 | 1830 | 1.08 | 1.10 |
| -5M | 925/593 | ---/145 | 221 | 0.94 | 1.03 |
| 220 mil disk thermal checked off | | | | | |
| -6M | 889/562 | ---/282 | 1830 | 1.09 | 1.15 |
| 160 mil disk thermal checked off initially | | | | | |
| -7R[b] | 921/612 | 929/599 | 1800 | 1.24 | 1.28 |
| -8R[b] | 901/563 | ---/560 | 14 | | |
| thermal shock failure | | | | | |
| -9R[b] | 902/593 | 732/612 | 60 | 1.02 | 1.13 |
| -10R[b] | 908/588 | 834/174 | 60 | 1.06 | 1.17 |
| -11R[b] | 940/605 | 962/566 | 1800 | 1.17 | 1.22 |
| -12R[b] | 936/594 | 957/581 | 1800 | 1.23 | 1.27 |
| -13M-1 | 901/609 | -/- | 600 | 1.11 | 1.04 |
| -13M-2 | -/- | -/- | 600 | 1.11 | 1.04 |
| -13M-3 | -/- | 607/589 | 600 | 1.04 | 0.98 |
| -14M-1 | 874/874 | -/- | 600 | 1.11 | 1.07 |
| -14M-2 | -/- | -/- | 600 | 1.08 | 1.02 |
| -14M-3 | -/- | 611/554 | 600 | 1.03 | 1.00 |
| -15M-1 | 908/809 | -/- | 600 | 1.48 | 1.41 |
| -15M-2 | -/- | -/- | 600 | 1.41 | 1.35 |
| -15M-3[b] | -/- | 809/801 | 600 | 1.38 | 1.32 |
| -16M[c] | 926/803 | 849/452 | 1800 | 1.03 | 0.99 |
| -17M[c] | 950/825 | 864/396 | 90 | 0.92 | 0.86 |
| -18MA[c] | 926/806 | -/- | 70 | 0.92 | 0.88 |
| -18MB[c] | -/- | 903/202 | 1730 | 1.08 | 1.04 |

[c] Final length refers to measurement after exposure, thickness refers to measurement after sectioning.

| Material Sample No. | T °F | Gross Recession Mils | Material Recession Mils | Degradation Mode | Exposure Time Seconds | Recession Rate[d] (Mils) (30 Min) | Description of Motion Picture Film Coverage |
|---|---|---|---|---|---|---|---|
| $HfB_{2.1}$ (A-2) | | | | | | | |
| -1M | 4150 | -3 | 31 | Oxidation | 1800 | 31 | little activity, uniform oxidation, crack formed in oxide coating |
| -2M | 5195 | -43 | 29 | Oxidation | 1830 | 29 | front face showed cold core, hot oxide rim, sunburst formation |
| -3M | 6200 | --- | 261 | Melting | 82 | 5742 | uniform melting undercutting of sides |
| -4M | 5425 | 223 | 271 | Oxidation | 1830 | 266 | sunburst formation, oxide melting |
| -5M | 5940 | --- | (320) | Th. Shock + Melting | 221 | 1791 | oxidation, thermal shock of disk followed by uniform melting |
| -6M | 5380 | --- | (120) | Th. Shock + Oxid. | 1830 | 118 | initial oxidation followed by thermal shock |
| -7R | 4140 | -4 | 13 | Oxidation | 1800 | 13 | speckled surface on heating, little activity |
| -8R | .... | --- | --- | Th. Shock | 14 | .... | thermal shock failure |
| -9R | 5535 | 170 | 141 | Melting | 60 | 4028 | melting from center to edges |
| -10R | 5410 | 368 | 384 | Melting | 60 | 11520 | rapid melting and recession |
| -11R | 5180 | -82 | 39 | Oxidation | 1800 | 39 | oxide melting, uniform oxidation |
| -12R | 4788 | -21 | 11 | Oxidation | 1800 | 11 | oxide melting, uniform oxidation |
| -13M-1 | 4200 | | | Oxidation | 600 | | Speckled front face, center appeared hotter than edges. |
| -13M-2 | 4210 | | | Oxidation | 600 | | Initial oxide breaking off in spots, center core still apparent. |
| -13M-3 | 4515 | -6 | 20 | Oxidation | 600 | 20 | Center core, oxide breaking off edges, some melting of oxide. |
| -14M-1 | 4660 | | | Oxidation | 600 | | Speckled front face, center core hotter than edges. |
| -14M-2 | 4920 | | | Oxidation | 600 | | Initial oxide breaking off front face. |
| -14M-3 | 5040 | -37 | 20 | Oxidation | 600 | 20 | Slight melting of oxide layer which appeared to be barely hanging onto front face. |
| -15M-1 | 2930 | | | Oxidation | 600 | | Little activity, hotter center core. |
| -15M-2 | 3095 | | | Oxidation | 600 | | Little activity, uniform appearance. |
| -15M-3 | 3175 | -1 | 4 | Oxidation | 600 | 4 | Little activity. |
| -16M | 5405 | -24 | 51 | Oxidation | 1800 | 51 | Pre-oxide flaking off sides, edge melting, sunburst formation. |
| -17M | 6240 | 195 | 169 | Melting | 90 | 3380 | Oxide melted, burned off, material melted. |
| -18MA | 6225 | --- | --- | Melting | 70 | --- | Oxide melted, burned off, material melted, solidified in sunburst. |
| -18MB | 5235 | 224 | 304 | Oxidation | 1730 | 304 | |

[d] Recession rates converted to 30 minutes on linear basis.

# TABLE 3

## SUMMARY OF ARC PLASMA EXPOSURES OF $ZrB_2$(A-3)

| Material Sample No. Assumed Emittance at λ = 0.65μ | Mach No. | $P_e$ atm | $i_e$ BTU/lb | D (in) | $q_{cw}$ BTU/ft²sec | T °R obs | $q_r$ Surface Radiation BTU/ft²sec | $\epsilon_N$ Computed Normal Emittance | Initial Length (thickness (mils) | Final Length* (thickness (mils) | Exposure Time (seconds) | Calculated Temperature Ratio T(CALC)/T(OBS) Cold Wall Heat Transfer Coefficient | Fay and Riddell Heat Transfer Coefficient |
|---|---|---|---|---|---|---|---|---|---|---|---|---|---|
| $ZrB_2$(A-3) ε = 0.57 | | | | | | | | | | | | | |
| -1M | 0.52 | 1.17 | 5945 | 0.492 | 860 | 6125 | 210 | 0.32 | 1063/1063 | 742/733 | 84 | 1.06 | 1.06 |
| -4M | 0.33 | 1.07 | 3990 | 0.492 | 560 | 4965 | 114 | 0.40 | 1062/1062 | 1061/1048 | 1860 | 1.14 | 1.10 |
| -17M | 0.35 | 1.07 | 3215 | 0.492 | 348 | 4179 | 31 | 0.22 | 1052/1052 | 1063/1047 | 1860 | 1.20 | 1.22 |
| -20M | 0.42 | 1.11 | 4665 | 0.492 | 840 | 6035 | 177 | 0.28 | 1059/1059 | 877/855 | 90 | 1.03 | 0.97 |
| -24M | 0.35 | 1.07 | 3375 | 0.492 | 750 | 9385 | 208 | 0.54 | 1057/1057 | 1076/1028 | 1860 | 1.17 | 1.13 |
| -23M | 0.32 | 1.06 | 3345 | 0.493 | 460 | 4475 | 51 | 0.27 | 1048/1048 | 1058/1040 | 1860 | 1.16 | 1.15 |
| -10R[b] | 3.2 | 0.02 | 9530 | 0.491 | 520 | 4835 | 103* | 0.40 | 1045/1045 | 1057/1027 | 1802 | 1.30 | 1.09 |
| -2R[b] | 3.2 | 0.014 | 14260 | 0.491 | 327 | 9000 | 132* | 0.52 | 1062/1062 | 1042/1004 | 1800 | 1.17 | 1.12 |
| -5R[b] | 3.2 | 0.012 | 13470 | 0.491 | 286 | 8120 | 132* | 0.41 | 1062/1062 | ----/1025 | 1800 | 1.08 | 1.06 |
| -30R[b] | 3.2 | 0.063 | 9380 | 0.491 | 458 | 9685 | 328* | 0.68 | 1066/1066 | 896/850 | 1464 | 1.09 | 1.05 |
| -11R[b] | 3.2 | 0.107 | 9270 | 0.491 | 950 | 9940 | 171* | 0.29 | 1063/1063 | 732/728 | 51 | 1.21 | 1.12 |
| -15R[b] | 3.2 | 0.168 | 8500 | 0.491 | 790 | 9780 | 289* | 0.54 | 1069/1069 | 879/869 | 98 | 1.18 | 1.10 |
| -56M | 0.36 | 1.08 | 3368 | 0.756 | 388 | 4670 | 110 | 0.49 | 733/720 | 738/717 | 1800 | 1.09 | 1.06 |
| -51M | 0.32 | 1.06 | 4935 | 0.750 | 475 | 4875 | 170 | 0.44 | 718/713 | 737/703 | 1800 | 1.15 | 1.13 |
| -52M-1 | 0.36 | 1.08 | 3765 | 0.426 | 465 | 5000 | 215 | 0.69 | 297/291 | ---/--- | 600 | 1.00 | 0.98 |
| -52M-2 | 0.36 | 1.08 | 3765 | 0.426 | 465 | 4975 | 195 | 0.68 | ---/--- | ---/--- | 600 | 1.02 | 0.99 |
| -52M-3 | 0.36 | 1.08 | 3765 | 0.426 | 465 | 5320 | 222 | 0.59 | ---/--- | ---/245 | 600 | 0.96 | 0.91 |
| -53M-1 | 0.36 | 1.08 | 3870 | 0.426 | 510 | 5285 | 185 | 0.60 | 308/310 | ---/--- | 600 | 1.09 | 1.03 |
| -53M-2 | 0.36 | 1.08 | 3870 | 0.426 | 510 | 5610 | 182 | 0.53 | ---/--- | ---/--- | 600 | 0.99 | 0.97 |
| -53M-3 | 0.36 | 1.08 | 3870 | 0.426 | 510 | 5565 | 264 | 0.54 | ---/--- | 351/331 | 600 | 0.99 | 0.98 |
| -54M-1 | 0.21 | 1.03 | 2835 | 0.426 | 365 | 4375 | 83 | 0.48 | 303/289 | ---/--- | 600 | 1.13 | 1.09 |
| -54M-2 | 0.21 | 1.03 | 2835 | 0.426 | 365 | 4355 | 45 | 0.28 | ---/--- | ---/--- | 600 | 1.08 | 1.04 |
| -54M-3 | 0.21 | 1.03 | 2835 | 0.426 | 365 | 4760 | 85 | 0.38 | ---/--- | 338/280 | 600 | 1.04 | 1.00 |
| -1MC | 0.31 | 1.06 | 4560 | 0.491 | 475 | 5190 | 113 | 0.34 | 421/104 | ---/ 71 | 1800 | 1.09 | 1.11 |
| -2MC | 0.29 | 1.05 | 3230 | 0.491 | 365 | 4930 | 176 | 0.63 | 422/181 | ---/ 87 | 1800 | 1.03 | 1.02 |
| -3MC | 0.31 | 1.06 | 3380 | 0.491 | 460 | 5170 | 236 | 0.75 | 429/102 | 448/ 71 | 1800 | 1.03 | 0.99 |
| -4MC | 0.33 | 1.07 | 4560 | 0.491 | 610 | 6340 | 404 | 0.83 | 424/104 | ---/ 0 | 64 | 0.93 | 0.90 |

[b] Transmissivity factor equals 0.86 for sapphire window.

* Surface radiation values may be low due to requirements for critical alignment caused by utilization of one-half inch diameter sample.

* Final Length is based on measurement prior to sectioning, thickness refers to length after sectioning.

| Material Sample No. | T °F | Gross Recession mils | Material Recession mils | Degradation Mode | Exposure Time seconds | Recession Rate* (mils) (30 min) | Description of Motion Picture Film Coverage |
|---|---|---|---|---|---|---|---|
| $ZrB_2$ (A-3) | | | | | | | |
| -3M | 5665 | 321 | 330 | Melting | 84 | 7062 | boride melting |
| -4M | 4505 | 1 | 14 | Oxidation | 1860 | 15 | solid oxide, little activity, few liquid drops, sunburst |
| -17M | 3710 | -11 | 5 | Oxidation | 1860 | 5 | |
| -20M | 5675 | 102 | 204 | Melting | 90 | 6080 | boride melting |
| -24M | 4095 | -19 | 29 | Oxidation | 1860 | 28 | oxide melting, sunburst formation |
| -23M | 4015 | -7 | 8 | Oxidation | 1860 | 8 | oxide solid, little activity noted |
| -10R | 4375 | -12 | 18 | Oxidation | 1802 | 18 | uniform oxidation |
| -2R | 4540 | 10 | 46 | Oxidation | 1800 | 46 | uniform oxidation, some liquid bubbles |
| -5R | 4660 | --- | 37 | Oxidation | 1800 | 37 | uniform oxidation, little activity |
| -30R | 5195 | 170 | 216 | Oxid. + Melting | 1464 | 266 | initial oxidation followed by uniform melting |
| -11R | 5680 | 341 | 335 | Melting | 51 | 11825 | uniform melting, rapid recession |
| -15R | 5320 | 490 | 480 | Melting | 98 | 8816 | uniform melting, recession |
| -56M | 4210 | 1 | 3 | Oxidation | 1800 | 3 | Hot oxide spot developed in center, then rest of front face giving mottled appearance. |
| -51M | 4415 | -19 | 10 | Oxidation | 1800 | 10 | Little activity, mottled appearance of oxide. |
| -52M-1 | 4630 | | | Oxidation | 600 | | Slight melting at edges, heavy oxide flaked off front face. |
| -52M-2 | 4515 | | | Oxidation | 600 | | Initial oxide broke away, new oxide formed and broke away, edge melting. |
| -52M-3 | 4860 | | 46 | Oxidation | 600 | 46 | Sunburst formed, slight melting, no further flaking. |
| -53M-1 | 4825 | | | Oxidation | 600 | | Melting, sunburst formation. |
| -53M-2 | 5150 | | | Oxidation | 600 | | Initial oxide broke away, melting and sunburst formation followed. |
| -53M-3 | 5155 | -45 | 79 | Oxidation | 600 | 79 | Oxide broke off again, melting and sunburst formation followed as before. |
| -54M-1 | 3915 | | | Oxidation | 600 | | Sunburst formation, oxide melting. |
| -54M-2 | 4095 | | | Oxidation | 600 | | Little activity. |
| -54M-3 | 4300 | -29 | 9 | Oxidation | 600 | 9 | No film coverage. |
| - 1MC | 4690 | --- | 33 | Oxidation | 1800 | 33 | Speckled front face, some oxide melting. |
| - 2MC | 4470 | --- | 14 | Oxidation | 1800 | 14 | Oxide chipping and melting off front face giving mottled appearance. |
| - 3MC | 4710 | -19 | 31 | Oxidation | 1800 | 31 | Oxide chipping and melting, uniform oxide buildup with some melting at edges. |
| - 4MC | 5680 | --- | 164 | Melting | 64 | 2870 | Rapid melting. |

* Recession rate converted to 30 minutes on linear basis.

# TABLE 4

## SUMMARY OF ARC PLASMA EXPOSURES OF $HfB_2$ + SiC(A-4)

| Material Sample No. Assumed Emittance at λ = 0.65μ | Mach No. | $P_e$ atm | $i_e$ BTU/lb | D (in) | $q_{cw}$ BTU/ft²sec | T °R obs | $q_r$ Surface Radiation BTU/ft²sec | $\epsilon_N$ Computed Normal Emittance | Initial Length/thickness (mils) | Final Length*/thickness (mils) | Exposure Time (seconds) | Calculated Temperature Ratio T(CALC)/T(OBS) Cold Wall Heat Transfer Coefficient | Fay and Riddell Heat Transfer Coefficient |
|---|---|---|---|---|---|---|---|---|---|---|---|---|---|
| $HfB_2$ + SiC (A-4) | | | | | | | | | | | | | |
| ε = 0.60 | | | | | | | | | | | | | |
| -1M | 0.35 | 1.08 | 3915 | 0.505 | 570 | 3910 | 61 | 0.47 | 966/686 | 968/680 | 1830 | 1.44 | 1.38 |
| -2M | 0.36 | 1.08 | 5105 | 0.505 | 670 | 5480 | 208 | 0.49 | 999/675 | 986/643 | 1830 | 1.10 | 1.08 |
| -3M | 0.38 | 1.09 | 6510 | 0.505 | 930 | 6080 | 260 | 0.40 | 989/674 | 610/277 | 439 | 1.09 | 1.06 |
| -4M | 0.36 | 1.08 | 5410 | 0.505 | 900 | 5620 | 203 | 0.43 | 959/644 | 507/175 | 1608 | 1.14 | 1.07 |
| -2-1M | 0.42 | 1.11 | 6245 | 0.477 | 935 | 6405 | 390 | 0.49 | 1108/776 | 448/505 | 1100 | 1.03 | 1.00 |
| -2-2M | 0.31 | 1.06 | 3435 | 0.487 | 510 | 3630 | 58 | 0.71 | 1107/790 | 1111/787 | 1830 | 1.48 | 1.41 |
| -2-3M | 0.35 | 1.08 | 5365 | 0.474 | 680 | 5250 | 192 | 0.54 | 1109/772 | 944/639 | 1830 | 1.16 | 1.15 |
| -2-4M | 0.38 | 1.09 | 5565 | 0.477 | 915 | 5650 | 333 | 0.69 | 1112/787 | 947/600 | 1830 | 1.14 | 1.09 |
| -2-5M | 0.38 | 1.09 | 6715 | 0.477 | 1005 | 6370 | 434 | 0.56 | 1103/770 | 534/211 | 120 | 1.05 | 1.00 |
| -2-6R† | 3.2 | 0.023 | 11400 | 0.478 | 506 | 5650 | 271 | 0.56 | 1102/780 | 1117/767 | 1800 | 1.10 | 0.98 |
| -2-7R† | 3.2 | 0.026 | 17040 | 0.475 | 610 | 5760 | 355 | 0.68 | 1109/791 | 1116/767 | 1800 | 1.16 | 1.09 |
| -2-8R† | 3.2 | 0.027 | 13540 | 0.478 | 700 | 5940 | 408 | 0.70 | 1103/781 | 1087/738 | 1800 | 1.15 | 0.99 |
| -2-9R† | 3.2 | 0.023 | 8920 | 0.475 | 402 | 5140 | 211 | 0.64 | 1105/765 | 1113/742 | 1800 | 1.14 | 1.01 |
| -2-10R† | 3.2 | 0.022 | 7560 | 0.488 | 314 | 3540 | 59 | 0.80 | 1099/773 | 1100/770 | 1800 | 1.55 | 1.38 |

†Transmissivity factor equals 0.86 for sapphire window.

*Final length is based on measurement prior to sectioning; thickness refers to length after sectioning.

| Material Sample No. | T °F | Gross Recession mils | Material Recession mils | Degradation Mode | Exposure Time seconds | Recession Rate* mils/sec / mils/30 min | Description of Motion Picture Film Coverage |
|---|---|---|---|---|---|---|---|
| $HfB_2$ + SiC (A-4) | | | | | | | |
| -1M | 3450 | -2 | 6 | Oxidation | 1830 | ----/6 | surface activity, liquid bubbles at edges |
| -2M | 5020 | 13 | 32 | Oxidation | 1830 | ----/31 | liquid oxide formation |
| -3M | 5620 | 389 | 397 | Melting | 139 | ----/5141 | liquid oxide, composite melting |
| -4M | 5160 | 459 | 469 | Oxid + Melt | 1608 | ----/525 | liquid oxide, sunburst formation, melting, some flaking off of oxide |
| -2-1M | 5945 | 260 | 271 | Oxidation | 1100 | ----/444 | initial oxide melting, erosion at angle to face, solid oxide formed |
| -2-2M | 3170 | -4 | 3 | Oxidation | 1830 | ----/3 | |
| -2-3M | 4790 | 165 | 133 | Oxidation | 1830 | ----/131 | initial oxide melting, erosion at angle to face, solid oxide formed |
| -2-4M | 5190 | 165 | 187 | Oxidation | 1830 | ----/184 | heated from top towards bottom, liquid oxide, erosion at angle, sunburst formation |
| -2-5M | 5810 | 569 | 559 | Melting | 120 | ----/8385 | rapid oxide melting, recession at angle, sunburst formation |
| -2-6R | 5190 | -15 | 13 | Oxidation | 1800 | ----/13 | |
| -2-7R | 5300 | -7 | 24 | Oxidation | 1800 | ----/24 | |
| -2-8R | 5480 | 16 | 43 | Oxidation | 1800 | ----/43 | |
| -2-9R | 4680 | -8 | 23 | Oxidation | 1800 | ----/23 | |
| -2-10R | 3080 | -1 | 3 | Oxidation | 1800 | ----/3 | |

*Recession rate converted to 30 minutes on linear basis.

# TABLE 5

## SUMMARY OF ARC PLASMA EXPOSURES OF BORIDE Z (A-5)

| Material Sample No. Assumed Emittance at $\lambda = 0.65\mu$ | Mach No. | $P_e$ atm | $i_e$ BTU/lb | D (in) | $q_{cw}$ BTU/ft²sec | $T_R$ °R obs | $q_r$ Surface Radiation BTU/ft²sec | $\epsilon_N$ Computed Normal Emittance | Initial Length/thickness (mils) | Final Length*/thickness (mils) | Exposure Time (seconds) | Calculated Temperature Ratio T(CALC)/T(OBS) Cold Wall Heat Transfer Coefficient | Fay and Riddell Heat Transfer Coefficient |
|---|---|---|---|---|---|---|---|---|---|---|---|---|---|
| Boride Z (A-5) $\epsilon = 0.60$ | | | | | | | | | | | | | |
| -1M | 0.30 | 1.05 | 3660 | 0.490 | 370 | 4515 | 116 | 0.59 | 723/679 | 725/676 | 970 | 1.14 | 1.16 |
| -2M | 0.54 | 1.19 | 4525 | 0.485 | 890 | ---- | --- | ---- | 695/670 | ---/653 | 11 | --- | ---- |
| -3M | 0.32 | 1.06 | 3005 | 0.482 | 410 | 4405 | --- | ---- | 674/639 | 680/617 | 1830 | 1.14 | 1.11 |
| -4M | 0.30 | 1.05 | 2500 | 0.490 | 350 | 3380 | 39 | 0.64 | 705/663 | 705/659 | 1830 | 1.40 | 1.35 |
| -5M | 0.36 | 1.08 | 5075 | 0.485 | 700 | 5605 | 356 | 0.77 | 736/690 | -----/505 | 33 | 1.08 | 1.06 |
| -6M | 0.42 | 1.11 | 4875 | 0.485 | 660 | 5710 | 335 | 0.67 | 719/695 | -----/603 | 40 | 1.05 | 1.04 |
| -7R+ | 3.2 | 0.025 | 12120 | 0.491 | 539 | 5630 | 359 | 0.76 | 1037/703 | 768/469 | 1800 | 1.14 | 1.01 |
| -8R+ | 3.2 | 0.013 | 9200 | 0.482 | 262 | 4250 | 112 | 0.73 | 1028/690 | 1051/680 | 1800 | 1.26 | 1.19 |
| -9R+ | 3.2 | 0.011 | 10410 | 0.482 | 192 | 3080 | 43 | 1.02 | 1036/675 | 1037/665 | 1800 | 1.64 | 1.61 |
| -11R+ | 3.2 | 0.031 | 14450 | 0.490 | 701 | 5620 | 250 | 0.55 | 1030/697 | 530/210 | 100 | 1.22 | 1.09 |
| -10R+ | 3.2 | 0.017 | 11620 | 0.485 | 389 | 5490 | 312 | 0.73 | 1027/697 | 1045/--- | 1800 | 1.08 | 0.98 |
| -12R+ | 3.2 | 0.011 | 13860 | 0.490 | 316 | 5335 | 306 | 0.80 | 1032/670 | 1058/--- | 1800 | 1.07 | 1.00 |

+Transmissivity factor equals 0.86 for sapphire window.

* Final Length is based on measurement prior to sectioning, thickness refers to length after sectioning.

| Material Sample No. | $T_{s_F}$ | Gross Recession mils | Material Recession mils | Degradation Mode | Exposure Time seconds | Recession Rate* (mils)/(30 min) | Description of Motion Picture Film Coverage |
|---|---|---|---|---|---|---|---|
| Boride Z (A-5) | | | | | | | |
| -1M | 4055 | -2 | 3 | Oxidation | 970 | 6 | little oxidation |
| -2M | ----- | --- | 17 | Th. Shock | 11 | ----- | immediate thermal shock failure |
| -3M | 3945 | -6 | 22 | Oxidation | 1830 | 22 | little oxidation |
| -4M | 3920 | 0 | 4 | Oxidation | 1830 | 4 | little oxidation |
| -5M | 5145 | --- | 185 | Th. Shock | 33 | ----- | specimen cracked, liquid oxide formed, spallation |
| -6M | 5250 | --- | 92 | Th. Shock | 40 | ----- | specimen cracked, liquid oxide formed, spallation |
| -7R | 5170 | 269 | 234 | Oxidation | 1800 | 234 | |
| -8R | 3790 | -23 | 10 | Oxidation | 1800 | 10 | |
| -9R | 2620 | -1 | 10 | Oxidation | 1800 | 10 | |
| -11R | 5160 | 500 | 487 | Melting | 100 | 8770 | |
| -10R | 5030 | -18 | --- | Th. Shock+Oxid | 1800 | ----/---- | radial crack 1/4" from face, little activity |
| -12R | 4875 | -26 | --- | Th. Shock+Oxid | 1800 | ----/---- | thermal shock of front face on heat-up, chipped non-uniformly, radial crack 1/4" from front, little activity |

*Recession rates converted to 30 minutes on linear basis.

# TABLE 6

## SUMMARY OF ARC PLASMA EXPOSURES OF $HfB_2$ + 20% SiC (A-7)

| Material Sample No. Assumed Emittance at λ = 0.65μ | Mach No. | P e atm | i e BTU/lb | D (in) | q cw BTU/ft²sec | T °R obs | $q_r$ Surface Radiation BTU/ft²sec | [a] N Computed Normal Emittance | Initial Length/Thickness (mils) | Final Length[b]/Thickness (mils) | Exposure Time (seconds) | Calculated Temperature Ratio T(CALC)/T(OBS) Cold Wall Heat Transfer Coefficient | Fay and Riddell Heat Transfer Coefficient |
|---|---|---|---|---|---|---|---|---|---|---|---|---|---|
| $HfB_{2,1}$ + 20 w/o SiC(A-7) | | | | | | | | | | | | | |
| ε = 0.60 | | | | | | | | | | | | | |
| -1M | 0.42 | 1.11 | 9690 | 0.488 | 810 | 6220 | 336 | 0.48 | 540/523 | ---/413 | 56 | 1.02 | 1.00 |
| -2M | 0.36 | 1.08 | 5055 | 0.488 | 715 | 5260 | 224 | 0.62 | 535/520 | ---/363 | 1740 | 1.16 | 1.12 |
| -3MA | 0.39 | 1.09 | 2970 | 0.488 | 665 | 6055 | 318 | 0.90 | 552/544 | ---/444[c] | 200 | 0.89 | 0.82 |
| -3MB | 0.39 | 1.09 | 2970 | 0.488 | 665 | 5205 | 198 | 0.57 | ---/--- | 420/363 | 1600 | 1.04 | 0.95 |
| -4M | 0.36 | 1.08 | 5200 | 0.488 | 755 | 5340 | 230 | 0.60 | 537/536 | ---/309 | 1800 | 1.16 | 1.12 |
| -5MA* | 0.15 | 1.01 | 5010 | 0.435 | 655 | 6405 | 335 | 0.42 | 936/926 | ---/--- | 50 | 0.93 | 0.86 |
| -5MB* | 0.15 | 1.01 | 5010 | 0.435 | 655 | 5490 | 112 | 0.26 | ---/--- | 710/640 | 1750 | 1.09 | 1.00 |
| -6M* | 0.71 | 1.34 | 3390 | 0.430 | 750 | 5595 | 246 | 0.53 | 912/909 | 849/811 | 264 | 1.02 | 0.98 |
| -7MA* | 0.15 | 1.01 | 6210 | 0.431 | 740 | 6595 | 318 | 0.36 | 918/921 | ---/--- | 50 | 0.96 | 0.90 |
| -7MB* | 0.15 | 1.01 | 6210 | 0.431 | 740 | 5560 | 57 | 0.13 | ---/--- | 592/539 | 750 | 1.13 | 1.06 |
| -23M1 | 0.33 | 1.06 | 4380 | 0.429 | 627 | 5420 | 209 | 0.51 | 923/922 | ---/--- | 1800 | 1.07 | 1.04 |
| -23M11 | 0.33 | 1.06 | 4550 | 0.429 | 583 | 5470 | 214 | 0.51 | ---/--- | ---/--- | 1800 | 1.06 | 1.05 |
| -23M111 | 0.33 | 1.06 | 4530 | 0.429 | 583 | 5500 | 212 | 0.49 | ---/--- | ---/--- | 1800 | 1.05 | 1.04 |
| -23M1V | 0.33 | 1.06 | 4370 | 0.429 | 603 | 5700 | 250 | 0.50 | ---/--- | 789/729 | 1800 | 1.01 | 0.99 |
| -24M1 | 0.36 | 1.07 | 3980 | 0.427 | 550 | 5170 | 198 | 0.59 | 895/883 | ---/--- | 1800 | 1.08 | 1.07 |
| -24M11 | 0.36 | 1.08 | 3970 | 0.427 | 551 | 5365 | 233 | 0.60 | ---/--- | ---/--- | 1800 | 1.04 | 1.03 |
| -24M111 | 0.36 | 1.07 | 3950 | 0.427 | 561 | 5400 | 226 | 0.57 | ---/--- | ---/--- | 1800 | 1.04 | 1.02 |
| -24M1V | 0.36 | 1.08 | 3950 | 0.427 | 571 | 5365 | 214 | 0.55 | ---/--- | 792/728 | 1800 | 1.05 | 1.03 |
| -25M1 | 0.24 | 1.03 | 4890 | 0.426 | 498 | 4945 | 169 | 0.60 | 928/921 | ---/--- | 1800 | 1.15 | 1.16 |
| -25M11 | 0.27 | 1.04 | 4700 | 0.426 | 505 | 5090 | 186 | 0.49 | ---/--- | ---/--- | 1418 | 1.11 | 1.12 |
| -25M111 | 0.28 | 1.04 | 4960 | 0.426 | 487 | 5215 | 193 | 0.55 | ---/--- | ---/--- | 1800 | 1.08 | 1.12 |
| -25M1V | 0.27 | 1.04 | 4910 | 0.426 | 495 | 5390 | 219 | 0.55 | ---/--- | ---/--- | 1800 | 1.05 | 1.08 |
| -25MV | 0.27 | 1.04 | 4610 | 0.426 | 498 | 5435 | 197 | 0.48 | ---/--- | ---/--- | 1800 | 1.03 | 1.05 |
| -25MVI | 0.26 | 1.04 | 4350 | 0.426 | 513 | 5435 | 211 | 0.51 | ---/--- | ---/--- | 1800 | 1.03 | 1.02 |
| -25MVII | 0.27 | 1.04 | 4780 | 0.426 | 508 | 5435 | 196 | 0.48 | ---/--- | ---/--- | 1800 | 1.04 | 1.06 |
| -25MVIII | 0.26 | 1.04 | 4420 | 0.426 | 507 | 5500 | 226 | 0.52 | ---/--- | ---/--- | 1800 | 1.03 | 1.02 |
| -25MIX | 0.27 | 1.04 | 4520 | 0.426 | 518 | 5585 | 235 | 0.51 | ---/--- | ---/--- | 1800 | 1.01 | 1.01 |
| -25MX | 0.26 | 1.04 | 4500 | 0.426 | 493 | 5700 | 262 | 0.53 | ---/--- | ---/--- | 1800 | 0.98 | 0.99 |
| -25MXI | 0.26 | 1.04 | 4500 | 0.426 | 483 | 5710 | 262 | 0.52 | ---/--- | 469/332 | 1800 | 0.97 | 0.98 |
| -30M | 0.25 | 1.03 | 5030 | 0.437 | 587 | 5375 | 216 | 0.55 | 666/664 | 322/321 | 1800 | 1.09 | 1.08 |
| -31M | 0.15 | 1.01 | 5580 | 0.438 | 487 | 4650 | 110 | 0.50 | 686/685 | ---/260 | 1800 | 1.23 | 1.23 |
| -32M | 0.21 | 1.02 | 5740 | 0.438 | 618 | 5615 | 253 | 0.54 | 687/687 | 576/516 | 1800 | 1.07 | 1.06 |
| -36MH | 0.21 | 1.02 | 3600 | 0.437 | 513 | 4370 | 89 | 0.19 | 699/107[d] | ---/94[d] | 1081 | 1.23 | 1.16 |
| -37MH | 0.21 | 1.02 | 3640 | 0.438 | 495 | 4225 | 80 | 0.53 | 690/403[d] | ---/398[d] | 1080 | 1.28 | 1.21 |
| -40M | 0.26 | 1.04 | 4390 | 0.438 | 495 | 4665 | 125 | 0.56 | 689/96[d] | ---/82[d] | 1800 | 1.19 | 1.19 |
| -41M | 0.27 | 1.04 | 4400 | 0.438 | 502 | 5000 | 150 | 0.51 | 687/397[d] | ---/335[d] | 1800 | 1.12 | 1.12 |
| -44MS | 0.26 | 1.04 | 4360 | 0.437 | 493 | 3250 | 36 | 0.69 | 684/93[d] | 684/93 | 1800 | 1.71 | 1.71 |
| -45MS | 0.26 | 1.04 | 4580 | 0.427 | 522 | 3345 | 46 | 0.78 | 690/395[d] | 690/395 | 1800 | 1.69 | 1.68 |

* Preoxidized samples

[b] Final length refers to sample length prior to sectioning; thickness refers to section length.

[c] Estimated.

[d] Nose to in-depth temperature measurement station.

| Material Sample No. | °T °F | Gross Recession (mils) | Material Recession (mils) | Degradation Mode | Exposure Time seconds | Recession Rate[e] mils/30 min | Description of Motion Picture Film Coverage |
|---|---|---|---|---|---|---|---|
| $HfB_{2,1}$ + 20% SiC (A-7) | | | | | | | |
| -1M | 5760 | --- | 110 | Melting | 56 | 3530 | Sunburst formed, rapid melting at angle. |
| -2M | 4800 | --- | 157 | Melt. + Oxid. | 1740 | 162 | Gradual heatup, rapid melting, solidified in sunburst. |
| -3MA | 5595 | --- | 100[c] | Melting | 200 | 900[c] | Sunburst formed, oxide melting. |
| -3MB | 4745 | --- | 81[c] | Oxidation | 1600 | 91[c] | Solidified sunburst, little change. |
| -4M | 4880 | --- | 227 | Melt. + Oxid. | 1800 | 227 | Rapid melting, solidified in sunburst, little change. |
| -5MA | 5945 | --- | --- | Melting | 50 | --- | Rapid melting, rapid recession. |
| -5MB | 5030 | 286 | 286 | Oxidation | 1750 | 286 | Solidified in sunburst. |
| -6M | 5135 | 63 | 98 | Oxid. + Melt. | 264 | 668 | Rotating and vibrating of sample, continuous oxide melting. |
| -7MA | 6135 | --- | --- | Melting | 50 | --- | Rapid melting. |
| -7MB | 5100 | 326 | 382 | Oxidation | 1750 | 382 | Solidified in sunburst. |
| -23M1 | 4960 | --- | --- | Melt. + Oxid. | 1800 | --- | Rapid melting, solidified in sunburst, little activity. |
| -23M11 | 5010 | --- | --- | Oxidation | 1800 | --- | Intact from cycle I. |
| -23M111 | 5040 | --- | --- | Oxidation | 1800 | --- | Intact from cycle II. |
| -23M1V | 5240 | 134 | 193 | Oxidation | 1800 | 48 | Intact from cycle III, some oxide chipped away. |
| -24M1 | 4710 | --- | --- | Melt. + Oxid. | 1800 | --- | Melting, solidified in sunburst, little activity. |
| -24M11 | 4905 | --- | --- | Oxidation | 1800 | --- | Intact from cycle I. |
| -24M111 | 4940 | --- | --- | Oxidation | 1800 | --- | Intact from cycle II. |
| -24M1V | 4905 | 103 | 153 | Oxidation | 1800 | 19 | Intact from cycle III. |
| -25M1 | 4485 | --- | --- | Melt. + Oxid. | 1800 | --- | Considerable melting, solidified after several minutes. |
| -25M11 | 4630 | --- | --- | Melt. + Oxid. | 1418 | --- | Oxide melting and chipping, sunburst formed, some oxide melting. |
| -25M111 | 4755 | --- | --- | Melt. + Oxid. | 1800 | --- | Same behavior as cycle II. |
| -25M1V | 4930 | --- | --- | Oxidation | 1800 | --- | Slight melting and spalling of oxide, little change. |
| -25MV | 4975 | --- | --- | Oxidation | 1800 | --- | No change from cycle IV. |
| -25MVI | 4975 | --- | --- | Oxidation | 1800 | --- | Slight melting and spalling of oxide, little change. |
| -25MVII | 4975 | --- | --- | Oxidation | 1800 | --- | No change from cycle VI. |
| -25MVIII | 5040 | --- | --- | Oxidation | 1800 | --- | No change from cycle VII, oxide buildup on sides. |
| -25MIX | 5125 | --- | --- | Oxidation | 1800 | --- | Slight melting and chipping of oxide at edges. |
| -25MX | 5240 | --- | --- | Oxidation | 1800 | --- | No change from cycle IX. |
| -25MXI | 5250 | 456 | 589 | Oxidation | 1800 | 53 | Slight melting of oxide at edges. |
| -30M | 4915 | 344 | 343 | Melt. + Oxid. | 1800 | 343 | Melting, solidified in sunburst, some slight oxide melting. |
| -31M | 4190 | --- | 425 | Melt. + Oxid. | 1800 | 425 | Slow melting, eventually solidified, some oxide melting. |
| -32M | 5155 | 111 | 171 | Melt. + Oxid. | 1800 | 171 | Melting, solidified in sunburst. |
| -36MH | 3910 | --- | 13 | Oxidation | 1081 | 22 | Hot spot 1/8" diam. at nose, little activity. |
| -37MH | 3765 | --- | 10 | Oxidation | 1080 | 17 | |
| -40M | 4205 | --- | 14 | Oxidation | 1800 | 14 | Very slight oxide melting spread from edges inward. |
| -41M | 4540 | --- | 62 | Oxidation | 1800 | 62 | Slow oxide melting from edges inward. |
| -44MS | 2790 | 0 | 0 | Oxidation | 1800 | 0 | |
| -45MS | 2885 | 0 | 0 | Oxidation | 1800 | 0 | Little visible. |

[c] Estimated

[e] Converted to 30 minutes on a linear basis.

# TABLE 7

## SUMMARY OF ARC PLASMA EXPOSURES OF $HfB_2$ + 20% SiC (A-7)

| Material Sample No. Assumed Emittance at $\lambda$ = 0.65μ | Mach No. | $P_e$ atm | $i_e$ BTU/lb | D (in) | $q_{cw}$ BTU/ft²sec | T °R obs | $q_r$ Surface Radiation BTU/ft²sec | $\epsilon_N$ Computed Normal Emittance | Initial Length Thickness (mils) | Final Length* Thickness (mils) | Exposure Time (seconds) | Calculated Temperature Ratio T(CALC)/T (OBS) Cold Wall Heat Transfer Coefficient | Fay and Riddell Heat Transfer Coefficient |
|---|---|---|---|---|---|---|---|---|---|---|---|---|---|
| $HfB_{2,1}$ + 20% SiC(A-7) $\epsilon$ = 0.60 | | | | | | | | | | | | | |
| -26RI | 3.2 | 0.086 | 10710 | 0.438 | 547 | 3500 | 26 | 0.41 | 1001/686 | ---/--- | 1800 | 1.82 | 1.81 |
| -26RII | 3.2 | 0.085 | 10890 | 0.438 | 547 | 3750 | 37 | 0.40 | ---/--- | ---/--- | 1800 | 1.70 | 1.70 |
| -26RIII | 3.2 | 0.085 | 10840 | 0.438 | 547 | 3750 | 49 | 0.53 | ---/--- | ---/--- | 1800 | 1.70 | 1.70 |
| -26RIV | 3.2 | 0.085 | 10800 | 0.438 | 547 | 3785 | 59 | 0.61 | ---/--- | 1005/681 | 1400 | 1.69 | 1.69 |
| -27RI | 2.2 | 0.209 | 7320 | 0.438 | 596 | 5455 | 76 | 0.18 | 1001/686 | ---/--- | 1800 | 1.15 | 1.14 |
| -27RII | 2.2 | 0.205 | 7360 | 0.438 | 604 | 5440 | 224 | 0.54 | ---/--- | ---/--- | 1800 | 1.16 | 1.14 |
| -27RIII | 2.2 | 0.197 | 7100 | 0.438 | 604 | 5370 | 212 | 0.54 | ---/--- | ---/--- | 1800 | 1.17 | 1.14 |
| -27RIV | 2.2 | 0.196 | 7150 | 0.438 | 596 | 5360 | 210 | 0.54 | ---/--- | 988/677 | 1800 | 1.17 | 1.15 |
| -28RI | 3.2 | 0.066 | 10320 | 0.427 | 499 | 3535 | 32 | 0.44 | 1206/898 | ---/--- | 1800 | 1.76 | 1.73 |
| -28RII | 3.2 | 0.066 | 10530 | 0.427 | 499 | 3660 | 34 | 0.40 | ---/--- | ---/--- | 1800 | 1.71 | 1.69 |
| -28RIII | 3.2 | 0.072 | 10200 | 0.427 | 489 | 3650 | 32 | 0.38 | ---/--- | ---/--- | 1800 | 1.70 | 1.69 |
| -28RIV | 3.2 | 0.072 | 10500 | 0.427 | 498 | 3840 | 60 | 0.59 | ---/--- | ---/--- | 1800 | 1.63 | 1.62 |
| -28RV | 3.2 | 0.072 | 10200 | 0.427 | 498 | 5180 | 136 | 0.40 | ---/--- | ---/--- | 1800 | 1.20 | 1.19 |
| -28RVI | 3.2 | 0.072 | 10300 | 0.427 | 498 | 5285 | 160 | 0.44 | ---/--- | ---/--- | 1800 | 1.18 | 1.17 |
| -28RVII | 3.2 | 0.062 | 9420 | 0.427 | 498 | 5285 | 154 | 0.42 | ---/--- | ---/--- | 1800 | 1.17 | 1.12 |
| -28RVIII | 3.2 | 0.062 | 10470 | 0.427 | 498 | 5415 | 152 | 0.38 | ---/--- | ---/--- | 1800 | 1.15 | 1.13 |
| -28RIX | 3.2 | 0.065 | 10210 | 0.427 | 487 | 6065 | 158 | 0.25 | ---/--- | ---/--- | 1479 | 1.02 | 1.01 |
| -28RX | 3.2 | 0.065 | 10790 | 0.427 | 489 | 3760 | 77 | 0.82 | ---/--- | ---/--- | 1800 | 1.66 | 1.65 |
| -28RXI | 3.2 | 0.065 | 10440 | 0.427 | 498 | 5190 | 113 | 0.33 | ---/--- | ---/--- | 1800 | 1.20 | 1.18 |
| -28RXII | 3.2 | 0.070 | 9980 | 0.427 | 480 | 5275 | 124 | 0.34 | ---/--- | ---/--- | 1800 | 1.17 | 1.16 |
| -28RXIII | 3.2 | 0.070 | 9880 | 0.427 | 480 | 5310 | 151 | 0.40 | ---/--- | 1210/883 | 1150 | 1.16 | 1.15 |
| -29RI | 2.2 | 0.165 | 7380 | 0.427 | 552 | 3470 | 47 | 0.69 | 1182/877 | ---/--- | 1800 | 1.79 | 1.76 |
| -29RII | 2.2 | 0.165 | 7510 | 0.427 | 552 | 3750 | 44 | 0.47 | ---/--- | ---/--- | 1800 | 1.66 | 1.64 |
| -29RIII | 2.2 | 0.167 | 7560 | 0.427 | 541 | 4410 | 72 | 0.40 | ---/--- | ---/--- | 1800 | 1.40 | 1.39 |
| -29RIV | 2.2 | 0.167 | 7810 | 0.427 | 549 | 4760 | 175 | 0.73 | ---/--- | ---/--- | 1800 | 1.31 | 1.31 |
| -29RV | 2.2 | 0.167 | 8290 | 0.427 | 555 | 4250 | 88 | 0.57 | ---/--- | ---/--- | 1800 | 1.48 | 1.49 |
| -29RVI | 2.2 | 0.166 | 7630 | 0.427 | 552 | 4525 | 94 | 0.48 | ---/--- | ---/--- | 1800 | 1.37 | 1.36 |
| -29RVII | 2.2 | 0.166 | 7650 | 0.427 | 547 | 4910 | 179 | 0.66 | ---/--- | ---/--- | 1800 | 1.27 | 1.26 |
| -29RVIII | 2.2 | 0.168 | 7720 | 0.427 | 555 | 4760 | 153 | 0.63 | ---/--- | ---/--- | 1800 | 1.31 | 1.30 |
| -29RIX | 2.2 | 0.168 | 7840 | 0.427 | 561 | 4795 | 221 | 0.89 | ---/--- | ---/--- | 1800 | 1.31 | 1.30 |
| -29RX | 2.2 | 0.168 | 7580 | 0.427 | 547 | 4760 | 151 | 0.63 | ---/--- | ---/--- | 1800 | 1.30 | 1.29 |
| -29RXI | 2.2 | 0.168 | 7850 | 0.427 | 552 | 4410 | 118 | 0.66 | ---/--- | 1167/828 | 1800 | 1.41 | 1.41 |
| -33R | 3.2 | 0.105 | 9840 | 0.427 | 590 | 3435 | 37 | 0.57 | 957/650 | 957/645 | 1542 | 1.88 | 1.85 |
| -34R | 3.2 | 0.169 | 8040 | 0.427 | 720 | 5465 | 198 | 0.47 | 1229/920 | 1242/889 | 1200 | 1.21 | 1.15 |
| -35R | 3.2 | 0.180 | 9030 | 0.427 | 791 | 5810 | 270 | 0.50 | 1224/921 | 931/606 | 90 | 1.17 | 1.13 |

*Final length refers to measurement after exposure, thickness refers to suction length.

| Material Sample No. | T °F | Gross Recession (mils) | Material Recession (mils) | Degradation Mode | Exposure Time seconds | Recession Rate* mils/30 min | Description of Motion Picture Film Coverage |
|---|---|---|---|---|---|---|---|
| $HfB_{2,1}$ + 20% SiC (A-7) | | | | | | | |
| -26RI | 3040 | --- | --- | Oxidation | 1800 | --- | Left edge grew hotter throughout run. |
| -26RII | 3290 | --- | --- | Oxidation | 1800 | --- | Oxide formed inward from left edge. |
| -26RIII | 3290 | --- | --- | Oxidation | 1800 | --- | Left side hotter than rest of face. |
| -26RIV | 3325 | 4 | 5 | Oxidation | 1400 | 1 | No change from cycle III. |
| -27RI | 4995 | --- | --- | Oxidation | 1800 | --- | Light oxide formed. |
| -27RII | 4980 | --- | --- | Oxidation | 1800 | --- | No change from cycle I, slight oxide chipping. |
| -27RIII | 4910 | --- | --- | Oxidation | 1800 | --- | No change from cycle II. |
| -27RIV | 4900 | 13 | 9 | Oxidation | 1800 | 2 | No change from cycle III. |
| -28RI | 3075 | --- | --- | Oxidation | 1800 | --- | Uniform heating, little activity. |
| -28RII | 3200 | --- | --- | Oxidation | 1800 | --- | Uniform heating, little activity. |
| -28RIII | 3190 | --- | --- | Oxidation | 1800 | --- | Uniform heating, one spot near edge oxidized. |
| -28RIV | 3380 | --- | --- | Oxidation | 1800 | --- | Bright oxide spot near edge, patches on face. |
| -28RV | 4720 | --- | --- | Oxidation | 1800 | --- | Oxide covered most of front face. |
| -28RVI | 4825 | --- | --- | Oxidation | 1800 | --- | Intact from cycle V, little activity. |
| -28RVII | 4815 | --- | --- | Oxidation | 1800 | --- | Some oxide chipping, little activity. |
| -28RVIII | 4955 | --- | --- | Oxidation | 1800 | --- | Intact from cycle VII, some additional oxidation. |
| -28RIX | 5605 | --- | --- | Oxidation | 1479 | --- | Intact from cycle VIII, little activity. |
| -28RX | 3300 | --- | --- | Oxidation | 1800 | --- | Most of oxide broke off, patchy oxide formed. |
| -28RXI | 4730 | --- | --- | Oxidation | 1800 | --- | Some chipping at edges, little activity. |
| -28RXII | 4815 | --- | --- | Oxidation | 1800 | --- | Intact from cycle XI, oxide covered most of face. |
| -28RXIII | 4850 | -4 | 15 | Oxidation | 1150 | 1 | Some oxide broke off, little activity. |
| -29RI | 3010 | --- | --- | Oxidation | 1800 | --- | Little activity, uniform heating. |
| -29RII | 3290 | --- | --- | Oxidation | 1800 | --- | Slight hot spot at center. |
| -29RIII | 3950 | --- | --- | Oxidation | 1800 | --- | Hot spot more apparent and growing. |
| -29RIV | 4300 | --- | --- | Oxidation | 1800 | --- | Oxide covering most of sample. |
| -29RV | 3790 | --- | --- | Oxidation | 1800 | --- | Most of oxide broke off, spotty oxide remaining. |
| -29RVI | 4065 | --- | --- | Oxidation | 1800 | --- | Oxide thickest at top edge. |
| -29RVII | 4450 | --- | --- | Oxidation | 1800 | --- | Some oxide broke off, surface nonuniformly oxidized. |
| -29RVIII | 4300 | --- | --- | Oxidation | 1800 | --- | Some oxide broke off, surface nonuniformly oxidized. |
| -29RIX | 4335 | --- | --- | Oxidation | 1800 | --- | Some oxide broke off top, heavy oxide on bottom. |
| -29RX | 4300 | --- | --- | Oxidation | 1800 | --- | Bottom oxide broke off, heavier oxide remained on top. |
| -29RXI | 3950 | 25 | 49 | Oxidation | 1800 | 4 | Oxide broke away almost completely, reformed slowly. |
| -33R | 2975 | 0 | 5 | Oxidation | 1542 | 6 | Uniform heating, little activity. |
| -34R | 5005 | -13 | 31 | Oxidation | 1200 | 46 | Slight oxide melting at edges. |
| -35R | 5350 | 293 | 315 | Melting | 90 | 6300 | Rapid melting and recession. |

*Converted to 30 minutes on a linear basis.

# TABLE 8

## SUMMARY OF ARC PLASMA EXPOSURES OF $HfB_2$ + 20%SiC (A-7)

| Material Sample No. Assumed Emittance at λ = 0.65μ | Mach No. | $P_s$ atm | $i_e$ BTU/lb | $p_s$ (in) | $q_{cw}$ BTU/ft²sec | $T_{obs}$ °R | $q_r$ Surface Radiation BTU/ft²sec | $\epsilon_N$ Computed Normal Emittance | Initial Length/Thickness (mils) | Final Length*/Thickness (mils) | Exposure Time (seconds) | Calculated Temperature Ratio T(CALC)/T(OBS) Cold Wall Heat Transfer Coefficient | Fay and Riddell Heat Transfer Coefficient |
|---|---|---|---|---|---|---|---|---|---|---|---|---|---|
| $HfB_{2.1}$ + 20%SiC(A-7) | | | | | | | | | | | | | |
| ε = 0.60 | | | | | | | | | | | | | |
| -38RH | 2.2 | 0.128 | 8280 | 0.437 | 497 | 3015 | 27 | 0.70 | 1000/93** | 1000/93 | 1800 | 2.03 | 2.23 |
| -39RH | 2.2 | 0.162 | 6540 | 0.437 | 487 | 3170 | 34 | 0.72 | 994/391** | 995/390 | 1812 | 1.88 | 2.02 |
| -42R | 2.2 | 0.138 | 7140 | 0.437 | 498 | 3080 | 27 | 0.64 | 1001/96** | 1001/96 | 1800 | 1.96 | 1.92 |
| -43R | 2.2 | 0.134 | 7520 | 0.437 | 503 | 3190 | 34 | 0.70 | 1001/395** | 1002/394 | 1800 | 1.91 | 1.88 |
| -46RS | 2.2 | 0.169 | 5750 | 0.440 | 503 | 3680 | 47 | 0.54 | 1001/93** | 1001/93 | 1200 | 1.60 | 1.53 |
| -47RS | 2.2 | 0.169 | 6290 | 0.440 | 489 | 3615 | 40 | 0.50 | 1001/395** | 1009/399 | 1800 | 1.64 | 1.61 |
| -48RH | 2.2 | 0.145 | 7030 | 0.975 | 492 | 3000 | 25 | 0.65 | 1000/96** | 1001/95 | 1800 | 2.01 | 1.99 |
| -49RHS | 2.2 | 0.162 | 6800 | 0.975 | 512 | 3280 | 34 | 0.63 | 1001/100** | 1001/100 | 1800 | 1.85 | 1.82 |
| -50RH | 2.2 | 0.150 | 7250 | 0.975 | 492 | 3090 | 30 | 0.70 | 1001/399** | 1001/399 | 1800 | 1.96 | 1.96 |
| -51RHS | 2.2 | 0.162 | 6510 | 0.975 | 497 | 3155 | 30 | 0.64 | 1000/395** | 1002/393 | 1800 | 1.90 | 1.86 |
| -52MI | 0.25 | 1.03 | 4020 | 0.437 | 455 | 3850 | 85 | 0.82 | 692/690 | ----/--- | 1800 | 1.40 | 1.40 |
| -52MII | 0.26 | 1.03 | 4110 | 0.437 | 455 | 4370 | 152 | 0.88 | ----/--- | ----/--- | 1800 | 1.24 | 1.24 |
| -52MIII | 0.25 | 1.03 | 4140 | 0.437 | 450 | 5185 | 199 | 0.59 | ----/--- | ----/--- | 1800 | 1.05 | 1.05 |
| -52MIV | 0.26 | 1.03 | 4180 | 0.437 | 442 | 4830 | 117 | 0.46 | ----/--- | ----/--- | 1800 | 1.12 | 1.13 |
| -52MV | 0.26 | 1.03 | 4160 | 0.437 | 450 | 5125 | 163 | 0.50 | ----/--- | ----/--- | 1800 | 1.06 | 1.06 |
| -52MVI | 0.26 | 1.03 | 4350 | 0.437 | 450 | 5150 | 182 | 0.55 | ----/--- | ----/--- | 1800 | 1.06 | 1.08 |
| -52MVII | 0.26 | 1.03 | 4180 | 0.437 | 450 | 5215 | 209 | 0.60 | ----/--- | ----/--- | 1800 | 1.04 | 1.05 |
| -52MVIII | 0.26 | 1.03 | 4400 | 0.437 | 450 | 5170 | 199 | 0.59 | ----/--- | ----/361 | 1430 | 1.06 | 1.07 |
| -38RR | 2.2 | 0.263 | 7290 | 0.437 | 880 | 5240 | 227 | 0.64 | 1001/93** | ----/--- | 1800 | 1.30 | 1.32 |
| -39RRI | 3.2 | 0.053 | 8810 | 0.437 | 885 | 3415 | 39 | 0.61 | 995/390** | ----/--- | 1800 | 2.02 | 1.83 |
| -39RRII | 3.2 | 0.105 | 7290 | 0.437 | 937 | 4745 | 199 | 0.83 | ----/--- | ----/366 | 375 | 1.44 | 1.34 |
| -46RR | 3.2 | 0.109 | 7540 | 0.440 | 988 | 3570 | 47 | 0.62 | 1001/93** | 1001/92 | 1800 | 1.94 | 1.65 |

* Final length refers to sample length prior to sectioning; thickness refers to section length.

** Nose to in-depth temperature measurement station.

| Material Sample No. | T °F | Gross Recession (mils) | Material Recession (mils) | Degradation Mode | Exposure Time seconds | Recession Rate* mils/30 min | Description of Motion Picture Film Coverage |
|---|---|---|---|---|---|---|---|
| $HfB_{2.1}$ + 20%SiC(A-7) | | | | | | | |
| -38RH | 2555 | 0 | 0 | Oxidation | 1800 | 0 | No activity. |
| -39RH | 2710 | -1 | 1 | Oxidation | 1812 | 1 | No activity. |
| -42R | 2620 | 0 | 0 | Oxidation | 1800 | 0 | Little visible. |
| -43R | 2730 | -1 | 1 | Oxidation | 1800 | 1 | No activity. |
| -46RS | 3220 | 0 | 0 | Oxidation | 1200 | 0 | Little activity, hottest at sample-shroud interface. |
| -47RS | 3155 | -8 | 0 | Oxidation | 1800 | 0 | Little activity, shroud hotter than sample. |
| -48RH | 2540 | -1 | 1 | Oxidation | 1800 | 1 | No activity. |
| -49RHS | 2820 | 0 | 0 | Oxidation | 1800 | 0 | No activity. |
| -50RH | 2630 | 0 | 0 | Oxidation | 1800 | 0 | No activity. |
| -51RHS | 2695 | -2 | 2 | Oxidation | 1800 | 2 | No activity |
| -52MI | 3390 | -- | -- | Oxidation | 1800 | --- | Little visible, edges began to oxidize. |
| -52MII | 3910 | -- | -- | Oxidation | 1800 | --- | Edge chipping and droplets, oxide buildup from edge inward. |
| -52MIII | 4725 | -- | -- | Oxidation | 1800 | --- | Oxide melted, broke off, slow melting continued. |
| -52MIV | 4370 | -- | -- | Oxidation | 1800 | --- | Considerable melting, solidified in sunburst. |
| -52MV | 4665 | -- | -- | Oxidation | 1800 | --- | Initial melting of oxide. |
| -52MVI | 4690 | -- | -- | Oxidation | 1800 | --- | Initial melting and chipping of oxide. |
| -52MVII | 4755 | -- | -- | Oxidation | 1800 | --- | Intact from cycle VI, little activity. |
| -52MVIII | 4710 | -- | 329 | Oxidation | 1430 | 41 | Intact from cycle VII, little activity. |
| -38RR | 4780 | -- | -- | Oxidation | 1800 | --- | 3/8" diam. hot spot oxidized at nose. |
| -39RRI | 2955 | -- | -- | Oxidation | 1800 | --- | Little activity. |
| -39RRII | 4285 | -- | 24 | Oxidation | 375 | 115 | 3/8" diam. hot spot. |
| -46RR | 3110 | 0 | 1 | Oxidation | 1800 | 1 | Little activity. |

*Converted to 30 minutes on a linear basis.

# TABLE 9

## SUMMARY OF ARC PLASMA EXPOSURES OF $ZrB_2$ + 20%SiC (A-8)

| Material Sample No. Assumed Emittance at λ = 0.65μ | Mach No. | $P_s$ atm | $i_e$ BTU/lb | D (in) | $q_{cw}$ BTU/ft²sec | T °R obs | $q_r$ Surface Radiation BTU/ft² sec | ε N Computed Normal Emittance | Initial Length/Thickness (mils) | Final Length*/Thickness (mils) | Exposure Time (seconds) | Calculated Temperature Ratio T(CALC)/T(OBS) Cold Wall Heat Transfer Coefficient | Fay and Riddell Heat Transfer Coefficient |
|---|---|---|---|---|---|---|---|---|---|---|---|---|---|
| $ZrB_{2.1}$ + 20% SiC(A-8) ε= 0.60 | | | | | | | | | | | | | |
| -1M | 0.47 | 1.14 | 5650 | 0.489 | 850 | 5975 | 293 | 0.49 | 418/410 | 272/255 | 22 | 1.07 | 1.05 |
| -2M | 0.45 | 1.12 | 5070 | 0.489 | 725 | 6045 | 306 | 0.49 | 397/397 | 236/212 | 34 | 1.01 | 1.00 |
| -3M | 0.35 | 1.07 | 4865 | 0.489 | 655 | 6055 | 363 | 0.57 | 407/393 | 106/86 | 78 | 0.98 | 0.96 |
| -4MA | 0.32 | 1.06 | 3915 | 0.489 | 515 | 5995 | 110 | .92 | 407/399 | ---/--- | 285 | 1.38 | 1.35 |
| -4MB | 0.32 | 1.06 | 3915 | 0.489 | 515 | 5995 | 358 | 0.63 | ---/--- | 271/257 | 42 | 0.93 | 0.91 |
| -5M | 0.62 | 1.25 | 3070 | 0.426 | 605 | 4935 | 162 | 0.58 | 880/873 | 698/649 | 1800 | 1.09 | 1.06 |
| -6M | 0.70 | 1.33 | 3320 | 0.426 | 735 | 5850 | 269 | 0.49 | 885/873 | 185/96 | 43 | 0.97 | 0.93 |
| -7MA | 0.17 | 1.02 | 3680 | 0.426 | 445 | 5500 | 288 | 0.60 | 886/880 | ---/--- | 280 | 0.96 | 0.92 |
| -7MB | 0.17 | 1.02 | 3680 | 0.426 | 445 | 5060 | 33 | 0.11 | ---/--- | 682/616 | 1520 | 1.05 | 1.00 |
| -8M | 0.10 | 1.01 | 5160 | 0.426 | 380 | 4640 | 167 | 0.77 | 852/838 | 854/831 | 1800 | 1.17 | 1.15 |
| -9M | 0.10 | 1.01 | 5230 | 0.426 | 350 | 3620 | 56 | 0.69 | 890/886 | 895/876 | 1800 | 1.47 | 1.48 |
| -10MA | 0.09 | 1.01 | 3970 | 0.426 | 240 | 3295 | 34 | 0.61 | 891/881 | ---/--- | 200 | 1.45 | 1.47 |
| -10MB | 0.09 | 1.01 | 3970 | 0.426 | 240 | 3165 | 28 | 0.59 | ---/--- | 891/877 | 1600 | 1.51 | 1.53 |
| -11M | 0.17 | 1.01 | 3710 | 0.426 | 350 | 3805 | 61 | 0.62 | 882/879 | 887/869 | 1800 | 1.34 | 1.33 |
| -12MA | 0.70 | 1.35 | 3130 | 0.426 | 715 | 4945 | 188 | 0.67 | 891/889 | ---/--- | 660 | 1.12 | 1.08 |
| -12MB | 0.70 | 1.35 | 3130 | 0.426 | 715 | 5550 | 285 | 0.64 | ---/--- | 888/842 | 9 | 1.00 | 0.96 |
| -13MA | 0.44 | 1.12 | 3140 | 0.426 | 485 | 5985 | 278 | 0.46 | 860/852 | ---/--- | 40 | 0.87 | 0.86 |
| -13MB | 0.44 | 1.12 | 3140 | 0.426 | 485 | 4775 | 114 | 0.47 | ---/--- | 796/779 | 1760 | 1.10 | 1.08 |
| -14MA | 0.21 | 1.01 | 4490 | 0.426 | 425 | 5630 | 268 | 0.57 | 881/867 | ---/--- | 160 | 0.96 | 0.98 |
| -14MB | 0.21 | 1.01 | 4490 | 0.426 | 425 | 4900 | 159 | 0.59 | ---/--- | 839/787 | 1640 | 1.11 | 1.13 |
| -15MI | 0.13 | 1.00 | 9160 | 0.427 | 367 | 4810 | 181 | 0.72 | 788/687 | ---/--- | 1800 | 1.12 | 1.14 |
| -15MII | 0.13 | 1.00 | 4830 | 0.427 | 385 | 5000 | 199 | 0.68 | ---/--- | ---/--- | 1800 | 1.08 | 1.07 |
| -15MIII | 0.13 | 1.00 | 5260 | 0.427 | 392 | 5160 | 218 | 0.65 | ---/--- | ---/--- | 1800 | 1.06 | 1.07 |
| -15MIV | 0.13 | 1.00 | 4850 | 0.427 | 389 | 5000 | 195 | 0.66 | ---/--- | ---/661 | 1800 | 1.08 | 1.08 |
| -17M | 0.15 | 1.01 | 5700 | 0.427 | 503 | 5340 | 218 | 0.57 | 607/604 | 538/494 | 1800 | 1.08 | 1.08 |
| -18M | 0.13 | 1.01 | 6070 | 0.427 | 445 | 5045 | 185 | 0.61 | 788/681 | 692/654 | 1800 | 1.13 | 1.15 |
| -19M | 0.14 | 1.00 | 4650 | 0.427 | 380 | 3685 | 58 | 0.67 | 686/681 | 688/675 | 1800 | 1.43 | 1.45 |
| -20M | 0.15 | 1.00 | 5730 | 0.427 | 410 | 4720 | 170 | 0.73 | 687/684 | 701/682 | 1800 | 1.18 | 1.22 |
| -25M | 0.13 | 1.01 | 5280 | 0.426 | 360 | 3620 | 50 | 0.62 | 98/96** | ---/88 | 1800 | 1.48 | 1.53 |
| -26M | 0.13 | 1.01 | 5430 | 0.435 | 370 | 3575 | 46 | 0.60 | 398/395** | ---/389 | 1800 | 1.51 | 1.56 |
| -29MS* | 0.13 | 1.00 | 5530 | 0.425 | 358 | 3820 | 58 | 0.58 | 99/96** | ---/88 | 1800 | 1.40 | 1.45 |
| -30MS | 0.13 | 1.01 | 4840 | 0.437 | 350 | 3000 | 29 | 0.76 | 688/395** | 690/389 | 1800 | 1.76 | 1.79 |
| -40M | 0.46 | 1.13 | 4950 | 0.489 | 870 | 5975 | 282 | 0.47 | 323/324 | 189/171 | 28 | 1.05 | 1.00 |
| -41M | 0.42 | 1.10 | 5130 | 0.489 | 800 | 6055 | 285 | 0.45 | 305/297 | 155/139 | 29 | 1.03 | 0.99 |
| -42M | 0.35 | 1.07 | 4625 | 0.488 | 690 | 6090 | 350 | 0.54 | 306/296 | 248/235 | 40 | 0.98 | 0.94 |
| -43MA | 0.33 | 1.07 | 4255 | 0.489 | 605 | 4125 | 99 | 0.73 | 303/292 | ---/--- | 80 | 1.39 | 1.34 |
| -43MB | 0.33 | 1.07 | 4255 | 0.489 | 605 | 6125 | 366 | 0.55 | ---/--- | 250/234 | 40 | 0.94 | 0.91 |

* Encased in Poco (B-10) graphite shroud which ablated completely in 500 sec.

* Final length refers to sample length prior to sectioning; thickness refers to section length.
** Nose to in-depth temperature measurement station.

| Material Sample No. | $T_F$ °F | Gross Recession (mils) | Material Recession (mils) | Degradation Mode | Exposure Time seconds | Recession Rate* mils/30 min | Description of Motion Picture Film Coverage |
|---|---|---|---|---|---|---|---|
| $ZrB_{2.1}$ + 20% SiC(A-8) | | | | | | | |
| -1M | 5515 | 146 | 155 | Melting | 22 | 12680 | Large drops melting and blowing off. |
| -2M | 5585 | 161 | 185 | Melting | 34 | 9790 | Large drops melting and blowing off |
| -3M | 5595 | 291 | 307 | Melting | 78 | 7092 | Slow heatup, rapid melting |
| -4MA | 3535 | --- | --- | Oxidation | 285 | --- | Slow heatup, some liquid at edges |
| -4MB | 5445 | 136 | 142 | Melting | 42 | 6070 | Rapid melting |
| -5M | 4475 | 182 | 224 | Oxidation | 1800 | 224 | Oxide melting continuously |
| -6M | 5390 | 700 | 777 | Melting | 43 | 32526 | Rapid melting |
| -7MA | 5140 | --- | --- | Melting | 280 | --- | Oxide formed and melted |
| -7MB | 4600 | 204 | 264 | Oxidation | 1520 | 264 | Solidified in sunburst |
| -8M | 4180 | -2 | 7 | Oxidation | 1800 | 7 | Little activity, some oxide melting at edges |
| -9M | 3160 | -5 | 10 | Oxidation | 1800 | 10 | Little activity |
| -10MA | 2835 | --- | --- | Oxidation | 200 | --- | Little visible |
| -10MB | 2705 | 0 | 4 | Oxidation | 1600 | 4 | Little visible |
| -11M | 3345 | -5 | 10 | Oxidation | 1800 | 10 | Little activity, some small bubbles on surface |
| -12MA | 4485 | --- | --- | Oxidation | 660 | --- | Sample loose on sting, sunburst formed |
| -12MB | 5090 | 3 | 247 | Melting | 9 | 39600 | Rapid melting |
| -13MA | 5525 | --- | --- | Melting | 40 | --- | Edges melted, sunburst formation |
| -13MB | 4315 | 64 | 73 | Oxidation | 1760 | 73 | Solidified in sunburst |
| -14MA | 5170 | --- | --- | Melting | 160 | --- | Melting |
| -14MB | 4440 | 42 | 80 | Oxidation | 1640 | 80 | Solidified in sunburst |
| -15MI | 4350 | --- | --- | Oxidation | 1800 | --- | Edge oxide melted, central unoxidized cold spot. |
| -15MII | 4540 | --- | --- | Oxidation | 1800 | --- | Slight spalling of oxide, center oxidized slowly |
| -15MIII | 4700 | --- | --- | Oxidation | 1800 | --- | No change from cycle II |
| -15MIV | 4540 | --- | 26 | Oxidation | 1800 | 7 | No change from cycle III |
| -17M | 4880 | 69 | 110 | Oxidation | 1800 | 110 | Melting, solidified in sunburst |
| -18M | 4585 | 96 | 27 | Oxidation | 1800 | 27 | Edges melted, solidified, some small bubbles |
| -19M | 3225 | -2 | 6 | Oxidation | 1800 | 6 | Hotter at edges, some edge melting |
| -20M | 4260 | -4 | 2 | Oxidation | 1800 | 2 | Heavy oxide formed slowly from edges to center |
| -25M | 3160 | --- | 8 | Oxidation | 1800 | 8 | Little activity. |
| -26M | 3115 | --- | 6 | Oxidation | 1800 | 6 | Little activity. |
| -29MS | 3360 | --- | 8 | Oxidation | 1800 | 8 | Little activity. |
| -30MS | 2540 | -2 | 6 | Oxidation | 1800 | 6 | Little activity. |
| -40M | 5515 | 134 | 153 | Melting | 28 | 9830 | Large drops melting and blowing off |
| -41M | 5595 | 150 | 158 | Melting | 29 | 9800 | Large drops melting and blowing off |
| -42M | 5630 | 58 | 61 | Melting | 40 | 2750 | Rapid melting, large chunks flying off |
| -43MA | 3665 | --- | - | Oxidation | 80 | --- | Small bubbles, uniform heating. |
| -43MB | 5665 | 53 | 58 | Melting | 40 | 2520 | Rapid melting |

*Converted to 30 minutes on a linear basis.

# TABLE 10

## SUMMARY OF ARC PLASMA EXPOSURES OF $ZrB_2$ + 20%SiC (A-8)

| Material Sample No. Assumed Emittance at λ = 0.65μ | Mach No. | $P_e$ atm | $h_e$ BTU/lb | D (in) | $q_{cw}$ BTU/ft²sec | $T_R$ °R obs | $q_r$ Surface Radiation BTU/ft²sec | $\epsilon_N$ Computed Normal Emittance | Initial Length/Thickness (mils) | Final Length*/Thickness (mils) | Exposure Time (seconds) | Calculated Temperature Ratio T(CALC)/T(OBS)) Cold Wall Heat Transfer Coefficient | Fay and Riddell Heat Transfer Coefficient |
|---|---|---|---|---|---|---|---|---|---|---|---|---|---|
| $ZrB_{2.1}$ + 20%SiC(A-8) ε = 0.60 | | | | | | | | | | | | | |
| -16RI | 2.2 | 0.159 | 6780 | 0.427 | 452 | 4780 | 49 | 0.20 | 1081/688 | ---/--- | 1800 | 1.23 | 1.24 |
| -16RII | 2.2 | 0.159 | 6730 | 0.427 | 446 | 4815 | 155 | 0.61 | ----/--- | ---/--- | 1800 | 1.22 | 1.23 |
| -16RIII | 2.2 | 0.159 | 7170 | 0.427 | 452 | 4900 | 185 | 0.68 | ----/--- | ---/--- | 1800 | 1.21 | 1.23 |
| -16RIV | 2.2 | 0.159 | 7170 | 0.427 | 452 | 4400 | 81 | 0.46 | ----/--- | 1000/661 | 1800 | 1.35 | 1.37 |
| -21RA | 3.2 | 0.095 | 10300 | 0.427 | 575 | 3335 | 32 | 0.55 | 1144/838 | ---/--- | 400 | 1.93 | 1.91 |
| -21RB | 3.2 | 0.095 | 10300 | 0.427 | 575 | 5740 | 187 | 0.37 | ----/--- | 549/271 | 33 | 1.12 | 1.11 |
| -22RA | 3.2 | 0.130 | 8210 | 0.427 | 647 | 4020 | 61 | 0.50 | 1128/812 | ---/--- | 145 | 1.61 | 1.53 |
| -22RB | 3.2 | 0.130 | 8210 | 0.427 | 647 | 5525 | 178 | 0.41 | ----/--- | 699/330 | 55 | 1.17 | 1.12 |
| -23RA | 3.2 | 0.155 | 8140 | 0.427 | 711 | 4145 | 77 | 0.55 | 1132/822 | ---/--- | 50 | 1.59 | 1.51 |
| -23RB | 3.2 | 0.155 | 8140 | 0.427 | 711 | 5490 | 187 | 0.44 | ----/--- | 538/209 | 51 | 1.20 | 1.14 |
| -24RA | 3.2 | 0.170 | 9130 | 0.427 | 748 | 4145 | --- | ---- | 1115/799 | ---/--- | 35 | 1.63 | 1.58 |
| -24RB | 3.2 | 0.170 | 9130 | 0.427 | 748 | 5715 | 182 | 0.36 | ----/--- | 406/138 | 55 | 1.18 | 1.15 |
| -27R | 2.2 | 0.117 | 7970 | 0.426 | 452 | 3335 | 22 | 0.38 | 1000/96** | 1006/89 | 1800 | 1.80 | 1.81 |
| -28R | 2.2 | 0.111 | 7350 | 0.426 | 452 | 4080 | 53 | 0.41 | 1001/396** | 1009/388 | 1810 | 1.46 | 1.43 |
| -31RS | 2.2 | 0.226 | 7390 | 0.440 | 440 | 3080 | 30 | 0.71 | 979/93** | 981/90 | 1800 | 1.93 | 2.04 |
| -32RS | 2.2 | 0.228 | 7270 | 0.440 | 437 | 3225 | 31 | 0.61 | 1004/397** | 1003/392 | 1800 | 1.83 | 1.94 |
| -33R | 3.2 | 0.057 | 9000 | 0.427 | 423 | 3190 | 23 | 0.47 | 938/622 | 941/612 | 1800 | 1.87 | 1.82 |
| -34R | 3.2 | 0.063 | 10160 | 0.427 | 480 | 4725 | 131 | 0.56 | 819/503 | 825/496 | 1800 | 1.31 | 1.29 |

* Final length refers to measurement after exposure, thickness refers to length after sectioning.
** Nose to in-depth temperature measurement station.

| Material Sample No. | $V_F$ | Gross Recession (mils) | Material Recession (mils) | Degradation Mode | Exposure Time seconds | Recession Rate* mils/30 min | Description of Motion Picture Film Coverage |
|---|---|---|---|---|---|---|---|
| $ZrB_{2.1}$ + 20%SiC(A-8) | | | | | | | |
| -16RI | 4320 | --- | --- | Oxidation | 1800 | --- | Little activity, oxide formed on top half. |
| -16RII | 4355 | --- | --- | Oxidation | 1800 | --- | Oxide broke off, spotty oxide reformed. |
| -16RIII | 4440 | --- | --- | Oxidation | 1800 | --- | Oxide broke off, reformed on bottom, then top. |
| -16RIV | 3940 | 1 | 27 | Oxidation | 1800 | 7 | Intact from cycle III, oxide grew uniform, broke in spots. |
| -21RA | 2875 | --- | --- | Oxidation | 400 | --- | Little activity. |
| -21RB | 6280 | 995 | 567 | Melting | 33 | 40500 | Sudden rapid melting. |
| -22RA | 3560 | -- | --- | Oxidation | 145 | --- | Uniform heating, slow heatup to edge melting. |
| -22RB | 5065 | 469 | 482 | Melting | 55 | 15700 | Melted from edges to center, rapid melting. |
| -23RA | 3685 | --- | --- | Oxidation | 50 | --- | Slow heatup to melting. |
| -23RB | 5030 | 594 | 613 | Melting | 51 | 21500 | Rapid melting. |
| -24RA | 3685 | --- | --- | Oxidation | 35 | --- | Heated to melting. |
| -24RB | 5255 | 649 | 661 | Melting | 55 | 21600 | Rapid melting. |
| -27R | 2875 | -6 | 7 | Oxidation | 1800 | 7 | Little activity. |
| -28R | 3620 | -8 | 8 | Oxidation | 1810 | 8 | Oxide formed from top to center, bottom unoxidized. |
| -31RS | 2620 | -2 | 3 | Oxidation | 1800 | 3 | Little activity, shroud slightly colder than sample. |
| -32RS | 2765 | 1 | 5 | Oxidation | 1800 | 5 | Little activity, oxidation at sample-shroud interface. |
| -33R | 2740 | -3 | 10 | Oxidation | 1800 | 10 | Little activity. |
| -34R | 4265 | -6 | 7 | Oxidation | 1800 | 7 | Non-uniform oxide buildup from left to right. |

*Converted to 30 minutes on a linear basis

# TABLE 11

## SUMMARY OF ARC PLASMA EXPOSURES OF $HfB_{2.1}$ +35 v/o SiC(A-9)

| Material Sample No. Assumed Emittance at $\lambda = 0.65\mu$ | Mach No. | $P_e$ atm | $i_e$ BTU/lb | D (in) | $q_{cw}$ BTU/ft²sec | T °R obs | $q_r$ Surface Radiation BTU/ft²sec | $\epsilon_N$ Computed Normal Emittance | Initial Length thickness (mils) | Final Length* thickness (mils) | Exposure Time (seconds) | Calculated Temperature Ratio T(CALC)/T(OBS) Cold Wall Heat Transfer Coefficient | Fay and Riddell Heat Transfer Coefficient |
|---|---|---|---|---|---|---|---|---|---|---|---|---|---|
| $HfB_{2.1}$ + 35 v/o SiC (A-9) | | | | | | | | | | | | | |
| $\epsilon = 0.60$ | | | | | | | | | | | | | |
| -1M | 0.48 | 1.14 | 5700 | 0.489 | 910 | 6050 | 327 | 0.51 | 523/505 | 229/222 | 78 | 1.07 | 1.03 |
| -2M | 0.45 | 1.12 | 4700 | 0.489 | 730 | 6300 | 369 | 0.50 | 522/510 | ---/279 | 133 | 0.96 | 0.93 |
| -4MA | 0.36 | 1.08 | 4610 | 0.489 | 645 | 4370 | 132 | 0.77 | 662/661 | ----/--- | 135 | 1.35 | 1.31 |
| -4MB | 0.36 | 1.08 | 4610 | 0.489 | 645 | 5870 | 366 | 0.66 | ----/--- | ----/280 | 118 | 1.00 | 0.98 |
| -5M | 0.33 | 1.07 | 3665 | 0.489 | 530 | 4000 | 140 | 0.76 | 575/553 | 544/503 | 1800 | 1.24 | 1.20 |
| - 6M | 0.10 | 1.01 | 4730 | 0.426 | 410 | 4040 | 65 | 0.52 | 437/424 | ---/418 | 1800 | 1.34 | 1.28 |
| - 7M | 0.13 | 1.01 | 3690 | 0.426 | 355 | 3860 | 69 | 0.66 | 436/428 | 438/425 | 1800 | 1.32 | 1.28 |
| - 8MA | 0.59 | 1.23 | 2640 | 0.426 | 530 | 4125 | 66 | 0.48 | 443/421 | ---/--- | 200 | 1.23 | 1.19 |
| - 8MB | 0.59 | 1.23 | 2640 | 0.426 | 530 | 3995 | 52 | 0.43 | ---/--- | 479/420 | 1600 | 1.28 | 1.23 |
| - 9MA | 0.10 | 1.01 | 4110 | 0.426 | 450 | 5525 | 260 | 0.59 | 433/428 | ---/--- | 360 | 0.98 | 0.90 |
| - 9MB | 0.10 | 1.01 | 4110 | 0.426 | 450 | 5285 | 134 | 0.37 | ---/--- | 201/183 | 1440 | 1.02 | 0.94 |
| -10MA | 0.27 | 1.05 | 4130 | 0.426 | 535 | 6010 | 274 | 0.45 | 432/426 | ---/--- | 75 | 0.93 | 0.91 |
| -10MB | 0.27 | 1.05 | 4130 | 0.426 | 535 | 5500 | 181 | 0.42 | ---/--- | 318/263 | 1725 | 1.02 | 1.00 |
| -11M | 0.28 | 1.05 | 5330 | 0.426 | 700 | 6195 | 279 | 0.40 | 373/367 | 55/ 0 | 142 | 0.99 | 0.97 |
| -12M | 0.10 | 1.01 | 4140 | 0.426 | 550 | 5825 | 260 | 0.48 | 431/425 | 87/ 51 | 418 | 0.97 | 0.85 |
| -13M | 0.36 | 1.08 | 3410 | 0.426 | 450 | 5115 | 138 | 0.43 | 431/421 | ---/297 | 1800 | 1.03 | 1.02 |
| -14MA | 0.21 | 1.02 | 3700 | 0.426 | 470 | 4370 | 109 | 0.63 | 439/432 | ---/--- | 200 | 1.23 | 1.18 |
| -14MB | 0.21 | 1.02 | 3700 | 0.426 | 470 | 5605 | 268 | 0.58 | ---/--- | 274/227 | 208 | 0.96 | 0.92 |
| -15M | 0.19 | 1.01 | 3520 | 0.426 | 410 | 4050 | 79 | 0.62 | 428/422 | 425/413 | 1800 | 1.38 | 1.24 |

*Final length is based on measurement prior to sectioning; thickness refers to length after sectioning.

| Material Sample No. | T °F | Gross Recession mils | Material Recession mils | Degradation Mode | Exposure Time seconds | Recession Rate* mils/sec / mils/30 min | Description of Motion Picture Film Coverage |
|---|---|---|---|---|---|---|---|
| $HfB_{2.1}$ + 35 v/o SiC (A-9) | | | | | | | |
| -1M | 5630 | 294 | 283 | Melting | 78 | 3.63/6530 | Immediate melting, rapid recession |
| -2M | 5840 | --- | 231 | Melting | 133 | 1.74/3130 | Slow heat-up followed by melting |
| -4MA | 3910 | --- | 1+ | Oxidation | 135 | ----/5+ | Slow heat-up, slight surface activity, then melting and rapid recession |
| -4MB | 5410 | --- | 380 | Melting | 118 | 3.22/5800 | |
| -5M | 3540 | 31 | 50 | Oxidation | 1800 | ----/50 | Slow heat-up, liquid at edges, then some melting at one edge, solidified, sunburst formed and frone, some additional surface activity |
| - 6M | 3580 | --- | 6 | Oxidation | 1800 | 6 | Little activity, slight oxide melt at edges. |
| - 7M | 3400 | -2 | 3 | Oxidation | 1800 | 3 | Little activity. |
| - 8MA | 3645 | --- | --- | Oxidation | 200 | | Little activity, slight oxide melt at edges. |
| - 8MB | 3535 | -36 | 1 | Oxidation | 1600 | 1 | |
| - 9MA | 5065 | --- | --- | Oxidation | 360 | | Oxide melted, solidified in sunburst. |
| - 9MB | 4825 | 232 | 245 | Oxidation | 1440 | 245 | |
| -10MA | 5550 | --- | --- | Oxidation | 75 | | Rapid melting of oxide, solidified in sunburst. |
| -10MB | 5040 | 114 | 163 | Oxidation | 1725 | 163 | |
| -11M | 5735 | 320 | 367 | Melting | 142 | 468½ | Rapid melting and recession. |
| -12M | 5365 | 344 | 374 | Melting | 418 | 1611 | Oxide melting, considerable recession. |
| -13M | 4655 | --- | 124 | Oxidation | 1800 | 124 | Oxide melted, solidified in sunburst. |
| -14MA | 3910 | --- | --- | Oxidation | 200 | 1774 | Slight edge melt, then rapid melting. |
| -14MB | 5145 | 161 | 205 | Melting | 208 | | |
| -15M | 3590 | 9 | 9 | Oxidation | 1800 | 9 | Little activity, hot rim around edge. |

+Estimated.

+Estimated
*Recession rate converted to 30 minutes on linear basis.

# TABLE 12

## SUMMARY OF ARC PLASMA EXPOSURES OF $ZrB_2$ + 14% SiC+30%C(A-10)

| Material Sample No. Assumed Emittance at λ = 0.65μ | Mach No. | $P_e$ atm | $i_e$ BTU/lb | D (in) | $q_{cw}$ BTU/ft²sec | T °R obs | $q_r$ Surface Radiation BTU/ft²sec | $\epsilon_N$ Computed Normal Emittance | Initial Length* thickness (mils) | Final Length* thickness (mils) | Exposure Time (seconds) | Calculated Temperature Ratio T(CALC)/T(OBS) Cold Wall Heat Transfer Coefficient | Fay and Riddell Heat Transfer Coefficient |
|---|---|---|---|---|---|---|---|---|---|---|---|---|---|
| $ZrB_2$ + SiC + C (A-10) ε = 0.60 | | | | | | | | | | | | | |
| -1M | 0.36 | 1.08 | 9045 | 0.499 | 765 | 5630 | 300 | 0.64 | 881/876 | 709/696 | 34 | 1.10 | 1.05 |
| -2M | 0.35 | 1.07 | 4755 | 0.499 | 665 | 5570 | 315 | 0.70 | 857/848 | 374/346 | 182 | 1.07 | 1.04 |
| -3M | 0.33 | 1.06 | 3280 | 0.499 | 540 | 4915 | 104 | 0.53 | 859/849 | 762/735 | 1800 | 1.19 | 1.12 |
| -4M | 0.32 | 1.06 | 4075 | 0.497 | 620 | 5330 | 101 | 0.27 | 858/850 | 582/504 | 1800 | 1.07 | 1.02 |
| -5M | 0.36 | 1.08 | 9250 | 0.499 | 765 | 5570 | 312 | 0.69 | 857/856 | 195/162 | 162 | 1.11 | 1.07 |
| -6M | 0.31 | 1.06 | 2920 | 0.499 | 485 | 3425 | 48 | 0.74 | 861/858 | 883/851 | 1800 | 1.50 | 1.41 |
| -7R[+] | 3.2 | 0.025 | 12570 | 0.499 | 490 | 5430 | 309 | 0.76 | 1165/854 | 1171/827 | 1800 | 1.16 | 1.05 |
| -8R[+] | 3.2 | 0.031 | 13670 | 0.499 | 637 | 5705 | 289 | 0.57 | 1165/844 | 1025/715 | 1800 | 1.17 | 1.05 |
| -9R[+] | 3.2 | 0.222 | 10260 | 0.480 | 1010 | 5525 | 224 | 0.51 | 1162/852 | 612/277 | 32 | 1.31 | 1.25 |
| -10R[+] | 3.2 | 0.127 | 9290 | 0.497 | 764 | 5525 | 250 | 0.57 | 942/622 | 632/300 | 37 | 1.23 | 1.14 |
| -11R[+] | 3.2 | 0.084 | 10560 | 0.499 | 686 | 5535 | 329 | 0.75 | 1163/852 | 1157/816 | 1800 | 1.21 | 1.13 |
| -12R[+] | 3.2 | 0.011 | 14370 | 0.497 | 328 | 5500 | 336 | 0.78 | 972/647 | 977/636 | 1800 | 1.05 | 0.98 |
| -13MA | 0.21 | 1.02 | 4210 | 0.499 | 410 | 4025 | 92 | 0.74 | 855/844 | -/- | 1300 | 1.33 | 1.32 |
| -13MB | 0.21 | 1.02 | 4210 | 0.499 | 410 | 4105 | 120 | 0.90 | -/- | 859/840 | 500 | 1.30 | 1.30 |
| -14M | 0.56 | 1.20 | 3405 | 0.499 | 560 | 5285 | 240 | 0.65 | 858/851 | 936/825 | 1800 | 1.02 | 1.01 |
| -15M | 0.60 | 1.24 | 3020 | 0.492 | 580 | 3840 | 65 | 0.62 | 787/782 | 789/774 | 1800 | 1.38 | 1.33 |
| -16MA | 0.70 | 1.33 | 3240 | 0.499 | 725 | 5135 | 230 | 0.70 | 856/854 | -/- | 1150 | 1.09 | 1.03 |
| -16MB | 0.70 | 1.33 | 3240 | 0.499 | 725 | 5525 | 330 | 0.75 | -/- | 719/714 | 63 | 1.02 | 0.96 |
| -17MA | 0.24 | 1.03 | 4315 | 0.426 | 540 | 5850 | 315 | 0.87 | 824/826 | -/- | 100 | 0.97 | 0.94 |
| -17MB | 0.24 | 1.03 | 4315 | 0.426 | 540 | 4730 | | | -/- | 564/566 | 1700 | 1.19 | 1.16 |
| -18MA | 0.21 | 1.03 | 3560 | 0.426 | 535 | 5850 | 293 | 0.53 | 820/825 | -/- | 45 | 0.93 | 0.87 |
| -18MB | 0.21 | 1.03 | 3560 | 0.426 | 535 | 5060 | 163 | 0.53 | -/- | 703/685 | 1755 | 1.08 | 1.01 |
| -19MA | 0.18 | 1.01 | 5200 | 0.426 | 450 | 5390 | 251 | 0.63 | 824/817 | -/- | 38 | 1.04 | 1.06 |
| -19MB | 0.18 | 1.01 | 5200 | 0.426 | 450 | 5150 | 206 | 0.63 | -/- | 814/773 | 1762 | 1.09 | 1.11 |
| -20M | 0.15 | 1.01 | 4430 | 0.425 | 365 | 4105 | 105 | 0.79 | 823/822 | 825/816 | 1800 | 1.28 | 1.29 |
| -21MA | 0.75 | 1.36 | 3210 | 0.426 | 825 | 4240 | 89 | 0.59 | 815/810 | -/- | 45 | 1.35 | 1.27 |
| -21MB | 0.75 | 1.36 | 3210 | 0.426 | 825 | 5685 | 228 | 0.46 | -/- | 192/162 | 99 | 1.00 | 0.95 |
| -22MA | 0.70 | 1.29 | 3230 | 0.425 | 730 | 4160 | 91 | 0.65 | 823/818 | -/- | 217 | 1.35 | 1.29 |
| -22MB | 0.70 | 1.29 | 3230 | 0.425 | 730 | 5700 | 263 | 0.53 | -/- | 312/288 | 104 | 0.99 | 0.94 |

[+]Transmissivity factor equals 0.86 for sapphire window.

*Final length is based on measurement prior to sectioning; thickness refers to length after sectioning.

| Material Sample No. | T °F | Gross Recession mils | Material Recession mils | Degradation Mode | Exposure Time seconds | Recession Rate* (mils)/(mils) (sec) (30 min) | Description of Motion Picture Film Coverage |
|---|---|---|---|---|---|---|---|
| $ZrB_2$ + SiC + C (A-10) | | | | | | | |
| -1M | 5170 | 172 | 180 | Melting | 34 | 5.29/9520 | immediate melting, sunburst late in run |
| -2M | 5110 | 483 | 502 | Melting | 182 | 2.76/4970 | immediate melting, sunburst formation |
| -3M | 4055 | 97 | 114 | Oxidation | 1800 | ----/114 | surface activity, sunburst formed and frose, little change |
| -4M | 4870 | 276 | 346 | Oxidation | 1800 | ----/346 | melting, sunburst formed and frose, some additional oxide melting |
| -5M | 5110 | 662 | 696 | Melting | 162 | 4.30/7740 | melting, rapid recession |
| -6M | 2965 | -22 | 7 | Oxidation | 1800 | ----/7 | no film coverage |
| -7R | 4970 | -6 | 27 | Oxidation | 1800 | ----/27 | uniform heating, some undercutting |
| -8R | 5245 | 140 | 129 | Melt + Oxid. | 1800 | ----/129 | one side heated faster, melted slightly, recession at angle, undercutting |
| -9R | 5065 | 550 | 575 | Melting | 32 | 18.9/32,400 | rapid melting and recession |
| -10R | 5065 | 310 | 322 | Melting | 37 | 8.7/15,660 | rapid melting and recession |
| -11R | 5075 | 6 | 36 | Oxidation | 1800 | ----/36 | uniform heating, some slight melting |
| -12R | 5044 | -5 | 11 | Oxidation | 1800 | ----/11 | uniform heating, little activity |
| -13MA | 3565 | | | Oxidation | 1300 | 4 | Poor exposure. |
| -13MB | 3645 | - 4 | 4 | Oxidation | 500 | | |
| -14M | 4825 | - 78 | 26 | Oxidation | 1800 | 26 | Initial melting, sunburst formation, oxide continued to melt. |
| -15M | 3400 | - 2 | 8 | Oxidation | 1800 | 8 | Droplets continuously shot out from center to edges. |
| -16MA | 4675 | | | Oxidation | 1150 | | Droplets formed followed by rapid melting of oxide. |
| -16MB | 5065 | 137 | 140 | Melting | 63 | 3543 | |
| -17MA | 5390 | | | Melting | 100 | | Rapid melting, solidified in sunburst, little additional activity. |
| -17MB | 4270 | 240 | 260 | Oxidation | 1700 | 260 | |
| -18MA | 5390 | | | Melting | 45 | | Rapid melting, solidified in sunburst, little additional activity. |
| -18MB | 4600 | 117 | 140 | Oxidation | 1755 | 140 | |
| -19MA | 4930 | --- | --- | Melting | 38 | | Front face melted, solidified in sunburst, additional |
| -19MB | 4690 | 10 | 44 | Oxidation | 1762 | 44 | oxide melting. |
| -20M | 3645 | - 2 | 6 | Oxidation | 1800 | 6 | Little activity, slight edge melt. |
| -21MA | 3780 | --- | --- | Oxidation | 45 | 11782 | Sample loose on sting, melting, rapid recession. |
| -21MB | 5225 | 623 | 648 | Melting | 99 | | |
| -22MA | 3700 | --- | --- | Oxidation | 217 | 9173 | Sample loose on sting, melting, rapid recession. |
| -22MB | 5240 | 511 | 530 | Melting | 104 | | |

*Recession rates converted to 30 minutes on linear basis.

# TABLE 13

## SUMMARY OF ARC PLASMA EXPOSURES OF $ZrB_2$ + 14% SiC + 30%C(A-10)

| Material Sample No. Assumed Emittance at $\lambda = 0.65\mu$ | Mach No. | $P_e$ atm | $i_e$ BTU/lb | D (in) | $q_{cw}$ BTU/ft²sec | T °R obs | $q_r$ Surface Radiation BTU/ft²sec | $\epsilon_N$ Computed Normal Emittance | Initial Length Thickness (mils) | Final Length* Thickness (mils) | Exposure Time (seconds) | Calculated Temperature Ratio T(CALC)/T (OBS) Cold Wall Heat Transfer Coefficient | Fay and Riddell Heat Transfer Coefficient |
|---|---|---|---|---|---|---|---|---|---|---|---|---|---|
| $ZrB_2$ + SiC + C (A-10) | | | | | | | | | | | | | |
| $\epsilon = 0.60$ | | | | | | | | | | | | | |
| -23MI | 0.21 | 1.02 | 3850 | 0.431 | 414 | 5090 | 161 | 0.51 | 822/820 | ---/--- | 1800 | 1.04 | 1.03 |
| -23MII | 0.21 | 1.02 | 4000 | 0.431 | 412 | 5060 | 158 | 0.51 | ---/--- | ---/--- | 1800 | 1.05 | 1.05 |
| -23MIII | 0.21 | 1.02 | 4150 | 0.431 | 402 | 5035 | 156 | 0.52 | ---/--- | ---/--- | 1800 | 1.06 | 1.06 |
| -23MIV | 0.21 | 1.02 | 3960 | 0.431 | 386 | 5035 | 157 | 0.52 | ---/--- | 822/757 | 1800 | 1.04 | 1.05 |
| -24MI | 0.20 | 1.02 | 4390 | 0.426 | 407 | 4085 | 75 | 0.57 | 826/825 | ---/--- | 1800 | 1.31 | 1.33 |
| -24MII | 0.20 | 1.02 | 4150 | 0.426 | 398 | 4710 | 141 | 0.61 | ---/--- | ---/--- | 1800 | 1.13 | 1.14 |
| -24MIII | 0.21 | 1.02 | 3870 | 0.426 | 396 | 4785 | 147 | 0.60 | ---/--- | ---/--- | 1800 | 1.08 | 1.07 |
| -24MIV | 0.21 | 1.02 | 4080 | 0.426 | 402 | 4920 | 170 | 0.62 | ---/--- | ---/--- | 1800 | 1.08 | 1.08 |
| -24MV | 0.21 | 1.02 | 4500 | 0.426 | 398 | 4865 | 151 | 0.57 | ---/--- | ---/--- | 1800 | 1.10 | 1.13 |
| -24MVI | 0.21 | 1.02 | 4350 | 0.426 | 394 | 4965 | 169 | 0.59 | ---/--- | ---/--- | 1800 | 1.07 | 1.10 |
| -24MVII | 0.24 | 1.02 | 4780 | 0.426 | 394 | 4990 | 175 | 0.60 | ---/--- | ---/--- | 1800 | 1.08 | 1.14 |
| -24MVIII | 0.23 | 1.02 | 4550 | 0.426 | 398 | 5010 | 169 | 0.57 | ---/--- | ---/--- | 1800 | 1.07 | 1.11 |
| -24MIX | 0.23 | 1.02 | 4150 | 0.426 | 406 | 5025 | 180 | 0.60 | ---/--- | ---/--- | 1800 | 1.06 | 1.08 |
| -24MX | 0.23 | 1.02 | 4400 | 0.426 | 394 | 5000 | 176 | 0.60 | ---/--- | ---/--- | 1800 | 1.07 | 1.10 |
| -24MXI | 0.23 | 1.02 | 3990 | 0.426 | 398 | 5045 | 187 | 0.61 | ---/--- | ---/--- | 1800 | 1.04 | 1.06 |
| -24MXII | 0.23 | 1.02 | 4310 | 0.426 | 425 | 5125 | 188 | 0.58 | ---/--- | 835/721 | 1800 | 1.05 | 1.07 |
| -27MA | 0.24 | 1.03 | 5160 | 0.437 | 511 | 6150 | 234 | 0.35 | 689/693 | ---/--- | 70 | 0.93 | 0.95 |
| -27MB | 0.24 | 1.03 | 5160 | 0.437 | 511 | 5535 | 173 | 0.39 | ---/--- | 574/541 | 1730 | 1.04 | 1.05 |
| -28MA | 0.74 | 1.35 | 3500 | 0.437 | 598 | 5930 | 181 | 0.31 | 690/685 | ---/--- | 250 | 0.93 | 0.93 |
| -28MB | 0.74 | 1.35 | 3500 | 0.437 | 598 | 5195 | --- | --- | ---/--- | ---/114 | 562 | 1.07 | 1.07 |
| -34MH | 0.18 | 1.01 | 3950 | 0.437 | 416 | 4105 | 68 | 0.51 | 691/103** | ---/85** | 1800 | 1.29 | 1.37 |
| -35MH | 0.18 | 1.01 | 3500 | 0.437 | 420 | 3760 | 62 | 0.54 | 686/393** | 690/388** | 1800 | 1.32 | 1.36 |
| -36M | 0.23 | 1.02 | 3870 | 0.437 | 400 | 3840 | 52 | 0.51 | 690/95** | 694/89** | 1800 | 1.37 | 1.37 |
| -39M | 0.21 | 1.02 | 3990 | 0.425 | 400 | 4740 | 92 | 0.39 | 692/197** | ---/381** | 1800 | 1.11 | 1.12 |
| -42MS | 0.21 | 1.03 | 4000 | 0.437 | 393 | 3020 | 27 | 0.69 | 693/103** | 694/101 | 1800 | 1.74 | 1.75 |
| -43MS | 0.21 | 1.03 | 4040 | 0.437 | 403 | 3055 | 26 | 0.63 | 688/400** | 693/397 | 1800 | 1.73 | 1.74 |

* Final length refers to measurement after exposure, thickness refers to length after sectioning

** Nose to in-depth temperature measurement station.

| Material Sample No. | T °F | Gross Recession (mils) | Material Recession (mils) | Degradation Mode | Exposure Time seconds | Recession Rate* mils/30 min | Description of Motion Picture Film Coverage |
|---|---|---|---|---|---|---|---|
| $ZrB_2$ + SiC + C (A-10) | | | | | | | |
| -23MI | 4630 | --- | --- | Melt. + Oxid. | 1800 | --- | Edges melted, sunburst formed, slight oxide melting. |
| -23MII | 4600 | --- | --- | Oxidation | 1800 | --- | Intact from cycle I, little activity. |
| -23MIII | 4575 | --- | --- | Oxidation | 1800 | --- | Intact from cycle II, little activity. |
| -23MIV | 4575 | 0 | 63 | Oxidation | 1800 | 16 | Intact from cycle III, little activity. |
| -24 MI | 3625 | --- | --- | Oxidation | 1800 | --- | Hotter at edges. |
| -24MII | 4250 | --- | --- | Oxidation | 1800 | --- | Oxide formed over face, some bubbles at edge. |
| -24MIII | 4325 | --- | --- | Oxidation | 1800 | --- | Heavy oxide covered face. |
| -24MIV | 4460 | --- | --- | Oxidation | 1800 | --- | Little change, slight oxide melting. |
| -24MV | 4405 | --- | --- | Oxidation | 1800 | --- | Little change, oxide grew heavier. |
| -24MVI | 4505 | --- | --- | Oxidation | 1800 | --- | Little change, slight oxide melting. |
| -24MVII | 4530 | --- | --- | Oxidation | 1800 | --- | Little change, slight oxide melting. |
| -24MVIII | 4550 | --- | --- | Oxidation | 1800 | --- | Little change, oxide heavier. |
| -24MIX | 4565 | --- | --- | Oxidation | 1800 | --- | Little change. |
| -24MX | 4540 | --- | --- | Oxidation | 1800 | --- | Little change. |
| -24MXI | 4585 | --- | --- | Oxidation | 1800 | --- | Little change. |
| -24MXII | 4665 | -9 | 104 | Oxidation | 1800 | 9 | Little change. |
| -27MA | 5690 | --- | --- | Melting | 70 | --- | Melted from edges to center |
| -27MB | 5075 | 115 | 141 | Oxidation | 1730 | 141 | Solidified in sunburst. |
| -28MA | 5470 | --- | --- | Melting | 250 | --- | Small droplets, oxide melted, considerable recession. |
| -28MB | 4735 | --- | 571 | Oxidation | 562 | 1265 | Solidified in sunburst. |
| -34MH | 3645 | --- | 18 | Oxidation | 1800 | 18 | Hot spot 1/4" diameter at nose, little activity. |
| -35MH | 3500 | -4 | 5 | Oxidation | 1800 | 5 | Hot spot 1/8" diameter at nose, little activity. |
| -36M | 3380 | -4 | 6 | Oxidation | 1800 | 6 | Little visible, slightly hotter at edges. |
| -39M | 4280 | --- | 16 | Oxidation | 1800 | 16 | Little visible, hotter at edges, oxide on front face. |
| -42MS | 2560 | -1 | 2 | Oxidation | 1800 | 2 | Little visible. |
| -43MS | 2595 | -5 | 3 | Oxidation | 1800 | 3 | Little visible. |

*Converted to 30 minutes on a linear basis.

# TABLE 14

## SUMMARY OF ARC PLASMA EXPOSURES OF $ZrB_2$ + 14%SiC + 30%C (A-10)

| Material Sample No. Assumed Emittance at λ = 0.65μ | Mach No. | $P_e$ atm | $i_e$ BTU/lb | D (in) | $q_{cw}$ BTU/ft²sec | T °R obs | $q_r$ Surface Radiation BTU/ft²sec | $\epsilon_N$ Computed Normal Emittance | Initial Length/Thickness (mils) | Final Length*/Thickness (mils) | Exposure Time (seconds) | Calculated Temperature Ratio T (CALC)/T (OBS) Cold Wall Heat Transfer Coefficient | Fay and Riddell Heat Transfer Coefficient |
|---|---|---|---|---|---|---|---|---|---|---|---|---|---|
| $ZrB_2$ + SiC + C (A-10) | | | | | | | | | | | | | |
| ε = 0.60 | | | | | | | | | | | | | |
| -25RI | 2.2 | 0.117 | 8070 | 0.437 | 492 | 4865 | 160 | 0.61 | 1001/682 | ---/--- | 1800 | 1.25 | 1.24 |
| -25RII | 2.2 | 0.117 | 8310 | 0.437 | 498 | 4955 | 194 | 0.68 | ---/--- | ---/--- | 1800 | 1.24 | 1.23 |
| -25RIII | 2.2 | 0.120 | 7800 | 0.437 | 498 | 5050 | 214 | 0.70 | ---/--- | ---/--- | 1800 | 1.21 | 1.18 |
| -25RIV | 2.2 | 0.120 | 8160 | 0.437 | 498 | 5190 | 235 | 0.69 | ---/--- | 1002/658 | 1600 | 1.18 | 1.17 |
| -26RI | 2.2 | 0.242 | 7650 | 0.437 | 460 | 4895 | 126 | 0.60 | 1000/679 | ---/--- | 1800 | 1.31 | 1.40 |
| -26RII | 2.2 | 0.240 | 7750 | 0.437 | 452 | 4955 | 202 | 0.71 | ---/--- | ---/--- | 1800 | 1.21 | 1.30 |
| -26RIII | 2.2 | 0.240 | 7900 | 0.437 | 460 | 5110 | 216 | 0.67 | ---/--- | ---/--- | 1800 | 1.18 | 1.27 |
| -26RIV | 2.2 | 0.240 | 7900 | 0.437 | 452 | 5135 | 224 | 0.69 | ---/--- | ---/--- | 1800 | 1.17 | 1.26 |
| -26RV | 2.2 | 0.236 | 7610 | 0.437 | 460 | 5110 | 220 | 0.69 | ---/--- | ---/--- | 1800 | 1.17 | 1.25 |
| -26RVI | 2.2 | 0.236 | 7580 | 0.437 | 469 | 5135 | 227 | 0.70 | ---/--- | ---/--- | 1800 | 1.17 | 1.24 |
| -26RVII | 2.2 | 0.236 | 8140 | 0.437 | 460 | 5155 | 219 | 0.66 | ---/--- | ---/--- | 1800 | 1.17 | 1.26 |
| -26RVIII | 2.2 | 0.236 | 7570 | 0.437 | 437 | 5180 | 219 | 0.65 | ---/--- | ---/--- | 1800 | 1.15 | 1.23 |
| -26RIX | 2.2 | 0.236 | 7890 | 0.437 | 437 | 5190 | 231 | 0.68 | ---/--- | ---/--- | 1800 | 1.15 | 1.24 |
| -26RX | 2.2 | 0.236 | 7650 | 0.437 | 455 | 5205 | 229 | 0.66 | ---/--- | ---/--- | 1800 | 1.15 | 1.23 |
| -26RXI | 2.2 | 0.236 | 7580 | 0.437 | 469 | 5190 | 236 | 0.69 | ---/--- | ---/596 | 951 | 1.16 | 1.23 |
| -30RA | 3.2 | 0.090 | 10440 | 0.426 | 551 | 3650 | 33 | 0.40 | 1128/822 | ---/--- | 428 | 1.75 | 1.75 |
| -30RB | 3.2 | 0.090 | 10440 | 0.426 | 551 | 5455 | 196 | 0.47 | ---/--- | 1138/796 | 1241 | 1.17 | 1.17 |
| -31RA | 3.2 | 0.105 | 10510 | 0.426 | 596 | 3650 | 44 | 0.53 | 1128/818 | ---/--- | 300 | 1.78 | 1.78 |
| -31RB | 3.2 | 0.105 | 10510 | 0.426 | 596 | 4910 | 123 | 0.45 | ---/--- | 473/138 | 30 | 1.32 | 1.32 |
| -32RA | 3.2 | 0.135 | 9520 | 0.426 | 656 | 3590 | 64 | 0.62 | 1119/809 | ---/--- | 35 | 1.83 | 1.80 |
| -32RB | 3.2 | 0.135 | 9520 | 0.426 | 656 | 4605 | 133 | 0.63 | ---/--- | 434/115 | 40 | 1.43 | 1.41 |
| -33RA | 3.2 | 0.145 | 7950 | 0.426 | 682 | 5490 | --- | --- | 1128/821 | ---/--- | 30 | 1.19 | 1.13 |
| -33RB | 3.2 | 0.145 | 7950 | 0.426 | 682 | 4780 | 129 | 0.52 | ---/--- | 419/102 | 40 | 1.36 | 1.29 |
| -36RH | 2.2 | 0.147 | 7250 | 0.437 | 492 | 3715 | 69 | 0.77 | 1010/102** | 1012/97 | 1800 | 1.63 | 1.76 |
| -37RH | 2.2 | 0.144 | 7710 | 0.437 | 482 | 3695 | 74 | 0.85 | 995/393** | 996/390 | 1800 | 1.64 | 1.80 |
| -40R | 2.2 | 0.147 | 6320 | 0.437 | 495 | 4935 | 173 | 0.62 | 1003/95** | 1004/89 | 1800 | 1.21 | 1.16 |
| -41R | 2.2 | 0.147 | 6460 | 0.425 | 495 | 5110 | 211 | 0.66 | 1000/399** | 1014/382 | 1800 | 1.17 | 1.13 |
| -44RS | 2.2 | 0.226 | 7400 | 0.440 | 495 | 4675 | 125 | 0.56 | 993/96** | 995/85 | 1800 | 1.30 | 1.35 |
| -45RS | 2.2 | 0.229 | 7470 | 0.440 | 498 | 5110 | 202 | 0.63 | 996/394** | 1001/380 | 1800 | 1.19 | 1.24 |
| -46RH | 2.2 | 0.155 | 7220 | 0.975 | 501 | 3025 | 22 | 0.56 | 1007/105** | 1007/104 | 1800 | 2.00 | 2.01 |
| -47RHS | 2.2 | 0.167 | 6010 | 0.969 | 507 | 4745 | 138 | 0.58 | 1004/100** | 1007/87 | 1800 | 1.25 | 1.21 |
| -48RH | 2.2 | 0.155 | 6350 | 0.975 | 492 | 2970 | 20 | 0.55 | 1005/402** | 1005/401 | 1800 | 2.01 | 1.97 |
| -49RHS | 2.2 | 0.167 | 6010 | 0.975 | 522 | 4130 | 99 | 0.73 | 983/391** | 983/388 | 1800 | 1.45 | 1.40 |
| -48RRA | 3.2 | 0.109 | 6980 | 0.976 | 654 | 5525 | 286 | 0.65 | 1004/402 | ---/--- | 425 | 1.15 | 1.05 |
| -48RRB | 3.2 | 0.117 | 8040 | 0.976 | 864 | 5535 | 286 | 0.65 | ---/--- | ---/--- | 180 | 1.24 | 1.10 |
| -48RRC | 3.2 | 0.125 | 8730 | 0.976 | 871 | 5525 | 281 | 0.64 | ---/--- | 938/--- | 33 | 1.25 | 1.14 |

* Final length refers to measurement after exposure, thickness refers to measurement after sectioning.

** Nose to in-depth temperature measurement station

| Material Sample No. | T °F | Gross Recession (mils) | Material Recession (mils) | Degradation Mode | Exposure Time seconds | Recession Rate* mils/30 min | Description of Motion Picture Film Coverage |
|---|---|---|---|---|---|---|---|
| $ZrB_2$ + SiC + C (A - 10) | | | | | | | |
| -25RI | 4405 | --- | --- | Oxidation | 1800 | ---- | Uniform oxide buildup, little activity. |
| -25RII | 4495 | --- | --- | Oxidation | 1800 | ---- | Some oxide chipping, little activity. |
| -25RIII | 4590 | --- | --- | Oxidation | 1800 | ---- | Oxide cracked, some chipping. |
| -25RIV | 4730 | -1 | 24 | Oxidation | 1800 | 6 | Large pieces of oxide broke off, surface reoxidized. |
| -26RI | 4135 | --- | --- | Oxidation | 1800 | ---- | Spotty oxide buildup. |
| -26RII | 4495 | --- | --- | Oxidation | 1800 | ---- | Oxide grew more uniform. |
| -26RIII | 4650 | --- | --- | Oxidation | 1800 | ---- | Little change from cycle II, some chipping at edges. |
| -26RIV | 4675 | --- | --- | Oxidation | 1800 | ---- | Oxide chipped off center and edges. |
| -26RV | 4650 | --- | --- | Oxidation | 1800 | ---- | Oxide breaking off and melting. |
| -26RVI | 4675 | --- | --- | Oxidation | 1800 | ---- | Uniform oxide, little activity. |
| -26RVII | 4695 | --- | --- | Oxidation | 1800 | ---- | Some oxide broke off edges, little activity. |
| -26RVIII | 4720 | --- | --- | Oxidation | 1800 | ---- | Intact from cycle VII. |
| -26RIX | 4730 | --- | --- | Oxidation | 1800 | ---- | Intact from cycle VIII. |
| -26RX | 4745 | --- | --- | Oxidation | 1800 | ---- | Intact from cycle IX, some spalling of heavy oxide. |
| -26RXI | 4730 | --- | 83 | Oxidation | 951 | 8 | Intact from cycle X. |
| -30RA | 3190 | --- | --- | Oxidation | 428 | ---- | Oxide formed from edges into center |
| -30RB | 4995 | -10 | 26 | Oxidation | 1241 | 36 | Oxide covered face |
| -31RA | 3190 | --- | --- | Oxidation | 300 | ---- | Oxide slowly melted from edges into center |
| -31RB | 4450 | 655 | 680 | Melting | 30 | 3710 | Rapid melting |
| -32RA | 3130 | --- | --- | Oxidation | 35 | ---- | Heated to melting |
| -32RB | 4145 | 685 | 694 | Melting | 40 | 16600 | Rapid melting |
| -33RA | 5030 | --- | --- | Melting | 30 | ---- | Heated to melting |
| -33RB | 4320 | 709 | 719 | Melting | 40 | 18400 | Rapid melting |
| -36RH | 3255 | -2 | 5 | Oxidation | 1800 | 5 | Hot spot 1/4" diam. oxidized at nose. |
| -37RH | 3235 | -1 | 3 | Oxidation | 1800 | 3 | Hot spot 1/4" diam. oxidized at nose. |
| -40R | 4475 | -1 | 6 | Oxidation | 1800 | 6 | Non-uniform oxide buildup, grew heavier. |
| -41R | 4650 | -14 | 17 | Oxidation | 1800 | 17 | Speckled surface, gradual oxide buildup. |
| -44RS | 4215 | - 2 | 11 | Oxidation | 1800 | 11 | Oxide gradually spread over sample, not shroud. |
| -45RS | 4650 | - 5 | 14 | Oxidation | 1800 | 14 | Oxide grew over top half of shroud and most of sample. |
| -46RH | 2565 | 0 | 1 | Oxidation | 1800 | 1 | Hot spot 1/4" diam. oxidized at nose. |
| -47RHS | 4285 | - 3 | 13 | Oxidation | 1800 | 13 | Small hot spot grew to 1/2" diam. at nose. |
| -48RH | 2510 | 0 | 1 | Oxidation | 1800 | 1 | Little activity. |
| -49RHS | 3670 | 0 | 3 | Oxidation | 1800 | 3 | Small hot spot 1/2" diam. at nose. |
| -48RRA | 5065 | --- | --- | Oxidation | 425 | ---- | Heavy oxide melting continuously, then |
| -48RRB | 5065 | --- | --- | Oxidation | 180 | ---- | solidified eventually leaving an unoxidized |
| -48RRC | 5065 | 66 | --- | Oxidation | 33 | ---- | spot at center. |

*Converted to 30 minutes on a linear basis.

# TABLE 15

## SUMMARY OF DEPLETION DEPTHS OBSERVED AFTER ARC PLASMA EXPOSURES OF BORIDE COMPOSITES

| Material Sample No. | Temperature (°F) | Depletion Depth(mils) | Time (sec) | Depletion Rate (mils/hour) |
|---|---|---|---|---|
| $HfB_2$+20%SiC(A-4) | | | | |
| -2M | 5020 | 11 | 1830 | 22 |
| -2-2M | 3170 | 10 | 1830 | 20 |
| -2-3M | 4790 | 26 | 1830 | 51 |
| -2-4M | 5190 | 32 | 1830 | 63 |
| -2-6R | 5190 | 26 | 1800 | 52 |
| -2-7R | 5300 | 52 | 1800 | 104 |
| -2-8R | 5480 | 49 | 1800 | 98 |
| $HfB_{2.1}$+35%SiC(A-9) | | | | |
| -1M* | 5610 | 130 | 78 | 6020 |
| -2M* | 5840 | 80 | 133 | 2170 |
| -4M* | 5410 | 70 | 251 | 996 |
| -5M | 3540 | 13 | 1800 | 26 |
| -7M | 3400 | 3 | 1800 | 6 |
| -8M | 3535 | 5 | 1800 | 10 |
| -9M | 4825 | 90 | 1800 | 180 |
| -10M | 5040 | 31 | 1800 | 62 |
| -13M* | 4655 | 41 | 1800 | 82 |
| -14M | 5145 | 8 | 408 | 71 |
| -15M | 3590 | 3 | 1800 | 6 |

*Melting occurred, depletion measurement unlikely to be dependable.

| Material Sample No. | Temperature (°F) | Depletion Depth(mils) | Time (sec) | Depletion Rate (mils/hour) |
|---|---|---|---|---|
| $HfB_{2.1}$+20%SiC(A-7) | | | | |
| -1M* | 5760 | 115 | 56 | 7410 |
| -2M | 4800 | 80 | 1740 | 166 |
| -3M | 4880 | 54 | 1800 | 108 |
| -4M* | 5030 | 140 | 1750 | 288 |
| -6M | 5135 | 65 | 264 | 885 |
| -7M | 5100 | 80 | 1750 | 165 |
| -23M | 5060 | 140 | 7200 | 70 |
| -24M | 4865 | 130 | 7200 | 65 |
| -25M | 4945 | 34 | 19418 | 6 |
| -26R | 4235 | 2 | 6800 | 1 |
| -27R | 4945 | 1 | 7200 | 1 |
| -29R | 3975 | 2 | 19800 | 1 |
| -30M* | 4915 | 27 | 1800 | 54 |
| -31M* | 4190 | 47 | 1800 | 94 |
| -32M* | 5155 | 100 | 1800 | 200 |
| -33R | 2975 | 0 | 1542 | 0 |
| -34R | 5005 | 0 | 1200 | 0 |
| -35R | 5350 | 130 | 90 | 5200 |
| -36MH | 3910 | 21 | 1081 | 70 |
| -37MH | 3765 | 10 | 1080 | 33 |
| -38RH | 2710 | 0 | 1812 | 0 |
| -39M | 4205 | 45 | 1800 | 90 |
| -41M | 4540 | 39 | 1800 | 78 |
| -42R | 2610 | 0 | 1800 | 0 |
| -43R | 2730 | 0 | 1800 | 0 |
| -45M | 4400 | 33 | 14030 | 8 |

*Melting occurred, depletion measurement unlikely to be dependable.

| Material Sample No. | Temperature (°F) | Depletion Depth(mils) | Time (sec) | Depletion Rate (mils/hour) |
|---|---|---|---|---|
| $ZrB_{2.1}$+20%SiC(A-8) | | | | |
| -3M* | 5585 | 100 | 34 | 10590 |
| -4M | 5445 | 120 | 327 | 1320 |
| -5M | 4475 | 5 | 1800 | 10 |
| -7M | 4600 | 6 | 1800 | 12 |
| -8M | 4180 | 3 | 1800 | 6 |
| -9M | 3160 | 1 | 1800 | 2 |
| -10M | 2705 | 0 | 1800 | 0 |
| -11M* | 3545 | 3 | 1800 | 6 |
| -12M* | 5090 | 70 | 669 | 376 |
| -13M | 4315 | 11 | 1760 | 22 |
| -15M | 4535 | 3 | 7200 | 2 |
| -16R | 4265 | 2 | 7200 | 1 |
| -17M | 4880 | 20 | 1800 | 40 |
| -18M | 4585 | 1 | 1800 | 2 |
| -19M | 3225 | 3 | 1800 | 6 |
| -20M* | 4260 | 6 | 1800 | 12 |
| -22R | 5065 | 17 | 200 | 306 |
| -25M | 3160 | 1 | 1800 | 2 |
| -26M | 3115 | 1 | 1800 | 2 |
| -27R | 2875 | 1 | 1800 | 2 |
| -28R | 3620 | 1 | 1810 | 2 |
| -29MS | 3360 | 1 | 1800 | 2 |
| -30MS | 2540 | 0 | 1800 | 0 |
| -33R | 2730 | 1 | 1800 | 2 |
| -34R | 4265 | 0 | 1800 | 0 |

*Melting occurred, depletion measurement unlikely to be dependable.

| Material Sample No. | Temperature (°F) | Depletion Depth(mils) | Time (sec) | Depletion Rate (mils/hour) |
|---|---|---|---|---|
| $ZrB_2$+SiC+C (A-10) | | | | |
| -1M* | 5170 | 5 | 34 | 530 |
| -2M* | 5110 | 6 | 182 | 119 |
| -3M | 4055 | 13 | 1800 | 26 |
| -4M | 4870 | 5 | 1800 | 10 |
| -7R* | 4970 | 42 | 1800 | 84 |
| -8R* | 5245 | 28 | 1800 | 56 |
| -12P | 5040 | 28 | 1800 | 56 |
| -13M | 3565 | 8 | 1800 | 16 |
| -14M | 4825 | 9 | 1800 | 18 |
| -15M* | 3400 | 8 | 1800 | 16 |
| -16M | 5065 | 10 | 1213 | 30 |
| -18M | 4600 | 17 | 1755 | 35 |
| -19M | 4690 | 13 | 1762 | 27 |
| -20M* | 3645 | 13 | 1800 | 26 |
| -21M* | 5225 | 15 | 144 | 380 |
| -22M | 5240 | 8 | 321 | 90 |
| -23M | 4595 | 20 | 7200 | 10 |
| -24M | 4410 | 12 | 21600 | 2 |
| -25R | 4555 | 14 | 7200 | 7 |
| -26R | 4420 | 13 | 18951 | 2 |
| -27M | 5075 | 8 | 1730 | 17 |
| -28M | 4735 | 12 | 562 | 77 |
| -30R | 4995 | 10 | 1241 | 29 |
| -34MH | 3645 | 12 | 1800 | 24 |
| -35MH | 3500 | 8 | 1800 | 16 |
| -37RH | 3235 | 0 | 1800 | 0 |
| -38M | 3380 | 5 | 1800 | 10 |
| -39M | 4280 | 11 | 1800 | 22 |
| -40R | 4475 | 10 | 1800 | 20 |
| -41R | 4650 | 6 | 1800 | 12 |
| -42MS | 2560 | 0 | 1800 | 0 |
| -43MS | 2595 | 0 | 1800 | 0 |
| -44RS | 4215 | 6 | 1800 | 12 |
| -45RS | 4650 | 7 | 1800 | 14 |

*Melting occurred, depletion measurement unlikely to be dependable.

# TABLE 16

## SUMMARY OF ARC PLASMA EXPOSURES OF RVA(B-5)

| Material Sample No. Assumed Emittance at λ = 0.65μ | Mach No. | $P_e$ atm | $i_e$ BTU/lb | D (in) | $q_{cw}$ BTU/ft²sec | T °R obs | $q_r$ Surface Radiation BTU/ft²sec | $\epsilon_N$ Computed Normal Emittance | Initial Length thickness (mils) | Final Length* thickness (mils) | Exposure Time (seconds) | Calculated Temperature Ratio T(CALC)/T(OBS) Cold Wall Heat Transfer Coefficient | Fay and Riddell Heat Transfer Coefficient |
|---|---|---|---|---|---|---|---|---|---|---|---|---|---|
| RVA(B-5) $\epsilon$ = 0.85 (Below 3000°F), 0.75(3000° - 3500°F), 0.65 (Above 3500°F) | | | | | | | | | | | | | |
| -2M | 0.33 | 1.07 | 3560 | 0.500 | 550 | 5040 | 143 | 0.47 | 1016/1016 | 687/701 | 120 | 1.06 | 1.02 |
| -3M | 0.30 | 1.08 | 2745 | 0.500 | 340 | 4500 | 78 | 0.40 | 1032/1032 | 851/837 | 120 | 1.03 | 1.01 |
| -5M | 0.39 | 1.10 | 6495 | 0.500 | 1030 | 6180 | --- | ----- | 1028/1028 | 822/830 | 58 | 1.05 | 1.00 |
| -6M | 0.49 | 1.15 | 6320 | 0.500 | 1080 | 6250 | 291 | 0.40 | 972/972 | 730/743 | 55 | 1.04 | 0.99 |
| -7M | 0.43 | 1.12 | 6225 | 0.500 | 810 | 5830 | 242 | 0.44 | 1007/1007 | 789/783 | 66 | 1.06 | 1.05 |
| -1R† | 3.20 | 0.187 | 12230 | 0.486 | 1138 | 5165 | 167* | 0.49* | 1083/1083 | 889/900 | 85 | 1.35 | 1.27 |
| -2R† | 3.20 | 0.029 | 9580 | 0.487 | 261 | 4110 | 57* | 0.42* | 1049/1049 | 749/741 | 600 | 1.20 | 1.21 |
| -3R† | 3.20 | 0.018 | 15600 | 0.487 | 487 | 4865 | 120* | 0.45* | 1064/1064 | 716/737 | 600 | 1.20 | 1.10 |
| -4R† | 3.20 | 0.163 | 7640 | 0.487 | 608 | 4665 | 100* | 0.44* | 1044/1044 | 687/665 | 300 | 1.26 | 1.21 |
| -5R† | 3.20 | 0.017 | 13570 | 0.486 | 326 | 4470 | 65* | 0.34* | 999/999 | 528/533 | 900 | 1.18 | 1.15 |
| -6R† | 3.20 | 0.016 | 14000 | 0.487 | 317 | 4570 | 98* | 0.47* | 991/991 | 689/690 | 600 | 1.15 | 1.13 |
| -7R† | 3.20 | 0.299 | 10950 | 0.486 | 979 | 5890 | 167* | 0.29* | 1044/1044 | 851/839 | 108 | 1.14 | 1.14 |
| -1M° | 0.35 | 1.08 | 4405 | 0.500 | 570 | ---- | --- | ----- | 993/993 | ---/695 | 108 | ---- | ----- |
| -4M° | 0.36 | 1.08 | 5965 | 0.500 | 750 | ---- | --- | ----- | 991/991 | 973/982 | 4 | ---- | ----- |
| -11M | 0.31 | 1.06 | 3740 | 0.741 | 435 | 4375 | 111 | 0.65 | 932/930 | 709/708 | 120 | 1.17 | 1.12 |
| -12M | 0.32 | 1.07 | 4900 | 0.741 | 529 | 4630 | 160 | 0.74 | 948/940 | 696/688 | 120 | 1.19 | 1.15 |
| -13M | 0.34 | 1.07 | 7030 | 0.741 | 640 | 4995 | 186 | 0.64 | 931/930 | 628/630 | 120 | 1.19 | 1.20 |
| -14R† | 3.2 | 0.012 | 10850 | 0.741 | 241 | 4010 | 92 | 0.76 | 1265/942 | 860/570 | 1200 | 1.26 | 1.14 |
| -15R† | 3.2 | 0.024 | 10930 | 0.741 | 455 | 4500 | 159 | 0.82 | 1262/939 | 841/543 | 900 | 1.30 | 1.11 |
| -16R† | 3.2 | 0.218 | 10060 | 0.739 | 979 | 5855 | 454 | 0.82 | 1233/929 | 797/490 | 300 | 1.17 | 1.07 |
| -23M | 0.10 | 1.00 | 2690 | 0.502 | 167 | 3725 | 58 | 0.64 | 683/679 | 522/521 | 180 | 1.12 | 1.12 |
| -24M | 0.13 | 1.00 | 3510 | 0.502 | 250 | 4105 | 89 | 0.67 | 683/680 | 568/561 | 120 | 1.14 | 1.14 |
| -25M | 0.15 | 1.00 | 2090 | 0.503 | 126 | 3420 | 41 | 0.64 | 684/678 | 586/584 | 180 | 1.08 | 1.13 |
| -26M | 0.15 | 1.00 | 1770 | 0.503 | 73 | 3035 | 27 | 0.68 | 674/670 | 572/573 | 361 | 1.05 | 1.18 |
| -27M | 0.15 | 1.00 | 1360 | 0.502 | 91 | 2995 | 27 | 0.71 | 665/663 | 554/534 | 300 | 1.05 | 1.08 |
| -28R† | 3.2 | 0.005 | 5280 | 0.503 | 34 | 2165 | 3 | 0.29 | 1000/701 | 971/669 | 1800 | 1.40 | 1.60 |
| -29R† | 3.2 | 0.008 | 11590 | 0.504 | 117 | 2780 | 20 | 0.71 | 1001/676 | 852/521 | 1800 | 1.50 | 1.63 |
| -30R† | 3.2 | 0.011 | 13950 | 0.502 | 211 | 3465 | 46 | 0.68 | 1002/680 | 708/387 | 1200 | 1.43 | 1.46 |
| -31M | 0.10 | 1.00 | 2530 | 0.501 | 135 | 3285 | 39 | 0.71 | 670/1980** | 534/69 | 240 | 1.15 | 1.18 |
| -32M | 0.10 | 1.00 | 2930 | 0.502 | 135 | 3475 | 36 | 0.53 | 671/4640** | 598/388 | 180 | 1.13 | 1.20 |

** Nose to in-depth temperature measurement station

†Transmissivity factor equals 0.86 for pyrex window.
*Surface radiation values may be low due to requirements for critical alignment caused by utilization of one-half inch diameter sample.
°Test terminated before temperature and surface radiation could be measured.

*Final Length is based on measurement prior to sectioning; thickness refers to length after sectioning.

| Material Sample No. | T °F | Gross Recession mils | Material Recession mils | Degradation Mode | Exposure Time seconds | Recession Rate* (mils/sec) / (mils/10 min) | Description of Motion Picture Film Coverage |
|---|---|---|---|---|---|---|---|
| RVA (B-5) | | | | | | | |
| -2M | 4580 | 329 | 315 | Oxidation | 120 | 2.63/4734 | uniform heating, rapid side recession |
| -3M | 4040 | 181 | 195 | Oxidation | 120 | 1.63/2934 | uniform heating, rapid side recession |
| -5M | 5720 | 206 | 198 | Oxidation | 58 | 3.41/6138 | uniform heating, rapid front and side recession |
| -6M | 5790 | 242 | 229 | Oxidation | 55 | 4.16/7488 | uniform heating, rapid front and side recession, some vibration |
| -7M | 5370 | 218 | 224 | Oxidation | 66 | 3.39/6102 | uniform heating, rapid front and side recession, some vibration |
| -1R | 4705 | 164 | 153 | Oxidation | 85 | 1.80/3240 | uniform heating and recession, rounding of edges |
| -2R | 3650 | 300 | 308 | Oxidation | 600 | 0.51/918 | |
| -3R | 4405 | 348 | 327 | Oxidation | 600 | 0.55/990 | uniform heating and recession |
| -4R | 4205 | 357 | 379 | Oxidation | 300 | 1.26/2268 | uniform heating, some side recession |
| -5R | 4010 | 471 | 466 | Oxidation | 900 | 0.52/936 | uniform heating, some side recession, rapid side recession |
| -6R | 4110 | 302 | 301 | Oxidation | 600 | 0.50/900 | uniform heating, some side recession |
| -7R | 5430 | 193 | 205 | Oxidation | 108 | 1.90/3420 | uniform heating and recession, rounding of edges |
| -1M | (4290)° | --- | 298 | Oxidation | 108 | 2.76/4968 | terminated due to rapid ablation, sample blown away |
| -4M | (4740)° | 18† | 9 | Oxidation | 9 | 1.00/1800 | terminated due to rapid ablation, sample blown away |
| -11M | 3915 | 223 | 222 | Oxidation | 120 | 1.85/3330 | uniform recession, slight surface activity |
| -12M | 4170 | 252 | 252 | Oxidation | 120 | 2.10/3780 | uniform recession, slight surface activity |
| -13M | 4525 | 303 | 300 | Oxidation | 120 | 2.50/4500 | uniform recession, slight surface activity |
| -14R | 3520 | 405 | 372 | Oxidation | 1200 | 0.31/558 | |
| -15R | 4040 | 421 | 396 | Oxidation | 900 | 0.41/792 | |
| -16R | 5395 | 436 | 439 | Oxidation | 300 | 1.46/2630 | Uniform recession. |
| -23M | 3265 | 161 | 148 | Oxidation | 180 | 0.88/1580 | Rough, speckled surface, uniform heating. |
| -24M | 3645 | 115 | 119 | Oxidation | 120 | 0.99/1785 | Rough, speckled surface, uniform heating. |
| -25M | 2960 | 98 | 94 | Oxidation | 180 | 0.52/940 | Rough, speckled surface, uniform heating. |
| -26M | 2575 | 102 | 97 | Oxidation | 361 | 0.27/483 | Speckled face, little visible. |
| -27M | 2535 | 111 | 129 | Oxidation | 300 | 0.43/774 | Rough, speckled surface, uniform heating. |
| -28R | 1705 | 29 | 32 | Oxidation | 1800 | 0.018/32 | Little visible. |
| -29R | 2320 | 149 | 155 | Oxidation | 1800 | 0.086/155 | Rough, speckled surface, uniform heating, gradual recession. |
| -30R | 3005 | 294 | 293 | Oxidation | 1200 | 0.24/440 | Rough surface, uniform heating, gradual recession. |
| -31M | 2825 | 136 | 129 | Oxidation | 240 | 0.54/968 | Little visible. |
| -32M | 3015 | 73 | 76 | Oxidation | 180 | 0.42/760 | Speckled heating. |

*Gross recession is overestimated because of chipping or erosion of back face.
°Temperatures estimated based on Cold Wall Heat Transfer Coefficient Calculations of 5518°R and 6030°R corrected by mean ratio T(CALC)/T(OBS) of 1.16 to 4750°R and 5200°R or 4290°F and 4740°F.

*Recession rate converted to 10 minutes on linear basis.

# TABLE 17

## SUMMARY OF ARC PLASMA EXPOSURES OF PG(B-6)

| Material Sample No. Assumed Emittance at $\lambda$ = 0.65μ | Mach No. | $P_e$ atm | $i_e$ BTU/lb | D (in) | $q_{cw}$ BTU/ft²sec | T °R obs | $q_r$ Surface Radiation BTU/ft²sec | $q_N$ Computed Normal Emittance | Initial Length thickness (mils) | Final Length* thickness (mils) | Exposure Time (seconds) | Calculated Temperature Ratio T(CALC)/T(OBS) Cold Wall Heat Transfer Coefficient | Fay and Riddell Heat Transfer Coefficient |
|---|---|---|---|---|---|---|---|---|---|---|---|---|---|
| "C" Axis Perpendicular to Arc | | | | | | | | | | | | | |
| PG (B-6) | | | | | | | | | | | | | |
| ε = 0.75 | | | | | | | | | | | | | |
| -1M | 0.31 | 1.06 | 2970 | 0.487 | 390 | 4320 | 73 | 0.44 | 1160/1160 | 1000/1000 | 120 | 1.11 | 1.08 |
| -2M | 0.33 | 1.07 | 3955 | 0.489 | 540 | 5150 | 139 | 0.42 | 1154/1154 | 861/882 | 120 | 1.04 | 1.01 |
| -3M | 0.35 | 1.08 | 4580 | 0.489 | 670 | 4990 | 131 | 0.44 | 999/999 | 865/856 | 61 | 1.14 | 1.10 |
| Delaminated on "C" Plane after Test | | | | | | | | | | | | | |
| -4M | 0.38 | 1.09 | 6665 | 0.486 | 810 | 4990 | 166 | 0.56 | 906/906 | 800/796 | 44 | 1.24 | 1.24 |
| -5M | 0.39 | 1.10 | 6750 | 0.487 | 980 | 5660 | 208 | 0.43 | 904/904 | 718/708 | 60 | 1.14 | 1.10 |
| -6M | 0.46 | 1.14 | 5710 | 0.488 | 940 | 5490 | 151 | 0.35 | 853/853 | 665/672 | 53 | 1.14 | 1.09 |
| -7M | 0.38 | 1.09 | 7320 | 0.486 | 870 | 5490 | 148 | 0.34 | 980/980 | 797/802 | 62 | 1.16 | 1.16 |
| Delaminated on "C" Plane after Test | | | | | | | | | | | | | |
| -1R† | 3.2 | 0.020 | 15640 | 0.487 | 504 | 4565 | 87* | 0.42* | 1090/1090 | 696/704 | 900 | 1.29 | 1.19 |
| -2R† | 3.2 | 0.015 | 14730 | 0.489 | 330 | 4175 | 65* | 0.45* | 1091/1091 | 481/527 | 1200 | 1.27 | 1.24 |
| -3R† | 3.2 | 0.299 | 16380 | 0.488 | 1216 | ---- | ---- | ---- | 1078/1078 | ----/1069 | ---- | ---- | ---- |
| Delaminated on "C" Plane | | | | | | | | | | | | | |
| -4R† | 3.2 | 0.187 | 8440 | 0.485 | 852 | 5110 | 75* | 0.23* | 1084/1084 | 639/628 | 300 | 1.25 | 1.16 |
| -6R† | 3.2 | 0.017 | 13500 | 0.488 | 328 | 4140 | 57* | 0.40* | 1111/1111 | 811/834 | 600 | 1.28 | 1.24 |
| -7R† | 3.2 | 0.187 | 8860 | 0.488 | 1008 | ---- | ---- | ---- | 1111/1111 | ----/1094 | ---- | ---- | ---- |
| Delaminated on "C" Plane | | | | | | | | | | | | | |
| ε = 0.65 | | | | "C" Axis Parallel to Arc | | | | | | | | | |
| -8M | 0.33 | 1.07 | 3825 | 0.486 | 550 | 5800 | 173 | 0.32 | 617/456 | 302/230 | 120 | 0.94 | 0.91 |
| -9M | 0.28 | 1.05 | 2255 | 0.486 | 290 | 4640 | 79 | 0.36 | 622/465 | 545/387 | 97 | 0.95 | 0.93 |
| -10M | 0.35 | 1.08 | 4355 | 0.486 | 690 | 6420 | 228 | 0.32 | 547/390 | 342/227 | 72 | 0.94 | 0.89 |
| -11M | 0.42 | 1.11 | 5925 | 0.486 | 1170 | 7150 | 464 | 0.37 | 582/421 | 278/208 | 66 | 0.94 | 0.87 |
| -12M | 0.33 | 1.07 | 2705 | 0.486 | 530 | 5780 | 151 | 0.28 | 533/375 | 339/204 | 95 | 0.88 | 0.81 |
| -8R† | 3.2 | 0.030 | 13900 | 0.486 | 921 | 5555 | 233 | 0.56 | 619/460 | 462/316 | 300 | 1.13 | 1.06 |
| -9R† | 3.2 | 0.189 | 7190 | 0.486 | 764 | 5850 | 268 | 0.53 | 554/395 | 324/168 | 150 | 1.11 | 1.02 |
| -10R† | 3.2 | 0.208 | 9750 | 0.487 | 1013 | 6135 | 342 | 0.56 | 588/427 | 300/154 | 210 | 1.14 | 1.08 |
| -11R† | 3.2 | 0.228 | 11310 | 0.487 | 1238 | 6480 | 431 | 0.57 | 626/464 | 279/138 | 210 | 1.16 | 1.08 |
| -12R† | 3.2 | 0.053 | 8230 | 0.487 | 451 | 4860 | 143 | 0.58 | 547/357 | 231/97 | 600 | 1.21 | 1.12 |

†Transmissivity factor equals 0.86 for sapphire window.

*Final length is based on measurement prior to sectioning, thickness refers to length after sectioning.

*Surface radiation values may be low due to requirements for critical alignment caused by utilization of one-half inch diameter sample.

| Material Sample No. | T °F | Gross Recession mils | Material Recession mils | Degradation Mode | Exposure Time seconds | Recession Rate* (mils)/(sec) / (mils)/(30 min) | Description of Motion Picture Film Coverage |
|---|---|---|---|---|---|---|---|
| PG (B-6) "A" Plane | | | | | | | |
| -1M | 3860 | 160 | 160 | Oxidation | 120 | 1.33/2394 | uniform heat-up, side recession observed |
| -2M | 4690 | 293† | 272 | Oxidation | 120 | 2.27/4086 | heat-up from sides to center parallel to "A" axis, side recession observed, sample moved during test |
| -3M | 4530 | 134 | 143 | Oxid + Th. Shock | 61 | 2.34/4212 | heat-up parallel to "A" axis, side recession, some sample vibration |
| -4M | 4530 | 106 | 110 | Oxidation | 44 | 2.50/4500 | heat-up parallel to "A" axis, side recession, some sample vibration |
| -5M | 5200 | 186 | 196 | Oxidation | 60 | 3.27/5886 | heat-up parallel to "A" axis, side recession, some sample vibration |
| -6M | 5030 | 188 | 181 | Oxidation | 53 | 3.41/6138 | heat-up parallel to "A" axis, side recession, some sample vibration, indication of surface reaction nonuniformity |
| -7M | 5030 | 183 | 178 | Oxid + Th. Shock | 62 | 2.87/5166 | |
| -1R | 4105 | 394 | 386 | Oxidation | 900 | 0.43/774 | heat-up parallel to "A" axis, uniform recession, indication of liquid on top side |
| -2R | 3715 | 610† | 564 | Oxidation | 1200 | 0.47/846 | heat-up parallel to "A" axis, uniform recession |
| -3R | ---- | --- | --- | Th. Shock | ---- | ----/--- | heat-up parallel to "A" axis, fracture almost immediate |
| -4R | 4650 | 445 | 456 | Oxidation | 300 | 1.52/2736 | heat-up parallel to "A" axis, uniform recession |
| -6R | 3680 | 300† | 277 | Oxidation | 600 | 0.46/828 | heat-up parallel to "A" axis, lustrous surface, uniform recession |
| -7R | ---- | --- | --- | Th. Shock | ---- | ----/---- | heat-up parallel to "A" axis, thermal shock after 25 mil sector had heated up |
| PG (B-6) "C" Plane | | | | | | | |
| -8M | 5340 | 315† | 226 | Oxidation | 120 | 1.88/3384 | uniform heating, hourglass oxidation |
| -9M | 4180 | 77 | 78 | Oxidation | 97 | 0.80/1440 | uniform heating, hourglass oxidation |
| -10M | 5760 | 205 | 163 | Oxidation | 72 | 2.26/4068 | uniform heating, hourglass oxidation |
| -11M | 6690 | 304† | 213 | Oxidation | 66 | 3.23/5814 | uniform heating, hourglass oxidation, surface activity |
| -12M | 5320 | 194† | 171 | Oxidation | 95 | 1.80/3240 | uniform heating, hourglass oxidation, surface activity |
| -8R | 5095 | 157† | 144 | Oxidation | 300 | 0.48/864 | uniform recession |
| -9R | 5390 | 230 | 227 | Oxidation | 150 | 1.51/2718 | heated from edges to center, no side heating, uniform recession |
| -10R | 5675 | 288 | 273 | Oxidation | 210 | 1.30/2340 | uniform recession, little side heating |
| -11R | 6020 | 347 | 326 | Oxidation | 210 | 1.55/2794 | uniform recession, little side heating |
| -12R | 4400 | 316 | 290 | Oxidation | 600 | 0.48/870 | gradual side heat-up, hourglass recession |

†Gross recession is overestimated because of chipping or erosion of back face.

*Recession rate converted to 30 minutes on linear basis.

# TABLE 18

## SUMMARY OF ARC PLASMA EXPOSURES OF BPG(B-7)

| Material Sample No. Assumed Emittance at λ = 0.65μ | Mach No. | $P_e$ atm | $i_e$ BTU/lb | D fin | $q_{cw}$ BTU/ft²sec | T °R obs | $q_r$ Surface Radiation BTU/ft²sec | $\epsilon_N$ Computed Normal Emittance | Initial Length/thickness (mils) | Final* Length/thickness (mils) | Exposure Time (seconds) | Calculated Temperature Ratio T(CALC)/T(OBS) Cold Wall Heat Transfer Coefficient | Fay and Riddell Heat Transfer Coefficient |
|---|---|---|---|---|---|---|---|---|---|---|---|---|---|
| | "C" Axis Perpendicular to Arc | | | | | | | | "C" Axis Perpendicular to Arc | | | | |
| BPG (B-7) | | | | | | | | | | | | | |
| ε = 0.75 | | | | | | | | | | | | | |
| -1M | 0.30 | 1.05 | 2955 | 0.487 | 370 | 4010 | 46 | 0.37 | 876/876 | 746/746 | 120 | 1.19 | 1.16 |
| -2M | 0.33 | 1.07 | 3965 | 0.486 | 530 | 5040 | 98 | 0.32 | 828/828 | 494/482 | 119 | 1.06 | 1.03 |
| -3M | 0.36 | 1.08 | 4745 | 0.483 | 550 | 5120 | 129 | 0.39 | 839/839 | 594/599 | 90 | 1.08 | 1.08 |
| | Delaminated on "C" Plane after Test | | | | | | | | | | | | |
| -4M | 0.36 | 1.08 | 6500 | 0.483 | 760 | 5400 | 165 | 0.41 | 799/799 | 567/575 | 75 | 1.13 | 1.14 |
| | Incipient Delamination on "C" Plane | | | | | | | | | | | | |
| -1R† | 3.2 | 0.192 | 8370 | 0.483 | 736 | 4940 | 102* | 0.36* | 874/874 | 482/508 | 300 | 1.25 | 1.20 |
| | Delaminated on "C" Plane after Test | | | | | | | | | | | | |
| -2R† | 3.2 | 0.187 | 8600 | 0.487 | 852 | 5265 | --- | ---- | 888/888 | 816/787 | 57 | 1.21 | 1.13 |
| | Delaminated on "C" Plane after 5 Seconds | | | | | | | | | | | | |
| -4R† | 3.2 | 0.020 | 15200 | 0.487 | 478 | 4910 | 109* | 0.39* | 848/848 | 537/539 | 600 | 1.18 | 1.10 |
| -5R† | 3.2 | 0.022 | 14700 | 0.487 | 501 | 4920 | 109* | 0.39* | 873/873 | ---/520 | 900 | 1.19 | 1.10 |
| -6R† | 3.2 | 0.017 | 13890 | 0.486 | 321 | 4270 | 55* | 0.35* | 785/785 | 521/547 | 600 | 1.23 | 1.21 |
| ε = 0.65 | "C" Axis Parallel to Arc | | | | | | | | "C" Axis Parallel to Arc | | | | |
| -5M | 0.33 | 1.07 | 3540 | 0.486 | 500 | 5690 | 161 | 0.32 | 501/342 | 329/197 | 82 | 0.93 | 0.90 |
| -6M | 0.28 | 1.05 | 2230 | 0.482 | 310 | 4695 | 75 | 0.32 | 500/349 | 392/239 | 120 | 0.95 | 0.92 |
| -7M | 0.35 | 1.08 | 4815 | 0.482 | 710 | 6300 | 228 | 0.38 | 495/339 | 275/170 | 70 | 0.94 | 0.91 |
| -8M | 0.38 | 1.09 | 5745 | 0.482 | 910 | 6405 | 331 | 0.41 | 489/344 | 229/147 | 64 | 1.00 | 0.95 |
| -9M | 0.32 | 1.06 | 3215 | 0.482 | 480 | 5610 | 164 | 0.35 | 506/343 | 307/175 | 96 | 0.92 | 0.88 |
| -8R† | 3.2 | 0.030 | 12000 | 0.486 | 441 | 5380 | 230 | 0.58 | 456/272 | 271/121 | 300 | 1.12 | 1.08 |
| -9R† | 3.2 | 0.139 | 7230 | 0.486 | 636 | 5510 | 210 | 0.48 | 500/347 | 353/195 | 150 | 1.14 | 1.08 |
| -10R† | 3.2 | 0.158 | 7260 | 0.484 | 781 | 5565 | 222 | 0.49 | 503/347 | 359/206 | 120 | 1.17 | 1.06 |
| -11R† | 3.2 | 0.208 | 9960 | 0.487 | 960 | 6290 | 368 | 0.55 | 431/272 | 259/106 | 120 | 1.12 | 1.06 |
| -12R† | 3.2 | 0.014 | 12340 | 0.486 | 371 | 5080 | 176 | 0.60 | 518/345 | 297/159 | 900 | 1.14 | 1.03 |

†Transmissivity factor equals 0.86 for pyrex window.
*Surface radiation values may be low due to requirements for critical alignment caused by utilization of one-half inch diameter sample.

*Final length is based on measurement prior to sectioning; thickness refers to length after sectioning.

| Material Sample No. | T °F | Gross Recession mils | Material Recession mils | Degradation Mode | Exposure Time seconds | Recession Rate* (mils)/(sec) / (mils)/(30 min) | Description of Motion Picture Film Coverage |
|---|---|---|---|---|---|---|---|
| BPG (B-7) "A" Plane | | | | | | | |
| -1M | 3550 | 130 | 130 | Oxidation | 120 | 1.08/1944 | heat-up from sides to center parallel to "A" axis, side recession observed |
| -2M | 4580 | 334 | 346 | Oxidation | 119 | 2.91/5238 | heat-up from sides to center, side recession |
| -3M | 4660 | 245 | 240 | Oxid + Th. Shock | 90 | 2.67/4806 | heat-up from sides to center, side recession |
| -4M | 4940 | 232 | 224 | Oxid + Th. Shock | 75 | 2.99/5382 | heat-up from sides to center, side recession |
| -1R | 4480 | 392† | 366 | Oxid + Th. Shock | 300 | 1.22/2196 | heat-up parallel to "A" axis, uniform recession |
| -2R | 4805 | 72 | 101 | Oxid + Th. Shock | 57 | 1.77/3186 | delaminated after 40 mil sector heated up |
| -4R | 4450 | 311 | 309 | Oxidation | 600 | 0.52/936 | heat-up parallel to "A" axis, uniform recession |
| -5R | 4460 | --- | 553 | Oxidation | 900 | 0.61/936 | heat-up parallel to "A" axis, uniform recession, some surface activity on front face |
| -6R | 3810 | 264† | 238 | Oxidation | 600 | 0.40/720 | heat-up parallel to "A" axis, uniform recession, bands noted on front face |
| BPG (B-7) "C" Plane | | | | | | | |
| -5M | 5230 | 172† | 143 | Oxidation | 82 | 1.77/3186 | uniform heating, hourglass oxidation |
| -6M | 4235 | 108 | 110 | Oxidation | 120 | 0.92/1656 | no film coverage |
| -7M | 5840 | 220† | 169 | Oxidation | 70 | 2.41/4338 | uniform heating, hourglass oxidation, speckled surface |
| -8M | 5945 | 260† | 197 | Oxidation | 64 | 3.09/5562 | uniform heating, hourglass oxidation, speckled surface |
| -9M | 5150 | 199† | 168 | Oxidation | 96 | 1.75/3150 | no film coverage |
| -8R | 4920 | 185† | 151 | Oxidation | 300 | 0.50/900 | uniform heating, recession |
| -9R | 5050 | 147 | 152 | Oxidation | 150 | 1.01/1818 | little activity, uniform recession |
| -10R | 5105 | 144 | 141 | Oxidation | 120 | 1.18/2124 | little activity, uniform recession |
| -11R | 5830 | 172 | 168 | Oxidation | 120 | 1.40/2520 | uniform heating, recession |
| -12R | 4620 | 221 | 186 | Oxidation | 900 | 0.21/372 | uniform heating, recession |

†Gross recession is overestimated because of chipping or erosion at back face.

*Recession rate converted to 30 minutes on linear basis.

# TABLE 19

## SUMMARY OF ARC PLASMA EXPOSURES OF Si/RVC(B-8)

| Material Sample No. Assumed Emittance at λ = 0.65μ | Mach No. | $P_e$ atm | $h_e$ BTU/lb | D (in) | $q_{cw}$ BTU/ft²sec | $T_R$ °R | $q_r$ Surface Radiation BTU/ft²sec | $\epsilon_N$ Computed Normal Emittance | Initial Length/Thickness (mils) | Final Length* Thickness (mils) | Exposure Time (seconds) | Calculated Temperature Ratio T(CALC)/T(OBS) Cold Wall Heat Transfer Coefficient | Fay and Riddell Heat Transfer Coefficient |
|---|---|---|---|---|---|---|---|---|---|---|---|---|---|
| Si/RVC(B-8) ε = 0.70 | | | | | | | | | | | | | |
| -1M | 0.36 | 1.08 | 4670 | 0.503 | 720 | 6180 | 292* | 0.42 | 714/717 | 494/489 | 73 | 0.95 | 0.90 |
| -2M | 0.33 | 1.07 | 4230 | 0.502 | 615 | 5840 | 257* | 0.47 | 696/691 | 522/519 | 77 | 0.96 | 0.92 |
| -3M | 0.32 | 1.07 | 3790 | 0.505 | 555 | 5750 | 280* | 0.54 | 715/710 | 541/531 | 75 | 0.94 | 0.90 |
| -4M | 0.31 | 1.06 | 3270 | 0.505 | 475 | 4230 | 100 | 0.66 | 731/739 | 729/727 | 240 | 1.21 | 1.16 |
| -5MA | 0.31 | 1.06 | 3720 | 0.503 | 470 | 4250 | 94 | 0.62 | 724/729 | ---/--- | --- | 1.23 | 1.20 |
| | After 735 seconds, temperature and radiation changed to -5MB | | | | | | | | | | | | |
| -5MB | 0.31 | 1.06 | 3720 | 0.503 | 470 | 5370 | 148* | 0.38 | ---/--- | 509/528 | 785 | 0.97 | 0.95 |
| -6MA | 0.32 | 1.06 | 3910 | 0.503 | 510 | 4150 | 90* | 0.65 | 692/693 | ---/--- | --- | 1.29 | 1.26 |
| | After 90 seconds, temperature and radiation changed to -6MB | | | | | | | | | | | | |
| -6MB | 0.32 | 1.06 | 3910 | 0.503 | 510 | 5510 | 220* | 0.51 | ---/--- | 500/520 | 185 | 0.97 | 0.95 |
| -7R† | 3.2 | 0.013 | 8850 | 0.502 | 210 | 3200 | 53 | 1.08 | 1031/735 | 1030/714 | 1800 | 1.51 | 1.43 |
| -8R† | 3.2 | 0.023 | 9390 | 0.502 | 415 | 4800 | 174 | 0.70 | 1041/749 | 701/488 | 500 | 1.18 | 1.03 |
| -9R† | 3.2 | 0.026 | 10090 | 0.505 | 590 | 5220 | 217 | 0.62 | 1034/725 | 768/451 | 500 | 1.17 | 0.98 |
| -10R† | 3.2 | 0.018 | 8850 | 0.503 | 310 | 4450 | 125 | 0.68 | 1031/680 | 747/491 | 750 | 1.19 | 1.07 |
| -11R† | 3.2 | 0.138 | 10170 | 0.503 | 693 | 5250 | 275 | 0.77 | 1032/720 | 760/435 | 200 | 1.23 | 1.20 |
| -12R† | 3.2 | 0.213 | 10560 | 0.502 | 968 | 6030 | 526 | 0.85 | 1027/719 | 679/369 | 160 | 1.16 | 1.11 |
| -13MA | 0.35 | 1.07 | 3260 | 0.507 | 445 | 4215 | 82 | 0.55 | 725/723 | ---/--- | 680 | 1.20 | 1.17 |
| -13MB | 0.15 | 1.07 | 3260 | 0.507 | 445 | 5235 | 128 | 0.36 | ---/--- | 362/335 | 124 | 0.97 | 0.94 |
| -14M | 0.10 | 1.01 | 5480 | 0.503 | 480 | 5540 | 196 | 0.44 | 707/708 | 342/339 | 196 | 1.00 | 0.93 |
| -15MA | 0.20 | 1.03 | 3120 | 0.503 | 295 | 3635 | 57 | 0.69 | 704/705 | ---/--- | 30 | 1.28 | 1.28 |
| -15MB | 0.20 | 1.03 | 3120 | 0.503 | 295 | 3530 | 45 | 0.62 | ---/--- | 704/701 | 1770 | 1.52 | 1.32 |
| -16M | 0.17 | 1.02 | 2520 | 0.504 | 220 | 3200 | 19 | 0.39 | 701/762 | 754/754 | 1800 | 1.53 | 1.33 |
| -17M | 0.38 | 1.07 | 2920 | 0.503 | 397 | 4235 | 90 | 0.60 | 721/729 | 458/349 | 530 | 1.15 | 1.12 |
| -18M | 0.29 | 1.05 | 3190 | 0.505 | 462 | 5570 | 59 | 0.77 | 723/728 | 725/718 | 1800 | 1.36 | 1.35 |
| -19MA | 0.18 | 1.02 | 3160 | 0.505 | 324 | 3730 | 71 | 0.78 | 716/713 | ---/--- | 100 | 1.28 | 1.24 |
| -19MB | 0.18 | 1.02 | 3160 | 0.503 | 321 | 3475 | 54 | 0.79 | ---/--- | 715/704 | 1700 | 1.37 | 1.33 |
| -20R† | 2.2 | 0.103 | 6240 | 0.500 | 227 | 3075 | 28 | 0.67 | 1054/740 | 1054/728 | 1800 | 1.60 | 1.71 |
| -21R† | 2.2 | 0.109 | 6300 | 0.506 | 262 | 3056 | 28 | 0.68 | 1027/696 | 1024/684 | 1800 | 1.66 | 1.75 |

* Surface radiation values might be in error since severe side erosion caused a significant change in specimen diameter.

† Transmissivity factor equals 0.86 for sapphire window.

Final length is based on measurement after exposure; thickness refers to specific sample.

| Material Sample No. | $h_w$ BTU/lb | Gross Recession (mils) | Material Recession (mils) | Degradation Mode | Exposure Time (seconds) | Recession Rate* mil units/sec to 10 min | Description of Motion Picture, Film Coverage |
|---|---|---|---|---|---|---|---|
| Si/SiC (B-8) | | | | | | | |
| -1M | 5720 | 220 | 228 | RVC Oxidation | 73 | 3, 12/5620 | Coating melted and burned off, hourglass recession. |
| -2M | 5580 | 174 | 172 | RVC Oxidation | 77 | 2, 24/3020 | Coating melted and burned off, hourglass recession. |
| -3M | 5490 | 174 | 177 | RVC Oxidation | 75 | 2, 39/1290 | Coating melted and burned off, hourglass recession. |
| -4M | 5720 | 2 | 12 | SiC Oxidation | 240 | ----/90 | Coating melted but remained on front face. |
| -5MA | 579 | --- | 10† | SiC Oxidation | 735 | ----/25† | Coating melted and remained, then burned off, hourglass recession. |
| -5MB | 4910 | 215 | 191 | RVC Oxidation | 50 | ----/---- 3, 82, 6876 | |
| -6MA | 1690 | --- | 10† | SiC Oxidation | 90 | ----, 200† | Coating melted and remained, then burned off, Hourglass recession. |
| -6MB | 5050 | 192 | 163 | RVC Oxidation | 65 | ----/---- 2, 50/4515 | |
| -7R | 2710 | 1 | 21 | SiC Oxidation | 1800 | ----/21 | |
| -8R | 4310 | 340 | 261 | Oxidation | 500 | ----/940 | |
| -9R | 1760 | 266 | 274 | Oxidation | 500 | ----/985 | |
| -10R | 1990 | 281 | 298 | Oxidation | 750 | ----/715 | |
| -11R | 1790 | 272 | 285 | RVC Oxidation | 200 | 1, 38/2565 | Immediate coating failure, uniform recession. |
| -12R | 5570 | 348 | 350 | RVC Oxidation | 160 | 2, 11/3938 | Immediate coating failure, uniform recession. |
| -13MA | 3755 | -- | --- | SiC Oxidation | 680 | ----/21 | Liquid on face and edges. |
| -13MB | 4775 | 363 | 388 | RVC Oxidation | 124 | 3, 06/5516 | Coating failed, rapid ablation. |
| -14M | 5080 | 365 | 373 | RVC Oxidation | 196 | 1, 86/3352 | Immediate coating failure, graphite ablation. |
| -15MA | 3175 | --- | --- | SiC Oxidation | 30 | ----/---- | Liquid at edges. |
| -15MB | 3070 | 0 | 4 | SiC Oxidation | 1770 | ----/4 | No failure. |
| -16M | 2730 | 7 | 8 | SiC Oxidation | 1800 | ----/8 | Little visible, no failure. |
| -17M | 4775 | 263 | 380 | RVC Oxidation | 530 | 0, 70/1263 | Bubbles at edges, failed near top edge and spread across face. |
| -18M | 3110 | 2 | 10 | SiC Oxidation | 1800 | ----/10 | Bubbles at edges, no failure. |
| -19MA | 3270 | --- | --- | SiC Oxidation | 100 | ----/---- | Small bubbles on face and edges |
| -19MB | 3015 | 1 | 9 | SiC Oxidation | 1700 | ----/9 | No failure. |
| -20R | 2615 | 0 | 12 | SiC Oxidation | 1800 | ----/12 | Little activity. |
| -21R | 2595 | 1 | 12 | SiC Oxidation | 1800 | ----/12 | Little activity. |

† Estimated.

Recession rates converted to thirty minutes on linear basis.

# TABLE 20

## SUMMARY OF ARC PLASMA EXPOSURES OF PT0178(B-9)

| Material Sample No. Assumed Emittance at λ = 0.65μ | Mach No. | $P_s$ atm | $i_s$ BTU/lb | D (in) | $q_{cw}$ BTU/ft²sec | T °R obs | $q_r$ Surface Radiation BTU/ft²sec | $\epsilon_N$ Computed Normal Emittance | Initial Length thickness (mils) | Final Length* thickness (mils) | Exposure Time (seconds) | Calculated Temperature Ratio T(CALC)/T(OBS) Cold Wall Heat Transfer Coefficient | Fay and Riddell Heat Transfer Coefficient |
|---|---|---|---|---|---|---|---|---|---|---|---|---|---|
| PT0178 (B-9) | | | | | | | | | | | | | |
| ε = 0.75 | | | | | | | | | | | | | |
| -1M | 0.28 | 1.05 | 1665 | 0.495 | 580 | 5375 | 193* | 0.49 | 1083/1084 | 786/759 | 83 | 0.81 | 0.70 |
| -2M | 0.24 | 1.03 | 2285 | 0.495 | 285 | 4650 | 94* | 0.43 | 1098/1104 | 832/829 | 100 | 0.93 | 0.90 |
| -3M | 0.29 | 1.05 | 3960 | 0.495 | 570 | 5410 | 211* | 0.52 | 1100/1104 | 844/808 | 67 | 1.00 | 0.95 |
| -4M | 0.31 | 1.06 | 4770 | 0.495 | 780 | 6280 | 260* | 0.36 | 1089/1091 | 817/815 | 58 | 0.94 | 0.87 |
| -5M | 0.33 | 1.07 | 5590 | 0.495 | 940 | 6445 | 375* | 0.46 | 1078/1080 | 799/801 | 54 | 0.97 | 0.90 |
| -6R+ | 3.2 | 0.011 | 12190 | 0.495 | 271 | 4250 | 133 | 0.87 | 1377/1083 | 909/607 | 1000 | 1.23 | 1.15 |
| -7R+ | 3.2 | 0.023 | 10800 | 0.495 | 443 | 4680 | 197 | 0.87 | 1450/1115 | 978/718 | 550 | 1.24 | 1.10 |
| -8R+ | 3.2 | 0.028 | 12990 | 0.495 | 590 | 5180 | 283 | 0.84 | 1473/1127 | 925/677 | 500 | 1.21 | 1.07 |
| -9R+ | 3.2 | 0.050 | 16050 | 0.495 | 763 | 5500 | 368 | 0.85 | 1350/1091 | 937/675 | 400 | 1.22 | 1.08 |
| -10R+ | 3.2 | 0.213 | 11440 | 0.495 | 1035 | 6355 | 625 | 0.81 | 1165/1096 | 525/260 | 190 | 1.11 | 1.06 |

*Surface radiation values might be in error since severe side erosion caused a significant change in specimen diameter.
+Transmissivity factor equals 0.86 for sapphire window.

*Final length is based on measurement prior to sectioning, thickness refers to length after sectioning.

| Material Sample No. | T °F | Gross Recession mils | Material Recession mils | Degradation Mode | Exposure Time | Recession Rate* mils/sec / mils/30 min | Description of Motion Picture Film Coverage |
|---|---|---|---|---|---|---|---|
| PT0178 (B-9) | | | | | | | |
| -1M | 4915 | 297 | 325 | Oxidation | 83 | 3.92/7050 | rapid heat-up of entire specimen, hourglass recession |
| -2M | 4190 | 266 | 275 | Oxidation | 100 | 2.75/4950 | rapid hourglass recession |
| -3M | 4950 | 256 | 296 | Oxidation | 67 | 4.42/7950 | rapid hourglass recession |
| -4M | 5820 | 272 | 276 | Oxidation | 58 | 4.76/8570 | rapid hourglass recession |
| -5M | 5985 | 279 | 279 | Oxidation | 54 | 5.17/9300 | rapid hourglass recession |
| -6R | 3790 | 468 | 476 | Oxidation | 1000 | ----/857 | |
| -7R | 4220 | 472 | 497 | Oxidation | 550 | ----/1298 | |
| -8R | 4720 | 548 | 450 | Oxidation | 500 | ----/1620 | |
| -9R | 5040 | 413 | 416 | Oxidation | 400 | ----/1872 | |
| -10R | 5895 | 640 | 836 | Oxidation | 190 | 4.40/7920 | rounding of nose, uniform recession |

*Recession rate converted to 30 minutes on linear basis.

# TABLE 21

## SUMMARY OF ARC PLASMA EXPOSURES OF AXF-5Q POCO (B-10) and GLASSY CARBON (B-11)

| Material Sample No. Assumed Emittance at λ = 0.65μ | Mach No. | $P_e$ atm | $i_e$ BTU/lb | D (in) | $q_{cw}$ BTU/ft²sec | T °R obs | $q_r$ Surface Radiation BTU/ft²sec | $\epsilon_N$ Computed Normal Emittance | Initial Length* thickness | Final Length* thickness | Exposure Time (seconds) | Calculated Temperature Ratio T(CALC)/T(OBS) Cold Wall Heat Transfer Coefficient | Fay and Riddell Heat Transfer Coefficient |
|---|---|---|---|---|---|---|---|---|---|---|---|---|---|
| **AXF-5Q (B-10) POCO Graphite** | | | | | | | | | | | | | |
| ε = 0.75 | | | | | | | | | | | | | |
| -1M | 0.30 | 1.06 | 3485 | 0.501 | 400 | 4820 | 140 | 0.55 | 826/831 | 629/629 | 103 | 1.03 | 1.02 |
| -2M | 0.36 | 1.08 | 6370 | 0.501 | 625 | 6040 | 345 | 0.55 | 840/842 | 605/604 | 76 | 0.97 | 1.01 |
| -3M | 0.33 | 1.07 | 5180 | 0.501 | 575 | 5600 | 210 | 0.46 | 824/830 | 610/618 | 81 | 1.00 | 1.01 |
| -4M | 0.38 | 1.09 | 5210 | 0.501 | 860 | 6260 | 305 | 0.42 | 836/843 | 643/644 | 61 | 0.97 | 0.92 |
| -5M | 0.42 | 1.11 | 9195 | 0.501 | 1060 | 6580 | 515 | 0.59 | 837/841 | 678/679 | 44 | 1.03 | 1.05 |
| -6M | 0.31 | 1.06 | 3530 | 0.501 | 335 | 4800 | 120 | 0.48 | 836/843 | 645/646 | 84 | 1.00 | 1.03 |
| -7R† | 3.2 | 0.025 | 14370 | 0.502 | 638 | 4980 | 217 | 0.75 | 1179/842 | 619/483 | 800 | 1.28 | 1.13 |
| -8R† | 3.2 | 0.015 | 12760 | 0.500 | 364 | 4360 | 132 | 0.78 | 1170/830 | 730/384 | 900 | 1.28 | 1.18 |
| -9R† | 3.2 | 0.034 | 16380 | 0.502 | 902 | 5380 | 312 | 0.79 | 1163/840 | 681/415 | 550 | 1.29 | 1.12 |
| -10R† | 3.2 | 0.218 | 10890 | 0.502 | 1102 | 5810 | 487 | 0.91 | 1128/836 | 573/308 | 250 | 1.22 | 1.15 |
| -11R† | 3.2 | 0.220 | 11620 | 0.501 | 1180 | 6225 | 356 | 0.50 | 1127/836 | 403/118 | 300 | 1.16 | 1.09 |
| -12R† | 3.2 | 0.010 | 11915 | 0.502 | 184 | 3070 | 38 | 0.91 | 1133/854 | 750/461 | 1500 | 1.55 | 1.57 |
| -13R† | 3.2 | 0.006 | 10570 | 0.502 | 104 | 2805 | 20 | 0.69 | 1131/843 | 933/638 | 1800 | 1.59 | 1.57 |
| **Glassy Carbon(B-11) Grade 2000** | | | | | | | | | | | | | |
| ε = 0.55 | | | | | | | | | | | | | |
| -1M | 0.31 | 1.06 | 3630 | 0.500 | 505 | 5450 | 193 | 0.46 | 506/135 | ---/--- | 45 | 1.01 | 0.97 |
| -2M | 0.29 | 1.05 | 3015 | 0.500 | 440 | 5450 | 219 | 0.53 | 565/135 | ---/31 | 35 | 0.95 | 0.91 |
| -3M | 0.20 | 1.03 | 3785 | 0.500 | 360 | 5000 | 147 | 0.50 | 525/135 | 521/10 | 54 | 1.04 | 1.04 |
| -4M | 0.16 | 1.02 | 3300 | 0.500 | 300 | * | * | * | 471/132 | ---/--- | ---- | ---- | ---- |

†Transmissivity factor equals 0.86 for sapphire window.
*Immediate thermal shock failure on exposure to jet.

* Final length is based on measurement prior to sectioning; thickness refers to length after sectioning.

| Material Sample No. | T °F | Gross Recession mils | Material Recession mils | Degradation Mode | Exposure Time seconds | Recession Rate mils/sec / mils/30 min | Description of Motion Picture Film Coverage |
|---|---|---|---|---|---|---|---|
| **POCO Graphite** | | | | | | | |
| -1M | 4360 | 197 | 202 | Oxidation | 103 | ---/3531 | uniform heating, slight hourglass recession |
| -2M | 5580 | 235 | 238 | Oxidation | 76 | ---/5638 | uniform heating, hourglass recession |
| -3M | 5140 | 214 | 212 | Oxidation | 81 | ---/4710 | uniform heating, slight hourglass recession |
| -4M | 5806 | 193 | 199 | Oxidation | 61 | ---/5862 | uniform heating, hourglass recession, speckled surface |
| -5M | 6120 | 159 | 162 | Oxidation | 44 | ---/6626 | rapid heating, rapid hourglass recession |
| -6M | 4340 | 191 | 197 | Oxidation | 84 | ---/4221 | uniform heating, hourglass recession, speckled surface |
| -7R | 4520 | 560 | 559 | Oxidation | 800 | ---/808 | |
| -8R | 3900 | 440 | 444 | Oxidation | 900 | ---/888 | |
| -9R | 4920 | 482 | 425 | Oxidation | 550 | ---/1390 | |
| -10R | 5350 | 577 | 529 | Oxidation | 250 | 2.12/3816 | uniform recession |
| -11R | 5765 | 724 | 718 | Ablation | 300 | 4308 | Uniform heating, recession, |
| -12R | 2610 | 383 | 393 | Ablation | 1500 | 472 | Uniform heating, recession, |
| -13R | 2345 | 198 | 205 | Ablation | 1800 | 205 | Uniform heating, recession, |
| **Glassy Carbon(B-11) Grade 2000** | | | | | | | |
| - 1M | 4990 | --- | --- | Oxidation | 45 | ---- | Hourglass recession; edges melted, then rear of specimen melted, then front face melted. |
| - 2M | 4990 | --- | 104 | Oxidation | 35 | 5349 | Hourglass recession. |
| - 3M | 4540 | 4 | 125 | Oxidation | 54 | 4167 | Hourglass recession. |
| - 4M | ---- | --- | --- | Th. Shock | ---- | ---- | Thermal shocked immediately. |

*Recession rates converted to 30 minutes on linear basis.

# TABLE 22

## SUMMARY OF ARC PLASMA EXPOSURES OF HfC + C(C-11)

| Material Sample No. Assumed Emittance at $\lambda$ = 0.65$\mu$ | Mach No. | $P_e$ atm | $i_e$ BTU/lb | D (in) | $q_{cw}$ BTU/ft$^2$ sec | T obs °R | $q_r$ Surface Radiation BTU/ft$^2$ sec | $\epsilon_N$ Computed Normal Emittance | Initial Length/Thickness (mils) | Final Length*/Thickness (mils) | Exposure Time (seconds) | Calculated Temperature Ratio T(CALC)/T (OBS) Cold Wall Heat Transfer Coefficient | Fay and Riddell Heat Transfer Coefficient |
|---|---|---|---|---|---|---|---|---|---|---|---|---|---|
| HfC + C (C-11) $\epsilon$ = 0.60 | | | | | | | | | | | | | |
| -1M | 0.35 | 1.07 | 4670 | 0.456 | 635 | 5710 | 353 | 0.71 | 407/407 | 486/348 | 1185 | 1.03 | 1.01 |
| -2M | 0.36 | 1.08 | 5320 | 0.456 | 715 | 5515 | 309 | 0.71 | 406/401 | 390/323 | 1800 | 1.11 | 1.10 |
| -3M | 0.37 | 1.09 | 5790 | 0.456 | 755 | 6580 | 538 | 0.61 | 416/408 | 237/208 | 66 | 0.95 | 0.95 |
| -4M | 0.36 | 1.08 | 5200 | 0.456 | 755 | 6710 | 465 | 0.49 | 408/404 | 262/256 | 45 | 0.92 | 0.90 |
| -5M | 0.33 | 1.07 | 3860 | 0.464 | 495 | 5250 | 244 | 0.68 | 413/412 | 443/362 | 1800 | 1.04 | 1.03 |
| -7R | 3.2 | 0.221 | 10230 | 0.464 | 889 | 6345 | 388 | 0.51 | 711/400 | 515/363 | 60 | 1.11 | 1.09 |
| -8R | 3.2 | 0.192 | 10100 | 0.463 | 801 | 6320 | 368 | 0.49 | 712/394 | 479/0 | 100 | 1.09 | 1.07 |
| -9R | 3.2 | 0.125 | 11770 | 0.459 | 709 | 5360 | 266 | 0.69 | 714/405 | 681/365 | 300 | 1.27 | 1.27 |
| -10R | 3.2 | 0.066 | 11850 | 0.459 | 614 | 5335 | 276 | 0.73 | 714/405 | 726/385 | 1800 | 1.24 | 1.19 |
| -11R | 3.2 | 0.011 | 14370 | 0.459 | 315 | 5240 | 250 | 0.71 | 714/401 | 734/381 | 1800 | 1.09 | 1.04 |
| -12R | 3.2 | 0.017 | 15420 | 0.459 | 756 | 6005 | 303 | 0.50 | 714/396 | 600/286 | 180 | 1.16 | 0.97 |
| -13M | 0.62 | 1.25 | 2590 | 0.456 | 565 | 4865 | 195 | 0.74 | 479/428 | 442/364 | 766 | 1.05 | 1.00 |
| -14M | 0.43 | 1.12 | 3490 | 0.455 | 435 | 5640 | 237 | 0.50 | 407/383 | 407/346 | 1800 | 0.96 | 0.94 |
| -15M | 0.15 | 1.01 | 2830 | 0.455 | 235 | 4325 | 65 | 0.39 | 481/415 | 529/368 | 1800 | 1.05 | 1.05 |
| -16M | 0.17 | 1.02 | 3570 | 0.426 | 310 | 4900 | 105 | 0.39 | 423/395 | 499/349 | 1800 | 1.01 | 1.02 |
| -17M | 0.14 | 1.01 | 3400 | 0.426 | 295 | 4820 | 88 | 0.35 | 439/437 | 481/405 | 1800 | 1.01 | 1.00 |
| -18MA | 0.21 | 1.03 | 6480 | 0.426 | 740 | 6675 | 409 | 0.44 | 439/438 | ---/--- | 60 | 0.95 | 0.93 |
| -18MB | 0.21 | 1.03 | 6480 | 0.426 | 740 | 5850 | 158 | 0.29 | ---/--- | 262/208 | 1740 | 1.08 | 1.06 |
| -19R | 3.2 | 0.029 | 9160 | 0.427 | 750 | 6055 | 303 | 0.48 | 752/441 | 734/410 | 45 | 1.11 | 0.89 |
| -20R | 3.2 | 0.180 | 9040 | 0.427 | 791 | 6175 | 329 | 0.48 | 751/440 | 523/201 | 120 | 1.10 | 1.07 |
| -21M | 0.27 | 1.04 | 6330 | 0.440 | 660 | 5800 | 283 | 0.53 | 451/450 | 431/404 | 1800 | 1.07 | 1.08 |
| -22M | 0.28 | 1.04 | 5960 | 0.439 | 708 | 5730 | 288 | 0.57 | 444/451 | 417/382 | 1800 | 1.09 | 1.08 |
| -23M | 0.30 | 1.05 | 6130 | 0.440 | 748 | 5570 | 240 | 0.53 | 459/453 | 416/374 | 1800 | 1.13 | 1.13 |
| -24R | 2.2 | 0.204 | 8000 | 0.440 | 633 | 5645 | 266 | 0.56 | 752/441 | 768/409 | 1800 | 1.14 | 1.13 |
| -25R | 2.2 | 0.204 | 8610 | 0.439 | 748 | 5690 | 269 | 0.55 | 753/445 | 746/412 | 1800 | 1.18 | 1.18 |
| -26R | 2.2 | 0.200 | 8340 | 0.439 | 699 | 5620 | 256 | 0.55 | 755/448 | 767/416 | 1800 | 1.17 | 1.15 |

* Final length refers to measurement after exposure, thickness refers to length after sectioning.

| Material Sample No. | T °F | Gross Recession (mils) | Material Recession (mils) | Degradation Mode | Exposure Time seconds | Recession Rate* mils/30 min | Description of Motion Picture Film Coverage |
|---|---|---|---|---|---|---|---|
| HfC + C (C-11) | | | | | | | |
| -1M | 5250 | -79 | 59 | Melt, + Oxid. | 1185 | 630 | Melting, sunburst formed. |
| -2M | 5055 | 16 | 78 | Melt, + Oxid. | 1800 | 78 | Melting, sunburst formed at angle, some molten droplets. |
| -3M | 6120 | 179 | 200 | Melting | 66 | 5455 | Rapid melting. |
| -4M | 6250 | 146 | 148 | Melting | 45 | 5920 | Rapid melting. |
| -5M | 4790 | -30 | 50 | Oxidation | 1800 | 50 | Heavy oxide, small sunburst, hotter at edges. |
| -7R | 5885 | 196 | 37 | Melting | 60 | 1110 | Melting throughout run. |
| -8R | 5860 | 233 | 394 | Melting | 100 | 7092 | Melting. |
| -9R | 4900 | 33 | 40 | Melt, + Oxid. | 300 | 240 | Sunburst formed, little additional activity. |
| -10R | 4875 | -12 | 20 | Oxidation | 1800 | 20 | Slow heatup, sides grew colder as oxide thickened. |
| -11R | 4780 | -10 | 20 | Oxidation | 1800 | 20 | Slow heatup, sides grew colder as oxide thickened. |
| -12R | 5545 | 114 | 110 | Melting | 180 | 1100 | Melting throughout run. |
| -13M | 4405 | 37 | 64 | Oxidation | 766 | 152 | Heavy oxide, some edge chipping. |
| -14M | 5180 | -30 | 37 | Oxidation | 1800 | 37 | Heavy oxide, some edge chipping. |
| -15M | 3865 | -48 | 47 | Oxidation | 1800 | 47 | Puffy oxide, some edge chipping. |
| -16M | 4440 | -76 | 46 | Oxidation | 1800 | 46 | Extremely heavy oxide. |
| -17M | 4360 | -42 | 32 | Oxidation | 1800 | 32 | Heavy oxide, some edge chipping. |
| -18MA | 6215 | --- | --- | Melting | 60 | --- | Rapid melting. |
| -18MB | 5390 | 177 | 230 | Oxidation | 1740 | 230 | Solidified in sunburst, little activity. |
| -19R | 5595 | -18 | 31 | Melt, + Oxid. | 45 | 1240 | Slow melting, sample fractured and fell. |
| -20R | 5715 | 228 | 239 | Melting | 120 | 3585 | Continuous melting. |
| -21M | 5340 | 20 | 46 | Oxidation | 1800 | 46 | Melted into sunburst, oxide continued to melt slowly. |
| -22M | 5270 | 27 | 69 | Oxidation | 1800 | 69 | Melted into sunburst, oxide continued to melt slowly. |
| -23M | 5110 | 43 | 79 | Oxidation | 1800 | 79 | Melted into sunburst, oxide continued to melt slowly. |
| -24R | 5185 | -16 | 32 | Oxidation | 1800 | 32 | Uniform oxidation, little activity. |
| -25R | 5230 | 7 | 32 | Oxidation | 1800 | 32 | Uniform oxidation, little activity. |
| -26R | 5160 | -12 | 32 | Oxidation | 1800 | 32 | Uniform oxidation, little activity. |

* Recession rates converted to thirty minutes on linear basis.

# TABLE 23

## SUMMARY OF ARC PLASMA EXPOSURES OF ZrC+C(C-12)

| Material Sample No. Assumed Emittance at $\lambda = 0.65\mu$ | Mach No. | $P_e$ atm | $h_e$ BTU/lb | D (in) | $q_{cw}$ BTU/ft²sec | T °R | $q_r$ Surface Radiation BTU/ft²sec | $\epsilon_N$ Computed Normal Emittance | Initial Length*/thickness (mils) | Final Length*/thickness (mils) | Exposure Time | Calculated Temperature Ratio T(CALC)/T(OBS) Cold Wall Heat Transfer Coefficient | Fay and Riddell Heat Transfer Coefficient |
|---|---|---|---|---|---|---|---|---|---|---|---|---|---|
| ZrC + C (C-12) | | | | | | | | | | | | | |
| $\epsilon = 0.60$ | | | | | | | | | | | | | |
| -1M | 0.33 | 1.07 | 3925 | 0.464 | 500 | 5310 | 256 | 0.69 | 412/406 | 444/359 | 1800 | 1.03 | 1.02 |
| -2M | 0.34 | 1.07 | 4070 | 0.464 | 575 | 5480 | 287 | 0.68 | 406/399 | 414/343 | 1800 | 1.03 | 1.00 |
| -3M | 0.36 | 1.08 | 4580 | 0.464 | 660 | 6430 | 378 | 0.67 | 411/404 | 387/379 | 23 | 0.92 | 0.89 |
| -4M | 0.33 | 1.07 | 4330 | 0.464 | 575 | 5420 | 292 | 0.72 | 407/403 | 415/353 | 1800 | 1.05 | 1.03 |
| -5M | 0.34 | 1.07 | 4460 | 0.464 | 620 | 5320 | 280 | 0.74 | 407/407 | 381/341 | 1800 | 1.09 | 1.07 |
| -6M | 0.35 | 1.08 | 4955 | 0.464 | 625 | 6500 | 361 | 0.43 | 417/408 | 331/317 | 44 | 0.91 | 0.91 |
| -7M | 0.31 | 1.06 | 3495 | 0.464 | 430 | 4965 | 199 | 0.70 | 417/411 | 426/370 | 1800 | 1.05 | 1.04 |
| -7R† | 3.2 | 0.084 | 11100 | 0.463 | 775 | 5415 | 303 | 0.75 | 711/411 | 721/202 | 1800 | 1.27 | 1.18 |
| -8R† | 3.2 | 0.224 | 11520 | 0.464 | 1012 | 6125 | 342 | 0.52 | 710/414 | ---/ 0 | 23 | 1.20 | 1.17 |
| -9R† | 3.2 | 0.218 | 10380 | 0.464 | 870 | 6235 | 316 | 0.44 | 713/403 | 435/ 0 | 20 | 1.13 | 1.11 |
| -10R† | 3.2 | 0.093 | 11030 | 0.464 | 548 | 5490 | 319 | 0.75 | 713/404 | 723/372 | 1800 | 1.17 | 1.17 |
| -11R† | 3.2 | 0.011 | 13320 | 0.464 | 383 | 5225 | 270 | 0.77 | 713/404 | 723/370 | 1800 | 1.14 | 1.02 |
| -12M | 0.62 | 1.26 | 2720 | 0.425 | 560 | 5230 | 219 | 0.62 | 444/443 | 478/354 | 1800 | 0.99 | 0.96 |
| -14M | 0.44 | 1.12 | 3425 | 0.426 | 535 | 5420 | 252 | 0.62 | 439/428 | 449/386 | 1800 | 1.00 | 0.98 |
| -15M | 0.15 | 1.01 | 2750 | 0.427 | 235 | 4360 | 65 | 0.38 | 481/468 | 536/404 | 1800 | 1.03 | 1.04 |
| -16MA | 0.17 | 1.02 | 3490 | 0.426 | 315 | 4890 | 76 | 0.28 | 449/452 | ---/--- | 150 | 1.01 | 1.02 |
| -16MB | 0.17 | 1.02 | 3490 | 0.426 | 315 | 4630 | 48 | 0.22 | ---/--- | 453/422 | 1650 | 1.07 | 1.07 |
| -17M | 0.21 | 1.03 | 3190 | 0.426 | 700 | 6785 | 214 | 0.22 | 285/227 | ---/ 0 | 65 | 0.90 | 0.85 |
| -18R† | 3.2 | 0.130 | 12110 | 0.427 | 650 | 5835 | 255 | 0.47 | 748/442 | 762/393 | 1350 | 1.15 | 1.19 |

†Transmissivity factor equals 0.86 for sapphire window.

*Final length is based upon measurement prior to sectioning; thickness refers to length after sectioning.

| Material Sample No. | T °F | Gross Recession mils | Material Recession mils | Degradation Mode | Exposure Time seconds | Recession Rate* (mils)/(sec) / (mils)/(30 min) | Description of Motion Picture Film Coverage |
|---|---|---|---|---|---|---|---|
| ZrC + C (C-12) | | | | | | | |
| -1M | 4850 | -32 | 47 | Oxidation | 1800 | ----/47 | droplets and whiskers at edges in small sunburst, heavy oxide coating |
| -2M | 5020 | -8 | 56 | Oxidation | 1800 | ----/56 | sunburst formation, recession at slight angle |
| -3M | 5970 | 24 | 25 | Melting | 23 | 1.09/1960 | rapid melting, specimen fell off sting |
| -4M | 4960 | -8 | 50 | Oxidation | 1800 | ----/50 | droplets and whiskers, small sunburst |
| -5M | 4860 | 26 | 66 | Oxidation | 1800 | ----/66 | sunburst formation of droplets and whiskers |
| -6M | 6040 | 86 | 91 | Melting | 44 | 2.07/3725 | rapid melting, specimen tilted when melting began |
| -7M | 4505 | -9 | 41 | Oxidation | 1800 | ----/41 | little activity, heavy oxide formed |
| -7R | 4955 | - 10 | 209* | Oxidation | 1800 | 209 | little activity |
| -8R | 5665 | --- | 614* | Melting | 23 | 36000 | rapid melting |
| -9R | 5775 | 278 | 404* | Melting | 20 | 36000 | rapid melting |
| -10R | 5030 | - 10 | 32 | Oxidation | 1800 | 32 | speckled appearance due to graphite flakes, uniform heating and recession |
| -11R | 4765 | - 10 | 34 | Oxidation | 1800 | 34 | same as 10R |
| -12M | 4770 | - 34 | 89 | Oxidation | 1800 | 89 | heavy oxide, sample loose on stinger, rotating and vibrating |
| -14M | 4960 | - 10 | 42 | Oxidation | 1800 | 42 | heavy oxide, sample loose on stinger |
| -15M | 3900 | - 55 | 64 | Oxidation | 1800 | 64 | puffy oxide formed |
| -16MA | 4430 | --- | --- | Oxidation | 150 | 30 | heavy oxide formed |
| -16MB | 4170 | - 4 | 30 | Oxidation | 1650 | | |
| -17M | 6325 | --- | 227 | Melting | 65 | 6286 | rapid melting and recession |
| -18R | 5375 | - 14 | 49 | Oxidation | 1350 | 65 | gradual oxide formation, little activity |

*Broken specimens, could not be measured accurately.

*Recession rates converted to thirty minutes on linear basis.

# TABLE 24

## SUMMARY OF ARC PLASMA EXPOSURES OF JTA(D-13)

| Material Sample No. Assumed Emittance at λ = 0.65μ | Mach No. | $P_e$ atm | $i_e$ BTU/lb | D (in) | $q_{cw}$ BTU/ft²sec | T °R obs | $q_r$ Surface Radiation BTU/ft²sec | $\epsilon_N$ Computed Normal Emittance | Initial Length/thickness (mils) | Final Length*/thickness (mils) | Exposure Time (seconds) | Calculated Temperature Ratio T(CALC)/T(OBS) Cold Wall Heat Transfer Coefficient | Fay and Riddell Heat Transfer Coefficient |
|---|---|---|---|---|---|---|---|---|---|---|---|---|---|
| JTA (D-13) | | | | | | | | | | | | | |
| ε = 0.75 | | | | | | | | | | | | | |
| -21M | 0.42 | 1.11 | 2515 | 0.489 | 730 | 4550 | 54 | 0.26 | 1015/1015 | 1000/992 | 132 | 1.13 | 0.98 |
| -22M | 0.32 | 1.06 | 3075 | 0.488 | 460 | 4210 | 60 | 0.40 | 1050/1050 | 1048/977 | 1830 | 1.18 | 1.12 |
| -23M | 0.33 | 1.07 | 4510 | 0.486 | 600 | ---- | --- | ---- | 1050/1050 | ----/--- | 6 | ---- | ---- |
| Four Disks Thermal Shocked Off Front | | | | | | | | | Four Disks Thermal Shocked Off Front | | | | |
| -24M | 0.12 | 1.06 | 4575 | 0.490 | 490 | ---- | --- | ---- | 1032/1032 | ----/--- | 11 | ---- | ---- |
| Six Disks Thermal Shocked Off Front | | | | | | | | | Six Disks Thermal Shocked Off Front | | | | |
| -1M | 0.32 | 1.07 | 3395 | 0.488 | 450 | 4210 | 65 | 0.44 | 986/674 | 975/628 | 1830 | 1.20 | 1.16 |
| -2M | 0.34 | 1.07 | 4920 | 0.488 | 660 | 5450 | 202 | 0.49 | 997/673 | 547/210 | 274 | 1.05 | 1.03 |
| -3M | 0.38 | 1.09 | 6425 | 0.488 | 980 | ---- | --- | ---- | 1011/693 | ----/--- | 21 | ---- | ---- |
| Three Disks Thermal Shocked Off Front | | | | | | | | | Three Disks Thermal Shocked Off Front | | | | |
| -4M | 0.36 | 1.08 | 4320 | 0.488 | 660 | 5020 | 190 | 0.64 | 998/645 | 466/125 | 214 | 1.12 | 1.07 |
| -5M | 0.38 | 1.09 | 5110 | 0.488 | 930 | ---- | --- | ---- | 978/658 | ----/--- | 6 | ---- | ---- |
| Four Disks Thermal Shocked Off Front | | | | | | | | | Four Disks Thermal Shocked Off Front | | | | |
| -6M | 0.36 | 1.08 | 4765 | 0.488 | 810 | 5080 | 135 | 0.43 | 992/673 | 709/369 | 87 | 1.18 | 1.08 |
| -7R† | 3.2 | 0.074 | 9520 | 0.488 | 506 | 5125 | 238 | 0.73 | 1000/681 | 977/637 | 1800 | 1.12 | 1.08 |
| -8R† | 3.2 | 0.164 | 7310 | 0.490 | 770 | 5765 | --- | ---- | 1005/713 | 449/132 | 180 | 1.07 | 0.97 |
| -9R† | 3.2 | 0.151 | 7260 | 0.489 | 771 | 5765 | 514 | 0.60 | 1003/692 | 425/97 | 180 | 1.07 | 0.96 |
| -10R† | 3.2 | 0.208 | 9110 | 0.488 | 945 | 6125 | 461 | 0.70 | 998/663 | 657/312 | 120 | 1.10 | 1.03 |
| -31MX | 0.33 | 1.07 | 5110 | 0.496 | 635 | 5210 | 170 | 0.49 | 691/682 | 215/198 | 175 | 1.10 | 1.10 |
| -32MXA | 0.33 | 1.07 | 4215 | 0.496 | 630 | 5215 | 190 | 0.55 | 680/678 | ---/--- | 300 | 1.07 | 1.02 |
| -32MXB | 0.33 | 1.07 | 4215 | 0.496 | 630 | 4395 | --- | ---- | ---/--- | 118/108 | 1500 | 1.26 | 1.21 |
| -33MXA | 0.31 | 1.06 | 3855 | 0.495 | 540 | 4845 | 184 | 0.71 | 689/682 | ---/--- | 200 | 1.10 | 1.06 |
| -33MXB | 0.31 | 1.06 | 3855 | 0.495 | 540 | 4395 | 86 | 0.49 | ---/--- | 426/381 | 1600 | 1.21 | 1.16 |
| -34MXA | 0.31 | 1.06 | 3780 | 0.495 | 490 | 4705 | 175 | 0.76 | 689/677 | ---/--- | 300 | 1.11 | 1.08 |
| -34MXB | 0.31 | 1.06 | 3780 | 0.495 | 490 | 4415 | 99 | 0.55 | ---/--- | 411/395 | 1500 | 1.18 | 1.15 |
| -35MXA | 0.33 | 1.07 | 4250 | 0.495 | 625 | 5160 | 192 | 0.58 | 692/684 | ---/--- | 200 | 1.08 | 1.03 |
| -35MXB | 0.33 | 1.07 | 4250 | 0.495 | 625 | 4365 | --- | ---- | ---/--- | 87/58 | 238 | 1.27 | 1.22 |
| -36MX | 0.35 | 1.08 | 4960 | 0.495 | 780 | 5340 | 164 | 0.43 | 695/686 | 92/82 | 143 | 1.11 | 1.08 |
| -37MX | 0.36 | 1.08 | 5805 | 0.496 | 860 | 6190 | 164 | 0.34 | 690/680 | 391/304 | 63 | 1.00 | 0.96 |
| -38MX | 0.35 | 1.08 | 5145 | 0.495 | 825 | 5635 | 162 | 0.39 | 693/679 | 127/105 | 132 | 1.11 | 1.05 |
| -39MX | 0.36 | 1.08 | 5505 | 0.495 | 820 | 5955 | 134 | 0.23 | 721/677 | 228/203 | 100 | 1.02 | 0.98 |
| -40MX | 0.36 | 1.08 | 5735 | 0.495 | 845 | 5955 | 114 | 0.19 | 696/687 | ---/246 | 102 | 1.05 | 0.99 |
| -41MX | 0.36 | 1.08 | 5395 | 0.495 | 830 | 5310 | 124 | 0.33 | 693/682 | ---/206 | 111 | 1.14 | 1.09 |
| -42M** | 0.71 | 1.33 | 3100 | 0.435 | 650 | 6020 | 220 | 0.36 | 845/836 | 471/412 | 51 | 0.88 | 0.85 |
| -43MA** | 0.37 | 1.08 | 3160 | 0.437 | 445 | 5645 | 246 | 0.59 | 862/880 | ---/--- | 110 | 0.91 | 0.90 |
| -43MB** | 0.37 | 1.08 | 3160 | 0.437 | 445 | 4635 | --- | ---- | ---/--- | 371/330 | 1690 | 1.12 | 1.10 |
| -44MA** | 0.37 | 1.08 | 3340 | 0.433 | 500 | 5490 | 235 | 0.57 | 893/896 | ---/--- | 80 | 0.93 | 0.91 |
| -44MB** | 0.37 | 1.08 | 3340 | 0.433 | 500 | 4480 | --- | ---- | ---/--- | 277/246 | 1750 | 1.14 | 1.11 |
| -45MA** | 0.36 | 1.08 | 3060 | 0.435 | 380 | 4810 | 164 | 0.65 | 862/861 | ---/--- | 35 | 1.00 | 1.00 |
| -45MB | 0.36 | 1.08 | 3060 | 0.435 | 380 | 4525 | --- | ---- | ---/--- | 717/654 | 1765 | 1.06 | 1.07 |

**Preoxidized 30 minutes at 1650°C.

†Transmissivity factor equals 0.86 for sapphire window.

*Final length is based on measurement prior to sectioning; thickness refers to length after sectioning.

| Material Sample No. | T °F | Gross Recession mils | Material Recession mils | Degradation Mode | Exposure Time seconds | Recession Rate* (mils)/(30 min) | Description of Motion Picture Film Coverage |
|---|---|---|---|---|---|---|---|
| JTA (D-13) | | | | | | | |
| -21M | 4090 | 15 | 23 | Oxidation | 132 | 314 | no film coverage |
| -22M | 3750 | 2 | 73 | Oxidation | 1830 | 72 | no film coverage |
| -23M | ---- | --- | -- | Th. Shock | 6 | ---- | no film coverage |
| -24M | ---- | --- | -- | Th. Shock | 11 | ---- | no film coverage |
| -1M | 3750 | 11 | 46 | Oxidation | 1830 | 45 | no film coverage |
| -2M | 4990 | 450 | 463 | Oxidation | 274 | 3042 | hot liquid oxide, sunburst formation, apparent cooling of front face |
| -3M | ---- | --- | --- | Th. Shock | 21 | ---- | rapid oxidation, thermal shock failure |
| -4M | 4560 | 532 | 520 | Oxidation | 214 | 4378 | liquid oxide continually boiled off |
| -5M | ---- | --- | --- | Th. Shock | 6 | ---- | thermal shock failure |
| -6M | 4620 | 283 | 304 | Oxidation | 87 | 6290 | liquid oxide continually boiled off |
| -7R | 4669 | 23 | 44 | Oxidation | 1800 | 44 | no film coverage |
| -8R | 5305 | 556 | 581 | Oxidation | 180 | 5810 | oxide melting, rapid recession, formed rounded nose |
| -9R | 5305 | 578 | 595 | Oxidation | 180 | 5950 | oxide melting, rapid recession, formed rounded nose |
| -10R | 5665 | 341 | 351 | Oxidation | 120 | 5265 | oxide melting, rapid recession, formed rounded nose |
| -31MX | 4750 | 476 | 484 | Oxidation | 175 | | Sunburst formation. oxide continued to melt. |
| -32MXA | 4795 | --- | --- | Oxidation | 300 | 4978 | Sunburst formation, slow melting of oxide |
| -32MXB | 3935 | 570 | 570 | Oxidation | 1500 | 570 | throughout run. |
| -33MXA | 4385 | --- | --- | Oxidation | 200 | | Same as 32MX. |
| -33MXB | 3935 | 263 | 301 | Oxidation | 1400 | 301 | |
| -34MXA | 4245 | --- | --- | Oxidation | 300 | | Same as 32MX. |
| -34MXB | 3955 | 276 | 282 | Oxidation | 1500 | 282 | |
| -35MXA | 4700 | --- | --- | Oxidation | 200 | | Same as 31MX. |
| -35MXB | 3905 | 605 | 626 | Oxidation | 238 | 2572 | |
| -36MX | 4880 | 603 | 604 | Oxidation | 143 | 7603 | Front surface melted throughout run. |
| -37MX | 5730 | 299 | 376 | Oxidation | 63 | 10742 | Rapid melting. |
| -38MX | 4975 | 566 | 574 | Oxidation | 132 | 7827 | Front surface melted throughout run, recession at angle. |
| -39MX | 5495 | 493 | 474 | Oxidation | 100 | 8532 | First gradual melting of front face, then rapid melting. |
| -40MX | 5495 | --- | 441 | Oxidation | 102 | 7782 | Same as 39MX. |
| -41MX | 4850 | --- | 476 | Oxidation | 111 | 7719 | Same as 39MX. |
| -42M | 5460 | 372 | 424 | Melting | 51 | 14965 | Immediate melting. |
| -43MA | 4985 | --- | --- | Melting | 110 | | Oxide melting, solidified in sunburst, some |
| -43MB | 3975 | 491 | 550 | Oxidation | 1690 | 550 | additional melting. |
| -44MA | 5030 | --- | --- | Melting | 50 | | Oxide melting, solidified in sunburst. |
| -44MB | 4020 | 616 | 650 | Oxidation | 1750 | 650 | |
| -45MA | 4150 | --- | --- | Melting | 35 | | Oxide melting, solidified in sunburst. |
| -45MB | 4065 | 145 | 207 | Oxidation | 1765 | 207 | |

*Recession rate converted to 30 minutes on linear basis.

# TABLE 25

## SUMMARY OF ARC PLASMA EXPOSURES OF JTA(D-13)

| Material Sample No. Assumed Emittance at $\lambda$ = 0.65 $\mu$ | Mach No. | $P_e$ atm | $i_e$ BTU/lb | D (in) | $q_{cw}$ BTU/ft$^2$sec | T °R obs | $q_r$ Surface Radiation BTU/ft$^2$sec | $\epsilon_N$ Computed Normal Emittance | Initial Length/Thickness (mils) | Final Length*/Thickness (mils) | Exposure Time (seconds) | Calculated Temperature Ratio T(CALC)/T (OBS) Cold Wall Heat Transfer Coefficient | Fay and Riddell Heat Transfer Coefficient |
|---|---|---|---|---|---|---|---|---|---|---|---|---|---|
| JTA (D-13) $\epsilon$ = 0.75 | | | | | | | | | | | | | |
| -48MXI | 0.15 | 1.01 | 4070 | 0.504 | 380 | 4225 | 98 | 0.65 | 689/684 | ---/--- | 1800 | 1.19 | 1.15 |
| -48MXII | 0.17 | 1.01 | 4270 | 0.504 | 379 | 4480 | 122 | 0.64 | ---/--- | ---/--- | 1800 | 1.13 | 1.12 |
| -48MXIII | 0.17 | 1.01 | 4670 | 0.504 | 376 | 4545 | 139 | 0.69 | ---/--- | ---/--- | 1800 | 1.12 | 1.13 |
| -48MXIV | 0.17 | 1.01 | 4610 | 0.504 | 370 | 4715 | 143 | 0.62 | ---/--- | 637/566 | 1800 | 1.08 | 1.09 |
| -49RXI | 3.2 | 0.057 | 9590 | 0.503 | 440 | 4765 | 162 | 0.67 | 1025/685 | ---/--- | 1800 | 1.21 | 1.16 |
| -49RXII | 3.2 | 0.057 | 9600 | 0.503 | 446 | 4910 | 174 | 0.64 | ---/--- | ---/--- | 1800 | 1.17 | 1.13 |
| -49RXIII | 3.2 | 0.057 | 9700 | 0.503 | 440 | 4980 | 184 | 0.64 | ---/--- | ---/--- | 1800 | 1.16 | 1.11 |
| -49RXIV | 3.2 | 0.055 | 9420 | 0.503 | 440 | 4835 | 176 | 0.69 | ---/--- | 976/640 | 1800 | 1.19 | 1.13 |

Note: Samples all cut from cylindrical billet perpendicular to billet axis (pressing direction).

*Final length refers to measurement after exposure, thickness refers to length after sectioning.

| Material Sample No. | T °F | Gross Recession (mils) | Material Recession (mils) | Degradation Mode | Exposure Time seconds | Recession Rate* mils/30 min | Description of Motion Picture Film Coverage |
|---|---|---|---|---|---|---|---|
| JTA (D-13) | | | | | | | |
| -48MXI | 3765 | --- | --- | Oxidation | 1800 | --- | Oxide formed, slow melting in irregular manner. |
| -48MXII | 4020 | --- | --- | Oxidation | 1800 | --- | No change from cycle I, slight oxide melting. |
| -48MXIII | 4085 | --- | --- | Oxidation | 1800 | --- | No change from cycle II, slight oxide melting. |
| -48MXIV | 4255 | 52 | 118 | Oxidation | 1800 | 30 | No change from cycle III, slight oxide melting. |
| -49RXI | 4305 | --- | --- | Oxidation | 1800 | --- | Slow, spotty oxide buildup to uniform layer. |
| -49RXII | 4450 | --- | --- | Oxidation | 1800 | --- | No change from cycle I, some edge chipping. |
| -49RXIII | 4520 | --- | --- | Oxidation | 1800 | --- | No change from cycle II, slight edge chipping. |
| -49RXIV | 4375 | 49 | 45 | Oxidation | 1800 | 11 | No change from cycle III, slight edge chipping. |

*Converted to thirty minutes on a linear basis.

# TABLE 26

## SUMMARY OF ARC PLASMA EXPOSURES OF KT-SiC(E-14)

| Material Sample No. Assumed Emittance at λ = 0.65μ | Mach No. | $P_e$ atm | $i_e$ BTU/lb | D (in) | $q_{cw}$ BTU/ft²sec | T °R obs | $q_r$ Surface Radiation BTU/ft²sec | $\epsilon_N$ Computed Normal Emittance | Initial Length/Thickness (mils) | Final Length/Thickness (mils) | Exposure Time (seconds) | Calculated Temperature Ratio T(CALC)/T(OBS) Cold Wall Heat Transfer Coefficient | Fay and Riddell Heat Transfer Coefficient |
|---|---|---|---|---|---|---|---|---|---|---|---|---|---|
| KT-SiC(E-14) | | | | | | | | | | | | | |
| ε = 0.76 | | | | | | | | | | | | | |
| -1M | 0.32 | 1.06 | 3090 | 0.490 | 480 | 3850 | 95 | 0.53 | 983/983 | 993/983 | 1835 | 1.32 | 1.25 |
| -2M | 0.35 | 1.07 | 3170 | 0.490 | 348 | 3495 | 23 | 0.33 | 992/992 | 998/989 | 1800 | 1.39 | 1.43 |
| -3M | 0.39 | 1.10 | 3280 | 0.491 | 810 | 3740 | 56 | 0.61 | 984/984 | 994/980 | 656 | 1.39 | 1.33 |
| -4M | 0.33 | 1.07 | 4155 | 0.491 | 600 | 4130 | 60 | 0.44 | 841/841 | 860/834 | 1835 | 1.35 | 1.29 |
| -5M | 0.36 | 1.08 | 4910 | 0.490 | 810 | 4850 | 101 | 0.39 | 988/674 | ---/249 | 165 | 1.24 | 1.17 |
| -6M | 0.36 | 1.08 | 4285 | 0.490 | 710 | 4885 | 151 | 0.56 | 991/680 | ---/0 | 124 | 1.18 | 1.11 |
| -7M | 0.35 | 1.08 | 3130 | 0.490 | 540 | 4255 | 90 | 0.58 | 990/678 | 989/656 | 1830 | 1.22 | 1.15 |
| | Longitudinal Crack | | | | | | | | | | | | |
| -8M | 0.35 | 1.08 | 4135 | 0.490 | 520 | 4105 | 58 | 0.66 | 985/678 | 969/644 | 1830 | 1.32 | 1.31 |
| | Longitudinal Crack | | | | | | | | | | | | |
| -1R* | 3.2 | 0.075 | 9720 | 0.489 | 487 | 3325 | 41 | 0.71 | 991/676 | 985/668 | 1800 | 1.80 | 1.75 |
| -2R* | 3.2 | 0.163 | 7200 | 0.491 | 781 | 5000 | 183 | 0.62 | 990/669 | 312/15 | 160 | 1.28 | 1.16 |
| -3R* | 3.2 | 0.068 | 11360 | 0.490 | 607 | 3640 | 69 | 0.83 | 991/675 | 976/668 | 1800 | 1.74 | 1.65 |
| -4R* | 3.2 | 0.150 | 7690 | 0.487 | 691 | 4910 | 220 | 0.81 | 990/681 | 417/100 | 170 | 1.29 | 1.21 |
| -5R* | 3.2 | 0.068 | 11710 | 0.491 | 687 | 3630 | 66 | 0.81 | 990/672 | 979/656 | 800 | 1.78 | 1.67 |
| -6R* | 3.2 | 0.100 | 11820 | 0.490 | 697 | 4885 | 212 | 0.79 | 990/685 | 517/202 | 200 | 1.34 | 1.30 |
| -7R* | 3.2 | 0.097 | 10880 | 0.490 | 652 | 3500 | 59 | 0.84 | 990/679 | 979/655 | 1800 | 1.84 | 1.77 |

*Transmissivity factor equals 0.86 for sapphire window.

*Final length is based on measurement prior to sectioning; thickness refers to length after sectioning.

| Material Sample No. | T °F | Gross Recession mils | Material Recession mils | Degradation Mode | Exposure Time seconds | Recession Rate* (mils)/(30 min) | Description of Motion Picture Film Coverage |
|---|---|---|---|---|---|---|---|
| KT-SiC (E-14) | | | | | | | |
| -1M | 3190 | -10 | 0 | Oxidation | 1835 | 0 | liquid present, bubbling, droplets swept to outside rim |
| -2M | 3035 | -3 | 3 | Oxidation | 1800 | 3 | no film coverage |
| -3M | 3280 | -10 | 4 | Oxidation | 656 | 11 | liquid present, bubbling, droplets swept to outside rim |
| -4M | 3670 | 1 | 7 | Oxidation | 1835 | 7 | no film coverage |
| -5M | 4190 | --- | 425 | Oxid + Vapor | 165 | 4627 | rapid ablation |
| -6M | 4425 | --- | 460 | Oxid + Vapor | 124 | 9874 | surface activity, liquid oxide, rapid ablation |
| -7M | 3795 | 1 | 22 | Oxidation | 1830 | 22 | liquid oxide, bubbling due to gas evolution |
| -8M | 3645 | 16 | 34 | Oxidation | 1830 | 35 | liquid oxide, bubbling due to gas evolution |
| -1R | 2865 | 6 | 8 | Oxidation | 1800 | 8 | no film coverage |
| -2R | 4840 | 678 | 654 | Oxid + Vapor | 160 | 7388 | rapid recession |
| -3R | 3180 | 15 | 7 | Oxidation | 1800 | 7 | no film coverage |
| -4R | 4480 | 973 | 881 | Oxid + Vapor | 170 | 6047 | uniform heating, sudden brightening, then rapid vaporization |
| -5R | 3170 | 11 | 16 | Oxidation | 800 | 36 | uniform heating, little activity |
| -6R | 4425 | 473 | 465 | Oxid + Vapor | 200 | 4347 | heated from edge to center, rapid recession by vaporization |
| -7R | 3040 | 11 | 24 | Oxidation | 1800 | 24 | uniform heating, little activity |

*Recession rate converted to 30 minutes on linear basis.

# TABLE 27

## SUMMARY OF ARC PLASMA EXPOSURES OF JT0 992(F-15)

| Material Sample No. Assumed Emittance at λ = 0.65μ | Mach No. | $P_e$ atm | $i_e$ BTU/lb | D /in | $q_{cw}$ BTU/ft²sec | T °R obs | $q_r$ Surface Radiation BTU/ft²sec | $\epsilon_N$ Computed Normal Emittance | Initial Length/thickness (mils) | Final Length*/thickness (mils) | Exposure Time (seconds) | Calculated Temperature Ratio T(CALC)/T(OBS) Cold Wall Heat Transfer Coefficient | Fay and Riddell Heat Transfer Coefficient |
|---|---|---|---|---|---|---|---|---|---|---|---|---|---|
| JT0992 (F-15) | | | | | | | | | | | | | |
| ε = 0.75 | | | | | | | | | | | | | |
| -1M | 0.43 | 1.12 | 5340 | 0.487 | 870 | 6160 | 289 | 0.42 | 1038/1038 | 462/420 | 377 | 0.99 | 0.99 |
| -2M | 0.35 | 1.07 | 2105 | 0.486 | 430 | 3930 | 104 | 0.93 | 1033/1033 | ---/999 | 1173 | 1.15 | 1.06 |
| -3M | 0.40 | 1.10 | 4285 | 0.487 | 770 | 5390 | 348 | 0.87 | 1054/1054 | 735/692 | 300 | 1.07 | 1.04 |
| -4M | 0.40 | 1.10 | 4900 | 0.488 | 860 | 5370 | 227 | 0.58 | 1034/1034 | 618/553 | 480 | 1.12 | 1.09 |
| -5M | 0.49 | 1.14 | 3540 | 0.487 | 740 | 5030 | 160 | 0.53 | 1063/1063 | 645/619 | 485 | 1.11 | 1.09 |
| -6M | 0.36 | 1.08 | 4155 | 0.487 | 660 | 4600 | 242 | 1.14 | 1016/1016 | 970/953 | 161 | 1.22 | 1.17 |
| -4R† | 3.2 | 0.013 | 7380 | 0.489 | 151 | 4270 | 46* | 0.29* | 1010/1010 | 969/957 | 1800 | 1.01 | 0.99 |
| -8R† | 3.2 | 0.014 | 9220 | 0.485 | 218 | 4845 | 97* | 0.37* | 990/990 | 995/968 | 1800 | 0.98 | 0.94 |
| -6R† | 3.2 | 0.014 | 13730 | 0.489 | 308 | 5380 | 184* | 0.46* | 1000/1000 | 1000/971 | 1800 | 0.97 | 0.94 |
| -5R† | 3.2 | 0.027 | 14550 | 0.487 | 500 | 5685 | 213* | 0.43* | 988/988 | 860/865 | 1200 | 1.03 | 0.98 |
| -1R† | 3.2 | 0.187 | 9240 | 0.489 | 950 | 6015 | 114* | 0.18* | 1005/1005 | 667/668 | 135 | 1.10 | 1.01 |
| -2R† | 3.2 | 0.287 | 9190 | 0.488 | 1145 | 6090 | 393* | 0.60* | 994/994 | 597/594 | 110 | 1.13 | 1.05 |
| -3R† | 3.2 | 0.163 | 8470 | 0.489 | 790 | ---- | --- | ---- | 971/971 | ---/--- | ---- | ---- | ---- |
| | Four Disks Thermal Shocked Off Front | | | | | | | | | | | | |
| -7R† | 3.2 | 0.013 | 9600 | 0.488 | 224 | ---- | --- | ---- | 1012/1012 | ---/--- | ---- | ---- | ---- |
| | Two Disks Thermal Shocked Off Front | | | | | | | | | | | | |

†Transmissivity factor equals 0.86 for sapphire window.
*Surface radiation values may be low due to requirements for critical alignment caused by utilization of one-half inch diameter samples.

*Final length is based on measurement prior to sectioning, thickness refers to length after sectioning.

| Material Sample No. | T °F | Gross Recession mils | Material Recession mils | Degradation Mode | Exposure Time seconds | Recession Rate* (mils) (30 min) | Description of Motion Picture Film Coverage |
|---|---|---|---|---|---|---|---|
| JT0991 (F-15) | | | | | | | |
| -1M | 5700 | 576 | 618 | Oxid + Melting | 377 | 2948 | liquid formation, bubbling, oxide stringers, sunburst configuration |
| -2M | 3470 | --- | 34 | Oxidation | 1173 | 52 | oxide formation, little activity, sample vibration |
| -3M | 4930 | 319 | 362 | Oxid + Melting | 300 | 2172 | liquid oxide, stringers, sunburst configuration |
| -4M | 4910 | 416 | 481 | Oxid + Melting | 480 | 1804 | no film coverage |
| -5M | 4570 | 418 | 444 | Oxid + Melting | 485 | 1648 | no film coverage |
| -6M | 4140 | 46 | 61 | Oxid + Melting | 161 | 1118 | no film coverage |
| -4R | 3810 | 41 | 53 | Oxidation | 1800 | 53 | little activity, slight oxidation |
| -8R | 4385 | -5 | 22 | Oxidation | 1800 | 22 | little activity, slight oxidation |
| -6R | 4920 | 0 | 29 | Oxidation | 1800 | 29 | little activity, slight oxidation |
| -5R | 5225 | 128 | 123 | Oxidation | 1200 | 185 | uniform heating, oxide melting, sunburst formation, uniform recession |
| -1R | 5555 | 336 | 337 | Oxid + Melting | 135 | 449 | oxide melting, recession |
| -2R | 5630 | 397 | 400 | Oxid + Melting | 110 | 6544 | oxide melting, recession |
| -3R | ---- | --- | --- | Th. Shock | ---- | ---- | delamination |
| -7R | ---- | --- | --- | Th. Shock | ---- | ---- | delamination |

*Recession rate converted to 30 minutes on linear basis.

# TABLE 28

## SUMMARY OF ARC PLASMA EXPOSURES OF JT0981(F-16)

| Material Sample No. Assumed Emittance at λ = 0.65μ | Mach No | $P_e$ atm | $I_e$ BTU/lb | D (in) | $q_{cw}$ BTU/ft²sec | T °R obs | $q_r$ Surface Radiation BTU/ft²sec | $q_N$ Computed Normal Emittance | Initial Length/thickness (mils) | Final Length*/thickness (mils) | Exposure Time (seconds) | Calculated Temperature Ratio T(CALC)/T(OBS) Cold Wall Heat Transfer Coefficient | Fay and Riddell Heat Transfer Coefficient |
|---|---|---|---|---|---|---|---|---|---|---|---|---|---|
| JT0981 (F-16) | | | | | | | | | | | | | |
| ε = 0.75 | | | | | | | | | | | | | |
| -21M | 0.30 | 1.05 | 2565 | 0.489 | 460 | ---- | --- | ---- | 1077/1077 | ---/--- | 7 | ---- | ---- |
| | One Disk Thermal Shocked Off Front | | | | | | | | | | | | |
| -22M | 0.32 | 1.06 | 3230 | 0.490 | 460 | 4330 | 60 | 0.36 | 1055/1055 | ---/--- | 1830 | 1.16 | 1.10 |
| | Thermal Shocked After Test | | | | | | | | | | | | |
| -23M | 0.33 | 1.07 | 4510 | 0.489 | 600 | ---- | --- | ---- | 1041/1041 | ---/--- | 6 | ---- | ---- |
| | Five Disks Thermal Shocked Off Front | | | | | | | | | | | | |
| -24M | 0.33 | 1.07 | 4510 | 0.490 | 600 | ---- | --- | ---- | 1073/1073 | ---/--- | 6 | ---- | ---- |
| | Six Disks Thermal Shocked Off Front | | | | | | | | | | | | |
| -2M | 0.36 | 1.08 | 4460 | 0.488 | 710 | 5570 | --- | ---- | 1000/662 | ---/162 | 115 | 1.03 | 0.98 |
| | One 136 Mil Thick Disk Thermal Shocked Off Front | | | | | | | | | | | | |
| -3M | 0.34 | 1.08 | 3900 | 0.488 | 670 | 5940 | 187 | 0.32 | 1000/631 | 774/400 | 70 | 0.93 | 0.88 |
| -4M | 0.35 | 1.08 | 3475 | 0.488 | 640 | 5650 | 192 | 0.46 | 998/565 | 603/266 | 148 | 0.99 | 0.92 |
| -5M | 0.32 | 1.06 | 2485 | 0.490 | 390 | 4370 | 61 | 0.35 | 1000/692 | 900/586 | 1830 | 1.06 | 1.01 |
| -6M | 0.34 | 1.07 | 4730 | 0.490 | 670 | ---- | --- | ---- | 997/675 | ---/--- | 173 | ---- | ---- |
| | Five Disks Thermal Shocked Off Front | | | | | | | | | | | | |
| -7M | 0.38 | 1.09 | 6160 | 0.488 | 950 | ---- | --- | ---- | 986/642 | ---/--- | 8 | ---- | ---- |
| | Three Disks Thermal Shocked Off | | | | | | | | | | | | |
| -8R† | 3.2 | 0.075 | 9650 | 0.489 | 512 | ---- | --- | ---- | 1017/676 | ---/--- | 13 | ---- | ---- |
| | Thermal Shock Failure | | | | | | | | | | | | |
| -9R† | 3.2 | 0.075 | 9120 | 0.488 | 523 | 5155 | 251 | 0.75 | 998/696 | 975/655 | 1800 | 1.12 | 1.06 |
| -1R† | 3.2 | 0.179 | 7430 | 0.489 | 747 | 5525 | 253 | 0.57 | 1014/694 | 659/338 | 150 | 1.11 | 1.03 |
| -10R† | 3.2 | 0.179 | 7430 | 0.488 | 751 | 5605 | 274 | 0.59 | 1013/675 | 626/299 | 126 | 1.10 | 1.01 |
| | Apparent Surface Delamination | | | | | | | | | | | | |
| -11R† | 3.2 | 0.208 | 9350 | 0.489 | 950 | 6070 | 395 | 0.62 | 996/667 | ---/--- | 100 | 1.12 | 1.05 |
| | Four Disks Thermal Shocked Off Front | | | | | | | | | | | | |

†Transmissivity factor equals 0.86 for sapphire window.

*Final length is based on measurement prior to sectioning, thickness refers to length after sectioning.

| Material Sample No. | T °F | Gross Recession mils | Gross Recession mils | Degradation Mode | Exposure Time seconds | Recession Rate* (mils) (30 min) | Description of Motion Picture Film Coverage |
|---|---|---|---|---|---|---|---|
| JT0981 (F-16) | | | | | | | |
| -21M | ---- | --- | --- | Th. Shock | 6 | | |
| -22M | 3870 | --- | --- | Oxid + Th. Shock | 1830 | ---- | |
| -23M | ---- | --- | --- | Th. Shock | 6 | ---- | no film coverage |
| -24M | ---- | --- | --- | Th. Shock | 6 | ---- | |
| -2M | 5110 | --- | 364 | Th. Shock + Oxid | 115 | 5697 | thermal shock, oxidation, bubbling |
| -3M | 5480 | 226 | 231 | Oxidation | 70 | 5939 | boiling of liquid oxide |
| -4M | 4990 | 395 | 299 | Oxidation | 148 | 3636 | boiling of liquid oxide |
| -5M | 3910 | 100 | 106 | Oxidation | 1830 | 108 | no film coverage |
| -6M | ---- | --- | --- | Th. Shock | 173 | ---- | thermal shock |
| -7M | ---- | --- | --- | Th. Shock | 8 | ---- | thermal shock |
| -8R | ---- | --- | --- | Th. Shock | 13 | | |
| -9R | 4695 | 23 | 41 | Oxidation | 1800 | 41 | little activity, uniform oxidation |
| -1R | 5065 | 355 | 356 | Oxid + Melting | 150 | 4272 | oxide melted, melting and rapid recession followed |
| -10R | 5145 | 391 | 376 | Oxid + Melting | 126 | 5173 | oxide melted, melting and rapid recession followed |
| -11R | 5610 | --- | --- | Th. Shock + Oxid + Melting | 100 | ---- | front face thermal shocked off during heat-up, but stuck to specimen, liquid formed, then front face flew off and melting continued. |

*Recession rate converted to 30 minutes on linear basis.

TABLE 29

SUMMARY OF ARC PLASMA TESTS IN NITROGEN TO MEASURE THE MELTING POINTS OF MOLYBDENUM AND TUNGSTEN

Mo (Accepted Melting Point = 5220°R, $\epsilon_{\lambda = 0.65} = 0.30$)

Measured Value (Model 500) = 5250 ± 30°R
Measured Value (ROVERS ) = 5190 ± 30°R

W (Accepted Melting Point = 6570°R, $\epsilon_{\lambda = 0.65} = 0.41$)

Measured Value (Model 500) = 6850 ± 110°R
Measured Value (ROVERS ) = 6710 ± 70°R

# TABLE 30

## SUMMARY OF ARC PLASMA EXPOSURES OF $WSi_2$ ON W (G-18)

| Material Sample No. Assumed Emittance at $\lambda = 0.65\mu$ | Mach No. | $P_e$ atm | $i_e$ BTU/lb | D (in) | $q_{cw}$ BTU/ft²sec | T °R | $q_r$ Surface Radiation BTU/ft²sec | $\epsilon_N$ Computed Normal Emittance | Initial Length/Thickness (mils) | Final Length*/Thickness (mils) | Exposure Time (seconds) | Calculated Temperature Ratio T(CALC)/T(OBS) Cold Wall Heat Transfer Coefficient | Fay and Riddell Heat Transfer Coefficient |
|---|---|---|---|---|---|---|---|---|---|---|---|---|---|
| $WSi_2$/W(G-18) $\epsilon$ = 0.60(below 3500°F), 0.55(above 3500°F), 0.40(bareW) | | | | | | | | | | | | | |
| -1M | 0.28 | 1.05 | 2440 | 0.505 | 305 | 3435 | 36 | 0.55 | 761/464 | 768/464 | 1519 | 1.34 | 1.31 |
| -2M | 0.28 | 1.05 | 2330 | 0.504 | 320 | 3360 | 34 | 0.57 | 750/448 | 787/437 | 1830 | 1.36 | 1.31 |
| -3M | 0.29 | 1.05 | 2260 | 0.504 | 330 | 3445 | 37 | 0.53 | 765/449 | 773/447 | 1830 | 1.33 | 1.27 |
| -4M | 0.30 | 1.05 | 2785 | 0.505 | 460 | 3535 | 44 | 0.60 | 763/449 | 779/442 | 1830 | 1.43 | 1.34 |
| -5M | 0.28 | 1.05 | 2680 | 0.504 | 240 | 3085 | 25 | 0.59 | 754/445 | 758/444 | 1830 | 1.46 | 1.80 |
| -6RA† | 3.2 | 0.082 | 7200 | 0.504 | 498 | 3290 | 27 | 0.49 | 765/455 | ---/--- | 700 | 1.90 | 1.76 |
| After 700 seconds arc conditions changed to 6RB | | | | | | | | | | | | | |
| -6RB† | 3.2 | 0.082 | 8310 | 0.504 | 554 | 3245 | 27 | 0.52 | ---/--- | 764/437 | 1100 | 1.86 | 1.71 |
| -7RA† | 3.2 | 0.158 | 8020 | 0.505 | 781 | 4035 | 71 | 0.57 | 764/454 | ---/--- | 300 | 1.69 | 1.55 |
| After 300 seconds, material began burning and conditions changed to 7RB. This may be due to burn off of the 5 mil coating of $WSi_2$. | | | | | | | | | | | | | |
| -7RB† | 3.2 | 0.158 | 8020 | 0.505 | 781 | 5880 | 170 | 0.30 | ---/--- | 719/404 | 50 | 1.20 | 1.10 |
| -8RA† | 3.2 | 0.158 | 7410 | 0.505 | 775 | 3965 | 61 | 0.53 | 761/466 | ---/--- | 270 | 1.70 | 1.54 |
| After 270 seconds, material began burning and conditions changed to 8RB. This may be due to burn off of the 5 mil coating of $WSi_2$. | | | | | | | | | | | | | |
| -8RB† | 3.2 | 0.158 | 7410 | 0.505 | 775 | 6055 | 142 | 0.25 | ---/--- | 471/191 | 280 | 1.15 | 1.05 |
| -9R† | 3.2 | 0.033 | 13400 | 0.503 | 649 | 5975 | 212 | 0.35 | 756/452 | 548/267 | 800 | 1.23 | 1.10 |
| -10RA†3.2 | | 0.023 | 11420 | 0.505 | 458 | ---- | 62 | ---- | 757/441 | ---/--- | 110 | ---- | ---- |
| After 110 seconds, arc conditions changed to 10RB | | | | | | | | | | | | | |
| -10RB†3.2 | | 0.018 | 7200 | 0.505 | 224 | 4330 | 31 | 0.31 | ---/--- | 509/207 | 1090 | 1.28 | 1.19 |
| -11M | 0.36 | 1.08 | 5205 | 0.504 | 785 | 6375 | 164 | 0.21 | 471/451 | ---/345 | 77 | 1.68 | 1.61 |
| -12M | 0.34 | 1.07 | 4095 | 0.503 | 560 | 5510 | 143 | 0.33 | 487/464 | ---/426 | 29 | 1.10 | 1.07 |
| -13M | 0.30 | 1.06 | 4265 | 0.504 | 525 | 6310 | --- | ---- | 464/437 | 301/272 | 127 | 0.95 | 0.94 |
| -14M | 0.26 | 1.04 | 3485 | 0.504 | 440 | 5035 | 82 | 0.27 | 455/452 | ---/--- | 1032 | 1.06 | 1.02 |
| -17M | 0.21 | 1.02 | 3150 | 0.504 | 320 | 3640 | 42 | 0.51 | 104/102** | ---/98 | 1800 | 1.34 | 1.33 |
| -18M | 0.21 | 1.02 | 3280 | 0.504 | 316 | 3490 | 33 | 0.47 | 201/200** | ---/199 | 1800 | 1.40 | 1.41 |
| -19MS | 0.21 | 1.02 | 3380 | 0.500 | 310 | 2880 | 23 | 0.71 | 440/95** | ---/95 | 1800 | 1.70 | 1.70 |
| -20MS | 0.21 | 1.02 | 3160 | 0.500 | 306 | 2970 | 27 | 0.74 | 147/200** | ---/300 | 1800 | 1.63 | 1.62 |
| -21M | 0.28 | 1.04 | 3600 | 0.503 | 396 | 3775 | 54 | 0.57 | 450/453 | 450/453 | 1800 | 1.37 | 1.37 |
| -22M | 0.15 | 1.01 | 4390 | 0.505 | 344 | 3895 | 66 | 0.61 | 454/448 | 458/448 | 1800 | 1.33 | 1.34 |
| -23RA† | 2.2 | 0.232 | 8180 | 0.505 | 699 | 3670 | 52 | 0.61 | 764/461 | ---/--- | 900 | 1.79 | 1.75 |
| -23RB† | 2.2 | 0.232 | 8180 | 0.505 | 699 | 4035 | 63 | 0.51 | ---/--- | ---/--- | --- | 1.66 | 1.62 |
| -23RC† | 2.2 | 0.232 | 8180 | 0.505 | 699 | 4735 | 102 | 0.43 | ---/--- | 741/428 | 166 | 1.41 | 1.38 |
| -24R† | 2.2 | 0.248 | 7460 | 0.505 | 653 | 3455 | 41 | 0.61 | 761/450 | 760/449 | 300 | 1.86 | 1.82 |

†Transmissivity factor equals 0.86 for sapphire window.

* Final length refers to measurement after exposure, thickness refers to measurement after sectioning.

** Nose to in-depth temperature measurement station

| Material Sample No. | T °F | Gross Recession mils | Material Recession mils | Degradation Mode | Exposure Time seconds | Material Sample No. (mils)/(sec) / (mils)/(30 min) | Description of Motion Picture Film Coverage |
|---|---|---|---|---|---|---|---|
| $WSi_2$/W (G-18) | | | | | | | |
| -1M | 2975 | -7 | +2 | $WSi_2$-Oxid | 1519 | ----/0 | uniform oxidation, slight bubbling at edges, coating intact |
| -2M | 2900 | -7 | 11 | $WSi_2$-Oxid | 1830 | ----/11 | uniform oxidation, coating intact |
| -3M | 2985 | -8 | 2 | $WSi_2$-Oxid | 1830 | ----/2 | uniform oxidation, coating intact |
| -4M | 3075 | -16 | 7 | $WSi_2$-Oxid | 1830 | ----/7 | uniform oxidation, coating intact |
| -5M | 2635 | -4 | 1 | $WSi_2$-Oxid | 1830 | ----/1 | uniform oxidation, coating intact |
| -6RA | 2830 | 1 | 18 | $WSi_2$-Oxid | 700 | ----/18 | no film coverage |
| -6RB | 2785 | 1 | 18 | $WSi_2$-Oxid | 1100 | ----/18 | |
| -7RA | 3575 | (10) | (10) | $WSi_2$-Oxid | 300 | ----/(60)* | no film coverage |
| -7RB | 5420 | 38 | 40 | W-Oxid | 50 | 0,80/1440 | |
| -8RA | 3505 | (10) | (10) | $WSi_2$-Oxid | 270 | ----/(67)* | uniform heating, coating failed followed by uniform recession |
| -8RB | 5595 | 180 | 168 | W-Oxid | 280 | 0,98/1710 | |
| -9R | 5515 | 208 | 185 | W-Oxid | 800 | ----/416 | no film coverage |
| -10RA | ---- | (30) | (30) | W-Oxid | 110 | ----/(492)* | no film coverage |
| -10RB | 3870 | 118 | 104 | W-Oxid | 1090 | ----/337 | |
| -11M | 5915 | --- | 106 | W-Oxid | 77 | 1,30/2480 | rapid heat-up, coating burned off, hourglass recession |
| -12M | 5050 | --- | 38 | W-Oxid | 29 | 1,31/2360 | rapid heat-up, coating burned off, hourglass recession |
| -13M | 5850 | 163 | 168 | W-Oxid | 127 | 1,30/2360 | rapid heat-up, coating burned off, hourglass recession |
| -14M | 4575 | --- | --- | $WSi_2$-Oxid | 1032 | ----/---- | coating melted, then solidified, then failed in one spot near edge which eventually spread over entire specimen |
| -17M | 3180 | --- | 4 | $WSi_2$-Oxid, | 1800 | ---/4 | Little activity, |
| -18M | 3030 | --- | 1 | $WSi_2$-Oxid, | 1800 | ---/1 | Little activity, some molten droplets at edge, |
| -19MS | 2420 | --- | 0 | $WSi_2$-Oxid, | 1800 | ---/0 | Little visible, |
| -20MS | 2410 | --- | 0 | $WSi_2$-Oxid, | 1800 | ---/0 | Little visible, |
| -21M | 3315 | 0 | 0 | $WSi_2$-Oxid, | 1800 | ---/0 | Some bubbling at edges, uniform heating, no coating failure, |
| -22M | 3435 | -1 | 0 | $WSi_2$-Oxid, | 1800 | ---/0 | Hot spots at edge well into run, no apparent failure, |
| -23RA | 3210 | --- | --- | $WSi_2$-Oxid, | 900 | ---/8 | Little visible, |
| -23RB | 3575 | --- | --- | W-Oxid, | --- | ---/--- | Probable coating failure, |
| -23RC | 4275 | 23 | 23 | W-Oxid, | 166 | 0,11/206 | Tungsten exposed, |
| -24R | 2995 | 1 | 1 | $WSi_2$-Oxid, | 1800 | ---/1 | Little activity, |

*Recession rate converted to 30 minutes on linear basis.

[a]Estimated.

TABLE 31

SUMMARY OF $W_5Si_3$ ZONE WIDTHS FORMED ON $WSi_2$/W(G-18) DURING ARC PLASMA TESTS

| Test | Temperature (°F) | Time (sec) | Width (mils) |
|---|---|---|---|
| $WSi_2$/W(G-18) | | | |
| -1M | 2975 | 1519 | 0.40 |
| -2M | 2900 | 1830 | 0.40 |
| -3M | 2985 | 1830 | 0.30 |
| -4M | 3075 | 1830 | 0.55 |
| -5M | 2625 | 1830 | 0.15 |
| -6R | 2830/2785 | 1800 | 0.40 |
| -17M | 3180 | 1800 | 1.70 |
| -18M | 3030 | 1800 | 1.15 |
| -21MS | 3315 | 1800 | 1.55 |
| -22MS | 3435 | 1800 | 3.20 |
| -24R | 2995 | 1800 | 1.20 |

# TABLE 32

## SUMMARY OF ARC PLASMA EXPOSURES OF Sn-Al ON Ta-10W (G-19)

| Material Sample No. Assumed Emittance at $\lambda = 0.65\mu$ | Mach No. | $P_e$ atm | $h_e$ BTU/lb | D (in) | $q_{cw}$ BTU/ft²sec | T °R obs | $q_r$ Surface Radiation BTU/ft²sec | $\epsilon_N$ Computed Normal Emittance | Initial Length/Thickness (mils) | Final Length* (Thickness (mils) | Exposure Time (seconds) | Calculated Temperature Ratio T(CALC)/T(OBS) Cold Wall Heat Transfer Coefficient | Fay and Riddell Heat Transfer Coefficient |
|---|---|---|---|---|---|---|---|---|---|---|---|---|---|
| Sn-Al/Ta-W(G-19) $\epsilon = 0.67$(Sn-Al), 0.50(Ta-W) | | | | | | | | | | | | | |
| -1M | 0.32 | 1.06 | 2880 | 0.516 | 390 | 5550 | 194 | 0.44 | 528/368 | 393/244 | 140 | 0.92 | 0.89 |
| Coating Failed - Melting of Ta Observed | | | | | | | | | | | | | |
| -2M | 0.24 | 1.04 | 1360 | 0.516 | 160 | 2565 | 11 | 0.54 | 512/347 | 518/332 | 1930 | 1.38 | 1.35 |
| -3M | 0.28 | 1.05 | 2135 | 0.516 | 270 | 3200 | 31 | 0.63 | 500/355 | 510/352 | 1831 | 1.34 | 1.31 |
| -4M | 0.29 | 1.05 | 2980 | 0.516 | 350 | 3370 | 39 | 0.64 | 530/378 | 542/367 | 1830 | 1.43 | 1.41 |
| -5M | 0.30 | 1.05 | 3230 | 0.516 | 460 | 5770 | 250 | 0.48 | 520/347 | 375/220 | 83 | 0.93 | 0.89 |
| Coating Failed - Melting of Ta Observed | | | | | | | | | | | | | |
| -6R† | 3.2 | 0.061 | 8740 | 0.516 | 514 | 5355 | 67 | 0.17 | 530/371 | ---/258 | 240 | 1.20 | 1.11 |
| Coating Failed - Melting of Ta Observed | | | | | | | | | | | | | |
| -7R† | 3.2 | 0.050 | 7100 | 0.516 | 355 | 3580 | 42 | 0.54 | 483/329 | ---/317 | 1800 | 1.54 | 1.45 |
| -8R† | 3.2 | 0.011 | 11440 | 0.515 | 209 | 4130 | 91 | 0.46 | 525/361 | 500/322 | 400 | 1.29 | 1.27 |
| Coating Failed - Melting of Ta Observed | | | | | | | | | | | | | |
| -9R† | 3.2 | 0.010 | 10520 | 0.515 | 188 | 3325 | 35 | 0.61 | 524/342 | 525/342 | 1800 | 1.41 | 1.43 |
| -10R† | 3.2 | 0.011 | 7940 | 0.516 | 116 | 3075 | 25 | 0.59 | 516/346 | 519/336 | 1800 | 1.41 | 1.45 |
| -11R† | 3.2 | 0.010 | 7220 | 0.516 | 94 | 2965 | 21 | 0.58 | 513/351 | 516/338 | 1804 | 1.38 | 1.45 |
| -12R† | 3.2 | 0.011 | 9400 | 0.516 | 132 | 3230 | 30 | 0.59 | 529/360 | 532/352 | 1800 | 1.39 | 1.45 |

†Transmissivity factor equals 0.86 for sapphire window.

*Final length is based on measurements prior to sectioning; thickness refers to length after sectioning.

| Material Sample No. | T °F | Gross Recession mils | Material Recession mils | Degradation Mode | Exposure Time seconds | Recession Rate* (mils/sec) / (mils/30 min) | Description of Motion Picture Film Coverage |
|---|---|---|---|---|---|---|---|
| Sn-Al on Ta-10W(G-19) | | | | | | | |
| -1M | 5090 | 135 | 124 | Ta-10W Melting | 140 | ----/1595 | |
| -2M | 2105 | -6 | 15 | Sn-Al Oxid | 1830 | ----/15 | little activity, coating did not fail |
| -3M | 2740 | -10 | 23 | Sn-Al Oxid | 1831 | ----/23 | surface activity, some liquid bubbles, no coating failure |
| -4M | 2910 | -12 | 11 | Sn-Al Oxid | 1830 | ----/11 | surface activity, some liquid bubbles, no coating failure |
| -5M | 5310 | 145 | 127 | Ta-10W Melting | 83 | ----/2753 | coating melted 20 seconds into run, totally burned off at 30 seconds and tantalum melted severely till run ended at 83 seconds |
| -6R | 4895 | --- | 121 | Ta-10W Melting | 240 | ----/908 | coating formed small bubble which grew, then specimen surface brightened |
| -7R | 3120 | --- | 12 | Sn-Al Oxid | 1800 | ----/12 | little activity |
| -8R | 3470 | 25 | 39 | Ta-10W Melting | 400 | ----/176 | metal melted |
| -9R | 2845 | -1 | 20 | Sn-Al Oxid | 1800 | ----/20 | uniform oxidation, little activity |
| -10R | 2615 | -3 | 10 | Sn-Al Oxid | 1800 | ----/10 | little activity, uniform heating |
| -11R | 2505 | -3 | 13 | Sn-Al Oxid | 1800 | ----/13 | little activity, uniform heating |
| -12R | 2770 | -3 | 16 | Sn-Al Oxid | 1800 | ----/16 | little activity, uniform heating |

*Recession rates converted to 30 minutes on linear basis.

# TABLE 33

## SUMMARY OF ARC PLASMA EXPOSURES OF W+Zr+Cu(G-20) and W+Ag(G-21)

| Material Sample No. Assumed Emittance at λ = 0.65μ | Mach No. | $P_o$ atm | $i_e$ BTU/lb | D (in.) | $q_{cw}$ BTU/ft²sec | T °R obs | $q_r$ Surface Radiation BTU/ft²sec | $\epsilon_N$ Computed Normal Emittance | Initial Length/thickness (mils) | Final Length*/thickness (mils) | Exposure Time (seconds) | Calculated Temperature Ratio T(CALC)/T(OBS) Cold Wall Heat Transfer Coefficient | Fay and Riddell Heat Transfer Coefficient |
|---|---|---|---|---|---|---|---|---|---|---|---|---|---|
| W+Zr+Cu(G-20) | | | | | | | | | | | | | |
| ε = 0.40 | | | | | | | | | | | | | |
| -1M | 0.22 | 1.03 | 2970 | 0.413 | 315 | 5005 | 104 | 0.35 | 445/437 | ---/290 | 157 | 1.03 | 1.03 |
| -2M | 0.13 | 1.01 | 3030 | 0.435 | 170 | 3805 | 41 | 0.42 | 504/500 | 398/388 | 324 | 1.22 | 1.30 |
| -3M | 0.15 | 1.01 | 1700 | 0.427 | 95 | 2640 | 6 | 0.26 | 521/491 | 404/401 | 1800 | 1.42 | 1.52 |
| -4MA | 0.15 | 1.01 | 1620 | 0.431 | 130 | 2900 | 18 | 0.54 | 462/458 | ---/--- | 1425 | 1.34 | 1.35 |
| -4MB | 0.15 | 1.01 | 1620 | 0.431 | 130 | 3420 | 30 | 0.47 | ---/--- | 408/405 | 182 | 1.14 | 1.15 |
| -5MA | 0.15 | 1.01 | 1670 | 0.412 | 135 | 3395 | 28 | 0.45 | 420/414 | ---/--- | 400 | 1.16 | 1.17 |
| -5MB | 0.15 | 1.01 | 1670 | 0.412 | 135 | 2775 | --- | ---- | ---/--- | 340/333 | 1400 | 1.42 | 1.44 |
| -6MA | 0.15 | 1.01 | 1830 | 0.412 | 155 | 3325 | 51 | 0.54 | 431/427 | ---/--- | 500 | 1.24 | 1.24 |
| -6MB | 0.15 | 1.01 | 1830 | 0.412 | 155 | 2880 | --- | ---- | ---/--- | 280/262 | 1300 | 1.43 | 1.44 |
| -7R† | 3.2 | 0.075 | 9280 | 0.412 | 489 | 5815 | 215 | 0.40 | 836/520 | 808/477 | 1800 | 1.15 | 1.13 |
| -8RA† | 3.2 | 0.135 | 11980 | 0.428 | 662 | 5855 | 406 | 0.74 | 755/438 | ---/--- | 41 | 1.25 | 1.29 |
| -8RB† | 3.2 | 0.135 | 11980 | 0.428 | 662 | 5665 | 442 | 0.91 | ---/--- | 502/181 | 459 | 1.29 | 1.33 |
| -9R | 3.2 | 0.100 | 10680 | 0.425 | 584 | 5760 | 237 | 0.46 | 755/433 | 738/411 | 775 | 1.22 | 1.23 |
| W+Ag(G-21) | | | | | | | | | | | | | |
| ε = 0.40 | | | | | | | | | | | | | |
| -1M | 0.23 | 1.03 | 2330 | 0.509 | 310 | 4770 | 81 | 0.33 | 474/466 | 179/0 | 250 | 1.01 | 0.97 |
| -2M | 0.18 | 1.01 | 2330 | 0.519 | 230 | 3690 | 43 | 0.49 | 473/461 | ---/300 | 503 | 1.26 | 1.23 |
| -3M | 0.13 | 1.01 | 2790 | 0.508 | 150 | 2740 | 15 | 0.56 | 466/455 | 467/452 | 1800 | 1.64 | 1.72 |
| -4M | 0.15 | 1.01 | 2360 | 0.510 | 210 | 3475 | 35 | 0.51 | 470/461 | ---/298 | 624 | 1.32 | 1.29 |
| -5M | 0.13 | 1.01 | 2760 | 0.519 | 210 | 3510 | 44 | 0.61 | 459/439 | ---/301 | 460 | 1.35 | 1.34 |
| -6M | 0.15 | 1.01 | 2000 | 0.514 | 160 | 3005 | 20 | 0.52 | 450/445 | ---/387 | 1800 | 1.41 | 1.40 |

†Transmissivity factor equals 0.86 for sapphire window.

*Final length is based on measurement prior to sectioning, thickness refers to length after sectioning.

| Material Sample No. | T °F | Gross Recession mils | Material Recession mils | Degradation Mode | Exposure Time seconds | Material Sample No. (mils)/(sec) (mils)/(30 min) | Description of Motion Picture Film Coverage |
|---|---|---|---|---|---|---|---|
| W+Zr+Cu(G-20) | | | | | | | |
| -1M | 4545 | --- | 147 | Melting | 157 | 1685 | Immediate melting of front face. |
| -2M | 3345 | 106 | 112 | Melting | 324 | 622 | Material melting out of front face, uniform melting. |
| -3M | 2180 | 97 | 90 | Oxidation | 1800 | 90 | Little visible. |
| -4MA | 2440 | --- | --- | Oxidation + | 1425 | | |
| -4MB | 2960 | 54 | 53 | Melting | 182 | 59 | Little visible, some apparent melting. |
| -5MA | 2935 | --- | --- | Melting + | 400 | | |
| -5MB | 2315 | 80 | 81 | Oxidation | 1400 | 81 | Little visible, some apparent melting. |
| -6MA | 2865 | --- | --- | Melting + | 500 | | |
| -6MB | 2420 | 151 | 165 | Oxidation | 1300 | 165 | Little visible, some apparent melting. |
| -7R | 5355 | 28 | 43 | Oxidation | 1800 | 43 | Heavy buildup on front, some oxide chipping off. |
| -8RA | 5395 | --- | --- | Melting | ---- | 925 | Heavy oxide, some melting, visible recession. |
| -8RB | 5205 | 253 | 257 | Oxidation | 500 | | |
| -9R | 5300 | 17 | 22 | Oxidation | 775 | 51 | Heavy buildup with oxide chipping off. |
| W+Ag(G-21) | | | | | | | |
| -1M | 4310 | 295 | 466 | Melting | 250 | 3355 | Little activity, rapid melting, hourglass recession. |
| -2M | 3230 | --- | 161 | Melting | 503 | 576 | Little visible, some apparent melting. |
| -3M | 2280 | - 1 | 3 | Oxidation | 1800 | 3 | Little visible, some apparent melting or ablation. |
| -4M | 3015 | --- | 163 | Melt, or Ablat. | 624 | 182 | Little visible. |
| -5M | 3050 | --- | 138 | Ablation | 460 | 540 | Little visible. |
| -6M | 2545 | --- | 58 | Ablation | 1800 | 58 | Little visible, apparent ablation. |

# TABLE 34

## SUMMARY OF ARC PLASMA EXPOSURES OF $SiO_2$+68.5 w/o W(H-22)

| Material Sample No. Assumed Emittance at λ = 0.65μ | Mach No. | $P_s$ atm | $i_s$ BTU/lb | D (in) | $q_{cw}$ BTU/ft²sec | T °R obs | $q_r$ Surface Radiation BTU/ft²sec | $\epsilon_N$ Computed Normal Emittance | Initial Length/thickness (mils) | Final Length*/thickness (mils) | Exposure Time (seconds) | Calculated Temperature Ratio T(CALC)/T(OBS) Cold Wall Heat Transfer Coefficient | Fay and Riddell Heat Transfer Coefficient |
|---|---|---|---|---|---|---|---|---|---|---|---|---|---|
| $SiO_2$+68.5%W(H-22) | | | | | | | | | | | | | |
| ε = 0.80 | | | | | | | | | | | | | |
| -1MA | 0.32 | 1.06 | 3670 | 0.507 | 470 | 4700 | 104 | 0.45 | 679/672 | ---/--- | 250 | 1.08 | 1.06 |
| -1MB | 0.32 | 1.06 | 3670 | 0.507 | 470 | 4850 | 132 | 0.51 | ---/--- | 681/662 | 1550 | 1.05 | 1.03 |
| -2MA | 0.33 | 1.07 | 4110 | 0.507 | 580 | 4965 | 143 | 0.50 | 704/700 | ---/--- | 600 | 1.08 | 1.04 |
| -2MB | 0.33 | 1.07 | 4110 | 0.507 | 580 | 4785 | 118 | 0.48 | ---/--- | 692/681 | 957 | 1.13 | 1.08 |
| -3MA | 0.36 | 1.08 | 4730 | 0.507 | 670 | 5640 | 240 | 0.50 | 688/684 | ---/--- | 150 | 1.00 | 0.97 |
| -3MB | 0.36 | 1.08 | 4730 | 0.507 | 670 | 5270 | 181 | 0.50 | ---/--- | 448/428 | 1650 | 1.07 | 1.04 |
| -4MA | 0.36 | 1.08 | 5500 | 0.507 | 780 | 5665 | 256 | 0.53 | 680/654 | ---/--- | 65 | 1.05 | 1.01 |
| -4MB | 0.36 | 1.08 | 5500 | 0.507 | 780 | 5345 | --- | ---- | ---/--- | 243/226 | 1735 | 1.11 | 1.07 |
| -5MA | 0.37 | 1.09 | 6170 | 0.507 | 840 | 5695 | 276 | 0.56 | 707/697 | ---/--- | 100 | 1.07 | 1.05 |
| -5MB | 0.37 | 1.09 | 6170 | 0.507 | 840 | 5450 | --- | ---- | ---/--- | 0/0 | 931 | 1.13 | 1.10 |
| -6MA | 0.38 | 1.08 | 4690 | 0.507 | 640 | 5315 | 200 | 0.53 | 691/682 | ---/--- | 150 | 1.05 | 1.02 |
| -6MB | 0.38 | 1.08 | 4690 | 0.507 | 640 | 5165 | 172 | 0.51 | ---/--- | 592/574 | 1650 | 1.08 | 1.05 |
| -7R† | 3.2 | 0.086 | 10580 | 0.507 | 526 | 4635 | 171 | 0.79 | 993/688 | 493/181 | 230 | 1.28 | 1.27 |
| -8R† | 3.2 | 0.011 | 13780 | 0.507 | 302 | 4525 | 164 | 0.83 | 980/677 | 645/346 | 350 | 1.17 | 1.10 |
| -9R† | 3.2 | 0.009 | 9800 | 0.507 | 184 | 3790 | 79 | 0.81 | 996/670 | 839/535 | 1800 | 1.23 | 1.16 |
| -10R† | 3.2 | 0.009 | 13100 | 0.508 | 230 | 4210 | 125 | 0.85 | 973/607 | 609/276 | 600 | 1.18 | 1.14 |
| -11R† | 3.2 | 0.004 | 12440 | 0.508 | 209 | 4025 | 95 | 0.77 | 987/687 | 700/392 | 1200 | 1.20 | 1.07 |

†Transmissivity factor equals 0.86 for sapphire window.

*Final Length is based on measurement prior to sectioning; thickness refers to length after sectioning.

| Material Sample No. | T °F | Gross Recession mils | Material Recession mils | Degradation Mode | Exposure Time seconds | Recession Rate* mils/sec / mils/30 min | Description of Motion Picture Film Coverage |
|---|---|---|---|---|---|---|---|
| $SiO_2$+68.5%W(H-22) | | | | | | | |
| -1MA | 4240 | --- | --- | Oxidation | 250 | | little activity, uniform heating, small hot bursts |
| -1MB | 4390 | - 2 | 10 | Oxid+Flow | 1550 | 10 | kept appearing on front surface |
| -2MA | 4505 | --- | --- | Oxidation | 600 | | uniform heating, small hot bursts, slight melting |
| -2MB | 4325 | 12 | 19 | Oxid+Flow | 957 | 22 | at edges |
| -3MA | 5100 | --- | --- | Oxidation | 150 | | uniform heating, small hot bursts, edge melting |
| -3MB | 4810 | 240 | 256 | Oxid+Flow | 1650 | 256 | |
| -4MA | 5205 | --- | --- | Oxidation | 65 | | liquid around edge, visible recession |
| -4MB | 4885 | 437 | 428 | Oxid+Flow | 1735 | 428 | |
| -5MA | 5235 | --- | --- | Oxidation | 100 | | liquid around edge, visible recession, |
| -5MB | 4970 | 707 | 697 | Oxid+Flow | 991 | 1217 | burned through sting hole |
| -6MA | 4855 | --- | --- | Oxidation | 150 | | uniform heating, small hot bursts |
| -6MB | 4705 | 99 | 108 | Oxid+Flow | 1650 | 108 | |
| -7R | 4175 | 500 | 507 | Oxid+Flow | 230 | 3968 | rapid recession, possible melting |
| -8R | 4065 | 335 | 331 | Oxid+Flow | 350 | 1702 | slight rounding of edges, visible length recession |
| -9R | 3530 | 157 | 135 | Oxid+Flow | 1800 | 135 | slight rounding of edges, little activity |
| -10R | 3750 | 364 | 331 | Oxid+Flow | 600 | 993 | slight rounding of edges, visible length recession |
| -11R | 3565 | 287 | 295 | Oxid+Flow | 1200 | 443 | slight rounding of edges, visible length recession |

*Recession rate converted to 30 minutes on linear basis.

TABLE 35

# SUMMARY OF ARC PLASMA EXPOSURES OF $SiO_2$ + 60 w/o W(H-23)

| Material Sample No. Assumed Emittance at λ = 0.65μ | Mach No. | $P_s$ atm | $I_e$ BTU/lb | D (in) | $q_{cw}$ BTU/ft²sec | T °R obs | $q_r$ Surface Radiation BTU/ft²sec | $\epsilon_N$ Computed Normal Emittance | Initial Length/thickness (mils) | Final Length*/thickness (mils) | Exposure Time (seconds) | Calculated Temperature Ratio T(CALC)/T(OBS) Cold Wall Heat Transfer Coefficient | Fay and Riddell Heat Transfer Coefficient |
|---|---|---|---|---|---|---|---|---|---|---|---|---|---|
| $SiO_2$-60W(H-23) ε = 0.40 | | | | | | | | | | | | | |
| -1M | 0.32 | 1.07 | 4490 | 0.505 | 515 | 4860 | 160 | 0.61 | 703/710 | 686/662 | 1830 | 1.25 | 1.24 |
| -2M | 0.30 | 1.06 | 3380 | 0.505 | 485 | 4455 | 125 | 0.68 | 687/700 | 718/683 | 1830 | 1.24 | 1.22 |
| -3M | 0.29 | 1.05 | 3005 | 0.504 | 340 | 3995 | 75 | 0.63 | 686/690 | 696/688 | 1039 | 1.31 | 1.30 |
| -4M | 0.26 | 1.04 | 2310 | 0.505 | 200 | 3805 | 65 | 0.66 | 700/711 | 702/699 | 1065 | 1.19 | 1.22 |
| -5M | 0.37 | 1.08 | 6010 | 0.505 | 755 | 5520 | 260 | 0.59 | 688/698 | 563/525 | 1087 | 1.23 | 1.22 |
| -6MA | 0.46 | 1.13 | 5060 | 0.506 | 840 | 5750 | 285 | 0.55 | 723/724 | ---/--- | 60 | 1.17 | 1.12 |
| | After 60 seconds, temperature and radiation changed to -6MB | | | | | | | | | | | | |
| -6MB | 0.46 | 1.13 | 5060 | 0.506 | 840 | 5095 | 190 | 0.60 | ---/ | 438/423 | 1740 | 1.32 | 1.27 |
| -7MA | 0.49 | 1.14 | 5230 | 0.506 | 895 | 5780 | 274 | 0.52 | 709/713 | ---/--- | 60 | 1.18 | 1.14 |
| | After 60 seconds, temperature and radiation changed to -7MB | | | | | | | | | | | | |
| -7MB | 0.49 | 1.14 | 5230 | 0.506 | 895 | 5120 | 154 | 0.48 | ---/ | 245/217 | 1740 | 1.34 | 1.28 |
| -8R† | 3.2 | 0.023 | 10860 | 0.506 | 475 | 4480 | 128 | 0.57 | 1006/699 | 634/320 | 325 | 1.44 | 1.37 |
| -9R† | 3.2 | 0.014 | 11330 | 0.506 | 324 | 4590 | 118 | 0.56 | 1007/699 | 460/155 | 600 | 1.35 | 1.24 |
| -10R† | 3.2 | 0.007 | 9260 | 0.506 | 228 | 3920 | 66 | 0.59 | 1060/707 | 904/593 | 1800 | 1.45 | 1.27 |
| -11R† | 3.2 | 0.004 | 10230 | 0.505 | 154 | 3620 | 53 | 0.66 | 1008/733 | 990/715 | 1800 | 1.45 | 1.32 |
| -12R† | 3.2 | 0.025 | 14830 | 0.506 | 616 | 4960 | 158 | 0.55 | 1008/697 | 338/19 | 300 | 1.47 | 1.32 |
| -15MA | 0.37 | 1.08 | 5440 | 0.506 | 855 | 5765 | 291 | 0.56 | 694/686 | ---/--- | 60 | 1.19 | 1.13 |
| -15MB | After 60 seconds | | | | | 5080 | 110 | 0.35 | ---/--- | 377/318 | 1226 | 1.35 | 1.23 |
| -16MA | 0.36 | 1.08 | 5150 | 0.506 | 845 | 5750 | 268 | 0.52 | 705/691 | ---/--- | 60 | 1.17 | 1.11 |
| -16MB | After 60 seconds | | | | | 5140 | 86 | 0.26 | ---/--- | 380/304 | 1740 | 1.31 | 1.24 |
| -17MA | 0.35 | 1.08 | 4330 | 0.506 | 700 | 5450 | 218 | 0.53 | 702/682 | ---/--- | 60 | 1.16 | 1.10 |
| -17MB | After 60 seconds | | | | | 5120 | 171 | 0.53 | ---/--- | 611/582 | 1740 | 1.24 | 1.17 |
| -18MA | 0.32 | 1.08 | 3679 | 0.505 | 560 | 4850 | 151 | 0.57 | 704/692 | ---/--- | 200 | 1.22 | 1.16 |
| -18MB | After 200 seconds | | | | | 4740 | 136 | 0.58 | ---/--- | 685/663 | 1600 | 1.24 | 1.19 |
| -19MA | 0.33 | 1.07 | 4260 | 0.506 | 630 | 5190 | 179 | 0.52 | 688/686 | ---/--- | 100 | 1.19 | 1.14 |
| -19MB | After 100 seconds | | | | | 5020 | 157 | 0.53 | ---/--- | 627/615 | 1700 | 1.24 | 1.18 |
| -20MA | 0.33 | 1.07 | 3980 | 0.505 | 595 | 5110 | 170 | 0.53 | 702/698 | ---/--- | 100 | 1.19 | 1.14 |
| -20MB | After 100 seconds | | | | | 4820 | 135 | 0.53 | ---/--- | 697/647 | 1700 | 1.26 | 1.20 |
| -21R† | 3.2 | 0.008 | 13160 | 0.505 | 173 | 3995 | 69 | 0.58 | 1009/692 | 715/391 | 1800 | 1.16 | 1.12 |
| -22R† | 3.2 | 0.009 | 14120 | 0.504 | 295 | 4340 | 108 | 0.65 | 1005/689 | 494/169 | 500 | 1.22 | 1.13 |
| -23R† | 3.2 | 0.017 | 13010 | 0.506 | 411 | 4450 | 111 | 0.60 | 1010/695 | 540/223 | 300 | 1.28 | 1.16 |
| -24R† | 3.2 | 0.016 | 7620 | 0.507 | 218 | 3760 | 63 | 0.67 | 1000/697 | 954/643 | 1800 | 1.27 | 1.18 |

†Transmissivity factor equals 0.86 for sapphire window.

*Final Length is based on measurement prior to sectioning; thickness refers to length after sectioning.

| Material Sample No. | T °F | Gross Recession mils | Material Recession mils | Degradation Mode | Exposure Time seconds | Recession Rate* mils/sec / mils/30 min | Description of Motion Picture Film Coverage |
|---|---|---|---|---|---|---|---|
| $SiO_2$-60W(H-23) | | | | | | | |
| -1M | 4400 | 17 | 48 | Oxidation | 1830 | ----/68 | slight surface activity |
| -2M | 3995 | ~31 | 17 | Oxidation | 1830 | ----/17 | slight surface activity |
| -3M | 3535 | ~10 | 2 | Oxidation | 1039 | ----/3 | some flaking and liquid late in run |
| -4M | 3345 | ~2 | 12 | Oxidation | 1065 | ----/21 | slight bubbling at edge, little activity |
| -5M | 5040 | 125 | 173 | Oxidation | 1087 | ----/287 | uniform oxidation at angle to cylinder axis, sagging of specimen due to fracture at sting, eventually fell off |
| -6MA | 5290 | --- | --- | Oxidation | 60 | | some surface activity and melting |
| -6MB | 4635 | 285 | 301 | Oxid + Flow | 1740 | ----/301 | |
| -7MA | 5320 | --- | --- | Oxidation | 60 | | slight surface activity and melting |
| -7MB | 4660 | ~14 | 496 | Oxid + Flow | 1740 | ----/496 | |
| -8R | 4220 | 372 | 379 | Oxidation | 325 | ----/2196 | |
| -9R | 4130 | 547 | 544 | Oxidation | 600 | ----/1632 | |
| -10R | 3460 | 96 | 114 | Oxidation | 1200 | ----/114 | |
| -11R | 3160 | 18 | 18 | Oxidation | 1800 | ----/18 | |
| -12R | 4600 | 701 | 678 | Oxidation | 300 | ----/4068 | |
| -15MA | 5400 | --- | --- | Oxidation | 60 | ----/---- | melting, recession at angle |
| -15MB | 4620 | 317 | 368 | Oxid + Flow | 1226 | ----/368 | |
| -16MA | 5295 | --- | --- | Oxidation | 60 | ----/---- | melting, recession at angle |
| -16MB | 4580 | 325 | 387 | Oxid + Flow | 1740 | ----/387 | |
| -17MA | 4990 | --- | --- | Oxidation | 60 | ----/---- | no film coverage |
| -17MB | 4650 | 91 | 100 | Oxid + Flow | 1740 | ----/100 | |
| -18MA | 4390 | --- | --- | Oxidation | 200 | ----/---- | slight surface activity |
| -18MB | 4280 | 19 | 29 | Oxid + Flow | 1600 | ----/29 | |
| -19MA | 4730 | --- | --- | Oxidation | 100 | ----/---- | surface activity |
| -19MB | 4560 | 61 | 71 | Oxid + Flow | 1700 | ----/71 | |
| -20MA | 4650 | --- | --- | Oxidation | 100 | ----/---- | surface activity |
| -20MB | 4360 | 5 | 51 | Oxid + Flow | 1700 | ----/51 | |
| -21R | 3535 | 294 | 301 | Oxidation | 1800 | 301 | uniform heating and recession |
| -22R | 3080 | 511 | 520 | Oxidation | 500 | 1073 | uniform heating, considerable recession |
| -23R | 3990 | 470 | 470 | Oxidation | 300 | 2820 | uniform heating, considerable recession |
| -24R | 3300 | 46 | 54 | Oxidation | 1800 | 54 | uniform heating, little activity |

*Recession rate converted to 30 minutes on linear basis.

# TABLE 36

## SUMMARY OF ARC PLASMA EXPOSURES OF Hi-20Ta-2Mo(I-23)

| Material Sample No. Assumed Emittance at λ = 0.65μ | Mach No | $P_e$ atm | $i_s$ BTU/lb | D (in) | $q_{cw}$ BTU/ft²sec | T °R obs | $q_N$ Surface Radiation BTU/ft²sec | $q_N$ Computed Normal Emittance | Initial Length/thickness (mils) | Final Length*/thickness (mils) | Exposure Time (seconds) | Calculated Temperature Ratio T(CALC)/T(OBS) Cold Wall Heat Transfer Coefficient | Calculated Temperature Ratio T(CALC)/T(OBS) Bay and Riddell Heat Transfer Coefficient |
|---|---|---|---|---|---|---|---|---|---|---|---|---|---|
| Hf-20Ta-2Mo(I-23) ε = 0.55 | | | | | | | | | | | | | |
| -1M | 0.35 | 1.08 | 3295 | 0.508 | 530 | 4655 | 112 | 0.61 | 880/578 | 889/553 | 1830 | 1.17 | 1.11 |
| -2M | 0.28 | 1.05 | 1725 | 0.509 | 230 | 3030 | 29 | 0.73 | 750/436 | 763/434 | 952 | 1.35 | 1.31 |
| -3M | 0.28 | 1.05 | 2585 | 0.514 | 385 | 4050 | 50 | 0.39 | 760/449 | 770/434 | 1830 | 1.21 | 1.15 |
| -4M | 0.28 | 1.05 | 2270 | 0.508 | 320 | 3785 | 50 | 0.52 | 741/428 | 761/416 | 1830 | 1.22 | 1.17 |
| -5M | 0.31 | 1.05 | 2600 | 0.503 | 400 | 3895 | 64 | 0.59 | 741/457 | 750/444 | 1830 | 1.27 | 1.20 |
| -6M | 0.30 | 1.05 | 2865 | 0.505 | 420 | 3715 | 54 | 0.60 | 720/413 | 729/405 | 1830 | 1.37 | 1.31 |
| -7R+ | 3.2 | 0.063 | 7870 | 0.508 | 455 | 4090 | 72 | 0.55 | 724/414 | 732/402 | 1800 | 1.49 | 1.38 |
| -8R+ | 3.2 | 0.151 | 7400 | 0.505 | 753 | ---- | --- | ---- | 753/447 | 306/0 | 10 | ---- | ---- |
| | Sample melted | | | | | | | | Sample melted | | | | |
| -9R+ | 3.2 | 0.022 | 11250 | 0.514 | 337 | 4855 | 122 | 0.47 | 744/432 | 719/326 | 1800 | 1.21 | 1.14 |
| -10R+ | 3.2 | 0.017 | 9180 | 0.502 | 258 | 3425 | 62 | 0.96 | 728/424 | 733/402 | 1800 | 1.59 | 1.49 |
| -11R+ | 3.2 | 0.017 | 10600 | 0.515 | 297 | 3860 | 72 | 0.69 | 753/446 | 764/418 | 1800 | 1.47 | 1.37 |
| -12R+ | 3.2 | 0.018 | 12710 | 0.507 | 378 | 4360 | 112 | 0.66 | 865/560 | 877/534 | 1800 | 1.39 | 1.25 |
| -13M | 0.26 | 1.04 | 2975 | 0.505 | 585 | 4370 | 116 | 0.68 | 435/436 | 447/412 | 1830 | 1.16 | 1.11 |
| -14M | 0.29 | 1.05 | 3965 | 0.509 | 615 | 5290 | 230 | 0.63 | 442/439 | ---/--- | 30 | 1.09 | 1.07 |
| -15M | 0.32 | 1.06 | 3735 | 0.505 | 515 | 5320 | 226 | 0.60 | 430/421 | 370/353 | 1830 | 1.04 | 1.04 |
| -21M | 0.21 | 1.03 | 4790 | 0.742 | 435 | 4860 | 156 | 0.59 | 679/672 | 694/666 | 1800 | 1.15 | 1.12 |
| -22M | 0.26 | 1.03 | 4920 | 0.743 | 470 | 5045 | 177 | 0.58 | 674/666 | 678/640 | 1800 | 1.13 | 1.11 |
| -23MA | 0.24 | 1.03 | 4470 | 0.492 | 500 | 5070 | 188 | 0.61 | 645/642 | ---/--- | 40 | 1.12 | 1.10 |
| -23MB | 0.24 | 1.03 | 4470 | 0.492 | 500 | 5780 | 278 | 0.53 | ---/--- | 0/0 | 10 | 0.98 | 0.97 |
| -24M | 0.19 | 1.01 | 3990 | 0.487 | 430 | 5080 | 169 | 0.54 | 434/425 | ---/392 | 1800 | 1.07 | 1.04 |
| -25M | 0.23 | 1.03 | 5400 | 0.487 | 580 | 5710 | 281 | 0.50 | 677/650 | 445/407 | 13 | 1.08 | 1.04 |
| -1MC | 0.29 | 1.05 | 3220 | 0.501 | 425 | 5220 | 233 | 0.67 | 443/ 97 | ---/51 | 1800 | 1.08 | 0.97 |
| -2MC | 0.30 | 1.05 | 3350 | 0.503 | 505 | 5310 | 206 | 0.55 | 440/ 93 | ---/24 | 1800 | 1.02 | 0.97 |
| -3MCA | 0.31 | 1.06 | 3380 | 0.499 | 510 | 5415 | 193 | 0.48 | 441/100 | ---/--- | 1560 | 1.08 | 0.95 |
| -3MCB | 0.31 | 1.06 | 3380 | 0.499 | 510 | 5795 | 214 | 0.40 | ---/--- | ---/ 0 | 15 | 0.94 | 0.89 |
| -4MC | 0.31 | 1.06 | 3560 | 0.503 | 480 | 5395 | 212 | 0.53 | 437/ 99 | ---/ 0 | 1800 | 1.01 | 0.98 |

+Transmissivity factor equals 0.86 for sapphire window.

*Final Length refers to sample length prior to sectioning; thickness refers to section length.

| Material Sample No. | T °F | Gross Recession mils | Material Recession mils | Degradation Mode | Exposure Time seconds | Recession Rate mils/sec / mils/30 min | Description of Motion Picture Film Coverage |
|---|---|---|---|---|---|---|---|
| Hf-20Ta-2Mo (I-23) | | | | | | | |
| -1M | 4195 | -9 | 25 | Oxidation | 1830 | ----/25 | some surface activity, speckling, little oxidation |
| -2M | 2570 | -13 | 2 | Oxidation | 952 | ----/4 | no film coverage |
| -3M | 3590 | -10 | 15 | Oxidation | 1830 | ----/15 | little activity |
| -4M | 3325 | -20 | 12 | Oxidation | 1830 | ----/12 | little activity |
| -5M | 3435 | -7 | 13 | Oxidation | 1830 | ----/13 | little activity |
| -6M | 3255 | -9 | 8 | Oxidation | 1830 | ----/8 | little activity |
| -7R | 3630 | -8 | 120 | Oxidation | 1800 | ----/12 | uniform heating, little activity |
| -8R | (4440)+ | 447 | 447 | Melting | 10 | ---/80460 | |
| -9R | 4395 | 25 | 106 | Oxid + Melting | 1800 | ----/106 | began melting, then stopped and little activity followed |
| -10R | 2965 | -5 | 22 | Oxidation | 1800 | ----/22 | |
| -11R | 3400 | -11 | 24 | Oxidation | 1800 | ----/24 | |
| -12R | 3900 | -12 | 26 | Oxidation | 1800 | ----/26 | |
| -13M | 3910 | -12 | 24 | Oxidation | 1830 | ----/24 | melting at edges, sunburst formation |
| -14M | 4830 | --- | --- | Oxid + Th. Shock | 30 | ----/-- | rapid melting, recession, possible thermal shock |
| -15M | 4860 | 60 | 68 | Oxidation | 1830 | ----/67 | sunburst formation, oxide melting |
| -21M | 4400 | -15 | 6 | Oxidation | 1800 | | Droplets at edges, little activity. |
| -22M | 4585 | - 4 | 26 | Oxidation | 1800 | | Droplets at edges, little activity. |
| -23MA | 4610 | --- | --- | Oxidation | 40 | 44200 | Sunburst formed, rapid melting. |
| -23MB | 5520 | 445 | 442 | Melting | 18 | | |
| -24M | 4620 | --- | 33 | Oxidation | 1800 | | Slow melting of oxide continuously. |
| -25M | 5250 | 232 | 243 | Melting | 13 | 33646 | Rapid melting. |
| -1MC | 4760 | --- | 46 | Oxidation | 1800 | 46 | Sunburst formation, edges appeared hotter than center until heavy oxide built up. |
| -2MC | 4850 | --- | 69 | Oxidation | 1800 | 69 | Sunburst formation, small spot at center and edges hotter until heavy oxide built up. |
| -3MCA | 4955 | --- | --- | Oxidation | 1560 | 114 | Sunburst formation, oxide melting. |
| -3MCB | 5335 | --- | 100 | Melting | 15 | | |
| -4MC | 4935 | --- | 99 | Oxidation | 1800 | 99 | Sunburst formation, oxide melting. |

+Temperature estimated based on Col. Wall Heat Transfer Coefficient Calculation of 6100°R corrected by mean ratio T(CALC)/T(OBS) of 1.24 to 4920°R or 4460°F.

*Recession rate converted to 30 minutes on linear basis.

# TABLE 37

## SUMMARY OF ARC PLASMA EXPOSURES OF Hf-20Ta-2Mo (I-23)

| Material Sample No. Assumed Emittance at $\lambda$ = 0.65μ | Mach No. | $P_e$ atm | $i_e$ BTU/lb | D (in) | $q_{cw}$ BTU/ft²sec | T °R ohs | $q_r$ Surface Radiation BTU/ft²sec | $\epsilon_N$ Computed Normal Emittance | Initial Length/Thickness (mils) | Final* Length/Thickness (mils) | Exposure Time (seconds) | Calculated Temperature Ratio T(CALC)/T (OBS) Cold Wall Heat Transfer Coefficient | Fay and Riddell Heat Transfer Coefficient |
|---|---|---|---|---|---|---|---|---|---|---|---|---|---|
| Hf - 20Ta - 2Mo (I-23) $\epsilon$ = 0.55 | | | | | | | | | | | | | |
| -26MI | 0.28 | 1.05 | 3640 | 0.450 | 438 | 4965 | 152 | 0.53 | 914/914 | ---/--- | 1800 | 1.08 | 1.07 |
| -26MII | 0.29 | 1.05 | 3860 | 0.450 | 458 | 5265 | 187 | 0.52 | ---/--- | ---/--- | 1800 | 1.04 | 1.03 |
| -26MIII | 0.29 | 1.05 | 4020 | 0.450 | 462 | 5265 | 172 | 0.48 | ---/--- | ---/--- | 1800 | 1.05 | 1.05 |
| -26MIVA | 0.28 | 1.05 | 3890 | 0.450 | 450 | 5370 | 174 | 0.44 | ---/--- | ---/--- | 1350 | 1.02 | 1.01 |
| -26MIVB | 0.28 | 1.05 | 3370 | 0.450 | 386 | 5000 | 147 | 0.50 | ---/--- | 880/745 | 450 | 1.04 | 1.03 |
| -27MI | 0.30 | 1.05 | 3180 | 0.450 | 390 | 4065 | 79 | 0.62 | 948/947 | ---/--- | 1800 | 1.26 | 1.25 |
| -27MII | 0.29 | 1.05 | 3300 | 0.450 | 400 | 4370 | 130 | 0.70 | ---/--- | ---/--- | 1800 | 1.19 | 1.18 |
| -27MIII | 0.30 | 1.05 | 3300 | 0.450 | 410 | 4755 | 180 | 0.75 | ---/--- | ---/--- | 1276 | 1.10 | 1.08 |
| -27MIV | 0.30 | 1.05 | 3510 | 0.450 | 392 | 3825 | 207 | 0.81 | ---/--- | ---/--- | 1320 | 1.08 | 1.09 |
| -27MV | 0.30 | 1.05 | 3420 | 0.450 | 430 | 5020 | 213 | 0.71 | ---/--- | ---/--- | 1800 | 1.05 | 1.04 |
| -27MVI | 0.30 | 1.05 | 3340 | 0.450 | 418 | 4870 | 188 | 0.63 | ---/--- | ---/--- | 1800 | 1.08 | 1.06 |
| -27MVII | 0.30 | 1.05 | 3300 | 0.450 | 415 | 4940 | 176 | 0.63 | ---/--- | 915/809 | 1800 | 1.06 | 1.04 |
| -30M | 0.26 | 1.04 | 4030 | 0.396 | 470 | ---- | --- | --- | 706/700 | ---/111 | 9 | --- | ---- |
| -31M | 0.21 | 1.02 | 3620 | 0.390 | 370 | 4665 | 112 | 0.50 | 693/685 | 701/638 | 1800 | 1.12 | 1.12 |
| -32M | 0.23 | 1.02 | 4080 | 0.395 | 415 | 4940 | 174 | 0.62 | 718/714 | 715/640 | 1800 | 1.10 | 1.11 |
| -37MH | 0.30 | 1.05 | 3460 | 0.499 | 648 | ---- | --- | --- | 665/95** | ---/0 | 8 | --- | ---- |
| -38MH | 0.21 | 1.02 | 3220 | 0.513 | 435 | 4690 | 101 | 0.44 | 752/398** | 770/350 | 1800 | 1.12 | 1.05 |
| -41M | 0.28 | 1.04 | 3760 | 0.399 | 443 | ---- | --- | --- | 717/108** | ---/ 0 | 8 | --- | ---- |
| -42M | 0.31 | 1.05 | 3190 | 0.390 | 430 | ---- | --- | --- | 944/398** | ---/350 | 9 | --- | ---- |
| -45MS | 0.30 | 1.05 | 3700 | 0.450 | 445 | 3715 | 44 | 0.49 | 793/102** | 804/ 91 | 1800 | 1.45 | 1.44 |
| -46MS | 0.30 | 1.05 | 3760 | 0.450 | 470 | 4210 | 72 | 0.49 | 794/395** | 802/382 | 1800 | 1.30 | 1.28 |
| -53MH | 0.19 | 1.02 | 3560 | 0.503 | 452 | 4505 | 128 | 0.66 | 721/117** | 725/ 60 | 1800 | 1.19 | 1.21 |
| -54M | 0.28 | 1.04 | 3800 | 0.504 | 455 | 4665 | 136 | 0.61 | 764/107** | 779/ 65 | 1800 | 1.17 | 1.14 |
| -55M | 0.28 | 1.04 | 3820 | 0.507 | 455 | 4870 | 156 | 0.59 | 795/406** | 812/370 | 1800 | 1.12 | 1.10 |

* Final length refers to measurement after exposure; thickness refers to section length.
** Nose to in-depth temperature measurement station.

| Material Sample No. | T °F | Gross Recession (mils) | Material Recession (mils) | Degradation Mode | Exposure Time seconds | Recession Rate* mils/30 min | Description of Motion Picture Film Coverage |
|---|---|---|---|---|---|---|---|
| Hf-20Ta-2Mo(I-23) | | | | | | | |
| -26MI | 4505 | --- | --- | Oxid.+Melt. | 1800 | --- | Oxidized rapidly, sunburst formed, edge melting continued. |
| -26MII | 4805 | --- | --- | Oxid.+Melt. | 1800 | --- | Oxide broke off, new sunburst formed, slow melting continued. |
| -26MIII | 4805 | --- | --- | Oxidation | 1800 | --- | Slight spalling, continuous slow melting. |
| -26MIVA | 4910 | --- | --- | Oxidation | 1350 | --- | Slight spalling, continuous slow melting. |
| -26MIVB | 4540 | 34 | 169 | Oxidation | 450 | 42 | |
| -27MI | 3605 | --- | --- | Oxidation | 1800 | --- | Edges hotter than center. |
| -27MII | 3910 | --- | --- | Oxidation | 1800 | --- | Uniform oxide formed, edges melted, small sunburst. |
| -27MIII | 4295 | --- | --- | Oxid.+Melt. | 1276 | --- | Oxide broke off, slowly melted into sunburst. |
| -27MIV | 4365 | --- | -- | Oxidation | 1320 | --- | Slight melting of oxide, ' ,le change. |
| -27MV | 4560 | --- | --- | Oxid.+Melt. | 1800 | --- | Most of oxide broke off, oxide melted into sunburst. |
| -27MVI | 4410 | --- | --- | Oxid.+Melt. | 1800 | --- | Some oxide broke off, continuous oxide melting. |
| -27MVII | 4480 | 33 | 138 | Oxid.+Melt. | 1800 | 21 | Pieces of oxide broke off, continuous oxide melting. |
| -30M | --- | --- | 589 | Melting | 9 | 117800 | Rapid melting. |
| -31M | 4205 | -8 | 47 | Oxidation | 1800 | 47 | Edge melting, sunburst formation, slow melting. |
| -32M | 4480 | 3 | 74 | Oxidation | 1800 | 74 | Edge melting, sunburst formation, slow melting. |
| -37MH | --- | --- | 95 | Melting | 8 | 21400 | Rapid melting. |
| -38MH | 4230 | 18 | 48 | Oxidation | 1800 | 48 | Oxidized over 3/8" diam. spot, slow melting |
| -41M | --- | --- | 108 | Melting | 8 | 24300 | Rapid melting. |
| -42M | --- | --- | 398 | Melting | 9 | 79600 | Rapid melting. |
| -45MS | 3255 | -11 | 11 | Oxidation | 1800 | 11 | Little visible. |
| -46MS | 3750 | -8 | 13 | Oxidation | 1800 | 13 | Little visible. |
| -53MH | 4045 | -4 | 57 | Oxidation | 1800 | 57 | Rough, heavy oxide over entire nose. |
| -54M | 4205 | -15 | 42 | Oxidation | 1800 | 42 | Edges melting continuously, small sunburst. |
| -55M | 4410 | -17 | 36 | Oxidation | 1800 | 36 | Edges melting continuously, small sunburst. |

*Recession rate converted to 30 minutes on linear basis.

# TABLE 38

## SUMMARY OF ARC PLASMA EXPOSURES OF Hf-20Ta-2Mo (I-23)

| Material Sample No. Assumed Emittance at $\lambda = 0.65\mu$ | Mach No. | $P_e$ atm | $i_e$ BTU/lb | D (in) | $q_{cw}$ BTU/ft²sec | $T_R$ °R obs | $q_r$ Surface Radiation BTU/ft²sec | $\epsilon_N$ Computed Normal Emittance | Initial Length/Thickness (mils) | Final* Length/Thickness (mils) | Exposure Time (seconds) | Calculated Temperature Ratio T(CALC)/T(OBS) Cold Wall Heat Transfer Coefficient | Fay and Riddell Heat Transfer Coefficient |
|---|---|---|---|---|---|---|---|---|---|---|---|---|---|
| Hf - 20Ta - 2Mo (I-23) $\epsilon = 0.55$ | | | | | | | | | | | | | |
| -28RI | 2.2 | 0.132 | 7590 | 0.451 | 403 | 4795 | 141 | 0.57 | 1229/910 | ---/--- | 1800 | 1.24 | 1.27 |
| -28RII | 2.2 | 0.132 | 7450 | 0.451 | 394 | 4715 | 141 | 0.61 | ---/--- | ---/--- | 1800 | 1.25 | 1.28 |
| -28RIII | 2.2 | 0.132 | 7410 | 0.451 | 394 | 4500 | 113 | 0.59 | ---/--- | ---/--- | 1820 | 1.31 | 1.34 |
| -28RIV | 2.2 | 0.137 | 7900 | 0.451 | 403 | 4585 | 126 | 0.61 | ---/--- | 1225/855 | 1800 | 1.30 | 1.35 |
| -29RI | 2.2 | 0.195 | 7400 | 0.451 | 354 | 4325 | 109 | 0.66 | 1275/951 | ---/--- | 1800 | 1.33 | 1.45 |
| -29RII | 2.2 | 0.195 | 7400 | 0.451 | 354 | 4455 | 121 | 0.65 | ---/--- | ---/--- | 1800 | 1.30 | 1.41 |
| -29RIII | 2.2 | 0.195 | 7400 | 0.451 | 354 | 4630 | 136 | 0.63 | ---/--- | ---/--- | 1800 | 1.25 | 1.36 |
| -29RIV | 2.2 | 0.195 | 7330 | 0.451 | 360 | --- | --- | --- | ---/--- | ---/910 | 310 | --- | --- |
| -33R | 2.2 | 0.141 | 6060 | 0.390 | 360 | 4290 | 83 | 0.52 | 1027/709 | 1039/690 | 1800 | 1.32 | 1.35 |
| -34R | 2.2 | 0.151 | 8000 | 0.390 | 409 | 4870 | 130 | 0.49 | 1029/721 | 1056/709 | 1800 | 1.23 | 1.31 |
| -35R | 3.2 | 0.057 | 9580 | 0.391 | 440 | 4070 | 59 | 0.46 | 1040/728 | 1050/717 | 1800 | 1.51 | 1.49 |
| -36RA | 3.2 | 0.080 | 9150 | 0.391 | 509 | 3975 | 56 | 0.48 | 1106/787 | ---/--- | 313 | 1.59 | 1.56 |
| -36RB | 3.2 | 0.080 | 9150 | 0.391 | 509 | 4940 | 167 | 0.60 | ---/--- | 1121/763 | 380 | 1.28 | 1.26 |
| -39RH | 2.2 | 0.137 | 6740 | 0.504 | 412 | 4080 | 94 | 0.72 | 982/97** | 988/75 | 1800 | 1.44 | 1.56 |
| -40RH | 2.2 | 0.132 | 6950 | 0.505 | 388 | 4070 | 99 | 0.77 | 1025/403** | 1025/381+ | 1800 | 1.43 | 1.57 |
| -43R | 2.2 | 0.140 | 7690 | 0.400 | 403 | 4440 | 118 | 0.64 | 1065/109** | 1087/ 83 | 1800 | 1.34 | 1.40 |
| -44R | 2.2 | 0.132 | 6800 | 0.401 | 403 | 5070 | 180 | 0.58 | 1276/394** | 1306/365 | 1800 | 1.16 | 1.17 |
| -47RS | 2.2 | 0.222 | 7340 | 0.440 | 498 | 4735 | 152 | 0.64 | 1018/102** | 1033/65 | 1800 | 1.31 | 1.35 |
| -48RS | 2.2 | 0.229 | 7090 | 0.440 | 498 | 4735 | 152 | 0.64 | 1061/399** | 1078/373+ | 1800 | 1.30 | 1.34 |
| -49RH | 2.2 | 0.111 | 7480 | 1.000 | 408 | 4185 | 101 | 0.70 | 1167/205** | 1175/182+ | 1800 | 1.42 | 1.44 |
| -50RHS | 2.2 | 0.115 | 5750 | 1.000 | 402 | 4280 | 106 | 0.67 | 1217/98** | 1230/73+ | 1800 | 1.34 | 1.30 |
| -51RH | 2.2 | 0.114 | 6900 | 1.000 | 398 | 4255 | 123 | 0.80 | 1280/397** | 1295/373+ | 1800 | 1.38 | 1.38 |
| -52RHS | 2.2 | 0.118 | 5890 | 1.000 | 398 | 4420 | 128 | 0.71 | 1348/399** | 1358/373+ | 1803 | 1.30 | 1.27 |

* Final length refers to measurement after exposure; thickness refers to section length.
** None to in-depth temperature measurement station.
+ Estimated.

| Material Sample No. | T °F | Gross Recession (mils) | Material Recession (mils) | Degradation Mode | Exposure Time seconds | Recession Rate mils/30 min | Description of Motion Picture Film Coverage |
|---|---|---|---|---|---|---|---|
| Hf-20Ta - 2Mo(I-23) | | | | | | | |
| -28RI | 4335 | --- | --- | Oxidation | 1800 | --- | Heavy oxide buildup. |
| -28RII | 4255 | --- | --- | Oxidation | 1800 | --- | Some oxide broke off, reformed. |
| -28RIII | 4040 | --- | --- | Oxidation | 1820 | --- | Some oxide broke off, reformed. |
| -28RIV | 4125 | 4 | 55 | Oxidation | 1800 | 14 | Some oxide broke off, reformed. |
| -29RI | 3865 | --- | --- | Oxidation | 1800 | --- | Uniform oxide buildup. |
| -29RII | 3995 | --- | --- | Oxidation | 1800 | --- | Oxide broke off, reformed uniformly. |
| -29RIII | 4170 | --- | --- | Oxidation | 1800 | --- | Oxide broke off, reformed uniformly. |
| -29RIV | --- | --- | 41 | Oxidation | 310 | 13 | Oxide broke off, reformed uniformly. |
| -33R | 3830 | -12 | 19 | Oxidation | 1800 | 19 | Slow, uniform oxidation. |
| -34R | 4410 | -27 | 12 | Oxidation | 1800 | 12 | Some oxide melted at edges, little activity. |
| -35R | 3610 | -10 | 11 | Oxidation | 1800 | 11 | Little activity. |
| -36RA | 3515 | --- | --- | Oxidation | 313 | --- | Little activity. |
| -36RB | 4480 | -15 | 24 | Oxidation | 380 | 62 | Oxide continuously melted at edges |
| -39RH | 3620 | -6 | 22+ | Oxidation | 1800 | 22+ | Light oxide slowly formed over 1/4" diam. spot. |
| -40RH | 3610 | 0 | 22+ | Oxidation | 1800 | 22 | Light oxide slowly formed over 1/4" diam. spot. |
| -43R | 3980 | -22 | 26 | Oxidation | 1800 | 26 | Oxidized uniformly, little activity. |
| -44R | 4610 | -30 | 29 | Oxidation | 1800 | 29 | Oxidized uniformly, little activity. |
| -47RS | 4275 | -15 | 37 | Oxidation | 1800 | 37 | Shroud relatively cold, sample oxidized uniformly. |
| -48RS | 4275 | -17 | 26+ | Oxidation | 1800 | 26+ | Shroud relatively cold, sample oxidized uniformly. |
| -49RH | 3725 | -8 | 23+ | Oxidation | 1800 | 23+ | Light oxide formed over 1/4" diam. spot. |
| -50RHS | 3820 | -13 | 25+ | Oxidation | 1800 | 25+ | Oxidized over 3/8" diam. spot. |
| -51RH | 3795 | -15 | 24+ | Oxidation | 1800 | 24+ | Little visible. |
| -52RHS | 3960 | -10 | 26 | Oxidation | 1803 | 26+ | Oxidized over 1/2" diam. spot. |

+ Estimated.

* Recession rate converted to 30 minutes on linear basis.
+ Estimated.

# TABLE 39

## SUMMARY OF ARC PLASMA EXPOSURES OF Ir ON C (I-24)

| Material Sample No. Assumed Emittance at λ = 0.65μ | Mach No. | $P_e$ atm | $i_e$ BTU/lb | D (in) | $q_{cw}$ BTU/ft²sec | T °R obs | $q_r$ Surface Radiation BTU/ft²sec | $\epsilon_N$ Computed Normal Emittance | Initial Length Thickness (mils) | Final* Length Thickness (mils) | Exposure Time (seconds) | Calculated Temperature Ratio T(CALC)/T(OBS) Cold Wall Heat Transfer Coefficient | Fay and Riddell Heat Transfer Coefficient |
|---|---|---|---|---|---|---|---|---|---|---|---|---|---|
| Ir/Graphite (I-24) ε = 0.30 | | | | | | | | | | | | | |
| -9M | 0.31 | 1.06 | 3450 | 0.521 | 525 | 6455 | 93 | 0.11 | 702/702 | 393/330 | 105 | 0.93 | 0.89 |
| -10MA | 0.20 | 1.02 | 2985 | 0.521 | 345 | 4825 | 90 | 0.35 | 681/607 | ---/--- | 400 | 1.13 | 1.09 |
| -10MB | 0.20 | 1.02 | 2985 | 0.521 | 345 | 4680 | 61 | 0.27 | ---/--- | ---/** | 1400 | 1.16 | 1.12 |
| -11M | 0.16 | 1.02 | 3620 | 0.525 | 310 | 4590 | 91 | 0.44 | 684/684 | 679/598 | 1800 | 1.22 | 1.21 |
| -13M | 0.16 | 1.02 | 3140 | 0.523 | 310 | 4995 | 99 | 0.34 | 695/695 | ---/** | 1800 | 1.09 | 1.05 |
| -16M | 0.15 | 1.00 | 4185 | 0.521 | 310 | 4640 | 88 | 0.40 | 695/695 | 690/647 | 1800 | 1.06 | 0.98 |
| -17R+ | 3.2 | 0.002 | 8550 | 0.521 | 98 | 3980 | 62 | 0.53 | 999/1005 | 1003/1005 | 1800 | 1.25 | 1.13 |
| -19RA+ | 3.2 | 0.008 | 12260 | 0.519 | 302 | 5395 | 122 | 0.31 | 1001/1006 | ---/--- | 30 | 1.21 | 1.07 |
| -19RB+ | 3.2 | 0.008 | 12260 | 0.519 | 302 | 4800 | 197 | 0.79* | ---/--- | 672/665 | 900 | 1.11 | 0.98 |
| -22RA+ | 3.2 | 0.016 | 12980 | 0.525 | 506 | 5780 | 79 | 0.15 | 990/999 | ---/--- | 12 | 1.27 | 1.10 |
| -22RB+ | 3.2 | 0.016 | 12980 | 0.525 | 506 | 5100 | 276 | 0.87* | ---/--- | 901/913 | 120 | 1.18 | 1.01 |
| -24R+ | 3.2 | 0.004 | 9190 | 0.520 | 155 | 4605 | 98 | 0.46 | 1000/1004 | 995/1007 | 1800 | 1.20 | 1.07 |
| -30R | 3.2 | 0.004 | 12220 | 0.518 | 194 | 4875 | 109 | 0.41 | 1019/1026 | 1027/1023 | 1800 | 1.22 | 1.10 |
| -4M | 0.18 | 1.02 | 2810 | 0.520 | 287 | 4810 | 76 | 0.30 | 695/697 | 692/693 | 600 | 1.09 | 1.06 |
| -12M | 0.17 | 1.01 | 2950 | 0.519 | 257 | 4575 | 46 | 0.22 | 701/700 | 699/698 | 1800 | 1.14 | 1.13 |
| -18M | 0.18 | 1.02 | 2930 | 0.521 | 287 | 4590 | 94 | 0.45 | 701/701 | 698/698 | 1200 | 1.15 | 1.13 |
| -23M | 0.18 | 1.01 | 2750 | 0.536 | 288 | 4615 | 98 | 0.46 | 699/698 | 696/694 | 1800 | 1.13 | 1.09 |
| -36M° | 0.21 | 1.02 | 3450 | 0.520 | 310 | 4645 | 92 | 0.42 | 699/699 | 695/695 | 1800 | 1.09 | 1.10 |
| -37M° | 0.27 | 1.04 | 3300 | 0.520 | 355 | 4855 | 118 | 0.46 | 688/688 | 694/--- | 1800 | 1.07 | 1.06 |
| -3R+ | 2.2 | 0.106 | 6230 | 0.507 | 250 | 4445 | 69 | 0.38 | 1001/688 | 981/--- | 1800 | 1.34 | 1.40 |
| -25R+ | 2.2 | 0.099 | 5650 | 0.515 | 201 | [illegible] | 43 | 0.44 | 1002/702 | 997/897 | 600 | 1.48 | 1.57 |
| -27R+ | 2.2 | 0.097 | 5790 | 0.521 | 196 | 3725 | 43 | 0.44 | 1002/703 | 1002/702 | 1200 | 1.58 | 1.58 |
| -29R+ | 2.2 | 0.097 | 5900 | 0.525 | 190 | 3820 | 43 | 0.43 | 1017/712 | 1011/705 | 1795 | 1.47 | 1.58 |
| -36MRA** | 0.20 | 1.02 | 3160 | 0.520 | 300 | 4450 | 103 | 0.56 | 695/695 | ---/--- | --- | 1.12 | 1.11 |
| -36MRB** | 0.42 | 1.10 | 3250 | 0.520 | 515 | 5310 | 233 | 0.62 | ---/--- | /--- | 889 | 1.03 | 0.99 |

+ Transmissivity factor equals 0.86 for sapphire window.
* After coating burned off, pyrometer was sighting the graphite substrate. Emittance of 0.75 was used for the Poco Graphite (B-10).
° Coating composition 50% $HfO_2$-50% Ir, ε = 0.50 at λ = 0.65μ.
** Reruns, conditions gradually changed from (A) to (B).

** Too distorted to measure due to partial coating burn-off and irregular graphite ablation.
* Final length refers to sample length prior to sectioning; thickness refers to section length.

| Material Sample No. | T °F | Gross Recession mils | Material Recession mils | Degradation Mode | Exposure Time seconds | Recession Rate* mils/30 min | Description of Motion Picture Film Coverage |
|---|---|---|---|---|---|---|---|
| Ir/Graphite(I-24) | | | | | | | |
| -9M | 5995 | 309 | 372 | Melting+C Ablation | 105 | 6377 | Front face melted, coating burn-off continued to sides, Some molten Ir on carbon. |
| -10MA | 4365 | --- | 33* | Ir Ablation | 400 | 149 | Dark spots on front face grew during run, one edge |
| -10MB | 4220 | --- | --- | C Ablation | 1200 | | melted and formed hole which spread across front face. |
| -11M | 4130 | - 5 | 86 | Oxidation | 1800 | 86 | Dark spots kept forming and disappearing except for one in center which grew near end of run. |
| -13M | 4535 | --- | --- | Ir+C Ablation | 1400 | ---- | Coating melted off front face in an irregular manner leaving large hole. |
| -16M | 4180 | - 5 | 48 | Oxidation | 1800 | 48 | Dark spots formed and disappeared; center patch expanded to edge, then most of front face as coating burned off. |
| -17R | 3520 | - 4 | 0 | Oxidation | 1800 | 0 | Uniform heating, little activity. |
| -19RA | 4935 | --- | 31* | Ir Melting | 30 | 1188 | Coating gradually melted off front face then sides. |
| -19RB | 4340 | 329 | 308 | C Ablation | 900 | 616 | Graphite ablation. |
| -22RA | 5320 | --- | 26* | Ir Melting | 12 | 3900 | Rapid melting of coating from front and sides. |
| -22RB | 4640 | 89 | 60 | C Ablation | 120 | 900 | Graphite ablation. |
| -24R | 4145 | 5 | - 3 | Oxidation | 1800 | 0 | Uniform heating, little activity. |
| -30R | 4415 | - 8 | 3 | Oxidation | 1800 | 3 | Uniform heating, little activity. |
| -4M | 4350 | 3 | 4 | Oxidation | 600 | 12 | Little activity. |
| -12M | 4115 | 2 | 2 | Oxidation | 1800 | 2 | Little visible, slightly mottled appearance. |
| -18M | 4130 | 3 | 3 | Oxidation | 1200 | 4 | Little activity, uniform heating. |
| -23M | 4155 | 3 | 5 | Oxidation | 1600 | 5 | Little activity, uniform heating. |
| -36M | 4185 | 4 | 4 | Oxidation | 1800 | 4 | Little activity, some roughening of surface. |
| -37M | 4375 | - 6 | --- | Oxidation | 1800 | ---- | Uniform heating, some roughening of surface. |
| -3R | 3985 | 20 | --- | Melting | 1800 | ---- | Coating failed around edge, not in center. |
| -25R | 3345 | 5 | 5 | Oxidation | 600 | 15 | Uniform heating, little activity. |
| -27R | 3335 | 0 | 1 | Oxidation | 1200 | 2 | Uniform heating, little activity. |
| -29R | 3360 | 6 | 7 | Oxidation | 1795 | 7 | Uniform heating, little activity. |
| -36MRA | 3990 | --- | --- | Oxidation | --- | ---- | Droplets and hot spots at edges. |
| -36MRA | 4850 | --- | --- | Melting | 889 | ---- | Apparent failure near edge spread inward. |

*Based on original coating thickness

*Recession rate converted to 30 minutes on linear basis.

TABLE 40

SUMMARY OF IN-DEPTH TEMPERATURE EXPOSURES OF $ZrB_2$(A-3)

| Material Sample No. Assumed Emittance at $\lambda = 0.65\mu$ | Nose Thickness (Inches) | $h_e$ BTU/lb. | $q_{cw}$ BTU/ft²sec | $^oT$ $^oR$ Surface | $^oT^*$ $^oR$ In-Depth | Time (Seconds) |
|---|---|---|---|---|---|---|
| $ZrB_2$(A-3) $\epsilon = 0.57$ | | | | | | |
| -1MC | 0.104 | 4540 | 475 | 4500 | ---- | 200 |
| | | | | 4710 | ---- | 350 |
| | | | | 4850 | ---- | 425 |
| | | | | 4920 | ---- | 520 |
| | | | | 5040 | ---- | 600 |
| | | | | 5080 | ---- | 700 |
| | | | | 5110 | ---- | 1300 |
| | | | | 5150 | ---- | 1500 |
| | | | | 5150 | ---- | 1800 |
| -2MC | 0.101 | 3230 | 365 | 4590 | 3160 | 180 |
| | | | | 4560 | 3160 | 350 |
| | | | | 4370 | 3130 | 500 |
| | | | | 4490 | 3160 | 600 |
| | | | | 4750 | 3220 | 900 |
| | | | | 4770 | 3300 | 1000 |
| | | | | 4810 | 3340 | 1350 |
| | | | | 4790 | 3280 | 1650 |
| | | | | 4910 | 3310 | 1750 |
| | | | | 4930 | 3400 | 1800 |
| -3MC | 0.102 | 3380 | 460 | 4770 | ---- | 80 |
| | | | | 4960 | ---- | 160 |
| | | | | 5030 | 3810 | 600 |
| | | | | 4980 | 3740 | 700 |
| | | | | 5010 | 3700 | 1000 |
| | | | | 5060 | 3720 | 1275 |
| | | | | 5150 | 3740 | 1600 |
| | | | | 5170 | 3760 | 1800 |
| -4MC | 0.104 | 4580 | 610 | 6340 | 4420 | 20 |
| | Rapid Melting | | | 6340 | ---- | 63.8 |

*Assuming $\epsilon = 1.00$ at in-depth temperature measurement station.

TABLE 41

SUMMARY OF IN-DEPTH TEMPERATURE EXPOSURES OF $HfB_{2.1}$ +20%SiC(A-7)

| Material Sample No. Assumed Emittance at $\lambda = 0.65\mu$ | Nose Thickness (Inches) | $h_e$ BTU/lb. | $q_{cw}$ BTU/ft²sec | $^oT$ $^oR$ Surface | $^oT^*$ $^oR$ In-Depth | Time (Seconds) |
|---|---|---|---|---|---|---|
| $HfB_{2.1}$ +20%SiC(A-7) $\epsilon = 0.60$ | | | | | | |
| -36MH | 0.109 | 3500 | 513 | 4210 | 3950 | 249 |
| | | | | 4370 | 3980 | 690 |
| -37MH | Sighting hole became blocked, no further measurements. | | | | | |
| | 0.405 | 3640 | 495 | 4070 | 3610 | 350 |
| | | | | 4230 | 3670 | 671 |
| -38RH | Sighting hole became blocked, no further measurements. | | | | | |
| | 0.100 | 8280 | 497 | 3070 | ---- | 600 |
| | | | | 3050 | ---- | 1200 |
| | | | | 3050 | ---- | 1800 |
| -39RH | 0.401 | 6540 | 487 | 3230 | 2780 | 600 |
| | | | | 3200 | 2880 | 1200 |
| | | | | 3190 | 2860 | 1800 |
| -40M | 0.100 | 4390 | 495 | 4095 | 3620 | 459 |
| | | | | 4175 | 3840 | 660 |
| | | | | 4340 | 3950 | 985 |
| | | | | 4580 | 3970 | 1278 |
| | | | | 4645 | 3990 | 1555 |
| | | | | 4670 | 3970 | 1670 |
| -41M | 0.397 | 4400 | 502 | 3950 | 3150 | 333 |
| | | | | 4230 | 3550 | 651 |
| | | | | 4565 | 3660 | 1084 |
| | | | | 4665 | 3660 | 1259 |
| | | | | 4870 | 3690 | 1536 |
| | | | | 5010 | 3810 | 1695 |
| -42R | 0.102 | 7140 | 498 | 3110 | ---- | 600 |
| | | | | 3110 | 2860 | 1000 |
| | | | | 3110 | 2860 | 1500 |
| -43R | 0.400 | 7520 | 503 | 3230 | 2680 | 600 |
| | | | | 3230 | 2690 | 1200 |
| | | | | 3260 | 2700 | 1800 |
| -44MS | 0.101 | 4360 | 493 | 3250 | 3070 | 666 |
| | | | | 3230 | 3070 | 958 |
| | | | | 3230 | 3060 | 1036 |
| | | | | 3230 | 3050 | 1273 |
| | | | | 3230 | 3050 | 1545 |
| | | | | 3220 | 3060 | 1727 |
| -45MS | 0.399 | 4580 | 522 | 3350 | 2780 | 136 |
| | | | | 3305 | 2790 | 367 |
| | | | | 3270 | 2750 | 678 |
| | | | | 3260 | 2740 | 962 |
| | | | | 3250 | 2750 | 1293 |
| | | | | 3230 | 2740 | 1700 |
| -46RS | 0.097 | 5750 | 503 | 3450 | 3120 | 600 |
| | | | | 3730 | 3160 | 1200 |
| -47RS | 0.400 | 6290 | 489 | 3660 | 2910 | 600 |
| | | | | 3580 | 2860 | 1200 |
| | | | | 3660 | 2830 | 1800 |
| -48RH | 0.100 | 7030 | 492 | 3030 | 2900 | 600 |
| | | | | 3000 | 2850 | 1200 |
| | | | | 2970 | 2840 | 1800 |
| -50RH | 0.401 | 7250 | 492 | 2970 | 2800 | 600 |
| | | | | 2950 | 2750 | 1200 |
| | | | | 2940 | 2780 | 1800 |
| -49RHS | 0.101 | 6800 | 512 | 3320 | 3000 | 600 |
| | | | | 3310 | 3000 | 1200 |
| | | | | 3310 | 3010 | 1800 |
| -51RHS | 0.399 | 6510 | 497 | 3200 | 2670 | 600 |
| | | | | 3190 | 2660 | 1200 |
| | | | | 3180 | 2640 | 1800 |

*Assuming $\epsilon = 1.00$ at in-depth temperature measurement station.

TABLE 42

SUMMARY OF IN-DEPTH TEMPERATURE EXPOSURES OF $ZrB_{2.1}$ +20%SiC(A-8)

| Material Sample No. Assumed Emittance at $\lambda = 0.65\mu$ | Nose Thickness (Inches) | $h_e$ BTU/lb. | $q_{cw}$ BTU/ft²sec | $^oT$ $^oR$ Surface, | $^oT^*$ $^oR$ In-Depth | Time (Seconds) |
|---|---|---|---|---|---|---|
| $ZrB_{2.1}$ +20%SiC(A-8) $\epsilon = 0.60$ | | | | | | |
| -25M | 0.096 | 5280 | 360 | 3580 | 3190 | 467 |
| | | | | 3620 | 3280 | 674 |
| | | | | 3510 | 3270 | 976 |
| | | | | 3490 | 3250 | 1255 |
| | | | | 3470 | 3230 | 1535 |
| | | | | 3560 | 3310 | 1735 |
| -26M | 0.395 | 5430 | 370 | 3560 | 3080 | 765 |
| | | | | 3570 | 3070 | 958 |
| | | | | 3560 | 3060 | 1275 |
| | | | | 3580 | 3060 | 1552 |
| | | | | 3560 | 3060 | 1748 |
| -27R | 0.102 | 7970 | 452 | 3050 | 2950 | 600 |
| | | | | 3140 | 2960 | 1200 |
| | | | | 3380 | ---- | 1800 |
| -28R | 0.400 | 7350 | 452 | 3010 | 2680 | 600 |
| | | | | 3220 | 2680 | 1200 |
| | | | | 4140 | 2680 | 1800 |
| -29M | 0.096 | 5330 | 358 | 3960 | 3350 | 350 |
| | | | | 3930 | 3260 | 405 |
| | Poco(B-10) Graphite shroud completely ablated. | | | | | 500 |
| | | | | 3790 | 3250 | 666 |
| | | | | 3740 | 3290 | 985 |
| | | | | 3710 | 3260 | 1268 |
| | | | | 3710 | 3260 | 1725 |
| -30M | 0.395 | 4840 | 350 | 3000 | 2470 | 185 |
| | | | | 2990 | 2550 | 649 |
| | | | | 2975 | 2550 | 940 |
| | | | | 2975 | 2550 | 1251 |
| | | | | 2990 | 2580 | 1551 |
| | | | | 2975 | 2570 | 1703 |
| -31R | 0.095 | 7390 | 440 | 3110 | 2830 | 600 |
| | | | | 3110 | 2820 | 1200 |
| | | | | 3110 | 2820 | 1800 |
| -32R | 0.399 | 7270 | 437 | 3260 | 2720 | 600 |
| | | | | 3240 | 2720 | 1200 |
| | | | | 3260 | 2720 | 1800 |

*Assuming $\epsilon = 1.00$ at in-depth temperature measurement station.

TABLE 43

SUMMARY OF IN-DEPTH TEMPERATURE EXPOSURES OF $ZrB_2$+SiC+C(A-10)

| Material Sample No. Assumed Emittance at $\lambda$ = 0.65$\mu$ | Nose Thickness (inches) | $i_e$ BTU/lb. | $q_{cw}$ BTU/ft$^2$sec | $^oT$ R Surface | $^oT^*$ R In-Depth | Time (Seconds) |
|---|---|---|---|---|---|---|
| $ZrB_2$+SiC+C(A-10) $\epsilon$ = 0.6c | | | | | | |
| -36MH | 0.102 | 3950 | 416 | 3930 | 3620 | 352 |
| | | | | 3975 | 3690 | 658 |
| | | | | 3910 | 3690 | 956 |
| | | | | 4110 | 3770 | 1253 |
| | | | | 3975 | 3620 | 1545 |
| | | | | 3975 | 3630 | 1685 |
| -35MH | 0.391 | 3500 | 420 | 3840 | 3290 | 340 |
| | | | | 3840 | 3270 | 661 |
| | | | | 3880 | 3310 | 940 |
| | | | | 3940 | 3300 | 1252 |
| | | | | 3940 | 3330 | 1541 |
| | | | | 3960 | 3320 | 1666 |
| -36RH | 0.109 | 7250 | 492 | 3110 | 2800 | 600 |
| | | | | 3370 | 3040 | 1200 |
| | | | | 3770 | 3280 | 1800 |
| -37RH | 0.393 | 7710 | 482 | 3160 | 2640 | 600 |
| | | | | 3260 | 2900 | 1200 |
| | | | | 3740 | 2980 | 1800 |
| -38M | 0.096 | 3870 | 400 | 3665 | 3480 | 377 |
| | | | | 3790 | 3490 | 639 |
| | | | | 3810 | 3520 | 950 |
| | | | | 3840 | 3540 | 1269 |
| | | | | 3840 | 3550 | 1571 |
| | | | | 3840 | 3550 | 1684 |
| -39M | 0.389 | 3990 | 400 | 4000 | 3010 | 370 |
| | | | | 4260 | 3280 | 665 |
| | | | | 4150 | 3360 | 939 |
| | | | | 4450 | 3430 | 1276 |
| | | | | 4710 | 3450 | 1545 |
| | | | | 4745 | 3440 | 1681 |
| -40R | 0.101 | 6320 | 495 | 4630 | 3370 | 600 |
| | | | | 4840 | 3430 | 1200 |
| | | | | 5020 | 3360 | 1800 |
| -41R | 0.400 | 6460 | 495 | 5130 | 2930 | 600 |
| | | | | 5210 | 2930 | 1200 |
| | | | | 4170 | 2930 | 1800 |
| -42MS | 0.102 | 4000 | 393 | 3020 | 2820 | 161 |
| | | | | 3000 | 2960 | 480 |
| | | | | 2990 | 2920 | 683 |
| | | | | 3000 | 2930 | 943 |
| | | | | 2945 | 2890 | 1264 |
| | | | | 2930 | 2890 | 1555 |
| | | | | 2920 | 2880 | 1700 |
| -43MS | 0.395 | 4040 | 403 | 2965 | 2540 | 218 |
| | | | | 3010 | 2600 | 665 |
| | | | | 2920 | 2530 | 961 |
| | | | | 2965 | 2560 | 1261 |
| | | | | 3010 | 2570 | 1545 |
| | | | | 3080 | 2600 | 1697 |
| -44RS | 0.094 | 7400 | 495 | 3850 | 3120 | 600 |
| | | | | 4670 | 3280 | 1200 |
| | | | | 4750 | 3220 | 1800 |
| -45RS | 0.399 | 7470 | 498 | 3880 | 2880 | 600 |
| | | | | 5130 | 2870 | 1200 |
| | | | | 5210 | 2870 | 1800 |
| -46RH | 0.108 | 7220 | 501 | 3050 | 2900 | 600 |
| | | | | 3060 | 3020 | 1200 |
| | | | | 3110 | 3020 | 1800 |
| -48RH | 0.404 | 6350 | 492 | 3030 | 2740 | 600 |
| | | | | 3010 | 2750 | 1200 |
| | | | | 3000 | 2770 | 1800 |
| -47RHS | 0.103 | 6010 | 507 | 4060 | 3040 | 600 |
| | | | | 4330 | 3140 | 1200 |
| | | | | 4830 | 3210 | 1800 |
| -49RHS | 0.392 | 6010 | 522 | 3210 | 2820 | 600 |
| | | | | 4150 | 2820 | 1200 |
| | | | | 4190 | 2830 | 1800 |

*Assuming $\epsilon$ = 1.00 at in-depth temperature measurement station.

TABLE 44

SUMMARY OF IN-DEPTH TEMPERATURE EXPOSURES OF RVA(B-5)

| Material Sample No. Assumed Emittance at $\lambda$ = 0.65$\mu$ | Nose Thickness (inches) | $i_e$ BTU/lb. | $q_{cw}$ BTU/ft$^2$sec | $^oT$ R Surface | $^oT^*$ R In-Depth | Time (Seconds) |
|---|---|---|---|---|---|---|
| RVA(B-5) $\epsilon$ = 0.85 (Below 3000°F), 0.75(3000°-3500°F), 0.65(Above 3500°F) | | | | | | |
| -31M | 0.202 | 2530 | 135 | 3280 | 2860 | 75 |
| | | | | 3320 | 2920 | 95 |
| | | | | 3310 | 3000 | 120 |
| | | | | 3300 | 3020 | 147 |
| | | | | 3310 | 3050 | 165 |
| | | | | 3310 | 3120 | 212 |
| | | | | 3310 | 3100 | 232 |
| -32M | 0.463 | 2930 | 135 | 3400 | 2730 | 105 |
| | | | | 3420 | 2760 | 115 |
| | | | | 3440 | 2780 | 130 |
| | | | | 3450 | 2815 | 145 |
| | | | | 3470 | 2835 | 160 |
| | | | | 3470 | 2845 | 170 |
| | | | | 3480 | 2850 | 180 |

*Assuming $\epsilon$ = 1.00 at in-depth temperature measurement station.

TABLE 45

SUMMARY OF IN-DEPTH TEMPERATURE EXPOSURES OF $WSi_2$/W(G-18)

| Material Sample No. Assumed Emittance at $\lambda$ = 0.65$\mu$ | Nose Thickness (inches) | $i_e$ BTU/lb. | $q_{cw}$ BTU/ft$^2$sec | $^oT$ R Surface | $^oT^*$ R In-Depth | Time (Seconds) |
|---|---|---|---|---|---|---|
| $WSi_2$/W(G-18) $\epsilon$ = 0.60 (Below 3500°F) | | | | | | |
| -17M | 0.102 | 3150 | 320 | 3620 | 3160 | 405 |
| | | | | 3620 | 3250 | 636 |
| | | | | 3630 | 3250 | 941 |
| | | | | 3650 | 3310 | 1245 |
| | | | | 3600 | 3310 | 1545 |
| | | | | 3600 | 3310 | 1682 |
| -18M | 0.200 | 3280 | 316 | 3490 | 2960 | 830 |
| | | | | 3470 | 3020 | 1130 |
| | | | | 3490 | 3070 | 1250 |
| | | | | 3490 | 3110 | 1560 |
| | | | | 3490 | 3110 | 1760 |
| -19MS | 0.096 | 3380 | 310 | 2880 | 2670 | 243 |
| | | | | 2850 | 2760 | 640 |
| | | | | 2815 | 2740 | 928 |
| | | | | 2860 | 2770 | 1260 |
| | | | | 2860 | 2770 | 1548 |
| | | | | 2860 | 2770 | 1672 |
| -20MS | 0.200 | 3160 | 306 | 2965 | 2720 | 157 |
| | | | | 2910 | 2690 | 359 |
| | | | | 2850 | 2670 | 678 |
| | | | | 2785 | 2640 | 958 |
| | | | | 2850 | 2660 | 1263 |
| | | | | 2770 | 2640 | 1545 |
| | | | | 2760 | 2620 | 1707 |

*Assuming $\epsilon$ = 1.00 at in-depth temperature measurement station.

TABLE 46

SUMMARY OF IN-DEPTH TEMPERATURE EXPOSURES OF Hf-20Ta-2Mo(I-23)

| Material Sample No., Assumed Emittance at λ = 0.65μ | Nose Thickness (inches) | $i_e$ BTU/lb. | $q_{cw}$ BTU/ft²sec | T °R Surface | T* °R In-Depth | Time (Seconds) |
|---|---|---|---|---|---|---|
| Hf-20Ta-2Mo(I-23) ε = 0.55 | | | | | | |
| -1MC | 0.097 | 3220 | 425 | 3890 | 3400 | 105 |
| | | | | 4230 | 3605 | 510 |
| | | | | 4665 | 3795 | 750 |
| | | | | 5085 | 3940 | 1200 |
| | | | | 5170 | 3920 | 1400 |
| | | | | 5220 | 3990 | 1800 |
| -2MC | 0.093 | 3350 | 505 | 4380 | 3625 | 150 |
| | | | | 4695 | 3740 | 275 |
| | | | | 4890 | 3740 | 400 |
| | | | | 5275 | 3900 | 600 |
| | | | | 5310 | 3740 | 800 |
| | | | | 5335 | 3810 | 900 |
| | | | | 5240 | 3760 | 1500 |
| | | | | 5310 | 3640 | 1800 |
| -3MC | 0.100 | 3380 | 510 | 5030 | 3840 | 80 |
| | | | | 5205 | 3890 | 380 |
| | | | | 5335 | 3900 | 515 |
| | | | | 5410 | 3920 | 1100 |
| | | | | 5415 | 4075 | 1330 |
| | | | | 5335 | 4280 | 1455** |
| | | | | 5340 | 4280 | 1560** |
| | | | | 5550 | 4500 | 1565 |
| | | | | 5670 | 4880 | 1570 |
| | | | | 5795 | (5240)+ | 1575 |
| -4MC | 0.099 | 3560 | 480 | 4770 | 3600 | 115 |
| | | | | 5330 | 3820 | 360 |
| | | | | 5195 | 3720 | 450 |
| | | | | 5385 | 3840 | 800 |
| | | | | 5265 | 3810 | 1200 |
| | | | | 5110 | 3810 | 1560 |
| | | | | 5195 | 3810 | 1800 |

*Assuming ε = 1.00 at in-depth temperature measurement station.

**Melting observed.

+Estimated

TABLE 47

SUMMARY OF IN-DEPTH TEMPERATURE EXPOSURES OF Hf-20Ta-2Mo(I-23)

| Material Sample No., Assumed Emittance at λ = 0.65μ | Nose Thickness (inches) | $i_e$ BTU/lb | $q_{cw}$ BTU/ft²sec | T °R Surface | T* °R In-Depth | Time (Seconds) |
|---|---|---|---|---|---|---|
| Hf-20Ta-2Mo ε = 0.55 | | | | | | |
| -53MH | 0.100 | 3560 | 452 | 4430 | 3640 | 319 |
| | | | | 4490 | 3700 | 638 |
| | | | | 4450 | 3690 | 941 |
| | | | | 4500 | 3670 | 1260 |
| | | | | 4460 | 3670 | 1553 |
| | | | | 4460 | 3690 | 1718 |
| -38MH | 0.398 | 3220 | 435 | 4550 | 3390 | 583 |
| | | | | 4490 | 3320 | 941 |
| | | | | 4440 | 3350 | 1259 |
| | | | | 4440 | 3330 | 1554 |
| | | | | 4480 | 3330 | 1712 |
| -39RH | 0.100 | 6740 | 412 | 4100 | 3580 | 600 |
| | | | | 4150 | 3600 | 1200 |
| | | | | 4160 | 3680 | 1800 |
| -40RH | 0.410 | 6950 | 388 | 4060 | 3270 | 600 |
| | | | | 4110 | 3285 | 1200 |
| | | | | 4150 | 3300 | 1800 |
| -54M | 0.106 | 3800 | 455 | 4640 | 3510 | 381 |
| | | | | 4610 | 3440 | 680 |
| | | | | 4630 | 3610 | 1274 |
| | | | | 4640 | 3550 | 1544 |
| | | | | 4650 | 3560 | 1740 |
| -55M | 0.408 | 3820 | 455 | 4760 | 3250 | 360 |
| | | | | 4800 | 3250 | 671 |
| | | | | 4850 | 3250 | 946 |
| | | | | 4870 | 3250 | 1256 |
| | | | | 4830 | 3260 | 1549 |
| | | | | 4800 | 3260 | 1731 |
| -43R | 0.120 | 7690 | 403 | 4270 | 3570 | 600 |
| | | | | 4390 | 3590 | 1200 |
| | | | | 4530 | 3560 | 1800 |
| -44R | 0.399 | 6800 | 403 | 4780 | ---- | 600 |
| | | | | 4960 | ---- | 1200 |
| | | | | 5190 | ---- | 1800 |
| -45MS | 0.099 | 3700 | 445 | 3580 | 3210 | 170 |
| | | | | 3630 | 3190 | 640 |
| | | | | 3650 | 3170 | 947 |
| | | | | 3670 | 3160 | 1264 |
| | | | | 3720 | 3190 | 1537 |
| | | | | 3700 | 3170 | 1703 |
| -46MS | 0.393 | 3760 | 470 | 3920 | 2800 | 350 |
| | | | | 3940 | 2790 | 680 |
| | | | | 3970 | 2790 | 943 |
| | | | | 4120 | 2790 | 1260 |
| | | | | 4180 | 2790 | 1543 |
| | | | | 4210 | 2790 | 1720 |
| -47RS | 0.102 | 7340 | 498 | 4480 | 3270 | 600 |
| | | | | 4650 | 3190 | 1200 |
| | | | | 4840 | 3160 | 1800 |
| -48RS | 0.400 | 7090 | 498 | 4500 | 2760 | 600 |
| | | | | 4650 | 2760 | 1200 |
| | | | | 4840 | 2720 | 1800 |
| -49RH | 0.206 | 7480 | 408 | 4100 | 3460 | 600 |
| | | | | 4220 | 3440 | 1200 |
| | | | | 4270 | 3460 | 1800 |
| -51RH | 0.400 | 6900 | 398 | 4230 | 3240 | 600 |
| | | | | 4290 | 3245 | 1200 |
| | | | | 4340 | 3240 | 1800 |
| -50RHS | 0.104 | 5750 | 402 | 4180 | 3420 | 600 |
| | | | | 4310 | 3420 | 1200 |
| | | | | 4370 | 3370 | 1800 |
| -52RHS | 0.398 | 5890 | 398 | 4370 | 2970 | 600 |
| | | | | 4450 | 2970 | 1200 |
| | | | | 4500 | 2980 | 1800 |

*Assuming ε = 1.00 at in-depth temperature measurement station.

TABLE 48

AVERAGED VALUES OF TOTAL NORMAL EMITTANCE AND RATIOS OF CALCULATED AND OBSERVED TEMPERATURES DERIVED FROM HOT GAS/COLD WALL ARC PLASMA TESTS

| Material/Code | | $\epsilon_N$ Computed Normal Emittance (Solid) | (Melting) | Calculated Temperature Ratio T(CALC)/T(OBS) - Cold Wall Heat Transfer Coefficient (Solid) | (Melting) |
|---|---|---|---|---|---|
| $HfB_{2.1}$ | A-2 | 0.45 | 0.39 | 1.16 | 0.98 |
| $ZrB_2$ | A-3 | 0.47 (0.500") | 0.39 (0.500") | 1.09 (0.500") | 1.08 (0.500") |
| $ZrB_2$ | A-3 | 0.57 (0.750") | ---- (0.750") | 1.12 (0.750") | ---- (0.750") |
| $HfB_2$ + 20 v/o SiC | A-4 | 0.62 | 0.48 | 1.22 | 1.07 |
| Boride Z | A-5 | 0.75 | ---- | 1.20 | ---- |
| $HfB_{2.1}$ + 20 v/o SiC | A-7 | 0.55 | 0.47 | 1.25 | 0.99 |
| $ZrB_{2.1}$ + 20 v/o SiC | A-8 | 0.59 | 0.50 | 1.34 | 1.02 |
| $HfB_{2.1}$ + 35 v/o SiC | A-9 | 0.55 | 0.52 | 1.17 | 0.99 |
| $ZrB_2$ + 14 v/o SiC + 30 v/o C | A-10 | 0.62 | 0.55 | 1.20 | 1.11 |
| RVA | B-5 | 0.52 (0.500") | 0.75 (0.740") | 1.17 (0.500") | 1.20 (0.740") |
| PG | B-6 | 0.41 $\perp$ to C | 0.41 $\parallel$ to C | 1.19 $\perp$ to C | 1.04 $\parallel$ to C |
| BPG | B-7 | 0.37 $\perp$ to C | 0.43 $\parallel$ to C | 1.18 $\perp$ to C | 1.03 $\parallel$ to C |
| Si/RVC | B-8 | 0.69 Coated | 0.56 Bare | 1.36 Coated | 1.07 Bare |

TABLE 48 (CONT)

AVERAGED VALUES OF TOTAL NORMAL EMITTANCE AND RATIOS OF CALCULATED AND OBSERVED TEMPERATURES DERIVED FROM HOT GAS/COLD WALL ARC PLASMA TE[illegible]

| Material/Code | | $\epsilon_N$ Computed Normal Emittance (Solid) | (Melting) | Calculated Tem[illegible] T(CALC)/T(OBS)-Cold wall Heat Transfer Coefficient (Solid) | (Melting) |
|---|---|---|---|---|---|
| PT0178 | B-9 | 0.65 | ---- | 1.07 | ---- |
| Poco Graphite | B-10 | 0.64 | ---- | 1.18 | ---- |
| Glassy Carbon | B-11 | 0.50 | ---- | 1.00 | ---- |
| HfC + C | C-11 | 0.57 | 0.50 | 1.10 | 1.05 |
| ZrC + C | C-12 | 0.60 | 0.42 | 1.08 | 1.01 |
| JTA | D-13 | 0.52 | 0.55 | 1.13 | 0.93 |
| KT-SiC | E-14 | 0.63 | ---- | 1.43 | ---- |
| JT0992 | F-15 | 0.48 | 0.60 | 1.04 | 1.08 |
| JT0981 | F-16 | 0.49 | 0.51 | 1.11 | 1.05 |
| $WSi_2/W$ | G-18 | 0.58 Coated | 0.32 Bare | 1.54 Coated | 1.13 Bare |
| Sn-Al/Ta-10W | G-19 | 0.59 Coated | 0.44 Bare | 1.4[illegible] Coated | 1.09 Bare |
| W + Zr + Cu | G-20 | 0.52 | 0.49 | 1.31 | 1.12 |
| W + Ag | G-21 | 0.54 | 0.33 | 1.35 | 1.01 |
| $SiO_2$ + 68.5 w/o W | H-22 | 0.61 | ---- | 1.12 | ---- |
| $SiO_2$ + 60 w/o W | H-23 | 0.56 | ---- | 1.27 | ---- |
| Hf-20Ta-2Mo | I-23 | 0.60 (0.500") | 0.45 (0.500") | 1.20 (0.500") | 1.00 (0.500") |
| | | 0.59 (0.750") | ---- (0.750") | 1.14 (0.750") | ---- (0.750") |
| Ir/C | I-24 | 0.36 Coated | 0.83 Bare | 1.21 Coated | 1.15 Bare |
| | | 0.51 Oxide Coated | 1.06 Oxide Coated | | |

TABLE 49

COMPUTED TEMPERATURES FOR $ZrB_2$ AND $HfB_2$ AFTER TWENTY SECONDS UNDER 10 MW ARC CONDITIONS

($i_e$ = 2000 BTU/lb, $P_e$ = 4.3 atm)

| Distance from Front Face mils | Cold Wall Heat Flux (BTU/ft$^2$sec) 800 | 1000 | 1200 |
|---|---|---|---|
| | $ZrB_2$ (density = 375 lbs/ft$^3$) | | |
| Radiation Equilibrium (Eqs. 2, 3) | 4530°F | 4640°F | 4715°F |
| 0 | 3221 | 3498 | 3708 |
| 250 | 2557 | 2814 | 3018 |
| 500 | 1887 | 2122 | 2318 |
| 1000 | 1029 | 1245 | 1437 |
| | $HfB_2$ (density = 625 lbs/ft$^3$) | | |
| Radiation Equilibrium (Eqs. 2, 3) | 4530°F | 4640°F | 4715°F |
| 0 | 3298 | 3571 | 3770 |
| 250 | 2577 | 2833 | 3030 |
| 500 | 1797 | 2034 | 2224 |
| 1000 | 461 | 688 | 902 |

# TABLE 50

## SUMMARY OF 10 MEGAWATT ARC HIGH FLUX

## EXPOSURE CONDITIONS AND RESULTS

| Material Sample No. Assumed Emittance at $\lambda = 0.65\mu$ $\epsilon = 0.60$ | $P_{plen}$ atm | $i_o$ BTU/lb | D in | $q_{cw}$ BTU/ft²sec | $T_R$ °R | Calculated Temperature Ratio T(CALC)/T(OBS) Cold Wall Heat Trans. Coefficient | Fay and Riddell Heat Trans. Coefficient | $T_{max}$ °F | Exposure Time seconds | Material Recession mils | Degradation Mode | Metallographic Features (Distance of Crack from) (Front Face - Mils) |
|---|---|---|---|---|---|---|---|---|---|---|---|---|
| $HfB_{2.1}$(A-2) | | | | | | | | | | | | |
| -HF-1 | 6.33 | 1965 | 0.875 | 785 | 4820 | 1.02 | 0.95 | 4360 | 20.1 | 21 | Th. Shock | Large Cracks* (70) |
| -HF-2 | 6.26 | 1930 | 0.875 | 695 | 3765 | 1.28 | 1.20 | 3505 | 20.1 | 1 | Oxidation | Fine Cracks* (90) |
| $HfB_{2.1}$(A-6) | | | | | | | | | | | | |
| -HF-20 | 6.57 | 2235 | 0.875 | 799 | 4068 | 1.27 | 1.19 | 3600 | 20.1 | -2 | Th. Shock | Large Cracks (380) |
| -HF-21 | 6.60 | 2030 | 0.875 | 733 | 3930 | 1.26 | 1.18 | 3470 | 20.1 | -1 | Oxidation | Large Cracks* (380) |
| $HfB_{2.1}$+20 v/o SiC(A-4) | | | | | | | | | | | | |
| -HF-25A | 4.76 | 2270 | 0.500 | 836 | 3700 | 1.41 | 1.27 | 3240 | 8.7 | -- | Oxidation | ---------- (---) |
| -HF-25B | 4.66 | 2300 | 0.500 | 836 | 4685 | 1.07 | 1.04 | 4425 | 20.0 | -- | Th. Shock | Large Cracks (300) |
| -HF-26 | 8.51 | 3895 | 0.500 | 1286 | 4920 | 1.31 | 1.31 | 4460 | 7.8 | -- | Th. Sh. +Melt | Large Cracks (160) |
| -HF-27A | 4.73 | 2170 | 0.500 | 835 | 3670 | 1.42 | 1.38 | 3210 | 10.9 | -- | Oxidation | ---------- (---) |
| -HF-27B | 4.80 | 2270 | 0.500 | 835 | 4320 | 1.21 | 1.17 | 3860 | 21.0 | 10 | Oxidation | Sound* (---) |
| -HF-28 | 7.22 | 3440 | 0.500 | 940 | 4165 | 1.34 | 1.30 | 3705 | 12.0 | 5 | Oxidation | Sound* (---) |
| -HF-35 | 6.57 | 2099 | 0.500 | 773 | ---- | ---- | ---- | ---- | 20.4 | 3 | Oxidation | Sound* (---) |
| -HF-36 | 7.42 | 2890 | 0.500 | 966 | 4630 | 1.02 | 1.02 | 4170 | 20.1 | 53 | Th. Shock | Large Crack (180) |
| -HF-37 | 7.06 | 2540 | 0.500 | 940 | 5250 | 1.05 | 1.03 | 4790 | 20.2 | 13 | Oxidation | Sound (---) |
| -HF-38 | 7.55 | 3013 | 0.500 | 1197 | 5540 | 1.08 | 1.05 | 5060 | 19.9 | 34 | Th. Shock | Large Crack (160) |
| $HfB_{2.1}$ + 20 v/o SiC(A-7) | | | | | | | | | | | | |
| -HF-18 | 4.63 | 2200 | 0.875 | 787 | 3960 | 1.30 | 1.21 | 3600 | 20.1 | 5 | Oxidation | Fine Cracks* (110) |
| -HF-19A | 4.74 | 2331 | 0.875 | 777 | 4040 | 1.29 | 1.22 | 3680 | 16.2 | -- | Oxidation | ---------- (---) |
| -HF-19B | 4.80 | 2335 | 0.875 | 840 | 4485 | 1.16 | 1.10 | 4025 | 20.1 | 0 | Th. Shock | Large Cracks ( 90) |
| -HF-32 | 7.26 | 2710 | 0.500 | 948 | 5070 | 1.11 | 1.08 | 4610 | 20.1 | 28 | Oxidation | Sound* (---) |
| -HF-33 | 8.47 | 3660 | 0.500 | 1306 | 5160 | 1.04 | 1.03 | 5700 | 20.1 | 340 | Th. Shock | Fin Cracks* (600) |
| -HF-34 | 6.83 | 2335 | 0.500 | 834 | 4990 | 1.06 | 1.03 | 4530 | 20.1 | 7 | Oxidation | Sound* (---) |
| $ZrB_2$(A-3) | | | | | | | | | | | | |
| -HF-5 | 2.47 | 4030 | 0.875 | 1120 | 6040 | 1.06 | 0.93 | 5480 | 16.2 | 32 | Th. Sh. +Melt | Large Cracks (300) |
| -HF-6 | 2.49 | 4065 | 0.875 | 1120 | 5870 | 1.08 | 0.96 | 5410 | 20.3 | 64 | Th. Sh. +Melt | Large Cracks (360) |
| -HF-7A | 2.44 | 2235 | 0.875 | 650 | ---- | ---- | ---- | ---- | 17.3 | -- | Oxidation | ---------- (---) |
| -HF-7B | 6.95 | 2540 | 0.875 | 960 | 5830 | 0.95 | 0.88 | 5370 | 20.3 | 65 | Th. Sh. +Melt | Large Cracks (210) |
| -HF-8 | 6.36 | 1968 | 0.875 | 800 | 4280 | 1.15 | 1.07 | 3820 | 20.3 | -- | Oxidation | ---------- (---) |
| -HF-13 | 6.54 | 2030 | 0.875 | 880 | 5190 | 0.97 | 0.89 | 4730 | 16.6 | 7 | Th. Shock | Large Cracks (360) |
| -HF-14 | 6.43 | 2030 | 0.875 | 849 | ---- | ---- | ---- | ---- | 20.1 | 1 | Th. Shock | Large Cracks (160) |
| -HF-15 | 6.31 | 2030 | 0.875 | 852 | 5130 | 0.98 | 0.91 | 4670 | 17.8 | 30 | Th. Shock | Large Cracks ( 90) |
| $ZrB_2$(Avco) | | | | | | | | | | | | |
| -HF-17 | 6.37 | 1964 | 0.875 | 714 | 3865 | 1.26 | 1.18 | 3425 | 20.1 | 12 | Oxidation | Fine Cracks* (length) |
| -HF-22 | 6.50 | 2130 | 0.875 | 811 | 4800 | 1.06 | 0.99 | 4340 | 15.6 | -4 | Th. Shock | Large Cracks (270) |
| Boride Z(A-5) | | | | | | | | | | | | |
| -HF-11 | 6.37 | 1965 | 0.875 | 714 | 4845 | 1.01 | 0.94 | 4385 | 14.6 | -- | Th. Shock | Large Cracks (250) |
| -HF-12 | 6.40 | 1965 | 0.875 | 747 | 4610 | 1.06 | 0.99 | 4160 | 12.0 | 6 | Th. Shock | Large Cracks (250) |
| $ZrB_{2.1}$ + 20 v/o SiC(A-8) | | | | | | | | | | | | |
| -HF-23A | 6.57 | 2200 | 0.875 | 787 | 4160 | 1.23 | 1.16 | 3700 | 20.1 | -- | Oxidation | ---------- (---) |
| -HF-23B | 6.77 | 2370 | 0.875 | 852 | 4370 | 1.21 | 1.14 | 3910 | 20.1 | -6 | Th. Shock | Large Cracks (length) |

*Samples examined by MDT dye penetrant (Table 12) yielding results in agreement with metallographic findings.
**$HfB_{2.1}$ + 20 v/o SiC(A-4)HF-35 showed a small surface crack but was otherwise sound.

TABLE 51

SPECIFICATION OF FLUX-SIZE THRESHOLDS FOR

THERMAL SHOCK FAILURES OF BORIDE CYLINDERS

| Material | No Thermal Shock Noted | | Thermal Shock Occurred | |
|---|---|---|---|---|
| | 1/2" Diam | 7/8" Diam | 1/2" Diam | 7/8" Diam |
| | ($q_{cw}$ $\frac{BTU}{ft^2 sec}$) / ($T_{max}$ °F) | | ($q_{cw}$ $\frac{BTU}{ft^2 sec}$) / ($T_{max}$ °F) | |
| $HfB_2$ (A-2) | ---------- | (695)/(3305)* | ---------- | (785)/(4360) |
| $HfB_2$ (A-6) | ---------- | (733)/(3470)* | ---------- | (799)/(3600) |
| $HfB_2$ + SiC (A-4) | (940)/(5170) | ---------- | ( 966)/(5170) | ---------- |
| $HfB_2$ + SiC (A-7) | (948)/(4610) | (787)/(3500)* | (1306)/(5780) | (840)/(4025) |
| $ZrB_2$ (A-3) | ---------- | (800)/(3820) | ---------- | (960)/(5370) |
| $ZrB_2$ (Avco) | ---------- | (714)/(3415)* | ---------- | (811)/(4340) |
| Boride Z (A-5) | ---------- | ---------- | ---------- | (714)/(4380)<br>(747)/(4160) |
| $ZrB_2$ + SiC (A-8) | ---------- | (787)/(3700) | ---------- | (852)/(3910) |

*Cracks revealed by NDT dye penetrant test and metallographic examinations of selected samples.

# TABLE 52

## SUMMARY OF ARC PLASMA EXPOSURES OF PIPE SPECIMENS IN THE TEN MEGAWATT ARC FACILITY

(Mach No. = 1.73, Stagnation Pressure 6.0 Atm.)

| Material Sample No. * | Position in Stream * | Enthalpy (BTU/lb) | Heat Flux (BTU/ft²sec) | Pipe Shear Stress (lbs/ft²) | °F | Emittance (λ = 0.65μ) | Sample Weight Pre-run/Post-run (grams) | Internal Diameter Pre-run/Post-run (inches) | Test Time (sec) |
|---|---|---|---|---|---|---|---|---|---|
| $HfB_{2.1}$+20%SiC(A-7) | | | | | | | | | |
| -1PP | UP | 3960 | 480 | 26.8 | *** | 0.60 | 34.44/34.46 | 0.608/0.610 | 10.00 |
| -2PP | DOWN | 3960 | 480 | 26.8 | 2270 | 0.60 | 36.18/36.18 | 0.606/0.608 | 10.00 |
| -3PP | UP | 3520 | 410 | 24.4 | *** | 0.60 | 35.29/35.10 | 0.607/0.608 | 10.02 |
| -4PP | DOWN | 3520 | 410 | 24.4 | 2270 | 0.60 | 35.27/35.27 | 0.606/0.608 | 10.02 |
| $ZrB_{2.1}$+20%SiC(A-8) | | | | | | | | | |
| -1PP | UP | 3960 | 480 | 26.8 | *** | 0.60 | 21.87/21.89 | 0.606/0.606 | 9.99 |
| -2PP | DOWN | 3960 | 480 | 26.8 | 2420 | 0.60 | 21.86/21.88 | 0.606/0.605 | 9.99 |
| -3PP | UP | 6000 | 590 | 26.4 | *** | 0.60 | 22.08/21.98 | 0.606/0.610 | 9.61 |
| -4PP | DOWN | 6000 | 590 | 26.4 | 4260 | 0.60 | 21.92/21.83 | 0.605/0.608 | 9.61 |
| $ZrB_2$+SiC+C(A-10) | | | | | | | | | |
| -1PP | UP | 3960 | 480 | 26.8 | *** | 0.60 | 17.94/17.94 | 0.606/0.605 | 10.05 |
| -2PP | DOWN | 3960 | 480 | 26.8 | 2600 | 0.60 | 18.73/18.74 | 0.606/0.605 | 10.05 |
| -3PP | UP | 6000 | 590 | 26.4 | *** | 0.60 | 18.13/18.08 | 0.606/0.609 | 6.93 |
| -4PP | DOWN | 6000 | 590 | 26.4 | 3960 | 0.60 | 18.40/18.37 | 0.606/0.605 | 6.93 |
| Si/RVC(B-8) | | | | | | | | | |
| -1PP | UP | 3895 | 472 | 26.5 | *** | 0.70 | 16.92/16.97 | 0.618/0.616 | 9.96 |
| -2PP | DOWN | 3895 | 472 | 26.5 | 3200 | 0.70 | 17.04/17.10 | 0.613/0.612 | 9.96 |
| -3PP | UP | 6000 | 590 | 26.4 | *** | 0.70 | 17.59/17.53 | 0.611/0.616 | 9.96 |
| -4PP | DOWN | 6000 | 590 | 26.4 | 4200 | 0.70 | 17.00/16.95 | 0.606/0.615 | 9.96 |
| KT-SiC(E-14) | | | | | | | | | |
| -3PP | UP | 3995 | 485 | 26.9 | *** | 0.70 | 12.54/12.54 | 0.602/0.602 | 10.00 |
| -4PP | DOWN | 3995 | 485 | 26.9 | 2420 | 0.70 | 12.49/12.50 | 0.601/0.604 | 10.00 |
| -5PP | UP | 6000 | 590 | 26.4 | *** | 0.70 | 12.52/12.22 | 0.601/----- | 9.96 |
| -6PP | DOWN | 6000 | 590 | 26.4 | 3920 | 0.70 | 12.48/12.26 | 0.602/----- | 9.96 |
| Hf-Ta-Mo(1-23) | | | | | | | | | |
| -1PP | UP | 3960 | 480 | 26.8 | *** | 0.55 | 46.78/----- | 0.629/** | 5.76 |
| -2PP | DOWN | 3960 | 480 | 26.8 | 3070 | 0.55 | 46.98/75.32* | 0.629/** | 5.76 |
| -3PP | UP | 3520 | 410 | 24.4 | *** | 0.55 | 44.40/44.44 | 0.641/0.633 | 4.73 |
| -4PP | DOWN | 3520 | 410 | 24.4 | >3000 | 0.55 | 45.50/38.71 | 0.632/0.623 | 4.73 |

*A single run consisted of a pair of samples denoted as "upstream" and "downstream".

* Combined weight of 1-23-1PP and -2PP.
** Sample melted and distorted.
*** No measurement made upstream, pyrometer sighted on 0.10" spot 1/2" inside rear of downstream sample.

| Material Sample No. | Visual Observations * | Description of Motion Picture Film Coverage ** |
|---|---|---|
| $HfB_{2.1}$+20%SiC(A-7) | | |
| -1PP | Series of radial cracks, longitudinal cracks 180° apart. | No activity visible. |
| -2PP | Series of radial cracks, several longitudinal cracks. | Underexposed, no activity visible. |
| -3PP | Half of sample severely cracked, half slightly cracked. | |
| -4PP | Cracked radially and longitudinally. | Hot spot around o-ring. |
| $ZrB_{2.1}$+20%SiC(A-8) | | |
| -1PP | Cracked longitudinally in half. | Overexposed, no features visible. |
| -2PP | One quarter cracked cleanly off. | |
| -3PP | Cracked radially and longitudinally. | Hot spot around o-ring, some sparks blowing back. |
| -4PP | Cracked radially and longitudinally. | Some liquid droplets. |
| $ZrB_2$+SiC+C(A-10) | | |
| -1PP | No visible cracks. | |
| -2PP | Cracked radially in half at o-ring. | Liquid continuously streaming back, some sparks blowing back. |
| -3PP | Cracked radially and longitudinally. | Liquid streaming back early in run, no activity near end. |
| -4PP | No visible cracks. | |
| Si/RVC(B-8) | | |
| -1PP | No visible cracks, coating inside burned off. | Hot spot near top and around o-ring. |
| -2PP | No visible cracks, streaks of silica inside. | Some liquid droplets, not spot around o-ring. |
| -3PP | No visible cracks, coating inside burned off. | |
| -4PP | No visible cracks, coating inside burned off. | Very hot around o-ring, then melted rapidly. |
| KT-SiC(E-14) | | Underexposed, no activity visible. |
| -3PP | Cracked longitudinally in half. | |
| -4PP | Cracked longitudinally in half. | **Camera was sighting inside rear of downstream sample. Descriptions thus apply to this sample's behavior. |
| -5PP | Cracked longitudinally in half and radially | |
| -6PP | Cracked longitudinally in thirds. | |
| Hf-Ta-Mo(1-23) | | |
| -1PP | Burned through at o-ring, eroded behind hole. | |
| -2PP | Large portion melted away, o-ring area degradation. | |
| -3PP | Little damage. | |
| -4PP | Burned through from o-ring back. | |

*Virtually all samples showed indications of heat effects where they came in contact with the o-rings of the sample holding fixture.

TABLE 53

SUMMARY OF MODEL DIMENSIONS BEFORE AND AFTER 15 SECOND EXPOSURE IN WAVE SUPERHEATER
(HEMISPHERICAL CAPS)

| Material ManLabs No/CAL No. | Sting No. | Initial Dimensions Diameter/Length/Wall mils | Final* Wall mils | Recession* Depth mils | Comments* |
|---|---|---|---|---|---|
| | | TEST (67-473) | | | |
| $ZrB_2$(A-3)-1-2 | 1 | 492/1021/139 | 142 | -3 | No change in structure |
| KT-SiC(E-14)-1-8 | 2 | 488/1000/135 | 117 | 18 | No change in structure |
| KT-SiC(E-14)-3-18 | 3 | 944/994/130 | 128 | 2 | Cap fractured on cooling longitudinal crack noted in holder may be due to expansion at sting. Microstructure showed Si melted. |
| Hf-20Ta-2Mo(I-23)-4-19 | 4 | 997/1167/129 | [illegible] | 3 | Melting at nose |
| W(G-18)Uncoated-X-11 | 5 | 491/992/152 | 153 | -1 | Nose was blue |
| RVA(B-5)-X-5 | 6 | 488/996/112 | 92 | 30 | No change in structure |
| JTA(D-13)-X-7 | 7 | 489/957/125 | 129 | -4 | No change in structure |
| JT0992(F-15)-X-9 | 8 | 490/945/96 | Thermal Shock | | Shocked during exposure |
| | | TEST (67-474) | | | |
| Hf-20Ta-2Mo(I-23)-1-12 | 1 | 491/1000/155 | 137 | 18 | Light oxide coating formed |
| $HfB_{2.1}$(A-2)-X-1 | 2 | 491/937/144 | 139 | 5 | Cap broke off at end of run |
| $HfB_2$+SiC(A-4)-X-4 | 3 | 492/963/154 | 159 | -5 | No change in structure |
| PG(B-6)-X-6 | 4 | 488/1061/122 | 104 | 8 | "C" axis perpendicular to cylinder axis, no change in structure |

TABLE 54

SUMMARY OF MODEL DIMENSIONS BEFORE AND AFTER 15 SECOND EXPOSURE IN WAVE SUPERHEATER
(HEMISPHERICAL CAPS)

| Material ManLabs No/CAL No. | Sting No. | Initial Dimensions Diameter/Length/Wall mils | Final* Wall mils | Recession* Depth mils | Comments* |
|---|---|---|---|---|---|
| BPG(B-7)-X-16 | 5 | 490/836/157 | 125 | 32 | "C" axis perpendicular to cylinder axis, no change in structure |
| JT0981(F-16)-X-10 | 6 | 488/946/141 | 122 | 19 | Light oxide coating formed |
| $ZrB_2$(A-3)-24-3 | 7 | 492/989/163 | Thermal Shock | | Shocked during exposure |
| Sn-Al/Ta-10W(G-19)-3-22 | 8 | 1001/1001/146 | 133** | 13 | Melted Sn at nose streamed back to sides and sting holder |

*Based on metallographic analysis.
**2 mil coating on outside and 8 mil coating on inside of Ta-10W.
+8 mil coating on both sides of 130 mil Ta-10W.

TABLE 55

CAMERA SETTINGS EMPLOYED IN WAVE SUPERHEATER EXPOSURES

| Run No. | Camera Number | Film Speed Frames/Sec | Focal Length of Lens | Aperature Stop | Shutter Speed Number | |
|---|---|---|---|---|---|---|
| -473 | 1 | 200 | 3 inch | f2.8 | 5 | Ektachrome EF |
| | 2 | 250 | 4 inch | f5.8 | 5 | Ektachrome EF |
| | 3 | 250 | 4 inch | f4.0 | 5 | EF |
| | 4 | 600 | 11 inch* | f5.6 | 40 | ER |
| -474 | 1 | 200 | 3 inch | f4.0 | 5 | Ektachrome ER |
| | 2 | 200 | 4 inch | f5.6 | 5 | Ektachrome EF |
| | 3 | 200 | 4 inch | f8.0 | 5 | ER |
| | 4 | 600 | 11 inch* | ---- | 40 | ER |

*Effective focal length.

TABLE 56

HEAT TRANSFER RESULTS

| | Run No. | 473 | 474 |
|---|---|---|---|
| $\frac{\Delta T}{\Delta t}$ | Rate of Temperature Rise - deg. F/sec | 780 | 880 |
| $\delta$ | Gage Thickness - in | 0.1260 | 0.1265 |
| T | Average Thermocouple Temp at Time of Reading - $^{o}F$ | 360 | 350 |
| c | Corresponding Specific Heat to T of Copper - BTU/lb - $^{o}F$ | 0.096 | 0.096 |
| $q_w$ | Indicated Heat Transfer Rate - BTU/$ft^2$-sec | 440 | 485 |
| $T_w$ | Gage Surface Temp - $^{o}F$ | 410 | 395 |
| $i_w$ | Gage Surface Enthalpy - BTU/lb | 210 | 205 |
| $i_s$ | Total Enthalpy of Stream at Time of Reading - BTU/lb | 1880 | 1870 |
| $q_{cw}$ | Cold Wall Heat Transfer Rate -BTU/$ft^2$sec | 495 | 545 |
| $i_e$ | Run Enthalpy - BTU/lb | 2200 | 2180 |
| $q_{cw}$ | Cold Wall Heat Transfer Rate Corrected to Run Enthalpy - BTU/$ft^2$sec | 580 | 635 |

TABLE 57

TEST CONDITIONS

| Run No. | 473 | 474 |
|---|---|---|
| Rotor Total Pressure - atm | 98.2 | 96.9 |
| Total Temperature - $^{o}R$ | 6740 | 6700 |
| Total Enthalpy - BTU/lb | 2200 | 2180 |
| Tunnel Reservoir Pressure - atm | 56.0 | 55.0 |
| Test Section Stagnation Pressure on Model Nose - atm | 1.15 | 1.15 |
| Free Stream Mach Number | 5.45 | 5.45 |
| Free Stream Density - $lbs/ft^3$ | $8 \times 10^{-5}$ | $8 \times 10^{-5}$ |
| Free Stream Pressure - psi | 0.65 | 0.64 |
| Free Stream Velocity - fps | 9700 | 9700 |

TABLE 58

WALL TEMPERATURE AND HEAT FLUX HISTORY FOR THE STAGNATION POINT OF A 0.500-INCH RADIUS HEMISPHERICAL NOSE WITH A THICKNESS OF 0.125 INCH

| Time | $T_w$ (°R) | $q_{AERO}$ | $-q_{RAD}$ | $q_{NET}$ |
|---|---|---|---|---|
| 0 | 560 | 464.1 | 0.026 | 464.1 |
| 0.5 | 1090 | 431.8 | 0.370 | 431.4 |
| 1.0 | 1302 | 418.9 | 0.753 | 418.1 |
| 1.5 | 1481 | 408.0 | 1.26 | 406.7 |
| 2.0 | 1650 | 397.7 | 1.94 | 395.7 |
| 2.5 | 1814 | 387.7 | 2.83 | 384.9 |
| 3.0 | 1972 | 378.0 | 3.96 | 374.1 |
| 3.5 | 2126 | 368.6 | 5.35 | 363.3 |
| 4.0 | 2274 | 358.4 | 7.01 | 351.4 |
| 4.5 | 2417 | 348.3 | 8.93 | 339.3 |
| 5.0 | 2554 | 338.5 | 11.14 | 327.3 |
| 6.0 | 2813 | 320.0 | 16.39 | 303.6 |
| 7.0 | 3051 | 303.0 | 22.7 | 280.3 |
| 8.0 | 3269 | 287.4 | 29.9 | 257.5 |
| 9.0 | 3468 | 273.3 | 37.9 | 235.4 |
| 10.0 | 3648 | 259.8 | 46.4 | 213.4 |
| 11.0 | 3808 | 246.3 | 55.0 | 191.3 |
| 13.0 | (4146)* | | | (146)* |
| 15.0 | (4405)* | | | (96)* |

*Estimated by hand calculations.

TABLE 59

WALL TEMPERATURE AND HEAT FLUX HISTORY FOR THE STAGNATION POINT OF A 0.250-INCH RADIUS HEMISPHERICAL NOSE WITH A THICKNESS OF 0.125 INCH

| Time | $T_w$ (°R) | $q_{AERO}$ | $-q_{RAD}$ | $q_{NET}$ |
|---|---|---|---|---|
| 0 | 560 | 653.0 | 0.026 | 653.0 |
| 0.5 | 1293 | 593.1 | 0.732 | 592.4 |
| 1.0 | 1576 | 568.7 | 1.62 | 567.1 |
| 1.5 | 1812 | 548.4 | 2.82 | 545.6 |
| 2.0 | 2032 | 529.4 | 4.47 | 524.9 |
| 3.0 | 2441 | 490.1 | 9.29 | 480.8 |
| 3.5 | 2629 | 471.0 | 12.5 | 458.5 |
| 4.0 | 2808 | 453.0 | 16.3 | 436.7 |
| 4.5 | 2978 | 435.8 | 20.6 | 415.2 |
| 5.0 | 3139 | 419.6 | 25.4 | 394.2 |
| 6.0 | 3434 | 389.8 | 36.4 | 353.4 |
| 7.0 | 3695 | 361.8 | 48.8 | 313.0 |
| 8.0 | 3919 | 335.0 | 61.8 | 273.3 |
| 9.0 | 4113 | 311.9 | 74.9 | 237.0 |
| 10.0 | 4279 | 292.1 | 87.8 | 204.3 |
| 11.0 | 4421 | 275.2 | 100.0 | 175.2 |
| 12.0 | (4576)* | | | (140)* |
| 13.0 | (4700)* | | | (112)* |
| 14.0 | (4800)* | | | (82)* |
| 15.0 | (4872)* | | | (67)* |

*Estimated by hand calculation.

UNCLASSIFIED
Security Classification

**DOCUMENT CONTROL DATA - R & D**

*(Security classification of title, body of abstract and indexing annotation must be entered when the overall report is classified)*

| | |
|---|---|
| 1. ORIGINATING ACTIVITY (Corporate author)<br>ManLabs, Inc.<br>21 Erie Street<br>Cambridge, Massachusetts 02139 | 2a. REPORT SECURITY CLASSIFICATION<br>UNCLASSIFIED<br>2b. GROUP<br>N/A |

3. REPORT TITLE

Stability Characterization of Refractory Materials under High Velocity Atmospheric Flight Conditions, Part III, Volume III: Experimental Results of High Velocity Hot Gas/Cold Wall Tests

4. DESCRIPTIVE NOTES (Type of report and inclusive dates)

April 1966 to July 1969

5. AUTHOR(S) (First name, middle initial, last name)

Larry Kaufman
Harvey Nesor

| | | |
|---|---|---|
| 6. REPORT DATE<br>February 1970 | 7a. TOTAL NO. OF PAGES<br>370 | 7b. NO. OF REFS<br>25 |
| 8a. CONTRACT OR GRANT NO.<br>AF33(615)-3859<br>b. PROJECT NO.<br>7312 Task 731201<br>7350 Tasks 735001 and 735002<br>c.<br>d. | 9a. ORIGINATOR'S REPORT NUMBER(S)<br>N/A<br>9b. OTHER REPORT NO(S) (Any other numbers that may be assigned this report)<br>AFML-TR-69-84, Part III, Volume III | |

10. DISTRIBUTION STATEMENT

This document is subject to special export controls and each transmittal to foreign governments or foreign nationals may be made only with prior approval of the Air Force Materials Laboratory (MAMC), Wright-Patterson AFB, Ohio.

| | |
|---|---|
| 11. SUPPLEMENTARY NOTES<br>N/A | 12. SPONSORING MILITARY ACTIVITY<br>Air Force Materials Laboratory (MAMC)<br>Air Force Systems Command<br>Wright-Patterson Air Force Base, Ohio |

13. ABSTRACT

The oxidation of refractory borides, graphites and JT composites, hypereutectic carbide-graphite composites, refractory metals, coated refractory metals, metal oxide composites, and iridium coated graphites in air over a wide range of conditions was investigated over the spectrum of conditions encountered during reentry or high velocity atmospheric flight, as well as those employed in conventional furnace tests. Elucidation of the relationship between hot gas/cold wall (HG/CW) and cold gas/hot wall (CG/HW) surface effects in terms of heat and mass transfer rates at high temperatures was a principal goal.

Arc plasma exposures have been performed at Mach Numbers between 0.1 and 3.2 stagnation pressures between 0.01 and 1.0 atm., stagnation enthalpies up to 16,000 BTU/lb, cold wall heat flux up to 1200 BTU/ft$^2$sec, exposure times up to 23,400 seconds and surface temperatures between 2100° and 6500°F. Data include material recession, metallographic and X-ray analysis, radiated heat flux and normal total emittance. In addition, color motion picture coverage was provided. Materials forming solid oxides show lower recessions in the HG/CW tests at a stated surface temperature than in CG/HW tests. The reverse is true for ablating materials. Temperature gradients of 800° to 1500°F through 30-50 mil oxides are observed. The practical implications of this finding are substantial (if the gradients exist under free flight conditions). Long-time cyclic exposures of diboride composites in the Model 500 and ROVERS facilities for trajectories typified by FDL-7MC provide a striking illustration of the reuse capability of boride composites for lifting reentry applications.

DD FORM 1 NOV 1473

UNCLASSIFIED
Security Classification

UNCLASSIFIED

Security Classification

## DOCUMENT CONTROL DATA - R & D

*(Security classification of title, body of abstract and indexing annotation must be entered when the overall report is classified)*

| | |
|---|---|
| 1. ORIGINATING ACTIVITY *(Corporate author)*<br>ManLabs, Inc.<br>21 Erie St.<br>Cambridge, Massachusetts 02139 | 2a. REPORT SECURITY CLASSIFICATION<br>UNCLASSIFIED<br>2b. GROUP |
| 3. REPORT TITLE | |
| 4. DESCRIPTIVE NOTES *(Type of report and inclusive dates)* | |
| 5. AUTHOR(S) *(First name, middle initial, last name)* | |

| | | |
|---|---|---|
| 6. REPORT DATE | 7a. TOTAL NO. OF PAGES | 7b. NO. OF REFS |
| 8a. CONTRACT OR GRANT NO.<br>b. PROJECT NO.<br>c.<br>d. | 9a. ORIGINATOR'S REPORT NUMBER(S)<br>9b. OTHER REPORT NO(S) *(Any other numbers that may be assigned this report)*<br>AFML-TR-69-84, Part III, Volume III | |

| | |
|---|---|
| 10. DISTRIBUTION STATEMENT | |
| 11. SUPPLEMENTARY NOTES | 12. SPONSORING MILITARY ACTIVITY |

13. ABSTRACT

This abstract is subject to special export controls and each transmittal to foreign governments or foreign nationals may be made only with prior approval of the Air Force Materials Laboratory (MAMC), Wright-Patterson AFB, Ohio.

DD FORM 1 NOV 68 1473

Security Classification

| 14. KEY WORDS | LINK A | | LINK B | | LINK C | |
|---|---|---|---|---|---|---|
| | ROLE | WT | ROLE | WT | ROLE | WT |
| oxidation | | | | | | |
| borides | | | | | | |
| graphites | | | | | | |
| J'T composites | | | | | | |
| refractory | | | | | | |
| metal oxide composites | | | | | | |
| reentry | | | | | | |
| high velocity atmospheric flight | | | | | | |
| stagnation enthalpies | | | | | | |
| cold wall heat flux | | | | | | |
| emittance | | | | | | |
| temperature gradients | | | | | | |
| trajectories | | | | | | |